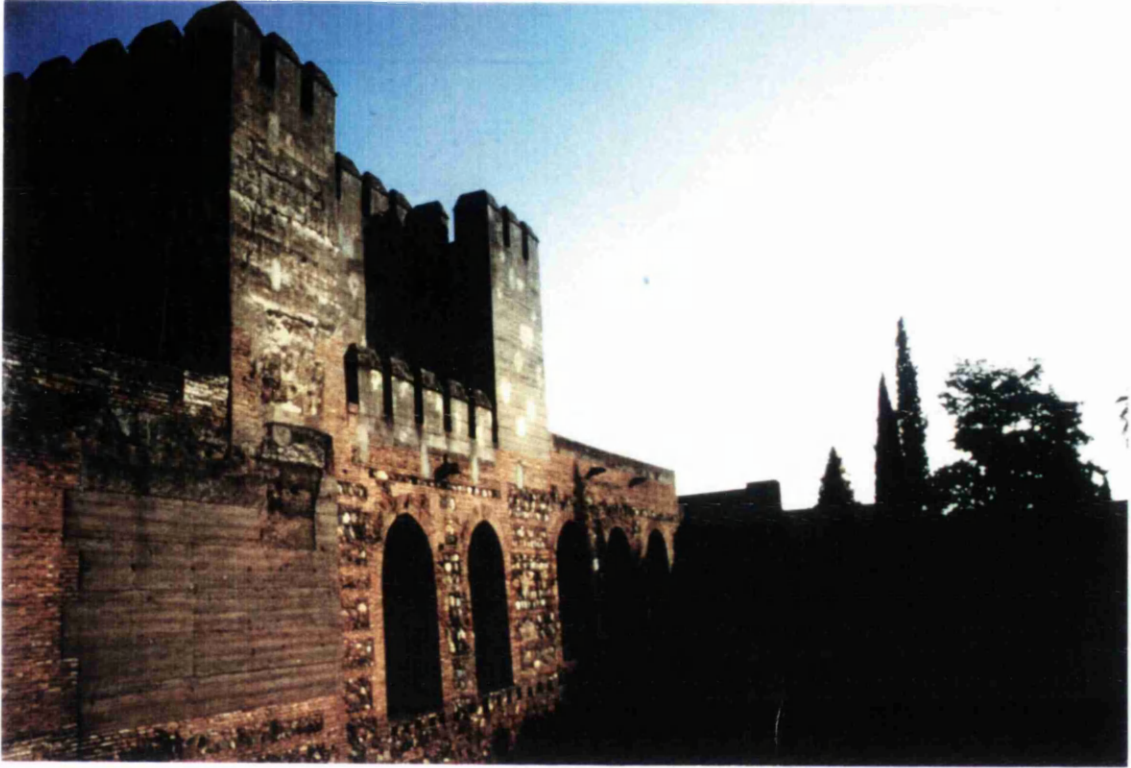


# **The Origin of the External Basins of the Betics, Southern Spain**

(and Their Use in Interpreting the Orogenic History)



*The Alhambra, Granada*

S.G.L. Stromberg B.Sc. (University of Liverpool)

A thesis submitted for the degree of Ph.D.

University of Glasgow

Department of Geology & Applied Geology.

July 1994.

**Vol. 1.**

ProQuest Number: 13833482

All rights reserved

INFORMATION TO ALL USERS

The quality of this reproduction is dependent upon the quality of the copy submitted.

In the unlikely event that the author did not send a complete manuscript and there are missing pages, these will be noted. Also, if material had to be removed, a note will indicate the deletion.



ProQuest 13833482

Published by ProQuest LLC (2019). Copyright of the Dissertation is held by the Author.

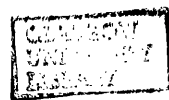
All rights reserved.

This work is protected against unauthorized copying under Title 17, United States Code  
Microform Edition © ProQuest LLC.

ProQuest LLC.  
789 East Eisenhower Parkway  
P.O. Box 1346  
Ann Arbor, MI 48106 – 1346



Her  
10,005  
Copy 1  
Vol 1



This thesis represents work carried out between October 1991 and July 1994.

I declare that this thesis is entirely my own work, except micropalaeontological studies which were jointly undertaken with M. Keen at the University of Glasgow. This thesis has not been submitted for a degree at any other institution.

Signed

S.G. Stromberg

**For Linda, Mum & Dad.**

### **Note on Thesis Organisation**

Because of the number of figures involved in this thesis the figures have been separated from the main text of the thesis. Consequently the thesis is presented as two volumes, Volume I contains the text of the Thesis and Volume II contains the figures and appendices. This allows easy cross referencing of the text, figures and appendices.

In addition this thesis is organised into 4 self contained parts;

*Overview*

*Part I The Guadalquivir Basin*

*Part II The Gibraltar Arc Flysch*

*Part III The use of the External Basins in the Interpretation of the Betic Orogen.*

Each part has its own separate system of chapter and figure organisation, this applies to both Volume I and Volume 2.

## Abstract

The Betic mountain chain of Southern Spain, together with the Rif Mountains of N.W. Africa forms the western-most extension of the Alpine mountain chain in Europe. The Orogen formed as a direct result of the interaction between the African and Iberian plates which took place from the late Cretaceous onwards. The origin of the Betics is far from understood and there are several conflicting hypotheses concerning the origin of the Orogen.

There are two major external basins to the Betic Orogen in Southern Spain, the Guadalquivir Basin and the Gibraltar Arc Flysch, and both provide important insights into its tectonic history.

The Guadalquivir Basin lies on the northern margin of the External Zone Tertiary fold-thrust belt of the Betic Orogen and south of the Palaeozoic Iberian Meseta. It can be subdivided into structurally distinct regions, an undeformed autochthonous basin which lies to the north of a deformed allochthonous basin. The origin of the Guadalquivir Basin (previously interpreted as being the foreland basin to the Orogen) is questioned. Structural sedimentological and provenance studies demonstrate that the Guadalquivir Basin is not a foreland basin because; 1. It formed as an integral part of the destruction of the Iberian passive margin during which time thin skinned thrusting generated a basin on the northern margin of the External Zones, 2. The fill and unconformities of this basin were controlled by eustasy rather than by the tectonic incursion of an orogenic wedge being driven onto the Iberian Margin, 3. The basin did not form by the downward flexure of the lithosphere in response to an orogenic load. Therefore the basin cannot be considered to be a true foreland basin. The clastic sedimentation in the Guadalquivir Basin was controlled by the emergence of the External Zone thrust sheet, during the late Miocene, which was related to the thin skinned thrusting. During this time the recycling of material, that had originally been derived from the Palaeozoic Iberian Meseta, took place. A thrusting event at the end of the Miocene/early Pliocene led to the destruction of the Guadalquivir Basin which was subdivided into the allochthon and autochthon seen today.

The Gibraltar Arc flysch nappes link the External Rif of North Africa to the External Zone of Southern Spain. The largest unit of the Gibraltar Arc is the Aljibe Flysch which can be subdivided into the Beneiza Flysch and Aljibe Arenites, which are Oligo-Miocene in age. The Beneiza Flysch is characterised by thin sandstones and siltstones that are interpreted to have been deposited by turbiditic currents. These pass rapidly upwards into the thick bedded and super-mature Aljibe Arenites, which are entirely dominated by water escape-structures. The contact between these two units marks a dramatic change in the depositional environment at the beginning of the Miocene. The Aljibe Flysch is interpreted as recording the development of a basin plain that became tectonically segregated at the beginning of the Miocene, at which time new and tectonically confined basins developed. Tectonic instabilities created elsewhere in the External Zone resulted in mobilisation of large amounts of sediment which was rapidly deposited in the newly created basins. The flysch units have subsequently been thrust westwards post-Lower Miocene during which time peridotites were emplaced into mid-crustal levels

Consideration of the tectonic and sedimentary history of the Guadalquivir Basin and Gibraltar Arc Flysch provides an important insight into the tectonic history of the Betic Orogen. Data collected during the study of these basins, combined with important new published data from the Alboran Sea and Ronda Peridotites, has resulted in the rejection of the widely accepted 'extensional collapse' model and in the identification of strike-slip tectonism and transcurrent movements as the main mechanism for the building of the Betic Orogen. Miocene transcurrent movements in the Betic area resulted in the break up the Iberian passive margin, the emplacement of metamorphic terranes and in the formation of thrusts in the Gibraltar Arc through a complicated history of transtension and transpression in the region of the Alboran sea.



# CONTENTS

## VOLUME 1

### OVERVIEW

1. THE BETIC OROGEN .....	3
1.1 Introduction .....	3
1.2 Plate Tectonic Setting .....	3
1.3 Tectonic Subdivision .....	4
1.3.1 Internal Zone .....	4
1.3.2 Nevado-Filabride Thrust Sheet .....	4
1.3.3 Alpujarride Thrust Complex .....	5
1.3.4 Malaguide Thrust Unit. ....	5
1.3.5 Internal Rif, N. Africa. ....	5
1.3.6 External Zone .....	6
1.3.7 Subdivision of the External Zone .....	6
1.3.8 The Alboran Sea .....	7
1.3.9 External Basins .....	7
1.4 Geological History: A comparison of hypotheses .....	8
1.4.1 Compressional Tectonism and Metamorphism. ....	8
1.4.2 Strike Slip Tectonism .....	9
1.4.3 Extensional Collapse .....	9
1.4.4 External Zone .....	10
1.4.5 External Basins. ....	11
2 ROLE OF BASINS IN INTERPRETING OROGENS .....	13
2.1 Classification of Basins. ....	13
2.2 The Classification of Neogene Basins of the Betic Orogen .....	15
2.2.1 External Foredeep Orogenic Basins .....	15
2.2.2 Rifted Continental Margin (Extensional) Basins .....	16
2.3 Basin Development in Relation to Orogens .....	17
2.3.1 Tectonics .....	18
2.3.2 Provenance .....	18
2.3.3 The Provenance History .....	20
2.4 External Basins of the Betics: Their Potential as an Orogenic Window .....	20
3 AIMS AND OBJECTIVES OF THESIS .....	21
3.1 Objectives. ....	21
3.2 Thesis Organisation. ....	21

### PART I

## THE GUADALQUIVIR BASIN

CHAPTER 1 INTRODUCTION .....	24
1.1 General Setting .....	24
1.2 Stratigraphic Setting .....	24
1.3 Previous Models for Basin Formation .....	25
1.4 Study Area .....	26
CHAPTER 2	
TECTONO-STRATIGRAPHIC ANALYSIS .....	28
2.1 Introduction .....	28
2.2 Data Sources .....	28
2.2.1 Maps .....	28
2.2.2 Seismic & Bore Hole Data .....	29

2.2.3 Field Data .....	30
2.3 Revisions .....	30
2.3.1 Revised Maps .....	30
2.3.2 A Revised Stratigraphy for the Guadalquivir Basin .....	31
2.4 Inferences .....	33
2.4.1 Nature of the Allochthonous / Autochthonous Boundary .....	33
2.4.2 Status of the Olistostrome .....	34
2.5 Cross-Sections .....	35
2.6 Chrono-Stratigraphy .....	36
2.7 Chrono-Stratigraphy Compared to Global Eustasy and Tectonism in the Betic Orogen .....	37
2.8 A Tectonic & Stratigraphic History for the Guadalquivir Basin .....	38
2.8.1 Mesozoic to Palaeogene. ....	38
2.8.2 Lower-Mid Miocene .....	38
2.8.3 Tortonian .....	39
2.9 Conclusions .....	40
 <b>CHAPTER 3</b>	
<b>SEDIMENTOLOGY &amp; PALAEOGEOGRAPHY .....</b>	<b>42</b>
3.1 Introduction .....	42
3.2 General Stratigraphy .....	42
3.3 Lower & Mid Miocene Facies Analysis .....	42
3.3.1 Thinly Bedded Facies .....	43
3.3.2 Thickly Bedded Marls .....	43
3.3.3 Laminated Diatomites .....	43
3.3.4 Boulder Facies .....	44
3.3.5 Facies Distributions and Associations .....	44
3.3.6 Facies Interpretations .....	44
3.4 Tortonian Facies Analysis .....	46
3.4.1 Thin Bedded Sandstones .....	46
3.4.2 Tabular Sandstones .....	47
3.4.3 Thick Bedded Sandstones .....	47
3.4.4 Cyclicity Observed in the Tortonian .....	48
3.4.5 Facies Interpretation .....	48
3.5 Lower Messinian Facies Analysis .....	51
3.5.1 Marls .....	52
3.5.2 Thin Bedded Calc-Lithic Arenites .....	52
3.5.3 Calc-Lithic Arenites .....	52
3.5.4 Bioclastic Grainstones .....	53
3.5.5 Conglomerates .....	53
3.5.6 Facies Interpretation .....	54
3.6 Upper Messinian Facies Analysis .....	57
3.6.1 Calc-Lithic Arenites. ....	58
3.6.2 Calc-Lithic Arenites With Thin Pebble Beds .....	58
3.6.3 Grey/Red Marls With Rootlets .....	58
3.6.4 Conglomerates .....	58
3.6.5 Facies Associations and Distributions .....	58
3.6.6 Facies Interpretation .....	59
3.7 Summary of the Palaeoenvironmental Evolution of the Guadalquivir basin .....	61
3.7.1 Lower Miocene Environment .....	61
3.7.2 Tortonian Environment .....	61
3.7.3 Lower Messinian Environment .....	62
3.7.4 Upper Messinian Environment .....	62
3.8 Palaeogeography of the Miocene Guadalquivir Basin .....	62
3.8.1 Shelf Break Margin .....	62
3.8.2 Ramp Margins .....	63
3.9 Allochthon & Autochthon: Part of the Same Basin ?? .....	64
3.10 Conclusions .....	64

<b>CHAPTER 4</b>	
<b>PROVENANCE OF THE GUADALQUIVIR</b>	
<b>BASIN SEDIMENTS .....</b>	<b>66</b>
4.1 Introduction .....	66
4.2 Quantitative Petrography .....	69
4.2.1 Samples .....	69
4.2.2 Methods .....	69
4.2.3 Assessment of Sediment Bias .....	72
4.2.4 Petrographic Characteristics in Relation to Plate Setting. ....	74
4.3 Clast Composition of Conglomerates .....	76
4.4 Palaeocurrent Data .....	76
4.4.1 Data .....	76
4.4.2 Transport Pathways .....	77
4.5 Geochemistry & Geochronology of Detrital White Micas .....	77
4.5.1 Geochemical Variation of White Micas .....	77
4.5.2 Samples .....	78
4.5.3 Methods .....	78
4.5.4 Geochemistry of the White Micas .....	79
4.5.5 Geochronology using Ar/Ar Dating Methods .....	80
4.5.6 Source of Metamorphic Detritus .....	82
4.6 Conclusions .....	82

<b>CHAPTER 5:</b>	
<b>STATUS OF THE GUADALQUIVIR BASIN .....</b>	
<b>85</b>	
5.1 Previous Interpretations .....	85
5.2 Characteristics of a Foreland Basin .....	85
5.2.1 Definition of a Foreland Basin .....	85
5.2.2 Evolution of a Foreland Basin .....	86
5.3 Stratigraphical Considerations of the Guadalquivir Basin .....	87
5.4 Status of the Guadalquivir Basin .....	88
5.4.1 Geographical Location and Geometry of the Basin .....	88
5.4.2 Mechanism of Formation of the Guadalquivir Basin .....	89
5.4.3 Classification of the Basin .....	90
5.5 Model for the Formation of the Basin .....	90

## PART II

### THE GIBRALTAR ARC FLYSCH BASIN

<b>CHAPTER 1</b>	
<b>INTRODUCTION .....</b>	
<b>93</b>	
1.1 General Geological Setting .....	94
1.2 Previous Interpretations .....	94
1.3 Study Area .....	94
<b>TECTONO-STRATIGRAPHIC HISTORY .....</b>	
<b>95</b>	
1.4 Cross-Section .....	95
1.4.1 Description .....	95
1.4.2 Interpretation .....	95
1.5 Stratigraphic Evolution .....	96
1.6 Conclusions .....	96
<b>CHAPTER 2</b>	
<b>SEDIMENTOLOGY &amp; PALAEOGEOGRAPHY</b>	
<b>OF THE ALJIBE FLYSCH .....</b>	
<b>98</b>	
2.1 Introduction .....	98
2.2 The Beneiza Flysch .....	98

2.2.1 Description .....	98
2.2.2 Interpretation .....	99
2.3 The Aljibe Arenites .....	99
2.3.1 General Characteristics .....	99
2.3.2 Logged Transects .....	99
2.3.4 Description of the Sedimentary Structures .....	100
2.3.5 The Idealised Sequence of Structures .....	102
2.3.6 Heterolithic Intervals .....	103
2.3.7. Interpretation of the Sedimentary Structures .....	103
2.3.8 Interpretation of the Idealised Sequence .....	106
2.3.9 Inferred Rates of Deposition .....	107
2.4 Beneiza Flysch to Aljibe Arenite Transition .....	108
2.5 Interpretation of the Aljibe Flysch .....	108
2.5.1 Deep Sea Depositional Systems .....	109
2.5.2 The Aljibe Flysch Compared to Deep Sea Depositional System .....	110
2.6 Conclusions .....	111

## CHAPTER 3

STATUS OF THE GIBRALTAR ARC .....	113
3.1 Interpretation of the Aljibe Flysch .....	113
3.2 Status of the Crust Prior to Deposition of the Aljibe Arenites .....	113
3.3 Nature of the Oligo-Miocene Tectonic Event .....	113
3.4 Timing of Thrusting in the Gibraltar Arc .....	114
3.5 Conclusions (A Model For Formation) .....	114

## PART III

### DISCUSSION:

## THE SIGNIFICANCE OF THE GUADALQUIVIR BASIN AND GIBRALTAR ARC FLYSCH TO THE EVOLUTION OF THE BETIC OROGEN

1 Introduction .....	117
2 Tectonic History Derived From the Study of the External Basins .....	117
3 The Alboran Domain .....	118
3.1 Ronda Peridotites .....	118
3.2 The Alboran Sea .....	120
4 A Rejection of the Extensional Collapse Model .....	122
5 The Case for Strike-Slip Tectonism .....	123
5.1 Plate Tectonic History .....	123
5.2 Strike-Slip Faults .....	123
5.3 Palaeomagnetic Rotations .....	123
6 The Betics as a History of Transtension-Transpression .....	125
7 A question of Terrane Tectonism ??? .....	125
8 Problems Associated With a Strike Slip Model .....	126
8.1 The Guadalquivir Basin Problem .....	126
8.2 The Betic Movement Zone Problem .....	127
9 A Model for the Evolution of the Betic Orogen .....	128
9.1 Cretaceous to Early Miocene (Fig. 8a) .....	128
9.2 Miocene (Fig. 8b) .....	128
9.3 Pliocene (Fig. 8c) .....	129
10 Unresolved Problems .....	129
11 Future work .....	130
12 Conclusions .....	131

THESIS CONCLUSIONS .....	133
The Guadalquivir Basin .....	133

The Gibraltar Arc Flysch Basins .....	134
ACKNOWLEDGEMENTS & REFERENCES .....	137

## VOLUME 2 FIGURES AND APPENDICES

### OVERVIEW: FIGURES

<i>Figure 1.1 The Alboran sea and surrounding mountain chains.</i> .....	159
<i>Figure 1.2. Successive positions of Africa relative to Europe.</i> .....	160
<i>Figure 1.3 The subdivision of the External Zone.</i> .....	161
<i>Figure 1.4 A summary of hypothesis proposed for the Betic Orogen.</i> .....	162

### PART I THE GUADALQUIVR BASIN: FIGURES

#### CHAPTER 1

INTRODUCTION: FIGURES .....	165
<i>Figure 1.1 The Baena-Montilla study area</i> .....	167
<i>Figure 1.2 Lithostratigraphic correlation diagram.</i> .....	168
<i>Figure 1.3 Basin development in the Betic Orogen.</i> .....	169
<i>Figure 1.4 Cross-section across the Guadalquivir Basin.</i> .....	170

#### CHAPTER 2

TECTONO-STRATIGRAPHIC ANALYSIS: FIGURES .....	171
<i>Figure 2.1 Seismic profile across the Guadalquivir Basin.</i> .....	172
<i>Figure 2.2 A revised stratigraphy for the autochthonous Guadalquivir Basin.</i> .....	173
<i>Figure 2.3 A panoramic S-N view across the Guadalquivir Basin.</i> .....	174
<i>Figure 2.4 Part of the allochthonous Guadalquivir Basin.</i> .....	175
<i>Figure 2.5 Deformed Tortonian sediments.</i> .....	176
<i>Figure 2.6 Photo and line diagram of the base of the Guadalquivir Basin.</i> .....	177
<i>Figure 2.7 Nature of the allochthonous-autochthonous boundary.</i> .....	178
<i>Figure 2.8 'Ollstostrome' mapped in a roadside outcrop.</i> .....	179
<i>Figure 2.9 Generalized cross-section.</i> .....	180
<i>Figure 2.10 Chronostratigraphic diagram.</i> .....	181
<i>Figure 2.11 Chrono-stratigraphy plotted against global eustasy and tectonism.</i> .....	182
<i>Figure 2.12 Tectonic and stratigraphic evolution.</i> .....	184

#### CHAPTER 3

SEDIMENTOLOGY & PALAEOGEOGRAPHY: FIGURES .....	185
<i>Figure 3.1 Lithostratigraphy of the Guadalquivir Basin.</i> .....	186
<i>Figure 3.2 The sub-Messinian unconformity.</i> .....	187
<i>Figure 3.3 Lower Miocene marls.</i> .....	188
<i>Figure 3.4 Lower Miocene boulder facies.</i> .....	190
<i>Figure 3.5 Thinly bedded facies.</i> .....	191
<i>Figure 3.6 Thickly bedded marls.</i> .....	191
<i>Figure 3.7 Laminated diatomites.</i> .....	192
<i>Figure 3.8(a) Diatom ooze.</i> .....	193
<i>Figure 3.8(b) Concinnodiscus sp.</i> .....	193
<i>Figure 3.9 Lenticular units in the boulder facies</i> .....	194
<i>Figure 3.10 Photomicrograph of calc-lithic arenite.</i> .....	194
<i>Figure 3.11 Photomicrograph of fine grained calc-lithic arenite.</i> .....	195

Figure 3.12 Photomicrograph of bioclastic marls. ....	195
Figure 3.13 Thin bedded and thick bedded, Tortonian sedimentary cycles. ....	196
Figure 3.14 Log of the tabular bedded facies. ....	197
Figure 3.15(a). Photo of thick bedded sandstones. ....	198
Figure 3.15(b) Sedimentary log of the thick bedded facies. ....	200
Figure 3.16 Cyclicity observed in the Tortonian. ....	201
Figure 3.17 Plot showing the production of asymmetrical and symmetrical bedforms. ....	202
Figure 3.18 Profile of a barrier beach. ....	203
Figure 3.19 Coarsening-upwards sequence produced by the progradation of a storm-dominated beach. ....	203
Figure 3.20 Sedimentary log of Lower Messinian sedimentary rocks. ....	204
Figure 3.21 Photomicrograph of fine grained calc-lithic arenite ....	205
Figure 3.22 Sedimentary log of lower Messinian fining up cycles. ....	206
Figure 3.23 Photomicrograph of calc-lithic arenite. ....	207
Figure 3.24 Diagram of mega-ripple bed ....	208
Figure 3.25 Sedimentary structures in calc-lithic arenite. ....	209
Figure 3.26 Photomicrographs of Bioclastic grainstones. ....	210
Figure 3.27 Log of channelised matrix supported conglomerate. ....	211
Figure 3.28 Lower Messinian conglomerates. ....	212
Figure 3.29 Erosional truncations in Lower Messinian conglomerates. ....	212
Figure 3.30 The formation of low-angle reactivation surfaces in sand waves ....	213
Figure 3.31 Palaeocurrent data from the Lower Messinian coastal fan deposits ....	214
Figure 3.32 Laminae picked out carbonaceous material. ....	215
Figure 3.33 Calc-lithic arenite with thin pebble horizons. ....	215
Figure 3.34 Sedimentary log of Upper Messinian conglomerates. ....	216
Figure 3.35 Conglomerates from the Upper Messinian Guadalquivir Basin. ....	217
Figure 3.36 Sedimentary log of Upper Messinian conglomerates. ....	218
Figure 3.37 Upper Messinian conglomerates. ....	219
Figure 3.38. Palaeocurrent data taken from Upper Messinian fluvial deposits. ....	220
Figure 3.39 Palaeo-bathymetry of the Guadalquivir Basin succession. ....	221
Figure 3.40 Palaeogeography during the Lower-Mid Miocene. ....	222
Figure 3.41 Palaeogeography during the Tortonian. ....	223
Figure 3.42 Palaeogeography during the Lower Messinian. ....	224
Figure 3.43 Palaeogeography during the Upper Messinian. ....	225
Figure 3.44 Two possible margin configurations. ....	226
Figure 3.45 A generalized palaeogeography. ....	227

## CHAPTER 4

PROVENANCE: FIGURES .....	228
Figure 4.1 Candidate source rocks. ....	229
Figure 4.2 Sample locations. ....	230
Figure 4.3 Obtaining a representative sample of the grain size population. ....	231
Figure 4.4 Variation of petrographic parameters. ....	232
Figure 4.5 Variation of petrographic parameters. ....	233
Figure 4.6 Variation of petrographic parameters. ....	234
Figure 4.7 Variation of petrographic parameters. ....	235
Figure 4.8 Variation of petrographic parameters. ....	236
Figure 4.9 Variation of petrographic parameters. ....	237
Figure 4.10 Occurrence of sedimentary lithics. ....	238
Figure 4.11 Petrographic ternary plots. ....	239
Figure 4.12 Qm, F, Lt plot for the Guadalquivir Basin. ....	241
Figure 4.13 Qp, Lvm, Lsm plot for the Guadalquivir Basin. ....	242
Figure 4.14 Lm, Lv, Ls plot for the Guadalquivir Basin. ....	243
Figure 4.15 Ternary plot for sedimentary lithics. ....	244
Figure 4.16 Lithological variation carbonte lithic-clasts. ....	245
Figure 4.17 Composition of clasts found in Messinian deposits. ....	246
Figure 4.18 Palaeocurrent data. ....	247
Figure 4.19 The Tschermak exchange for muscovite micas. ....	248
Figure 4.20 Modified graphical representation of the Tschermak exchange. ....	249
Figure 4.21 Sample locations for white micas. ....	250
Figure 4.22 Geochemical variation of white micas collected from the Betic Orogen. ...	251



Figure 4.23 K/Al variation across detrital white micas. ....	252
Figure 4.24 Provenance model. ....	253

## CHAPTER 5

STATUS OF THE GUADALQUIVIR BASIN: FIGURES .....	254
Figure 5.1 The 'generic' foreland basin. ....	255
Figure 5.2 Early 'flysch' stage of a foreland basin. ....	256
Figure 5.3 Late molasse stage of a foreland basin. ....	256
Figure 5.4 A simple foreland basin profile. ....	257
Figure 5.5 Complex foreland basins. ....	257
Figure 5.6 Comparison of the Guadalquivir Basin with the Apennine foreland basin. ....	259
Figure 5.7. Banks & Warburton (1991) Structural cross-section. ....	260
Figure 5.8. Theoretical response of the lithosphere to a load. ....	261
Figure 5.9 Tectonic evolution of the Betic Orogen. ....	262
Figure 5.10. Schematic diagram showing the evolution of the Betics. ....	264

## PART II

### THE GIBRALTAR ARC FLYSCH BASIN: FIGURES

## CHAPTER 1

### INTRODUCTION & TECTONO-STRATIGRAPHIC

HISTORY: FIGURES .....	266
Figure 1.1 Geology of the Gibraltar Arc .....	268
Figure 1.2 Stratigraphy of the Aljibe Flysch. ....	269
Figure 1.3 Study Area 1 for the Aljibe Flysch. ....	271
Figure 1.4 Transect 1 across the Aljibe Flysch. ....	272
Figure 1.5 Transects 2 & 3 across the Aljibe Flysch. ....	273
Figure 1.6 Transect 4 across the Aljibe Flysch. ....	274
Figure 1.7 Cross-section across Study Area 1. ....	275
Figure 1.8 Flysch nappes of the Gibraltar Arc. ....	276
Figure 1.9 Tectonic contacts in the Gibraltar Arc. ....	277
Figure 1.10 Genesis of the Gibraltar Arc. ....	279

## CHAPTER 2

### SEDIMENTOLOGY & PALAEOGEOGRAPHY

OF THE ALJIBE FLYSCH FIGURES .....	280
Figure 2.1 The Beneiza Flysch and the Aljibe Arenites. ....	281
Figure 2.2 Photomicrographs of sandstones from the Beneiza Flysch .....	282
Figure 2.3 Ichnofauna Chondrites. ....	283
Figure 2.4 Sedimentary log of part of the Beneiza Flysch .....	285
Figure 2.5 The ideal Bouma sequence. ....	286
Figure 2.6 Occurrence of complete and partial Bouma sequences. ....	287
Figure 2.7 Photomicrograph of Aljibe Arenite sandstones. ....	287
Figure 2.8 Sedimentary log of part of the Aljibe Arenites. ....	289
Figure 2.9 Summary lithological log, transect 2. ....	290
Figure 2.10 Summary lithological log, transect 3. ....	291
Figure 2.11 Dark laminae in the Aljibe Arenites. ....	293
Figure 2.12 Dish structured laminae. ....	295
Figure 2.13 Mega-dishes and associated vertical pillars. ....	296
Figure 2.14 Dish structured laminae that overlie micro-conglomerates. ....	298
Figure 2.15 Convolute overturned folds. ....	300
Figure 2.16 Convolute diapir emanating from a pillar. ....	302
Figure 2.17 Diapirs with disrupted tops. ....	304
Figure 2.18 Type A pillars and associated mega-dishes. ....	306
Figure 2.19 Sinuous pillar. ....	308
Figure 2.20 Bifurcating pillar. ....	310
Figure 2.21 Type C pillars. ....	312

Figure 2.22 Type D pillars. ....	314
Figure 2.23 Sandstone intrusion. ....	316
Figure 2.24 Downwards descending pillar. ....	318
Figure 2.25 Pillar found in the core of a diapir. ....	320
Figure 2.26 Sand mound. ....	322
Figure 2.27 Diffuse streaks found in zones of complete mixing. ....	324
Figure 2.28 Typical sequence of structures found in the Aljibe Arenites. ....	326
Figure 2.29 The idealised sequence of water escape structures. ....	327
Figure 2.30 Coarse sandstone passing directly into type B pillars. ....	329
Figure 2.31 Pillars passing directly into convolute diapirs. ....	331
Figure 2.32 Dish structured laminae passing directly into convolute diapirs. ....	333
Figure 2.33 Overturned pillars. ....	335
Figure 2.34 Heterolithic intervals, Aljibe Arenites. ....	336
Figure 2.35 Height distribution of pillars measured from the Aljibe Arenites. ....	337
Figure 2.36 The Benetza Flysch to Aljibe Arenites transition. ....	339

## PART III

### DISCUSSION:

### THE SIGNIFICANCE OF THE GUADALQUIVIR BASIN & GIBRALTAR ARC FLYSCH TO THE EVOLUTION OF THE BETIC OROGEN: FIGURES

Figure 1 The Alboran domain .....	341
Figure 2 Model for emplacement of the peridotites. ....	342
Figure 3 Proposed evolution of the western Mediterranean .....	344
Figure 4(a) Schematic cross-section across the Málagaide Complex and Los Reales Nappe. ....	345
Figure 4(b) Proposed geodynamic model for the extensional deformation in the Los Reales-Málagaide domain. ....	345
Figure 5 Time-averaged motion of Eurasia and Africa. ....	346
Figure 6 Rotation in simple shear zone. ....	347
Figure 7 Structural sections through the Betic Movement Zone. ....	348
Figure 8(a) Iberian margin 65-27 Ma. ....	349
Figure 8(b) Miocene evolution of the Betic Orogen. ....	351
Figure 8(c) Pliocene evolution Of the Betic orogen. ....	353

## APPENDICES

APPENDIX I	
SELECTED SEDIMENTARY LOGS	
FROM THE GUADALQUIVIR BASIN .....	354

APPENDIX II	
MICROPALAEONTOLOGY OF THE	
GUADALQUIVIR BASIN .....	380
Introduction .....	380
Methods .....	380
Micropalaeontology .....	380
Problems Associated With Allochthonous Specimens .....	380
Lower to Mid Miocene .....	381
Tortonian .....	381
Lower Messinian .....	382
Palaeo-bathymetry .....	382
Tabulation of data .....	383

## PLATES

<i>Plate I: Foraminifera</i> .....	393
<i>Plate II: Foraminifera</i> .....	395
<i>Plate III: Ostracods</i> .....	397

## APPENDIX III

### SELECTED SEDIMENTARY LOGS

FROM THE ALJIBE FLYSCH .....	399
Beneiza Flysch .....	402
Aljibe Arenites .....	405

## APPENDIX IV TABULATED DATA .....

425

Lower Miocene Boulder Facies From the Guadalquivir Basin .....	426
Quantitative Petrography of Samples from The Guadalquivir Basin .....	431
Clast Surveys for Conglomerates	
Found in the Messinian Guadalquivir Basin .....	436
Palaeocurrent Data .....	440
Mica Analysis .....	442
Measured Pillar Height from the Aljibe Arenites .....	449

## APPENDIX V

LOCATIONS, GRID REFERENCES AND MAPS .....	451
---	-----

***Volume 1***

***Text***

# **OVERVIEW**

*Perspective-  
Use it or Lose it  
If you turned to this page  
You're forgetting that what is going  
On around you is not reality  
Think about that !*

From 'Illustons' by Richard Bach

## OVERVIEW

This thesis aims to describe the tectonic and sedimentological relationships of two basins, the Guadalquivir Basin and the Gibraltar Arc Flysch basin, that lie on the periphery of the Betic mountain chain in southern Spain. These basins are believed to have been generated by the interaction between African and Iberian plates. The Betic orogen itself has been the subject of some controversy, and its tectonic history is not yet fully understood. It is believed that the basins in question may provide some insight into the development of the Orogen.

The purpose of this section is to highlight the tectonic setting of the orogen, the various hypotheses which have been proposed for its development and the main areas of disagreement between workers. This will provide a background for the discussion of the basins.

This section will then go on to describe how basins in general may be used in the interpretation of orogens and how the Guadalquivir and Gibraltar Arc Flysch basins might add to the tectonic interpretation of the Betic Orogen.

The final part of this section will clearly state the aims and objectives of this thesis.

### 1. THE BETIC OROGEN

#### 1.1 Introduction

The Betic mountain chain of Southern Spain (Fig. O.1), together with the Rif Mountains of NW. Africa, the Alboran sea and the Gibraltar Arc, forms the western-most extension of the Alpine mountain chain in Europe (Banda and Ansorge, 1980). The history of the Betics spans some 90 Ma., from the late Cretaceous to Pleistocene times. The orogen formed as a direct result of interaction between the Iberian and African plates (Dewey *et al.*, 1973, 1989; Kampschuur and Rondell, 1974; Torres-Roldán, 1979; Banda and Ansorge, 1980)

#### 1.2 Plate Tectonic Setting (Fig. O.2)

During the early part of the Cretaceous Iberia acted as a separate plate, moving independently of Africa & Europe as spreading in the north Atlantic occurred (Dewey *et al.*, 1973, 1989; Malod and Mauffret, 1990; Roest and Sirvastava, 1991). At some time before the Santonian (84 Ma.) Iberia attached itself to the African plate (Sirvastava *et al.*, 1990) welding the Moroccan and Oran Terrains to Africa (Dewey *et al.*, 1973). This resulted in a new active boundary in the Bay of Biscay, separating the African/Iberian plate from the Eurasian plate. Sirvastava (1990) proposed that at 42 Ma. this plate boundary shifted to the Pyrenean Arc, leading to compression between Eurasia and Africa and to the creation of the Pyrenean Alpine mountain chain. During this later period there was no movement in southern Iberia. At around 32 Ma. (lower Oligocene) the plate boundary jumped again to the Gibraltar Arc (Sirvastava *et al.*, 1990), creating a new active plate boundary between Eurasia/Iberia and Africa. However, no major movement occurred until 27 Ma. (Upper Oligocene), when Iberia rotated eastward into Africa (Dewey *et al.*, 1973) leading to compression and major strike slip movements between Africa and Iberia. The overall result was the subduction of the African Margin from 27 Ma. onwards. This subduction, and the interaction of Africa and Iberia is



thought to have been responsible for the formation of the Betic mountain chain.

### 1.3 Tectonic Subdivision (Fig. O.1)

In the past the Orogen which formed between Africa and Iberia has been described and discussed in terms of separate southern Spanish and North African components. This led to some confusion as to the tectonic subdivision of the Betic Orogen. An attempt, therefore, will be made to address the Betic orogen in terms of both of these components. This will produce a slightly modified tectonic subdivision.

The Betic orogen (and its north African counterpart) can be divided into four distinct tectonic Zones :-

1. *The Internal zone* of southern Spain and *Internal Rif* of north Africa.
2. *The External Zones*; which are divided into the Subbetic and Prebetic Subzones of southern Spain and the External Rif of north Africa. The Subbetic subzone is linked to the External Rif of north Africa by the Gibraltar Arc (Platt and Vissers, 1989; Doblas, 1989), which contains Oligocene Flysch nappes (Torres-Roldán, 1979; Platt and Vissers, 1989; Sanz-De-Galdeano, 1990).
3. *The Alboran Sea*; occupies the region between southern Spain and North Africa. It is a topographic low bounded by the high mountain chains of the Internal Zone, Gibraltar Arc and External Rif (Torres-Roldán, 1979; Banda & Ansorge, 1980; Sanz-De-Galdeano, 1990; Platt & Vissers 1989).
4. *The external basins*; are those basins which lie on the periphery of the orogen but are thought to have been generated by an orogenic mechanism. They include the Guadalquivir Basin on the southern margin of the orogen and the Gibraltar Arc Flysch deposits in the west. It is the external basins which are the subject of this dissertation.

#### 1.3.1 Internal Zone

The Internal Zone of the Betic Mountain chain, southern Spain, consists of a series of overthrust tectonic nappes (Egeler *et al.*, 1972 & Egeler & Simon, 1969). These tectonic nappes form three thrust sheets, stacked from bottom to top these are: the Nevado-Filabride (deepest), the Alpujarride (intermediate) and the Malaguide (highest). All are metamorphosed to varying degrees, but the lowest sheet, the Nevado-Filabride, is most consistently at higher grade than the higher Alpujarride and Malaguide thrust sheets.

#### 1.3.2 Nevado-Filabride Thrust Sheet

The Nevado-Filabride exhibits a polyphase metamorphism (Nijhus, 1964; Puga & Díaz-de-Frederico, 1978; Gomez-Pugnaire & Fernandez-Soler, 1987). Both Kampschuur *et al.*, (1974) and Torres-Roldán (1979) recognised 3 metamorphic facies, glaucophane-schist, greenschists and a greenschist and amphibolite facies. Kampschuur *et al.* (1974) attributed the glaucophane-schist facies to an old, pre-Alpine, D<sub>1</sub> metamorphic event that persisted into

Permo-Triassic times. A second more static metamorphism, D<sub>2</sub>, produced retrograde facies and a much later, Alpine, D<sub>3</sub> event gave rise to the glaucophane-schist amphibolite facies (Lagenberg, 1972). Torres-Roldán (1979), however, suggested that during the first Alpine metamorphism some of the rocks of the Nevado-Filabride were subjected to an abnormally low geothermal gradient. This was then subsequently overprinted by a change towards much lower pressures.

Some of the confusion in the interpretation of the metamorphic history was removed by the further subdivision of the Nevado-Filabride into two thrust nappes (Bakker *et al.*, 1989). (1). A lower low-pressure/low-temperature unit termed the Veleta Complex, is overthrust by (2) The Mulhacen Complex, which displays high-pressure/low-temperature metamorphism. Both units were subsequently overprinted by a medium grade metamorphism of low-pressure type.

Bakker *et al.* (1989) demonstrated that the Mulhacen complex underwent at least five phases of deformation related to continent to continent collision. This was followed by an intermediate metamorphism that was produced during crustal thinning and heterogeneous extension. Bakker *et al.* (1989) suggested that it was during this extension that units in the Alpujarride were juxtaposed against the Nevado-Filabride complex.

### 1.3.3 Alpujarride Thrust Complex

Early workers such as Egeler *et al.* (1969), Aldaya (1970) Boulin (1970) and Kornprobst (1974) considered the Alpujarride to be unaffected by Alpine metamorphism, since the medium-high grade assemblages present are usually associated with pre-Alpine orogenic cycles. However, Torres-Roldán (1979) demonstrated that the Alpujarride is characterised by an intermediate to low pressure kyanite/sillimanite assemblage overprinted by a lower pressure andalusite/sillimanite assemblage. This was interpreted as reflecting at least two major metamorphic events, the later one being syn-Alpine. Zeck *et al.* (1992) recorded uplift of 15-20 Km at rates of 5-10 Km/My in the final stages of orogenic development. Such high rates have been attributed to the slab detachment of the African plate from the base of the Iberian plate and associated diapirism in the upper-mantle.

### 1.3.4 Malaguide Thrust Unit.

Alpine metamorphism is confined to the lower most part of the Malaguide thrust unit (Egeler *et al.*, 1969), and has been correlated with metamorphism in the lower portions of the Alpujarride. They both display similar metamorphic assemblages (Torres-Roldán, 1979). Above this lower zone the rocks become progressively less affected by metamorphism (Egeler *et al.*, 1969; Torres-Roldán, 1979).

### 1.3.5 Internal Rif, N. Africa.

The Betic zone is continued across the Gibraltar Arc to form the Internal Rif of north west Africa (Kampschuur *et al.*, 1974). The Nevado-Filabride thrust unit is only found in the Betic Cordillera of southern Spain, while the Alpujarride thrust unit is similar to the Sebti unit of the Internal Rif. The Malaguide thrust unit has counterparts in both the Gomarides of the

Internal Rif and the Kabylas of the Tell mountains of North Africa (Sanz-De-Galdeano, 1990).

### 1.3.6 External Zone

The External zone of the Betic Orogen consists of unmetamorphosed Triassic to lower Miocene rocks (Garcia-Hernandez *et al.*, 1979) that form a complicated structural belt. These Rocks are dominantly sedimentary with some localised sub-marine volcanic and sub-volcanic mafic igneous units of early Cretaceous age (Kampschuur *et al.*, 1974; Garcia-Hernandez *et al.*, 1979). Juxtaposition of the Internal and External Zones took place during the Eocene to early Miocene Alpine shortening period (Garcia-Hernandez *et al.*, 1979; Sanz-De-Galdeano, 1990). Most shortening took place in the mid Miocene

The Triassic-Miocene cover of the External Zone has been detached and thrust northward on Triassic Evaporite décollements (Garcia-Hernandez *et al.*, 1979). Thrusting extends into the Guadalquivir Basin where rocks of the External Zone form an Olistostrome within lower Miocene sediments (García-Rossell, 1973). Compressive deformation initiated in the Early Oligocene resulted in uplift followed by flysch deposition, the flysch now forming an extensive part of the Gibraltar Arc. De-Smet (1984) and Leblanc & Oliver (1984) reported a substantial strike-slip component in the External Zone. However, Banks & Warburton (1991), used seismic data to demonstrate that all of the observable tectonic detachments of the eastern part of Internal Zone were thrust faults with a dominant transport direction to the north.

### 1.3.7 Subdivision of the External Zone (Fig O.3)

Blumenthal (1927) subdivided the External Zone into Prebetic and Subbetic Subzones based on palaeogeographic criteria. The Prebetic subzone consists principally of rocks of shallow marine origin while those of the Subbetic subzone are mainly of pelagic marine origin (Fig. O.3a) The Prebetic and Subbetic Subzones are separated by an Intermediate Unit of mixed stratigraphic origin that cannot be assigned to either.

The Subbetic and Prebetic Subzones also have very different structural styles and this has caused some confusion as to whether these divisions are stratigraphical or structural divisions. Structurally the Subbetic subzone is characterised by nappe features, contrasting with the much more shortened Prebetic subzone. Shortening of the order of 15-25 Km has been recorded by Dabrio & Lopez-Garrido (1970). The northern margin of the Prebetic subzone displays reverse faulting and imbricate structures which give way southwards to a much gentler fold/fault geometry. The southern margin of the Prebetic subzone is overthrust by the Subbetic subzone (Garcia-Hernandez *et al.*, 1979).

The palaeogeographic analysis of Garcia-Hernandez *et al.* (1979), Hermes (1978) and others has led to the further division of the Subbetic subzone into three units, the Subbetic Internal Unit, the Subbetic Middle Unit and the Subbetic External Unit (Fig. O.3a,b). The deposition of the Subbetic and Prebetic subzone and Intermediate Unit took place on an extended continental margin of Triassic terrestrial red beds and evaporites (Pacquet, 1969). Later extension resulted in the formation of two basins whose contents are now classified as the Subbetic Middle Unit and the Intermediate Unit, these basins were separated by a

palaeo-high which now forms the External Subbetic Unit. This basin and graben set was bounded to south by a platform, which forms the Internal Subbetic and to the north by the Prebetic subzone (see Fig O.3b).

In contrast to Garcia-Hernandez *et al.* (1979), Hermes (1978) and Dabrio & Lopez-Garrido (1970), Blankenship (1992) produced a structural/palaeogeographical interpretation based on seismic reflection profiles, subsurface well control and balanced cross-sections. (Fig. O.3c) This model regards the External Zone as a single basin, made up of the Intermediate Unit and Middle Unit of the Subbetic subzone bounded by two palaeo-highs, the Prebetic subzone to the north, and platformal sediments of the External and Internal Units to the south. Blankenship (1992) suggests that this basin subsequently underwent a total of 200km of shortening.

### 1.3.8 The Alboran Sea

The Alboran sea is unusual in that it forms a topographic low of thinned continental crust (Doblas *et al.*, 1989; Sanz de Galdeano, 1990 ) in what is essentially the core of the Betic orogen.

The area is underlain by continental crust and by anomalously low seismic velocity mantle (Banda *et al.*, 1980). It is broken by E-W trending horst and graben structures. Linear magnetic anomalies suggest the widespread presence of Neogene extrusive and intrusive igneous rocks (Galdeano *et al.*, 1974).

The Alboran sea, because of its peculiarities had been ignored by many workers until Torres-Roldán (1979) suggested that was a product of the extensional collapse of the orogen. Doblas *et al.* (1989), Platt *et al.* (1989) and Zeck *et al.* (1992) went on to suggest that its formation was driven by orogenic collapse which occurred when the lithospheric root of the orogen was removed and replaced by mantle. The upwelling of mantle caused doming in what is now the Betic Cordillera and gravity driven collapse in what is now the Alboran sea.

### 1.3.9 External Basins

**1. The Guadalquivir Basin;** lies on the northern margin of the Tertiary fold belt of the External Zone and south of the Palaeozoic Iberian Plate. It trends NE-SW and is terminated to the NE by the overthrust sequence of the External Zone. In this area NW-directed allochthonous units of the External Zone of the Betics have apparently overridden the basin (Banks & Warburton, 1991). To the SW the basin opens into the Gulf of Cadiz where sedimentation is continuing along the coastal strip between Huelva and Sanlúcar de Barrameda. There are two structurally distinct areas from which the stratigraphy of the basin has been reconstructed. One immediately south of the Iberian Plate is autochthonous. The other is south of the fault bounding the orogen, and is allochthonous. The basin fill is characterised by fine grained sediments, mainly marls with some sequences of finer grained sandstone and rare conglomerates (Martínez del Olmo *et al.*, 1984; Suárez Alba *et al.*, 1988). On the SE margin of the basin and extending along the length of the Guadalquivir basin there is a band of disrupted rocks referred to as an Olistostrome (Gracia Dueñas, 1969; Gracia Rosell, 1973; García Hernández *et al.*, 1980). This marks the contact between the basin and the External

Zone.

The Guadalquivir basin has been interpreted as being both the foreland basin to the Betic Orogen (Torres Roldán, 1979; Martínez del Olmo, 1984 and Suárez Alba *et al.*, 1988) and also as a series of piggy back style basins (Roldán García *et al.*, 1991). Sanz de Galdeano & Vera (1992) believe that the Guadalquivir basin began life as an open gulf, the North Betic Strait, which in mid Miocene time was converted to a foreland basin. The olistostrome has a highly sheared matrix and is interpreted as being emplaced by gravity sliding. Sanz de Galdeano & Vera (1992) report that this zone of gravity sliding existed as a 'highly mobile sector' along the southern margin of the North Betic Strait during the lower Miocene.

2. *The Gibraltar Arc Flysch*; links the External Rif of N. Africa with the External Zone of southern Spain and encloses the Alboran sea to the west. It consists of a series of flysch nappes which have been thrust westwards during the 'radial' collapse of the Betic Orogen (Platt & Vissers, 1989)

Sanz de Galdeano & Vera (1992) refer to this area as the 'Campo del Gibraltar Complex'. They suggested that it originated from materials originally deposited in the north Africa Flysch Trough which existed south and south-west of the Flyschs' present position. Tertiary turbidites and hemipelagites are reported within the Gibraltar Arc Flysch, while Bourgeois (1978) reports that part of these deposits were re-sedimented during the Burdigalian, forming tectono-sedimentary units.

#### **1.4 Geological History: A comparison of hypotheses**

In this section some attempt will be made to synthesize the varying models proposed for the development of the Betic Orogen. The conflicting evidence and arguments provided by various authors, summarised in Fig. O.4, will be highlighted in this section.

The Betic Orogen has been variously seen as compression dominant, as reflecting a large amount of strike slip between interacting plates and as an area that has undergone a large amount of extension during orogenic collapse. These alternative views will be discussed below. In addition the problems concerning the characteristics of the Subbetic/Prebetic Subzones of the External Zone and the external/peripheral basins will be examined.

##### **1.4.1 Compressional Tectonism and Metamorphism.**

Most authors agree that for at least part of its history the African/Iberian plate boundary acted as a major zone of compression as Africa and Iberia converged. The direction of dip of the subducting plate is still unclear, but Banda & Ansorge (1980) suggest that the African plate does not simply dip under Iberia and Davies *et al.* (1993) showed the Iberian plate steeply dipping under Africa.

The earliest metamorphism recorded in the orogen is late Cretaceous (85-65 Ma.) occurring in the Nevado-Filabride thrust unit (Doblas & Oyarzun, 1989; Bakker *et al.*, 1989; Monié *et al.*, 1991). This may have been brought about by burial during the attachment of Iberia to Africa, when the Oran and Moroccan terranes were accreted on to the Iberian plate (Dewey *et al.*, 1973; 1989). This is problematic since it would require the rocks to have been

buried for some 47 million years during the relatively inactive period in which the active plate margin lay in the Pyrenean trough, not between Africa and Iberia (Sirvastava *et al.*, 1990a; 1990b). It was not until the late Oligocene (27Ma) that the Iberian/African plate margins became active again. Many authors place the main uplift and exhumation of the Betic orogen at this time (Platt & Vissers, 1989; de Jong *et al.*, 1992) Bakker *et al.*, 1989).

However, the Nevado-Filabrides and Alpujarride tectonic subdivisions of the internal zone individually display very different structural and metamorphic histories (Bakker *et al.*, 1989). They cannot have been juxtaposed by simple thrust stacking and exhumation such as might have occurred in a purely compressional regime. Their association can be explained by either strike slip tectonism or by extensional collapse of the orogen.

#### 1.4.2 Strike Slip Tectonism

Egler (1969) demonstrated that the superimposed Nevado-Filabride Alpujarrides thrust sheets have very different structural and metamorphic histories that reflect at least two thrust phases.

One way of producing such juxtaposition is by strike slip tectonism. Several workers including De Smet (1984), LeBlanc (1984) and Andriex *et al.* (1971) have emphasised the importance of dextral strike slip faulting in the Subetics subzone of the External Zone (Fig O.1). LeBlanc and Oliver (1984) believe that the Internal Zone/External Zone boundary is a strike slip contact that originally separated the Iberian plate margin and the Alboran microplate/African plate margins. Platzman *et al.* (1993) and Allerton *et al.* (1993) also appealed to a large strike slip component, acting in the Betic orogen to explain palaeomagnetic rotations of structural blocks in both the Internal and External zones. Their data indicate a dextral shear regime acting on the Betic orogen and rotating blocks during the latest Oligocene and earliest Miocene. Blocks are unrotated in the latest Miocene indicating that relative movement had ceased by the latest Miocene.

#### 1.4.3 Extensional Collapse

Balyana & Garcia Duenas (1986), Garcia Duenas (1993), Doblas & Oyarzun (1989) and Platt (1983) have all observed extensional faults and low angle detachments within the Internal Zone. There is a widely held view that these are the product of large scale extension that occurred within the Betic Orogen.

Platt & Vissers (1989) suggested that the high grade Nevado-Filabride thrust sheet was exhumed by the extensional detachment of the overlying Alpujarride thrust sheet. It was proposed that simple thrust stacking during Oligocene (c. 27 Ma.) led to the burial and high grade metamorphism of the Nevado-Filabride thrust sheet. Subsequently as the northward progression of Africa slowed, the subducting African plate fell away from the base of the Iberian plate. This resulted in the diapiric upwelling of mantle below the Betic orogen. The net effect of this was a doming of the internal zone and the detachment of the Alpujarride thrust sheet exposing the high grade Nevado-Filabride thrust sheet. Extension progressed to such an extent that the Alboran sea opened up. Platt & Vissers (1989) placed the initial extensional event at 19 Ma. (Burdigalian). However, such an age is inconsistent with an uplift



date of 27 Ma. for the Nevado-Filabride thrust sheet obtained from the dating of Phengite grains (Bakker *et al.*, 1989). This implies that the Nevado-Filabride was exposed by the Burdigalian not buried by thrust stacking. Moreover Bakker *et al.* (1989) and de Jong *et al.* (1992) both placed the initial extension at between 27 Ma. and 24 Ma., and give an initial metamorphic burial age of pre 30 Ma. Zeck *et al.* (1992) placed the major uplift slightly later at between 23 Ma. and 19 Ma. and indicated that the minimum age of extension is constrained to before 19 Ma., when Burdigalian sediments sealed the detachment which separates the Alpujarride from the Malaguides.

Doblas and Oyarzun (1989) proposed a core complex style of extensional tectonism that is similar to the mechanism inferred by Platt and Vissers (1989). Doblas and Oyarzun (1989) envisaged a single extensional event starting much later between the Serravallian and Tortonian (15-6.5 Ma.) and continuing into the Messinian. De Jong *et al.*, (1992) used the step heating of phengite micas to give a  $^{40}\text{Ar}/^{39}\text{Ar}$  minimum age of 30 Ma. for the cooling of the main tectonic metamorphic phase. This was followed by a series of local events resetting the grains at 17-19 Ma., 13-15 Ma. and 8 -10 Ma. dates which were coeval with volcanism in the eastern Betics. These ages are interpreted as reflecting periods of crustal and sub-crustal extension. Two further ages of 18.5 Ma. and 21.5 Ma. represent periods of overthrusting and crustal thickening which separated the main extensional events.

Within the extensional collapse model there is a need to explain the juxtaposition of thrust sheets that have different tectonic and metamorphic histories. Platt and Vissers (1989) do not take this into account, and their model would require the removal of at least 12 Km of crust from between the Nevado-Filabride and Alpujarride thrust sheets for it to be consistent with the metamorphic and tectonic schemes proposed by other workers.

It is possible that extensional collapse can be combined with strike slip tectonism to explain the formation of extensional features and yet remain consistent with the tectonic and metamorphic data

Most workers have seen the External zones and External basins as separate geological problems, and have not fully linked them to the mechanisms of the Betic Orogen, as discussed above. As a consequence the geological problems concerning the External Zones and External Basins will be discussed separately below:

#### 1.4.4 External Zone

The External zone was formed from a Mesozoic sedimentary sequence which was detached from its Palaeozoic basement and thrust northwards onto the Iberian craton. It is composed of Triassic to Miocene aged rocks (Blankenship, 1991). The External Zones have been subdivided into the Subbetic and Prebetic Subzones (Fig O.1 , O.3) which consist respectively of basinal and shelf facies. (Garcia-Hernandez, 1980; Banks and Warburton (1991) They are therefore defined mainly in terms of their palaeogeographic regime (Fig. O.3) although they appear to have an additional tectonic significance, with the Prebetic subzone dominating in western Iberia and the Subbetic subzone found in eastern Iberia overthrusting the Guadalquivir Basin (Fig O.1). However there is some dispute about the true Palaeogeographic position of these units (see section 1.1 & Fig O.3) and about the timing and amount of

transport during thrusting. Blankenship (1991) demonstrated a series of duplex structures in the External Zone which host 200 Km of nappe displacement. This is disputed by others (Reichter, 1993; Sanz de Galdeano *et al.*, 1993; Molina and Ruiz-Ortiz (1993); Garcia Hernandez, 1980) who suggest that the External zone has only been locally displaced by 10-15 Km and remains broadly in its original stratigraphical position.

#### 1.4.5 External Basins.

The external basins are those lying on the periphery of the Orogen but considered to have been generated by it. There are two possible external basins associated with the Betic Orogen; the Guadalquivir Basin and the Gibraltar Arc Flysch (see section 1.1 and Fig O.1). It is these basins that form the main subject of this thesis.

The origins of these basins must be considered in light of the timing of tectonic and metamorphic events referred to above. If the extensional collapse of the orogen started between 27-25 Ma., as isotopic dating suggests, then the origin of both the Guadalquivir and the Gibraltar Arc Flysch basins is problematic

Sanz de Galdeano & Vera (1992), Martin del Olmo (1984), Suárez Alba *et al.*, (1988) and Torres Roldán (1979) all regard the Guadalquivir Basin as the foreland basin to the Betic mountain chain. However there is no trace of the basin before 27 Ma. at which time, according to many authors, the extensional collapse of the orogen began. Sanz de Galdeano & Vera (1992) suggest that the Guadalquivir basin originally existed as a proto-Guadalquivir basin, filled by marls and olistostromes, and in the mid Miocene was converted to a true foreland/foredeep type of basin. Almost all the authors, including Sanz de Galdeano & Vera (1992) agree that by the time the foreland Guadalquivir Basin was supposed to be forming the orogen was actually undergoing extension. One would expect a true foreland basin to form during the compressional phase (Allen *et al.*, 1986). During extensional collapse it is more likely that any foreland basin be destroyed as it is overridden by the spreading edge of the collapsing orogen. It is not clear what kind of basin might be expected on the external margins of a collapsing orogen. Moreover, recent work by Roca & Desegaulx (1992) suggests that in the east of the orogeny the equivalent of the Guadalquivir basin emerges from the overthrust external zone to form the Valencia trough. This trough is shown to be an extensional basin, disrupted late on its history by compressional thrusting and this may be a more likely origin for the Guadalquivir basin. The present southern margin of the present Guadalquivir Basin is marked by a broad band of disrupted rock, referred to as an 'olistostrome'. The 'olistostrome' appears to be allochthonous making the southern margin of the Guadalquivir Basin a tectonic rather than stratigraphic contact.

There is little published about either the sedimentology or origin of the Gibraltar Arc Flysch. However, it is known that deposition of the Flysch spans at least the Oligo/Miocene (Bourgeois, 1978). Platt & Vissers (1989) imply that the Gibraltar Arc was thrust out radially during extensional collapse. Thrusting appears to be coincident with the deposition of the Flysch and it is not clear what relationship there was between this and the extensional collapse of the Betic Orogen.

It can be seen from the above that there are several points that need to be addressed before the tectonic history of the Betic Orogen can be resolved :-

1. How does the earliest phase of Cretaceous metamorphism (65 Ma.) relate to the proposed main phase of thrust stacking at around 30 Ma., and what happened during the intervening 47 million years between these two events?
2. When precisely did extensional collapse of the Orogen begin and how did it progress?
3. Was the extensional collapse phase solely responsible for exhumation of the high grade Nevado-Filabride thrust sheet or did some uplift occur during an earlier phase of thrust stacking?
4. How much displacement has occurred in the External Zone: what is the timing of this displacement, and is it related to an extensional or compressional regime within the orogen?
5. How do the external basins fit into the orogenic scenario? Is the formation of the Guadalquivir and Gibraltar Arc Flysch basins linked to tectonism in the Betic Orogen or are they unrelated, and merely disrupted by orogenic events late in their history?
6. Is the olistostrome found along the southern margin of the Guadalquivir basin, a sedimentary unit, or was it emplaced tectonically?

## 2 ROLE OF BASINS IN INTERPRETING OROGENS

Basins are of considerable value in interpreting orogens, and this value depends on the recognition of the relationship between the orogen and the basin. A number of classification schemes have been proposed. The general principles of these schemes are discussed before a suitable scheme is selected to provide a rigorous framework for discussing the Guadalquivir and Gibraltar Arc Flysch basins of the Betic Orogen.

### 2.1 Classification of Basins.

Basins are essentially formed in areas of prolonged subsidence of the Earth's surface. Such subsidence may be driven by a variety of processes which are ultimately related to those which cause the lithosphere to subside. The lithosphere is divided into a series of plates which move relative to each other and interact at their margins. Plate margins can be classified as divergent, convergent, constructive, destructive or strike slip. Excellent reviews of plate boundaries can be found in most basic textbooks, and will not be discussed further.

Because basins are related to subsidence of the lithosphere which is primarily caused by plate interaction, those schemes which classify basins in terms of their plate tectonic setting seem to be the most useful:-

Dickinson (1974) emphasized both the position of the basin in relation to the plate margin and the type of plate margin closest to the basin. By this scheme Dickinson (1974) recognised five major basin types:-

1. Oceanic Basins.
2. Rifted continental basins or extensional basins.
3. Arc trench systems.
4. Suture belts, or orogens.
5. Intracontinental basins.

A sixth type was added to this list by Reading (1982) who suggested that strike slip/transform margin basins were a separate and distinct category that needed to be added to the scheme of Dickinson (1974).

Many basins associated with suture belts or orogens (type 4 of Dickinson, 1974), have been studied in detail leading to a variety of subdivisions:

Besly (1988) recognised that basins within orogenic belts could be classified in terms of their position relative to the orogen. Similar to Bally & Snelson (1980) Besly's work (1988) was based on the position of Carboniferous basins in northwest Europe relative to the Variscan Orogenic belt and differentiated basin types:-

**Table 1.** Basin classification scheme of Bally & Snelson (1980)**1. Basins located on rigid lithosphere not associated with formation of megasutures.**

- 1.1 Related to formation of oceanic crust
  - 1.1.1 *Rifts*
  - 1.1.2 *Oceanic Transform fault associated basins*
  - 1.1.3 *Oceanic abyssal plains*
  - 1.1.4. *Atlantic type passive margins which straddle continental & oceanic crust.*
    - 1.1.4.1 Overlying earlier rift systems
    - 1.1.4.2 Overlying earlier transform systems
    - 1.1.4.3 Overlying earlier back arc basins of (3.2.1) and (3.2.2) type
- 1.2 Located on pre-Mesozoic continental lithosphere
  - 1.2.1 *Cratonic basins*
    - 1.2.1.1 Located on earlier rift grabens
    - 1.2.1.2 Located on former backarc basins of (3.2.1) type.

**2. Perisutural basins on rigid lithosphere associated with formation of compressional megasuture**

- 2.1 Deep sea trench or moat on oceanic crust adjacent to B-subduction margin
- 2.2 *Foredeep and underlying platform sediments*, or moat on continental crust adjacent to A-subduction zones.
  - 2.2.1 Ramp with buried grabens but with little or no blockfaulting
  - 2.2.2 Dominated by block faulting
- 2.3 *Chinese-type basins* associated with distal blockfaulting related to compressional megasuture and without associated A-subduction margin.

**3. Episutural basins located and mainly contained in compressional megasuture**

- 3.1 Associated with B-subduction zone
  - 3.1.1 *Forearc basins*
  - 3.1.2 *Circum Pacific backarc basins*
    - 3.1.2.1 Back arc basins floored by oceanic crust and associated with B-subduction
    - 3.1.2.2. Back arc basins floored by continental or intermediate crust, associated with B-subduction
- 3.2 Backarc basins, associated with continental collision on concave side of A-subduction arc
  - 3.2.1 On continental crust or *Pannonian-type* basins
  - 3.2.2 On transitional and oceanic crust or *W. Mediterranean* type basins
- 3.3 Basins related to episutural megashear systems
  - 3.3.1 *Great basin-type* basin
  - 3.3.2 *California-type* basins

**1. Internal Basins**, which are entirely allochthonous and have undergone extensive deformation and metamorphism, or are early post orogenic features located within the internal allochthon

**2. Peripheral basins**, are initially located in the orogenic foreland, but at later stages of orogeny become involved in deformation and low grade metamorphism. The fills of such basins are now preserved in allochthonous or para-autochthonous positions.

**3. External Basins**, are autochthonous in more distal positions in the foreland, and have fills which were affected only by moderate or slight deformation in the latest stages of orogeny, and are unmetamorphosed

Perhaps the most detailed and comprehensive scheme is that of Bally & Snelson (1980).

This emphasized the characteristics of lithospheric behaviour rather than the 'geographical' relationships of Dickinson (1974) and in many respects is an elaboration of both the Dickinson (1974) and Besly (1988) views. This scheme is summarised in Table 1, it divides the basins into those associated with either major suture belts on compressive margins or those associated with non-compressive margins. The basins of compressive margins are subdivided into perisutural and episutural basins. Perisutural basins are associated with compressional megasutures, but do not occur within megasutures, while episutural basins are basins located within compressional megasutures. Perisutural basins are equivalent to the External and peripheral basins defined by Besly (1988) while Episutural basins are equivalent to Internal Basins.

The scheme of Bally & Snelson (1980) is considered to provide the most comprehensive classification of basins, and will be used when considering basins in relation the Betic orogen.

## 2.2 The Classification of Neogene Basins of the Betic Orogen

Sanz de Galdeano & Vera (1992) subdivided the Neogene Betic Orogenic basin into internal and external basins under a scheme comparable to that of Besly (1988) referred to above. The internal basins are early post orogenic features that are contained within the internal allochthon. They include the Granada Basin, the Almeria basin and others which thought to have formed during the extensional collapse of the orogen (Platt & Vissers, 1989). The external basins include the Guadalquivir basin and possibly also the Gibraltar Arc flysch. The Guadalquivir basin is interpreted to be a foredeep basin produced by the downwards flexure of the Iberian margin as it was overridden by the African plate, creating a depocentre on the northern margin of the orogen (Sanz de Galdeano & Vera, 1992).

Under the scheme of Bally & Snelson (1980) the Betic Orogen is a type-A subduction margin, that is, a collisional margin involving continental crust. The basin types defined by Sanz de Galdeano & Vera (1992) are equivalent to episutural type 3.3 (internal) and perisutural, type 2.2 (external) of Bally & Snelson (1980), Table 1. However, there is some debate as to whether the Guadalquivir Basin is an external, orogenic foredeep type of basin as suggested by Sanz de Galdeano & Vera (1992) or an extended continental margin basin resembling the Valencia Trough and not associated with the Betic megasuture. Because this is a major point of confusion external (foredeep) and extensional (rifted continental margin) basins will be compared to highlight their characteristic differences.

### 2.2.1 External Foredeep Orogenic Basins

Foredeep or foreland basins are defined as sedimentary basins lying between the front of an orogen and the adjacent craton (Allen *et al.*, 1986). Foreland basins develop at the front of active thrust belts, where the transport direction is toward the basin (Allen *et al.*, 1986). The progression of these thrusts causes the overridden foreland lithosphere to flex downwards, creating a depocentre. Dickinson (1974) proposed two genetic classes of foreland basin:-

1. *Peripheral basins*, are situated against the outer-arc of the orogen during continent-continent subduction (type A-subduction of Bally & Snelson, 1980; Table 1)

2. *Retro-arc basins*; are situated behind a magmatic arc and linked with subduction of oceanic lithosphere (type B-subduction of Bally & Snelson, 1980; Table 1).

Where a basin lies ahead of the active thrust front it is termed a 'foredeep' basin, where it rides on top of the moving thrust sheet, and behind the thrust front it is a 'thrust sheet top' basin (Ori & Friend, 1984) or a 'piggy back basin'.

However, foreland basins vary greatly from these simple models, particularly in terms of the state of the lithosphere supporting the basin and it is important to know what kind of crust a basin evolves from (Allen *et al.*, 1986).

The foreland basin is filled by detritus from the overriding orogen as this is uplifted and subject to denudation. The first deposits are often fine grained and are commonly turbidites as in the Hecho Group of the Pyrenees (Labaume *et al.*, 1985) and the Palaeozoic foreland basin of Quebec (Hiscott *et al.*, 1988). Later deposits are dominated by shallow water or continental coarse-grained Molasse-type deposits. Molasse foreland basins are predominantly filled with terrigenous sediments and are commonly coarse grained (Homewood *et al.*, 1986). The Silwalik sub-Himalayan basin (Graham *et al.*, 1975) is a good example of a molasse. However, the term molasse is often confused since it has been used for both tectonofacies and lithofacies, which must clearly be differentiated in any description of a foreland basin. Miall (1978) has interpreted the typical deposition pattern of foreland basins and related it to orogenic growth. The early deepwater stage indicates the onset of growth of the orogen, when topography was subdued and sedimentary delivery rates low. The Molasse stage occurs later when a mountain belt has grown to its 'steady state' size when rapid erosion counter balances uplift. It is during this stage that the basin is filled by molasse type deposits that are derived from the orogen. Allen *et al.* (1986) suggest that the early stage may reflect the loading of an initially stretched lithosphere. For a normal unstretched crust, emergence and the shedding of a clastic wedge accompanies the onset of shortening. For a progressively thinner crust the onset of rapid clastic sedimentation is increasingly delayed as it awaits the emergence of the orogenic belt above sea level.

### 2.2.2 Rifted Continental Margin (Extensional) Basins

Lithospheric stretching produces an evolutionary sequence from intracontinental rifts to passive margins. Rifting occurs at sites of crustal extension characterised by high heat flows and volcanic activity. Rifting may operate by an active or passive mechanism:-

*Active Rifting*; in which a thermal plume acting on the base of the lithosphere causes updoming and crustal thinning.

*Passive Rifting*; tensional stresses acting on the crust causing lithospheric thinning and the passive upwelling of the asthenosphere.

Passive continental margins that have been extended or rifted are characterised by seaward thickening prisms of marine sediment overlying a faulted basement consisting of syn-rift sequences. Post-rift seaward thickening prisms are formed of shallow water deposits. The uniform stretching model of McKenzie (1978) has been widely applied to the initial extension of passive margins (LePichon & Sibuet, 1981). In this model stretching of the whole

lithosphere occurs instantaneously, resulting in crustal thinning, asthenosphere upwelling and the formation of listric rotational faults in the region of crustal thinning. Other authors have appealed to asymmetrical stretching of the lithosphere (Coward, 1986; Wernicke, 1985; Lister 1989), leading to a basin and range complex. Basin and range complexes such as the Basin and Range of Colorado, North America (Wernicke, 1985; Lister 1989) lead to the formation of exposed metamorphic core complexes flanked by listric rotational faults seated on a major zone of detachment.

Following the initial rifting and deposition of syn-rift sediments, the thinned crust subsides (this is the drifting phase of Allen & Allen (1986)). There are several mechanisms which have been postulated to cause such subsidence and basin formation in the post-rift phase (Allen & Allen, 1986):-

1. *Subsidence due to sediment loading*; sedimentary loads enhance the tectonically driven subsidence. But this alone cannot cause sufficient subsidence to explain the thick sequences of shallow water deposits that may occur on a passive margin.
2. *Subsidence due to phase changes*; such as that from gabbro to denser eclogite at the base of the lithosphere.
3. *Subsidence due to creep of ductile lower crust*; thought to be caused by unequal ductile loading across the margin.
4. *Subsidence due to cooling following lithospheric thinning*; the upwelling of the asthenosphere is followed by thermal contraction.

Allen & Allen (1986) summarised the geological characteristics of extended passive margins, which are as follows:-

1. They overlie earlier rift systems which are generally sub-parallel or less commonly at high angles to the ocean margin.
2. An early syn-rift phase of sedimentation can be differentiated from a later drifting phase, the two are often separated by an unconformity.
3. Some passive margins exhibited considerable sub-aerial relief at the end of rifting (leading to major unconformities).
4. Some passive margins are underlain by linked extensional fault systems.
5. The drifting phase is characterised by gravity-controlled deformation such as salt tectonics, mud diapirism, slumps, slides, listric growth faults etc.

Two general kinds of passive margin have been differentiated, starved margins 2-4 Km thick, and nourished margins 5-12 km thick (Allen & Allen, 1986), the formation of these are dependent on sediment supply and amount of sub-aerial relief generated at the end of the rifting phase.

### **2.3 Basin Development in Relation to Orogens**

If basin configuration is largely a product of plate configuration, type and relative motions of the plate margin then 'the basin geometry and tectonic style is directly related to plate tectonic forces that have occurred through its history'. The interaction of plates tends to



produce large amounts of detritus generated by volcanic activity, by denudation of thickened crustal welts and by gravity sliding from disrupted plate margins. It therefore seems likely that detritus produced at plate margins will be concentrated in basins or depocentres that are generated by the plate interactions.

From these inferences, by analysis of the tectonic history and fill history of the basin the local plate configuration and their history of interaction can be partly or wholly deduced. Basin analysis may resolve a part of the tectonic history of a plate margin which cannot be resolved using tectonic and metamorphic data alone. Such studies are best made in the light of analogues from other basins/plates such as the Himalayas or the Alpine mountain chain, which have been documented.

In order to analyse a basin's history the tectonic style and provenance of the sediments (source) of the basin must be determined. Changes in the tectonic style and provenance history can be used to track the history of plate interaction and development of an orogen.

### 2.3.1 Tectonics

The tectonic style of a basin is related to the overall tectonic regime which governs a plate boundary. It can be easily determined by basin analysis whether a basin has been formed in a compressional, extensional, or strike slip regime. Many basinal areas demonstrate a change in style reflecting a change in tectonic style. Houseknecht (1986) described the evolution of the Atoka formation of the Arkoma Basin in south-central USA from a passive margin to a foreland basin. Stratigraphical analysis of the basinal sediments and the identification of regional unconformities was used to pin-point the exact time when this transition took place. Similar data may be used to give an indication of when the onset of orogenic mountain uplift took place. Unconformities can be further used to identify periods of tectonic activity and generated instability within an orogen. Uplift in a basin and correlative unconformities may denote the propagation of the thrust front of the orogen, likewise subsidence may denote lithospheric flexure of the foreland, also generated by propagation of the thrust front.

When considering an orogenic foreland basin it is important to differentiate between foredeep and piggyback basins and determine whether there is a transition from the former to the latter. Such knowledge can fix the position of a thrust front and through this the geological history of the orogen.

It may be that the observed tectonic style of an orogenic basin, internal or external is incompatible with the supposed configuration of the orogen at the time of the basin formation. Recognition of this may lead to the reappraisal of the tectonic history of an orogen.

### 2.3.2 Provenance

Provenance studies aim to constrain the location of sediment source areas for a basin and define the pathways by which sediment is transferred from source to deposition (Haughton *et al.*, 1991). In order to achieve this many geological disciplines, including mineralogy, geochemistry, geochronology sedimentology and petrography are integrated into a basin analysis framework.

In order to determine the provenance of a sedimentary package contained within a known stratigraphic interval, three main tools are used:-

1. *Palaeocurrent*; the palaeocurrent is determined from a variety of sedimentary structures including pebble imbrication, current lineations and cross-bedding. A large data base is required to reduce the error inherent in such measurements, and to identify a regional rather than local flow. The palaeocurrent is used to determine the dispersal pattern within a basin and to trace that pattern back to a source block.
2. *Petrography*; is used to determine the mineralogy of the sediment, and is most commonly applied to siliciclastic rocks. The mineralogy of the sediment is a product of the character and nature of denudation of the source. Dickinson *et al.* (1983), Graham *et al.* (1986), Allen *et al.* (1991) and Ingersoll (1977) have all shown that quantitative petrology can be used to determine the source of the sediment, and ultimately the plate tectonic setting (Fig O.5).
3. *Maturity*, is a qualitative measure of the degree to which the sediment has undergone weathering before and during transport and may indicate the time span between denudation and deposition. The most mature sediments are typically well sorted, with well rounded grains and lack the more epigenetically unstable grains, such as mafic minerals. The most mature sediments are quartz arenites, containing more than 90% quartz. Maturity is important because (1) it can distort the provenance of a sediment if the source indicator minerals are lost and (2) gives an indication of the number of transport/deposition cycles a sediment has been through.

Quantitative provenance methods can be used to interpret the characteristics of the source and the nature of the sedimentary basin:

They may identify palaeogeography and tectonic setting. Provenance is often incorporated into palaeogeographic reconstructions, particularly in areas of complex tectonics. Bluck (1983) and Dempster & Bluck (1989) used provenance to demonstrate that Ordovician sedimentary rocks that are found in faulted contact with Dalradian rocks in Scotland did not originate from the Dalradian. This is despite the fact the Dalradian is known to have been undergoing uplift at the time of sedimentation. This led to the re-interpretation of Ordovician palaeogeography of Scotland. Dickinson *et al.* (1983) demonstrated that there is a clear relationship between the petrography, provenance and the plate tectonic setting of north American Phanerozoic sandstones on a series of ternary plots (Fig. O.5)

They may identify the source blocks of the sediments that fill the basin. The mineralogy of the sediment provides important constraints on the mineralogy of the source area. It gives an indication of what terrains or metamorphic belts were exposed at the time of sediment derivation. Evans & Magne Rajetzky (1991) have used provenance to construct a record of Alpine metamorphic and structural events.

They may identify igneous evolution. A detrital record may be all that remains of some crustal blocks and higher crustal levels. Provenance may be the only means of determining the evolution of ancient plate margins. A more complete picture of magmatism can be derived

by looking at both provenance and the remains of arc basement (Longman *et al.*, 1979; Leitch & Willis, 1982).

They may identify crustal evolution. Fine grained sediments can sample a large continental area (Haughton *et al.*, 1991) and have been used to trace the evolution of the upper crust. Trace element analysis can be used to infer the composition of the upper crust and isotopic data can constrain the pattern of crustal growth.

### 2.3.3 The Provenance History

Changes in provenance through the history of a basin can be used to map changes in the nature of the source. This can give an indication of what terrain was exposed at what time, and also from which crustal level it originated. A foreland basin fill can be looked at in terms of provenance and can be treated as a 'recording' of orogenic evolution. Graham *et al.* (1986) used the Sphinx Conglomerate of south-west Montana to map the changing provenance in a foreland basin. These data were used to deduce the terrain evolution of the Madison Range of the Rocky Mountains. Allen (1991) analysed Torridonian detritus and inferred the timing of mantle contribution to the Laurentian crust in north west Scotland. Rapson (1965), examined Jurassic and Cretaceous rocks in the south west Rocky Mountains and was able to trace the unroofing history of the Nevadan-Laramide fold thrust belt in the southern Canadian Cordillera. A recent advance has been the use of single grain analysis to determine provenance, an example is the isotopic age dating of single detrital micas in sediments (Kelley & Bluck, 1989; 1992).

## 2.4 External Basins of the Betics: Their Potential as an Orogenic Window

From the discussion in section 1.1.4 it can be seen that the evolution of the Betic Orogen is far from fully understood. The external basins (the Guadalquivir Basin and the Gibraltar Arc Flysch basin) are an integral part of the Betic orogenic history. Most of the studies of these external basins of the Betic Orogen have been very generalized, with few data to support their interpretations. There has been no attempt to link the development of the external basin to that of the Betic Orogen. By utilizing the techniques outlined in section 1.2.3 it may be possible to resolve some of the conflicting hypotheses proposed for the Betic Orogen and to determine the timing of some of the orogenic events. Clearly there are two questions that must be addressed in trying to produce such a basin-orogen linkage.

1. How are the basins classified under the scheme of Bally & Snelson (1980)
- 2 What is the provenance and provenance history of the basins, and how does it relate to the source, and to the tectonic history of the source?

### 3 AIMS AND OBJECTIVES OF THESIS

In this section the aims and objectives of the research that is the subject of this thesis will be summarised:-

The main aim of the conducted research has been to utilize data from the external basins of the Betic Orogen, the Guadalquivir and Gibraltar Arc Flysch basins, to critically evaluate the conflicting hypotheses which have been proposed to explain the tectonic evolution of the Betics. In order to achieve this there are several objectives that must be reached:

#### 3.1 Objectives.

- 1 The basins' classifications under the scheme of Bally & Snelson (1980), as outlined in Table 1., must be determined
2. The sedimentology of the basins' must be described and some attempt made to establish a palaeogeography.
3. The provenance and provenance history of the basins needs to be determined.

From these three objectives it should be possible to determine whether or not the basins are truly linked to the orogen, as proposed by Sanz de Galdeano & Vera (1992), or whether they are merely coincidental with the orogenic history of the Betics. If the basins are tied in with the orogenic history then some attempt will be made to trace the development of the orogen using the tectonic and provenance history of the basins. If the basins are not considered to be orogenic, then there may be important inferences which can be made about the overall plate tectonic history and timing of the orogenic assembly.

#### 3.2 Thesis Organisation.

The thesis is organised into three parts. Part I deals with the Guadalquivir basin, its tectonic/ stratigraphic setting, provenance and palaeogeography. From this the status of the Guadalquivir basin is assessed relative to the basin classification scheme of Bally & Snelson. Part II is similar in format to Part I and deals with the Gibraltar Arc Flysch basin. Part III places both basins in context with the Betic orogen and assesses implications for the interpretation of the orogenic history of southern Spain. The current literature will be assessed in the light of this interpretation

# ***PART I***

# ***THE GUADALQUIVIR***

# ***BASIN***

*Qui non ha vista Sevilla, non ha vista marravilla*

*(Who hasn't seen Sevilla, has seen no wondrous thing)*

*Andalucían saying*

# ***Chapter 1***

## ***Introduction***

## CHAPTER 1 INTRODUCTION

### 1.1 General Setting

The Guadalquivir Basin lies on the northern margin of the External Zone of the Tertiary fold thrust belt of the Betic Orogen and south of the Palaeozoic Iberian Meseta (Fig 1.1). It has a NEE-SWW orientation and is bounded to the SE by the overthrust sequence of the Prebetic Subzone, a subdivision of the External Zone fold thrust belt. Here NW directed allochthonous units of the Prebetic Subzone have apparently overridden the Guadalquivir basin to rest directly on the Iberian Massif and its Mesozoic cover (Fig. 1.1). Recent work by Roca and Desegaulx (1992) suggests that the Guadalquivir basin emerges to the E from beneath the overthrust zone to form the Valencia Trough. To the SWW the basin opens into the Gulf of Cadiz where sedimentation is continuing on the shelf and along the coastal strip between Huelva and Sanlúcar de Barrameda.

There are two structurally distinct regions within the Guadalquivir Basin:

- 1 *The Undeformed Allochthonous Basin*, lies to the north of the allochthonous Guadalquivir thrust front (Fig. 1.1).
- 2 *The Deformed Allochthonous Basin*, lies to the south of the thrust front. It is transported (along with parts of the External Zone) northwards over the autochthonous part of the basin (Sanz de Galdeano & Vera, 1992; Blankenship, 1991). The basin behind the thrust front now forms a complex pattern of outcropping allochthonous basin and External Zone sediments (Fig 1.1).

The allochthonous part of the basin contains bands of disrupted rocks that has been described as an olistostrome (Fig 1.1) (García Duenas, 1969; García Hernández *et al.*, 1980; Sanz de Galdeano & Vera, 1992). Both the allochthonous and autochthonous parts of the basin are characterised by a fill dominated by fine grained sediments (mainly marls) with some coarse grained sandstones and more locally conglomerates (Sanz de Galdeano & Vera, 1992; Roldán García & Rodríguez Fernández, 1991)

The whole of the Guadalquivir region is presently undergoing uplift, and much of the exposure of Tertiary sediments in the basin is created by erosion of poorly defined terraces which record this emergence.

### 1.2 Stratigraphic Setting

The general relationship of the stratigraphy of the Guadalquivir basin to that of the External Zone is shown in Figure 1.2. This litho-stratigraphic summary has been constructed using the stratigraphy defined by Roldán García (1985a,b). The Guadalquivir basin fill rests unconformably on rocks of the External Zone and is divided by several unconformities which were generated in the Serravallian, Tortonian and Messinian. In places, the autochthonous Guadalquivir Basin is overthrust by rocks of both the External Zone and the allochthonous Guadalquivir Basin. Olistostromes are found mainly in the lower Miocene (Aquitania to Serravallian) and appear to be most abundant in the region around the thrust front of the

emergent External Zone. Sanz de Galdeano and Vera (1992) divided the Guadalquivir basin fill up into two distinct sub-basinal units, the North Betic Strait of the Proto- Guadalquivir Basin (Lower and Middle Miocene) and the Foreland Guadalquivir Basin (Upper Miocene) (Figs. 1.2, 1.3). The Proto-Guadalquivir basin formed as the North Betic Strait in the Lower Miocene which then evolved into a Foredeep type of basin during the Middle Miocene (Fig 1.3). The olistostromes are considered to be intercalated with sediments belonging to the Foredeep Basin of the North Betic Strait (Sanz de Galdeano and Vera; 1992).

### 1.3 Previous Models for Basin Formation

The most complete, and certainly the most recent, model for the development of the Guadalquivir Basin is that of Sanz de Galdaeno & Vera (1992). However the model is not consistent with new data presented in this thesis. It is nevertheless the best model published, and can be summarised as follows:

In Burdigalian times the Subbetic underwent a WNW, ESE compression, during which time a marine basin appeared within the Subbetic. This basin formed the North Betic Strait connecting the Atlantic Ocean to the Mediterranean and evolved during the Mid Miocene. As a result of continued deformation in the Subbetic a mobile sector appeared on the southern border of the North Betic Strait in which huge olistostromes formed. These olistostromes are interpreted as reflecting important re-sedimentation on the Subbetic thrust front. Towards the mid Miocene a new depocentre developed near the southern margin of the North Betic Strait, forming a foredeep to the Guadalquivir basin (Fig. 1.3)

During the Mid Miocene the mobile sector of the North Betic Strait continued to receive olistostromic masses, indicating a continued processes of structural disorganisation in the Subbetic subzone. In central and western sectors of the mobile area the depocentre was displaced towards the NW to occupy the area of the present Guadalquivir Basin. The last movement of olistostrome masses occurred during the Serravallian.

In Tortonian times the North Betic Strait was interrupted as the Prebetic subzone suffered a N & NW displacement. The mobile sector disappeared and the North Betic Strait was transformed into the Foreland Guadalquivir Basin. This basin continued to subside in the Messinian until finally major uplift of the Betic chain ended communication between the Atlantic and Mediterranean.

A number of other authors have produced models which deal with specific aspects of the Guadalquivir Basins history. Suárez Alba *et al.*, (1989) recognised a Neogene Guadalquivir Foreland Basin and produced a cross-section (Fig 1.4). Using seismic facies analysis and field studies, turbidite sediments were identified in the Guadalquivir Basin. In all, six turbidite bodies were identified. These showed a westward progradation with a palaeo-flow axial to the basin. However no morphological palaeo-talus or preferential sediment supply was identified.

Roldan Garcia & Rodriguez Fernandez identified several units in the allochthonous part of the basin. These have been interpreted as being piggy back basins which developed over thrust sheets that moved northwards during the mid-upper Serravallian & Tortonian.

This thesis will re-evaluate these models and their evidence in the light of new field



outcrop and map data. The new data will be used to generate several alternative models for the formation of the Guadalquivir Basin that are more consistent with the observed field relationships.

#### **1.4 Study Area**

The Guadalquivir Basin has been studied in the area around Montilla, Cordoba Province (Fig. 1.1) This area was selected because it contains reasonable exposure of both the allochthonous and autochthonous parts of the Guadalquivir Basin. It is also covered by three well constrained Geological maps (Roldán García *et al.*, 1985a,b; Leyva Cabello, 1973). Other areas were found to be poorly exposed and with no published maps available. The locations of sections recorded in sedimentary logs and from which samples were taken are shown on the maps in Foldouts 1,2 and 3. These are modified from published maps of Roldán García *et al.*, (1985a,b) and Leyva Cabello (1973).

***Chapter 2***  
***Tectono-***  
***Stratigraphic***  
***Analysis***

---

## CHAPTER 2

### TECTONO-STRATIGRAPHIC ANALYSIS

#### 2.1 Introduction

The allochthonous and autochthonous parts of Guadalquivir basin have been studied in detail in the area of Baena and Montilla (Fig. 1.1). The exposure in this area is generally poor, but field observations have been combined with geological maps seismic sections and bore-hole data to produce a reasonably well constrained tectono-stratigraphic history

The study is based on three published geological maps, those of Roldán-García *et al.* (1985a,b) and Leyva Cabello (1973). A seismic section and bore-holes (Fig. 2.1), located within the study area (Fig. 1.1), have been combined with outcrop observations to produce revised maps (Foldouts 1,2 & 3). The lithologies and sedimentary facies of the Guadalquivir basin are reinterpreted in Chapter 3, and have been used in conjunction with these maps to produce a revised stratigraphy (Fig. 2.2). The revised maps, seismic section and boreholes have been used to construct three detailed cross-sections (Foldouts 4,5 & 6). Cross-sections, maps, and field data have been used to outline a chrono-stratigraphy which is compared to the global eustasy curve and known tectonism of the Betic Orogen. The result is a new tectono-stratigraphic history for the area.

The allochthonous and autochthonous parts of the Guadalquivir basin have been previously interpreted as being two separate basins that developed contemporaneously with thrusting (Sanz de Galdeano & Vera, 1992; Roldán García & Rodríguez Fernández, 1991). However, sedimentological analysis (Chapter 3) demonstrates that the sediments in the allochthonous and autochthonous portions of the Guadalquivir Basin are almost identical in terms of their facies, facies associations and petrography. Detailed provenance analysis (Chapter 4) have also revealed that sediments in the allochthonous and autochthonous basin have the same source in the Spanish Meseta. Because of these similarities the allochthonous and autochthonous basins are considered to have been part of same basin for much of the Miocene and not two separate basins.

#### 2.2 Data Sources

In order to construct a tectono-stratigraphic history of the Guadalquivir basin several data sources have been combined.

##### 2.2.1 Maps

Three 1:50.000 geological maps published by the Instituto Geológico y Minero España cover the study area (Roldán-García *et al.*, 1985a,b; Leyva Cabello, 1973). These are the Baena sheet, ref. 967/17-39, the Montilla sheet, ref. 966.16-39 and the Espejo sheet, ref. 944/16-38. The maps were produced mainly through the use of colour aerial photography and satellite imaging. Because of poor exposure it was found that the maps could not be improved by conventional mapping. However, where appropriate, critical geological boundaries have been checked, and, where necessary, modifications have been made.

From the inspection of the maps (Foldouts 1,3 & 3) it was found that the study area could be divided into two distinct geological zones (Fig. 1.1), an allochthonous zone and an autochthonous zone. The autochthonous zone is characterised by lower Aquitanian to Messinian sedimentary rocks which are largely undeformed and generally flat lying. The allochthonous zone consists of Mesozoic and Palaeogene rocks of the External Zone that are found together with Lower Miocene rocks that are similar in character to rocks found in the autochthonous zone. These rocks are often intensely deformed and are cut by numerous faults. The boundary between these two zones broadly coincides with the boundary suggested by Sanz de Galdeano & Vera (1992) and Roldan Garcia *et al.* (1985b) that separates the allochthonous and autochthonous parts of the Guadalquivir Basin.

### 2.2.2 Seismic & Bore Hole Data

A seismic line, published by Blankenship (1992), and shown in Figure 2.1 passes through the study area 8 Km west of Baena (Fig. 1.1). This line crosses both the allochthonous and autochthonous parts of the Guadalquivir Basin. The line is constrained by boreholes situated at Nueva Carteya (37°36'N, 04°25'W) and Rio Guadalquivir (27°31'N, 04°15'W) (Fig. 1.1 & Foldout 1) the successions of these boreholes are shown in Table 2.1.

**Table 2.1** Results of Boreholes drilled at Nueva Carteya and Rio Guadalquivir

Rio Guadalquivir H-1		Nueva Carteya 1	
Depth to top of (m)	Age	Depth to top of (m)	Age
0-206	Miocene	Unknown	Miocene
206-256	Eocene	Unknown	Cretaceous
256-932	Lower Cretaceous	Unknown	Jurassic
1668-2070	Middle Jurassic	Unknown	Triassic
2070-3774	Lower Jurassic	Unknown	
		3227	<b>Thrust</b>
<b>Thrust</b>		3227m-3554	Miocene
3774-3849	Upper Palaeocene- Middle Eocene		
3849-4346	Lower Cretaceous		
4346-4709	Upper Jurassic		
<b>Thrust</b>			
4709-4984	Upper Palaeocene- Middle Eocene		
4984-5069	Red beds		

From Blankenship (1993)

From the interpretation of the seismic line and the borehole data, several important observations can be made:-

1 The borehole at Nueva Carteya and the seismic line show a series of thrust nappes composed of folded Mesozoic rocks of the External Zone. At Nueva Carteya the borehole encountered 327m of Lower Miocene strata at a depth of 3227m below the thrust nappes. This clearly demonstrates that rocks of the External Zone are thrust over Miocene sedimentary rocks of the Guadalquivir Basin.

**2** At the northern end of the seismic line there is an undisturbed Lower Miocene to Upper Miocene succession. This is the autochthonous part of the Guadalquivir Basin. The base of the Guadalquivir basin succession rests on Triassic rocks which rest in turn upon the Palaeozoic basement of the Iberian Foreland.

From these observations it can be deduced that the allochthonous rocks are thrust over the autochthonous part of the Guadalquivir Basin, and that the thrusting movements were at least post-Lower-Miocene in this area, but may have started earlier elsewhere. The autochthonous part of the basin is believed to lie below the thrust nappes (Fig. 2.1) (Blankenship, 1992).

However, the seismic section does not resolve the issue of whether or not the thrusts cut through the Upper Miocene sediments of the Guadalquivir Basin. Blankenship (1992) suggested that the thrusts are blanketed by Tertiary sediments of the Guadalquivir river basin but conceded that there was no field data to support this view (Blankenship, 1993). Because of poor exposure and extensive cultivation it seems unlikely that the thrusts can be observed directly. However, it may be possible to resolve this question by the analysis of Geological maps (Section 2.4).

### *2.2.3 Field Data*

Field data collected from the study area are mainly in the form of sedimentary logs and petrographic analyses of samples (Chapter 3 & Appendix I). The sites from which the logs and samples were derived are shown on the maps in Foldouts 1, 2 & 3.

Field studies and sample collections were restricted by the poor exposure found in this intensively cultivated area. Despite this restriction the Miocene to upper Messinian sediments have been logged and over 100 samples have been collected. The logged sections and samples have been located on Foldouts 1, 2 & 3.

The field data have been used to determine lithologies and facies, and to interpret depositional environments and palaeogeography of the Guadalquivir Basin. The field data are fully interpreted in Chapter 3 and will not be discussed further here. The lithological and environmental interpretations have been incorporated into the stratigraphic revision (Fig. 2.2) discussed in section 2.3.

## **2.3 Revisions**

The seismic section, bore holes and field data have been used to produce revised geological maps and a revised stratigraphy.

### *2.3.1 Revised Maps*

The principal amendments to the maps have been the identification of: 1) the external zone thrust front and 2) the allochthonous and autochthonous portions of the Guadalquivir Basin succession, and the boundary between them (Foldouts 1, 2 & 3). Minor revisions to geological boundaries have also been made where it was found to be appropriate. Figure 2.3 shows a panoramic view of the External Zone thrust front and the allochthonous and autochthonous portions of the Guadalquivir basin.

The External Zone thrust front has been marked on previously published maps and cross-sections (Garcia Hernandez *et al.*, 1989; Roldán-Garcia *et al.*, 1985a,b; Sanz de Galdeano & Vera, 1992; Blankenship, 1992). It divides rocks of the overthrust External Zone from those of the Guadalquivir Basin. In the Baena Montilla study area this boundary is marked by a series of thrust contacts which are defined by a dramatic change in topography from a gently undulating, low lying land in the north to high mountains in the south (Fig. 2.3). The mountains in the south are characterised by largely undeformed Mesozoic and Palaeogene limestones that are found in normal stratigraphic sequence, except where cut by thrusts. The lower land is formed by rocks of the allochthonous zone characterised by a complicated outcrop pattern of Mesozoic and Palaeogene rocks of the External Zone and Lower to Mid Miocene rocks of the Guadalquivir Basin (Fig. 2.4). Geological juxtapositions in this area are commonly out of stratigraphic sequence. In places, rocks of the External Zone are thrust over Lower Miocene sedimentary rocks of the allochthonous Guadalquivir Basin. An example of this is seen in the Baena Klippe (Foldout 1) where Palaeogene rocks are thrust over Lower Miocene rocks.

The boundary between the allochthonous and autochthonous units of the Guadalquivir Basin (Foldouts 2 & 3) separates the flat lying undeformed sequence of Upper Miocene sedimentary rocks from deformed and faulted External Zone rocks and lower to Mid Miocene sedimentary rocks of the allochthonous zone. The boundary can also be seen on seismic sections (Fig. 2.1), separating rocks in the south that are cut by thrusts from rocks in the north that appear to be unaffected by thrusting.

The allochthonous/autochthonous boundary shown in Foldouts 2 & 3 has been marked on the maps where deformed Mesozoic, Palaeogene, and lower to Mid Miocene rocks were found juxtaposed against the undeformed Upper Miocene sequence. In places this boundary has been inferred across areas of non-exposure. Parts of the allochthonous zone are so intensely deformed that individual stratigraphic units could not easily be identified. This relationship is seen in the NE corner of Foldout 2 and the SE corner of Foldout 3. In these areas (Localities 81-91, Foldout 3) outcrops of Mid Miocene and Upper Miocene rocks have been found which are similar to rocks found in the autochthonous part of the Guadalquivir Basin (Fig. 2.5). This has also been observed by Leyva Cabello (1973). This indicates that the allochthonous part of the Guadalquivir Basin contains mid and Upper Miocene sedimentary rocks which are important to arguments presented in section 2.4.

### 2.3.2 A Revised Stratigraphy for the Guadalquivir Basin

It is not the purpose of this section to construct a new, alternative stratigraphy for the Baena Montilla region. The aim is to revise the stratigraphy of the autochthonous (undeformed) Guadalquivir basin succession using the seismic sections, bore hole data, field data and revised geological maps. No attempt has been made to revise the stratigraphy of the External Zone as it is not the main subject of this thesis.

The main revisions that have been made to the stratigraphy are to the thicknesses, lithologies and environmental interpretations of the stratigraphic units defined by Roldán-Garcia *et al.* (1985a,b) and Leyva Cabello (1973). The new lithological and environmental

interpretations are based on the field and petrographic studies that are discussed in Chapter 3. The revised maps (Foldouts 1,2 & 3) and sedimentary logs (Appendix I) have been used to identify unconformities in the Guadalquivir basin. These were found to coincide with unconformities identified by Roldán-García *et al.* (1985a,b) and Leyva Cabello (1973). The final revision has been to remove the 'Olistostrome' from the stratigraphy. The reasons for this are discussed in section 2.4. The revised stratigraphy for the Guadalquivir Basin is summarised in Figure 2.2.

The Guadalquivir Basin in the Baena Montilla region is a minimum of 700m and a maximum of 1Km thick. The base of the basin fill is of Aquitanian age (Roldán-García *et al.*, 1985a,b) and rests unconformably on deformed Palaeogene and Mesozoic marls and limestones of the External Zone (Fig. 2.6). The limestones dip steeply to the W while the marls are effectively horizontally bedded. The limestones below the marls have a surface that is irregular over 10m. Deep depressions are commonly filled by limestone boulders (Fig. 2.6). This palaeo-topography resembles karst surfaces described by Jackus (1977), Legrand & Stringfield (1973), Sweeting (1973) and reviewed by Esteban & Klappa (1983). As a consequence the palaeo-topography has been tentatively interpreted as a palaeo-karst indicating sub-aerial exposure. The surface is exposed in only one locality (Location 9, Foldout Map 1, Ref. 522 340), consequentially the karst could not be fully characterised.

The lower and Mid Miocene rocks of the Guadalquivir basin are dominated by diatom and globigerinid marls indicating that deposition took place in a pelagic sea-way. The upper parts of the marl sequence (Serravallian) are dissected by channelised marine debris flows. These are unconformably overlain by between 25 and 50 metres of Tortonian sandstones that are intercalated with marls. Sandstone facies analysis indicates that deposition during the Tortonian took place on a shallow marine shelf. Beach deposits are locally present. Another unconformity separates the Tortonian sandstones from distinctive lower Messinian calc-lithic sandstones which are also interbedded with marls (Fig. 2.2). The calc-lithic arenites have been interpreted as having been deposited on a tidally dominated shallow marine shelf with both lagoonal and patch reef environments. They are overlain unconformably by upper Messinian conglomerates that were deposited in coastal fan deltas fed by an extensive fluvial system. This succession is overlain by deposits of the Quaternary Guadalquivir river basin.

To summarise, in the Baena Montilla region the rocks of the Guadalquivir basin rest unconformably on rocks of the external zone. Prior to the development of the basin the external zone was deformed and at least part of it appears to have been sub-aerially exposed. Three unconformities have been identified in the basin succession, at the base of the Tortonian, between the Tortonian and Messinian and in the Messinian. Overall the Guadalquivir basin succession is a shallowing up sequence, progressing from pelagic marine deposits in the Aquitanian to fluvial deposits in the Messinian. Minor fluctuations within this sequence are observed in the Tortonian and Messinian.

The allochthonous part of the Guadalquivir Basin has been transported northward over the autochthonous part of the basin, as is supported by seismic sections (Fig. 2.1). If the allochthonous and autochthonous zones were originally part of the same basin, as indicated by sedimentological and provenance data (Chapter 3 & 4), then the basin would have

extended much further south. This would place the southern margin of the Miocene Guadalquivir Basin much further south than the present external zone thrust front.

## 2.4 Inferences

From the revised maps and stratigraphy important inferences can be made concerning the nature of the Allochthonous/Autochthonous boundary and the status of the olistostrome described by Garcia Duenas (1969), Garcia Hernandez *et al.* (1980) and Sanz de Galdeano & Vera (1992).

### 2.4.1 Nature of the Allochthonous/Autochthonous Boundary

Geological contacts along the boundary separating the allochthonous zone deposit from the autochthonous Guadalquivir Basin sequence (Foldout Maps 2 & 3) are not stratigraphically consistent. To explain this the Upper Miocene rocks must either unconformably overlie the Allochthonous sheet or else the boundary must represent a tectonic contact (i.e. thrust).

The seismic section (Fig. 2.1) and interpretation of Blankenship (1992) shows that the boundary between the allochthonous and autochthonous zones is a thrust contact. The autochthonous rocks of the Guadalquivir basin can be extrapolated below the allochthon. However it is not clear in these sections whether the thrusts cut the Upper Miocene succession or whether the Upper Miocene blankets the thrusts (as suggested by Blankenship (1992)). Several key observations have been made that resolve this question:-

- 1 The study area is divided into two distinct zones (Fig. 1.1, Foldout 2). In the western portion of the Baena Montilla region, Upper Miocene rocks of the autochthonous Guadalquivir basin are exposed. By contrast the eastern portion of the area is dominated by allochthonous rocks belonging to the Guadalquivir Basin and the External Zone (Fig. 2.7a). The autochthonous rocks are exposed in the Rio Guadajoz river valley which is topographically lower than the area to the east in which the allochthonous rocks are exposed (Fig. 2.7a). Other N-S trending river valleys found along the E-W allochthonous thrust front also contain exposures of autochthonous Guadalquivir Basin rocks. This observation may be interpreted in one of two ways, in structural or in stratigraphical terms. If the allochthonous rocks were thrust northward following the deposition of Upper Miocene sediments then autochthonous rocks would lie beneath the allochthonous thrust sheet. The underlying autochthonous Upper Miocene rocks would have then been exposed by rivers cutting down through the allochthonous thrust sheet (Fig. 2.7b). An alternative hypothesis to this is that the present river systems follow the course of older Miocene palaeo-valleys. Sub-aerial exposure occurring at the end of the Lower Miocene and following a phase of thrusting would have led to the formation of river valleys along the thrust front margin. These valleys would have been subsequently filled by Upper Miocene marine sediments. However the first rocks seen in Upper Miocene above the candidate unconformity are marine and not fluvial, and there is no evidence for the substantial sub-aerial exposure that would have been required to create such large valleys.

2. Another important observation is that both Mid and Upper Miocene rocks occur



within the allochthonous zone. These have been deformed and transported along with the rest of the allochthonous sheet (Fig. 2.5). Therefore thrusting must have taken place after the deposition of the Upper Miocene sediments.

In conclusion it seems likely that the boundary between the allochthonous and autochthonous units is a thrust contact. This view is supported by seismic data. Thrusting must have taken place after the deposition of the Upper Miocene sediments and therefore the thrusts must somehow cut Upper Miocene sediments.

#### 2.4.2 Status of the Olistostrome

Olistostromes are stratigraphic units which are generally separated from overlying and underlying formations by depositional contacts (Hsu, 1974). They are distinct from melanges which are tectonic units bounded by shear surfaces (Hsu, 1974). Olistostromes may range from boulder beds to graded turbidites and are developed on a local scale. In contrast, melanges are usually developed on a regional scale. Melange terranes show different degrees of severity of fragmentation and mixing, grading from internally coherent allochthonous slabs to broken formations on to pervasively sheared and intimately mixed melanges.

The southern margin of the present Guadalquivir basin is marked by a band of disrupted rock interpreted as an 'olistostrome' (Garcia Rosell, 1973). It marks the boundary between the allochthonous and autochthonous units of the Guadalquivir Basin (Sanz de Galdeano & Vera, 1992). Sanz de Galdeano & Vera (1992) suggested that the 'olistostromes' formed during Lower Miocene times and were shed from a mobile front that was created as the thrust fronts of the External Zone encroached on the North Betic Strait of the Guadalquivir Basin. However, field and map observations indicate that these deposits are not 'olistostromes' but tectonic 'melanges'.

The 'olistostromes' of Garcia Rosell (1973) and Sanz de Galdeano & Vera (1992) are of a regional scale, developed along the entire allochthonous front defining the southern limit of the present Guadalquivir Basin. They contain huge slabs of External Zone material, mainly consisting of Triassic deposits (Fig. 2.4). The most disrupted rocks are found close to the allochthonous/autochthonous boundary, interpreted as a thrust front. This description alone is closer to the definition of a melange than that of an olistostrome, the latter tending to be more locally developed and with sedimentary contacts (Hsu, 1974).

No 'olistostrome' type material was found intercalated with the Lower Miocene marls in the Baena, Montilla region, even in localities where abundant 'olistostromes' are close by. Sanz de Galdeano & Vera (1992) clearly state that the 'olistostrome' was deposited during the Lower Miocene into the Guadalquivir Basin. If it were deposited during the Lower Miocene then it should be found intercalated with contemporaneous sediments, namely the marls. This is not the case in the Baena Montilla region.

There are more detailed observations that can be made about the 'Olistostrome'. Figure 2.9 shows a roadside exposure of 'Olistostrome' which consists of intimately mixed material of many lithological types. Some blocks are similar in character to the autochthonous Upper Miocene deposits of the Guadalquivir Basin. In particular conglomerates dominated by limestone clasts have only been found elsewhere in Messinian deposits of the Guadalquivir

Basin, and are thought to have been generated from the denudation of External Zone rocks (Chapter 4). Other areas of the Baena Montilla region previously mapped as 'olistostromes' (Roldán-García *et al.*, 1985a,b; Leyva Cabello, 1973) have been found to contain deformed Upper Miocene sediments (Fig. 2.5). In general the olistostromes are dominated by Triassic red marls and by evaporite deposits.

From these observations several things can be deduced concerning the nature of the 'olistostromes': They have formed much later than was suggested by Sanz de Galdeano & Vera (1992) as material incorporated into them indicates a post-Messinian age. In outcrop this often forms a pervasively mixed formation, comprising rocks ranging in age from Triassic to Messinian. It is difficult to envisage how such a mixed unit could have formed by normal sedimentary processes. Triassic marls and evaporites are known to form the decollement horizon of thrusts in the External Zone (García Hernández *et al.*, 1979; Banks and Warburton, 1991), and this, taken with the observation that the most disrupted rocks are close the allochthonous/autochthonous thrust boundary, suggests that the 'olistostromes' are associated with thrusts. Allerton *et al.* (1993) also show Triassic material between Jurassic and Cretaceous allochthons in their cross-sections (Fig. O.1)

Blankenship (1993) noted that no Jurassic carbonates found have been in the 'olistostromes'. This is surprising since other authors (Sanz de Galdeano & Vera, 1992) insist that the 'olistostromes' were derived from External Zone thrust sheets that encroached on the basin. If this were the case then Jurassic carbonates, which are stratigraphically higher level than the Triassic, would have been exposed first. Thus Jurassic material should have been shed before the Triassic.

In conclusion, it seems likely that the so called 'olistostromes' formed along post Messinian thrusts. As the external zone was thrust northward on Triassic Evaporite decollements, material from the base and front of the thrust sheets was sheared off and mixed with Triassic red marls. This material included Upper Miocene deposits of the Guadalquivir Basin and so the thrusting must have taken place after the Messinian. If the 'olistostromes' are associated with thrusting and are tectonically produced then they should be termed 'melanges' according to the definition of Hsu (1974). Thus, the 'olistostromes' have been re-defined as 'melanges' and have been removed from the stratigraphy of the Guadalquivir basin.

## 2.5 Cross-Sections

Three geological cross-sections, with their locations shown on Figure 1.1, have been drawn for the Baena, Montilla region (Foldouts 4, 5 & 6). These incorporate data taken from the revised geological maps (Foldouts 1,2 & 3), the seismic (Fig. 2.1) and borehole data (Table 2.1) of Blankenship (1992) and new field data (Appendix I). One is orientated E-W (Foldout 4) and the other two S-N (Foldouts 5 & 6). The symbols and key are as for the revised geological maps in Foldouts 1, 2 & 3.

The E-W cross-section in Foldout 4 extends from the allochthonous unit in the east to the autochthonous unit in the west. The autochthonous Guadalquivir rocks are exposed in a river valley the significance of which has been discussed in section 2.4 (Fig. 2.7). In this

section the allochthonous thrust over the autochthonous unit, as can be seen in the seismic section (Fig. 2.1). The allochthonous unit in the east consists of a series of overthrust nappes composed of Mesozoic and Palaeogene rocks of the External Zone. These are overlain unconformably by Lower Miocene rocks of the Guadalquivir Basin fill, which are also cut by the thrusts. The Lower Miocene rocks are folded near the thrust fronts. Within the allochthon the Baena Klippe overlies the high level thrust separating the folded Palaeogene rocks from Mesozoic rocks below. This may be a remnant of a roof thrust that formed as part of a duplex system. The deformed Palaeogene rocks are overlain unconformably by Lower Miocene rocks which form the base of the Guadalquivir Basin fill (Fig. 2.6). The autochthon in the west is composed largely of flat lying sedimentary rocks of the Guadalquivir Basin. Unconformities have been identified within this sediment pile, between the Mid Miocene and Tortonian, between the Tortonian and Messinian and within the Messinian. Upper Messinian rocks are too thin to be shown on the cross-section. The autochthonous Guadalquivir basin deposits may overlie Triassic rocks belonging to the external zone (not shown on cross-section), as indicated on the seismic section of Blankenship (1992) in Figure 2.1. Both the allochthonous and autochthonous rocks rest on the Palaeozoic basement of the Iberian Foreland.

The south-north cross-section in Foldout 5 is a section across the map in Foldout 1. This covers the allochthonous zone only (Fig. 1.1). In the area considered this is similar in character to the allochthonous part of the cross-section in Foldout 4. The Baena Klippe is shown in a south-north section, on which the folded Palaeogene rocks can be clearly seen. The folds are overturned and have axial traces that trend E-W. To the north the Klippe overthrusts Lower Miocene rocks of the Guadalquivir basin.

The south-north cross-section 3, foldout 6 is a section across the maps in Foldout 2 & 3. The southern half of the section is composed of sediments of the autochthonous Guadalquivir Basement. To the north the allochthon is downfaulted against these rocks. The allochthonous rocks are highly deformed here and individual stratigraphic units could not be differentiated. However, they are known to include Tortonian rocks (Fig. 2.5). An undulating topography in this area has been interpreted as reflecting folding (Leyva Cabello, 1973). These folds have in turn been interpreted as thrust tip folds that hide blind thrusts. The allochthon is thrust over autochthonous Upper Miocene rocks to north, these rocks, because of poor exposure, are only known as Upper Miocene rocks. They clearly belong to the Guadalquivir Basin fill.

From these individual cross-sections a generalized south north cross-section has describing the southern margin of the Guadalquivir Basin has been produced (Fig. 2.9). Klippes are interpreted as being remnants of roof thrusts to a duplex system while melanges are shown associated with the thrust faults. This summary section forms the basis for constructing a tectonic/stratigraphic history for the Baena Montilla region (Section 2.8).

## 2.6 Chrono-Stratigraphy

The chrono-stratigraphy of the autochthonous Guadalquivir basin fill is shown in the form of a Wheeler (1958) type chrono-stratigraphic diagram (Fig. 2.10). In this the stratigraphic units are plotted in terms of their vertical and lateral continuity through time. In Figure 2.10

relative time is shown on the left *y* axis, thickness on the right *y* axis and lateral continuity on the *x* axis. The time scale is adjusted to thickness. Unconformities and related hiatuses, shown in the diagram, are plotted in time and space. A hiatus is defined as a space-time value of non-deposition (i.e. places where stratigraphy is missing) and is thought to develop during a regressive/transgressive episode.

The chrono-stratigraphic diagram has been constructed for the autochthonous Guadalquivir Basin succession from the revised geological maps (Foldouts 1,2 & 3), cross-sections (Foldouts 4,5 & 6) and new field data (Appendix I). The southern part of this diagram is well constrained, while the resolution to the north is restricted by poor exposure. Part of the stratigraphy is missing where allochthonous rocks are downfaulted against the autochthonous Guadalquivir Basin deposits. Unconformities and inferred hiatuses identified in the basin are shown. Most of the unconformities involve small time-gaps, although the Messinian (6.5 Ma.) unconformity cuts out the Tortonian in the south. The exact age of the base of the Guadalquivir Basin is unknown but has been estimated as Aquitanian (Roldán-García *et al.*, 1985a,b). If this is correct then part of the Aquitanian is missing and the hiatus is much larger than shown in Figure 2.10. There is evidence that a Karst surface developed before deposition of the Aquitanian (section 2.3) and this supports the hypothesis that the floor of the Guadalquivir Basin is a much larger hiatus than shown.

Hiatuses in the Guadalquivir basin are produced by regressive transgressive cycles that may, or may not have involved sub-aerial exposure. It is important to know whether these cycles are a product of tectonism, global eustasy or a combination of both.

## **2.7 Chrono-Stratigraphy Compared to Global Eustasy and Tectonism in the Betic Orogen**

In order to determine the relative influences of eustasy and tectonism on the sedimentation of the Guadalquivir Basin the chrono-stratigraphy has been plotted against both the Global Eustasy curve of Haq *et al.* (1987) and tectonism observed in the Betic Orogen (Fig. 2.11).

The basal deposits of the Guadalquivir Basin are Aquitanian pelagic marls that rest unconformably on Palaeogene limestones. These limestones were folded and subject to sub-aerial exposure that resulted in karstification prior to the deposition of the Aquitanian. The unconformity is dated at between 19 & 23 Ma. (Roldán-García *et al.*, 1985a,b) which means that the limestones were probably deformed before 23 Ma., during the Oligocene. The timing of the deformation coincides with the start of extension in the Betic orogen (see Overview, Fig. O.4). The 19-23 Ma. unconformity also coincides with a major sea-level fall that marks the base of super cycle TB2 of Haq *et al.* (1987). It may be that the sea level fall was amplified by the compression and uplift of the External Zones, to produce substantial sub-aerial exposure at this time. The karst surface was subsequently flooded and a pelagic seaway established, with the deposits coinciding with the transgressive part of cycle TB2.1 of Haq *et al.* (1987).

Other unconformities in the Guadalquivir Basin do not seem to reflect tectonism, but do appear to correlate reasonably well with sea-level falls. In particular the Tortonian hiatus correlates with a large sea level fall at the base of super-cycle TB3 of Haq *et al.* (1987) which

produced major sequence boundaries world wide. A compressive event is recorded in the Betic orogen at the base of the Tortonian by Ott & Estevou & Montenat (1990), but this has not been recognised by other workers. However it led Sanz de Galdeano & Vera (1992) to attribute the emergence of internal basins in the Betic Cordillera to a combination of both the sea level fall at the base of supercycle TB3 and reported compression in the orogen.

The two unconformities in the Messinian appear to correlate with sea-level falls at the bases of cycles TB3.3 and TB3.4 of Haq *et al.* (1987). This correlation is supported by Sanz de Galdeano & Vera (1992) who also attribute the appearance of reefs and evaporites in the eastern Guadalquivir and Almeria basins to the same sea level falls.

The overall shallowing up of the Guadalquivir Basin (Section 2.3, Fig. 2.2) fits the known general trend in sea-level, falling during the Miocene.

Thus the sea-level curves, when compared with tectonism observed in the Betic orogen, suggest that the unconformity at the base of the Guadalquivir Basin succession reflects both tectonism and eustatic sea-level fall. Other unconformities appear to have been Eustatically driven, although compression may have influenced that at the base of the Tortonian. The overall Guadalquivir Basin succession can be tied into the general sea-level trend during the Miocene.

## **2.8 A Tectonic & Stratigraphic History for the Guadalquivir Basin**

From the data and discussion above a tectonic and stratigraphic history can be produced for the Guadalquivir Basin in the Baena-Montilla region. This is summarised in Table 2.2 and Figure 2.12. Figure 2.12 also gives an indication of the probable movements that Africa underwent in relation to Iberia during the Miocene.

### **2.8.1 Mesozoic to Palaeogene.**

The external zone consists mainly of limestones and marls deposited on a basin/graben topography during the Mesozoic and Palaeogene (Garcia Hernandez *et al.*, 1980; Blankenship, 1992). The basin graben structure of the Palaeozoic basement implies that the Iberian Margin was undergoing extension at this time. The amount of extension for the Iberian margin has not been determined. At the end of the Oligocene the Mesozoic/Palaeogene cover was folded, indicating a conversion from an extensional to a compressional regime.

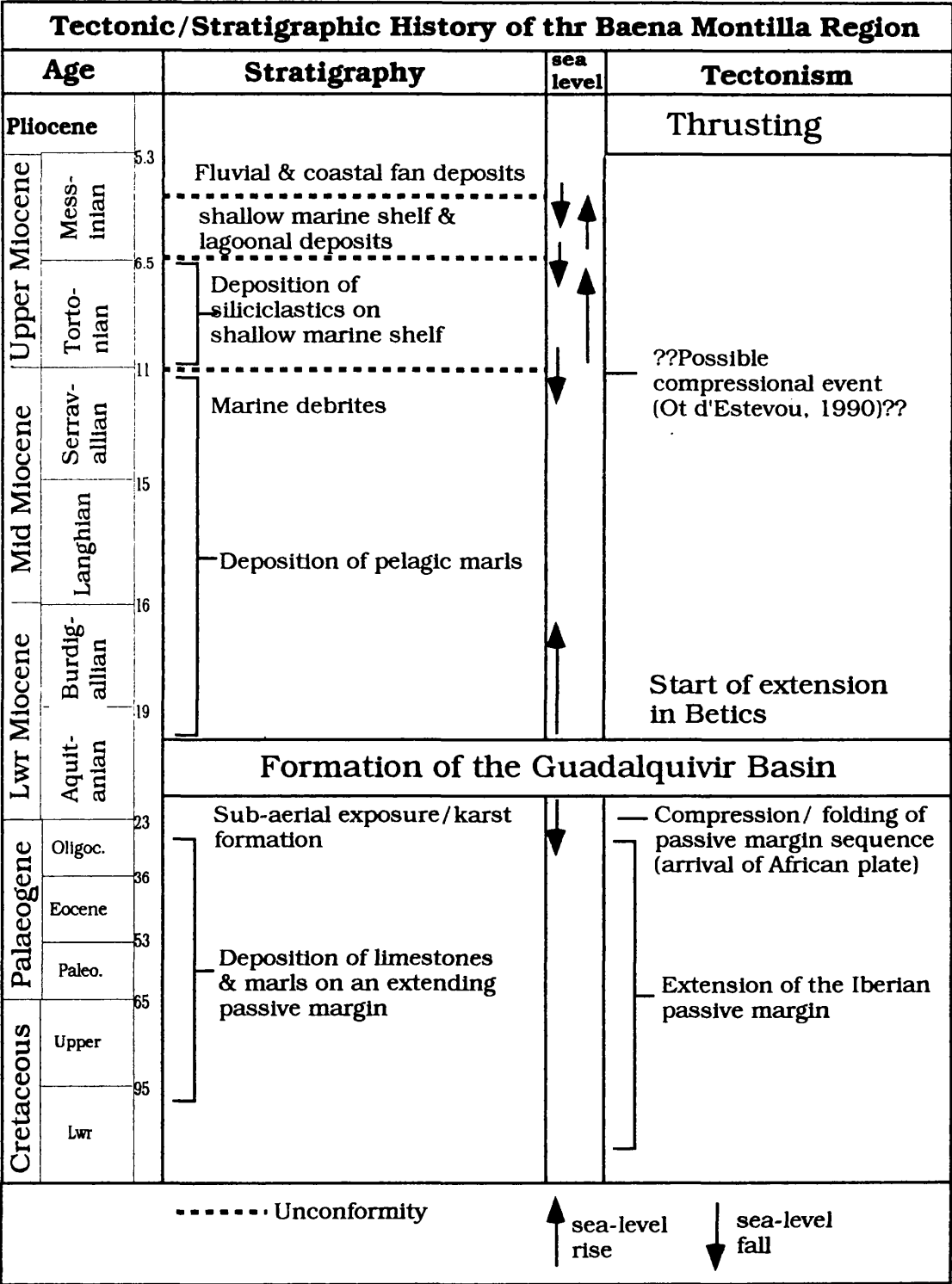
The Mesozoic Palaeogene cover may have been detached from its Palaeozoic basement during compression (Fig. 2.12a), but this is uncertain. Compression and uplift in the external zone combined with a major sea-level fall to produce substantial sub-aerial exposure. This resulted in karst erosion of Palaeogene limestones exposed in the area.

### **2.8.2 Lower-Mid Miocene**

A transgression over the Karst surface at the beginning of the Miocene brought with it the first deposits of the Guadalquivir basin. This may have resulted from a sea level rise coinciding with the subsidence of the passive margin formed as the northward progression of Africa slowed and the Betic Orogen underwent extension. Globigerinid and diatom marls were deposited in the basin, indicating that it formed a pelagic seaway during lower and Mid

Miocene times. Later on deposition in the basin was interrupted by debrites that were deposited prior to the formation of the Tortonian unconformity. The debrites may record the onset of the development of an unconformity elsewhere, this will be discussed in Chapter 3.

Table 2.2



2.8.3 Tortonian

A sea-level fall at the beginning of the Tortonian resulted in the formation the unconformity that now separates the Tortonian from the Mid Miocene. This may have been accentuated by the compression and uplift in the Betic orogen recorded by Ott d' Estevou, (1990). A transgression during the Tortonian led to the deposition of shallow marine siliciclastics.

Facies analysis of these rocks indicates deposition on a shallow marine storm dominated shelf. The end of the Tortonian is marked by another sea-level fall that resulted in an unconformity and the Tortonian hiatus.

#### **2.8.4 Messinian**

Messinian deposits unconformably overlie the Tortonian and Lower Miocene deposits and are dominated by shallow marine, lagoonal, coastal fan and fluvial deposits. The fluvial deposits are separated from the marine succession by an unconformity that developed during in the mid Messinian.

#### **2.8.5 Post Messinian (Pliocene )**

Renewed compression in the External Zone of the Betics orogen resulted in thrusting in Baena Montilla region which divided the Guadalquivir Basin into allochthonous and autochthonous units and formed the tectonic melanges. Thrusting may have been duplex style, with basal detachments and roof thrusts (Fig 2.12d). The cover was probably detached on Triassic evaporite deposits. Thrusts may have based on older detachments developed during the Oligo/Miocene shortening phase. Sedimentation in the Baena-Montilla region continues today as part of the Guadalquivir river basin

### **2.9 Conclusions**

From the study of the Baena-Montilla region several important facts concerning the origin and history of the Guadalquivir basin have been deduced.

1 The Guadalquivir basin developed between two compressional phases, that may or may not be related to tectonism in the Betic Orogen, but it is largely unaffected by tectonism during its Miocene history.

2 The Guadalquivir basin contains deposits, principally marls which are less than 1km thick. This indicates that the basin did not receive much detritus during its Miocene history.

3 Seismic data and stratigraphic relationships indicate that thrusting disrupted the Guadalquivir Basin at the end of the Miocene. Thrusting must have taken place after Messinian deposition.

4 Lithosomes in the Guadalquivir basin previously described as olistostromes are actually tectonic melanges. Their formation was associated with a post Messinian thrusting phase.

The Guadalquivir sedimentary rocks represents a basin fill that was largely passive, with unconformities being driven by eustatic sea-level falls. The basin deposits have previously been subdivided into the North Betic Strait and Foreland Basin successions on the strength of differing tectonic styles and the presence or absence of 'Olistostromes' (Sanz

de Galdeano & Vera, 1992). Because new data indicates that the basin has a passive fill and that there are no 'olistostromes' there now seems little point in making this distinction. Therefore, from a stratigraphic point of view, the Miocene fill of the Guadalquivir basin should not be subdivided.



***Chapter 3***  
***Sedimentology &***  
***Palaeogeography***

## CHAPTER 3

### SEDIMENTOLOGY & PALAEOGEOGRAPHY

#### 3.1 Introduction

This chapter aims to detail sedimentological investigations that have been carried out upon Miocene rocks of the Guadalquivir Basin. The Miocene rocks of the Basin has been split into four stratigraphical units bounded by unconformities. For each of these units facies and micropalaeontological analyses have been used to determine the environments of deposition which form the basis of palaeogeographical reconstructions. The micropalaeontology is fully outlined in Appendix II, and the results have been incorporated into the facies analysis in this chapter. Numbers of locations referred to in this chapter are given on the maps contained in Foldouts 1,2 & 3 and grid references refer to published Instituto Geológico Y Minero De España (IGME) maps (see Appendix 5).

#### 3.2 General Stratigraphy

This sedimentological investigation uses the stratigraphic framework of Roldán-García (1985a,b) and Leyva-Cabello (1973) which was determined from detailed bio-stratigraphical analysis. They recorded four unconformities within the Miocene rocks of the Guadalquivir Basin (Fig. 3.1) (Roldán-García *et al.*, 1985a,b; Leyva-Cabello, 1973. These have been dated as sub-Oligo/Miocene (21 Ma.), sub-Tortonian (11 Ma.), sub-Lower Messinian (7 Ma.) and Intra-Messinian (6 Ma.). The sub-Oligo/Miocene unconformity defines the base of the Guadalquivir Basin succession (Sanz-de-Galdeano, 1992) and separates the deformed Palaeogene rocks of the External Zone from marls belonging to the Guadalquivir Basin. This unconformity was observed in the field (Location 9, Foldout Map 1, Ref. 522 340) and is marked by a karst surface developed on Palaeogene limestones (Fig. 2.6). The Messinian unconformity can also be seen in outcrops (Location 44, Foldout Map 2, Ref. 514 325) and logged section, Fig. 3.2). At locality 44 (Ref. 514 325) the unconformity is seen to cut out Tortonian rocks leaving the Messinian rocks resting directly on Lower to Mid Miocene Marls. The other two unconformities, the Tortonian and the Intra-Messinian are not exposed and are not immediately apparent on Geological maps (Foldout Maps 1,2&3). However, the stratigraphy of Roldán-García (1985a,b) and Leyva-Cabello (1973) is partly based on bore-hole data and observations from other parts of the Guadalquivir Basin. For these reasons and because there is no evidence to suggest that these observations are incorrect, the unconformities are accepted as being present in the study area. For the purposes of sedimentological analysis the unconformities have been used to divide the stratigraphy into four successions (Fig. 3.1). Each succession is treated separately in terms of facies analysis, facies interpretation and interpretation of environments of deposition.

#### 3.3 Lower & Mid Miocene Facies Analysis

Aquitania to Serravallian rocks are exposed in both allochthonous and autochthonous portions of the Guadalquivir Basin and are lithologically and palaeontologically identical in

each, although they are best seen in the allochthonous portion (Foldout Map 1). The Aquitanian to Serravallian conformable succession unconformably overlies deformed Palaeogene rocks of the External Zone and are themselves cut by sub-Tortonian and sub-Messinian unconformities (Fig. 2.10). The maximum thickness of the succession (deduced from cross-sections of the study area) is 450m. The succession is dominated by clays, fine grained carbonates and partly indurated limestones (Fig. 3.3). Samples were found to contain both calcareous and siliceous microfossils (Appendix II), with the calcareous microfossils dominant. Taken as a whole the Lower-Mid Miocene rocks of the Guadalquivir Basin can be classified as marls, following the classification scheme of Berger (1974b). The succession terminates with erosionally based lenticular beds of stratified marls which contain boulders (Fig. 3.4).

Facies within the Lower-Mid Miocene succession are defined on the basis of calcareous and siliceous microfossils ratios, ratios of planktonic and benthonic fauna, presence or absence of laminae and nature of the laminae. Four facies are recognised within the succession, thinly bedded marls, thickly bedded marls, laminated diatomites and a boulder facies. All four facies are found in both allochthonous and autochthonous portions of the basin fill.

### 3.3.1 Thinly Bedded Facies

This facies, typified by exposures at location 23 (Foldout Map 1, Ref. 541 331), consists of marls with bedding less than 10cm thick (Fig. 3.5). Bed-bounding surfaces are typically planar or gently undulating (<1 cm undulation), carry clay partings and occasionally are marked by grove marks. Internally beds may contain planar lamination, or lack structures. The microfauna is dominated by planktonic Foraminifera typical of open ocean environments. Benthonic Foraminifera include *Gyroidina* sp. cf. *altiformis*, *Uvigerina peregrina*, *Cibicides* cf. *pachydeimisi* and *Cycammina* which indicate water depths greater than 200m (Appendix II). Ostracods present are dominated by *Cytherella* cf. *postdentikulata* which indicate circalittoral to upper bathyal environments. A small number of Ostracods (e.g. *Agrenocythere hazelae*) are more typical of Bathyal depths greater than 800m. A few Radiolaria and Diatoms are also present in this facies.

### 3.3.2 Thickly Bedded Marls;

Marls with beds thicker than 50 cm (Fig. 3.6) have been described at several localities and are best exposed at Location 31 (Foldout Map 1, Ref. 543 339). The beds lack structures and the Microfauna is dominated by Foraminifera with both planktonic and benthonic Forms. The benthonic forms include *Gyroidina* sp. cf. *altiformis*, *Pyrgo*, *Cibicides* cf. *pachydeimisi*, *Planulina* and *Cycammina* typical of upper bathyal, and outer-shelf environments with water depths of between 75m and 200m (Appendix II). Siliceous microfossils are absent

### 3.3.3 Laminated Diatomites

This facies, best exposed at Location 44 (Foldout Map 2, Ref. 514 325), is made up of alternating clay-rich and carbonate-rich laminae (Fig. 3.7) which range in thickness from few

millimetres up to several centimetres. The clay rich laminae are dominated by siliceous microfossils with abundant diatoms and a few radiolaria (Fig. 8a). The diatom flora is monospecific, dominated by *Concinodiscus* (Fig. 3.8b). By contrast the carbonate rich laminae are dominated by planktonic foraminifera which are typical of open oceanic environments and diatoms and radiolaria make up less than 30% of the microfossils.

### 3.3.4 Boulder Facies

This facies is best exposed in the allochthonous portion of the basin, particularly at Location 40 (Foldout Map 1, Ref. 530 334). Boulder fills are found in the autochthonous zone immediately beneath the sub Messinian and sub Tortonian unconformities and may actually define the sub-Tortonian surface (Fig. 3.1). The facies is characterised by large angular and sub-rounded blocks in an unstratified marl matrix (Fig. 3.4). The boulders consist of lithified marls and partly indurated fine grained limestones and are between 0.12 and 1.92m in diameter with an average of 0.54m (Appendix IV). The boulders and their matrix form stacked lenticular units that are 1.5m to 4m thick and are 3-15m wide (Appendix IV). A few of the lenticular units have a winged geometry with 10-50cm thick wings extending up to 2m from the margins of the lenticular units (Fig. 3.9).

### 3.3.5 Facies Distributions and Associations

Because of limited exposure it has not been possible to assess the lateral or vertical distribution of the facies nor to determine facies associations. However, all four facies are present in both the allochthonous and autochthonous portions of the basin. The Lower-Mid Miocene succession is remarkably similar in terms of lithologies, facies and micropalaeontology across the allochthonous autochthonous boundary. There is some indication that the boulder facies is limited to the upper parts of the succession, and seems to have developed immediately before the formation of the Tortonian unconformity and may even define the unconformity. This facies may either be 1) the pre unconformity facies, and therefore represents the onset of sea-level fall or 2) coincidental with the unconformity and therefore define the unconformity. Roldán-García *et al.* (1985a,b) noted that a 'brecciated facies' in the Langhian and Serravallian deposits of the Guadalquivir Basin and this is assumed to be the 'boulder facies'.

### 3.3.6 Facies Interpretations

Marls containing marine biota, including foraminifera, radiolaria and diatoms are associated with pelagic open marine environments (Scholle *et al.*, 1983). Pelagic sediments with abundant planktonic foraminifera, radiolaria and diatoms are associated with warm waters and with areas of high productivity, that are commonly associated with areas of upwelling. Present pelagic carbonate facies are confined to latitudes between 60° north and south (Berger, 1974; Davies & Gorsline, 1976). Rocks collected from the Lower-Mid Miocene succession of the Guadalquivir Basin show a surprising lack of the coccolith detritus that is so common in Miocene pelagic environments. In addition no agglutinated foraminifera are present in the assemblage suggesting the possibility of some other processes having affected

the microfaunal assemblage. Pelagic sediments are known to be winnowed by bottom currents and winnowing may destroy the more fragile biogenic components such as agglutinates. Current activity in the thin bedded facies is suggested by planar lamination and current lineation. Despite the possibility that more fragile fauna may be missing, the microfaunal assemblage still indicates that the marls were deposited in water depths ranging from circalittoral to bathyal (Appendix II). Clays within the marls are either evenly disseminated or form distinct laminae (Fig. 3.7) and indicate detrital terrigenous or volcanic input. Detrital input suggests a hemipelagic rather than a purely pelagic environment. The input of detrital material is known to be controlled by changes in ocean currents which vary according to climate and sea-level (Kennedy & Garrison, 1975). 'Contaminating' detritus such as clays is deposited in the central Pacific far from terrestrial sediment sources. This includes small amounts of fine grained, wind-blown quartz and large volumes of clay (Rex *et al.*, 1969). Thus the marls in the Lower-Mid Miocene succession may have been deposited in deep water environments, and yet still received some terrigenous detritus via surface winds.

Micropalaeontological analysis (Appendix II) suggests that the observed facies were deposited in varying water depths. The thin bedded and thick bedded facies are characterised by benthonic Foraminifera which indicate outer-shelf and bathyal environments in water depths of between 200m and 800m. The laminated diatomites consist of alternating diatom-rich clay laminae and foraminifera-rich carbonate laminae. The abundance of both of these indicate waters of high productivity. The diatoms are monospecific, consisting of *Concinodiscus*, known to favour oceanic warm waters (Hajos, 1973; Gombos, 1987). Diatoms are primary producers, while planktonic foraminifera and radiolaria are consumers feeding on diatoms. Certain species of diatoms are known to bloom periodically in oceans (Burckle, 1978) resulting in dramatic increases in the numbers of one or two species. Such an increase in producers may have led to a corresponding increase in the numbers of consumers such as foraminifera. A bloom would be followed by a rapid decline of diatoms, as population and consumption increased, leading to an increase in the deposition of diatom detritus. A reduction in the numbers of diatoms would result in a decline in the number of consuming foraminifera, as these could not be supported by the remaining diatoms. Thus, diatom blooms would be followed by increased deposition of diatom tests, while their decline would be closely followed by a rapid decline of foraminifera resulting in the mass deposition of foraminifera tests. The populations of diatoms and foraminifera would peak at slightly different times and this is ultimately responsible for the alternation of layers seen in the laminated diatomite facies. Against this background of cyclical deposition terrigenous clays were deposited via surface currents, but these were swamped by periodic increase in carbonates with the decline of expanded foraminifera populations. Similar laminated diatomites have been observed in deep sea cores (Haslett pers. comm.) and have been interpreted in a similar manner.

The upper part of the Lower/Mid Miocene succession has been dissected by erosional hollows that were later filled by boulder debris. The hollows have a 'channel form' with wing-like extensions. The deposits resemble debris-flows found in a bank margin facies of the

Devonian of the Rocky Mountains, Alberta Canada (Cook *et al.*, 1972). Such debris-flows are produced when carbonate slopes fail. Boulders that are produced raft in a mud slurry that may cut a channel down slope (Loucks *et al.*, 1985). Slope failure that may be related to a fall in sea-level, tectonic activity or over-steepening by deposition. The boulders in the Lower-Mid Miocene succession are lithologically similar to the marls and indurated limestones found beneath the debrites. Derivation of material from the underlying succession would require the erosion of Lower-Mid Miocene rocks. This could be achieved by a relative sea-level fall produced during tectonic uplift, eustasy or a combination of the two. The Tortonian unconformity (11 Ma.) is attributed to a major eustatic sea-level fall at the base of Super Cycle TB2 that may have been enhanced by uplift in the Betic Cordillera (Chapter 2.7). The development of debrites in the Mid Miocene may record the onset of this sea-level fall, and so mark the sub-Tortonian unconformity.

In summary, the lower to Mid Miocene succession of the Guadalquivir Basin is characterised by marls deposited in a hemipelagic sea-way with depths ranging from upper Bathyal (200m) to Bathyal (>800m). During the Mid Miocene debrites developed which may indicate the onset of the relative sea-level fall that ultimately led to the formation of the Tortonian unconformity.

### 3.4 Tortonian Facies Analysis

Tortonian sedimentary rocks are exposed in both the allochthonous and autochthonous portions of the basin where they consist of sandstones interbedded with marls. In the autochthonous part of the basin these are between 25m and 60m thick. In allochthonous portion the thickness of the Tortonian rocks is unknown, but they are known to be lithologically identical. Petrographically the sandstones are lithic arenites with lithic clasts forming 20-50% of the grains and between 20 and 90% (average 50%) of these are carbonate (Fig. 3.10). As a consequence of this large carbonate lithic component the sandstones have been termed calc-lithic arenites. Tortonian calc-lithic arenites also contain varying amounts of bioclastic material which include foraminifera, pelmatozoan fragments, shell fragments and ostracods. The microfaunal assemblages are described in Appendix II.

The Tortonian succession has been subdivided into three main facies, thin bedded sandstones, tabular sandstones and thick bedded sandstones, all of which show a range of sedimentary structures.

#### 3.4.1 Thin Bedded Sandstones

These sandstones form beds typically less than 20cm thick with planar bounding surfaces lacking flute marks or other sole structures.

The sandstones are predominantly fine grained calc-lithic arenites (Fig. 3.11). Bioclasts are foraminifera, pelmatozoa and shell fragments; Analysis (Appendix II) shows that the Foraminifera are dominated by planktonic forms, with a few benthonic forms, typified by *Cibicides cf. wallerstarfi*, suggesting that the sandstones were deposited in an upper bathyal environment with depths greater than 200m.

Internally the sandstones are characterised by low angle scours, planar lamination,

small hummocks, bioturbation or a lack internal structures. Any combination of these structures may occur in any one bed. In general the thin bedded sandstones form small (less than 1m) coarsening- and thickening- up cycles (Fig. 3.13). In these cycles, marls pass into thin 2-3cm sandstones which may be planar laminated or lack structures. The planar laminated sandstones may give way to thicker 10-20cm sandstone beds which contain low angle scours or small hummocks. These Hummocky/scoured beds may finally pass into planar laminated or structureless bioturbated beds in places. Hummocks in these cycles have 10-15cm amplitudes and consist of convex- and concave-up lamination that intersects at low angles. Laminae generally thicken towards the centres of the hummocks. The low angle scours are similar to the hummocks but only consist of concave-up laminae.

Interbedded marls also contain bioclasts including foraminifera, pelmatozoa and a few radiolaria, carbonate lithic grains and rare quartz grains in a carbonate mud matrix (Fig. 3.12). The foraminifera assemblage is dominated by planktonic forms typical of open oceanic environments.

### 3.4.2 Tabular Sandstones

This facies is characterised by tabular 20cm- 1m thick sandstone beds with planar or gently undulating (over 3cm) bounding surfaces. The beds are commonly massive but may contain low angle scours, hummocky cross-stratification, planar lamination or may be bioturbated (Fig. 3.14). Lithologically the sandstones are calc-lithic arenites with up to 20% of the clasts consisting of Bioclasts which include foraminifera, pelmatozoa, and shell fragments. The microfauna of this facies has been analysed (Appendix II) and the assemblage is dominated by planktonic foraminifera. Hummocky-cross stratification in this facies is similar to that in the thin-bedded facies, except that the hummocks have amplitudes of between 50cm and 1m. Low angle scours are similar to the hummocky cross-stratification but contain concave-up laminae only. Structures within the sandstones may grade vertically into each other and common transitions include planar lamination passing into structureless sandstones, structureless sandstones giving way to hummocks or bioturbation, bioturbation giving way to planar lamination, and bioturbation and hummocks changing to scour-dominated horizons.

### 3.4.3 Thick Bedded Sandstones

This facies is characterised by sandstone beds thicker than 1m and containing a range of sedimentary structures. Structures observed include planar lamination, gently dipping (<10°) planar lamination, low angle truncations and scours, trough cross-stratification, hummocky cross-stratification, ripple cross-lamination, convolute lamination and bioturbation (Fig. 3. 15). Lithologically the sandstones are fine, medium and coarse grained calc-lithic arenites that may fine upwards. The microfauna of this facies is dominated by ostracods and foraminifera. The Ostracods are typified by *Gymocytheridea meniscus*, *Cyprides* sp *torosa* and *Cytheridea expansa*, which are typical brackish forms (Appendix II). The foraminifera are dominated by near-shore or coastal benthonic forms such as *Ammonia* sp *becarri*, *Elphidium crispum* and *Elphidium "excavatum"*. Benthonic forms include *Stilostomella*,

*Frondicularia* and *Nonion boueanum* which are more typically associated with infralittoral and mid-shelf deposits, but these are present in much smaller numbers than the near shore coastal forms.

The thickest sandstones are dominated by planar and gently dipping planar lamination often occurring together (Fig. 3.15). Other sandstone beds are dominated by low angle scours, trough cross-stratification and hummocky cross-stratification. The trough cross-stratification is formed by troughs 50cm to 1m across. Hummocky cross-stratification and the low angle scours are similar to structures observed in the thin bedded and tabular facies, except for much larger amplitudes of between 75cm and 1.5m. The tops of the beds are commonly bioturbated. Common sequences of structures within this facies include planar lamination passing into inclined planar lamination which gives way to massive sandstones (Fig. 3.15). Planar lamination may pass upward into structureless and bioturbated sands (Log at Location 92, Ref. 522 343; Appendix I). Planar lamination, hummocks, scours and trough cross-stratification tend to occur together at the base of the thick-bedded facies, immediately above the tabular sandstone facies (Log at Location 5, Ref. 529 343 and 91, Ref. 521 348; Appendix I).

#### 3.4.4 Cyclicity Observed in the Tortonian

Overall the Tortonian succession can be split into 3-4 coarsening/thickening up cycles, one of which is seen at Location 5a (Ref. 529 343) (Fig. 3.16). In these cycles, marls pass up into thin bedded sandstones which give way in turn to tabular sandstones and finally thick bedded sandstones. The thickness of cycles varies between 6m and 25m, although the complete succession is not fully exposed at any one locality. All three facies types and cycles are found exposed in both the allochthonous and autochthonous zones of the Guadalquivir Basin fill. However the poor exposure has not allowed the correlation of these cycles across the basin.

#### 3.4.5 Facies Interpretation

The Tortonian succession consists of thickening up cycles of intercalated sandstones and marls yielding a microfauna that indicates a marine environment of deposition. The cycles are characterised by sequences of marls, marls with thin sandstones, tabular sandstones and thick bedded sandstones.

The thin bedded facies consists of fine grained sandstones containing a foraminiferal assemblage which is associated with upper bathyal and outer-shelf environments. The sandstone beds contain planar lamination, low-angle scours and hummocks which indicate a high energy environment in which unidirectional flows have interacted with the sediment. Bioturbation is also evident, and this may indicate quieter periods with reduced sedimentation rates and lower flow velocities.

The hummocks in this facies are morphologically similar to hummocky cross-stratification documented from a wide range of environments including rivers, estuaries, beach deposits, shallow marine shelf and distal shelf deposits (Harms *et al.*, 1975; Walker, 1983; 1985; Sun, 1990; Scott, 1992; Brenchley *et al.*, 1993). Despite this range of



environments, such structures are commonly attributed to the action of storm waves on shelf sands, in which high velocity oscillatory flows rework the sediment (Walker *et al.*, 1983; Brenchley, 1985; Duke *et al.*, 1991). However, such structures have also been shown to be deposited by either purely unidirectional flows or unidirectional flows with a combined weak oscillatory flow component (Sun, 1990; Myrow & Southard, 1992). The low angle scours in the thin bedded facies are similar to low angle cross lamination described by Corbett *et al.* (in press), which is attributed to unidirectional flows (Sun, 1990). Hummocky cross-stratification and low angle scours have been more fully documented by Myrow & Southard (1990) who refer to hummocks as symmetrical ripples and low angle scours as asymmetrical ripple forms. They experimentally determined the effects of varying combinations of oscillatory and unidirectional flow on the production of symmetrical and asymmetrical ripple forms (or hummocks and low angle scours) (Fig. 3.17). Smaller hummocks, similar to those observed in the thin bedded facies, are attributed to very weak oscillatory flows. Asymmetrical ripples or low angle scours are produced by unidirectional flows with only the weakest of oscillatory flows taking part in the processes. Using these data it seems likely that structures in these thin bedded sandstones were formed by unidirectional flows that produced the planar lamination, low angle scours and small hummocks.

The tabular sandstone facies consist of fine to medium grained sands whose faunal assemblage indicates an outer shelf environment. Low angle scours and hummocky cross-stratification are also present and are similar to structures found in the thin bedded facies, except that they have larger amplitude (50cm -1m). Increasing sizes of symmetrical and asymmetrical structures indicate an increase in the oscillatory flow component and higher orbital velocities (Fig. 3.17; Myro and Southard, 1990). Within this facies planar lamination often grades into low angle scours, hummocks and then into bioturbated or structureless sands. This transition is typical of sequences documented by Myrow & Southard (1990) in which strong unidirectional flows are reduced and give way to oscillatory flows which are maintained or may increase. Such series of planar lamination, hummocks/symmetrical ripples and bioturbation are typically found in tempestite deposits (Kreisa, 1981; Aligner, 1982; Sellacher, 1982; Brenchley, 1985). Tempestites are density currents generated by storm action on the shallower parts of the shelf, such currents have been observed in modern environments and are known to move sediment to depths of 200m or more (Komar *et al.*, 1972; Hickley *et al.*, 1985). Subsequent and substantial reworking of these sediments by oscillatory currents, generated by the lowering of wave base during storms, can occur at depths of up to 100m (Cacchione & Drake, 1982; Luteneuer, 1986; Drake & Cacchione, 1989). The micropalaeontology (Appendix II) indicates that the tabular sandstones were formed in depths less than 100m, and so within the influence of storm wave base and associated oscillatory currents.

An increasing oscillatory component is observed in the transition from the thin bedded sandstones to tabular sandstones (Fig. 3.14), reflecting an increase in the influence of storm wave base. In the more distal components of tempestites, oscillatory currents may be present but unidirectional flow and fall-out from suspension are the main mechanisms of deposition (Brenchley, 1985). More proximal deposits show a greater influence of oscillatory currents.

Thus, the increasing oscillatory component observed in the lower parts of the Tortonian cycles represents a transition from distal to more proximal tempestites. This inferred shift from distal thin bedded tempestites to more proximal deposits is also suggested by an increasing lithic component in the sandstones, decrease in the percentage of bioclasts (Appendix IV) and an increase in sandstone thickness. Such a shift from thin bedded sandstones to thicker tabular sandstones with planar lamination, low angle scours and hummocky cross-stratification has been documented in tempestite and wave-dominated cycles in the Ordovician Beach Formation, Bell Island, Newfoundland (Brenchley *et al.*, 1993) and these cycles are also thought to signify a shift from distal to more proximal deposits.

Thus it is likely that the thin bedded and tabular facies are outer shelf to upper bathyal sediments that have been deposited via storm induced density currents. The tabular facies shows an increase in the influence of oscillatory flows that indicates the influence of storm wave base, which can only occur at depths of less than 100m. This inferred shallowing is also indicated by the micropalaeontological analysis of samples from these facies (Appendix II).

The thick bedded facies consists of fine, medium and coarse-grained sands that display a wide range of structures characteristic of high energy environments. Micropalaeontological analysis (Appendix II) places the sandstones in a proximal, near-shore environment. The presence of trough cross-stratification, cross-stratification and mega-ripples indicates the influence of strong unidirectional currents (Harms *et al.*, 1975). Hummocky cross-stratification and low angle scours with amplitudes of between 1m and 2m, are typical of 'classical' hummocky cross-stratified deposits described by (Hamblin & Walker 1979; Dott & Bourgeois, 1982; Walker *et al.*, 1983; Duke *et al.*, 1991). Symmetrical wave ripples (Hummocks) of this scale are thought to have been produced by high velocity orbital currents with little or no unidirectional flow component (Fig. 3.17; Myrow & Southard, 1992). Such flows are strongly associated with the reworking of shallow marine deposits by oscillatory currents reflecting a wave base lowered during seasonal storms. Bioturbation within the sandstones of the thick bedded facies (Fig. 3.16) indicates that high energy events were separated by 'quiet periods'.

In shallow near-shore environments thick sandstones with a diverse range of high energy structures are associated with proximal beach environments (Clifton *et al.*, 1971; Schwartz *et al.*, 1973; Cant, 1974; Swift, 1975; Howard & Reineck, 1981; McCubbin, 1982). In beach environments deposits can be split into lower shoreface, transition zone, mid foreshore and back shore (Fig. 3.18).

The lower shoreface is characterised by sands that reflect storm and fair-weather conditions (Elliot, 1978 p 162-167) and these are typically dominated by hummocky cross-stratification, trough cross-stratification and tabular cross-lamination. Similar structures are observed in thick bedded facies found immediately above the tabular sandstone facies (Fig. 3.16) and are interpreted as indicating a shift from outer-mid shelf deposits to proximal shallow marine/lower shoreface deposits.

The transition zone of the shoreface is dominated by breaker surf and swash (Fig. 3.18) and by longshore current bed forms reflecting high energy flow. Deposits of the transition zone are dominated by planar laminae and current lineated beds with occasional ripples

(Hayes & Kana, 1976; Komar 1976). Thick sandstones observed at Location 93 (Ref. 521 343) (Fig. 3.15) are dominated in the lower parts by planar lamination with occasional tabular cross-laminae and ripple cross lamination indicating the migration of dune and ripple scale structures. In the mid-Foreshore mega-ripples may occur on the highest energy beaches (Clifton *et al.*, 1971; Hawley; 1982).

Internal structures of the foreshore are limited to low angle planar lamination (2-3°) that generally dip seaward (Thompson, 1937; Hoyt & Weimer, 1963). The thick bedded sandstones in the Tortonian (Fig. 3.15) display planar lamination that passes into inclined planar lamination. This is interpreted as a representing a shift from the transition zone, typified by planar lamination, to foreshore deposits containing inclined planar lamination. Structureless sands above this zone may have been deposited in a back-shore region (Fig. 3.18) since such zones are known to be devoid of high energy structures.

Thus, the sedimentary structures and micropalaeontology (Appendix II) indicate that the thick bedded facies is a product of deposition and sediment reworking that has taken place in a near-shore, high energy environment. Sedimentary structures, (Fig. 3.15), indicate that beach deposits may be present, indicating shoreface, foreshore and back-shore deposits.

The Tortonian succession is characterised by a number of thickening up cycles recording the transition from thin bedded facies, into a tabular facies which pass finally into thick bedded facies. Interpretation of these facies indicates that the cycles represent repeated transitions from distal outer shelf to proximal beach deposits. Similar cycles have been observed in modern progradational shorelines (Elliot, 1978). Progradation occurs when there is a constant sediment supply, stable sea-level and low to moderate subsidence rates (Bernard *et al.*, 1962). Repetition of such cycles, as is observed in the Tortonian, occurs when there is a reduction in sediment supply, rise in sea-level or increase in subsidence (Fischer, 1961; Kraft, 1971). On wave-dominated shelves, such as the Tortonian shelf, transitions from distal tempestites to proximal near-shore deposits, contained within upwards coarsening sequences are similar to transitions observed by Howard & Reineck (1981), Clifton *et al.*, (1971) and Davidson & Greenwood (1974, 1976). A striking example of this is the Jurassic Fernie-Kootenay Formation, Alberta, Canada (Fig. 3.19, Hamblin & Walker, 1979). In this succession tempestites pass into off-shore tabular sandstones that are dominated by hummocky cross-stratification and finally into shoreface and foreshore deposits. The Guadalquivir Tortonian succession is remarkably similar to cycles observed in the Fernie-Kootenay Formation which provides a good model for interpreting depositional cycles found in the Guadalquivir Basin Tortonian Shelf succession.

### 3.5 Lower Messinian Facies Analysis

The largest outcrop and best exposure of the Lower Messinian is in the autochthonous portion of the basin fill. Small outcrops of Messinian rocks are also present in the allochthonous portion of the basin fill which have lithologies and facies comparable with those in the autochthonous portion. The Lower Messinian is less than 150m (Roldán-García, 1985b) and is characterised by marls, calc-lithic arenites, bioclastic grainstones and conglomerates. It has been split into five distinct facies types; marls, thin bedded calc-lithic

arenites, calc-lithic arenites with high energy structures, bioclastic grainstones and conglomerates. The conglomerates can be subdivided into matrix-supported channel-fills and clast-supported groups.

### 3.5.1 Marls

The marls are carbonate muds with scattered quartz grains and bioclasts. The bioclasts are dominated by foraminifera, with rare pelmatozoan and shell fragments. The foraminiferal assemblage is characterised by both shallow-nearshore and open-marine shelf benthonic forms and indicates a mixing of faunas from different environments.

### 3.5.2 Thin Bedded Calc-Lithic Arenites

This facies is typified by planar-bounded calc-lithic arenite beds less than 20cm thick, intercalated with marls (Fig. 3.20). Sandstone beds in this facies lack internal stratification or other sedimentary structures. The calc lithic arenites consist of quartz grains, lithic grains and bioclasts in a fine grained carbonate matrix (Fig. 3.21). They are generally matrix-supported with an average of 40% of the rock matrix forming. Bioclasts can form up to 28% of the grains, with an average of 12%. They are dominated by foraminifera, with some ostracods present. The remaining clasts are lithic fragments, up to 90% of which are carbonate sedimentary lithics (Appendix IV). Ostracods in this facies (Appendix II) are dominated by *Cyprideis* sp. *torsa*, *Cytheridea* cf. *Expansa* and *Cyamocytheridea meniscus*, typical of brackish environments. The foraminiferal assemblage contains *Ammonia* sp. *becarri*, *Elphidium crispum* and *Elphidium "excavatum"* which are also associated with brackish environments, but in addition species more typical of open shelf environments are also present, although in smaller numbers.

The thin bedded facies often forms small 20- 50 cm fining up cycles (Fig. 3.22). These are characterised by sharp based calc-lithic arenites containing less than 40% marl matrix, passing up into sandy marls and finally into fine grained marls

### 3.5.3 Calc-Lithic Arenites

This facies is characterised by medium to coarse grained calc-lithic arenites with less than 10% marl matrix. Beds in this facies range from 20cm to several metres thick. Lithic clasts form 20% -50% of the clasts with monocrystalline quartz making up the remainder (Fig. 3.23). Up to 90% of the lithic components are sedimentary grains and more than 80% of these are carbonate. The arenites commonly display a range of structures, including mega-ripples bed forms, trough cross-stratification, tabular cross-stratification, hummocky cross-stratification and low angle scours.

Mega-ripples bed forms are best exposed at location 64, near Montilla (Foldout Map 2, Ref. 514 330) where they have been studied in some detail (Fig. 3.24). In outcrop they have wavelengths of between 1.5m and 6m. The foresets are commonly draped by marls that yield marine microfossils. In places the mega-ripples are scoured (Fig. 3.24) and the scoured surfaces are also filled by marls. Lenticular sandstones with erosional bounding surfaces are intercalated with the mega-ripples. Within the mega-ripples, foresets are defined by marl/

mud drapes which are sometimes in closely spaced pairs or bundles (Fig. 3.24). Lower angle marl/mud-draped set boundaries separate mega-ripples and truncate the high angle foresets. The microfauna from mega-rippled sandstones is dominated by foraminifera and ostracods. The foraminiferal assemblage is dominated by *Ammonia gp. Becarri*, a near shore/brackish form, but also contains *Nodosaria* which is more typical of infralittoral and circalittoral deposits. The ostracod assemblage is dominated by open shelf forms such as *Aurila* and *Xestoleberis*, but in contrast to the foraminiferal assemblage the brackish forms are absent. Overall, the microfaunal assemblage indicates derivation from both shallow marine shelf and nearshore/brackish environments (Appendix II).

Other outcrops of calc-lithic arenites, such as those at location 97 & 65 (Foldout Map 2, Refs. 522 351 & 517 332) contain trough cross-stratification, tabular cross-stratification, hummocky cross-stratification, low angle scours and bioturbated horizons (Fig. 3.25). Troughs are 50cm-1m long and up to 50cm deep. Foresets often dip in opposite directions, forming herringbone cross-stratification in sets 40-50cm high. The hummocky cross-stratification consists of convex-up and concave-up laminae intersecting at low angles (10-15°). The laminae tend to thicken towards the centres of the hummocks which have amplitudes 1-2m. Low angle scours are similar to the hummocks, except they consist of concave-up laminae only. The micropalaeontological analysis (Appendix II) of samples taken from this facies has revealed a diverse assemblage of ostracods and foraminifera. The ostracods are dominated by *Cytheridea expansa*, *Cytheridea gp torosa* and *Cyamocytheridea meniscus*, which are all brackish forms. In addition, however, ostracods more typical of open shelf environments (*Nonurocytheris*, *seminulum* and *Nonurocytheris laevigata*) and of outershelf/upper bathyal environments (*Aurilla*) are also present although in smaller numbers than the brackish forms. *Ilocypris* was also found in some of the samples, and this is usually associated with freshwater. The foraminiferal assemblage (Appendix II) is dominated by planktonic forms, but benthonic forms such as *becarri*, *Bolivina*, *Cibicides* and *Nodosaria* indicate a mixture of upper-bathyal, shelf and near-shore varieties.

#### 3.5.4 Bioclastic Grainstones

Lithologies in this facies are dominated by bioclasts and lithic grains in a carbonate mud matrix but are always clast supported (Fig. 3.26). The rocks are poorly sorted and bioclasts consist of foraminifera, bryozoa, echinoderm fragments, shell fragments and calcareous algae. The last are dominated by the encrusting forms *Lithothamnium*, *Lithophyllum*, and *Archaeolithothamnium*.

#### 3.5.5 Conglomerates

Two types of conglomerate are recognised in the Lower Messinian deposits of the allochthonous and autochthonous portions of the Guadalquivir Basin fill, a matrix-supported marine conglomerate and a clast supported conglomerate.

The matrix-supported conglomerate, typified by exposure at location 99 (Foldout map 3, Ref. 510 344), is dominated by limestone, calc-lithic arenite and chert clasts. The conglomerate forms a lenticular body with an erosional base cutting into bedded calc-lithic

arenites. The margins of the body interfinger with calc-lithic arenite (Fig. 3.27) and conglomerate beds thin and pinch out away from the main body. The matrix-supported conglomerate, at location 99 (Ref. 510 349), is a maximum of 2m thick, and is overlain by 25cm of marls which are followed by bioclastic grainstones.

The clast-supported-conglomerate, dominated by limestone clasts, is extensively exposed in a disused quarry at location 9 (Foldout Map 2, Ref. 522 340). The conglomerate at this locality can be subdivided into two separate units (Fig. 3.28). The lower unit has a marl matrix that yields a marine microfauna. This is overlain by a conglomerate with a sandier matrix lacking any marine microfauna. The two conglomerates are separated by a 50cm marl which locally contains rootlets. The lower conglomerate contains large erosional truncations (Fig. 3.29) that forming mega trough like structures. Troughs are up to 15m deep and 20m-60m wide. The marl matrix of this lower unit contains both foraminifera and ostracod faunas that indicate a marine influence.

### 3.5.6 Facies Interpretation

In general the faunal assemblages of the Lower Messinian deposits indicate a strong brackish influence with a few samples yielding freshwater fauna. The foraminiferal, and ostracod assemblages imply a protected, brackish, shallow-water environment, and the presence of conglomerates with rootleted horizons suggests a near coastal situation. However, microfossils that indicate a protected brackish environment were also found in sandstones containing high energy structures typical of open shelf environments. Most samples with brackish faunas were also found to contain mid-shelf and outer-shelf faunas. Consequently, it appears that both brackish and open-shelf sediments and faunas are being reworked and mixed. Before such processes can be considered the facies must be interpreted individually

Calc-lithic arenites similar to those in the Tortonian contain structures such as trough cross-stratification, tabular cross-stratification and hummocky cross-stratification typical of high energy regimes. In places tabular cross-stratification sets form herringbone cross strata indicating bi-directional current flows. Such patterns of changes in flow direction are commonly associated with tidal currents. Large scale trough cross-stratification indicates the migration of lunate ripples and dunes. Large amplitude hummocky cross-stratification, also occurs within these 'high energy' deposits. Symmetrical ripples or hummocks of this scale are produced in oscillatory flows, with high orbital velocities and have little or no unidirectional flow component (Fig. 3.17; Myrow & Southard, 1991). Such oscillatory flows are most commonly produced by the lowering of wave base during storms which rework shelf sediments (Hamblin & Walker 1979; Dott & Bourgeois, 1982; Walker *et al.*, 1983; Duke *et al.*, 1991). Thus despite the faunal indications, the sandstones were deposited on an open storm dominated shallow marine shelf.

At one locality (Fig. 3.24) stacked mega-ripples are present in calc-lithic arenite rocks with a dominantly open-shelf faunal assemblage. The mega-ripples are characterised by bundled mud-draped foresets and low angle set bounding surfaces. Such structures are characteristic, although not definitive, features of tidal deposits (de Raaf & Boersma, 1971; Reineck & Singh, 1973 p97-102). Mud drapes in tidal deposits are associated with deposition

of suspended sediment during slack water, between ebb and flow currents, and paired mud drapes together with their changes in frequency are attributed to ebb-flood and neap-spring cycles (Allen, 1982). Low angle truncation surfaces, termed 'reactivation surfaces' are the product of asymmetrical ebb-flood cycles (Allen, 1980) (Fig. 3.30). During the dominant flow stage, which may either be the ebb or flood stage, mega-ripples migrate in the direction of flow. During the reversed, subordinate, flow if the current is not strong enough to produce ripple migration the ripple face may be eroded. Reactivation surfaces form at a lower angle than the foresets and so truncate them. During slack water, suspended mud particles are deposited on the reactivation surfaces. In the marine environment mega-ripples often form on the surfaces of tidal sand-ridges with wavelengths 10 to 15 km (Reineck, 1963; Houbolt, 1968). However, in open shelf settings, mud drapes and low-angle erosion surfaces may not necessarily reflect tidal periodicities, they are just as likely to be formed by a combination of abnormally high suspended sediment concentration and low current velocities over a longer period (McCave, 1970). Such conditions may immediately follow a storm. Further evidence of storm activity is reflected in the scours and lenticular sandstones of the mega-rippled deposits of the Lower Messinian. These features indicate erosion followed by mud deposition from suspension, a characteristic of storm cycles (Brenchley *et al.*, 1993). Despite this ambiguity the herringbone cross-bedding clearly indicates reversals of flow directions as in tidal currents. When features are taken together it seems likely that the Lower Messinian sediments were influenced by tidal currents.

Thus it seems that structures found within the calc-lithic arenites do indicate the deposition of sediments on a shallow marine shelf, during the Lower Messinian. These sediments were reworked by storm and tidal currents, producing a complex series of sedimentary structures.

Poorly-sorted bioclastic grainstones are typically found in shoals or patch reef environments. 'High energy' skeletal shoals are found on bank margins and intercalated with mid shelf deposits. Skeletal shoals fringing the bank margin on the sea-ward side, reflect a high energy zone of wave shoaling (Wilson, 1975). Shoals developed in Pennsylvanian and Wolfcampian limestones in West Texas are interpreted as shelf deposits worked into patches by wave shoaling processes (Kerr, 1977). Both bank margin shoals and mid shelf shoals form in shallow water, high energy zones and are characterised by bioclastic grainstones, wackestones and packstones with foraminifera, echinoderms, bryozoa, calcareous algae and shell fragments in varying proportions.

Deposits that share some characteristics of shoal deposits occur in patch reef environments. Facies sequences that record the growth of patch reef mounds can be split into three phases (Wilson, 1975). Bioclastic lime muds with thin skeletal sands are overlain by lime muds. These pass upwards into a well bedded mound cap containing encrusting algae and bioclastic debris including pelmatozoa, bryozoa and benthonic foraminifera. Facies sequences in the Lower Messinian at locations 44 (Ref. 514 325) and 61 (Ref. 506 334) (Appendix I) are similar to these patch reef facies sequences. Marls with thin calc-lithic arenite and bioclastic grainstones beds pass into algal-laminated and bioclastic grainstones. Because the skeletal shoal and patch reef cap deposits are so similar it has been impossible

to distinguish between the two environments. There is no evidence for bioherms and the bioclastic grainstones lack the internal stratification typical of high energy shoals. However, both types of environments are found in shallow waters and generally occur in mid-shelf positions.

Thus the Lower Messinian deposits reflect a shallow marine shelf that was influenced by both wave and tidal induced currents and on which skeletal shoals or patch reefs developed. These open-shelf deposits were separated from more proximal, lagoonal and brackish environments, implied by the faunal assemblage. Such environments are usually separated by a coralline barrier reef or by elongate sandbars that develop on the shelf margin. Ball (1967) observed that tidal sandbelts, in the Bahama Banks, separate open shelf margin deposits from lagoonal deposits. Such tidal bar belts may extend for up to 100Km along the shelf margin (Newell, 1955; Dravis, 1977; Palmer, 1979). Mega-ripples found in Lower Messinian rocks of the Guadalquivir Basin may have formed part of just such a tidal bar belt, that separated high energy deposits from lagoonal deposits. The skeletal sands, also found in the Lower Messinian, may have formed as shoals on the sea-ward side of the tidal bars, although mega-ripples and skeletal grainstones are not found together.

Finally, the conglomerates provide important evidence of Lower Messinian depositional environments.

The clast supported conglomerates form a facies sequence in which conglomerates containing marine microfossils give way to conglomerates with a barren sandy matrix. A rootlet horizon separates the two units providing evidence of sub-aerial exposure. Overall the facies sequence represents a transition from a marine to a sub-aerial conglomerate and so places the environment of deposition in coastal waters. Conglomerates within coastal fan deposits have been documented from the Devonian of Norway (Steel & Gloppen, 1980) and the Miocene of Turkey (Hayward, 1983). Coastal fans form where confined streams emerge into open coastal waters (Daily *et al.*, 1980) and indicate that fluvial systems were emerging onto a shelf. Alluvial fans that prograde into seas, generally emerge from a coast that has a high relief (Freidman & Sanders, 1978; Gvirtman & Buchbinder, 1978).

Large erosional truncations in the marine conglomerate (Fig. 3.29) may record shifting fan lobes similar to those recorded by Collinson (1978). Hummocky lobes in fjord fan deltas of British Columbia (Prior & Bornhold, 1988) are formed by coarse-grained depositional systems that develop close to the sediment source. However these lobes are rarely preserved and the erosional truncations are more likely to be products of chutes and channels radiating across the lobes. The transport of coarse stream debris across a fan produces chutes and channels which are best developed on the lower segment of the cone surface which is often submarine (Prior & Bornhold, 1988). These chutes are generally filled by cobbles that are of a size comparable to those in the Lower Messinian conglomerates.

The matrix-supported conglomerates are contained within a lenticular body with an erosional base cutting into marine calc-lithic arenites. This body has a channel like form and is overlain by a thin marls and skeletal calc-lithic arenites (Fig. 3.27). Thus a channel has been cut into the shelf deposits. Because the conglomerate interfingers with calc-lithic arenites of marine origin, the channel itself must have been part of a submarine channel



system. Submarine channels may form as part of a shelf by-pass system conducting coastal deposits to the shelf edge and often terminating in submarine canyon or shelf slope-break deposits. Such channels can be up to 50Km long and examples are recorded in the Cambro-Ordovician of Alberta, Canada (Stow, 1978), similar channels are noted by Whittaker (1974).

Overall the Lower Messinian represents a combination of fluvial/coastal fan, lagoonal and open-marine shelf deposits. The lagoonal and open shelf environment may have been separated by a tidal bars that developed on the shelf margin. Any model must be provide a sheltered lagoonal environment that contains brackish water and yet still allow the movement of brackish faunas onto the open shelf.

Lithic fragments in the arenites are dominated by sedimentary lithics (Chapter 4) which can only have been produced by the denudation of limestones in a sub-aerial environment. They have been transported onto the shelf and reworked by wave/tidal currents. An obvious conduit for this detritus is through the coastal fan delta in the Lower Messinian. Palaeocurrents (Fig. 3.31) suggest that the fan was channelling detritus to the west, placing the source, and thus the coastline, to the east. However this may only represent one lobe of a fan, and fans commonly have a splay of lobes which may give palaeocurrents that vary over 180°.

The coastal fan may have been the proximal part of a larger fan delta that prograded out on to the shelf. Delta systems include both lagoonal and marsh environments (Elliot, 1978, p120) in inter-distributary areas. If a delta was being built on the Lower Messinian shelf then the delta-front would have been subject to both wave and tide processes (as the shelf is known to have been). Modern examples of wave/tide dominated deltas are the Burdekin, Irrawaddy, Mekong, Niger and Chinoco deltas (Allen, 1965). In such deltas linear shore-parallel bars develop on the delta front in response to the expansion of tidal currents as they pass from the confines of channels onto the open shelf. These barriers protect a brackish lagoonal environment and separate it from the wave-dominated shelf (Oomkens, 1974). Bars are not continuous, but are breached by tidal channels which allow brackish water and sediment from the lagoons to be transported to the open shelf (Oomkens, 1974). The sediment 'flushing' processes would have been enhanced by the constant shifting of the channels and reworking of the barrier bar and inter-distributary lagoonal deposits. During major storms sediment and water from the open shelf would have been carried over the barrier bar or along the delta channel to form wash-over deposits containing open shelf marine faunas. The processes of sediment flushing and storm washover were ultimately responsible for producing the mixed faunal assemblage now observed in the Lower Messinian rocks.

### **3.6 Upper Messinian Facies Analysis**

Upper Messinian rocks are best exposed in the autochthonous portion of the Guadalquivir Basin fill, but are also found in the allochthon where they form part of the 'olistostrome' complex re-interpreted as a melange associated with late Miocene thrusting (Chapter 2). In the autochthon the Upper Messinian is a maximum of 50m thick, and is thought to be

bounded by unconformities (Roldán-García *et al.*, 1985b).

The succession is characterised by marls calc-lithic arenites and conglomerates. Four facies are recognised, fine to coarse grained calc-lithic arenites, calc-lithic arenites with thin conglomerates, grey and red marls with rootlets and conglomerates. Microfossils are absent.

### 3.6.1 Calc-Lithic Arenites.

This facies is characterised by fine-medium-coarse grained calc-lithic arenites. These are composed of monocrystalline quartz (60-80%) and lithic grains (20-40%) in a marl matrix. The lithic component of the arenites is dominated by sedimentary fragments (80-90%) of which 50-70% are marl. Metamorphic grains account for less than 10% of the total lithic population. The rocks contain cross-stratification, planar lamination, and low angle scours. Tabular cross-stratification may display asymptotic bases. The foresets are often picked out by drapes of carbonaceous material (Fig. 3.32) or by lines of small pebbles, which define sets 5-30cm thick. Low angle scours with wavelengths of 5-20cm are up to 10cm deep and are often filled by coarse calc-lithic arenites.

### 3.6.2 Calc-Lithic Arenites With Thin Pebble Beds

Commonly pebble beds are intercalated with the calc-lithic arenites (Fig. 3.33) and range from single pebble to several pebble thickness. These are laterally continuous for 15-30m. Pebbles are often imbricated and are commonly associated with ripple cross-lamination in the arenites.

### 3.6.3 Grey/Red Marls With Rootlets

Colour stratified marls at location 46 (Foldout Map 2, Ref. 511 338) are intercalated with conglomerates and calc-lithic arenites (Fig 3.34). The upper portions of the marls commonly contain rootlets and may contain carbonate nodules. The most common colour variation in stratification is red marls passing into mottled dark grey/light grey marls and finally into light grey marls which may contain rootlets and carbonaceous laminations.

### 3.6.4 Conglomerates

This facies is typified by pebble and cobble sized clasts (0.1-3.2cm) in a calc-lithic arenite matrix. The clasts may be rounded to sub-angular but are mostly rounded. They are dominated by quartzite, limestone and chert with a few calc-lithic arenite and metamorphic clasts present (A full clast survey is given in Appendix IV). The conglomerates are contained within bedded units with erosional bases, clasts are commonly imbricate and form cross-stratification (Fig. 3.35). The cross-strata form sets that are 5-50cm thick and yield bi-modal current directions. Coarsening-upward units range from coarse grained calc-lithic arenites to cobble sized clasts (Fig. 3.36). A few fining upward units are also present (Fig. 3.34).

In places the conglomerates are matrix supported, but these conglomerates also contain cross-strata yielding bi-modal current directions

### 3.6.5 Facies Associations and Distributions

The logs from locations 46 (Ref. 511 338) and 47 (Ref. 510 340), given in Appendix I and Figures 3.34 & 3.36, display the typical vertical facies distributions of the Upper Messinian succession. The calc-lithic arenites and conglomerates form both coarsening-up and fining-up sequences and the conglomerate beds (Fig. 3.37) almost always have erosional bases. The calc-lithic arenites containing ripple cross-lamination, tabular cross-lamination and carbonaceous material are often associated with thin pebble horizons and coarse grained sandstone beds. The marls almost always show a vertical colour stratification sequence with red marls overlain by grey marls, with a gradational contact between the two.

### 3.6.6 Facies Interpretation

The Upper Messinian rocks lack the microfauna typical of the underlying succession, and the evidence of rootlets and carbonaceous material suggests that the conglomerates were deposited in a sub-aerial environment. The colour stratification in the marls is similar to stratification in palaeosols of the Eocene Willwood Formation in the Big Horn Basin. The colour-stratified marls are interpreted as palaeosols considered to have developed on the overbank deposits of a fluvial system (Krauss & Brown, 1988). The colour stratification is evidence of pedogenesis, the upper grey horizon reflecting the concentration of organic matter and the red colouration the concentration of Fe sesquioxides below. Comparison with the Willwood Formation suggests that the Upper Messinian rocks contain fairly mature palaeosols and this must indicate that there was a substantial period of sub-aerial exposure during the Upper Messinian.

Because the palaeosols are intercalated with conglomerates, the conglomerates are also interpreted as having been deposited in a sub-aerial environment. Structures in the conglomerates such as cross-stratification indicate current deposition and the erosional bases indicate deposition as part of a channelised fluvial system. Coarse grained conglomerates that are intercalated with rocks that show evidence for subaerial exposure, are most commonly associated with fluvial braid-plain systems (Collinson, 1978).

Fluvial braid plain deposits can be divided into channels and bars that produce horizontally bedded imbricate gravel deposits that may appear massive where the texture is coarse and uniform (Boothroyd & Ashley, 1975; Church & Gilbert, 1975; Rust 1972, 1975). The channels are subject to the fastest flowing currents and consequentially this is where the largest clasts are imbricate (Rust 1972b). Numerous low sinuosity channels develop across the braid plain, and channel switching leads to cycles of channel abandonment and channel re-activation. Where channels are abandoned they become filled by sand, and the gravel floor is draped by sandy sediment which migrates during deposition as ripples and dunes (Williams & Rust, 1969).

Erosionally based conglomerates that fine upwards (Fig. 3.37) were probably deposited in channels. The coarse grained deposits were deposited on the floors of eroded channels and subsequent abandonment led to the deposition of finer sediment resulting in the fining up cycles. Ultimately, if the channel was not reactivated pedogenesis may have occurred, producing palaeosols and rootlets

Channels in braided plain systems are complemented by bars dominated by coarse

clastic deposition. Bars may be either longitudinal or transverse with respect to the channel axis. Both types of bar are characterised by coarsening up sequences and commonly contain cross-stratification (Ore, 1964; Bluck, 1976 ; Bluck, 1982).

In longitudinal bars, the coarse clasts are segregated as thin gravel sheets (Boothroyd & Ashley, 1975) and imbricate gravels form with the long axes of the clasts transverse to the current (McDonald & Banerjee, 1971, Boothroyd & Ashley, 1975). In longitudinal bars such imbrication tends to be unidirectional and is best developed at the heads of the bars (Bluck, 1974 ).

Transverse bars tend to produce extensive sets of cross-bedding as they migrate downstream (Ore, 1964; Smith, 1970). Such cross-bedding can be produced in any one of four ways; (i) migration of small deltas of sand and gravel on the bar front, (ii) migration of mega-ripples in channels cut through the bar, (iii) migration of sand ripples on the bar top and (iv) the migration of the steep margins of the bar (Bluck 1974). The orientations of foresets and of long axes of imbricated clasts is much more variable than in longitudinal bars (Bluck, 1974) and the cross-strata produced by the accreting margin of bar are the most variable of the cross-strata types. In modern deposits the large cross-strata of bar margins tend to dip away from the main channel (Bluck, 1974).

The Upper Messinian deposits contain coarsening up sequences of conglomerates (Fig. 3.37) with imbrication and cross-strata that is unidirectional in some beds and bi-directional in others. From the above discussion, the conglomerates can be interpreted as the products of deposition within migrating bars. There is evidence for both transverse bars and longitudinal bar deposits. Longitudinal bars are represented by segregated sands and conglomerates with unidirectional imbrication orientations and no large cross-strata, transverse bars by thicker conglomerates containing cross-strata with variable orientations.

Palaeocurrents have been measured from both cross-strata and imbricated clasts (Fig. 3.38). The cross-strata in the bars show the greatest variability while the imbricated clasts give a more consistent palaeocurrent direction. Palaeocurrents derived from imbricated clasts appear to be normal to those derived from cross-strata. This is consistent with the models of Ore (1964) and Bluck (1974; 1976) who demonstrated that cross-strata in transverse bars tend to be variable and dip away from the main channel. Imbrication is best developed in channels and longitudinal bars and in modern systems these give the most reliable palaeocurrent directions (Bluck, 1974; 1976). Thus, in the Upper Messinian the cross-strata are products of transverse bars whose margins migrated away from the channels while imbrication reflects currents acting on channel floors and on longitudinal bar fronts. Analysis of the imbricated clasts (Fig. 3.38) indicates that the streams flowed from the SW to the NE.

In conclusion, during the Upper Messinian the floor of the Guadalquivir Basin in the Baena-Montilla region was sub-aerially exposed. A braided fluvial plain developed that carried coarse clastic material from the SW to the NW, indicating a source which must have been in the External Zones. The nature of the conglomerates indicates that the hinterland feeding the braid-plain must have had some considerable relief. The clast compositions and palaeocurrents are more fully discussed in Chapter 4.

### 3.7 Summary of the Palaeoenvironmental

#### Evolution of the Guadalquivir basin

The Miocene Guadalquivir Basin succession is a progradational sequence in which there is a shift from an open marine seaway in the Lower Miocene to a terrestrial fluvial system in the Upper Messinian. A bathymetric curve illustrating this shift can be constructed from both facies interpretations and micropalaeontological analysis (Fig. 3.39). The Lower Miocene was deposited at bathyal depths (200-800m). This is limited by an unconformity and deposition at the beginning of the Tortonian marks a major shift to shallow-shelf depths (<200m). During the Tortonian the basin experienced rapid changes in water depth, fluctuating between outer-shelf and near-shore environments. During the Lower Miocene a mid-shelf to near-shore environment was established in the Baena-Montilla area and deposition became influenced by delta incursion and brackish waters. In the Upper Messinian there was another major shift of sea level, leading to local sub-aerial exposure and the establishment of a fluvial braid plain. From the bathymetric curve (Fig. 3.39) it can be seen that, overall, the Miocene Guadalquivir Basin sequence reflects a relative sea-level fall. This correlates with the general trends in global sea-level during the Miocene (Fig. 2.11) (Haq *et al.*, 1987), which led to the Mediterranean Messinian Salinity Crisis.

From facies interpretation, micropalaeontology and inferred sea-level change record the palaeoenvironmental evolution of the Guadalquivir Basin can summarised as a series of block diagrams (Figs. 3.40-3.43):

#### 3.7.1 Lower Miocene Environment

During the Lower Miocene the Guadalquivir Basin was dominated by an open seaway (Fig. 3.40) characterised by the deposition of pelagic biogenic detritus from the water column and fine grained terrigenous detritus via surface currents. The sea supported a diverse community of foraminifera, radiolaria and diatoms which bloomed periodically. During the Mid Miocene times the sea-floor was disrupted by the deposition of debrites the formation which may have been triggered by the onset of the sea-level fall that generated the Tortonian unconformity.

#### 3.7.2 Tortonian Environments

The Tortonian was dominated by the deposition and reworking of clastic material on a storm-dominated shelf fringed by coastline beach deposits (Fig. 3.41). Periodic storms induced density currents that deposited sands in waters on the outer margins of the shelf. The Tortonian seaway was typified by a fluctuating sea-level which caused periodic progradation of the shoreline followed by rapid flooding, leading to the formation of thickening and coarsening up cycles. The relative sea-level changes could have been brought about by fluctuating sediment supply, minor fluctuations in global sea-level or tectonic activity in the Betic Orogen. The base of the Tortonian succession has been interpreted to be a product of a major sea-level fall that was possibly amplified by tectonism in the Betics (Chapter 2, section 2.7). The cycles within the Tortonian represent smaller higher frequency fluctuations which

are not usually associated with tectonism or major eustatic changes. It is more likely that these minor fluctuations are controlled by a fluctuating sediment supply or very minor changes in the global sea-level curve.

### 3.7.3 Lower Messinian Environment

During the Lower Messinian a delta was built onto a storm/tide dominated shelf (Fig. 3.42). The delta deposits formed interdistributary bars separating brackish pools from the open shelf. Sediment was transported onto the shelf via tidal channels which also acted as a conduit for the transport of brackish faunas. In places skeletal debris was reworked into shoals which formed on the open shelf or on bar margins. Sediments were also transported from the open shelf into the brackish pools, probably as wash over deposits during storms but perhaps also via tidal channels which breached interdistributary bars.

### 3.7.4 Upper Messinian Environment

The Upper Messinian was marked by a major shift of the coastline basinward, resulting in sub-aerial exposure of the shelf (Fig. 3.43). Alluvial fans fed a braid plain dominated by anastomosing low sinuosity channels and bars that conducted coarse grained detritus from the hinterland to the coastline.

## 3.8 Palaeogeography of the Miocene Guadalquivir Basin

Using the environmental interpretations it is possible to construct a generalised palaeogeography for the Miocene Guadalquivir basin. However, before this can be assessed the configuration of the shelf and position of the coastline must be determined.

Broadly speaking a depositional margin can fall in one of two categories, a shelf with a marginal break or a ramp margin (Fig. 3.44). Shelf break margins and ramp margins have been reviewed by Van Wagoner *et al.* (1990) who devised a set of criteria for differentiating the two types:

### 3.8.1 Shelf Break Margin

A shelf break margin is characterised by

1. well defined shelf, slope and basin floor topography;
2. shelf dips less than  $0.5^{\circ}$ , slopes of  $4-6^{\circ}$ , with  $10^{\circ}$  dips along sub-marine canyon walls ;
3. a relatively abrupt shelf-break separating low-angle shelf deposits from much more steeply dipping slope deposits ;
4. a relatively abrupt transition from shallow water into much deeper water;
5. Incision in response to sea-level fall below the depositional-shoreline break if submarine canyons form; and
6. probable deposition of basin-floor submarine fans and slope fans

### 3.8.2 Ramp Margins

Ramp margins are characterised by

1. uniform, low angle dips of less than  $1^{\circ}$  with most dips less than  $0.5^{\circ}$
2. no abrupt changes in gradient separating relatively low dips from much steeper dips;
3. no abrupt changes in water depth from shallow water to much deeper water;
4. Incision to, but not below lowstand shoreline in response to a relative falls in sea-level and;
6. deposition of lowstand deltas and other shoreline sandstones in response to sea-level fall (basin floor submarine fans and slope fans unlikely to be deposited on the ramp margin).

In the Miocene Guadalquivir Basin succession we have evidence for deep-water pelagic deposits, in the Lower Miocene and shallow shelf deposits from the Tortonian onwards. There is no gradational change between these and they are never found together within coarsening up cycles. The above criteria suggest that there is shelf break separating the deep water deposits from shallow water deposits. There is also evidence for incision during the Mid Miocene in the form of debrite deposits. The debrites are intercalated with the deep water deposits and so incision must have occurred below depositional shoreline break, at or below the shelf break. In conclusion it appears that the evidence points strongly to the Miocene Guadalquivir Basin having a shelf break margin as opposed to a ramp style margin.

The relative position of the coastline can be determined by considering the palaeocurrent data and provenance indicators (Chapter 4). Palaeocurrent data from the braided stream deposits in the upper Messinian indicate that streams flowed from the SW towards the NE. Data from the coastal fan deposits in the Lower Miocene show palaeocurrents to the W although fan deposits can vary by as much as  $180^{\circ}$ . The most reliable palaeocurrents are those from the braided streams which would generally have flowed from the hinterland across the coastal plain towards the coastline, placing the hinterland to the S and the seaway to the north. In addition to the palaeocurrent data, provenance studies outlined in Chapter 4, indicate that a large proportion of the detritus came from the External Zones which would have been located to the south, this suggests that there was relief in this direction and this would also place the coastline south of the seaway.

In the final analysis it appears that the Miocene Guadalquivir Basin was rimmed by a shelf break that separated deep water from shallow water. Material was fed from south to north, from the External Zones to the shelf via braided streams and fan deltas. A generalized palaeogeography for the Miocene Guadalquivir Basin which takes into account the environmental interpretations outlined above is given in Figure 3.45.

### 3.9 Allochthon & Autochthon: Part of the Same Basin ??

One of the main questions arising from the tectonic, stratigraphical and sedimentological analysis of the rocks in the Baena-Montilla area is whether or not the allochthon and

autochthon were originally part of the same basin fill, or two separate basins juxtaposed during thrusting. There are several lines of evidence suggesting that a single basin existed prior to thrusting that extended much further south than the present Guadalquivir Basin does today.

1) There is no evidence for the structural segregation of the basin. Aquitanian to Messinian rocks are incorporated into the melange complex associated with late/post Miocene thrusting (Chapter 2, section 2.4) and thrusting previously interpreted as Mid Miocene, has been shown to be at least late Messinian (Chapter 2). So for the basins' Miocene history there is no evidence for a structural break.

2) Sedimentological analysis has shown that rocks with identical stratigraphical ages, microfaunal assemblages, lithologies and facies, are found in both the allochthon and autochthon. This is particularly apparent in the Lower-Mid Miocene and Tortonian.

43 The petrography and consequentially the provenance, of sedimentary rocks in the allochthon and autochthon are identical (Chapter 4).

Thus structural, sedimentological, palaeontological and lithological evidence indicates that the autochthon and allochthon elements within the Guadalquivir Basin formed a single basin that extended southward past the present boundary.

### 3.10 Conclusions

In conclusion the Miocene Guadalquivir succession formed in a single basin characterised by deepwater and shallow marine shelf deposits separated by a shelf break (Fig. 3.45). A fluvial braid plain dominated the southern part of the basin and channelled detritus from the External Zone to coastal delta systems. The detritus was reworked on the shelf by storm and tidal currents that led to the mixing of near shore and shelf faunas. Through the Miocene the coastline prograded northward out across the shelf in direct response to a relative sea-level fall that was most probably eustatically driven.



## ***Chapter 4***

# ***Provenance of the Guadalquivir Basin Sediments***

## CHAPTER 4

### PROVENANCE OF THE GUADALQUIVIR BASIN SEDIMENTS

#### 4.1 Introduction

Provenance studies are designed to identify the location and nature of a sediment source and the pathways by which sediments are dispersed (Haughton *et al.*, 1991). In order to produce a reliable fingerprint of the source several techniques must be employed. Before the implications of provenance data can be evaluated, the bias away from the source composition that may be inherent in the sedimentary rocks must be assessed. Such bias away from source composition can be brought about by hydraulic segregation (sorting), diagenesis and sediment recycling.

This chapter describes the methods and results of provenance studies of Miocene sedimentary rocks in the Guadalquivir Basin. These have been carried out to identify the nature of the source for sediments in the Guadalquivir Basin.

Three candidate sources can be identified; the Hercynian Massif to the north, the External Zone of the Betic Orogen and the Internal Zone of the Betic Orogen which are both to the south (Fig. 4.1).

The Hercynian Massif forms the northern margin of the Basin. It is characterised by a complex series of terranes that contain Precambrian, Ordovician, Devonian and Carboniferous metamorphosed and unmetamorphosed rocks (Anderson, 1978). The terranes have been affected by several Precambrian and Hercynian deformation and metamorphic episodes. Rocks present include, schists, amphibolites, gneisses, marbles, quartzites, shales, greywackes, conglomerates, limestones and sandstones (Martinez Garcia *et al.*, 1986). Numerous granites and granitoid bodies have invaded the terranes and these have been dated as pre-Hercynian, syn-Hercynian and post-Hercynian (Correge, 1978). Granites have been dated at between 310-318 m.y. (Correge, 1978) and include the Pedroches Batholith which dominates the southern margin of the Iberian Massif. As a consequence of the presence of the granitoid bodies, many of the rocks in the Hercynian Massif have been overprinted by contact metamorphism. The northern margin of the Guadalquivir Basin is characterised by late Miocene fan delta deposits which are believed to have emerged from the Hercynian hinterland (Juan Fernandez, pers. comm.). These fan deltas may have fed Hercynian detritus into the Guadalquivir Basin during the late Miocene.

The southern margin of the Guadalquivir Basin is formed by the External Zone of the Betic Orogen and is dominated by Triassic to Lower Miocene unmetamorphosed sedimentary rocks (Garcia Hernandez *et al.*, 1979). These represent sediments deposited on an extending plate margin present before the formation of the Betic Mountain Chain. The External Zone is dominated by marls and limestones deposited in shallow marine and pelagic marine environments. (Garcia Hernandez *et al.*, 1979; Blankenship, 1992). These rocks were deformed and thrust northward by movements that occurred in the Betic Orogen during latest Oligocene and Miocene times (Chapter 2).

The Internal Zone forms the metamorphic core of the Betic Orogen and consists of a

series of nappes metamorphosed to varying degrees, but generally characterised by a high pressure metamorphism (Egeler & Simon, 1969; Egeler *et al.*, 1972). The earliest recorded metamorphism is late Cretaceous (85-65 Ma.) (Doblas & Oyarzun, 1989; Bakker *et al.*, 1989; and Moiné *et al.*, 1991). A discussion concerning the complexity of Internal Zone metamorphism is given in the Overview (Section 1.3).

Provenance studies of the sedimentary rocks of the Guadalquivir Basin fill are aimed at assessing the contribution of each of these three sources to the basin. To fully characterise the sediments a multi-disciplinary approach has been adopted, including the use of petrography, geochemistry, geochronology and palaeocurrent data.

Petrography has been used to determine the general characteristics of sandstones in the Guadalquivir Basin succession, and an attempt has been made to assess any bias which may have been introduced during hydraulic segregation, diagenesis or sediment recycling. Taking the assessed bias into account, the petrography has been quantified and the framework composition been plotted on Q, F, Lt ternary plots. These give a general indication of the plate setting and plate configuration for the Guadalquivir Basin.

The quantitative petrographic data has been compared with the clast composition of conglomerates interpreted to have been deposited in fluvial braid plains and coastal fans that are thought to have fed marine sediments into the Basin (Chapter 3). These deposits also yield palaeocurrent data giving the general transport direction of the sediments.

Following general analysis of petrography and clast composition, attention has been focused on the metamorphic clasts of the sandstones. Geochemistry has been used to characterise detrital white micas which were compared with white micas derived from the Internal Zone of the Betic Orogen. The micas have also been dated, using single grain  $^{40}\text{Ar}/^{39}\text{Ar}$  isotopic dating techniques, to determine their age of cooling and thus their likely source.

All the data, from petrography, palaeocurrents, geochemistry and geochronology, are combined and an assessment of the sediment source made.

Table 4.1

<b>SAMPLE</b>	<b>AGE</b>	<b>ENVIRONMENT OF DEPOSITION</b>
GQ1	Upper Miocene	N margin fan deposits
GQ2	Upper Miocene	N margin fan deposits
GQ3	Tortonian	shallow marine shelf
GQ6	Tortonian	tempestites
GQ7	Tortonian	shallow marine shelf
GQ79(b)	Tortonian	tempestites
GQ93	Tortonian	tempestites
GQ97	Tortonian	shoreface/near coast
GQ99	Tortonian	tempestites
GQ100	Tortonian	shoreface/near coast
GQ101	Tortonian	shoreface/near coast
GQ103(a)	Tortonian	shoreface/near coast
GQ104	Tortonian	shoreface/near coast
GQ98	Tortonian	shoreface/near coast
GQ79(a)	Lwr Messinian	tidal/storm shelf
GQ77(b)	Lwr Messinian	marine conglomerate matrix
GQ78(b)	Lwr Messinian	brackish/lagoonal
GQ88	Lwr Messinian	brackish/lagoonal
GQ89	Lwr Messinian	brackish/lagoonal
GQ92	Lwr Messinian	tidal bar
GQ20	Lwr Messinian	tidal/storm shelf
GQ95	Lwr Messinian	tidal/storm shelf
GQ106	Lwr Messinian	tidal/storm shelf
GQ40	Lwr Messinian	tidal/storm shelf
GQ84	Lwr Messinian	brackish/lagoonal
GQ85	Lwr Messinian	brackish/lagoonal
GQ72	Upper Messinian	fluvial conglomerate matrix
GQ73	Upper Messinian	fluvial conglomerate matrix

**Table 4.1** Samples, from autochthonous and allochthonous portions of the Guadalquivir basin. All these samples have been used in petrographic studies which form part of a detailed provenance investigation of the Basin. Environmental interpretations are based on those given in Chapter 3

## 4.2 Quantitative Petrography

Petrography forms the foundation of this provenance study. It relies on the identification and quantification of minerals and clasts.

The petrographic framework mode of a sedimentary rock is the product of sedimentary processes, source composition and source mixing (Haughton *et al.*, 1991).

### 4.2.1 Samples

Samples were collected from Tortonian and Messinian sandstone units found in the Guadalquivir Basin succession exposed in the Baena-Montilla study area. Lower and Mid Miocene rocks were not included as they are dominated by marls and lack sandstones. To gain a representative view of the sandstones, samples were collected from all of the lithofacies that have been identified in allochthonous and autochthonous portions of the basin fill (Chapter 3). In addition, samples were collected from upper Miocene rocks found on the northern margin of the basin. These were deposited in large submarine and subaerial fans, thought to have been fed by detritus originating from the Hercynian Massif (Juan Fernandez pers. comm.). Sample locations are given on Figure 4.2. Samples represent the full range of environments believed to have existed in the Guadalquivir basin (Table 4.1)

### 4.2.2 Methods

The samples (Table 4.1) were impregnated with blue stained resin and thin-sectioned. To facilitate the identification of feldspars the sections were subsequently stained with barium chlorite and rhodizonate following the method of Bailey and Stevens (1960).

Point-counts of the framework modes of each thin section were conducted using a mechanised point-counting stage. The stage-advance was set to increment a distance equal to the average grain size. Two counts were conducted on each thin section. The first quantified the proportion of monocrystalline quartz (Qm), plagioclase (P), K-feldspar (K) and lithic fragments (Lt) in each sample. A total of 500 grains was counted. The second count was designed to provide a detailed inventory of the lithic fragments in terms of their metamorphic, volcanic and sedimentary components. The metamorphic component was split into metamorphic grain types, based on the method outlined by Rapson (1965) and Ingersoll & Suczek (1979). A total of 500 lithic fragments were counted and classified for each sample. Metamorphic grain types were recognised as follows;

**phyllitic schist (Ph.Sch)** fragments of micaceous rock with a distinct schistose fabric, (i.e. a well developed, finely spaced cleavage);

**quartz , mica and feldspar aggregate (Q-M-F Ag)** fragments of quartz, mica and feldspar aggregates lacking a distinct fabric;

**quartz, mica and feldspar tectonite (Q-M-F Tect)** fragments composed of quartz, mica and feldspar with a distinct fabric such as grain flattening, elongation or alignment;

**quartz and mica aggregate (Q-M Ag)** fragments containing only quartz and mica

lacking a distinct fabric;

**quartz mica tectonite (Q-M Tect)** fragments containing quartz and mica with a distinct fabric such as grain flattening, elongation or alignment;

**polycrystalline quartz tectonite (Qp Tect)** fragments of polycrystalline quartz in which grains are flattened, elongated or aligned to form a distinct fabric;

**Micas (Micas)** single mica grains;

**polycrystalline micas (Micas p)** fragments containing more than one mica grain, but without a schistose fabric;

**polycrystalline quartz** fragments of polycrystalline quartz lacking a distinct fabric;

**quartz and feldspar aggregate (Q-F Ag)** fragments containing quartz and feldspar but lacking a distinct fabric and

**contact metamorphic minerals (Contact meta)** minerals associated with the contact metamorphism of country rocks. The commonest is cordierite.

Sedimentary lithic fragments were also divided into generic lithic fragment types which are as follows;

**sandstone (Sand)** fragments containing identifiable quartz, feldspar and lithic grains of sedimentary origin;

**argillite other than marls (Argillite)** mud-rock fragments, excluding carbonate;

**polycrystalline carbonates (Carb pc)** carbonate fragments in which grains are identifiable;

**Marl (Marl)** carbonate mud rock in which separate grains could not be identified and

**Chert (Chert)** cryptocrystalline quartz fragments.

Framework modes, outlined above, were used to derive other modal values characterizing the rock sample, including the total number polycrystalline quartz grains (Qp), the total number of metamorphic lithic fragments (Lm), the total number of volcanic lithic fragments (Lv) the total number of sedimentary lithics (Ls), the total number of volcanic and meta-volcanic lithic fragments (Lvm) and the total number of sedimentary and meta-sedimentary lithic fragments (Lsm). These variables were calculated as follows;

$$Qp = Qp \text{ Tect} + Qp$$

$$Lm = Ph.Sch + Q-M-F \text{ Ag} + Q-M-F \text{ Tect} + Q-M \text{ Ag} + Q-M \text{ Tect} + \text{Micas} + \text{Mica p} + Q-F \text{ Ag} + \text{Contact Meta}$$

$$Lv = \text{Total number of hypabyssal volcanic grains}$$

$$Ls = \text{Sand} + \text{Argillite} + \text{Carb pc} + \text{Marl} + \text{Chert}$$

$$Lvm = Lv$$

$$Lsm = Lm + Ls$$

In addition to counting framework grains the individual grain sizes were measured. Measurement was made with a graduated ocular that was calibrated using a thin section glass with a millimetre scale etched upon it. To gain a representative sample of the grain-

Table 4.2

Sample	GQ 88	GQ89	GQ92	GQ 20
Age Facies	Messinian brackish	Messinian brackish	Messinian tidal bar	Messinian tidal/storm shelf
<b>Q-F-Lt count</b>				
Qm	224	313	240	364
P	18	12	13	3
K	12	5	0	5
Lt	246	170	247	127
Total feldspar	30	17	13	8
<b>Lithic count</b>				
<b>Meta lithics</b>				
Ph. Sch	0	0	0	0
Q-M-F Ag	20	19	15	13
Q-M-F Tect	0	0	0	0
Q-M A	20	73	12	28
Q-M Tect	0	0	3	9
Qp Tect	0	13	2	16
Micas	18	0	6	25
Mica p	0	13	2	19
Qp	38	75	25	131
Q-F-Ag	0	0	0	0
Contact Meta	0	0	0	0
<b>Volcanic Lithics</b>				
Hypabyssal	0	0	1	0
<b>Sed Lithics</b>				
Sand	14	15	0	5
Argillite	0	0	0	0
Carb pc	184	160	188	79
Marl	170	85	228	142
Chert	24	26	9	22
Unknown Lt	12	21	9	11
<b>Calculations</b>				
Qp	38	88	27	147
Lm	58	105	38	94
Lv	0	0	1	0
Ls	392	286	425	248
Lvm	0	0	1	0
Lsm	450	391	463	342
<b>Grain size</b>				
Mean (phi)	1.56	1.29	1.28	1.80
Sorting	0.91	0.75	0.68	0.52

**Table 4.2** Petrographic framework modal data for Upper Miocene sandstones of the Guadalquivir Basin. The full data set is given in Appendix IV.

size population the following method was employed (Bluck pers. comm.):

- (1) The longest axis of an arbitrary number of grains is measured (e.g. 10 grains) and their mean size is plotted against the number of grains counted (Fig. 4.3);
- (2) Step 1 is repeated and the mean for the new number of grains is plotted (10+10, the mean of 20 grains);
- (3) Steps are repeated and data plotted until the resultant graph produces a consistent mean (Fig. 4.3). Once the mean becomes consistent the population mean has been obtained and a representative sample of the population has been measured.

From the grain size population, sorting (standard deviation from the mean) was calculated using the Folk & Ward (1957) formulae:

$$\sigma\phi = \frac{\phi_{84} - \phi_{16}}{4} + \frac{\phi_{95} - \phi_{5}}{6.6}$$

where  $\sigma\phi$  = sorting

$\phi_n$  = percentile value  $\phi_n$  measured from cumulative frequency curves, plotted for the grain size population, at the  $n$ th percentage frequency.

A sample of the petrographic data set, outlining the count variables, is given in Table 4.2. The full data set can be found in Appendix IV. In addition to the point count data the stratigraphical age and environmental interpretation (derived from Chapter 3) is given for each sample. Estimates of the percentage of bioclastic grains and matrix is also given for each sample where appropriate.

#### 4.2.3 Assessment of Sediment Bias

The petrographic signature of the sedimentary rocks in a basin may not be a true reflection of the source, but may be 'biased' in some way. Bias can be brought about by hydraulic segregation and sediment recycling during transport or by diagenesis.

During transport and deposition grains are subject to attrition and hydraulic segregation. During prolonged transport and associated hydraulic action original polycrystalline fragments may be broken up into their component parts. Tortosa et al. (1991) demonstrated that polycrystalline quartz content decreases with grain size. Polycrystalline quartz is broken down into its component monocrystalline quartz grains by attrition. The smaller monocrystalline grains may then be hydraulically segregated into the finer sediment fraction. Thus the finer grain sizes may not accurately reflect the true lithic content of the source rock. This problem also applies to other polycrystalline lithic fragments. For example a sandstone lithoclast (indicative of a source in sedimentary rocks) composed of quartz feldspar and lithic fragments is easily broken up into monocrystalline quartz, feldspar and metamorphic lithic fragments, which may then be subject to hydraulic segregation. This is further complicated by the fact that grains that are less resistant to attrition, in particular feldspars and lithics, are lost during prolonged transport by attrition and hydraulic segregation processes (Morton, 1985).



Recycling is the processes by which sediments are reworked from one basin to another. During recycling hydraulic segregation and attrition processes are prolonged. This may bias the composition towards more mature grains that are less likely to discriminate the source (Luepke, 1984; Morton, 1985; Magne & Maure, 1990). Recycling may also result in a complex sediment mixture involving different sources (Haughton, 1991). Thus the data derived from recycled sediments seldom reflects the palaeotectonic setting of a sedimentary basin.

During burial, diagenetic changes take place in sedimentary rocks. The circulation of aggressive fluids through the rocks may dissolve certain minerals such as feldspars. Precipitation of other minerals, such as carbonate, may fill pores or replace minerals. Thus, any rocks that have undergone significant diagenetic alteration will not accurately reflect their source (Morton, 1984; Milliken, 1988; Humphreys et al., 1991).

Grain size and sorting of a sediment are directly related to processes of transport and hydraulic segregation (Haughton et al., 1991). Because of this relationship the bias inherent in the rocks of the Guadalquivir Basin can be assessed by comparing the occurrence of easily broken lithics with grain size and sorting variation within the sample population. The lithic components chosen for comparison are metamorphic lithics (Lm), sedimentary lithics (Ls) polycrystalline quartz (Qp) and monocrystalline quartz fragments (Qm). With increased sorting and finer grain sizes it is expected that there will be a reduction of Qp in favour of Qm and Ls in favour of Lm. These trends, if present will reflect the disaggregation of the grains and the sorting of the resultant components into the finer fractions. The lithic components of the sandstones can also be compared to the facies interpretations of the successions from which the samples were derived. Facies and the environments of deposition are closely tied to the overall hydraulic regime.

Figures 4.4-4.9 show the variation of Ls, Lm, Qp, Qm and Qm with mean grain size, sorting and facies for samples taken from the Guadalquivir Basin. For each plot a variety of regression lines were fitted. The best correlation co-efficient that could be obtained for any of the plots was 0.242 which, for the number of paired samples, is not a significant correlation, even at the 10% level. It is considered that overall the plots present a random distribution, and that there is no significant variation of the modal framework compositions with grain size, sorting or facies

There is, however, a distinct difference between samples taken from the Baena-Montilla region and samples taken from the northern margin fan deltas. Samples from the northern margin fans have higher amounts of Qp and Lm and significantly lower amounts of Ls (Fig. 4.4 & 4.5).

If sediment was being transported from northern-margin fan deposits to the Baena-Montilla region then the implication is that a large proportion of the Lm and Qp components were removed during transport. However, the Baena-Montilla rocks also have a large Ls component (Fig. 4.10) and it seems unlikely that Lm and Qp would be lost without there being a corresponding reduction in Ls, and this therefore implies different sources for the two areas. The full implications of these observations are assessed in the light of palaeocurrent and geochemical data.

Sediments that have largely been derived from older sedimentary rocks may have a

large sedimentary lithic (Ls) component. Rocks from the Baena-Montilla area are dominated by Ls fragments, which vary between 40% and 90% with an average of 69% (Fig. 4.10). By comparison, the northern margin rocks contain less than 5% Ls fragments. Thus, it appears that the southern part of the Guadalquivir Basin, in the Baena Montilla region, received detritus from older sedimentary rocks/or older basins, while the northern margin received detritus from the Hercynian Massif metamorphic terranes. This suggests that at least two sources contributed to the Guadalquivir Basin one of which was an older uplifted sedimentary basin.

The sedimentary rocks of the Guadalquivir Basin are largely uncemented and consequentially friable. There is no evidence for the feldspars or sedimentary lithic grains going over to clay minerals. Overall there is no evidence, in thin section or under the scanning electron microscope, for the dissolution of minerals or for the growth of new minerals. These rocks are not considered to have been buried to any great depth and diagenesis is not considered to have been a significant factor in controlling the framework composition modal values.

Several conclusions can be drawn concerning the nature of the sedimentary rocks in the Guadalquivir Basin and possible 'bias' introduced during transport and hydraulic sorting.

- (1) There is no significant variation of the modal compositions with grain size, sorting or facies. Therefore hydraulic transport processes are not considered to have induced a significant bias into the Guadalquivir sample populations.
- (2) There is a fundamental difference between sandstones found in the Baena-Montilla region of the Guadalquivir Basin and those on the northern margin. The northern margin is dominated by Lm and Qp while the Baena-Montilla region is dominated by Ls fragments.
- (3) There are two possible explanations for this difference; a) that Lm clasts have been lost during transport or b) that there were two or more sources contributing to the basin;
- (4) The Baena-Montilla sample population is dominated by Ls, and so the petrographic modal compositions do not reflect the original source of the metamorphic, volcanic and igneous detritus but indicate the destruction of earlier sedimentary rocks and/or basins.

It should also be noticed that sedimentary rocks in the allochthon could not be differentiated from those in the autochthon, using petrographic techniques. This is consistent with the invariance of facies across the two portions of the basin (Chapter 3) and as a consequence the allochthon and autochthon are considered to be parts of the same basin.

#### *4.2.4 Petrographic Characteristics in Relation to Plate Setting.*

While recognising the 'bias' inherent in determining provenance of sedimentary rocks, it is nevertheless possible to use framework modal data to give a general indication of the tectonic regime in which the sediments were deposited. Modal values were plotted on Q, F, Lt type

ternary plots and compared with published data on sediments for which the tectonic regime was known. Three plots have been employed (Fig. 4.11) Qm, F and Lt (Dickinson *et al.*, 1983); Qp, Lvm and Lsm (Ingersoll & Suczek, 1979) and Lm, Lv and Ls (Ingersoll & Suczek, 1979). Full explanations for these plots are provided in the references.

In the Qm, F, Lt plot (Fig. 4.12), the Baena-Montilla and northern margin compositions plot in the recycled orogenic field and vary between quartzose recycled and transitional recycled groups. Recycled orogenic detritus is derived from suture belts in which sedimentary, volcanic and metamorphic rocks are involved in uplift and thrusting. Tectonic settings include subduction complexes, suture belts of collisional orogens and thin-skinned foreland fold thrust belts along the flanks of arc or collisional orogens (Dickinson *et al.*, 1983). Quartzose recycled detritus indicates that the orogenic uplift involved sediments that were ultimately recycled from cratonic sources. Transitional recycled detritus also contains metamorphic and sedimentary detritus recycled directly from the orogen itself. The position on this plot of the Guadalquivir Basin data set comes as no surprise because of the proximity of the Betic Orogen. Older sedimentary rocks, that once formed part of the passive margin are known to have been involved in Betic Orogenic uplift. These rocks now form part of the External Zone fold thrust belt flanking the southern margin of the Guadalquivir Basin and sediment could easily have been derived from this zone.

The Qp, Lvm and Lsm plot of the data set (Fig. 4.13) displays a similar trend with data grouping in the suture belt field. Both the Qm, F and Lt plot (Fig. 4.12) and the Qp, Lvm and Lsm plot (Fig. 4.13) strongly suggest that Guadalquivir Basin sediments were derived from an orogenic suture belt, namely the Betic Orogen.

The Lm, Lv, Ls plot (Fig. 4.14) confirms this observation for the Baena Montilla data set and also eliminates the possible involvement of a subduction complex, clearly placing the sedimentary rocks in a suture belt setting. This plot also suggests the recycling of detritus from sedimentary rocks deposited on a rifted continental margin. This again is consistent with previous tectonic models in which an extending passive margin is known to have existed on the Iberian plate, prior to the formation of the Betic Orogen suture belt (Garcia Hernandez, 1979; Blankenship, 1992). However, in this plot the northern margin data plot near the Lm upper corner (Fig. 4.14) and outside the suture belt field. This supports the view that there is a fundamental difference in the source of detritus for the northern margin sedimentary rocks and that for the Baena-Montilla region.

While these plots confirm the general tectonic setting they fail to emphasize or utilize the dominant Ls fragments in the Baena-Montilla sedimentary succession. By analysing these fragments it may be possible to determine the nature of the sedimentary succession which formed the source for the Guadalquivir Basin sedimentary rocks. The Ls fragments have been plotted in terms of their sandstone, carbonate and chert components (Fig. 4.15). Clearly the population is dominated by carbonate fragments. These are made up of both polycrystalline carbonate and marl fragments in almost equal proportions (Fig. 4.16). Because the sandstones are dominated by carbonate lithic clasts they have been classified as calc-lithic arenites, the preferred term used elsewhere in this thesis. The External Zone foreland fold thrust belt is dominated by carbonate rocks (Fig. 1.2), but limestones are also

found in terranes of the Hercynian Massif (Martinez Garcia *et al.*, 1986) and carbonate lithoclasts could have been derived from either of these areas. In addition the lower part of the Guadalquivir Basin succession is dominated by marls dissected by channels containing debris-flows (Fig. 3.2; Chapter 3). Marl clasts could easily have been derived from within the Guadalquivir Basin.

In conclusion the petrographic framework modal data demonstrates that the sediments of the Guadalquivir Basin were derived from sedimentary and metamorphic rocks that formed part of a suture belt complex, which must have been the Betic Orogen. The carbonate fragments could have been recycled from the External Zone of the Betic Orogen, from the Hercynian Massif or from within the Guadalquivir Basin itself. Metamorphic lithic fragments could also have been recycled from the Hercynian Massif or from lithic sandstones in the External Zone. In order to resolve this ambiguity conglomerates in the Guadalquivir Basin succession have been analysed, together with their corresponding palaeocurrents. Geochemical and geochronological techniques have been employed to determine the ultimate source of the metamorphic lithic fragments.

### 4.3 Clast Composition of Conglomerates

Conglomerates are found in both Lower Messinian coastal fan deposits and Upper Messinian fluvial deposits of the Guadalquivir Basin succession exposed in the Baena-Montilla area (Figs 3.42 & 3.43). Clasts have been surveyed in both these deposits and their lithological components are summarised in Figure 4.17. The full data set is given in Appendix IV. The lower Messinian coastal fan deposits are dominated by limestone clasts, while the Upper Messinian deposits are predominantly quartzite and limestone clasts. Both conglomerate sequences contain calc-lithic arenite clasts, calc-lithic arenites are only found in Lower Messinian and Tortonian deposits of the Guadalquivir Basin.

The carbonate clastics, suggest that detritus was supplied from a limestone succession. This supports deductions made from the petrographic data. However, the conglomerates also contain meta-quartzite clasts which increase in frequency in the Upper Messinian. Quartzites are exposed in the Hercynian Massif (Martinez Garcia *et al.*, 1986) and are also found in conglomerates in the External Zone (Perez-Lopez, 1991) and the Alpujarride nappes of the Internal Zone of the Betic Orogen (J. Hughes pers. comm.). The presence of calc-lithic arenite clasts supports the view that recycling of Guadalquivir Basin sediments was taking place as calc-lithic arenites are only found with the Guadalquivir Basin fill.

Overall the conglomerate clast population reflects the same provenance as the sandstones.

### 4.4 Palaeocurrent Data

Palaeocurrent data from conglomerates in coastal fan and fluvial deposits provides a useful insight into the transport pathways and ultimately the locations of the sources relative to the Guadalquivir Basin.

#### 4.4.1 Data

Palaeocurrents have been determined from imbricated pebbles in Lower Messinian fan deposits and from both imbricated pebbles and cross-strata in the Upper Messinian Fluvial deposits. As discussed in Chapter 3, sections 3.5, 3.6 and 3.7, the most reliable data are those measured from imbricated clasts in the fluvial deposits. The cross strata in the fluvial deposits and the imbrication in the fan deposits can vary over 180°. Palaeocurrent data taken from fluvial imbricate clasts suggests that these were deposited by currents that flowed SSW to NNE (Fig. 4.18). Because the fluvial deposits are the products of low sinuosity streams (Chapter 3, section 3.7) this was almost certainly the dominant transport direction.

#### *4.4.2 Transport Pathways*

Conglomerates deposited by braided streams in the Baena-Montilla region of the Guadalquivir Basin have transported clasts from exposed External Zone Rocks in the south to a marine basin in the north (Chapter 3 section 3.8). This view is supported by the clast composition and palaeocurrent data. The conglomerates contain little metamorphic detritus, explaining the lack of metamorphic detritus in the Baena-Montilla sandstones. Thus, it appears that the carbonate fragments found in the Baena-Montilla area were derived from the limestone succession in the External Zone which must have fringed the southern margin of the Basin. However, carbonate material was also recycled within the Basin, as indicated by the calc-lithic arenite clasts. The northern margin deposits contain few sedimentary clasts and are dominated by metamorphic clasts believed to have been derived from the Hercynian Massif (Juan Fernandez pers. comm.). Thus, there is strong evidence for three separate sources contributing to the Guadalquivir Basin sediments, the External zone of the Betic Orogen, the Hercynian Massif, and recycled Guadalquivir Basin sediment.

### **4.5 Geochemistry & Geochronology of Detrital White Micas**

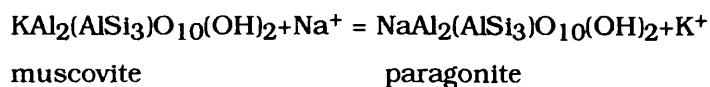
Attention is now focused on the metamorphic lithic clasts in the sedimentary rocks. Metamorphic detritus could have been sourced from the Hercynian Massif, from the Betic Internal zone or from a combination of the two. In order to discriminate between the two a geochemical characterisation of metamorphic minerals, known to vary with pressure and temperature conditions, was undertaken.

#### *4.5.1 Geochemical Variation of White Micas*

Detrital white micas were chosen in preference to other metamorphic minerals for geochemical analysis because;

- (1) they vary significantly with changing pressure and temperature in the muscovite-celadonite and muscovite-paragonite solid solution systems;
- (2) detrital white micas are surprisingly resistant minerals, compared to other abundant metamorphic minerals;
- (3) large amounts of white mica could be separated rapidly from the rocks. Other metamorphic minerals were found to be difficult to extract from the rocks, much less abundant, and are often highly altered;

- Chemically, white micas vary between muscovite-celadonite and muscovite-paragonite substitutions.



### 4.5.2 Samples

### 4.5.3 Methods

## **Part I: The Guadalquivir Basin**

through a Frantz Isodynamic separator in which micas are separated on the basis of their magnetic susceptibility, following standard procedures.

The resulting residue containing white micas was mounted in resin and analysed at the University of Glasgow using a Cameca SX50 electron microprobe. The data were reduced using ZAF techniques and cations per formula unit calculated on the basis of 22 oxygens. The  $\text{Fe}^{2+}/\text{Fe}^{3+}$  ratio was estimated by ratio, following the methods of Schumacher (1991)

Part of the data set is given in Table 4.3 and the full data set can be found in Appendix IV. The analysis of the white micas has given lower than normal (c90%) oxide totals. Good analysis usually gives totals of 94-96% the rest being made up by water molecules. These lower totals could have been caused by one of two factors; the mica surfaces may not have been perfectly flat, causing dispersion of the electron beam, or the micas may have been slightly altered during transport to the basin. However the mica analyses are within acceptable limits and, because the main area of interest is the ratio of the cations, little error

**Table 4.3**

	GQ21M.2	GQ21M.6	GQ21M.9	GQ21M.1	GQ5M.3
SiO <sub>2</sub>	44.35	59.44	43.47	3.91	6.03
TiO <sub>2</sub>	0.12	0.44	0.11	0.30	0.26
Al <sub>2</sub> O <sub>3</sub>	36.93	19.63	37.22	37.94	35.39
Cr <sub>2</sub> O <sub>3</sub>	0.00	0.05	0.04	0.00	0.03
MgO	0.78	0.56	0.83	0.36	0.86
CaO	0.01	0.03	0.44	0.01	0.06
MnO	0.03	0.05	0.00	0.00	0.02
Fe <sub>2</sub> O <sub>3</sub>	0.90	0.90	1.35	0.85	1.03
FeO	0.14	0.14	0.21	0.14	0.16
Na <sub>2</sub> O	1.95	0.14	3.02	0.41	0.70
K <sub>2</sub> O	5.00	8.75	3.48	6.24	5.49
Total	90.21	90.13	90.17	90.16	90.03
Si	6.03	8.12	8.15	5.92	6.20
Ti	0.01	0.01	0.00	0.03	0.03
Al	5.96	3.12	3.06	6.18	5.74
Cr	0.00	0.01	0.00	0.00	0.00
Mg	0.12	0.11	0.11	0.07	0.18
Ca	0.00	0.00	0.01	0.00	0.01
Mn	0.00	0.01	0.00	0.00	0.00
Fe <sub>3</sub>	0.09	0.09	0.12	0.09	0.10
Fe <sub>2</sub>	0.02	0.02	0.02	0.02	0.02
Na	0.52	0.04	0.04	0.11	0.19
K	0.87	1.53	1.53	1.10	0.96
Total	13.62	13.06	13.04	13.52	13.43

**Table 4.3.** Representative white mica compositions. Cations per formulae based on 22 oxygens.  $\text{Fe}^{+2}/\text{Fe}^{+3}$  estimated by ratio (a full data set is given in Appendix IV).

would be produced by the slightly lower than normal totals (T. Dempster, 1994 pers. comm.).

#### 4.5.4 Geochemistry of the White Micas

The detrital white micas of the Guadalquivir Basin and Internal zone contain little paragonite. However, there is a significant variation between muscovite and celadonite compositions.

The data collected have been plotted on a modified Tschermak substitution diagram in which  $\text{Mg}+\text{Fe}^{2+}$  is plotted against the  $\text{Si}/\text{Al}$  ratio (Fig. 4.22). The data fall into two distinct populations. Micas taken from the Guadalquivir Basin, including the northern margin samples tend towards muscovite compositions, while micas from the Internal Zone tend towards celadonite compositions. Clearly the Internal Zone micas form a distinct population when compared to the Guadalquivir Basin micas. Therefore, it seems unlikely that the Guadalquivir Basin micas were derived from the Internal Zone. The micas from the Baena-Montilla region (southern margin) of the Basin plot in same group as those of the northern margin micas, implying a similar source. Metamorphic clasts found in northern margin fan deposits are thought to have been derived from Hercynian terranes (Juan Fernandez pers. comm.) and it is likely that the Baena-Montilla micas were also ultimately from this source. The southern margin of the Hercynian Massif is dominated by granitic batholiths, and large areas of country rock have been affected by contact metamorphism. This explains the tendency for white micas from this source to approach muscovite compositions since these are more stable at high temperatures. The white micas in the Guadalquivir Basin could have been derived either from granites and/or metamorphic rocks in the Hercynian Massif.

This hypothesis can be tested by age dating the Micas, as the Betic Orogen and Hercynian Massif contain rocks of radically different ages.

#### 4.5.5 Geochronology using Ar/Ar Dating Methods

$^{40}\text{Ar}/^{39}\text{Ar}$  dating relies on the same principle as  $^{40}\text{K}/^{40}\text{Ar}$  dating.  $^{40}\text{K}$  decays to daughter elements  $^{40}\text{Ca}$  and  $^{40}\text{Ar}$ .  $^{40}\text{K}$  occurs naturally in rocks and so the ratio of  $^{40}\text{K}/^{40}\text{Ar}$  and the half life allow the age of closure of the isotopic system (i.e cooling) to be determined.

$^{40}\text{Ar}/^{39}\text{Ar}$  dating takes advantage of this system. A sample is irradiated to transform a proportion of  $^{39}\text{K}$  to  $^{39}\text{Ar}$ .  $^{39}\text{K}$  is a stable isotope of K occurring naturally in rocks. Following irradiation, the  $^{40}\text{Ar}/^{39}\text{Ar}$  ratio is determined. The  $^{40}\text{Ar}$  is the radiogenic product of  $^{40}\text{K}$  and  $^{39}\text{Ar}$  is produced from  $^{39}\text{K}$  during irradiation of the sample. The  $^{40}\text{Ar}/^{39}\text{Ar}$  is proportional to the  $^{40}\text{Ar}/^{40}\text{K}$  ratio and so proportional to the age. This is so because  $^{39}\text{Ar}$  is dependent upon the amount of  $^{39}\text{K}$  present in the sample and the  $^{39}\text{K}/^{40}\text{K}$  ratio is essentially consistent in nature. To determine the amount of  $^{39}\text{Ar}$  produced during irradiation a standard sample of accurately known K-Ar age is irradiated with the unknown. The age of the unknown is derived by comparison with the  $^{40}\text{Ar}/^{39}\text{Ar}$  of the flux of the monitor standard.

The great advantage of  $^{40}\text{Ar}/^{39}\text{Ar}$  over  $^{40}\text{K}/^{40}\text{Ar}$  is that only one isotopic analysis is required and the technique can be performed on single grains via laser probe analysis. A full review of  $^{40}\text{Ar}/^{39}\text{Ar}$  isotopic dating techniques can be found in McDougall & Harrison (1988).

Single micas were hand picked from the processed samples. The grains were then washed ultrasonically in distilled water and placed in specially designed aluminium containers, which were irradiated at Michigan State University Reactor. The micas were dated at the Scottish Universities Reactor Research Centre, East Kilbride by P. McConville using  $^{40}\text{Ar}/^{39}\text{Ar}$  isotopic laser probe analysis, following methods outlined by McConville *et al.*, (1988) and Kelley & Bluck (1989;1992)



Before the results of  $^{40}\text{Ar}/^{39}\text{Ar}$  dating can be considered, the reliability of the samples must be assessed. K can be lost by alteration during weathering and this loss will affect the amount of radiogenic Ar produced and ultimately distort the age determination. Because of this it is necessary to assess the mobility of K within a grain. Mobile K is compared with immobile framework elements such as Al and K loss is reflected as low K/Al ratios (Kelley & Bluck, 1992).

To assess K mobility 4 grains, 2 selected prior to irradiation and 2 selected following irradiation, were traversed by a series of electron microprobe analyses, a total of 23 analyses. A mean K/al ratio of 0.35 was determined with a standard deviation of 0.025 (7.2%). The variation within each grain is similar to the variation observed for all four grains (Fig. 4.23) apart from one analysis which varied by 0.065 (18.5%). This probably reflects an analysis taken close to a crack or cleavage plane. Overall, the population of K/Al ratios has a common composition and there is no evidence for significant K loss before or after irradiation. Based on this, the chance of analysing an area that has experienced K loss is less than 10% and so the isotopic ages are considered reliable.

In addition to the analysis for K loss, the mica grains have also been examined with a scanning electron microscope using back-scattered imaging. No zoning or compositional variation was observed. However the detrital grains are probably fragments of larger grains and these may have been compositionally zoned. On the basis of this mica population it is impossible to assess compositional variation within the original grains.

Due to difficulties during the irradiation of the samples, only a few grains could be accurately analysed. The results of these analyses (Table 4.4) may have been subject to hydrocarbon contamination, the probability of which is reflected in the larger than normal errors assigned to the analyses in Table 4 (P. McConville pers. comm.).

Because few mica ages were obtained and because the analyses may be subject to errors the results can only provide a very general indication of the range of ages for the Guadalquivir Basin mica population.

The ages determined for the micas vary between 1302 Ma. and 250 Ma. Even when large errors are taken into the account these are much older than the oldest metamorphic rocks recognised in the Betic Orogen, which are 85-65 Ma. (Bakker *et al.*, 1989; Molne *et al.*, 1989). However, the Hercynian Massif contains Pre-Cambrian to Carboniferous rocks. (Martinez Garcia *et al.*, 1986). Thus, if the mica isotopic ratios are a reflection of actual ages

then grains can only have come from the Hercynian Massif.

**Table 4.4**

Sample	Isotopic Age	Air Corrected Age	Fraction Radiogenic
GQ6	535 ± 28	251 ± 82	43%
GQ6	481 ± 17	328 ± 46	65%
GQ9	681 ± 47	263 ± 126	34%
GQ9	1224 ± 15	250 ± 45	66%
GQ9	1224 ± 34	1152 ± 42	92%
GQ14	961 ± 42	475 ± 73	43%
GQ21	1195 ± 58	267 ± 90	17%
GQ21	391 ± 24	270 ± 81	41%
GQ37	1316 ± 34	1302 ± 35	99%

**Table 4.4.**  $^{40}\text{Ar}/^{39}\text{Ar}$  ages (in Ma.) for individual detrital micas. Monitor J value=0.01211. Background correction on  $^{39}\text{Ar} \leq 30\%$ .

#### 4.5.6 Source of Metamorphic Detritus

In conclusion, the micas in the Guadalquivir Basin are geochemically distinct from those originating from the Internal Zone of the Betic Orogen. Micas in the Baena-Montilla region (southern margin) of the Basin are geochemically similar to micas found in northern margin fan deposits which are believed to have been derived from the Hercynian Massif. Isotopic dating, despite its unreliability, also suggests derivation from the Hercynian Massif as opposed to the Betic Orogen. In the final analysis it seems much more likely that the metamorphic detritus originated from the Hercynian Massif rather than from the Betic Orogen.

#### 4.6 Conclusions

Provenance data can be ambiguous and conclusions based on one method should be treated with some scepticism. However, the provenance of the Guadalquivir Basin sediments has been analysed using a variety of independent techniques and these results lead to the same conclusions:

- (1) Sedimentary rocks from the northern margin of the Basin are petrographically distinct from those in the Baena-Montilla region (southern margin). The northern margin rocks are dominated by metamorphic lithic clasts while those from the Baena Montilla region are dominated by sedimentary carbonate lithic clasts.
- (2) Within the Baena-Montilla region (southern margin) of the basin there is no difference between sedimentary rocks in the autochthon and those in the allochthon both are characterised by marls and calc-lithic arenites.
- (3) Sedimentary lithic clasts in the Guadalquivir Basin were mainly derived from the External zone and from within the Basin itself but with possible additions from the Hercynian Massif. This conclusion is supported by petrographic data, by conglomerate clast surveys and by palaeocurrent analysis.

- (4) It seems likely that metamorphic detritus was ultimately derived from the Hercynian Massif and is mainly concentrated along the northern margin of the basin. Little of this reached the southern margin (Baena-Montilla area) of the basin.
- (5) There is no evidence for the contribution of detritus from metamorphic rocks in the Internal Zone of the Betic Orogen.

Much of the sedimentary lithic detritus in the Guadalquivir Basin is believed to have been derived from the External Zone. Prior to its conversion to a foreland fold-thrust belt the External Zone formed part of an extending passive margin flanking the southern margin of the Iberian Plate. Presumably, the passive margin basin could have received detritus from the Hercynian Massif that formed part of the Iberian plate. Metamorphic detritus could have been subjected to recycling, first being deposited on the passive margin and then passed from the External Zone to the Guadalquivir Basin. During the recycling from the External Zone to the southern margin of the Guadalquivir basin, the northern margin of the basin would still have been receiving detritus directly from the Hercynian Massif. By this processes an asymmetric metamorphic detritus signature would have been generated across the basin, with the northern margin receiving metamorphic detritus directly from the Hercynian Massif while the southern margin mainly received sedimentary detritus with some recycled metamorphic fragments from the External Zone.

In the final analysis, three main sources of sediment have been identified, for the Mlocene of the Guadalquivir Basin the Hercynian Massif to the north, the External Zone to south, and detritus recycled from within the Guadalquivir Basin itself. Figure 4.24 is a provenance model for the Guadalquivir Basin which takes into account provenance data and the palaeogeographic reconstruction given in Chapter 3 (Fig. 3.45)

# ***Chapter 5***

## ***Status of the Guadalquivir Basin (a synthesis)***

---

**CHAPTER 5: STATUS OF THE GUADALQUIVIR BASIN****(a synthesis)****5.1 Previous Interpretations**

The Guadalquivir Basin has previously been interpreted as a foreland basin that formed as a foredeep in front of the Betic Orogen fold thrust belt (Martinez del Olmo, 1984; Suarez Alba *et al.*, 1988; Sanz de Galdeano and Vera, 1992). During thrusting the southern part of the basin is considered to have developed on top of the northward translating thrust sheet as a series of satellite basins (Roldan-Garcia, 1991). These basins are classified as 'piggy back' basins following the scheme of Ori & Friend (1984). The implication of these models is that the arrival of the orogenic wedge caused the downwards flexure of the Iberian Plate in front of it, creating a trench.

However, this interpretation of the Guadalquivir Basin as a 'Foreland Basin' is largely on the basis of its geographical position with respect to the orogenic thrust front. Under the classification scheme of Bally & Snelson (1980) the use of location alone is considered inadequate. Accurate classification must take into account lithospheric behaviour during basin formation.

**5.2 Characteristics of a Foreland Basin**

Important to the considerations of foreland basins are the criteria by which they are defined and the evolutionary patterns of sedimentation in them.

**5.2.1 Definition of a Foreland Basin**

A Foreland basin is most simply defined as a sedimentary basin lying between the front of a mountain chain and an adjacent craton (Allen *et al.*, 1986). However, this definition is based purely on geographical location and in addition many authors have implied distinct mechanisms of formation. To include this the definition can be extended to:

'a foreland basin is a basin that develops in front of an active orogenic belt as the response of flexurally competent lithosphere to loads applied during the emplacement of thrust sheets and to loads transmitted from the subduction zone.' (Waschbusch & Royden, 1992).

Foreland basins can be subdivided on the basis of the type of collisional margin (i.e. continent-continent or continent-oceanic) and lithosphere involved. The type of lithosphere is critical to basin formation, since the degree and rate of flexure and thus the rate of basin subsidence is dependent on the competence of the lithosphere being loaded (Watts and Cochran, 1974; Beaumont, 1978; Molanar, 1988; McNutt & Kogan, 1988).

Although this is reasonably clear, confusion has arisen in defining foreland basins from inferring geographical, geometrical or mechanistic properties in a single term. The failure to separate such properties has led to ambiguous definitions.

In order to remove this ambiguity, definition must be separated into two parts, generic and mechanistic. In the generic part the geographical location and overall geometry of the basin are important and in the mechanistic part it is the means by which the basin formed that is important. Generically, a foreland basin must be situated between the front of a mountain chain and adjacent craton and must display asymmetry with the deepest part of the basin lying immediately in front of the mountain chain (Fig. 5.1). In order to satisfy the mechanistic part of the definition, this geometry must have been brought about by the downward flexure of the lithosphere in response to the translation of the orogenic front on to the foreland (Beaumont, 1981)

Classic examples of basins that satisfy this definition can be found in the Molasse troughs of the Alpine Chain (Homewood *et al.*, 1986; Pfiffner, 1986; Puigdefabregas, 1986) the northwestern Himalayan Foredeep (Johnson *et al.*, 1986) and the Appalachian and Rocky Mountain basins of North America (Tankard, 1986).

The Guadalquivir Basin is evaluated in the light of this discussion.

### 5.2.2 Evolution of a Foreland Basin

Once a foreland basin has been identified, the history of the basin fill is critical to the understanding of the evolution of the basin and the tectonic history of its orogenic wedge.

The development of a foreland basin can be divided into two distinct phases related to the emergence of the translating fold thrust belt. During the 'pre-emergence stage' the subsiding foredeep is flanked by a submarine thrust belt and its clastic supply is typically derived from a distant or extra-orogenic source (Fig. 5.2). In the second 'post-emergence stage' the thrust belt itself becomes a major sediment contributor (Fig. 5.3). In Alpine foreland basins these stages are characterised by distinct phases termed 'flysch' and 'molasse' respectively (Hsu, 1970; Van Houten, 1974; Mitchell & Reading, 1986). Unfortunately these terms have become confused as they have been used for both lithofacies and tectonofacies. This situation has arisen because the early flysch stage of deposition is often caught up in the thrust tectonics of the later stages of basin evolution, as in the northern Apennine Basin, Italy (Ricci Lucchi, 1986). It is contended here that the terms should be restricted to lithofacies, but these need not be restricted to foreland basins. Essentially, the flysch stage is characterised by turbidites deposited in deep oceanic water. By contrast, the classical Alpine molasse forms at a later stage as the thrust belt emerges and is characterised by continental and shallow water deposits (Dzulinski & Smith, 1964). In the northern Apennine Basin the molasse is mostly the product of re-sedimentation into deeper water but is still thought to reflect emergence of the fold-thrust belt (Ricci Lucchi, 1986).

The geometry of a foreland basin is largely controlled by the rate at which the orogenic thrust belt is translated onto the foreland. In the simple case, such as the northern Alpine Molasse Basin (Homewood *et al.*, 1986), thrusts stack up on the margin of the basin and there is little migration of the depocentre (Fig. 5.4). If the thrust front migrates onto the foreland the basin may become divided and form a complex series of minor basins (Fig. 5.5), often on top of the translating thrust sheets. These are termed piggy-back basins (Ori & Friend, 1984). By this means a foreland basin can become divided into autochthonous and allochthonous

units as the depocentre migrates across the foreland..

In most cases, during deposition of the molasse the foreland basin is fed by the orogenic wedge stage and in the very last stages may become filled by metamorphic detritus from the internal orogen. By tracing the heavy mineral assemblage in the molasse deposits it may be possible to determine the unroofing history of the orogen itself.

### 5.3 Stratigraphical Considerations of the Guadalquivir Basin

Before the status of the Guadalquivir Basin can be assessed there several important stratigraphical considerations that need to be highlighted.

There is some variation in defining the base of the sequence which forms the Guadalquivir Basin. The Lower Miocene Marls (Fig. 2.2) at the base of the succession are regarded as the continuation of sedimentation in the External Zone by Roldán-García, (1985a,b) and Blankenship (1992). These rocks are considered to have been deposited on an extending passive margin (García Hernández *et al.*, 1980; Blankenship, 1992) destroyed by compressional tectonism during the Oligo-Miocene Betic orogeny.

Alternatively, Sanz de Galdeano & Vera (1992) suggest that the lower Miocene was deposited in part of a marine basin, the North Betic Strait, that was separate from both the External Zone passive margin sequence and the Guadalquivir Foreland Basin sequence. The Miocene succession was subdivided into these two separate basins (the lower Miocene North Betic Strait and the Upper Miocene Foreland Basin) on the basis of tectonic style and presence or absence of olistostromes (Sanz de Galdeano, 1992).

However, data presented in this thesis demonstrates that the Lower Miocene rocks of the Guadalquivir Basin were separated from those of the Oligocene External Zone by an important compressional deformation that resulted in substantial subaerial relief (Chapter 2, section 2.8). Therefore the lower Miocene Marls are distinct from sediments of the External Zone.

In this thesis the olistostromes are considered to be tectonic melanges associated with post-Messinian thrusting (see Chapter 2, section 2.4) and the Lower Miocene marls are separated from the Tortonian clastic rocks by an unconformity considered to have been generated by a eustatic sea-level fall rather than by a major tectonic event (see Chapter 2, section 2.7). Therefore there is no major tectonic break between the Lower and Upper Miocene parts of the Guadalquivir Basin. These data indicate that there cannot have been two distinct basins. If the Guadalquivir Basin is a foreland basin, as many suggest, then it seems likely that the Lower Miocene marls represent the 'pre-emergence' flysch stage and the Upper Miocene deposits the 'post emergence' molasse.

In conclusion, the Miocene Guadalquivir Basin, as defined here, formed in a compressional regime which was distinct from the extensional system that characterised the External Zone. The fill of the Basin is considered to have been relatively continuous, and punctuated only by unconformities generated during eustatic sea-level falls, as opposed to tectonic interactions.

## 5.4 Status of the Guadalquivir Basin

Before the Guadalquivir Basin can be classified in the Bally & Snelson (1980) scheme it must be determined whether or not it satisfies the generic (geography and geometry) and mechanistic criteria for the definition of a foreland basin as outlined in section 5.2.

### 5.4.1 Geographical Location and Geometry of the Basin

The Guadalquivir Basin is situated between the External fold thrust belt of the Betic Orogen and the cratonic Iberian Massif. In cross-section it appears to have a 'classic' foreland basin geometry. To highlight this similarity the cross-section of the Basin (derived in Chapter 2) can be compared with a cross-section across the Northern Apennine Basin (Fig. 5.6). Both basins can be subdivided into an allochthon and an autochthon and each is characterised by thrusting and 'olistostrome' or 'melange' type deposits (Fig. 5.6).

The fill of the Guadalquivir Basin is typical of fills in other foreland basins (Miall, 1978). Initial basin formation (Lower Miocene, Fig. 2.2) was characterised by sedimentation in deep oceanic waters (Chapter 3, section 3.3) equivalent to the 'pre-emergence flysch' deposits in other Alpine foreland basins (Labaume *et al.*, 1985, Ricci Lucchi, 1978). The sediments of the basin fill shallowed up through the Miocene, culminating in shallow-water and continental fluvial deposits (Fig. 2.2) equivalent to 'post emergence' molasse-stage deposits in Himalayan and Alpine foreland basins. (Perkash *et al.*, 1980, Houten, 1974). This transition from 'flysch' to 'molasse' is typical of many foreland basins (Allen *et al.*, 1986) although the Palaeozoic foreland basin of Quebec (Hiscott *et al.*, 1986) and the Cretaceous-Tertiary Magallanes basin of South America (Biddle *et al.*, 1986) remained essentially deep-water throughout their history.

The clastic deposits of the Guadalquivir Basin, which first appeared in the Tortonian, were derived from the External Zone fold thrust belt (Chapter 4, sections 4.4 & 4.6; Fig. 4.24). The arrival of clastic rocks is interpreted as reflecting the time when the External Zone fold-thrust belt became sub-aerially exposed and it marks the beginning of the 'post -emergence' (molasse) stage of the basin

Thus, the Guadalquivir Basin is a foreland basin in the 'generic' (geographic and geometric) sense and the fill is typical of many foreland basins. However, there are some important features that distinguish it from other foreland basins.

The location with respect to the orogenic wedge is far from clear. Balanced cross-sections, derived from seismic refraction data, (Banks & Warburton, 1991; Figure 6) show that the Guadalquivir Basin lies 50 Km from the orogenic wedge, close to the flexural bulge (Fig. 5.7). There is no evidence for the development of a Miocene basin immediately in front of the orogenic wedge where most subsidence due to lithospheric flexure would have occurred (Allen & Allen, 1990, page 99, section 4.2).

The basin fill is remarkably thin, less than 1 km. Of this fill, less than 150m is clastic (Chapter 3) none of it is derived from the metamorphic rocks of the internal orogen (Chapter 4, section 4.5). This is unusual when compared to other foreland basins which may contain between 1.5 Km and 6 Km of sediment, a large proportion of which is clastic and derived from the orogen (Allen *et al.*, 1986). Most foreland basins start as deep-water troughs in which



topography is relative subdued and sediment delivery rates low, leading to an under-filled basin (Miall, 1978). In later stages, as the fold-thrust belt emerges, rapid erosion leads to the rapid filling of the basin by orogenic material, some of which is of metamorphic origin. This rapid filling stage was never achieved in the Guadalquivir Basin, which appears to have been maintained as an under-filled basin throughout its history.

In the Banks & Warburton (1991) cross-section (Fig. 5.7) the Guadalquivir Basin is hardly detectable, manifesting itself as a thin cover of sedimentary rocks resting upon the detached External Zone. When the Basin is compared with the scale of the Orogen it appears considerably smaller than a Foreland Basin would be expected to be.

#### 5.4.2 Mechanism of Formation of the Guadalquivir Basin

Critical to the definition of a foreland basin is the mechanism by which it forms. A foreland basin develops in response to subsidence brought about by flexure of the lithosphere during its loading by an orogenic wedge. Consequentially, the foredeep of a foreland basin develops immediately in front of the orogenic fold thrust belt where subsidence is at its greatest (Fig. 5.8). This process takes place during compression brought about by the collision of two plates causing the orogen to be driven onto the foreland or flexing lithosphere (Allen *et al.*, 1986).

However, the Guadalquivir Basin did not form during the compressional phase of the orogen, but during its extensional phase (see Overview, Section 1.4). Hence, the Basin formed on the margin of an extending orogen. Extension in the internal part of the orogen manifested itself as thrusting at its margins in the External Zone and Gibraltar Arc Flysch (Platt & Vissers, 1989; page 543 & Fig. 6). Seismic refraction data suggest that the External Zone is a thin skin thrust belt with a fundamental detachment 8-10 Km below the top of basement (Banks & Warburton, 1991, page 280). The implication is that during extension in the Internal parts of the orogen thin slices of the External Zone were driven onto the Iberian Craton. This is shown in Figure 5.7 (Banks & Warburton, 1991).

A key question which now arises is whether enough material was emplaced on to the Iberian Massif during extension within the orogen to cause lithospheric flexure. Flexure may have occurred during compression of the orogen, but this ended in the Oligocene, before the formation of the Guadalquivir Basin. There is no evidence to suggest that a foreland basin existed before this time. It seems unlikely that the emplacement of material by thin skinned thrusting could have produced sufficient load to cause significant flexure of the lithosphere and basin subsidence. However, this requires the detailed modelling of the response of the Iberian Plate to loading by thin skinned thrust slices, and this is beyond the scope of this thesis.

When the position of the Guadalquivir Basin in relation to the flexural bulge is taken into account the question of flexure or non-flexure becomes irrelevant. Subsidence due to flexure decreases with distance from the orogenic belt (Kominz & Bond, 1982; 1986) and is almost negligible near the flexural bulge (Fig. 5.8). Indeed there is likely to be uplift on the flexural bulge rather than subsidence (Fig. 5.8)

Because of the involvement of orogenic extension, the loading of the Iberian Plate by thin skinned thrusting, and the position of the Guadalquivir Basin relative to the flexural

bulge, it is unlikely that basin subsidence was caused by lithospheric flexure during orogenic loading. Some other mechanism must be sought for the formation of the Guadalquivir Basin.

#### 5.4.3 Classification of the Basin

While the Guadalquivir Basin is 'generically' a foreland basin it is unlikely to have formed by the flexural response of the lithosphere to orogenic loading. Thus, by definition the Basin cannot be considered to be a true foreland basin. This makes classification of the basin under the Bally & Snelson (1980) scheme extremely difficult. Essentially it is a perisutural basin on rigid lithosphere associated with the formation of a compressional megasuture and so falls into type 2 basins of Bally & Snelson (1980) (Table 1, Overview). However it is not a trench or a foredeep and does not fall into the sub-classes of type 2 basins. The problem with the classification scheme is that it does not take into account the peculiarities of the Betic Orogen and its history of extension.

Indeed there is the difficulty of whether or not this sequence can be considered to have formed in a true basin at all. The Guadalquivir Basin is really just a fragment of thin cover of sedimentary rocks over the External Zone and flexural bulge of the Iberian Massif (Fig. 5.7). This cover formed as the External Zone, once an extending passive margin, was converted to a fold-thrust belt by compression at the edge of an extending orogenic welt. It may be that the Basin merely represents the final stages of the 'rolling up' of a passive margin sequence during the extension of an orogen.

In the final analysis, the Guadalquivir basin is almost impossible to classify using existing schemes, but it is certainly not a true foreland basin. It is considered to be a unique product of the peculiarities of the Betic Orogen and its formation.

### 5.5 Model for the Formation of the Basin

The Guadalquivir basin formed as part of an extending orogen, where the extension in the Internal Zone produced compression in the outer margins of the orogen (Fig. 5.9). The initiation of extension in the Internal Betic Zone is dated as 27-24 Ma. (Overview, Fig. O.4) which coincides with the compression and subaerial exposure of the External Zone (Chapter 2.8). The karst surface, formed as a result, represents the base of the Guadalquivir Basin succession which then developed during the Miocene.

Before the formation of the Guadalquivir Basin, rocks of the External Zone were deposited on an extended continental margin of Triassic terrestrial red beds and evaporites (see Overview, section 1.3). The External Zone formed as a series of grabens (see Overview, Fig. O.3). These have previously been interpreted as having been broken up by thrusting induced by compression as the African Plate accreted onto the Iberian margin (Garcia-Hernandez, 1979; Banks & Warburton, 1991; Blankenship, 1992). However, sedimentation in the External Zone is known to have continued into the latest Oligocene and maybe into the Lower Miocene without significant change in the basin configuration (Blankenship, 1992; Roldan Garcia *et al.*, 1985a,b). The earliest metamorphism recorded in the Internal Betic rocks is Cretaceous and compression is known to have continued through the Palaeogene (see Overview, Fig. O.4) during which time the External Zone maintained its profile. The first

compressional event in the External Zone is not recorded until the latest Oligocene (Chapter 2, section 2.9) the time when extension of the orogen was initiated. Thus, the passive margin basins were broken up and thrust onto the Iberian Massif during compression induced by extension of the Internal parts of the orogen.

The suggestion here is that the Passive Margin was not significantly influenced by tectonism in the Betic area until extension within the orogen was initiated. This implies that the orogenic wedge was not driven onto the Iberian margin during the Palaeogene compressional phase and that loading of Iberia did not take place until after extension had occurred. During extension Iberia was loaded by thin slices of detached External Zone rocks, but this load was probably insufficient for flexure of the lithosphere. If the loading of Iberia only took place during thin skinned thrusting, then this explains the absence of a foreland basin on the Iberian plate.

There is strong evidence that the Internal Zone of the Betic orogen did not generate sub-aerial relief during the Miocene as 1km of Miocene marine marls are found unconformably overlying metamorphic rocks of the Internal Zone (Rodriguez Fernandez, 1993; Fig. 3). Platt & Vissers (1989; page 543) suggest that the Betic orogen subsided below sea-level in response to crustal thinning during Miocene extension. It has been suggested that the Betics of southern Spain did not generate any sub-aerial relief until late Miocene or early Pliocene times (Bluck & Hughes pers. comm.). If this is correct then the lack of metamorphic detritus in the Guadalquivir Basin is explained since at the time of formation of the Guadalquivir Basin metamorphic rocks of the Internal Zone would have been covered by a marine basin.

In the final analysis it appears that the Guadalquivir Basin formed as an integral part of the destruction of the Iberian Passive margin during extension of the internal parts of the Orogen. Thin skinned thrusting generated a basin on the margin of the External Zone. The fill and unconformities of this basin were controlled by eustasy rather than tectonic incursion (Chapter 2, section 2.7) and clastic sedimentation by the emergence of External Zone thrust sheets during the late Miocene. The final thrusting event in the External Zone disrupted the Guadalquivir Basin succession and led to its division into the autochthon and allochthon seen today. This model is summarised in Figure 5.10 and provides a working hypothesis for discussion in Part III of this thesis.

# **PART II**

# **THE GIBRALTAR ARC**

# **FLYSCH BASIN**

*At first sight it looks like a sphinx, crouching on the waters edge,  
her hindquarters resting in Europe he head gazing over the sea  
and her forepaws stretching in front of her to form the most  
southerly part of our continent*

Alexander Dumas describing Gibraltar in 1846

***Chapter 1***  
***Introduction &***  
***Tectono- Stratigraphic***  
***History***

## Chapter 1: Introduction

### 1.1 General Geological Setting

The Gibraltar Arc is formed from a series of thrust nappes which link the External Rif of North Africa to the External Zone of southern Spain (Fig. 1.1). The Flysch nappes are generally referred to as the 'Campo del Gibraltar Complex' (Olmo-Sanz *et al.*, 1987; Fontbote *et al.*, 1986; Sanz de Galdeano & Vera, 1992) and make up a large part of the Gibraltar Arc. The Flysch deposits extend from Ubrique in the North to Tarifa on the southern peninsula of Spain.

The Flysch Nappes have been subdivided into numerous tectono-stratigraphic units, the largest of which is the Aljibe Flysch (Fig. 1.1) with a minimum stratigraphic thickness of 1400m (Olmo-Sanz *et al.*, 1987). It is this unit that is the subject of this part of the thesis. The Aljibe Flysch can be further subdivided into the Beneiza Flysch and the Aljibe Arenites (Fig. 1.2) which are of Oligo-Miocene age (Chauve, 1960; Didion, 1969)

The Beneiza Flysch is composed of arenites, limestones and marls that are interpreted as having been deposited as turbidites during the Oligocene (Olmo-Sanz *et al.*, 1987). The Aljibe Arenites, dated as Lower Miocene (Chauve, 1961; Didion, 1969), are composed of thick bedded quartz arenites and are characterised by graded bedding, planar lamination, convoluted lamination, dish structures, pillow structures and other water escape features (Bourgois, 1978; Olmo-Sanz *et al.*, 1987).

### 1.2 Previous Interpretations

The 'Campo del Gibraltar' complex which includes the Aljibe Flysch is considered to have originated from materials deposited in an Oligo-Miocene North Africa Flysch Trough that lay S-W of the present position of the Flysch (Sanz de Galdeano & Vera, 1992). Bourgois (1978) reported that the Aljibe Arenites were subject to important re-sedimentation processes during the Burdigalian, resulting in the formation of tectono-sedimentary units. The North African Flysch Trough was subsequently displaced westward during Miocene thrusting that is interpreted to have been induced by the extensional collapse of the Betic Orogen (see Part I, Chapter 5, Fig. 5.9) (Platt & Vissers, 1992)

### 1.3 Study Area

The Aljibe Flysch has been studied in two areas (Fig. 1.1), in the Cortes del Frontera region (study area 1), and in exposures found on the southern coast of Spain (study area 2). In the Cortes region a series of transect were made across the Flysch nappes (Figs. 1.4-1.6) and the resulting logs form the basis of this study. The coastal area provided excellent exposures of sedimentary structures in wave washed rocks. All location numbers refer to the locations given in Figures 1.4-1.6 and a sample of the logs generated from the transects is given in Appendix III.

## **Tectono-Stratigraphic History**

### **1.4 Cross-Section**

An E-W cross-section, located on Figure 1.3, drawn for the Cortes region (Fig. 1.7) incorporates data from published maps (Olmo-Sanz et al., 1987), the thrust transects (Figs. 1.4-1.6), the logged sections (Chapter 2) and other field observations.

#### *1.4.1 Description*

The cross-section features a series of thrust units. The eastern portion of the cross-section is characterised by nappes of Alpujarride and Malaguide rocks belonging to the Internal Zone (metamorphic rocks) of the Betic Orogen. The central sector contains deformed but unmetamorphosed Sub-Betic rocks belonging to the External Zone of the Betic Orogen. A full review of the Internal and External Zones of the Betic Orogen is given in the Overview (Section 1.3). The western portion of the cross-section consists of the Aljibe Flysch nappes, which form a series of imbricate thrust nappes (Fig. 1.8). Where the Malaguide rocks are found in tectonic contact with the Sub-Betic External Zone they form a series of upright, vertical beds. This zone is referred to as the Dorsal Zone (Olmo-Sanz et al., 1987) and consists of both Internal Zone and External Zone rocks together with thin slices of Flysch.

The axial traces of the folds and of the thrust contacts trend north-south and the dominant transport along the thrusts is interpreted to be to the West.

The Alpujarride, Malaguide, Subbetic, External Zone and Aljibe Flysch Units are separated by low angle tectonic contacts. No stratigraphic contacts have been observed between any of these units in the Gibraltar Arc. Thrust nappes in the Flysch are cut by a series of normal faults and in places the Flysch is down-faulted against Subbetic External Zone rocks. The thrust contacts are often characterised by thin slices of Triassic deposits that contain evaporitic horizons, particularly between the Flysch and Sub-Betic, External Zone Units (Fig. 1.9).

#### *1.4.2 Interpretation*

The low angle contacts between the tectonic units have been interpreted as being low angle detachment faults (Doblas & Oyarzun, 1989, Fig. 2, page 432; Platt & Vissers, 1989). It has been suggested that these are the product of extension during the diapiric rise of peridotites (Doblas & Oyarzun, 1989) which formed a core-complex flanked by a series of low-angle detachments (Fig. 1.10). Thrusting was generated within the Flysch Units as they were detached from the core complex peridotites and moved westward. The main zone of detachment, as in other parts of the Betic Orogen, appears to be in Triassic evaporite deposits which belong to the External Zone. The implication here is that, prior to this extensional event the Flysch Unit covered the External and Internal Zones of the Betic Orogen, extending eastwards past its present location

### **1.5 Stratigraphic Evolution**

The Flysch deposits are completely detached from their basement forming highly allochthonous units and stratigraphical contacts are only preserved within the nappes. As a consequence, the true stratigraphical relationship between the Flysch deposits and the External/Internal zones is unknown. Within the Flysch the Beneiza Flysch is conformably overlain by the Aljibe Arenites (Fig. 1.2). Other Flysch units in the Campo del Gibraltar complex form thin thrust slices between the Aljibe Flysch and the Sub-Betic External Zone units or Dorsal Zone. These units are so fragmented that it has been impossible to determine their true stratigraphical relationship with the Aljibe Flysch.

### **1.6 Conclusions**

The Gibraltar Arc is formed by a series of highly allochthonous units that have been thrust westward during extension related to the diapiric rise of a Peridotite core zone. The true stratigraphical relationship between the Aljibe Flysch and other tectonic units has not been observed, but it is thought that, prior to detachment, the Flysch formed a sedimentary cover that blanketed the Internal and External Zone rocks of the Betic Orogen.



***Chapter 2***  
***Sedimentology &***  
***Palaeogeography***  
***of the***  
***Aljibe Flysch***

## Chapter 2

### Sedimentology & Palaeogeography of the Aljibe Flysch

#### 2.1 Introduction

The Aljibe Flysch is the largest tectono-sedimentary unit found within the 'Campo del Gibraltar' complex (Fig. 1.1). This unit is formed from a series of imbricate flysch nappes that extend across the central sector of the Gibraltar Arc, from Algeciras in the south to Ubrique in the north, covering approximately 3000 Km<sup>2</sup>.

For the purposes of study the Aljibe Flysch unit can be divided into two distinct stratigraphical units, the Late Oligocene Beneiza Flysch, and Early Miocene Aljibe Arenites (Fig 1.2).

A series of E-W logged transects has been constructed for individual nappes of the Flysch deposits (Figs. 1.4-1.6). These form the framework for detailed sedimentological and palaeogeographical studies of the Aljibe Flysch and its sub-units.

#### 2.2 The Beneiza Flysch

The Late Oligocene sub-unit of the Aljibe Flysch is made up of monotonously bedded siltstones, sandstones, and mudstones of unknown total stratigraphical thickness (minimum 5 m.).

##### 2.2.1 Description

This sub-unit consists of thin (< 20cm) siltstones and tabular fine grained sandstones intercalated with marls (Fig. 2.1). Petrographically the sandstones are quartz and lithic arenites (Fig. 2.2). The lithic fragments are dominated (>70%) by sedimentary fragments and of the sedimentary lithic clasts more than 90% are carbonate lithic grains. The remaining lithic fragments are metamorphic or highly altered fragments.

The bounding surfaces of the tabular beds are planar with occasional sole markings. A simple ichnofauna may be found on bed surfaces which is most commonly entirely the branching form *Chondrittes* (Fig. 2.3). Internally the beds display convolute lamination, cross lamination or planar lamination but may be structureless (Fig. 2.4). Typically the sedimentary structures form complete or partial Bouma sequences. The complete Bouma sequence (Fig. 2.5) is composed of sole markings at the base of a massive or graded bed (A), passing upwards into planar laminated, convolute laminated or structureless sandstones (B), ripple cross lamination (C), planar lamination (D) and finally structureless siltstones (E).

In the Beneiza Flysch, of a total observed 137 upward-fining beds, only 13% displayed the complete Bouma sequence (A->E) the rest displaying partial sequences (Fig. 2.6). The most common partial Bouma sequence (46% of observed beds) included massive graded bed with sole marks passing into convolute lamination or planar lamination (A->B) and the sequence A,B,C was obtained in only 18% of beds.

### 2.2.2 Interpretation

Bouma sequences and partial Bouma sequences are typically observed in turbidite-deposited sediments (Walker 1967). Classically turbidites are characterised by repetitive interbedded sandstones and shales with planar tops and bases (Walker, 1984; page 172). No scouring or channelling occurs on the bases of such beds on a scale greater than a few centimetres. The sandstones tend to have sharp bases that grade upwards into fine sandstones, siltstones and mudstones, and the undersides of the beds may bear sole markings. Turbidite-deposited beds contain a combination of parallel lamination, ripple cross-lamination, convolute lamination and graded bedding (Walker 1967; Mutti & Ricci Lucchi, 1972, Walker 1978) which can ideally be described by a Bouma sequence.

The Beneiza Flysch sub-unit conforms to this general description of classical turbidites and the presence of complete and partial Bouma sequences suggests that it was deposited by turbidity currents. Turbidity currents are density currents of suspended sediment and water that flow downslope, driven by gravity acting on the density difference between the flow and the surrounding water mass (Walker, 1984). Such currents are known to operate in a wide range of environments, ranging from lakes and reservoirs to deep marine environments. Micropalaeontological analysis of the Beneiza Flysch (Chauve, 1960; Didion, 1969) suggests that deposition took place in deep oceanic waters.

## 2.3 The Aljibe Arenites

### 2.3.1 General Characteristics

The Aljibe Arenites represent the Lower Miocene sub-unit of the Aljibe Flysch tectono-sedimentary unit. This sub-unit has a stratigraphical thickness of 2-3Km and is composed of thick (up to 10 m) sandstones interbedded with marls and siltstones. Petrographically the sandstones are fine, medium and coarse grained quartz arenites, with more than 98% of the framework being well rounded quartz grains (Fig. 2.7). Sandstone beds may coarsen or fine upwards (Fig. 2.8). Internally the sandstones generally appear to be massive, except where exposed in wave washed rocks in coastal sections (Study Area 2; Fig 1.1) in which they are dominated by complex sediment fluidization structures (see 2.3.6). Rare planar cross-stratification, trough cross-stratification, planar lamination and bioturbation are also present in the sandstone beds.

### 2.3.2 Logged Transects

Two detailed logged transects have been constructed across a single folded thrust nappe (Fig. 1.5). These transects have been taken through opposite limbs of a syncline and utilize the Beneiza Flysch/Aljibe Arenite transition (Oligo-Miocene boundary) as the datum. Transect 2 (locations 40-50) is approximately 3000m long and Transect 3 (locations 58-65) is approximately 1500m long. The logged transects are summarised as lithological logs in Figures 2.9 & 2.10, full logs are given in Appendix III.

In Figures 2.9 & 2.10 the lithologies are divided into sandstones, heterolithic intervals and marl intervals against which sandstone bed thickness and sand percentage have been

plotted. Heterolithic intervals include thin sandstones and siltstones interbedded with marls in which the sandstones are no more than 3cm thick. Where sandstone beds are thicker they are classified as sandstones rather than being included in heterolithic intervals. The percentage sandstone has been calculated from the percentage sandstone per metre, and each metre interval has been overlapped by 25cm so that they reflect running averages. The logged transects contain considerable intervals of non-exposure as indicated on Figures 2.9 & 2.10.

In total 248 sandstone intervals have been observed within the logged transects and these have a minimum thickness of 3cm and a maximum of 900cm. The average thickness is 66cm with a standard deviation of 102cm. A total of 132 heterolithic and marl intervals have been observed with a minimum thickness of 1cm and a maximum of 1200cm with an average thickness of 60cm (standard deviation of 124 cm). In the logged transects the total observed sandstone interval thickness is 221m and the total observed thickness of heterolithic and marl intervals is 79m giving a sandstone/heterolithic ratio of 3:1. However, this ratio may be distorted due to the fact that the heterolithic intervals are less well exposed than the sandstone intervals.

Each logged section can be subdivided into a series of coarsening/thickening-up cycles 2 -30m thick. Cycles are shown in Figures 2.9 & 2.10 numbered as C1, C2, C3....etc. Cycles are more difficult to identify where they are cut by areas of non-exposure. Typically the bases of cycles are marked by dark grey marls, which pass into heterolithic intervals and then thick bedded sandstones. A few of the identified cycles appear to fine/thin upwards, notably cycle C16 in transect 3 (Fig. 2.10), but these are much rarer in comparison to the more normal coarsening/thickening up cycles. Within the cycles individual sandstone intervals, interpreted as being beds, most commonly fine upwards, although some may also coarsen upwards (Fig. 2.8). Grain sizes in these intervals range from fine sand ( $\phi$  3) to micro-conglomerates ( $\phi$  -1). Individual sandstone beds may have planar or erosional bases the latter with a relief of up to 50cm. No large-scale channels have been observed. The sandstone beds logged in Study Area 1 (Fig. 1.1) generally appear massive with rare examples of cross-stratification, trough cross-stratification, parallel lamination bioturbation and water escape structures. However, in wave-washed rocks in coastal exposures (Study Area 2; Fig. 1.1) they appear to be dominated by complex water escape features with primary depositional structures, such as cross-stratification, largely obscured.

These logged transect are typical of the Aljibe Arenites exposed throughout the Gibraltar Arc and the arenites show a surprising lack of facies variation over this wide area.

#### *2.3.4 Description of the Sedimentary Structures*

While the logged transects include sandstones that appear massive and structureless, wave washed surfaces of the same rocks exposed in coastal sections show a complex range of sedimentary structures. The structures are similar to water-escape structures described by Lowe (1975). Because of this similarity, the structures in study area 2 can be classified according to the scheme of Lowe (1975) which resolves water escape features into six basic types; dark laminae, dish structured laminae, convolute laminae, pillars, sand mounds and

diffuse structures.

*Dark laminae*; are mm (< 0.5cm) scale laminae which are picked out by heavy minerals clays and micas forming characteristic dark streaks. The dark laminae are often overlain by lighter bands of quartz and feldspar up to 5cm thick. The laminae vary from planar or gently undulating to complex 'stylolite' type laminae (Fig. 2.11).

*Dish structured laminae*; are formed by laterally discontinuous concave-upwards laminae (Fig. 2.12). The dishes are generally 2-5cm in section and are often separated from each other by vertical pillars. The dishes vary from gently undulating (Fig. 2.12) to deep, upward curving dishes 4-5cm deep (Fig. 2.13), termed mega-dishes by Lowe (1975). Dish structures are commonly associated with dark, flat laminae and pillars separate mega-dishes. Dishes are often found in fine medium grained sandstones that overlie massive coarse grained (micro-conglomerate) sandstones (Fig. 2.14).

*Convolute laminae*; are folded and deformed laminae picked out by concentrations of heavy minerals and clays. Convolutions range in scale from a few centimetres to metres. Three types of convolute lamination can be recognised; simple overturned folds (Fig. 2.15), diapirs (Fig. 2.16) and disrupted diapirs (Fig. 2.17).

*Overturned folds*; are simple fold structures characterised by steeply inclined, overturned synforms and antiforms. These are similar to sedimentary slump structures described by Helwig (1970) and Woodcock (1976).

*Diapirs*; are mushroom shaped convolutions that emanate from a point or pillar. Diapirs often contain pillars in their cores and can be stacked to form series.

*Discontinuous diapirs*; are those where the lamination becomes discontinuous and fragmented at their tops. (Fig. 2.17).

*Pillars*; are elongate and often diffuse streaks of massive, lighter coloured sand 1cm to 175cm high (mean height 20cm, with most being between 0-20cm). Five types of pillars can be recognised and classified according to the scheme outlined by Lowe (1975);

*Type A pillars*; are those associated with mega-dishes, forming between the upward curving margins of the dishes, these are generally small, less than 2cm in height (Fig. 2.18).

*Type B Pillars*; are unrelated to dishes and range from a few millimetres to metre scale. These may be straight or sinuous, or may bifurcate (Figs. 2.19, 2.20).

*Type C pillars*; are diffuse lenticular streaks, the free-surface pillars of Lowe (1975). They are associated with the upper layers of beds, where bedding surfaces can be interpreted (Fig. 2.21).

*Type D pillars*; are narrow irregular streaks 1-5cm in diameter. On the surfaces of the beds they form en-echelon sets (Fig. 2.22). Type D pillars have been termed stress pillars by Lowe (1975).

*Type E Pillars*; are intrusions or large dykes 10-30cm wide and up to 3m in length (Fig. 2.23). These are rare, and usually cross-cut other sedimentary structures. The margins of the intrusions are often picked out by concentrations of heavy minerals on bed surfaces. These intrusions may terminate as sandstone mounds on bedding surfaces.

*Other pillars not classified by Lowe (1975);*

1. Pillars of coarse sand that often appear to be downwards penetrating (Fig. 2.24).
2. Pillars found in the cores of diapirs (Fig. 2.25).

*Sand mounds*; are formed where intrusions break bedding surfaces (Fig. 2.26). Such mounds are commonly surrounded by concentric rings of heavy minerals.

*Diffuse Streaks*; are zones of complete mixing of dark and light sandstone, giving a mottled appearance (Fig. 2.27). Horizons of this type lack other well developed structures and are up to 70cm thick and laterally continuous for more than 10m.

### 2.3.5, The Idealised Sequence of Structures

The structures are not randomly distributed but are ordered into distinct sequences to form repeating cycles. A typical sequence is shown in Figure 2.28 from which an idealised sequence can be constructed (Fig. 2.29).

In this ideal sequence (Fig. 2.29) the base is marked by coarse grained (micro-conglomeratic) sandstone with or without convolute fold structures (A). This basal horizon passes up into dark laminae (B) which give way to dish structured laminae (C). At higher levels the dishes are commonly replaced by mega-dishes, usually associated with Type A pillars (D). The larger pillars of this horizon may develop into diapirs (E) and additional pillars are commonly found in the cores of the diapirs. The top of the sequence is marked by fine to medium grained sandstone in which free surface (Type C) pillars or diffuse streaks can be found (F).

While this ideal sequence is common in the Aljibe Arenites there are dramatic variations from the ideal cycle. Any part of the sequence A,B,C,D,E,F may be missed out (i.e A,B,E,F). Common variations include coarse sandstone passing directly into sandstones with Type B pillars or dykes (Fig 2.30) into which the coarse sandstone may be injected (Fig. 2.30). Other sequences may include only pillars passing into convolute diapirs (Fig. 2.31) or dishes passing directly into diapirs and missing out the pillar/mega-dish (D) stage (Fig. 2.32).

The larger pillars and dykes commonly cross-cut other water-escape structures. Many horizons contain only diffuse streaks and other structures cannot be recognised. Any of the structures described may be deformed, either overturned (Fig. 2.33) or folded into more complex features.

### 2.3.6 Heterolithic Intervals

The heterolithic intervals between the sandstone beds also display complex convolute structures (Fig. 2.34). They commonly show folding and faulting, injection structures such as small dykes, and complex sediment-mixing patterns (Fig. 2.34). The siltstones and mudstones of the heterolithic intervals often mix with the bases of overlying sandstones forming indistinct gradational boundaries. Overall the heterolithic intervals are rarely preserved as laminated or well bedded sediments and almost always display water escape structures.

### 2.3.7. Interpretation of the Sedimentary Structures

The structures described are identical to features described by Lowe (1975) which are interpreted as water escape structures.

Water-escape is the process by which water is expelled from sediments as they become consolidated during compaction. Water-escape most commonly occurs in sediments that are rapidly deposited to form a loosely packed sediment with a high porosity containing interstitial water (Nicholls *et al.*, 1994). Rapid deposition and loose packing is most commonly associated with the proximal parts of deep sea fans, with areas around the mouths of channels and with overbank deposits (Lowe, 1975; Allen, 1982).

The early consolidation of sediments involves a processes of fluid escape during which time the grains become more tightly packed. Fluid escape occurs by three basic mechanisms; seepage, liquefaction and fluidization, the interaction of these leads to the formation of the complex range of water escape structures.

Seepage is the slow movement of fluid through a sediment, and is the most common mechanism by which water is expelled from sediments (Lowe, 1975). It involves the slow upwards percolation of water in response to the pressure gradient induced by sediment loading. Seepage does not account for the formation of water escape features, unless flow rates are high, in which case a fluidized or liquefied state is approached (Lowe, 1975).

During liquefaction the grains are temporally suspended in response to a sudden increase in fluid flow rates and pore pressure. Following rapid suspension the sediment almost immediately begins to settle back through the fluid to re-establish the grain framework (Lowe, 1975). During this process a sudden loss of shear resistance is experienced by the sediment during which time it is easily deformed and 'slump' structures such as convolute folds may form. During liquefaction water-escape structures may form during the initial temporary fluidization stage and water escaping from liquefied beds may fluidise higher sedimentary layers. Beds that have undergone liquefaction are characterized by sandstone dykes, sand volcanoes and extrusions that are commonly found in association with slumps and mass flow structures (folds and convolute lamination).

A sediment becomes fluidized when the grains are suspended for longer periods by the upwards movement of pore fluids. By this processes the sediment is transformed from a body of granular material into a fluid-like state. Fluidization is likely to occur in coarse grained silts and sand sized material, while coarser sands and gravels and finer silts generally de-

water by seepage. Coarse sands and gravels are highly permeable and water escapes readily, preventing the high fluid pressures necessary for the high fluid velocities that cause fluidization from being established. Where coarse grained material is subject to higher fluid velocities the grains are often too heavy to be lifted and suspended (Lowe, 1975). Fine grained silts are relatively impermeable and as a result the movement of pore water is prevented (Lowe, 1975). If the fluid follows preferred escape paths, perhaps taking advantage of inherited weakness, the surrounding sediment will quickly become consolidated by losing water to the fluidization channel (Lowe, 1975). Where such fluidization channels form, convection cells of fluidized material may be set up (Kunii & Levenspiel, 1969).

Often there is no clear distinction between liquefaction and fluidization as there is a transition from one process to the other. Where fluidized horizons develop the surrounding sediment may become liquefied. As fluid velocities decrease a fluidized horizon may be converted to a liquefied horizon as the grains settle out to re-establish the grain frameworks. Lowe (1975) also infers that an initial but temporary period of fluidization is required to suspend grains in order to bring about the liquefaction of a sediment.

The process by which individual water-escape structures form, has been described in detail by Lowe (1975), and these explanations, with some modification, can be applied to water-escape structures in the Aljibe flysch;

*Dark laminae*; reflect the presence of horizontal fluidization paths where the fluid is forced to flow horizontally by the presence of permeability barriers. Micas and clay minerals become concentrated along the boundaries of the fluid channels. The concentrations of these minerals are enhanced if the fluid seeps into the sediment adjacent to the pathway. During seepage the more mobile grains, such as micas and clays, approaching the channel boundaries are sucked into the pores of the surrounding sediment, where they become trapped. This has the effect of further reducing the permeability of channel walls, and thus may serve to maintain fluidization longer.

In addition to clays and micas, dark laminae may be formed by heavy minerals. As the lighter and more mobile grains such as quartz and feldspar are fluidized the heavier, less mobile grains may settle out, accumulating below the lighter coloured fluidization paths (Lowe, 1975).

Elutriation may also play a part in segregating grains. Upwards escaping fluids move lighter minerals upwards, but heavier minerals may not be fluidized, and in effect behave as if liquefied, settling out from the main fluidized flow. By this process heavy minerals can settle through the fluid as the lighter minerals remain suspended and rise. If a denser, less permeable, layer is encountered by a rising fluid the denser layer may settle through the fluid as cohesive bodies (Nicholls *et al.*, 1994). If the upward flow decelerates the previously suspended, lighter, minerals also begin to settle. Thus, in irregular flows, where decelerating flows are common, bands of heavy or coarse material overlain by finer grained lighter material may form. This is important, because observed upward-fining cycles may actually be the products of intense water escape rather than reflecting primary depositional processes.

*Dish structures*; Lowe (1975) suggested that dishes form by the subsidence of sediment over the central parts of horizontal flow paths. In experiments, dishes have been observed



to form as denser material settles through a fluidized horizon (Nicholls *et al.*, 1994). Increased fluidization velocities lead to an increase in the curvature of the dishes as subsidence becomes more pronounced. The upwards-curving margins of the dishes form discontinuities where fluidization can be concentrated and it is at these points that horizontal flow is converted to vertical flow and pillars form. Further growth of the pillars may bend up the edges of the dishes, leading to more pronounced curvature and the formation of mega-dishes.

*Convolute laminae*; Diapiric structures have been produced experimentally by the gravitational deformation of layers of silicone, in which underlying lighter silicone rises and denser overlying silicone sinks (Ramberg, 1981). A similar process has been observed by Nicholls *et al.* (1994) in which non-fluidized layers sink into fluidized layers. Thus, fluidized sediment may rise up through a denser non fluidized layer, with flow usually initiated at a discontinuity. As the fluidized layer rises and the denser layer sinks the fluidized material may expand into overlying layers. The descending pillars observed in the Aljibe Arenites probably record the downward movement of non fluidized layers into the fluidized horizons. During diapiric expansion the flow velocity is reduced as the flow becomes less confined and sediment may begin to settle out. Once the fluidized flow is reduced to allow liquefaction to take over the expansion of the diapir stops allowing it to be preserved. If the expanding diapir reaches a less dense layer, or discontinuity, the fluidized mass may suddenly expand into the surrounding sediment, rupturing the top of the diapir. Diapirs may also periodically pinch off from the main body of the fluidized sediment, forming discreet rising bodies of material or a series of 'stacked diapirs'.

*Pillars*; Models for pillar growth have been developed by Lowe (1975). Pillars grow where horizontal fluidization is converted to vertical fluidization. This commonly occurs at discontinuities where fluidized sediment can be concentrated. This concentration results in the rapid growth of the pillars which propagate by erosion of the overlying sediment. During propagation the pillars may bifurcate. Lowe (1975) suggested that where a pillar of rising fluid reaches a permeability barrier a convection cell may be set up in which the elutriation of heavy minerals can take place. The precise mechanism by which different types of pillars form is more fully outlined by Lowe (1975).

*Sand mounds*; Where large intrusions (pillars) break through and extrude fluidized sediment onto the surface of a bed, sand mounds form. Mounds formed in this manner are referred to as sand volcanoes (Lowe, 1975; Nicholls *et al.*, 1994). In the Aljibe Arenites these are preserved on bedding surfaces as mounds surrounded by concentric rings of concentrated heavy minerals. Lowe (1975) suggested that heavy minerals are rolled up the sides of the conduits supplying the volcanoes, although this has never been proved experimentally. Concentric rings, such as those seen surrounding mounds in the Aljibe Arenites, may suggest several periods of activity of the volcanoes. Lowe (1975) cited this as evidence for the replenishment of interstitial water at depth.

*Total sediment mixing*; is represented by diffuse streaks. The layers containing these lack well defined structures and represent zones which have been completely fluidized. This requires large amounts of water, high fluid velocities and high permeability (Nicholls *et al.*, 1994)

### 2.3.8 Interpretation of the Idealised Sequence

The idealised sequence can be understood by considering the processes by which water escape is initiated and progresses. The following interpretation is based on the detailed account of the formation of water escape structures at different fluid flow rates given by Lowe (1975)

*Initiation*; While most sediments consolidate by gradual water seepage during compaction, some sedimentary units, such as those of the Aljibe Arenites, experience violent consolidation soon after or concurrent with deposition. Violent consolidation involves the expulsion of water by liquefaction and fluidization processes.

Rapid consolidation can be induced in two main ways; 1) by earthquake shock or 2) by rapid deposition leading to rapid loading and consolidation.

During earthquakes sediments with large volumes of interstitial fluid may become instantaneously liquefied, because of a change in packing of the grains. This releases water which may fluidize supradjacent layers.

The rapid deposition of sand and gravel initiates the consolidation of immediately underlying sediments. Water escaping from such layers may liquefy or fluidize supradjacent layers. Lowe (1975) considered loading consolidation a significant process that is much more common than initiation by earthquake shock. Loading consolidation is most profound where sands are dumped rapidly onto soft unconsolidated argillaceous substrates. The rate and magnitude of loading (and the corresponding fluidization velocities) bears a direct relationship to the depositional rate.

Heterolithic intervals (containing argillaceous material) in the Aljibe Arenites show evidence for significant water escape. It is suggested that these layers provided a significant proportion of the fluid responsible for the fluidization of the overlying sandstones. The base of the idealised sequence is commonly marked by coarse grained sediment and/or convolute folds. The coarse sands would have been highly permeable and would have thus acted as conduits for the transfer of water from the heterolithic strata to the fine and medium grained sands above, which would have been readily fluidized.

In other cases, water escaping from underlying layers may have first liquefied an immediately overlying layer. This would have reduced the shear resistance of the sediments so that the layer became prone to hydroplastic deformation. Subsequent folding of this layer squeezed out water which was added to the volume of fluid available for the fluidization of supradjacent layers (Fig. 2.37).

*Progress of consolidation*; Consolidation may progress in three ways; by slow seepage, by a gradual increase in fluid escape rates, or by a rapid increase in fluid escape rates followed by a gradual decline (Lowe, 1975). The idealised sequence (A,B,C,D,E,F; Fig. 2.29) can be best interpreted by considering the second case, that of the gradual increase of fluid escape rates.

In this scenario, water escaping from the lower layers of a sediment pile (i.e heterolithic intervals) would have been added to that contained in overlying layers. This would have resulted in an upwards increase in the volume of fluid available for fluidization and would be accompanied by an upward increase in fluid velocity as the water was expelled upwards

under increasing pressure. Flow would be enhanced by the consolidation of the lower layers, preventing the fluid from flowing back down through the sediment. Thus, the idealised water escape sequence (Fig. 2.29) represents a sequence of escape structures which evolve in response to upward increasing fluidization pressures and velocities.

Initially, at the base of the sediment pile, flat consolidation lamination begin to form and as the rate of fluid flow increases these laminae became more frequent and darker to form horizon B (Fig. 2.29). As the horizontal flow rates increase subsidence may occur over the horizontal flow paths leading to the formation of dishes between which small isolated pillars may appear (horizon C). At higher discharge rates, induced by the increasing volume of fluid, the flow becomes concentrated at local discontinuities (such as the margins of dishes). Where this occurs horizontal flow is converted to vertical flow, and the erosive propagation of pillars (horizon D) may occur. Upon reaching finer grained sediments, in the upper parts of the graded bed, the pillars may meet permeability barriers, and diapirs form which expand into the overlying fine grained sediment (horizon E). If the volume of fluid continues to increase the diapirs may rupture suddenly, releasing a large volumes of fluid into the uppermost layers. At this point complete fluidization may occur, leading to sediment mixing and the formation of the diffuse streaks (horizon F). Where the fluid breaks the surface of the bed, free surface pillars and extrusions form.

Where the fluidization velocity increases rapidly, rather than gradually, the dark laminae and dishes associated with lower fluid velocities may be missed out. The first structures seen may be dykes, pillars and diapirs. In extreme circumstances whole layers may become fluidized instantaneously or dykes, terminating in volcanoes, may form directly from the lower heterolithic or coarse grained intervals. Abrupt increases in fluid velocities are most common in finer-grained and clay-rich sands where permeability barriers are common (Lowe, 1975). Fluidization may not take place during initial compaction because of these low permeabilities. Increasing pore pressures during loading may lead to ruptures into which pore fluids rush. It is by this process that clastic dykes and sand volcanoes are thought to form (Lowe, 1975).

Large pillars and dykes often cut earlier fluidization structures and bedding surfaces. This suggests that initial consolidation and fluidization may leave a meta-stable framework with a large amount of residual pore fluid that cannot escape (Lowe, 1975). Continued consolidation and loading leads to increased pore pressures until a break occurs. The fluids then rush into the break and rapid fluidization leads to the formation of cross-cutting structures.

### **2.3.9 Inferred Rates of Deposition**

Water escape structures are known to form most readily in environments in which; 1) the episodic deposition of fine and medium grained sands, from aqueous currents of declining velocities takes place and 2) where alternate intervals of sand and mud are instantaneously deposited at an overall high mean sedimentation rate (Lowe, 1975; Nicholls *et al.*, 1994).

In Study Area 2 the Aljibe Arenites are composed of heterolithic intervals and sandstone horizons that are almost entirely dominated by water escape structures. Many

of the sandstone beds described from the logged sections (Appendix 3) appear to be normally graded, suggesting that they were deposited from currents with declining velocities. Little else about the mode of deposition can be determined as any primary depositional structures have been destroyed by water escape processes.

From the above observations and interpretations several facts about the rate of deposition and nature of consolidation can be deduced;

1) Abundant water escape structures are present in almost all of the sandstone beds exposed in study area 2 suggesting continuous rapid deposition for the Aljibe Arenites.

2) The largest cross-cutting dykes and pillars are less common than the early fluidization structures described in the idealised sequence (Fig. 2.35). This indicates that most of the fluid was expelled during initial deposition and that initial fluid transfer was extremely efficient.

The implication is that the arenites were deposited rapidly, from a source with a very specific sediment type, and that consolidation and water expulsion were, in effect, instantaneous.

#### **2.4 Beneiza Flysch to Aljibe Arenite Transition**

The boundary between the Beneiza flysch and the Aljibe Arenites, the sub-units of the Aljibe Flysch, can be directly observed in a road-cutting which is located on Fig. 1.1. Here the Aljibe Arenites have a sharp, non-gradational contact with the Beneiza Flysch (Fig. 2.36). Across the contact there is a dramatic change from thin bedded turbidites containing Bouma sequences to thick de-watered sandstones. There is no evidence for erosion of the underlying Beneiza Flysch along the base of the Aljibe Arenites.

#### **2.5 Interpretation of the Aljibe Flysch**

The Beneiza flysch is composed of thin sandstones that were periodically deposited from turbidity currents and thus represent moderate to low rates of deposition from a distal source. These are in contrast to the Aljibe Arenites which are dominated by thickly bedded sandstones that must have been deposited at sustained high rates.

Classical turbidites such as those of the Beneiza Flysch are associated with the distal parts of subaqueous depositional systems, most commonly submarine fans, fan deltas or basin plains (Bouma, 1962; Walker & Mutti, 1973; Hiscott, 1981, Walker, 1984.) Turbidity currents are initiated by the mobilisation of sediment in the more proximal parts of the depositional system, usually by mass movements such as slope failure and sediment slumping (Lowe 1976; Walker, 1978)

The proximal parts of these systems are dominated by mass flow deposits sustained by rapid sedimentation (Walker, 1978; Normark, 1978). Mass movements lead to the deposition of thick sand beds with a meta-stable grain framework and high water content. It is these beds, which are prone to liquefaction and fluidization that are responsible for initiating grain flows (coarse grained turbidites) which may evolve into classical turbidites

downslope (Lowe, 1976; Walker, 1984). As a consequence, sandstones that are dominated by water escape structures are interpreted as representing the transition between mass movement and turbidite deposits.

The micropalaeontological evidence (Chauve1960; Didion, 1969), and the fact that shallow marine and coastal deposits are absent, suggests that the Beneiza Flysch and Aljibe Arenites were deposited as part of a deep sea system in which rapid sedimentation, mass flow and turbidites all operated.

### 2.5.1 Deep Sea Depositional Systems

Deep water environments can be subdivided into three basic types; slope aprons, submarine fans and basin plains, each of which has a distinct facies architecture and spatial arrangement (Stow, 1992)

Slope aprons are deposited between the shelf break and basin floor. Deposition and erosion takes place on slopes of between 2-7°. Slope aprons may be constructive, building out into the basin plain by slope progradation (Piper *et al.*, 1976; Mullins *et al*, 1984) or destructive and dominated by slumping and sliding (Hill, 1984). Many slope aprons are cut by canyons which feed isolated lobes at the base of the slope (Carter, 1979). Overall upward coarsening sequences may result from distinct phases of slope progradation (Stow, 1992)

Where a slope apron develops on an active fault margin, very narrow thick sedimentary wedges may accumulate at the front of the slope as a result of confinement by down-faulting (Gawthorpe, 1986). Faulted aprons are dominated by slope parallel arrangements of coarse grained facies in which localised tectonic activity can produce fining upwards and symmetrical vertical sequences (Gawthorpe, 1986; Stow, 1992).

Submarine fans are distinctive and often isolated constructional features that form at the base of a slope where submarine canyons emerge (Stow, 1992) The radius of such features ranges from a few kilometres to tens of Kilometres. Submarine fans are complex systems in which distinct morphological elements can be recognised (Normark, 1978; Walker, 1978; Nilsen & Abbot, 1981, Piper and Normark, 1983). These elements have been reviewed by Stow (1992) and can be summarised as follows;

- a) Canyons and channels, tributary and distributary channels with meandering and straight segments, abandoned channels, half filled and buried channels.
- b) Irregular slumps, slides, and debris flow masses.
- c) Broad levees and lobes are found between the channels and build up at the ends of channels.
- d) Smooth current moulded interchannel and interslope areas dominated by turbidity currents.

These elements give rise to a complex facies architecture which includes debrites and conglomerates, thick bedded sandstones, slump structures, channelised sandstones and thin bedded turbiditic sandstones interbedded with shales (Ruiz-Ortiz, 1983; Piper & Normark, 1983; Prior & Bornhold, 1989).

Several fan types can be recognised, in which growth is controlled by slope morphology

and sediment supply. The end members of fan morphology are outlined by Stow (1992); *Radial fans* have a true fan morphology and develop from a single feeder channel. *Elongate fans* develop sub-parallel to the source area. They usually have an irregular upper fan dominated by slumping and complex networks of tributary networks. An elongate facies distribution develops with a high ratio of mud to sand. *Fan deltas* develop partly in shallow water and consequently contain proximal shallow water facies. Such fans also contain turbidites in their more distal portions.

Basin plains have a very gentle relief and often contain the distal portions of submarine fans. They include large areas of smooth or current modified sea floor dominated by thin turbidite deposited silts and fine sands. Two types of basin plain are recognised, undersupplied and oversupplied. Undersupplied basin plains are dominated by fine grained facies, siliciclastic and biogenic sediments with an overall thickness of less than 1 km. Oversupplied basin plains develop in tectonically active areas where syn-sedimentary faulting may take place. The basin plain is filled rapidly with sediments with mounded overlapping fill geometries and chaotic distributions of coarse and fine grained facies.

### 2.5.2 The Aljibe Flysch Compared to Deep Sea Depositional System

The Aljibe Flysch is characterised by what is an essentially simple facies architecture in which thin bedded turbidites (Beneiza Flysch) pass rapidly into thick bedded sandstones that were deposited at sustained high rates (Aljibe Flysch). The Aljibe Flysch lacks the facies diversity normally associated with fan deposits and lacks evidence of channels, interdistributary lobes, slump structures, or channel abandonment.

The Beneiza Flysch sub-unit is characterised by deposits similar to those found in distal parts of submarine fans or associated with underfilled basin plains where fine sands and silts deposited by turbidity currents are dominant. The Aljibe Arenites represent a thick accumulation of very rapidly deposited coarse sands, in which there is little facies variation. Such accumulations are most likely to have been deposited at the foot of slopes or in overfilled basin plains, where the basin is confined by active down-faulting. However, tectonically controlled deposits usually include large scale slump deposits, debrites and conglomerates which are absent from the Aljibe Arenites. In addition the channel systems that usually characterise the proximal parts of slope aprons are also missing.

There is a rapid transition from turbidites in the Oligocene Beneiza Flysch to rapidly deposited sandstones in the Miocene Aljibe Arenites. There is no evidence across this contact for the progradation that would be expected in a shift from distal turbidites to more proximal coarse grained sandstones. Also surprising is the fact that there is no facies common to both the Beneiza Flysch and Aljibe Arenites. The implication is that, across the Oligo-Miocene boundary there is a sudden and catastrophic change from a relatively quiet basin plain environment to one dominated by the rapid deposition of huge amounts of coarse grained sediment. If the Aljibe Arenites are a product of deposition in a tectonically confined basin then the Beneiza Flysch/Aljibe Arenites transition probably reflects the initiation of tectonic activity. At this time the basin plain was broken up by faulting. A large amount of sediment, that was originally deposited elsewhere, was mobilised and rapidly transported to the newly

created tectonically confined basin.

## **2.6 Conclusions**

In the final analysis it seems most likely that the Aljibe Flysch records the development of a basin plain that became tectonically segregated at the beginning of the Miocene. This tectonism created instabilities elsewhere which resulted in the mobilisation of large amounts of sediment. This was deposited in new tectonically confined basins in which a thick wedge of sediment with restricted facies accumulated.

However, this is problematic because there is no evidence for slumps, channels or conglomerates that would normally be associated with tectonically active deep sea basins. This doubt is further complicated by the fact that the Aljibe Flysch is now a highly allochthonous unit and, as a consequence, the configuration of the basement at the time of deposition is unknown. The relationship of the Aljibe Flysch to other tectono-sedimentary units is also unknown. Because the Aljibe Flysch can only be studied as an isolated tectonic sedimentary unit, any conclusions drawn must be treated as wholly speculative.

***Chapter 3***  
***Status of the Gibraltar***  
***Arc***



## Chapter 3

### Status of the Gibraltar Arc

#### 3.1 Interpretation of the Aljibe Flysch

The largest tectono-sedimentary unit of the Gibraltar Arc Flysch, the Aljibe Flysch Unit, records two distinct basinal phases. The Oligocene Beneiza Flysch sub-unit contains turbidites that were deposited in the distal portion of an open basin plain. By contrast the lower Miocene Aljibe Arenites represent the deposition of siliciclastic material into tectonically confined basins. The transition from the Beneiza Flysch to the Aljibe Arenites implies an important phase of basin re-configuration and, thus, may pin-point the occurrence of a major tectonic event at the beginning of the Miocene. Because the Aljibe Flysch is now highly allochthonous it is difficult to determine the precise nature of basin configuration by reference to the basin deposits alone. In order to fully understand the Gibraltar Arc Flysch Oligo-Miocene basins and place them in a meaningful tectonic framework it is necessary to determine;

1. The status of the crust prior to the creation of the Miocene confined basins.
2. The precise nature of the tectonic event that characterises the Oligo-Miocene boundary which is marked by the Beneiza Flysch-Aljibe Arenites transition.
3. The timing of thrusting that converted the Aljibe Flysch into the allochthonous Flysch Nappes that are observed in the Gibraltar Arc today.

#### 3.2 Status of the Crust Prior to Deposition of the Aljibe Arenites

The Beneiza Flysch is contemporaneous with Oligocene sediments of the Betic External Zone which represent sedimentation on an extended Iberian Passive Margin (Part I, Chapter 5.5). Sedimentation in the External Zones of the Betic Orogen is known to have continued into the latest Oligocene without significant change to the External Zone extensional basin configuration and it is suggested that the Iberian Passive Margin was not affected by Betic Tectonism until late Oligocene/early Miocene times (Part I, Chapter 5.5).

If the Beneiza Flysch is associated with deposition on the Iberian Margin then it is interpreted as deep-water sediments that were deposited on the distal portion of the Palaeogene Iberian Passive margin.

#### 3.3 Nature of the Oligo-Miocene Tectonic Event

It is generally accepted that extensional tectonism began in the Betics at the beginning of the Miocene (Overview 1.3.4; Fig O.4). This is supported by seismic sections constructed across the Alboran Sea which clearly demonstrate that the first sediments deposited in extensional basins are late Oligocene-early Miocene in age (Campillo *et al.*, 1992). Thus, it seems likely that the Beneiza Flysch/Aljibe Arenite (Oligo-Miocene) transition is coincident with the start of extension in the Betics. Extension resulted in the break up of the Iberian Passive Margin and the creation of confined extensional basins in the Gibraltar Arc region. Break up of the passive margin also led to the mobilisation of External Zone sediments (in this case mature arenites) that were rapidly transported to the newly created extensional basins.

There is no petrographic evidence for the deposition of material within the Aljibe Flysch derived from either the peridotites or metamorphic complexes that characterise the Internal Zone of the Betics. This suggests that they were not exposed during Lower Miocene times. Similar conclusions are drawn from provenance studies conducted in the Guadalquivir Basin (Part I, Chapter 4).

### **3.4 Timing of Thrusting in the Gibraltar Arc**

Thrusting of the flysch nappes clearly post-dates the deposition of the lower Miocene Aljibe Arenites. However, because these now form highly allochthonous units the precise timing of thrusting cannot be determined by reference to the flysch deposits alone. The timing and nature of the thrusting event will be discussed in the light of recent papers concerning the emplacement of the peridotites in Part III of this thesis.

### **3.5 Conclusions (A Model For Formation)**

The Aljibe Flysch (the largest tectonic unit of the Gibraltar Arc Flysch) records three distinctive phases of Betic tectonic history.

1. The Oligocene deposition of turbidites in the distal portion of the Iberian Passive Margin (External zones).
2. The start of extension in the lower Miocene led to the formation of confined basins into which sediment, mobilised from the Palaeogene Iberian Passive Margin, was deposited.
3. The Flysch units were subsequently thrust westward (post-lower Miocene).

This model has some important implications to the understanding of the evolution of the Betics. The history derived from the Aljibe Flysch is incompatible with the models of Platt & Vissers (1989) and Doblas & Oyarzun (1989) that are outlined in Chapter 1 (Introduction to the Gibraltar Arc) because;

1. The external Zone is unaffected by Betic tectonism prior to the start of extension in the Lower Miocene. Platt & Vissers (1989) model requires crustal stacking during the Palaeogene for which there is no evidence within the Mesozoic and Palaeogene succession of the Iberian Passive Margin. It is difficult to envisage how metamorphism of crustal blocks found in the Internal Zone could have taken place near the Iberian Margin without significantly affecting that margin.
2. Platt & Vissers (1989) and Doblas & Oyarzun (1989) suppose that extension and contemporaneous diapiric rise of the mantle (leading to peridotite emplacement) caused thrusting at the margins of the Betics. However, thrusting in the Gibraltar Arc clearly post dates the creation of extensional basins and actually leads to their destruction. In addition, the Flysch deposits contain no metamorphic or peridotite

detritus suggesting that during lower Miocene extension there was no exhumation of the peridotites or metamorphic core complexes.

The essence of the problem is that it is difficult to distinguish between the passive margin and extension that may have occurred during the building the Betic Orogen. It may be that the Aljibe Flysch, and other contemporaneous flysch units of the Gibraltar Arc, are unique in that they reflect the transition from a passive margin sequence to an orogenic sequence.

These problems will be further discussed in Part III of this Thesis where evidence from both the Guadalquivir Basin and Gibraltar Arc Flysch will be used to assess models proposed for the Betic Orogen. This will lead to the rejection of extensional collapse and simple core complex models and the consideration of alternative models.

# **PART III**

## **DISCUSSION:**

### ***The Significance of the Guadalquivir Basin and Gibraltar Arc Flysch to the Evolution of the Betic Orogen***

*"I am starting to see a bigger picture ,*

*I'm beginning to colour it in"*

Bigger Picture, the Waterboys, 1990

## **DISCUSSION: THE SIGNIFICANCE OF THE GUADALQUIVIR BASIN AND GIBRALTAR ARC FLYSCH TO THE EVOLUTION OF THE BETIC OROGEN**

### **1 Introduction**

Important insights into the tectonic history of the Betics, in particular Oligo-Miocene events, are recorded in the external basins of the Betic Orogen. They can be used to test the hypotheses which have been proposed for the tectonic evolution of the Betic Orogen. There is now a need to combine observations made in the External basins with data that have recently been published concerning the tectonic evolution of the Alboran Domain. Together these provide a unique insight into the Betic Orogen. A model must be sought to explain all of the data including those from the Betics collected by other workers, which may at first appear contradictory.

### **2 Tectonic History Derived From the Study of the External Basins**

The tectonic, sedimentary and palaeogeographic histories of the Guadalquivir Basin and Gibraltar Arc Flysch have been completely revised in this thesis. If these basins are linked to the Orogen then certain inferences can be drawn from the interpretation of these basins;

It has been demonstrated that the External Zones remained undisturbed throughout the Mesozoic and Palaeogene and were not affected by tectonic movements until the end Oligocene-early Miocene (Part I, Chapter 5.5; Part II, Chapter 3.2). The Mesozoic and Palaeogene rocks of the External Zone are known to have been deposited on an extended Iberian passive margin (Roldan Garcia, 1985a,b; Blankenship, 1992) which must have remained intact until latest Oligocene times .

The implication, derived from the re-interpretation of the external basins, that the Iberian margin was not significantly affected by Betic Tectonism until the early Miocene is problematic since the Internal Zone rocks were metamorphosed during Mesozoic and Palaeogene times (Egeler *et al.*, 1972; Bakker *et al.*, 1989; Monié, 1991; Zeck *et al.*, 1992; De Jong 1992). If metamorphism of these nappes took place on the Iberian Margin then it seems unlikely that the passive margin could have remained unaffected by the tectonism responsible for these metamorphic events. This will be discussed further in section 7 where terrane tectonism is considered as a possible mechanism in the building of the Betics.

It is generally accepted that the Betic Orogen was undergoing extension by the start of the Miocene (Overview, Section 1.4; Fig. 0.4). It has also been demonstrated that at the beginning of the Miocene the External Zone rocks (belonging to the Iberian passive margin) were subject to compression on their northern margin (Part I, Chapter 5.5), and to probable extension along their western margin (Part II, Chapter 3.3). This is interpreted as recording the break-up of the passive margin, which ultimately led to the formation of the Guadalquivir Basin in the north and to the formation of small confined extensional basins in the west (in the region now occupied by the Gibraltar Arc). Instabilities created in the External zone led to the mobilisation of sediment which was rapidly transported to the west and redeposited in the newly created basins (Part II, Chapter 3.3) Both basins have subsequently been subject

to compression and thrusting, resulting in the creation of allochthonous units. In the Guadalquivir Basin the thrusting is post Messinian (Part I, Chapter 2.8) while in the Gibraltar Arc it is post Lower Miocene (Part II, Chapter 3.4). The precise timing of these events is unknown, and it may be that the thrusting in both areas is tied to the same Betic compressional event, which would have been post Messinian (i.e. Pliocene).

It has been demonstrated that neither the Guadalquivir Basin nor the Gibraltar Arc Flysch contain detritus from the metamorphic rocks of the Internal Zone (Part I, Chapter 4; Part II, Chapter 2). This implies that the metamorphic blocks were not exposed or were not in their present positions during the depositional history of these basins. This suggests that the Internal Zones were exhumed or were emplaced into their present positions during the mid to late Miocene.

To summarise; it appears that the first major tectonic event did not take place in southern Iberia until the end of the Oligocene-early Miocene. This event was almost certainly extensional and at this time important new basins opened up along the northern and western margins of the External Zone. These basins were subsequently subject to compression which created allochthonous units. The timing of this compression is unclear, but it may have been late Miocene or even Pliocene.

The history derived from the Guadalquivir Basin and Gibraltar Arc Flysch can now be used to critically evaluate the conflicting hypotheses proposed for the Betic Orogen.

### **3 The Alboran Domain**

The understanding of the Alboran Domain (Fig. 1), which includes both the Alboran Sea and the Ronda peridotites is critical to the understanding of Betic tectonic history. Recent publications provide important clues concerning the history of the Alboran Sea and the related Betic tectonism.

There are two important pieces of evidence that must be discussed; The nature of the emplacement of the Ronda peridotites, and the interpretation of new seismic and bore hole data for the Alboran sea.

#### **3.1 Ronda Peridotites**

The outcropping Ronda peridotites are sub-continental upper mantle bodies emplaced within the Alpujarride units which are made up essentially of mid-crustal rocks recording Alpine metamorphism (Torné *et al.*, 1992; Grevillia & Remaidi, 1993). The peridotites are a suite of ultramafic rocks consisting mostly of lherzolites and harzburgites with minor amounts of dunites, pyroxenites, gabbros, and leucocratic dykes (Grevillia & Remaidi, 1993).

Classically, the peridotites are interpreted as having been exhumed by extension during diapiric upwelling of the mantle which produced the low angle detachments that characterise the Internal Betics (Doblas & Oyarzun, 1989; Part II, Chapter 1.4). However, this interpretation is questionable since it fails to explain how the peridotites became emplaced into mid-upper-crustal rocks. By contrast many authors have demonstrated that the mantle lithosphere slab was emplaced by large scale thrusting (Lundeen, 1978; Dickey *et al.*, 1979; Tubla & Cuevas, 1986, 1987; Balyana & García Dueñas, 1991). In addition the

thinning that has occurred in the Alboran Sea is considered to have been insufficient to be wholly responsible for the complete exhumation of the peridotites (Torné *et al.*, 1989.; Davies *et al.*, 1993; Tubia *et al.*, 1993).

Several models have been developed that better explain the emplacement of the peridotites, and these are critically examined below;

Torné *et al.* (1989) suggested that the peridotites were initially emplaced during the Palaeogene, coeval with the building of the Alboran domain. The peridotites were considered to constitute a slab of lithospheric mantle emplaced within units of the Alpujarride that rested on the Nevado Filabride units (Fig. 2), although how this was achieved is not made clear by Torné *et al.* (1989). The same model suggested that at a later stage crustal stacking, related to thrust stacking in the Gibraltar Arc and rifting in the Alboran sea unrooted and dismembered the peridotites, placing them in their present locations. While this model was an improvement on the purely extensional model of Doblas & Oyarzun (1989) it is still unsatisfactory because it is not clear how the initial phase of Palaeogene emplacement took place. Presumably if the mantle peridotites were emplaced above the Nevado Filabride unit then some process of thrust stacking is envisaged. A similar mechanism was suggested by Platt & Vissers (1989) who described the Palaeogene formation of a collisional ridge by crustal thickening. The emplacement of mantle bodies into the upper crust during the Palaeogene would have required considerable crustal reorganisation of the Iberian margin. However, this is inconsistent with data derived from the Guadalquivir Basin and Gibraltar Arc Flysch which clearly demonstrate that there was no major tectonic reorganisation of the Iberian Passive Margin during the Palaeogene (see section 2, this chapter).

Further progress in understanding has been made by Davies *et al.*, (1993) who used detailed petrographic and geochemical studies to support a model in which the peridotites formed above a subducting plate (Fig. 3). They considered that subduction took place during collision between Europe and Africa and that uplift at 85 Ma. uplifted the peridotites by an initial 150 km. In the absence of evidence for slow uplift of the peridotites, Davies *et al.*, (1993) considered that there was a tectonic hiatus between 80-25 Ma. This is a reasonable deduction as Sirvastava *et al.*, (1990a,b) and Roest & Sirvastava (1991) demonstrated that the main locus of plate boundary activity was in the Pyrenean trough and not between Africa and Iberia. At around 25 Ma. the plate boundary between Africa & Iberia became active again (Sirvastava *et al.*, 1990a,b) and Davies *et al.*, (1993) record a rapid uplift in the peridotites. They attributed this to slab detachment and emplacement of asthenosphere in the place of the subducted slab. This led to the rise of the crust, to lithospheric extension and nappe emplacement. Rapid cooling over the last 20 m.y. led to subsidence and the creation of the Alboran Sea (van Wees *et al.*, 1992).

By contrast Tubia *et al.*, (1993) have relied on the detailed structural analysis of the Gibraltar Arc and Alboran domain in order to produce a model for the emplacement of the peridotites. They have demonstrated that there is thinned continental crust above the Peridotites, suggesting emplacement by continental rifting. This extension is further supported by the presence of closely spaced isograds. During extension lower grade rocks were brought down against higher grade rocks. Tubia *et al.*, (1993) record stretching

lineations orientated to N110°E and a top to the E-S-E shear sense. It is suggested that the peridotites were uplifted by this extensional event and were subsequently emplaced into their present positions by thrusting. Lineations record a thrust transport direction to N70°E. The measured lineations are important because they suggest that extension and thrusting was sub-parallel to the trend of the Betics. If thrusting was produced by N-S convergence then the lineations should be perpendicular to the trend of the Betics.

Tubia *et al.* (1993) conclude that there were two tectonic phases involved in the emplacement of the peridotites, an early extensional phase (Fig. 4), and a later thrusting phase. The peridotites were first raised by extension, although they did not initially reach the surface. They were subsequently emplaced into the Gibraltar Arc by thrusting. Lineations oblique to the trend of the Betics are interpreted as indicating strike-slip tectonism. In this scenario extension is related to transtension and thrusting is related to transpression. Transcurrent tectonism is compatible with the strike-slip motion of Africa and Iberia from Jurassic to Tertiary times (Dewey, 1989). Overall this model is favoured by the data presented in this thesis because;

- 1 It is compatible with the tectonic history interpreted from the Gibraltar Arc Flysch basins. These record a phase of extension at the beginning of the Miocene followed by thrust stacking (Part II, Chapter 3). This model also places extension before compression, and this is compatible with the history deduced for the Gibraltar Arc (section 2, this chapter).
- 2 It explains the two phases of tectonism recorded by the Ronda peridotites, both of which are manifest both structurally (Tubia *et al.*, 1993) and petrographically (Davies *et al.*, 1993).
- 3 It does not require an initial Palaeogene compression and crustal thickening which, as is demonstrated throughout this thesis, is not recorded in the External Zone of the Iberian Passive Margin.
- 4 It is compatible with the strike-slip history recorded in the Alboran sea, outlined below.

### 3.2 The Alboran Sea

The Alboran sea is formed on continental crust thinned in a series of extensional grabens (Overview 1.3.3). The mechanism by which it formed has been the subject of some controversy, with many of the models proposed lacking the support of detailed structural data. Recently, Campillo *et al.* (1992) have deduced a tectonic history for the Alboran Sea from detailed seismic stratigraphy and bore hole data. The air gun profiles outlined by them represent the most detailed survey of the area to date.

Campillo *et al.* (1992) demonstrated that the first sediments deposited in the Alboran graben basins are of early Miocene age, indicating that extension was initiated at the beginning of the Miocene. Other workers have also concluded that extension started at the beginning of the Miocene (Overview 1.4; Fig O.4). This is consistent with tectonic histories derived for both the Guadalquivir Basin and Gibraltar Arc (Part I, Chapter 2; Part II, Chapter



3) which demonstrate that a major tectonic reorganisation took place at the beginning of the Miocene. Campillo *et al.* (1992) also described significant boundary parallel displacements along the northern and southern margins of the Alboran sea, indicating considerable strike-slip movements. Major decollements separate the sedimentary and Alboran Domain units from the underlying continental lithosphere and individualized complexed structures are recognized in the metamorphic nappes. From these observations a model of 'orogenic float', which favours the longitudinal transport of terranes along strike slip faults has been proposed, based on the models of Oldow (1990). Campillo *et al.*, (1992) deduced a detailed Miocene and Pliocene history for the Alboran sea incorporating the plate movement models developed by Sirvastava *et al.* (1990a). The principle elements of this are;

*Pre-Tortonian*, during the initiation of extension the western Alboran basins were created as a series of small deep faulted depressions. These are perhaps analogous the confined basins that believed to have formed during the break-up of the External Zone and in which the Aljibe Arenites were deposited (Part II, Chapter 3).

*The Tortonian* is marked by a series of transgressive deposits that onlap the structural highs. Normal faulting became active along the E & W boundaries of the Alboran Sea, while along the N-S margins transcurrent movements were predominant.

*The Messinian* marks a period of compressional tectonics and of global sea-level lowering. Transcurrent movements and extension occurred at the end of the Messinian.

*During the Pliocene*, transtensional movements resulted in the formation of small pull apart basins. Transtension continued throughout the Pliocene.

*During the Late Pliocene*, active strike-slip faulting also led to the formation of small pull-apart basins. The Alboran Ridge developed where such strike-slip faults were blocked by the development of positive flower structures (Campos, 1992)

*Finally in the Late Pliocene to Recent*, transtension was converted to transpression, resulting in structural inversions.

In summary, the Alboran Sea records transcurrent movements in which transtension, dominant in the Miocene, evolved towards transpression in the late Pliocene. In the Lower Miocene the formation of major decollements led to the strike-slip emplacement of metamorphic terranes.

The thrusting observed in the Gibraltar Arc (Part II, Chapter 3) has been dated as 'post Lower Miocene', but without an accurate control on its precise timing. It may be that the thrusting in the Gibraltar Arc and associated emplacement of the peridotites coincided with the change from transtension to transpression in the Pliocene, this, however, cannot be

proved from the data presented here.

#### **4 A Rejection of the Extensional Collapse Model**

The Miocene extension of the Betic orogen has previously been attributed to the collapse of an overthickened collisional ridge (Platt & Vissers, 1989). Such a model has formed the basis for the interpretation of data collected from the Betics by a number of workers.

However extensional collapse is incompatible with interpretations of the Gibraltar Arc Flysch, the Guadalquivir Basin succession and the Alboran domain, (see discussions above). These data and the reasons for rejecting the extensional collapse model can be summarised as follows:

**1** The extensional collapse model requires the presence of a collisional ridge prior to the onset of extension (Platt & Vissers, 1989). This implies that crustal thickening by thrust stacking occurred during the Palaeogene. However, data from the Guadalquivir Basin (Part I, Chapter 5), the Gibraltar Arc (Part II, Chapter 3) and observations made by García-Hernandez (1980) & Blankenship (1992) show that in the External Zone (part of the Iberian Passive Margin) sedimentation continued until the late Oligocene without significant disruption to the graben basin profile. There is no evidence for the disruption of the External Zone by compression during the Palaeogene and, therefore, it is unlikely that a collisional ridge formed prior the Miocene. At the end of the Oligocene or during the early Miocene the External Zone became disrupted by compression in the north (Part I, Chapter 5.5), and by extension in the west (Part III, Chapter 3.5). Both of these events coincide with the start of extension in the Internal parts of the Betics (Overview, Section 1.4). It is interpreted that the Iberian Passive margin became affected by Betic tectonism in the late Oligocene/ early Miocene. This movement was dominated by extension and therefore the first Betic event was extensional. There is no evidence for the pre-Miocene compression that would be required to build a collisional ridge.

**2** Data from the Ronda peridotites and Alboran Sea (section 3) suggest that Miocene extension was followed by a compression caused by the transition from transtension to transpression in an overall strike-slip regime. This interpretation is supported by observations made in the Gibraltar Arc which suggest that the formation of extensional basins during the early Miocene was followed by thrust stacking post-Mid Miocene (Part III, Chapter 3.5). This counters the extensional collapse model, which requires that thrust stacking occurred first and was followed by extension.

**3** The extensional collapse model does not adequately explain the major transcurrent movements that have been observed in both the Alboran Sea (Campillo *et al.*, 1992) and other parts of the Betic Orogen (Overview, Section 1.4.2).

Clearly the extensional collapse model of Platt & Vissers (1989) is inadequate for the Betic Orogen. There is a need for new, alternative models that take into account all of the

data collected from the Betics.

## 5 The Case for Strike-Slip Tectonism

There is a substantial weight of evidence for strike slip movements in the Betics. This can be found in the plate tectonic history, the observation of strike-slip faults and the presence of Alboran pull-apart basins and in palaeomagnetic rotations

### 5.1 Plate Tectonic History

The plate tectonic history deduced by Dewey (1989) and Sirvastava, (1990a;1990b) and outlined in the Overview (section 1.2) shows that from 27 Ma. Iberia rotated into Africa. Dewey (1989) reported that much of this movement was taken up by strike-slip faulting between Africa and Iberia. Stress fields derived from structural studies and outlined by Campillo *et al.* (1992) suggest substantial strike-slip movements along the southern border of Iberia during the Miocene. Roest (1990) also identified important strike-slip movements along the Azore-Gibraltar fracture zone, which is essentially the boundary between the African and Iberian plates.

### 5.2 Strike-Slip Faults

Andrieux *et al.* (1971) De Smet (1984) and Leblanc & Oliver (1984) have emphasised the importance of dextral strike-slip faulting in the Subbetic subzone of the External Zone. Leblanc & Oliver (1984) suggested that the Internal Zone-External Zone boundary is a strike slip contact that originally separated the Iberian plate from the African plate. Egeler & Simon (1969) also appealed to strike-slip movements as the main mechanism for the juxtaposition of the Nevado Filabride and Alpujarride thrust sheets, which have very different and contrasting structural and metamorphic histories.

The interpretation of recent seismic data from the Alboran Sea suggests that both the northern and southern margins of the Alboran Sea were dominated by strike slip tectonism during the Miocene and this eventually led to the formation of pull-apart basins in the Alboran Sea (Campillo *et al.*, 1992).

The evidence for strike-slip faulting has been largely ignored during the evolution of more popular models such as the extensional collapse (Platt & Vissers, 1989) and core-complex models (Doblas & Oyarzun, 1989). However, it is becoming increasingly difficult to ignore the accumulating weight of evidence for the presence of substantial strike-slip faulting in the Betic Orogen.

### 5.3 Palaeomagnetic Rotations

Platzman, (1992), Platzman *et al.* (1993) and Allerton *et al.* (1993) have all reported important palaeomagnetic rotations of structural blocks in the External Zone and Gibraltar Arc of the Spanish Betics and in the Rif Arc of north Africa. These rotations have occurred about vertical axes and are interpreted as reflecting movements on locally developed strike-slip faults.

Allerton *et al.* (1993) observed clockwise rotations of 200° since the latest Oligocene in the External Zone. Rotations are believed to have occurred during strike slip movements on

thrust boundaries. Allerton *et al.* (1993) suggested that rotations were a result of compressional deformation in the Betics induced by the oblique convergence of the African & Iberian margins. Compression and associated strike slip movements indicate a transpressional rather than a purely compressional regime.

Platzman (1992) and Platzman *et al.* (1993) recorded substantial rotation of structural blocks in the Gibraltar Arc and Rif Arc of Morocco. Clockwise rotations in the Gibraltar Arc contrast with anti-clockwise rotations in the Rif Arc.

Platzman (1992) rejected the hypothesis that the Betics developed in a zone of distributed dextral strike-slip, because in such a situation the rotations should be consistently counter-clockwise and they are not. Counter-clockwise rotations cannot be reconciled with a model of dextral strike slip.

Platzman (1992) pointed out that clockwise rotations in the north and counter clockwise rotations in the south could be accounted for if there were a strike slip emplacement of a microplate. This envisages the westward movement of an independent Alboran microplate which indented the margin of Africa (Andrieux *et al.*, 1971; Leblanc & Oliver, 1984; Boullin *et al.*, 1986). Andrieux *et al.* (1971) proposed that this westward movement was accommodated by right-lateral displacement along the northern boundary of the Alboran Sea and by left-lateral movement along the southern margin. This is consistent with the large strike faults observed along these margins (Campillo *et al.* (1992). However, Platzman (1992) rejects this model firstly on the grounds that at the tip of the plate indenter (in the region of the Gibraltar Arc) there should be no rotation, whereas there is a rotation, and secondly because the Alboran Sea has a non-rigid plate-like character and lacks a definable mechanism to drive the plate. This conclusion is made despite the fact that the rotation of Africa into Iberia may actually supply a plate-driving mechanism.

Platzman (1992) favours a model in which structural blocks are rotated as they are detached during the extensional collapse of an elongate collisional ridge, appealing to the model of Platt & Vissers (1989). Extensional collapse is interpreted to have produced dextral shear and clockwise rotations north of the ridge and counter clockwise rotations south of the ridge (Fig. 5).

However, while Platzmans' (1992) model is appealing, it fails to explain the formation of major strike-slip faults on the northern and southern margins of the Alboran Sea and also fails to take into account the oblique convergence of Africa and Iberia. Furthermore there is (as already highlighted) difficulty with the extensional collapse model since there is no evidence for the thrust stacking required for the formation of a collisional ridge prior to the Miocene extension.

In conclusion, there is a wide variety of geological data suggesting that strike-slip tectonism is an important mechanism in the formation of the Betic Orogen. Some of these may be incorporated in an extensional collapse model (Platzman, 1992). However, extensional collapse requires the formation of a collisional ridge prior to extension. There is no evidence, in either the external basins or the Alboran Sea, of a collisional ridge in southern Iberia existing prior to the initiation of extension.

## 6 The Betics as a History of Transtension-Transpression

Several workers, through the use of single-grain radiometric dating techniques, have identified repeated cycles of compression and extension in the metamorphic nappes of the Internal Zone.

De Jong *et al.* (1992) used  $\text{Ar}^{40}/\text{Ar}^{39}$  dating of single phengite grains to identify periods of extension and compression in the Nevado Filabride rocks of the Internal Zone. They also used step heating methods to identify a minimum age of cooling of 30 Ma. This event was followed by a series of local resetting events at 17-19 Ma., 13-15 Ma. and 8-10 Ma. which were each coeval with volcanism in the eastern Betics. These events are interpreted as reflecting periods of crustal and sub-crustal extension. Two further ages at 18.5 Ma. and 21.5 Ma. are interpreted to represent periods of overthrusting separating the main extension events.

Thus, the Miocene records a complex history of extensional and compressional episodes and not the simple conversion from thrust stacking to extension suggested by Platt & Vissers (1992). The history of repeated extension and compression is consistent with a strike-slip model, similar to that proposed by Tubia *et al.* (1993) and by Campillo *et al.* (1992) in which strike-slip is manifest as either transtension or transpression depending on the precise orientation of the transcurrent stress field at the time.

It is well known that suture zones form ideal strike-slip boundaries (Sylvester, 1988) in order to accommodate horizontal plate motions. Examples of strike-slip suture belts can be found in the Indo-Eurasian collision (Fitch, 1972; Karig, 1980; Tapponier *et al.*, 1986) and in the Semangko fault system, northern Sumatra (Page *et al.*, 1979; Hla & Maung, 1987). Orogen-parallel strike-slip faults are particularly well developed in present subduction arc complexes characterised by oblique convergence (Fitch, 1972; Oxbrugh, 1972; Saleeby, 1977).

If it is accepted that the Betic suture belt is the product of oblique convergence then it seems likely that much of the horizontal component of the displacement would have been accommodated by strike-slip movements. Strike-slip may have produced transtension or transpression depending on the arrangement of the stress field which would change in response to changes in the rate and angle of convergence.

## 7 A question of Terrane Tectonism ???

It can be demonstrated that the nappes of the Internal Zone have contrasting structural and metamorphic histories (Egeler & Simon, 1969) and have been recently juxtaposed (Andrieux, 1971; DeSmet, 1984; Leblanc & Oliver, 1984; Tubia *et al.*, 1993). In particular, the high pressure and low temperature metamorphic rocks of the Nevado Filabride (Kampschuur & Rondell, 1979) are juxtaposed against the low grade Alpujarride rocks (Torres-Roldan, 1979). The contact between these two units is characterised by mylonitic and cataclastic rocks (Platt & Behrmann, 1985). The extensional collapse models (Platt & Vissers, 1989) and core complex type models (Doblas & Oyarzun, 1989) do not adequately explain the juxtaposition of nappes that have very different tectonic and metamorphic histories. If the high grade Nevado-Filabride rocks were exhumed by extension alone, then up to 12 Km of crust would have had to be removed from between the Nevado Filabride and Alpujarride units in order that

the model should remain consistent with the metamorphic and tectonic schemes proposed for these two units (Overview, Section 1.4.3). There is no evidence in the Betics for such 'missing' crust.

One way to superimpose crustal blocks with very different histories is by the accretion of terranes onto the margin of Iberia. These blocks would have been metamorphosed and exhumed elsewhere and then transported to the Iberian margin during the Miocene. This is similar to the model proposed by Campillo *et al.* (1992) who favoured the longitudinal transport of terranes by strike slip faulting.

Discrete crustal fragments can be expelled sideways along strike slip faults of convergent margins, a process referred to as 'tectonic escape' (Burke & Sengor, 1986). This may have been the mechanism by which crustal blocks in the Internal Zone, were transported along strike slip faults parallel to the suture belt. Campillo *et al.* (1992) refer to discrete detached blocks in the Alboran sea as 'orogenic float' and also postulate a model of tectonic escape for their emplacement. An excellent review of tectonic escape can be found in Sylvester (1988).

In a tectonic domain composed of discrete blocks and subject to shortening individual blocks may move relative to one another. This results in the opening of large basins between the blocks as they are wedged away from each other by movements along strike slip faults (Fig. 6) (Hill, 1982; Wu & Wang, 1988). This may be the mechanism by which the Internal Basins (Overview, Section 2.2) opened during the Miocene. If this is so then the Internal Basins would represent transtensional 'pull-apart basins' rather than extensional 'domino fault-block' type basins, as suggested by Platt & Vissers (1989) and Doblas & Oyarzun (1989).

## **8 Problems Associated With a Strike Slip Model**

While the above discussion clearly favours strike slip faulting as the main mechanism for the building of the Betics, there are distinct problems and several contradictions associated with such a model.

### **8.1 The Guadalquivir Basin Problem**

It has been demonstrated that the Guadalquivir Basin is not a foreland basin, but is associated with the destruction of the Iberian Passive margin during the Miocene extension of the Betic Orogen (Part I, Chapter 5.5). The depositional history of the basin is marked first by compression at the end of the Oligocene. This resulted in deformation of the Mesozoic and Palaeogene External Zone sediments (Part I, Chapter 2.9). A second, post-Messinian, phase of compression resulted in the break up of the Guadalquivir Basin and in the creation of the autochthonous and allochthonous zones of the Orogen (Part I, Chapter 2.9).

The initial discussion, in Part I, Chapter 5, attributed the early Miocene compression in the region of the Guadalquivir Basin to thrusting induced at the margin of a collapsing collisional ridge, following the model of Platt & Vissers (1989). In this model the spreading of overthickened crust is alleged to cause extension in the Internal Zones and compression at its margins in the External Zone (Platt & Vissers, 1989).

However, this is inconsistent with the arguments presented above which demonstrate

that there is no evidence for the existence of a collisional ridge prior to the Miocene extension. Moreover, Miocene extension is attributed to transtension induced during major strike slip movement between the African and Iberian plates. If this is so then it becomes difficult to explain the late Oligocene compression of the northern External Zone because;

**1** If there is no collisional ridge, then spreading of the crust onto the Iberian margin (induced by extensional collapse) is unlikely.

**2** If transtension in a strike slip regime is the main mechanism, then tectonism would have been accommodated in a relatively narrow zone in the region of the Alboran Sea. It is difficult to envisage how transtension or transpression could have induced compression in the Guadalquivir Basin, which is some distance away from the zone of strike slip faulting.

One explanation is that the compression recorded along the northern margin of the External Zone (prior to the formation of the Guadalquivir Basin) may reflect the arrival of the terranes envisaged by Campillo *et al.* (1992). Because Africa was essentially converging with Iberia, albeit obliquely, space would be required to accommodate the terrane blocks. This space may have been created by the compression and thin skin thrusting of the External Zones. Thus, while extension is the main mechanism in the Alboran Domain the emplacement of terranes, which were in effect driven onto the Iberian Margin, produced compression in part of the External Zone. The inference here is that during the Miocene the External Zone was broken up by extension in the west and compression in the north.

The post-Messinian thrusting that caused the break up of the Guadalquivir Basin (Part I. Chapter 2.9) may record the time when transtension was converted to transpression, as the convergence between Africa and Iberia became less oblique and generated structural inversions (Campillo *et al.*, 1992). Pliocene compression and uplift has also been recorded along the eastern Iberian margin in the Valencia trough (Janssen *et al.*, 1993).

## 8.2 The Betic Movement Zone Problem

Within the Internal Zone of the Betic orogen the high grade Nevado Filabride unit is separated from the higher Betic nappes by a broad zone of heterogeneous ductile shear. This is characterised by mylonites passing upwards into cataclastic rocks (Fig. 7) and is known as the Betic Movement Zone (Platt & Behrmann, 1985). Extensional mylonites overlain by cataclastic rocks are characteristic of detachment faults as in the Basin & Range of California (Platt & Vissers, 1989). The Betic Movement Zone is therefore interpreted as the main zone of detachment that developed during the Miocene Extension of the Internal Zone (Platt & Vissers, 1989). The formation of mylonites in the Betic Movement Zone post-dates the high grade metamorphism of the Nevado Filabride unit. The transition from pre-mylonite amphibolites to cataclastic rocks is interpreted to reflect uplift during nappe emplacement (Platt & Behrmann, 1985). Quartz lineations in the Mylonites are orientated to the NNE and indicate elongation (i.e. extension) NNE-SSW (Platt & Behrmann, 1985).

The Betic Movement Zone has been interpreted to be the product of a detachment to

the NNE and SSW that was generated during extension and gravitational spreading of the Orogenic belt (Platt & Vissers, 1989). However, as discussed, there is no evidence for overthickened pre-extensional crust and the extensional collapse model fails to explain the initial juxtapositions of the Nevado Filabride and higher Betic nappes with different metamorphic and structural histories. While the strike-slip model provides an alternative to the extensional collapse model there is some difficulty in explaining the formation of the Betic Movement Zone by strike-slip movements alone.

One possible explanation is that strike slip movements were characterised by repeated phases of transtension and transpression, as suggested by Campillo *et al.* (1992). During transpression, the terranes that were emplaced laterally by strike slip faults were buried by thrust stacking. The Nevado Filabride rocks could have attained their metamorphic grade elsewhere, prior to terrane emplacement. This initial transpressional event resulted in the juxtaposition of the Nevado Filabride unit and the higher Betic nappes, with the Nevado Filabride being buried to some depth. During subsequent transtension a zone of detachment formed as the higher Betic nappes became extended. This resulted in the re-exposure of the Nevado Filabride rocks and in their uplift in response to unloading during detachment. Such a model allows for both the juxtaposition of nappes with very different histories as well as the uplift of the Nevado Filabride in a 'core complex' style detachment. Both of these can be integrated in an overall strike-slip model.

## 9 A Model for the Evolution of the Betic Orogen

From the above discussions and those found in Part I, Chapter 5 and Part II, Chapter 3, a 'best fit model' for the Betics can be derived. This takes into account new and important data from the Guadalquivir Basin, from the Gibraltar Arc Flysch and from the Alboran Domain. This model, for which there is compelling evidence, attempts to integrate the various lines of evidence from the Betic Orogen into an overall scenario of strike-slip movement.,.

### 9.1 Cretaceous to Early Miocene (Fig. 8a)

Prior to the Miocene the boundary between African and Iberian plates was largely inactive, with the main movements taking place in the Pyrenean trough between Iberia and Eurasia (Sirvastava *et al.*, 1990a). In effect southern Iberia experienced a tectonic hiatus between 65-27 Ma. (Campillo *et al.*, 1992). During this relatively quiet interval, deposition of the External Zone rocks took place on what was essentially an extended passive margin (Fig. 8a). There is no evidence for Betic tectonism affecting the Iberian Passive Margin at this time.

### 9.2 Miocene (Fig. 8b)

The beginning of the Miocene corresponded with the start of Betic Tectonism in southern Iberia as the plate boundary again became active and Africa rotated into Iberia (Sirvastava *et al.*, 1990a). The first events recorded were extension of the Alboran Domain and compression along the northern margin of the External Zone (in the region now occupied by the Guadalquivir Basin). Extension in the Alboran Domain is believed to have been brought about by the oblique convergence of Africa and Iberia resulting in strike-slip movements and



the development of a mainly transtensional regime. This extension resulted in the break up of the western parts of the External Zone and the formation of small and confined pull-apart basins into which sediment, mobilised from the External Zone, was rapidly deposited. This deposition is represented by the Aljibe Flysch of the Gibraltar Arc (Part II, Chapter 3). Compression along the northern margin of the External Zone is more difficult to explain but may have been induced by the arrival of metamorphic terranes which required buckling of the margin to accommodate them. These terranes, which now form the Internal Zones, are interpreted as having been emplaced by lateral movements along strike slip faults, perhaps by a 'tectonic escape' mechanism (Campillo *et al.*, 1992). Compression led to the formation of the Guadalquivir Basin, confined by the uplifting External Zone rocks.

Through the Miocene the Betic orogen mainly experienced transtensional movements, punctuated by periods of transpression. Repeated phases of transtension and transpression are reflected in the variations in the  $Ar^{40}/Ar^{39}$  isotope system in phengitic micas from the Internal Zone, implying local resetting (De Jong *et al.*, 1992). During early transpression, thrust stacking of the metamorphic terranes may have led to burial of the Nevado Filabride unit and the juxtaposition of the Nevado Filabride, Alpujarride and Malaguide terrane blocks.

During transtension, the Ronda peridotites were uplifted, although initially not all the way to the surface. The Nevado Filabride unit, buried during transpression, was uplifted to form a 'core complex' by the detachment of the higher Betic nappes. This detachment was associated with the formation of the Betic Movement Zone. Transtension also led to the formation of the Internal Zone basins, such as the Granada Basin, as a series of pull-apart basins. Strike-slip movements continued into the Pliocene.

### 9.3 Pliocene (Fig. 8c)

Towards the end of the Pliocene the convergence of Africa and Iberia became less oblique as Africa began to move in a more northerly direction (Campillo *et al.*, 1992). As a result the mainly transtensional became progressively more transpressional. Related compression resulted in tectonic inversions in the Gibraltar Arc and Alboran Sea. Thrusts formed the peridotites were emplaced into their present positions. The Guadalquivir Basin, became subdivided into the allochthonous and autochthonous zones present today.

## 10 Unresolved Problems

The above model is an attempt to fit various tectonic, metamorphic and sedimentary histories into an overall model of strike-slip tectonism. While this model is appealing and explains most of the features of the Betics, it contains several unresolved problems;

- 1 It is considered that extension in the Betic Orogen began at the beginning of the Miocene. This is true for the Alboran Domain, but in the area now occupied by the Guadalquivir Basin the first event was clearly compressional deformation. This has been explained by the arrival of metamorphic terranes on the southern margin of Iberia causing compression in the outer parts of the External Zone. However, such a model requires simultaneous extension in the western parts and compression in the northern parts of the

External Zone. It is difficult to see how this could have been achieved, even by the emplacement of terranes. Also, it seems unlikely that deformation would have been induced by strike-slip tectonism so far away from the main zone of strike-slip movement.

**2** Zeck *et al.* (1992) recorded very rapid uplift in the Internal Zones. It is difficult to envisage how such rapid uplift rates could have been induced by transtension alone and without the involvement of some other mechanism, such as the diapiric emplacement of hot mantle material at the base of the crust.

**3** There is no explanation of how the terranes originally obtained their metamorphic grade. This poses a fundamental question about the origins of the Internal Zones. If they are the remnants of an older subduction zone, where was this zone located and at what time was it active?

**4** It is suggested that the Betic Orogen records transtension, punctuated by periods of transpression, but the nature of these events and their precise timing is unknown. It is not known when thrust stacking of the Internal Zones took place or when they were exhumed. The timing of these events is vital to gaining an understanding of the Betic Orogen

**5** The crust in the Alboran sea is much thinner than could have been brought about by transtension alone. This poses the question of whether or not the Alboran Sea represents a micro-plate and, if it does, was it already thinned prior to its emplacement.

## **11 Future work**

This study has demonstrated how external basins may be of use in interpreting the history of an orogen. However the work presented represents a small parts of the basins studied. While the areas studied are considered to be representative of the basins in question it is now necessary to extend the study in both the Guadalquivir Basin and the Gibraltar Arc in order to fully test the hypotheses put forward.

In addition, there are several key questions that have arisen from discussions which need to be more fully investigated ;

**1** The establishment of the provenance and timing of emplacement of the metamorphic terranes of the Internal Zones is vital. These Zones have been subject to many studies including radiometric dating and the results of these studies and derived dates have been applied to the Betics as a whole. However, if these rocks are terranes then data, and more specifically, the radiometric dates may only apply to the terrane blocks and their place of origin only, and not to the Betic Orogen as a whole. The timing of emplacement is critical as this will pin point the time after which the radiometric dates become significant to the Betics.

**2** The exact timing of thrusting in the flysch nappes of the Gibraltar Arc and the Guadalquivir Basin is unknown. Indeed it is not even known whether or not thrusting in these two areas was contemporaneous. As the thrust events record a time of major structural

inversion, their exact chronology is critical to the understanding of the Betic Orogen.

Finally the Betic Orogen of southern Spain has received much attention and most models have been generated from data collected only from Spain. However, the Orogen also includes rocks found along the northern margin of Africa. Clearly there is also a need to study these in order to determine if the tectonic, metamorphic and sedimentary history is compatible with that deduced from southern Spain. This is an entirely unknown quantity and merits the initiation of major field investigations.

## **12 Conclusions**

The external basins of the Betic Orogen provide important insights into the tectonic history of the Orogen and in particular into Oligo-Miocene events. Data gained from the study of these basins have been used to test various hypotheses for the formation of the Orogen and these have led to the development of new models. The tectonic history derived from the study of the External Basins has been combined with important new data from the Alboran Sea and Ronda peridotites. This has resulted in the rejection of the widely accepted 'extensional collapse' model and in the identification of strike-slip tectonism and transcurrent movements as the main mechanism for the building of the Betic Orogen. Miocene transcurrent movements in the Betic area resulted in the break up the Iberian passive margin, the emplacement of metamorphic terranes, and in the formation of thrusts in the Gibraltar Arc through a complicated history of transtension and transpression in the region of the Alboran Sea.

# ***Thesis Conclusions***

---

## Thesis Conclusions

The Guadalquivir Basin and the Gibraltar Arc Flysch Basins are considered to be basins linked to the development of the Betic Orogen. Their tectonic and palaeogeographic histories are critical to gaining a full understanding of the Orogen.

The detailed study of both of these basins has led to a complete revision of their tectonic and palaeogeographic histories. These revisions can be summarised as follows;

### **The Guadalquivir Basin**

**1** The Guadalquivir Basin developed between two compressional phases, but was largely unaffected by tectonism during its Miocene history.

**2** Prior to the formation of the Guadalquivir Basin the External Zone was unaffected by Betic Tectonism. The External Zones maintained their passive margin basin profile until the onset of the late Oligocene/early Miocene compressional event that led to the formation of the Guadalquivir Basin. This suggests that the Hercynian Passive Margin was not subjected to Betic tectonism until early Miocene times.

**3** Seismic data and stratigraphic relationships indicate that thrusting disrupted the basin at the end of the Miocene following the deposition of Messinian sediments.

**4** Lithosomes in the Guadalquivir Basin previously described as 'olistostromes' are actually tectonic melanges and their formation was associated with the post-Messinian thrusting event (post basin).

**5** The Guadalquivir Basin contains deposits, principally marls, which are less than 1 Km thick indicating that the basin did not receive much detritus during its Miocene history.

**6** Sedimentological and micropalaeontological studies demonstrate that the Miocene Guadalquivir Basin formed as a single basin characterised by deepwater and shallow marine deposits separated by a shelf break. A fluvial braid plain dominated the southern part of the basin and channelled detritus from the External Zone to coastal fan deltas. The detritus was reworked on the shelf by storm and tidal currents that led to the mixing of near-shore and shelf faunas. Storm tempestite currents transported some of the detritus to the deeper parts of the basin. Through the Miocene the coastline prograded northwards across the shelf in direct response to a relative sea-level fall that was most probably eustatic. There is no evidence for the existence of a major turbidite basin, as is suggested by other authors.

**7** Detailed provenance studies indicate that sedimentary lithic clasts were mainly derived from the External Zones, part of the Palaeogene Iberian Passive Margin, and from within the basin itself. Some material was also derived from the Hercynian Massif.

**8** White mica geochemistry and geochronology indicates that metamorphic detritus was ultimately derived from the Hercynian Massif. Some of this may have been recycled from the External Zone, which would have received detritus from the Hercynian Massif prior to its break up and prior to the formation of the Guadalquivir Basin.

**9** There is no evidence for the derivation of material from the Internal Zone rocks of the Betic Orogen.

**10** While the Guadalquivir Basin geographically appears to be a foreland basin it is unlikely to have been formed by the flexural response of the lithosphere to orogenic loading. Thus, by definition, it cannot be considered to be a foreland basin.

**11** In the final analysis it can be demonstrated that the Guadalquivir Basin formed as an integral part of the destruction of the Iberian Passive Margin. Thin skinned thrusting generated a basin on the northern margin of the External Zones. The fill and unconformities of this basin were controlled by eustasy rather than by tectonic incursion, and clastic sedimentation was driven by the emergence of the External Zone thrust sheets during the late Miocene. A final Late Miocene thrusting event disrupted the Guadalquivir Basin and led to its division into the allochthon and autochthon.

### **The Gibraltar Arc Flysch Basins**

**1** The Gibraltar Arc is formed by series of highly allochthonous units that have been thrust westwards.

**2** The largest tectono-sedimentary unit of the Gibraltar Arc is the Aljibe Flysch. This flysch sequence consists of mainly quartz arenites deposited by turbidites and grain flows. They are often in upward coarsening sequences that terminate in sandstones with abundant dewatering features

**3** The Aljibe Flysch records the development of a turbidite dominated basin plain on the southern margin of the External Zones during the Oligocene. This became tectonically segregated at the beginning of the Miocene at which time restricted extensional basins formed.

**4** Tectonism related to the break up the basin plain, created instabilities elsewhere in the External Zone. This led to the mobilisation of large amounts of sediment that were rapidly deposited in the new tectonically confined basins in which thick wedges of sediment, with restricted facies, accumulated.

**5** The Gibraltar Arc sedimentary basins record the break up of the External Zones, and this may represent the tectonic transition from the Iberian Passive Margin to the Betic Orogen.

The tectonic and Palaeogeographic history, deduced for the Guadalquivir Basin and Gibraltar Arc Flysch basins have been used, in conjunction with data collected by other authors, to critically examine various models proposed for the evolution of the Betic Orogen. This can be summarised as follows.

- 1 There is no evidence for Betic tectonism affecting the Iberian Passive Margin prior to the supposed Miocene 'extensional collapse' event.
- 2 If Betic tectonism did not affect the Iberian Margin during the Palaeogene then it is unlikely that a collisional ridge formed prior to the Miocene. If this is the case then extension cannot have been caused by the collapse of an overthickened orogenic wedge.
- 3 There is a substantial weight of evidence for major strike slip movements having occurred in the Betic Orogen.
- 4 Many features of the Betic Orogen can be explained through a history of transtension and transpression that occurred in an overall strike-slip regime.
- 5 The Internal Zones of the Betic Orogen may have been emplaced as terrains during strike slip movements. A model of orogenic float and tectonic escape is envisaged for terrain emplacement.

From all of the above, a 'best fit' model for the Betic Orogen has been derived which can be summarised as follows;

- 1 Prior to the Miocene, Iberia existed as an extended passive margin that was unaffected by Betic tectonism.
- 2 The first orogenic event is recorded at the end of the Oligocene/ early Miocene.
- 3 The Orogen developed in response to the oblique convergence of Africa and Iberia resulting in strike slip movements and the development of a mainly transtensional regime.
- 4 Transtension resulted in the partial uplift of peridotite bodies and the formation of extensional basins in the regions of the Gibraltar Arc, Alboran Sea and Internal Zones.
- 5 Transtension was punctuated by periods of transpression during the Miocene. This resulted in the thrust stacking of metamorphic terrains that were emplaced along the strike slip margin and the emplacement of peridotites into mid crustal levels.
- 6 Towards the end of the Pliocene the convergence of Africa and Iberia became less oblique and the transtensional regime became progressively more transpressional. This resulted in

tectonic inversions in the Gibraltar Arc and Alboran Sea and the emplacement of the Peridotites into their present position.



# ***Acknowledgements & References***

## **Acknowledgements**

I would like to acknowledge NERC grant Ref: GT4/91/GS/51 for providing the financial support for this research.

I would also like to thank my supervisor, Brian Bluck, for his guidance and support, Juan Fernandez, Cessa Vesseras and Torr  s X for support in the field, Colin Braithwaite & Mike Keen for critical reviews and Mike Keen for collaboration on the micropalaeontological analysis. I would particularly like to thank the technical staff at the Dept. of Geology, Univ. of Glasgow, especially Douglas Maclean for his expert photographic work, Colin Farrow and Jim Kavanaugh for computer support work and Robert MacDonald for microprobe analysis. Thanks also goes to Paul McConville at SURCC for help with isotopic dating under particularly difficult circumstances. I also wish to thank John Hughes for providing some of the data used in this thesis and Andy Munro and Mark Osbourne for useful discussions over pints of beer. Thanks also to Andy Munro, Lynda Mitchell, Mark Wilkinson and Dave McGimpsey for three great years of climbing in Scotland, without these people madness would have surely set in.

Thanks also to the Powrie family for taking me in and looking after me in the last few months of writing up and putting up with me during a very fraught time.

---

## References

- Aldaya, F. (1970) La sucesión de etapas tectónicas en el dominio Alpujárride (Zona Bética provincia de Granada). *Cuadernos Geología*, **1** 159-181.
- Allen, J. R. L. (1965) Late quaternary Niger Delta, and adjacent areas; sedimentary environments and lithofacies. *Bulletin of the American Association of Petroleum Geologists*, **49** 547-600.
- Allen, J. R. L. (1980) Sand waves a model of origin and internal structure. *Marine Geology*, **26** 281-328.
- Allen, J. R. L. (1982) *Sedimentary Structures: Their Character and Physical Basis*. Elsevier, Amsterdam.
- Allen, P. (1991) Provenance research: Torridonian and Wealden. In: *Developments in Sedimentary Provenance Studies* (Ed. by P.D.W. Haugton, S.P. Todd and A.C. Morton), London Geological Society, London., 13-21.
- Allen, P. A. and Allen, J. R. (1990) *Basin Analysis; Principles and Applications*. Blackwell Scientific Publications, London, pp 451.
- Allen, P. A. and Homewood, P. (1986) *Foreland Basins*. IAS Special Publication, London, pp 453.
- Allen, P. A., Homewood, P. and Williams, G. D. (1986) Foreland basins: an introduction. In: *Foreland Basins*. (Ed. by P.A. Allen and P. Homewood), IAS Special Publication, London, 3-15.
- Allerton, S., Longergan, L., Platt, J. P., Platzman, E. S. and McClelland, E. (1993) Palaeomagnetic rotations in the eastern Betic Cordillera southern Spain. *Earth and Planetary Science Letters*, **119** 225-241.
- Anderson, J. G. C. (1978) *The structure of western Europe*. Pergamon Press, Oxford, pp 250.
- Andrieux, J., Fontbote, J. M. and Mattauer, M. (1971) Sur un modele explicaty de l'Arc de Gibraltar. *Earth and Planetary Science Letters*, **12** 191-198.
- Auboin, J. (1965) *Developments in Geotectonics*. Elsevier, Amsterdam, pp 335.
- Bailey, E. H. and Stevens, R. E. (1960) Selective staining of K-feldspar and plagioclase on rock slabs and in thin sections. *American Mineralogist*, **45** 1020-1027.
- Bakker, H. E., Jong, K. D., Helmers, H. and Biermann, C. (1989) The geodynamic evolution of the Internal Zone of the Betic Cordilleras (south-east Spain): a model based on structural analysis and geothermobarometry. *Journal of Metamorphic Geology*, **7** 359-381.
- Ball, M. M. (1967) Carbonate sandbodies of Florida and the Bahamas. *Journal of Sedimentary Petrology*, **37** 556-591.
- Bally, A. W. and Snelson, S. (1980) Realms of subsidence. In: *Facts and principles of world petroleum occurrence*. (Ed. by A.D. Miall), Canadian Society of Petroleum Geology., 9-75.
- Balyana, J. C. and Dueñas, V. G. (1991) Estructuración de los mantos Alpujárrides al W de Málaga (Béticas, Andalucía). *Geogaceta*, **9** (30-33),

- Balyana, J. C. and Garcia-Dueñas, V. (1986) Grandes fallas de contracción y de extensión implicadas en el contacto entre los dominios de Alborán y Sudibérico en el arco de Gibraltar. *Geogaceta*, **1** 19-21.
- Banda, E. and Ansorge, J. (1980) Crustal structure under the central and eastern part of the Betic Cordillera. *Geophysical Journal Royal Astronomical Society*, **63** 515-532.
- Banda, E., Gallart, J., Dueñas, V. G., Dañaberla, J. J. and Markis, J. (1993) Lateral variation of the crust in the Iberian peninsula. New evidence from the Betic Cordillera. *Tectonophysics*, **204** 221-256
- Banks, C. J. and Warburton, J. (1991) Mid-crustal detachment in the Betic system of southeast Spain. *Tectonophysics*, **191** 275-289.
- Beaumont, C. (1978) The evolution of foreland basins on viscoelastic lithosphere: theory and examples. *Geophysical Journal Royal Astronomical Society*, **55** 471-497.
- Beaumont, C. (1981) Foreland basins. *Geophysical Journal Royal Astronomical Society*, **65** 291-329.
- Berger, W. H. (1974b) Deep-sea sedimentation. In: *The geology of continental margins*. (Ed. by C.A. Burke and C.L. Drake), Springer Verlag, New York., 213-241.
- Berger, W. H. (1976) Biogenous deep sea sediments, production preservation and interpretation. In: *Treatise on Chemical Oceanography* (Ed. by J.P. Riley and R. Chester), Academic Press, London, 154-173.
- Bernard, H. A., LeBlanc, R. J. and Major, C. F. (1962) Recent and Pliocene geology of southeast Texas. In: *Geology. Gulf Coast and Central Texas and guidebook of excursion*. Houston Geol. Soc., 175-225.
- Besly, B. M. (1988) Late Carboniferous sedimentation in northwest Europe: an introduction. In: *Sedimentation in an Synorogenic Basin Complex*. (Ed. by B.M. Besly and G. Kelling), Chapman & Hall, New York, 1-8.
- Biddle, K. T., Uliana, M. A., Mitchum, R. M., Fitzgerald, M. G. and Wright, R. C. (1986) The stratigraphic and structural evolution of the central and eastern Magallanes Basin, southern South America. In: *Foreland Basins*. (Ed. by P.A. Allen and P. Homewood), Special Publication of the Int. Assoc. Sedim, London, 41-62.
- Blankenship, C. L. (1992) Structure and palaeogeography of the external Betic Cordillera, southern Spain. *Marine and Petroleum Geology*, **9** 256-264.
- Blankenship, C. L. (1993) Reply to Comments on 'Structure and palaeogeography of the External Betic Cordillera, southern Spain'. *Marine & Petroleum Geology*, **10** 514-522.
- Bluck, B. J. (1974) Structure and directional properties of some valley sandbar deposits in southern Iceland. *Sedimentology*, **21** 533-554.
- Bluck, B. J. (1976) Sedimentation in some Scottish rivers of low sinuosity. *Transactions of the Royal Society of Edinburgh*, **69** (18), 425-456.
- Bluck, B. J. (1982) Texture of Gravel Bars in Braided Streams. In: *Gravel-bed Rivers* (Ed. by R.D. Hey, J.C. Bathurst and C.R. Thorne), John Wiley & Sons Ltd, London., 339-355.
- Bluck, B. J. (1983) Role of the Midland Valley of Scotland in the Caledonian Orogeny. *Transactions of the Royal Society of Edinburgh: Earth Sciences*, **70** 29-46.

- Boothroyd, J. C. and Ashley, G. M. (1975) Processes, bar morphology and sedimentary structures on braided outwash fans, north eastern Gulf of Alaska. In: *Glaciofluvial and Glaciolacustrine Sedimentation*. (Ed. by A.V. Jopling and B.C. McDonald), Society of Economic Palaeontologists and Mineralogists. Special Publication, 193-222.
- Boullin, J. (1970) Les zones internes des Cordillères Bétiques de Málaga à Motril (Espagne méridionale). *Ann. Hébert et Haug*, **10** 1-235.
- Boullin, J. P., Durand-Delgas, M. and Oliver, P. (1986) Betic Riffian and Tyrrhenian arcs: Distinctive features, genesis and developmental stage. In: *The Origin of Arcs*. (Ed. by F.C. Weze), Elsevier, Amsterdam, 281-304.
- Bouma, A. H. (1962) *Sedimentology of Flysch Deposits*. Elsevier, Amsterdam, pp 168.
- Bourgois, J. (1978) *La Transversale de Ronda. Cordillères Bétiques Espagne. Données Géologiques Pour un Modèle d'Evolution de l'Arc de Gibraltar*, Université de Besançon, Ph.D.
- Brenchley, P. J. (1985) Storm influenced sandstone beds. *Geology*, **9** 369-396.
- Brenchley, P. J., Pickerill, R. K. and Stromberg, S. G. (1993) The role of wave-reworking on the architecture of storm-sandstone facies, Bell Island Group (Lower Ordovician), eastern Newfoundland. *Sedimentology*, **40** (3), 339-383.
- Burckle, L. H. (1978) Marine Diatoms. In: *Introduction to Marine Micropaleontology*. (Ed. by B.U. Haq and Boersma), Elsevier, New York, 245-267.
- Burke, K. and Sengor, A. M. C. (1986) Tectonic escape in the evolution of the continental crust. In: *Reflection Seismology-The Continental Crust*. (Ed. by M. Barazagar and I.D. Brown), American Geophysical Union, Geodynamics Series, 41-51.
- Blumenthal, M. M. (1927) Versuch einer tektonischen Gliederung der betischen Cordilleren von Central und Südwest (Andalusien). *Ecolagae Geol. Helv.*, **20** 487-532.
- Campillo, A. C., Maldonado, A. and Mauffret, A. (1992) Stratigraphic and tectonic evolution of the Western Alboran Sea: Late Miocene to recent. *Geo-Marine Letters*, **12** 165-172.
- Campos, J., Maldonado, J. D. and Campillo, A. C. (1992) Post Messinian evolutionary patterns of the Central Alboran Sea. *Geo-Marine Letters*, **12** 173-178.
- Cant, D. J. (1974) Development of shoreline shelf sand bodies in a Cretaceous epeiric sea deposit. *Journal of Sedimentary Petrology*, **44**, 173-185.
- Carter, R. M. (1979) Trench-slope channels from the New Zealand Jurassic: the Otekura formation, Sandy Bay, South Otago. *Sedimentology*, **26** 475.
- Chauve, P. (1960) Etude de quelques affleurements jurassiques de la région d'Alcala de los Gazules (province de Cadix, Espagne). *B.S.G.F.*, **7** (II), 345-351.
- Church, M. and Gilbert, R. (1975) Proglacial fluvial and lacustrine environments. In: *Glaciofluvial and Glaciolacustrine Sedimentation*. (Ed. by A.V. Jopling and B.C. McDonald), Society of Economic Palaeontologists and Mineralogists. Special Publication, 22-100.
- Clifton, H. E., Hunter, R. E. and Philips, R. L. (1971) Depositional structures and processes in the non-barred high-energy nearshore. *Journal of Sedimentary*

Collinson, J. D. (1978) Alluvial sediments. In: *Sedimentary Environments and Facies*. (Ed. by H.G. Reading), Blackwell Scientific Publications, London, 20-62.

Cook, H. E., McDaniel, P. N., Mountjoy, E. W. and Pray, L. C. (1972) Allochthonous carbonate debris flows at Devonian bank margins, Alberta, Canada. *Bulletin Canadian Petroleum Geology*, **20** 439-497.

Corbett, P. W. M., Stromberg, S. G., Brenchley, P. J. and Geehan, G. (in press) Laminaset geometries in fine grained shallow marine sequences: Core data from the Rannoch Fm. (North Sea) and outcrop data from the Kennilworth Member, Utah. *Sedimentology*, (in press).

Corretege, L. G. (1978) Summary of the characteristics of the granitic rocks in the Iberian Terranes. *International Conference on Iberian Terranes and their Regional Correlation*, Oviedo, Spain, IGCP.

Coward, M. P. (1986) Heterogeneous stretching, simple shear and basin development. *Earth and Planetary Science Letters*, **80** 325-336.

Dabrio, J. C. and Lopez-Garrido, A. C. (1970) Estructura en escamas del sector noroccidental de la Sierra de Cazorla (Zona Prebetica ) y del borde de la Depresión del Guadalquivir (Prov de Jaén). *Cuad. Geol. Univ. Granada*, **1** 149-157.

Daily, B., Moore, P. S. and Rust, B. R. (1980) Terrestrial marine transition in the cambrian rocks of Kangaroo Island, South Australia. *Sedimentology*, **27** 379-399.

Davidson-Arnott, R. G. D. and Greenwood, B. (1974) Bedforms and structures associated with bar topography in the shallow water environment, Kouchibouguac Bay, New Brunswick, Canada. *Journal of Sedimentary Petrology*, **44** 698-704.

Davidson-Arnott, R. G. D. and Greenwood, B. (1976) Facies relationships on a barred coast, Kouchibouguac Bay, New Brunswick, Canada. In: *Beach and Nearshore Sedimentation*. (Ed. by R.A. Davis and R.L. Ethington), SEPM, Tulsa, 149-168.

Davies, G. R., Nixon, P. H., Pearson, D. G. and Obata, M. (1993) Tectonic implications of graphitized diamonds from the Ronda peridotite massif, southern Spain. *Geology*, **21** 471-474.

Davies, T. A. and Gorsline, D. S. (1976) Oceanic sediments and sedimentary processes. In: *Chemical Oceanography*. (Ed. by J.P. Riley and R. Chester), Academic Press, London, 1-80.

De-Jong, K., Wijbrans, J. R. and Féraud, G. (1992) Repeated thermal resetting of phengites in the Mulhacen Complex (Betic Zone, southeastern Spain) shown by  $^{40}\text{Ar}/^{39}\text{Ar}$  step heating and single grain laser probe dating. *Earth and Planetary Science Letters*, **110** 173-191.

Dempster, T. J. (1992) Zoning and recrystallization of phengitic micas: implications for Metamorphic equilibration. *Contributions to Mineralogy and Petrology*, **109** 526-537.

Dempster, T. J. and Bluck, B. J. (1989) The age and origin of boulders in the Highland Border Complex: constraints on terrain movements. *Journal of the London Geological Society*, **147** 351-357.

De-Smet, M. E. M. (1984) Wrenching in the external zone of the Betic Cordillera, Southern Spain. *Tectonophysics*, **107** 57-73.

- Dewey, J. F., Helman, M. L., Turco, E. and Hutton, D. H. W. (1989) Kinematics of the western Mediterranean. In: *Alpine Tectonics*. (Ed. by M.P. Coward, D. Dietrich and R.G. Park), Spec. Publ. geol. Soc. London 45, 265-283.
- Dewey, J. F., Pitman-III, W. C., Ryan, W. B. F. and Bonnin, J. (1973) Plate tectonics and the Evolution of the Alpine System. *Bulletin of the Geological Society of America*, **84** 3137-3180.
- Dickey-Jr., J. S., Lundeen, M. T. and Obata, M. (1979) Geologic map of the Ronda ultramafic complex. *Geological Society American Chart Service*, **29** 1-4.
- Dickinson, W. R. (1974) Plate tectonics and sedimentation. In: *Tectonics and Sedimentation* (Ed. by W.R. Dickinson), Spec. Publ. Soc. Econ. Paleont. Mineral., Tulsa, Oklahoma.
- Dickinson, W. R., Beard, L. S., Brakenridge, G. R., Erjavec, J. L., Ferguson, R. C., Inman, K. F., Knepp, R. A., Lindberg, F. A. and Ryberg, P. T. (1983) Provenance of North American Phanerozoic sandstones in relation to tectonic setting. *Bulletin of the Geological Society of America*, **94** 222-235.
- Dickinson, W. R. and Seely, D. R. (1979) Structure and stratigraphy of forearc regions. *Bulletin of the American Association of Petroleum Geologists*, **63** (1), 2-31.
- Dickinson, W. R. and Valloni, R. (1980) Plate settings and provenance of sands in modern ocean basins. *Geology*, **8** 82-86.
- Didon, J. (1969) *Etude géologique du Campo de Gibraltar*, Paris, These.
- Doblas, M. and Oyarzun, R. (1989) Neogene extensional collapse in the western Mediterranean (Betic-Rif orogenic belt); Implications for the genesis of the Gibraltar Arc and magmatic activity. *Geology*, **17** 430-443.
- Dott, R. H. J. and Bourgeois, J. (1982) Hummocky cross stratification. Significance of its variable bedding sequences. *Bulletin of the Geological Society of America*, **93** 663-680.
- Dravis, J. J. (1977) *Holocene sedimentary depositional environments on the Eleuthra Bank, Bahamas*. Miami Fla. Univ. of Miami, M.Sc.
- Duke, W. L., Arnott, R. W. C. and Cheel, R. J. (1991) Shelf sandstones and hummocky cross-stratification: New insights on a stormy debate. *Geology*, **19** 625-628.
- Dzulynski, S. and Smith, A. J. (1964) Flysch Facies. *Ann. Soc. Geol. Pol.*, **34** 245-266.
- Egeler, C. G., Rondell, H. E. and Simon, O. J. (1972) Considerations on the grouping of the tectonic units of the Betic Zone, Southern Spain. *Estud. Geol.*, **27** 467-473.
- Egeler, C. G. and Simon, O. J. (1969) Sur la tectonique de la Zone Bétique (Cordillères Bétiques, Espagne). Etude basée sur les recherches dans le secteur compris entre Almería et Vélez Rubio. *Verh. K. Ned. Akad. Wet., Afd. Natuurkd., Reeks I.*, **25** (3), 90.
- Elliot, T. (1978) Siliciclastic shorelines, Tide dominated shorelines. In: *Sedimentary environments and facies*. (Ed. by H.G. Reading), Blackwell Scientific Publications, London, 182-188.
- Elliot, T. (1978b) Deltas. In: *Sedimentary environments and facies*. (Ed. by H.G. Read-

ing). Blackwell Scientific Publications, London., 113-154.

Esteban, M. and Klappa, C. F. (1983) Subaerial Exposure Environment. In: *Carbonate Depositional Environments*. (Ed. by P.A. Scholle D.G. Bebout C.H. Moore), American Association of Petroleum Geologists, Tulsa, Oklahoma, 1-55.

Fischer, A. G. (1961) Stratigraphic record of transgressing seas in the light of sedimentation on the Atlantic Coast of New Jersey. *Bulletin of the American Association of Petroleum Geologists*, **45** 1656-1666.

Fitch, T. J. (1972) Plate convergence, transcurrent faults and internal deformation adjacent to S.E. Asia and the Western Pacific. *Journal of Geophysical Research*, **77** 4430-4460.

Fontbote, J. M., Estevez, A., Navarro-Villa, F., Oroz-Co, M. and Sanz-de-Galdeano, C. (1986) *Mapa Geológico De España, 1:200.000 Algeciras 87. With Memoirs*. Solid Geology, 2nd Edition, Instituto Geológico Y Minero De España.

Friedman, G. M. and Sanders, J. E. (1978) *Principles of Sedimentology*. Wiley, New York, pp 792.

Galdeano, A., Cortillot, V., Le-Borgne, E., Le-Mouel, J. L. and Rossignol, J. C. (1974) An aeromagnetic survey of the southwest of the western Mediterranean. Description and tectonic implications. *Earth and Planetary science Letters*, **23** 323-336.

García-Dueñas, V. (1969) Les unités allochtones de la Zone Subbétique dans la transversale de Grenade (Cordillères Bétiques Espagne). *Rev. Géogr. Phys. Géol. Dynam.*, **11** 211-222.

García-Duenas, V., Balnyá, J. C. and Martínez-Martínez, J. M. (1994) Miocene extensional detachments in the outcropping basement of the northern Alboran Basin: Tectonic Implications. (pre-print).

García-Hernandez, M., Lopez-Garrido, A. C., Rivas, P., Sanz-de-Galdeano, C. and Vera, J. A. (1980) Mesozoic paleogeographic evolution of the External Zones of the Betic Cordillera. *Geologie En Mijnbouw*, **59** (2), 155-168.

García-Rossell, L. (1973) *Estudio geológica de la transversal Ubeda-Huelma y sectores adyacentes. Cordilleras Béticas (Prov. de Jaen)*. University of Granada, Spain, Ph.D.

Gawthorpe, R. L. (1986) Sedimentation during carbonate ramp-to-slope evolution in a tectonically active area: Bowland Basin (Dinantian), northern England. *Sedimentology*, **33** 185.

Gombos, A. M. (1975) Fossil diatoms from leg 7, Deep Sea Drilling Project. *Micropaleontology*, **21** (3), 306-333.

Gomez-Pugnaire, M. T. and Fernandez-Soler, J. M. (1987) High pressure metamorphism in metabasites from Betic Cordilleras (SE Spain) and its evolution during the Alpine orogeny. *Contributions to Mineralogy and Petrology*, **95** 231-244.

Graham, S. A., Dickinson, W. R. and Ingersoll, R. V. (1975) Himalayan-Bengal model for flysch dispersal in the Appalachian Ouachita system. *Bulletin of the Geological Society of America*, **86** 273-286.

Graham, S. A., Tolson, R. B., Decelles, P. G., Ingersoll, R. V., Bargar, E., Caldwell, M., Cavazza, W., Edwards, D. P., Follo, M. F., Handschy, J. F.,



- Lemke, L., Moxon, I., Rice, R., Smith, G. A. and White, J. (1986) Provenance modelling for Analysing source terrane evolution and controls on foreland sedimentation. *Special publication International Association of Sedimentologists*, **8** 425-436.
- Grevilla, F. and Remaidi, M. (1993) Field trip to the Ronda ultramafic massif; an example of asthenosphere lithosphere interaction. *Oftoliti*, **18** 21-35.
- Guidotti, C. V. (1984) Micas in metamorphic rocks. In: *Micas. Reviews in Mineralogy*. (Ed. by S.W. Bailey), Mineralogical society of America, 357-467.
- Gvirtzman, G. and Buchbinder, B. (1978) *Recent and Pleistocene Coral Reefs and Coastal Sediments of the Gulf of Elat*. International Association of Sedimentologists, Post Conference Guidebook, pp 161-191.
- Hajos, M. (1973) Mediterranean Diatoms. In: *Initial Reports of Deep Sea Drilling Projects* (Ed. by A.G. Kaneps), National Science Foundation, 944-971.
- Hamblin, A. P. and Walker, R. G. (1979) Storm-dominated shallow marine deposits: the Fernie-Kootenay (Jurassic) transition, southern Rocky Mountains. *Canadian Journal of Earth Sciences*, **16** 1673-1690.
- Haq, B. U., Hardenbol, J. and Vail, P. R. (1987) Chronology of fluctuating sea levels since the Triassic. *Science*, **235** 1156-1167.
- Harms, T.A. (1975) Depositional environments as interpreted from primary sedimentary structures and stratification sequences. *Society of Economic Paleontologists and Mineralogists Short Course notes*, **2** pp 161.
- Haughton, P. D. W., Todd, S. P. and Morton, A. C. (1991) Sedimentary provenance studies. In: *Developments in Sedimentary Provenance Studies*. (Ed. by P.D.W. Haughton, S.P. Todd and A.C. Morton), Geological Society, London, 1-11.
- Hawley, N. (1982) Internal structures on macrotidal beaches. *Journal of Sedimentary Petrology*, **52** 785-795.
- Hayes, M. O. and Kana, T. W. (1976) *Terrigenous Clastic Depositional Environments- Some Modern Examples*. Coastal Research Division, University of South Carolina.
- Hayward, A. B. (1983) Coastal alluvial fans and associated marine facies in the Miocene of S.W. Turkey. In: *Modern & Ancient Fluvial Systems*. (Ed. by J.D. Collinson and J. Lewin), I.A.S Special Publication, 323-336.
- Helwig, J. (1970) Slump folds and early structures, northeastern Newfoundland Appalachians. *Journal of Geology*, **78** 172-187.
- Hermes, J. J. (1978) The stratigraphy of the Sub-Betic and southern Prebetic of the Velez-Rubio Cravaca area and its bearing on transcurrent faulting in the Betic Cordilleras of Southern Spain. *Kon. Ned. Akad. Wet. Proc.*, **81** 1-54.
- Hill, D. P. (1982) Contemporary block tectonics. *Californian & Nevada Journal of Geophysical Research*, **87** 5433-5450.
- Hill, P. R. (1984) Sedimentary facies of the Nova Scotian upper and middle continental slope, offshore eastern Canada. *Sedimentology*, **31** 293-309.
- Hiscott, R. N., Pickering, K. T. and Beeden, D. R. (1986) Progressive filling of a confined Middle Ordovician foreland basin associated with the Taconic orogeny, Quebec Canada. In: *Foreland Basins*. (Ed. by P.A. Allen and P. Homewood) Special Publication of the International Association Sedimentologists, London, 309-326.

- Homewood, P., Allen, P. A. and Williams, G. D. (1986) Dynamics of the molasse basin of western Switzerland. In: *Foreland Basins* (Ed. by P.A. Allen and P. Homewood) Special Publication of the International Association Sedimentologists, 199-218.
- Houbolt, J. J. H. C. (1968) Recent sediment in the southern bight of the North Sea. *Geol. Mijnb.*, **47** 254-273.
- Houseknecht, D. W. (1986) Evolution from passive margin to a foreland basin: the Atoka Formation of the Arkoma Basin south-central U.S.A. In: *Foreland Basins* (Ed. by P.A. Allen and P. Homewood) Special Publication of the International Association Sedimentologists, London., 327-346.
- van-Houten, F. B. (1974) Northern Alpine molasse and similar Cenozoic sequences in southern Europe. In: *Modern and Ancient Geosynclinal Sedimentation*. (Ed. by Dott and Shaver) Special Publication of the Society of Economic Paleontologists and Mineralogists, Tulsa, 260-273.
- Howard, J. P. and Reineck, H. E. (1981) Deposition of high energy beach to offshore sequences: comparison with low energy sequences. *Bulletin of the American Association of Petroleum Geologist*, **65** 807-830.
- Hoyt, J. H. and Weimer, R. J. (1963) Comparison of modern and ancient beach deposits. *Bulletin of the American Association of Petroleum Geologists*, **47** 529-531.
- Hsü, K. J. (1974) Melanges and their distinction from olistostromes. *SEPM Special Publication*, **19** 321-333
- Hsü, K. J. (1970) The meaning of the word Flysch: a short historical research. *Special Paper Geological Association of Canada*, **7** 1-11.
- Humphreys, B., Morton, A. C., Hallsworth, C. R., Gatliff, R. W. and Riding, J. B. (1991) An intergrated approach to provenance studies: a case example from the Upper Jurassic of the Central Graben, North Sea. In: *Developments in Sedimentary Provenance studies* (Ed. by P.D.W. Haughton, S.P. Todd and A.C. Morton) Geological Society, London, 251-262.
- Ingersoll, R. V. (1978) Peterofacies and peterologic evolution of the late Cretaceous Fore-Arc Basin, northern and central California. *Journal of Geology*, **86** 335-352.
- Ingersoll, R. V. and Suczek, C. A. (1979) Petrology and provenance of Neogene sand from the Nicobar and Bengal fans, DSDP sites 211 and 218. *Journal of Sedimentary Petrology*, **49**.
- Jakucs, L. (1977) *Morphogenetics of karst regions*. John Wiley & Sons, New York, pp 284.
- Janssen, M. E., Torne, M., Cloetingh, S. and Banda, E. (1993) Pliocene uplift of the eastern Iberian margin: Inference from quantitative modelling of the Valencia Trough. *Earth and Planetary Science Letters*, **119** 585-597.
- Johnson, G. D., Reynolds, R. G. H. and Burbank, D. W. (1986) Late Cenozoic tectonics and sedimentation in the north-western foredeep: I Thrust ramping and associated deformation in the Potwar region. In: *Foreland Basins* (Ed. by P.A. Allen and P. Homewood) IAS Special Publication., London, 273-292.
- Kampschuur, W. and Rondell, H. E. (1974) The origin of the Betic Orogen, southern Spain. *Tectonophysics*, **27** 39-56.

- Karig, D. F. (1980) Material transport within accretionary prisms and the 'Harker' problem. *Journal of Geology*, **88** 27-39
- Kelley, S. and Bluck, B. J. (1989) Detrital mineral ages from the Southern Uplands using  $^{40}\text{Ar}$ - $^{39}\text{Ar}$  laser probe. *Journal of the Geological Society of London*, **146** 401-403.
- Kelley, S. P. and Bluck, B. J. (1992) Laser  $^{40}\text{Ar}$   $^{39}\text{Ar}$  ages for individual detrital muscovites in the Southern Uplands of Scotland, U.K. *Chemical Geology (Isotope Geosciences Section)*, **101** 143-156.
- Kennedy, W. J. and Garrison, R. E. (1975) Morphology and genesis of nodular chalks and hard grounds in Upper Cretaceous of Southern England. *Sedimentology*, **22** 311-386.
- Kerr, R. S. (1977) Development and diagenesis of a Lower Cretaceous bank complex. Edwards Limestone, north central Texas. In: *Cretaceous Carbonates of Texas and Mexico* (Ed. by D. Bebout and L. Loucks) Bureau of Economic Geology, Austin, Texas, 216-233.
- Komar (1976) *Beach Processes and Sedimentation*. Prentice Hall, New Jersey.
- Kornprobst, J. (1974) Contribution à l'étude pétrographique et structurale de la zone interne du Rif (Maroc septentrional). *Service géol Maroc. Mem.*, **25** 249.
- Kraft, J. C. (1971) Sedimentary facies and geologic history of a Holocene marine transgression. *Bulletin of the American Association of Petroleum Geologists*, **82** 2131-2158.
- Krauss, M. J. and Brown, T. M. (1988) Pedofacies analysis; A new approach to reconstructing ancient fluvial sequences. In: *Special Paper 216* (Ed. by Reindhardt W.R. Silgo) Geological Society of America, 143-152.
- Kriesa, R. D. (1981) Storm-generated sedimentary structures in subtidal marine facies in subtidal marine facies with examples from Middle and Upper Ordovician south-western Virginia. *Journal of Sedimentary Petrology*, **51** 823-848.
- Kunii, D. and Levenspiel, O. (1969) *Fluidization Engineering*. John Wiley, New York, pp 534.
- Lababe, P., Sérguret, P. and Seyve, C. (1985) Evolution of a turbiditic foreland basin and analogy with an accretionary prism: example from the South Pyrenean basin. *Tectonics*, **4** 661-686.
- Lagenberg, C. W. (1972) Polyphase deformation in the Sierra de Los Filbrides North of Lubrín, SE Spain. *Univ. Amsterdam, G.U.A. papers of Geology*, **1** 2475-2496.
- Le-Pichon, X. and Sibuet, J. C. (1981) Passive margins: a model of formation. *Journal of Geophysical Research*, **86** 3708-3720.
- Leblanc, D. and Oliver, P. H. (1984) Role of strike slip faulting in the Betic-Rifian orogeny. *Tectonophysics*, **101** 345.
- Legrand, H. E. and Stringfield, V. T. (1973) Karst Hydrology: a review. *Journal of Hydrology*, **20** 97-120.
- Leitch, E. C. and Willis, S. G. A. (1982) Nature and significance of plutonic clasts in Devonian conglomerates of the New England Fold Belt. *Journal of the Geological Society of Australia*, **29** 83-89.
- Leyva-Cabello, F. (1973) *Mapa Geológico De España, 1:50.000 Montilla. Sheet 966*.

Lister, G. S. and Davis, G. A. (1989) The origin of metamorphic core complexes and detachment faults formed during Tertiary continental extension in the northern Colorado River region, U.S.A. *Journal of Structural Geology*, **11** 65-94.

Longman, C. D., Bluck, B. J. and Van-Breeman, O. (1979) Ordovician conglomerates and the evolution of the Midland Valley. *Nature*, **344** 850-853.

Loucks, R. G., Brown, A. A., Achauer, C. W. and Budd, D. A. (1985) Carbonate gravity-flow sedimentation on low angle slopes off the Wolfcampian northwest shelf of the Delaware Basin. In: *Deep-Water Carbonates. Buidups, Turbidites, Debris Flows & Chalks. SEPM core workshop No. 6. New Orleans, March 23-24, 1985.* (Ed. by P.D. Crevello and P.M. Harris) Society of Economic Paleontologists and Mineralogists, 56-92.

Lowe, D. R. (1975) Water escape structures in coarse-grained sediments. *Sedimentology*, **22** 157-204.

Lowe, D. R. (1976) Grain flow and grain deposits. *Journal of Sedimentary Petrology*, **42** 157-183.

Luepke, G. (1984) *Stability of heavy minerals in sandstone*. Van Nostrand Reinhold, New York.

Lundeen, M. T. (1978) Emplacement of the Ronda Peridotite, Sierra Bermeza, Spain. *Bulletin of the Geological Society of America*, **89** 172-180.

Magne, M. A. and Maure, H. F. (1990) *Heavy Minerals in Colour*. Unwin Hyman, London.

Malod, J. A. and Mauffret, A. (1990) Iberian plate motions during the Mesozoic. *Tectonophysics*, **184** 261-278.

Martínez-Del-Olmo, W., Garcíá-Mallo, J., Leret-Verdú, G., Serrano-Oñate, A. and Suárez-Alba, J. (1984) Modelo tectosedimentario del Bajo Guadalquivir. I *Congreso Español de Geología*, **1** 199-213.

Martínez-García, E., Herranz, P., de-San-José, M. A., Perejon, A., Gonzalez-Casado, J. M., Pieren, A., Apalategui, O., Eguiluz, L. and Hernandez-Enrile, J. L. (1986) Geotraverse South (B-1). Excursion guidebook. *International conference on Iberian Terranes and their regional correlation*, Oviedo, Spain, IGCP.

Massonne, H. J. and Schreyer, W. (1987) Phengite geobarometry based on the limiting assemblage with K-feldspar, phlogopite and quartz. *Contributions to Mineralogy and Petrology*, **96** 212-224.

McCave, I. N. (1970) Deposition of fine grained suspended sediment from tidal currents. *Journal of Geophysical Research*, **75** 4151-4159.

McConville, P., Kelley, S. and Turner, G. (1988) Laser probe  $^{40}\text{Ar}/^{39}\text{Ar}$  analysis of Peace River shocked L6 chondrite. *Geochimica et Cosmochimica Acta*, **52** 2487-2499.

McCubbin, D. G. (1982) Barrier island and strand plain facies. In: *Sandstone Depositional Environments*. (Ed. by P.A. Scholle and D.R. Spearing) American Association of Petroleum Geologists, Memoir, **31**, 247-280.

McDonald, B. C. and Banerjee, I. (1971) Sediments and bedforms on a braided

---

outwash plain. *Canadian Journal of Earth Science*, **8** 1282-1301.

McDougall, I. and Harrison, T. M. (1988) *Geochronology and Thermochronology by the  $^{40}\text{Ar}/^{39}\text{Ar}$  method*. Oxford University Press, Oxford, pp 212.

McKensie, D. A. (1978) Some remarks on the development of sedimentary basins. *Earth & Planetary Science Letters*, **40** 25-32.

McNutt, M. K. and Kogan, M. G. (1987) Isostasy in the USSR 2. interpretation of admittance data. In: *The Composition, Structure, Dynamics of the Earth's Lithosphere-Asthenosphere System* (Ed. by F. Fuchs and C. Froixdeveaux) American Geophysical Union, Washington D.C, 309-327.

Miall, A. D. (1978) Tectonic and syndepositional deformation of molasse and other non-marine-paralic sedimentary basins. *Canadian Journal of Earth Sciences*, **15** 1613-1632.

Milliken, K. L. (1988) Loss of provenance information through subsurface diagenesis in Plio-Pleistocene sandstones, Northern Gulf of Mexico. *Journal of Sedimentary Petrology*, **58** 992-1002.

Mitchell, A. H. G. and Reading, H. G. (1986) Tectonics and Sedimentation. In: *Sedimentary Environments and Facies* (Ed. by H.G. Reading) Blackwell Scientific Publications, Oxford, 471-519.

Molina, J. M. and Ruiz-Ortiz, P. A. (1993) Comments on 'Structure and palaeogeography of the External Betic Cordillera, southern Spain' by C.L. Blankenship. *Marine and Petroleum Geology*, **10** 517-518.

Molnar, P. (1988) Continental tectonics in the aftermath of plate tectonics. *Nature*, **335** 131-137.

Monié, P., Galindo-Zaldivar, J., Gonzalez-Lodeiro, F., Goffé, B. and Jabaloy, A. (1991)  $^{39}\text{Ar}/^{40}\text{Ar}$  geochronology of Alpine tectonism in the Betic Cordilleras (southern Spain). *Journal of Geological Society London*, **148** 289-297.

Monié, P., Maluski, H., Saadallah, A. and Caby, R. (1988) New  $^{39}\text{Ar}$ - $^{40}\text{Ar}$  ages of Hercynian and Alpine thermotectonic events in Grande Kabylie (Algeria). *Tectonophysics*, **152** 53-69.

Morton, A. C. (1984) Stability of detrital heavy minerals in Tertiary sandstones from the North Sea basin. *Clay Minerals*, **19** 287-308.

Muang, H. (1987) Transcurrent movements in the Burma Andaman Sea region. *Geology*, **15** 911-912.

Mullins, H. T., Heath, K. C., Buren, M. V. and Newton, C. R. (1984) Anatomy of a modern open-ocean carbonate slope: northern Little Bahama Bank. *Sedimentology*, **31** 141-168.

Mutti, E. and Lucchi, F. R. (1972) Le torbiditi dell'Appennino settentrionale: introduzione all'analisi di facies. *Memorie della Società Geologica Italiana*, **11** 161-199.

Myrow, P. M. and Southard, J. B. (1991) Combined-flow model for vertical stratification sequences in shallow marine storm-deposited beds. *Journal of Sedimentary Petrology*, **51** 202-211.

Newell, N. P. (1955) Bahama platforms in the crust of the Earth, a symposium. *Geological Society of America, Special Paper*, pp 62.

- Nicholls, R. J., Sparks, R. S. J. and Wilson, C. J. N. (1994) Experimental studies of the fluidization of layered sediments and the formation of fluid escape. *Sedimentology*, **41** 233-254.
- Nijhus, H. J. (1964) *Plurifacial Alpine Metamorphisim in the South Eastern Sierra de los Filbrides, South of Lubrín, SE Spain*. Amsterdam, M.Sc.
- Nilsen, T. H. and Abott, P. L. (1981) Palaeogeography and sedimentology of Upper Creteceous Turbidites, San Diego California. *Bullettn of the American Association of Petroleum Geologists*, **65** 1256-1284.
- Normark, W. R. (1978) Fan valleys, channels and depositional lobes on modern submarine fans: Characters for recognition of sandy turbidite environments. *Bulletin of the American Association of Petroleum Geologists*, **62** 912-931.
- Oldow, J. S., Bally, A. W. and Avé-Lallemae, H. G. (1990) Transpression, orogenic float and lithosphere balance. *Geology*, **18** 991-994.
- Olmo-Sanz, A. D., Macia, J. G. d. P., Aldaya-Valverde, F., Montero, J. C., Duenas, V. G., Rossel, L. G., Galdeano, C. S. D., Fernández, M. O. and Roldán, R. T. (1987) *Mapa Geologico De España, 1:50.000 Cortes de la Frontera. Sheet 1.064 (14-45).With Memoirs*. Solid Geology Map, 1st Edition, Instituto Geológico Y Minero De España.
- Oomkens, E. (1974) Lithofacies realtions inn the late Quaternary Niger Delta Complex. *Sedimentology*, **21** 195-222.
- Ore, H. T. (1964) Some critera for the recognition of braided deposits. *Wyoming Contrributions to Geology*, **3** 1-14.
- Ori, G. G. and Friend, P. F. (1984) Sedimentary basins formed and carried piggy-back on active thrust sheets. *Geology*, **12** 475-478.
- Ott-d'Estevou, P. and Montenat, C. (1990) Le Bassin de Sorbas-Tabernas. *Doc. Trav. l'IGAL*, **12-13** 101-128.
- Oxbrugh, I. R. (1972) Plate tectonics and continetal collision. *Nature*, **239** 202-204.
- Page, B. G. N., Bennet, J. D., Caneron, N. R., Bridge, D., Jeffery, D. H., Keats, W. and Thaib, J. (1979) A review of the main structural and magmatic features of Northern Sumatara. *Journal of the Geological Society of London*, **136** 569-579.
- Palmer, M. S. (1979) *Holecene Facies Geometery of the Leeward Bank Margin. Tongue of the Ocean, Bahamas*. Miami Fla. Miami, M.Sc.
- Parkash, B., Sharma, R. P. and Roy, A. K. (1980) The Siwalik Group (molasse) sediments shed by collision of continental plates. *Sedimentary Geology*, **25** 127-159.
- Perez-Lopez, A. D. (1991) *El Trias de Facies Germanica del Sector Central de la Cordillera Betica*. University Granada, Spain, Ph.D.
- Pfiffner, O. A. (1986) Evolution ofthe north Alpine foreland basin in the Central Alps. In: *Foreland Basins* (Ed. by P.A. Allen and P. Homewood) IAS Special Publication, London, 219-228.
- Piper, D. J. W. and Normark, W. R. (1983) Turbidite depositional patterns and flow characteristics, Navy submarine Fan, California Borderland. *Sedimentology*, **30** 681-694.

- Piper, D. J. W., Normark, W. R. and Ingle, J. C. (1976) The Rio Dell formation: a Plio-Pleistocene basin slope deposits in Northern California. *Sedimentology*, **23** 309.
- Platt, J. P. and Behrmann, J. H. (1985) Structures and fabrics in a crustal-scale shear zone, Betic Cordillera, SE Spain. *Journal of Structural Geology*, **8** (1) 15-33.
- Platt, J. P. and Vissers, R. L. M. (1989) Extensional collapse of thickened continental lithosphere: A working hypothesis for the Alboran Sea and Gibraltar Arc. *Geology*, **17** 540-543.
- Platzman, E. S. (1992) Paleomagnetic rotations and the kinematics of the Gibraltar arc. *Geology*, **20** 311-314.
- Platzman, E. S., Platt, J. P. and Oliver, P. (1993) Palaeomagnetic rotations and fault kinematics in the Rif Arc of Morocco. *Journal of the Geological Society of London*, **150** 707-718.
- Powell, R. and Evans, J. A. (1983) A new geobarometer for the assemblage biotite-muscovite-chlorite-quartz. *Journal of Metamorphic Geology*, **1** 331-336.
- Prior, D. B. and Bornhold, B. D. (1988) Submarine morphology and processes of fjord fan deltas and related high gradient systems: modern examples from British Columbia. In: *Fan Deltas: Sedimentology and Tectonic Settings* (Ed. by Nemec and Steel) Blackie, London, 125-143.
- Prior, D. B. and Bornhold, B. D. (1989) Submarine sedimentation on a developing Holocene fan delta. *Sedimentology*, **36** 1053-1076.
- Puga, E. and Díaz-de-Frederico, A. (1978) Metemorfismo polifásico y deformaciones alpinas en el Complejo de Sierra Nevada (Cordillera Bética). Implicaciones geodinámicas. *Proceedings Reunión sobre la geodinámicas de la Cordillera Bética y Mar de Alborán*.
- Puigdefábregas, C., Muñoz, J. A. and Marzo, M. (1986) Thrust belt development in the eastern Pyrenees and related depositional sequences in the southern foreland basin. In: *Foreland Basins* (Ed. by P.A. Allen and P. Homewood) IAS Special Publication, London, 229-246.
- Raaf, J. F. M. and Boersma, J. R. (1971) Tidal deposits & their sedimentary structures. *Geol. Mijnb.*, **50** 479-503.
- Ramberg, H. (1981) *Gravity deformation and the Earth's crust*. Academic Press, London.
- Rapson, J. E. (1965) Petrography and derivation of Jurassic-Cretaceous clastic rocks, southern Rocky Mountains, Canada. *Bulletin of the American Association of Petroleum Geologists*, **49** 1426-1452.
- Reading, H. G. (1982) Sedimentary basins and global tectonics. *Proceedings of the Geological Association*, **93** 321-350.
- Rehault, J. P., Mousatt, E. and Fabbri, A. (1987) Structural evolution of the Tyrrhenian back-arc basin. *Marine Geology*, **74** 123-150.
- Reicheter, K. (1993) To balance or not? Comment on 'Structure and palaeogeography of the External Betic Cordillera, southern Spain' by C.L. Blankenship. *Marine and Petroleum Geology*, **10** 514-516.

Reineck, H. E. (1963) Sedimentgefüge in Bereich der südlicher Nordsee. *Abh. Senckenbergische Naturforsch Ges.*, **505** 1-138.

Reineck, H. E. and Singh, I. B. (1973) *Depositional Sedimentary Environments With Reference to Terrigenous Clastics*. Springer Verlag, Berlin, pp 439.

Rex, R. W. (1969) Eolian origin of sands of Hawaiian Islands and Pacific Pelagic Sediments. *Journal of Sedimentary Petrology*, **163** 277-279.

Ricci-Lucchi, F. (1986) The Oligocene to Recent foreland basins of the northern Apennines. In: *Foreland Basins* (Ed. by P.A. Allen and P. Homewood), IAS Special Publication, London, 105-140.

Roca, E. and Desegaulx, P. (1992) Analysis of the geological evolution and vertical movements in the València Trough area, western Mediterranean. *Marine and Petroleum Geology*, **9** 167-185.

Rodriguez-Fernandez, J. and Martin-Penela, J. (1993) Neogene evolution of the Campo de Dalias and the surrounding offshore areas-(Northeastern Alboran Sea). *Geodinamica Acta*, **6** (4), 225-270.

Roest, W. R. and Sirvastava, S. P. (1991) Kinematics of plate boundaries between Eurasia, Iberia and Africa in the North Atlantic from the Late Cretaceous. *Geology*, **19** 613-616.

Roldan-Garcia, F. J. and Rodriguez-Fernandez, J. (1991) Un ejemplo de cuenca piggyback asociada a la evolucion Neogena del frente de las Zonas Externas Béticas. *I Congreso del Grupo Español Terclero*, 73-94.

Roldán-Garcia, J. F. and Dívar-Rodríguez (1985b) *Mapa Geológico De España, 1:50.000 Montilla. Sheet 966. With Memoirs*. Solid Geology Map, 1st Edition, Instituto Geológico Y Minero De España.

Roldán-Garcia, J. F., Ruiz-Ortiz, P. A. and Molino-Cámara, J. M. (1985a) *Mapa Geológico De España, 1:50.000 Baena. Sheet 967. With Memoirs*. Solid Geology Map, 1st Edition, Instituto Geológico Y Minero De España.

Ruiz-Ortiz, P. A. (1983) A carbonate submarine fan in a fault-controlled basin of the Upper Jurassic, Betic-Cordillera, southern Spain. *Sedimentology*, **30** 33-49.

Rust, B. R. (1972) Structure and process in a braided river. *Sedimentology*, **18** 221-245.

Rust, B. R. (1972b) Pebble orientation in fluvial sediments. *Journal of Sedimentary Petrology*, **42** 384-388.

Rust, B. R. (1975) Fabric and structure in glaciofluvial gravels. In: *Glaciofluvial and Glaciolacustrine Sedimentation*. (Ed. by A.V. Jopling and B.C. McDonald) Society of Economic Palaeontologists and Mineralogists, Special Publication, 238-248.

Saidovia, K. M. (1967) Sediment stratigraphy and paleogeography of the Pacific Ocean by benthonic Foraminifera during the Quaternary. *Progress in Oceanography*, **4** 143-151.

Saleeby, J. B. (1977) Fracture zone tectonics, continental margin fragmentation and emplacement of the King Kaeah ophiolite belt. In: *North American Ophiolites*. (Ed. by R.G. Coleman and W.P. Irwin), Orogen Dept. of Geol. & Min. Ind. Bull., 141-160.

Sanz-De-Galdeano, C. (1990) Geologic evolution of the Betic Cordilleras in the



Western Mediterranean, Miocene to present. *Tectonophysics*, **172** 107-119.

Sanz-de-Galdeano, C., Algarra, A. M., Vera, J. A. and Rivas, P. (1993) Comments on 'Structure and palaeogeography of the External Betic Cordillera, southern Spain' by C.L. Blankenship. *Marine & Petroleum Geology*, **10** 518-519.

Sanz-de-Galdeano, C. and Vera, J. A. (1992) Stratigraphic record and palaeogeographical context of the Neogene basins in the Betic Cordillera, Spain. *Basin Research*, **4** 21-36.

Scholle, P. A., Artheur, M. A. and Ekdale, A. A. (1983) Pelagic Environments. In: *Carbonate Depositional Environments*. (Ed. by P.A. Scholle, D.G. Bebout and C.H. Moore) American Association of Petroleum Geologists, Tulsa, 619-691.

Schumacher, J. C. (1991) Empirical ferric iron corrections: necessity, assumptions, and effects on selected geothermobarometers. *Mineralogical Magazine*, **55** 3-18.

Schwartz, M. L. (1973) *Barrier Islands*. Dowden, Hutchinson & Ross, Stroudsburg, pp 451.

Scott, E. (1992) The palaeoenvironment and dynamics of the Rannoch-Etive nearshore and coastal succession, Brent Group, Northern North Sea. In: *Geology of the Brent Group* (Ed. by A.C. Morton, R.S. Hazeldine, M.R. Giles and S. Brown) Geological Society of London, London.

Seilacher, A. (1982) Distinctive features of sandy tempestites. In: *Cyclic and Event Stratification*. (Ed. by G. Einsele and A. Seilacher) Springer-Verlag, Berlin, 333-349.

Sirvastava, S. P., Roest, W. R., Kovacs, L. C., Oakey, G., Lévesque, S., Verhoef, J. and Macnab, R. (1990a) Motion of Iberia since the late Jurassic: Results from detailed aeromagnetic measurements in the Newfoundland Basin. *Tectonophysics*, **184** 229-260.

Sirvastava, S. P., Schouten, H., Roest, W. R., Kiltgord, K. D., Kovacs, L. C., Verhoef, J. and Macnab, R. (1990b) Iberian plate kinematics: a jumping plate boundary between Eurasia and Africa. *Nature*, **344** 756-759.

Sloss, L. L. (1963) Sequences in the cratonic interior of North America. *Bulletin of the Geological Society of America*, **74** 93-114.

Smith, N. D. (1970) The braided stream depositional environment; Comparison of the Platte River with some Silurian clastic rocks, North Central Appalachians. *Bulletin of the Geological Society of America*, **82** 3407-3420.

Steel, R. J. and Gloppen, T. G. (1980) Late Caledonian (Devonian basin formation, western Norway) signs of strike slip tectonics during infilling. In: *Sedimentation in Oblique Slip Mobile Zones*. (Ed. by P.F. Ballance and H.G. Reading) I.A.S. Special Publication, 79-103.

Stow, D. A. V. (1978) Deep Clastic Seas. In: *Sedimentary Environments and Facies*. (Ed. by H.G. Reading) Blackwell Scientific Publications, London, 399-444.

Stow, D. A. V. (1992) Deep-water environments: overview and commentary. In: *Deep-Water Turbidite Systems*. (Ed. by D. A. V. Stow) Blackwell Scientific Publications, Oxford, 182-202.

Suárez-Alba, J., Martínez-del-Olmo, W., Serrano-Oñate, A. and Leret-Verdú, G. (1988) Estructa del sistema Turbidítico De La Formación arenas Guadalquivir, Neogeno Del Valle del Guadalquivir. *Geogaceta*, **6** 1-23.

- Suczek, C. A. and Ingersoll, R. V. (1984) Petrology and provenance of cenozoic sand from the Indus cone and the Arabian basin, DSDP sites 221, 222 and 224. *Journal of Sedimentary Petrology*, **55** (3), 340-346.
- Sun, S. Q. (1990) Discussion of Swaley Cross-Stratification produced by unidirectional flow, Bencliff Grit (Upper Jurassic), Dorset, U.K. *Journal of the Geological Society, London*, **147** 396-400.
- Sweeting, M. M. (1973) *Karst Landforms*. Macmillan Publishers, London, pp 362.
- Swift, D. J. P. (1975) Barrier Island genesis evidence from the Middle atlantic Shelf of North America. *Sedimentary Geology*, **14** 1-43.
- Sylvester, A. G. (1988) Strike slip faults. *Bulletin of the Geological Society of America*, **100** 1666-1703.
- Tankard, A. J. (1986) On the depositional response to thrusting and lithospheric flexure: Examples from the Appalachian and Rocky Mountain basins. In: *Foreland Basins* (Ed. by P.A. Allen and P. Homewood) IAS Special Publication, London, 369-394.
- Tapponier, P., Peltzer, G. and Armijo, R. (1986) On the mechanics of collision between India & Asia. In: *Collision Tectonics* (Ed. by M.P. Coward and A.C. Reis) Geological Society of London, London, 115-157.
- Thompson (1937) Original structures of beaches, bars and lines. *Bulletin of the Geological Society of America*, **48** 723-752.
- Torné, M., Banda, E., Garcíá-Dueñas, V. and Balanyá, J. C. (1992) Mantle-lithosphere bodies in the Alboran crustal domain (Ronda peridotites, Betic-Rif orogenic belt). *Earth and Planetary Science Letters*, **110** 163-171.
- Torres-Roldán, R. L. (1979) The tectonic subdivision of the Betic Zone (Betic Cordilleras, Southern Spain): Its significance and one possible Geotectonic Scenario for the Westernmost Alpine Belt. *American Journal of Science*, **279** 19-51.
- Tortosa, A., Palomares, M. and Arribas, J. (1991) Quartz grain types in Holocene deposits from the Spanish Central System: some problems in provenance analysis. In: *Developments in Sedimentary Provenance Studies*. (Ed. by P.D.W. Haughton, S.P. Todd and A.C. Morton), London Geological Society, London, 138-175
- Tubia, J. M. and Cuevas, J. (1986) High temperature emplacement of the Los Reales peridotite nappe (Betic Cordillera, Spain). *Journal of Structural Geology*, **8** 473-482.
- Tubia, J. M. and Cuevas, J. (1987) Structure et cinématique liées à la mise en place de peridotites de Ronda (Cordillères Bétiques, Espagne). *Geodinamica Acta.*, **1** 59-69.
- Tubia, J. M. and Ibarguchi, J. J. G. (1991) Eclogites of the Ojén nappe a record of subduction in the Alpujarride complex (Betic Cordilleras, southern Spain). *Journal of the Geological Society of London*, **148** 801-804.
- Tubia, J. M., Navarro-Vilá, F. and Cuevas, J. (1993) The Málaga-Los Reales Nappe: an example of crustal thinning related to the emplacement of the Ronda peridotites (Betic Cordillera). *Physics of the Earth and Planetary Interiors*, **78** 343-354.
- Van-Wagoner, J. C., Mitchum, R. M., Campion, K. M. and Rahmanian, V. D. (1990) *Siliclastic Sequence Stratigraphy in Well Logs, Cores and Outcrops: Concepts for High-Resolution Correlation of Time and Facies*. American Association of Petroleum

---

Geologists, Tulsa, Oklahoma, pp 55.

Van-Wees, J. D., De-Jong, J. and Cloetingh, S. (1992) Two dimensional P-Tt modelling and the dynamics of extension and inversion in the Betic Zone (S.E. Spain). *Tectonophysics*, **203** 305-324.

Velde, B. (1965) Phengite micas: synthesis, stability, and natural occurrence. *American Journal of Science*, **263** 886-913.

Walker, R. G. (1967) Turbidite sedimentary structures and their relationship to proximal and distal depositional environments. *Journal of Sedimentary Petrology*, **37** 25-43.

Walker, R. G. (1978) Deep water sandstone facies and ancient submarine fans: models for exploration for stratigraphic traps. *Bulletin of the American Association of Petroleum Geologists*, **62** 932-966.

Walker, R. G. (1984) Turbidites and associated coarse clastic deposits. In: *Facies Models* (Ed. by R.G. Walker) Geological Association of Canada, Toronto.

Walker, R. G. (1985) Ancient examples of tidal sand bodies formed in open shallow seas. In: *Shelf Sands and Sandstone Reservoirs* (Ed. by R.W. Tillman) Tulsa.

Walker, R. G., Duke, W. L. and Leckie, D. A. (1983) Hummocky cross stratification. Significance of its variable bedding sequences. Discussion and reply. *Bulletin of the Geological Society of America*, **94** 1245-1251.

Walker, R. G. and Mutti, E. (1973) Turbidite facies and facies associations. In: *Turbidites and Deep Water Sedimentation*. (Ed. by G.V. Middleton and R.H. Bouma) Pacific Section of the Society of Economic Palaeontologists and Mineralogists. Short Course, 119-157.

Waschbusch, P. J. and Royden, L. H. (1992) Episodicity in foredeep basins. *Geology*, **20** 915-918.

Watts, A. B. and Cochrane, J. R. (1974) Gravity anomalies and flexure of the lithosphere along the Hawaiian Emperor seamount chain. *Gophysical Journal of the Astrological Society*, **38** 119-141.

Wernicke, B. (1985) Uniform-sense normal simple shear of the continental lithosphere. *Canadian Journal of Earth Sciences*, **22** 108-125.

Whittaker, J. (1974) Ancient submarine canyons and fan valleys. In: *Modern and Ancient Geosynclinal Sedimentation*. (Ed. by R.H. Dott and R.H. Shaver) Special Publication Society of Economic Palaeontologists and Mineralogists, 106-125.

Williams, P. F. and Rust, B. R. (1969) The sedimentology of a braided river. *Journal of Sedimentary Petrology*, **39** 649-679.

Wilson, J. L. (1975) *Carbonate Facies in Geologic History*. Springer-Verlag, New York, pp 439.

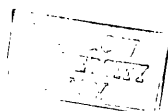
Woodcock, N. H. (1976) Ludlow series slumps and turbidites and the form of the Montgomery Trough, Powys, Wales. *Proceedings of the Geologists' Association*, **87** 165-191.

Wu, F. T. and Wang, P. (1988) Tectonics of western Yunnan Province, China. *Geology*, **16** 153-157.

Zeck, H. P., Molné, P., Villa, I. M. and Hansen, B. T. (1992) Very high rates of

---

cooling and uplift in the Alpine belt of the Betic Cordilleras, Southern Spain. *Geology*, **20**  
79-82.



# **The Origin of the External Basins of the Betics, Southern Spain**

(and Their Use in Interpreting the Orogenic History)



*The Alhambra, Granada*

**S.G.L. Stromberg B.Sc. (University of Liverpool)**

A thesis submitted for the degree of Ph.D.

University of Glasgow

Department of Geology & Applied Geology.

July 1994.

**Vol. 2.**



## ***Volume 2***

# ***Figures & Appendices***

# ***Overview***

## ***Figures***



Figure O.1 The Alboran sea and surrounding mountain chains.

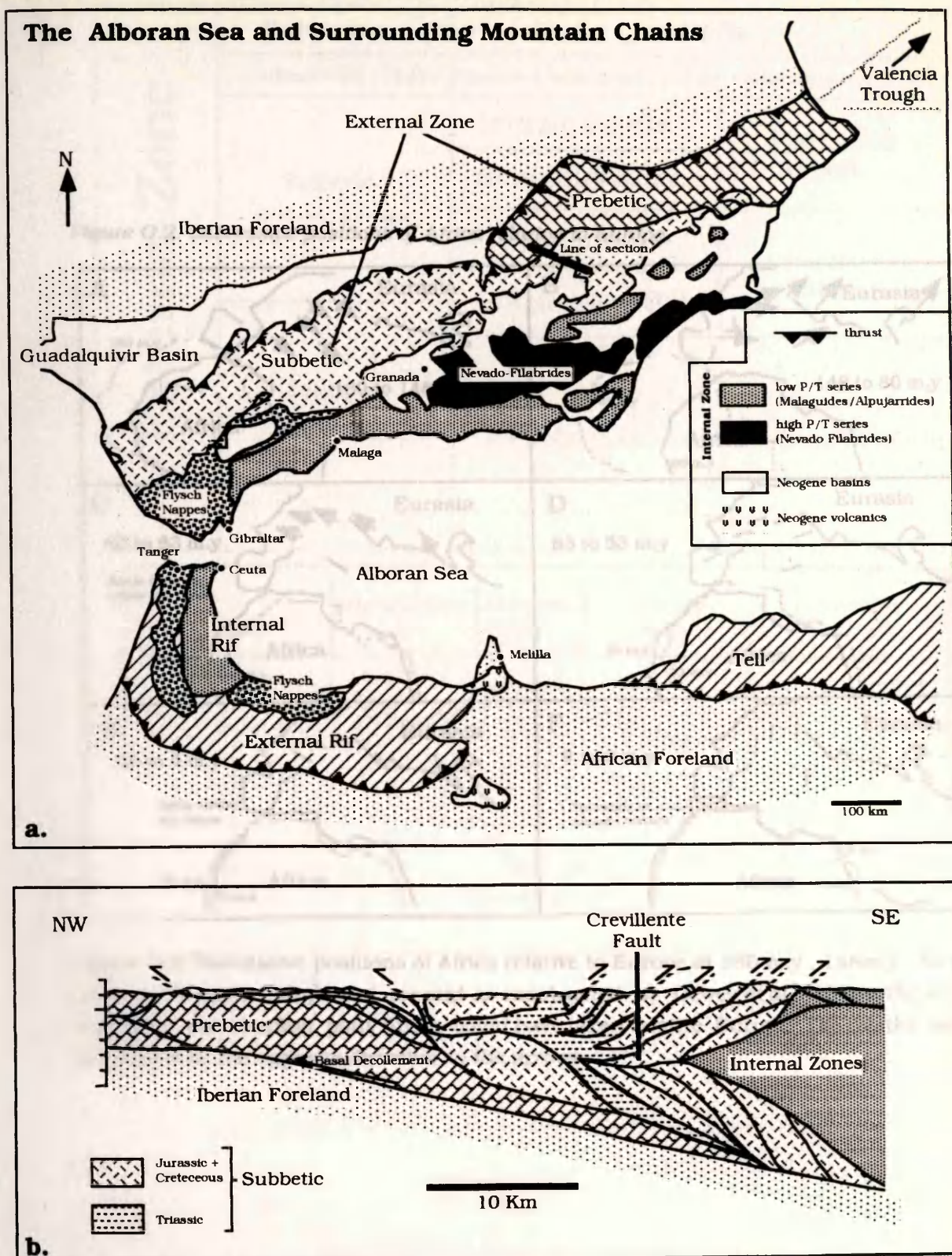


Figure O.1 (a) Alboran sea and surrounding mountain chains, modified from Platt & Vissers (1989) and Torres-Roldán (1979). (b) Structural cross section through the External Zone of the Eastern Betic Cordillera, from Allerton *et al.* (1993)



Figure O.3 The subdivision of the External Zone.

A.	Subzones	Units	
	Bulmenthal (1927)	García-Hernández (1979)	Blankenship (1991)
	Subetic (Pelagic marine)	Internal Subetic	Platformal
		External Subetic	Subetic

Figure O.2. Successive positions of Africa relative to Europe.

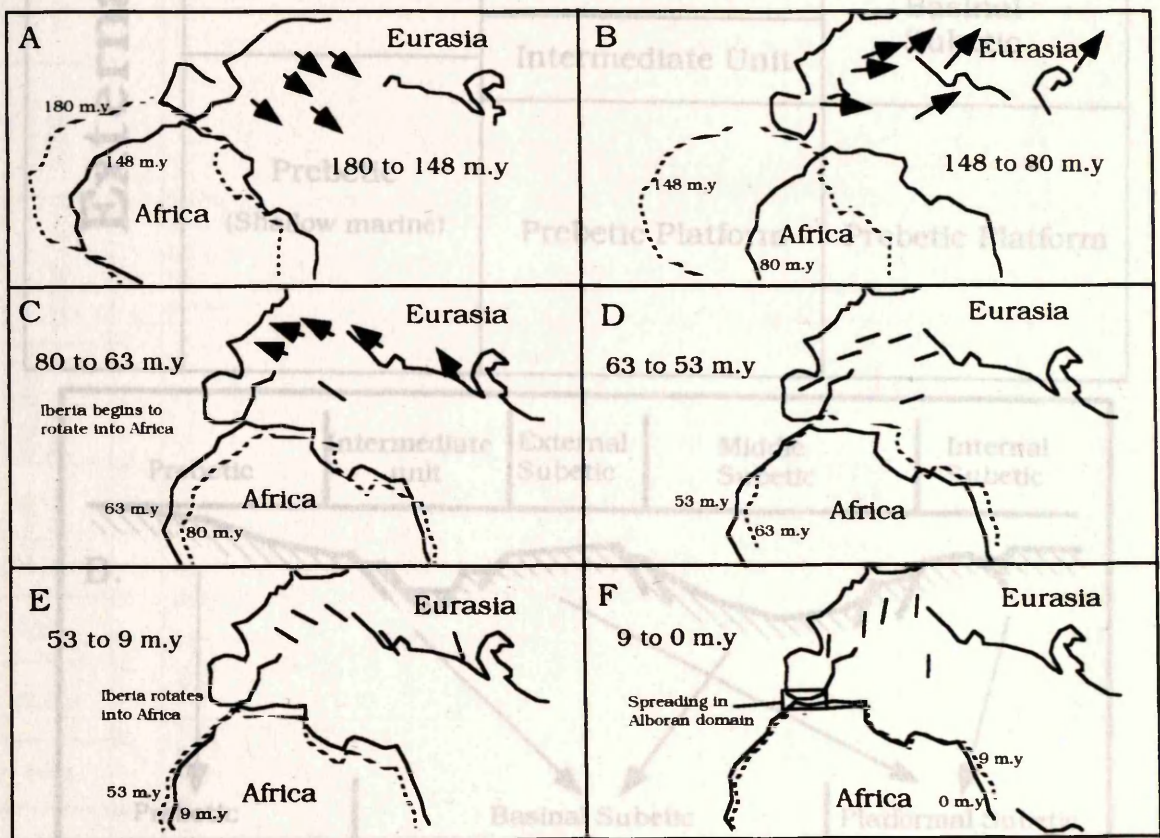


Figure O.2. Successive positions of Africa relative to Europe at 180 m.y., 148m.y., 80 m.y., 63 m.y., 53 m.y., 9 m.y., and present as constructed by Dewey *et al.* ((1973). The arrows represent the simplest path Africa could have taken relative Europe. The relative motion of Iberia is in the opposite direction to the arrows.

Figure O.3. A) shows the subdivision of the External Zone according to various authors. Equivalent units for each scheme are shown. A) relates to (B & C) which show the two contrasting models for the palaeogeography of the External Zone of the Betic Orogen: (B) shows the interpretation of García Hernández *et al.* (1980), C) shows the recent model of Blankenship (1992) which is much simpler and is based on borehole data and seismic reflection profiles. Equivalent units are shown by arrows. (Diagram after Blankenship (1992).



Figure. O.3 The subdivision of the External Zone.

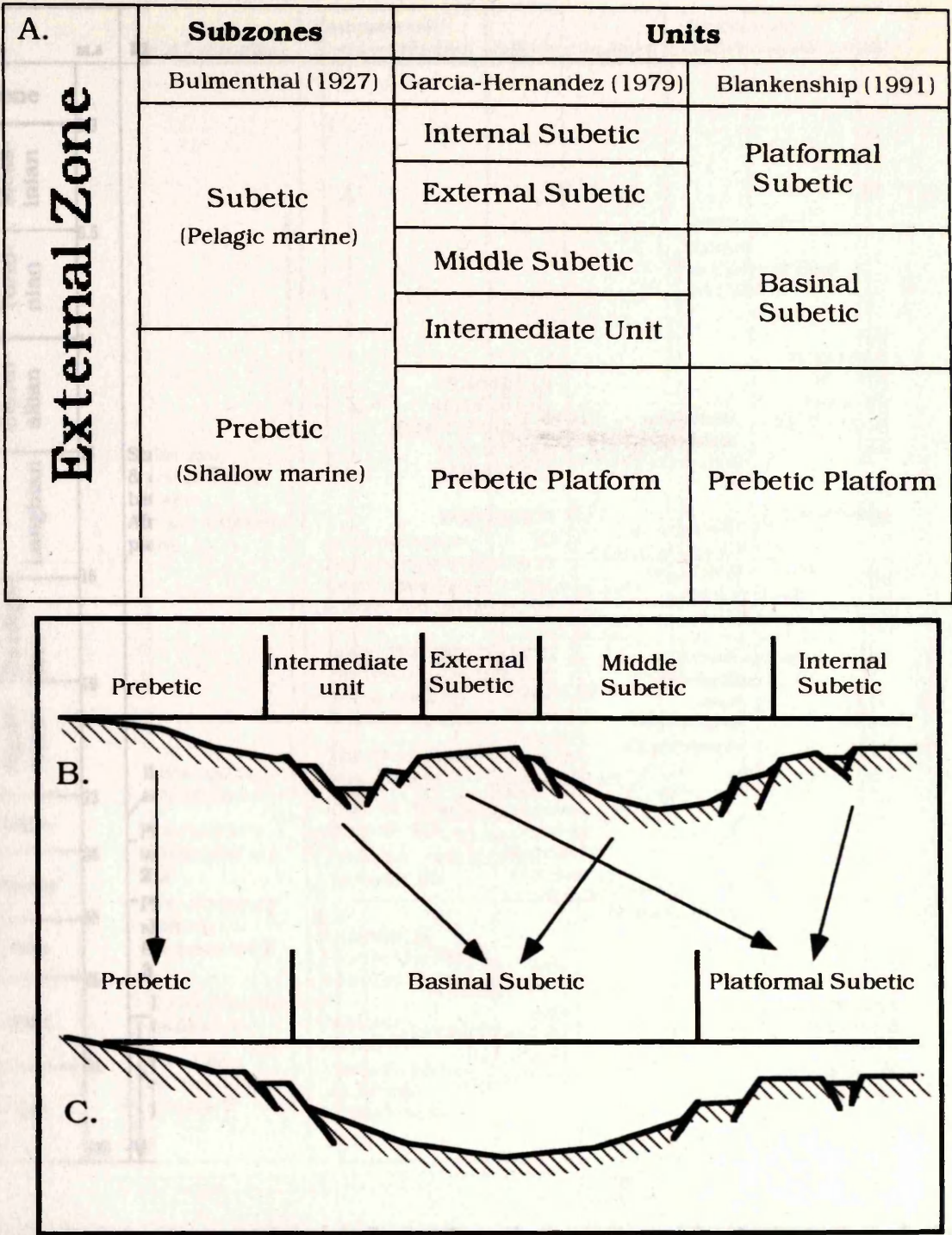


Figure. O.3. A) shows the subdivision of the External Zone according to various authors, Equivalent units for each scheme are shown. A) relates to (B & C) which show the two contrasting models for the palaeogeography of the External Zone of the Betic Orogen; B) shows the interpretation of Garcia Hernandez et al. (1980); C) shows the recent model of Blankenship (1992) which is much simpler and is based on borehole data and seismic reflection profiles. Equivalent units are shown by arrows. Diagram after Blankenship (1992).



Figure O.4 A summary of hypothesis proposed for the Betic Orogen.

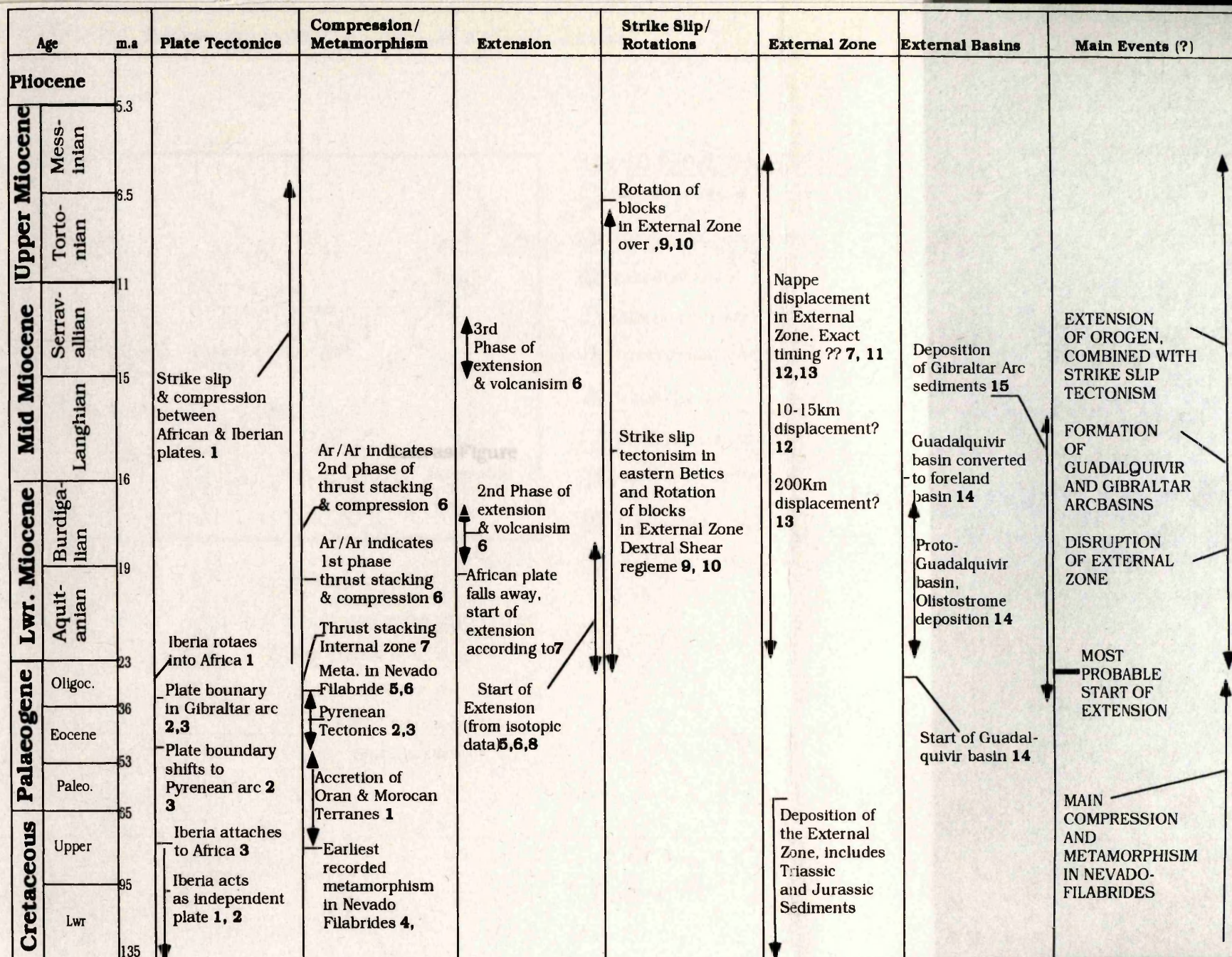


Figure O.4 A summary of the conflicting hypotheses proposed for the tectonic evolution of the Betic Orogen. Numbers (in bold) indicate the sources of the data which are as follows: 1 Dewey (1973), 2 Roest and Sirvastava (1990), 3 Sirvastava *et al.* (1990), 4 Moiné *et al.* (1991), 5 Bakker *et al.* (1989), 6 de Jong *et al.* (1992), 7 Platt & Vissers (1989), 8 Zeck *et al.* (1992), 9 Platzman *et al.* (1993), 10 Allerton *et al.* (1993), 11 Garcia Hernandez (1980), 12 Martinez & Ruitz Ortiz (1993), 13 Blankenship (1992), 14 Sanz de Galdeano & Vera (1993), 15 Bourgois (1973). Column on the right indicates the tectonic events most authors (1-15) agree with and therefore the most likely.



Figure O.4 A summary of hypothesis proposed for the Betic Orogen.

Figure O.5 Sedimentary rocks from known plate tectonic settings.

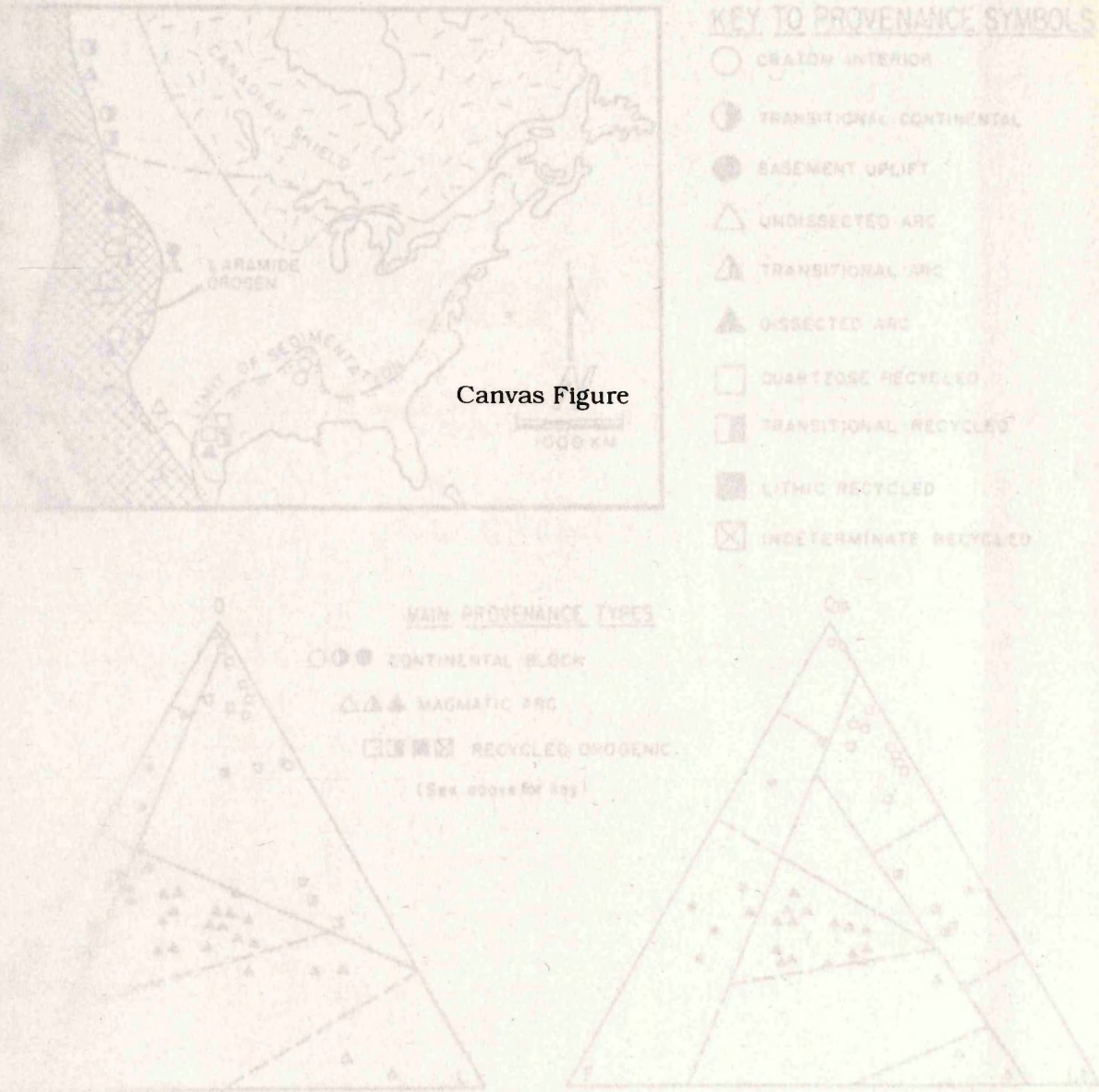


Figure O.4 A summary of the conflicting hypotheses proposed for the tectonic evolution of the Betic Orogen. Numbers (in bold) indicate the sources of the data which are as follows: 1 Dewey (1973), 2 Roest and Sirvastava (1990), 3 Sirvastava *et al.* (1990), 4 Moiné *et al.* (1991), 5 Bakker *et al.* (1989), 6 de Jong *et al.* (1992), 7 Platt & Vissers (1989), 8 Zeck *et al.* (1992), 9 Platzman *et al.* (1993), 10 Allerton *et al.* (1993), 11 Garcia Hernandez (1980), 12 Martinez & Ruitz Ortiz (1993), 13 Blankenship (1992), 14 Sanz de Galdeano & Vera (1993), 15 Bourgois (1973). Column on the right indicates the tectonic events most authors (1-15) agree with and therefore the most likely.



Figure O.5 Sedimentary rocks from known plate tectonic settings.

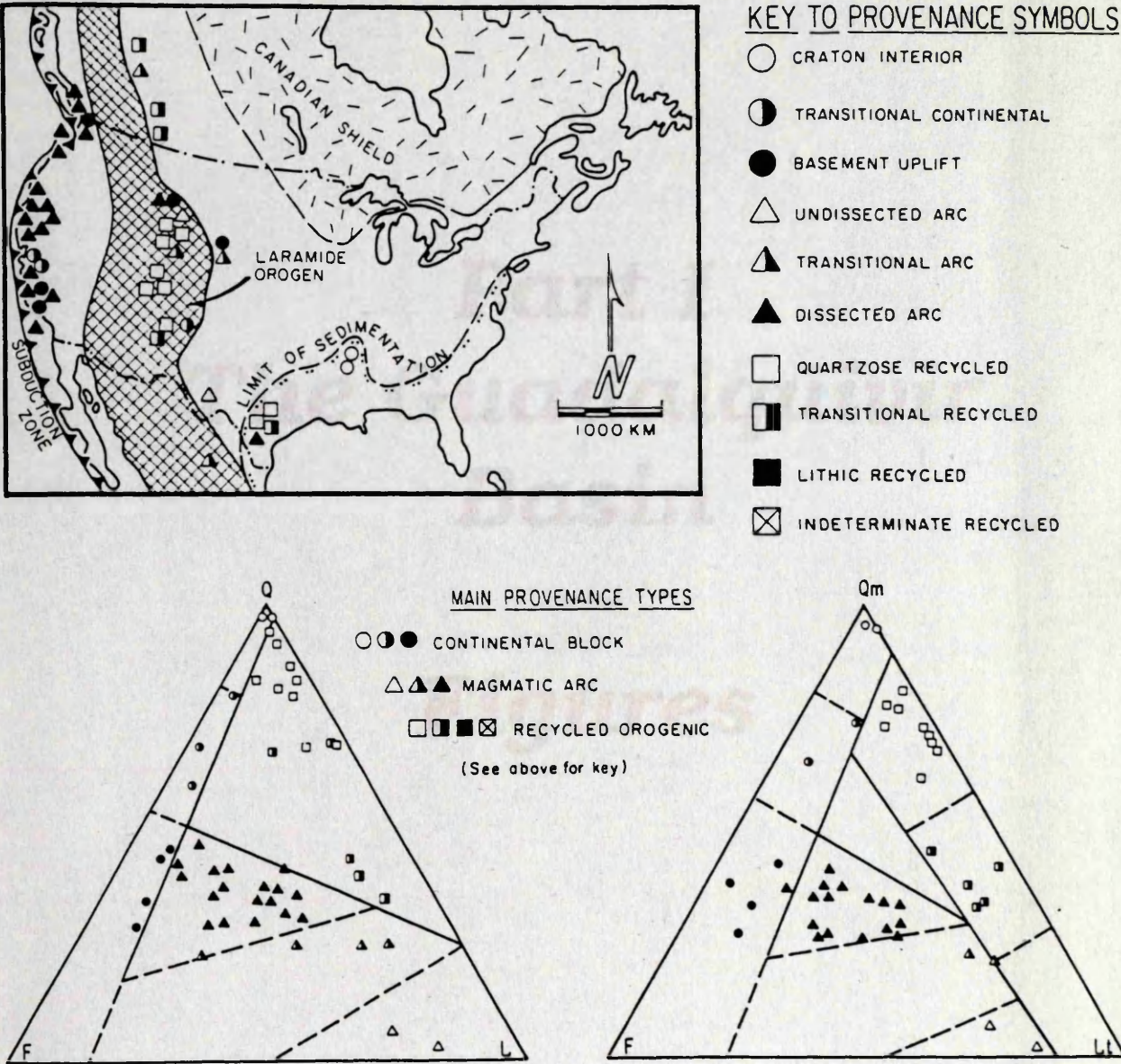


Figure O.5 Sedimentary rocks from known plate tectonic settings can be plotted in terms of their components. Such plots and quantitative petrology can be used to determine the general plate tectonic setting of other sedimentary rocks. Plot taken from Dickinson *et al.* (1983).



***Part I***  
***The Guadalquivir***  
***Basin***

***Figures***

# ***Chapter 1***

## ***Introduction***

***Figures***



Figure 1.1 Baena-Montilla study area for the Guadalquivir Basin. The area was selected on the basis of exposure and because it contains both autochthonous and allochthonous rocks. The area is constrained by three geological maps (Foldouts 1,2 & 3; Roldán García *et al.*, 1985a,b; Leyva Cabello, 1973). Seismic section (Fig. 2.1) and boreholes are located on the map.



Figure 1.1 The Baena-Montilla study area

# The Guadalquivir Basin & Chosen Study Area

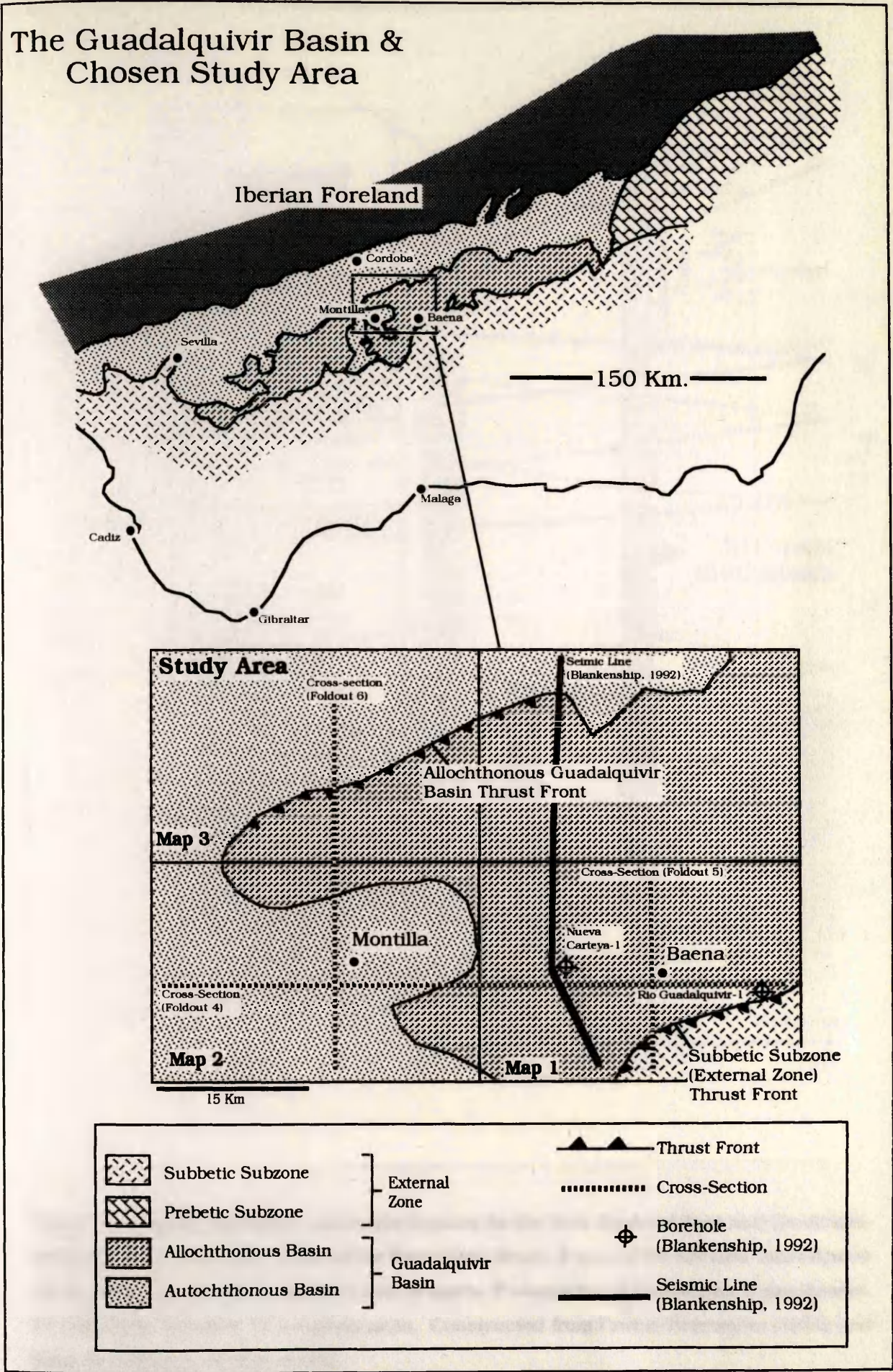




Figure 1.2 Lithostratigraphic correlation diagram.

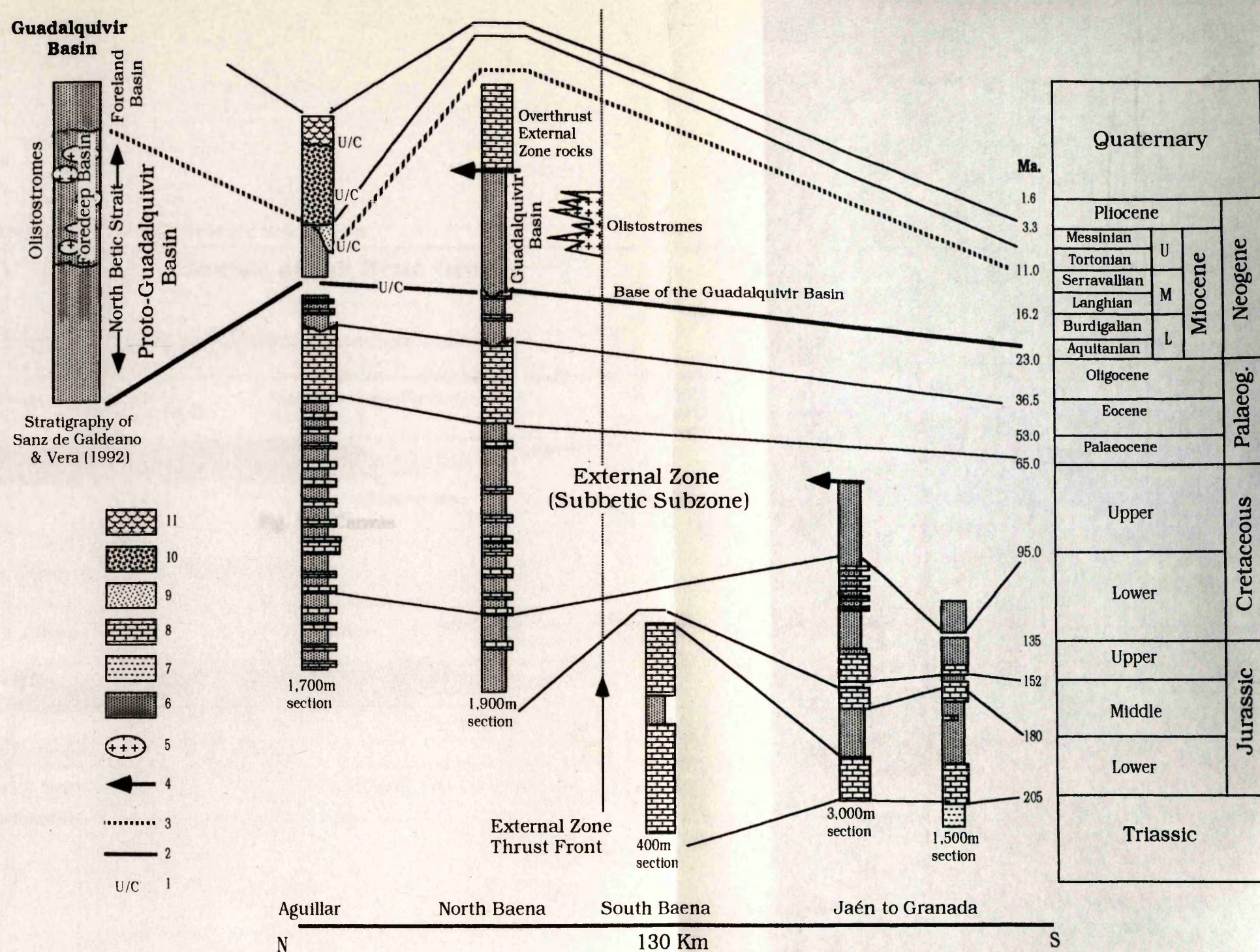


Figure 1.2 Lithostratigraphic correlation diagram for the Betic External Zone and Guadalquivir Basin; 1 unconformity, 2 base of the North Betic Strait, 3 base of the foreland Guadalquivir Basin, 4 thrust contact, 5 olistostromes, 6 marls, 7 evaporites, 8 limestones, 9 sandstones, 10 calc-lithic arenites, 11 conglomerates. Constructed from García Hernández (1980) and Sanz de Galdeano & Vera (1992).



Figure 1.4 Cross-section across the Guadalquivir Basin.

Figure 1.3 Basin development in the Betic Orogen.

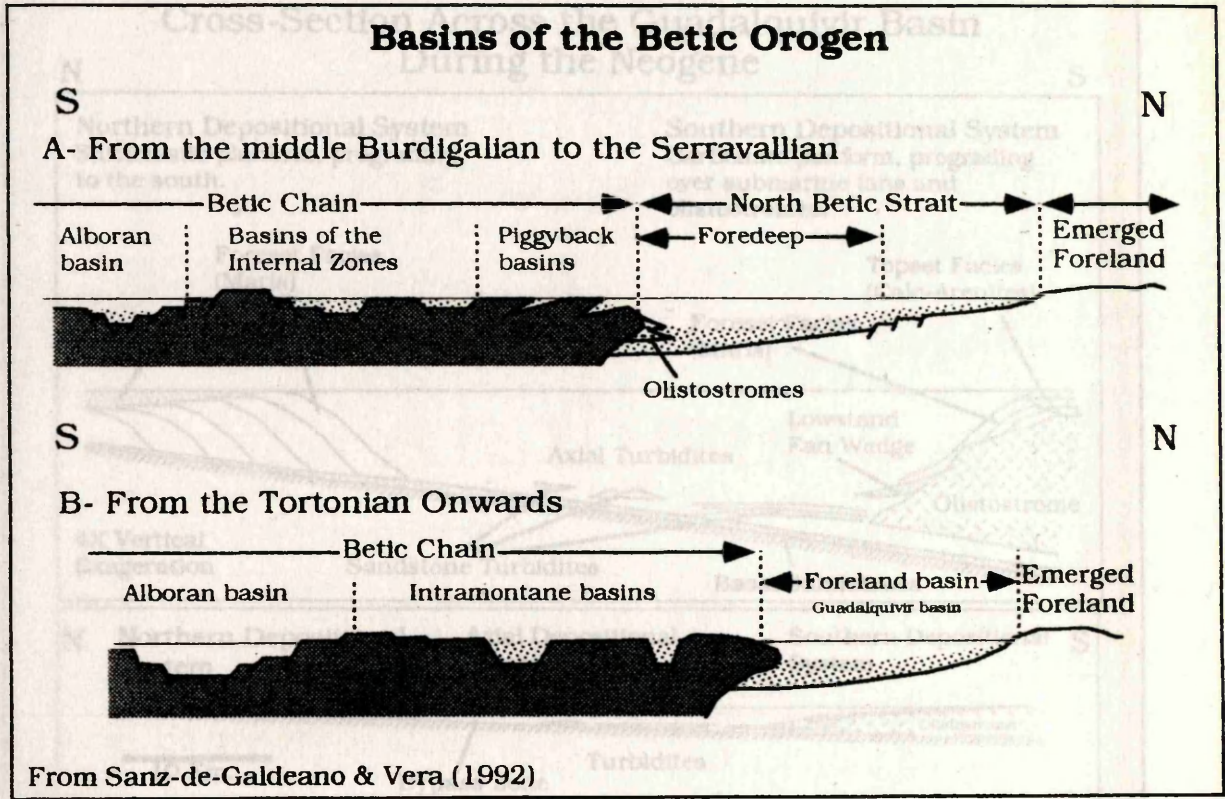


Figure 1.3 Basin development in the Betic Orogen during the Lower Miocene; (A) Burdigalian to Serravallian, (B) from the Tortonian onwards.

Figure 1.4 Cross-section across the Guadalquivir Basin, as interpreted by Suárez-Alba et al. (1992).



Figure 1.4 Cross-section across the Guadalquivir Basin.

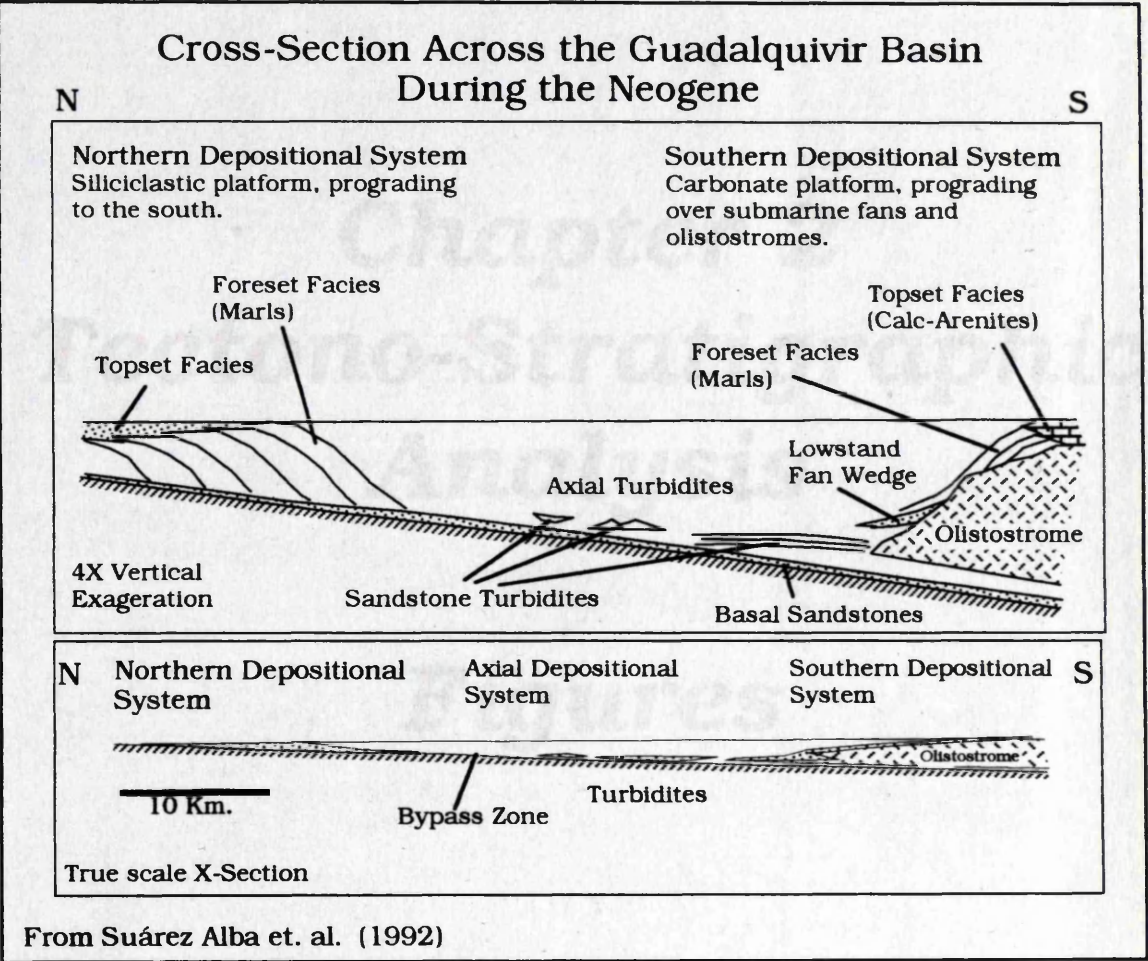


Figure 1.4 Cross-section across the Guadalquivir Basin, as interpreted by Suárez Alba *et al.* (1992).



**Chapter 2**  
**Tectono-Stratigraphic**  
**Analysis**

**Figures**

Figure 2.1 Seismic profile across the Guadalquivir Basin.

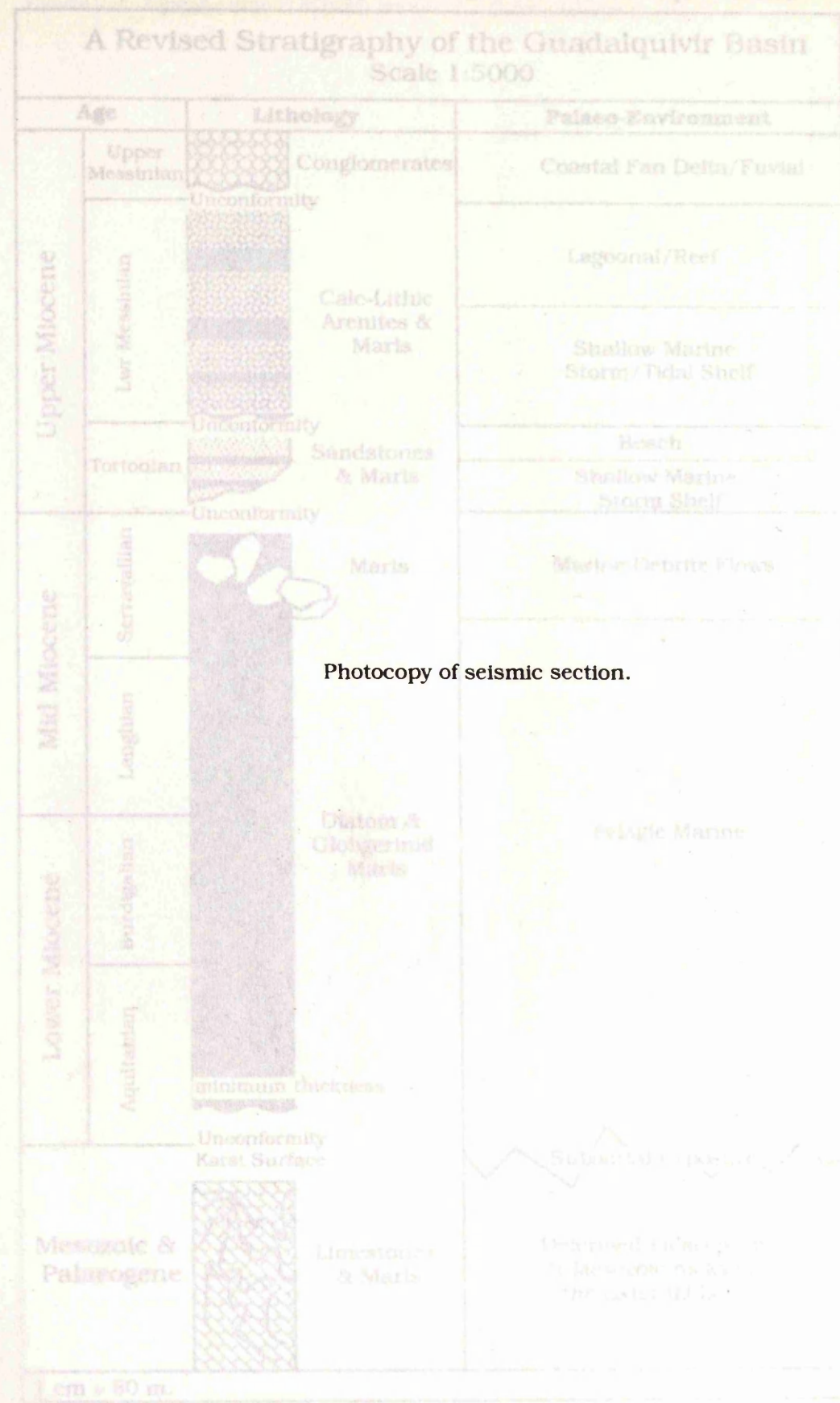


Figure 2.1 A revised stratigraphy for the autochthonous Guadalquivir Basin. Stratigraphy of the Guadalquivir Basin. Line of transect and constraining bore hole (Nueva Carteya) is located on Fig. 1.1. Seismic line and interpreted line drawing taken from Blankenship (1992).



Figure 2.1 Seismic profile across the Guadalquivir Basin.

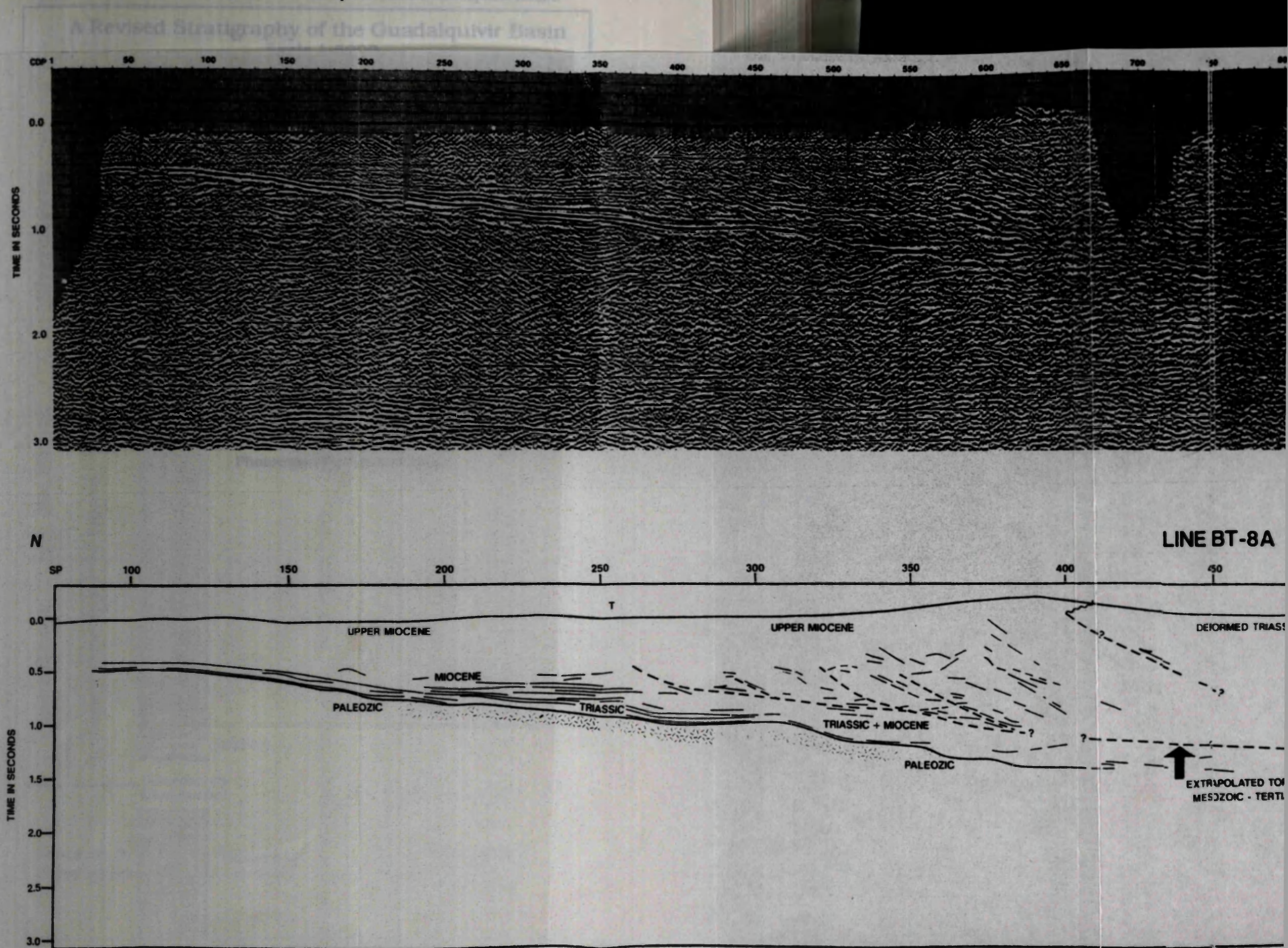
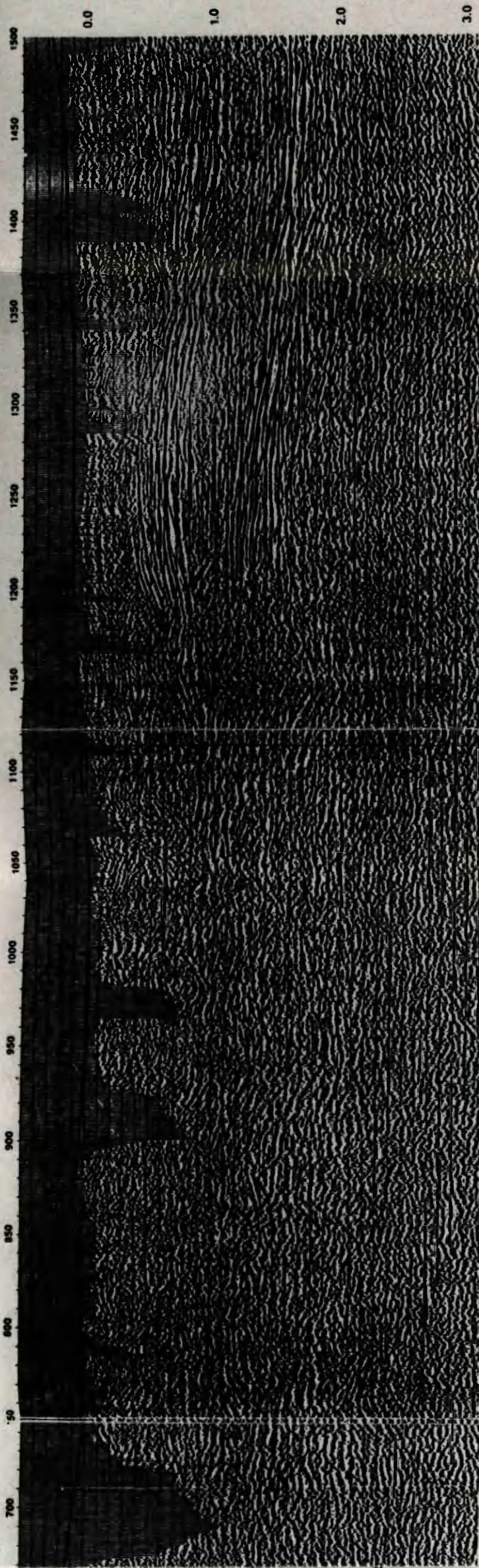


Figure 2.1 A revised stratigraphy for the autochthonous Guadalquivir Basin. Stratigraphy  
 Figure 2.1 Seismic profile and interpreted line drawing across the allochthon and autochthon of the Guadalquivir Basin. Line of transect and constraining bore hole (Nueva Carteya) is located on Fig. 1.1. Seismic line and interpreted line drawing taken from Blankenship (1992).



TIME IN SECONDS



LINE BT-8A

NUEVA CARTEYA



S

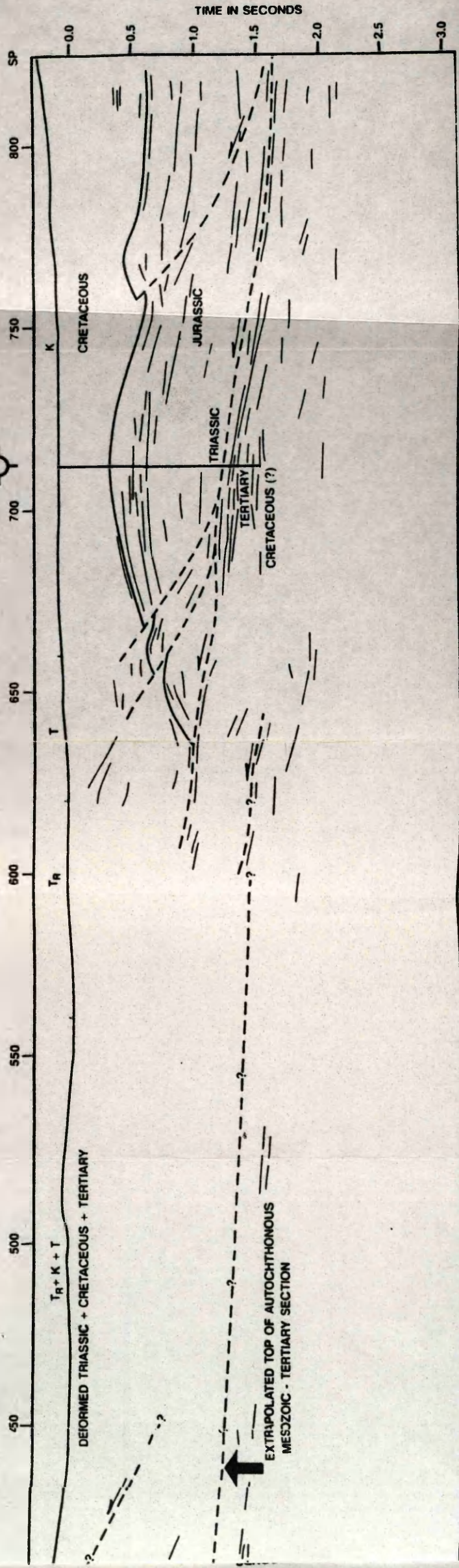




Figure 2.2 A revised stratigraphy for the autochthonous Guadalquivir Basin.

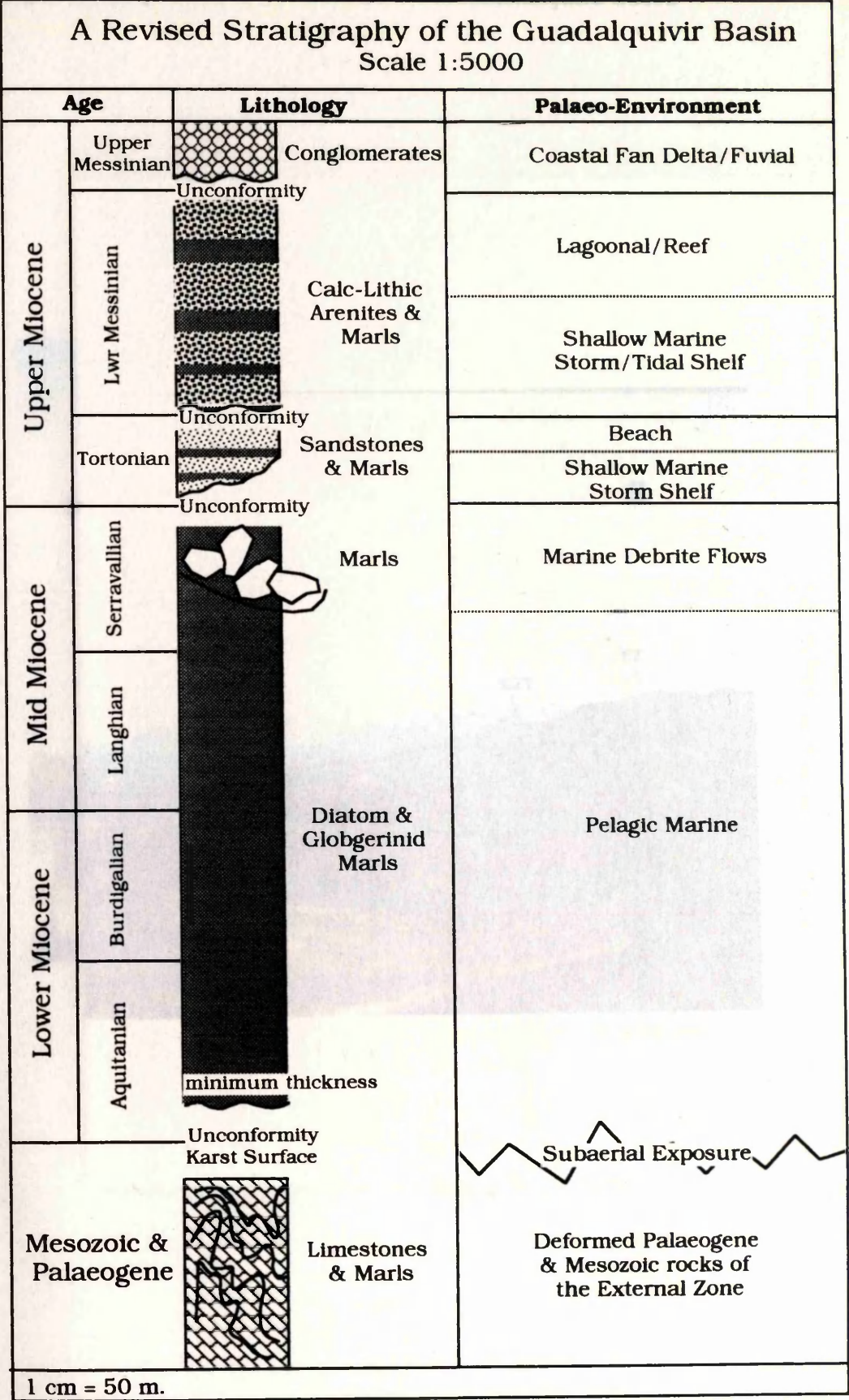


Figure 2.1 A revised stratigraphy for the autochthonous Guadalquivir Basin. Stratigraphy revised from Roldan Garcia et al., (1985a,b) and Leyva Cabello (1979) on the basis of field data, seismic sections (Fig. 2.1) and borehole data (Blankenship, 1992; 1993). Lithological and environmental interpretations are based on field and petrographic studies that are discussed in Chapter 3

Figure 2.3 A panoramic S-N view across the Guadalquivir Basin.

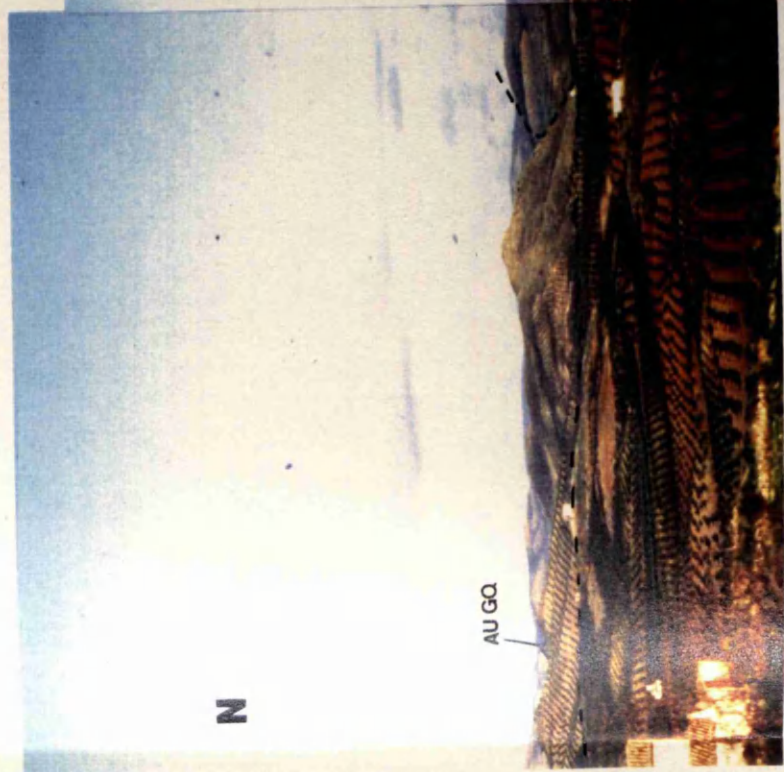
Part of the allochthonous Guadalquivir Basin.

Photo-montage foldout

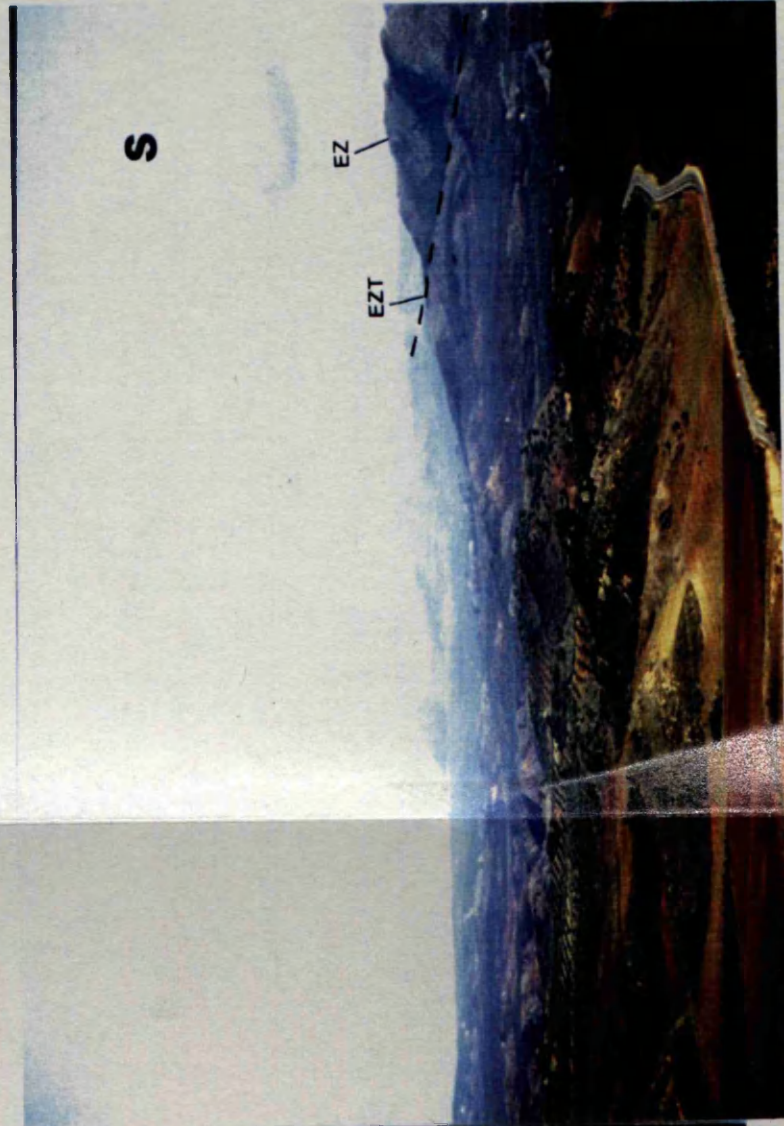
Part of the allochthonous Guadalquivir Basin showing Triassic and Jurassic strata of the External Zone and Lower Miocene strata of the External Zone and Lower Miocene strata of the External Zone. The width of the photo-montage foldout is approximately 20 m high.

Figure 2.3 A panoramic S-N view across the Guadalquivir Basin showing the External Zone (EZ), the External Zone thrust front (EZF), the allochthonous Guadalquivir Basin (ALGQ) and the autochthonous Guadalquivir Basin (AUGQ). Photo taken from Ref. 543 334, looking E.





N



S



Figure 2.4 Part of the allochthonous Guadalquivir Basin.



Figure 2.4 Part of the allochthonous Guadalquivir Basin showing Triassic (T) and Cretaceous (K) sediments of the External Zone and Lower-Mid Miocene marls of the Guadalquivir Basin. Section is approximately 20 m high.



Figure 2.5 Deformed Tortonian sediments.

A



B

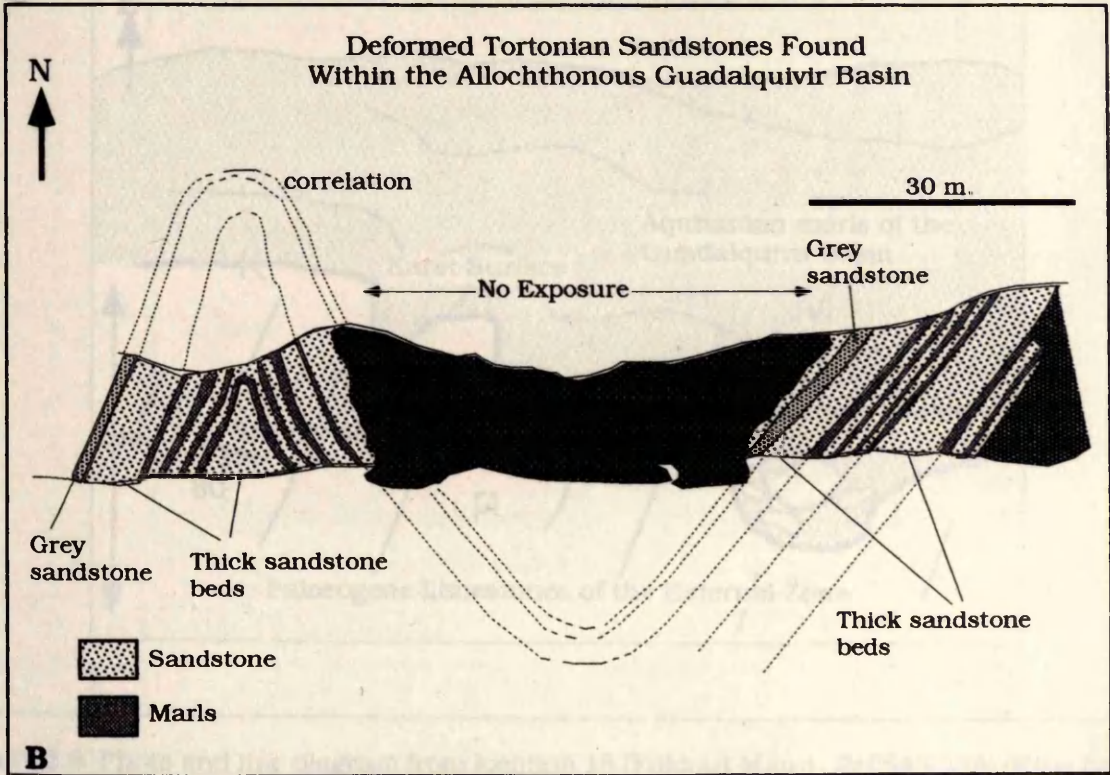


Figure 2.5 Deformed Tortonian sediments found in the allochthonous portion of the Guadalquivir Basin. (A) Photo of vertical Tortonian sandstones. (B) Line drawing of section of deformed Tortonian sediments. From location 5 (Ref 529 343).



Figure 2.6 Photo and line diagram of the base of the Guadalquivir Basin.

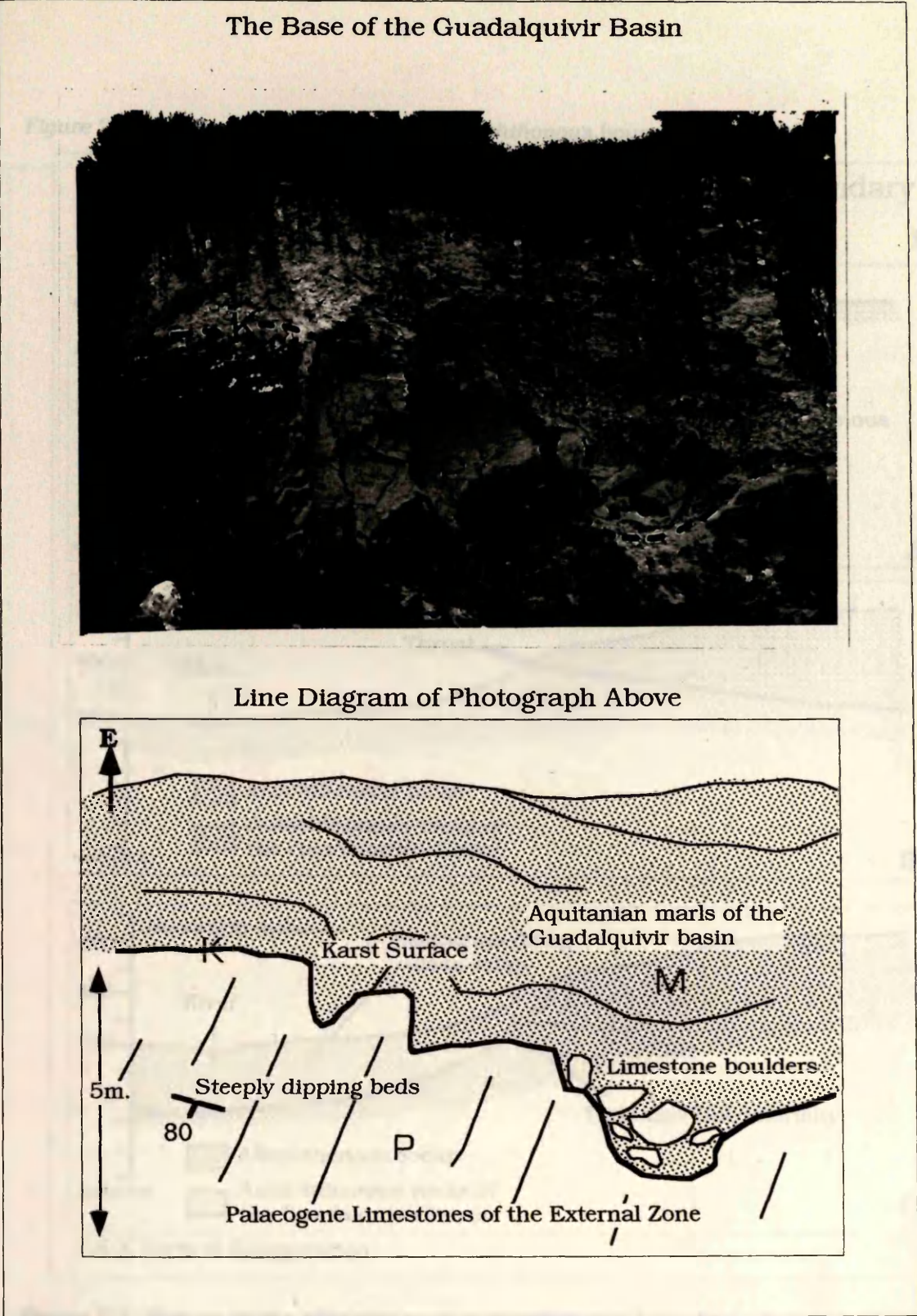


Figure 2.6 Photo and line diagram from location 18 (Foldout Map 1, Ref 543 334) of the base of the Guadalquivir Basin. Lower Miocene marls of the Guadalquivir Basin unconformably overlie deformed Palaeogene limestones of the External Zone. A karst surface characterises the unconformity and indicates that a substantial period of subaerial exposure separated the External Zone from marine sediments of the Guadalquivir Basin.



Figure 2.5 'Olistostrome' mapped over modern outcrops.

Figure 2.7 Nature of the allochthonous-autochthonous boundary.

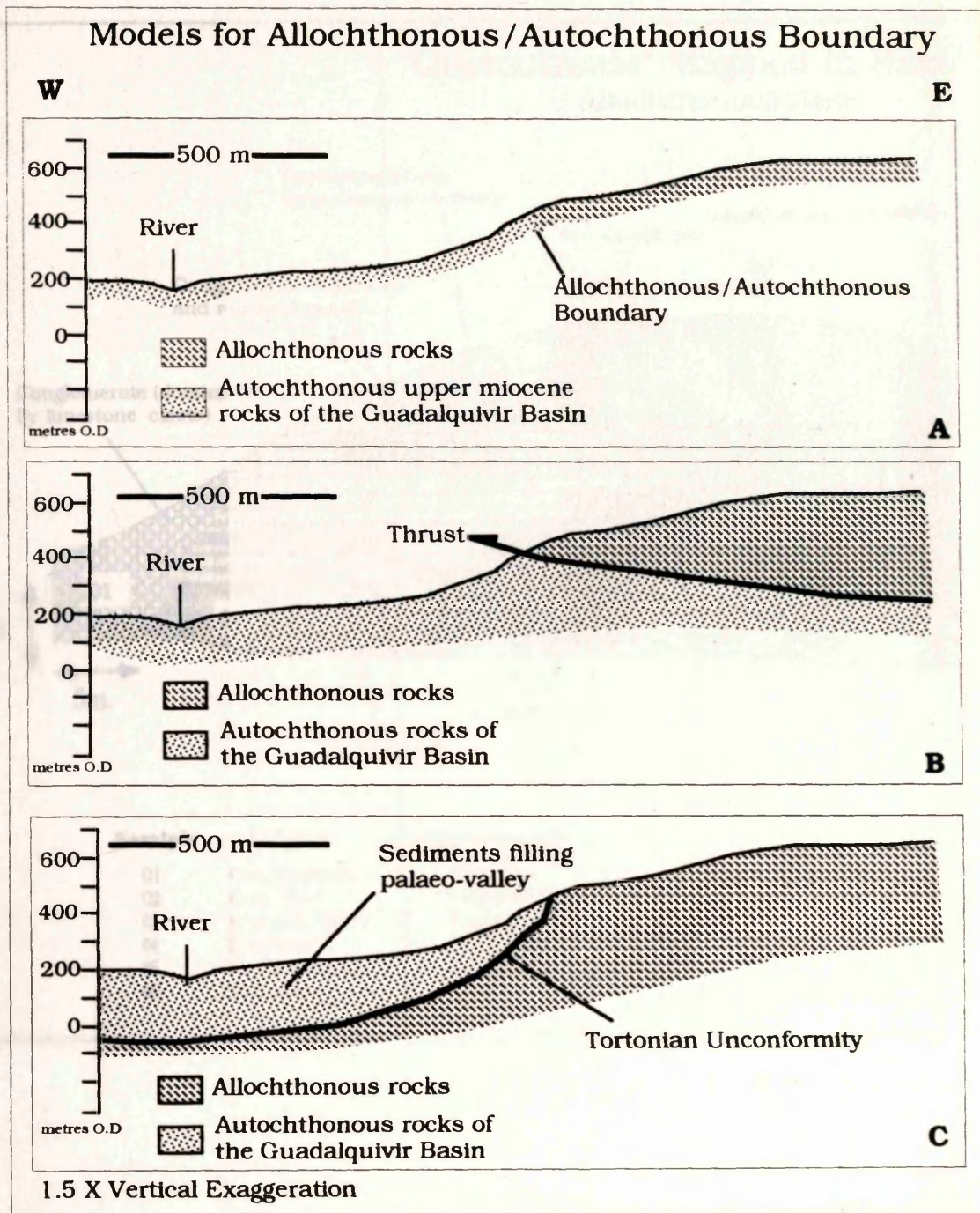


Figure 2.7 Nature of the allochthonous-autochthonous boundary. A: cross-section E-W across the autochthon-allochthon in the Baena-Montilla study area. B: the boundary as a thrust contact. C: the boundary as an unconformity inferring a palaeovalley.



Figure 2.8 'Olistostrome' mapped in a roadside outcrop.

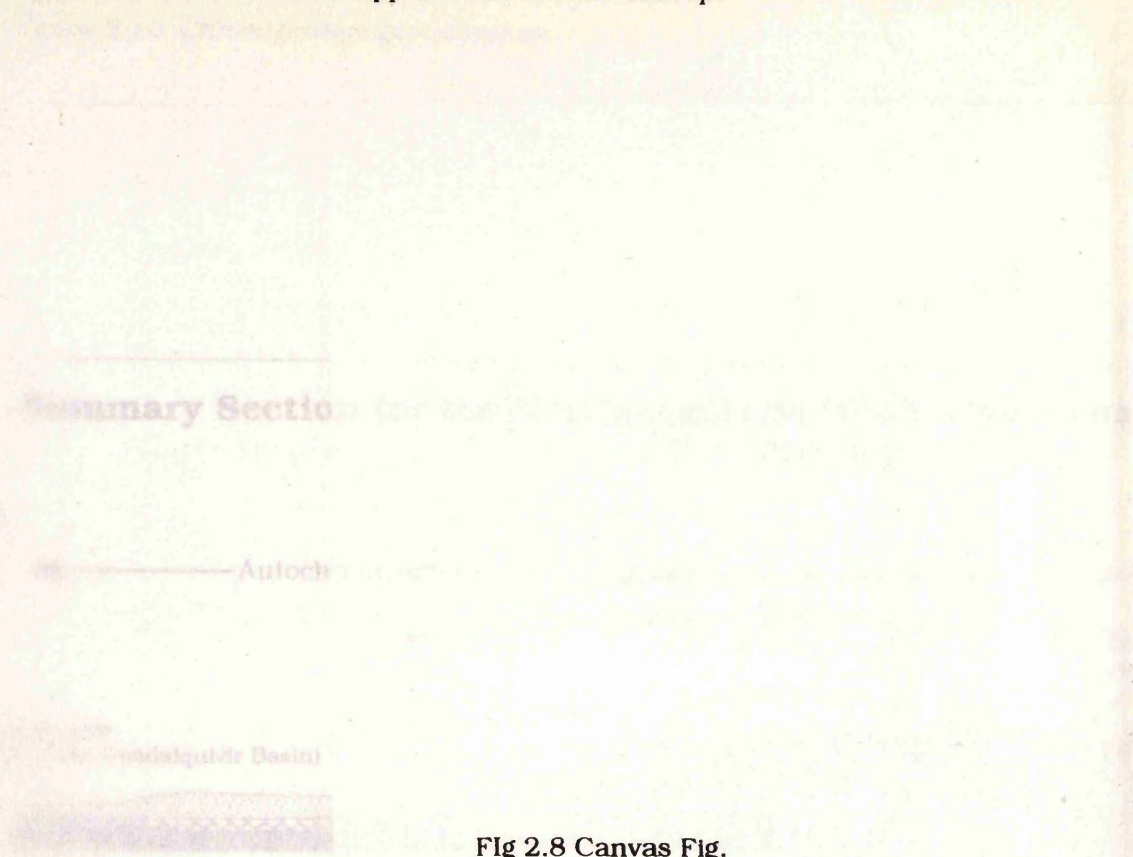
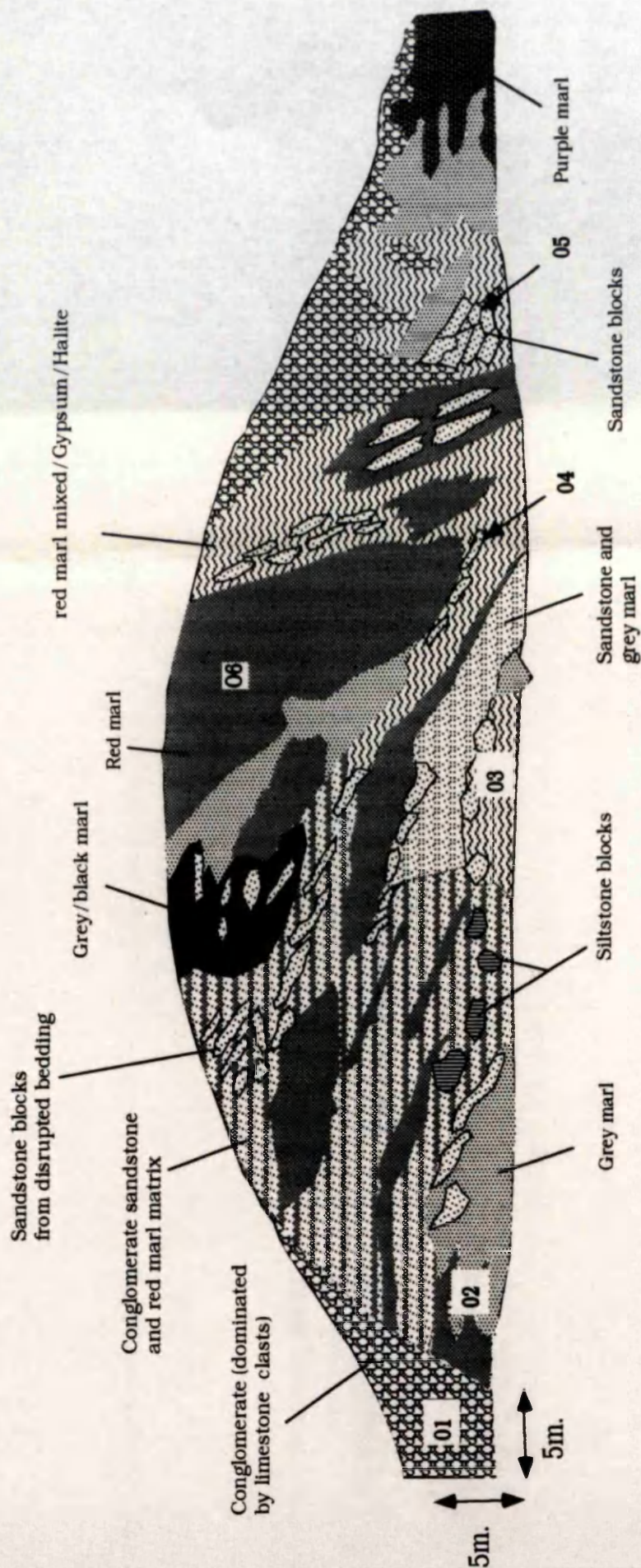


Fig 2.8 Canvas Fig.

Figure 2.8 'Olistostrome' mapped in a roadside outcrop (Baena-Allcaudete road 5Km from Allcaudete ). The 'olistostrome' consists of intimately mixed material of many lithological types. The 'olistostrome' contains rocks from both the External Zone and the Guadalquivir Basin. The youngest rocks are Messinian conglomerates, thought to belong to fluvial deposits of the Guadalquivir Basin. The 'olistostrome' has been re-interpreted as a melange that has a tectonic origin.

# "Olistostrome" Mapped in Roadcut Allochthonous Zone



Sample	Lithology	Stratigraphic age
01	Conglomerate	Messinian
02	Grey Marl	Unknown
03	Gypsum/Halite	Triassic
04	Sandstone	Tortonian
05	Red Sandstone	Triassic
06	Red marl	Triassic



Figure 2.9. Generalized cross-section.

Figure 2.10 Chronostratigraphic diagram.

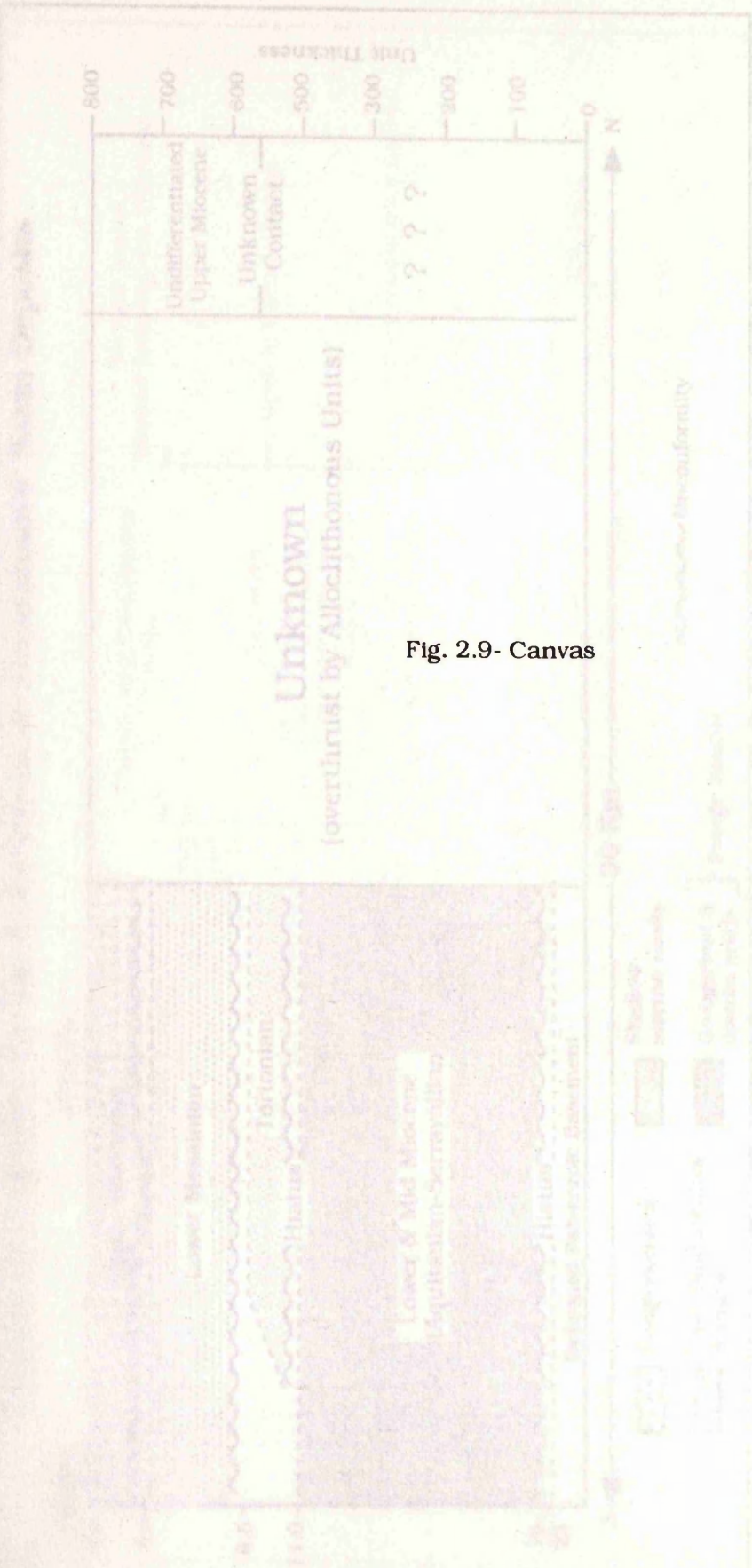
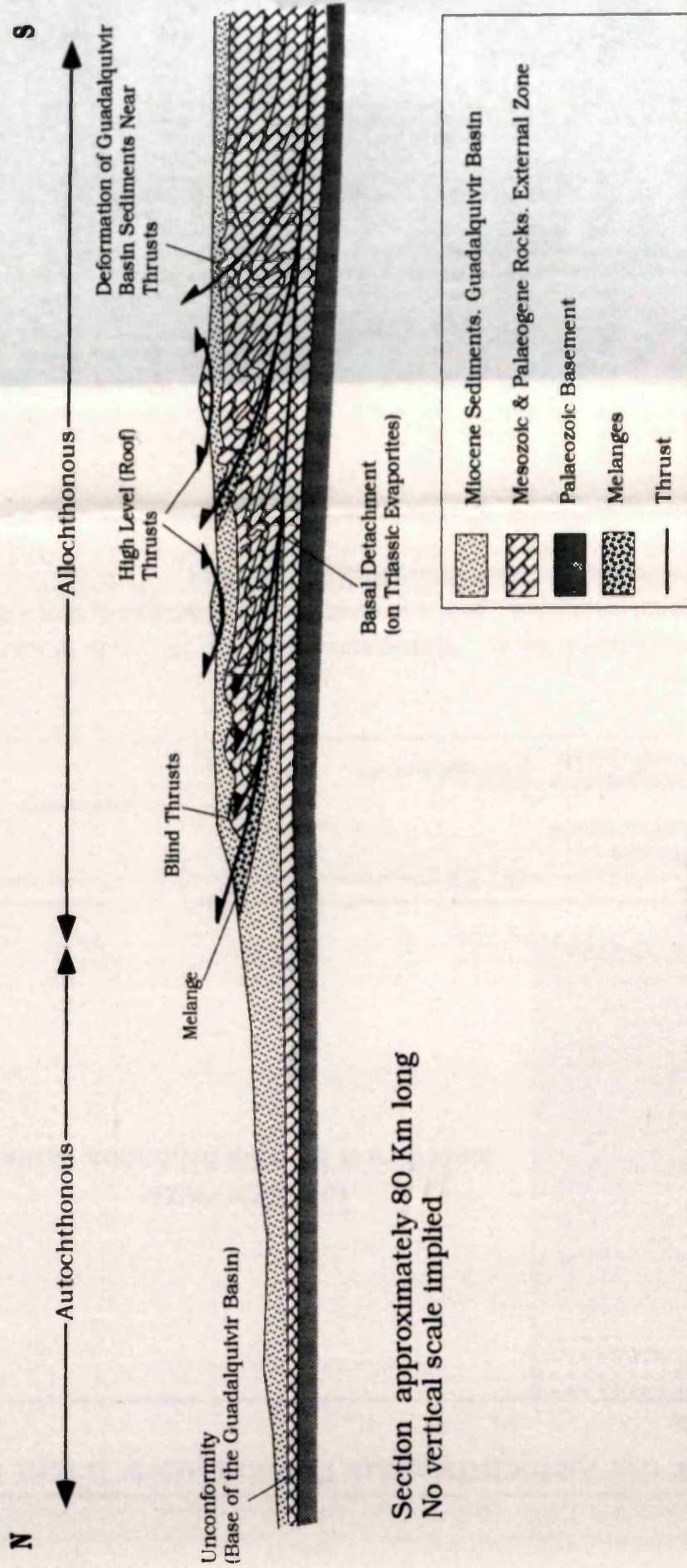


Fig. 2.9- Canvas

Figure 2.9. Generalized cross-section across the External Zone and Guadalquivir Basin of the Betic Orogen. The vertical axis is 'Unit Thickness' and the horizontal axis is 'Distance'. The section shows several geological units, including 'Undifferentiated Upper Miocene', 'Unknown Contact', 'Unknown (overthrust by Allochthonous Units)', 'Lower of Mid Miocene (Mullerian-Sarmiento)', 'Tortonian', 'Lower Miocene', and 'Basal Submarine Basement'. A legend on the right identifies symbols for 'Shale or sandstone', 'Conglomerate or breccia', and 'Basal Submarine Basement'.

Figure 2.9. Generalized cross-section across the External Zone and Guadalquivir Basin of the Betic Orogen.

# Summary Section for the Northern Margin of the Betic orogen and the Southern Margin of the Guadalquivir Basin



Section approximately 80 Km long  
No vertical scale implied

Constructed from Cross-Sections in Foldouts 4,5 & 6



Figure 2.11. Chrono-stratigraphy plotted against global eustasy and tectonism.

Figure 2.10 Chronostratigraphic diagram.

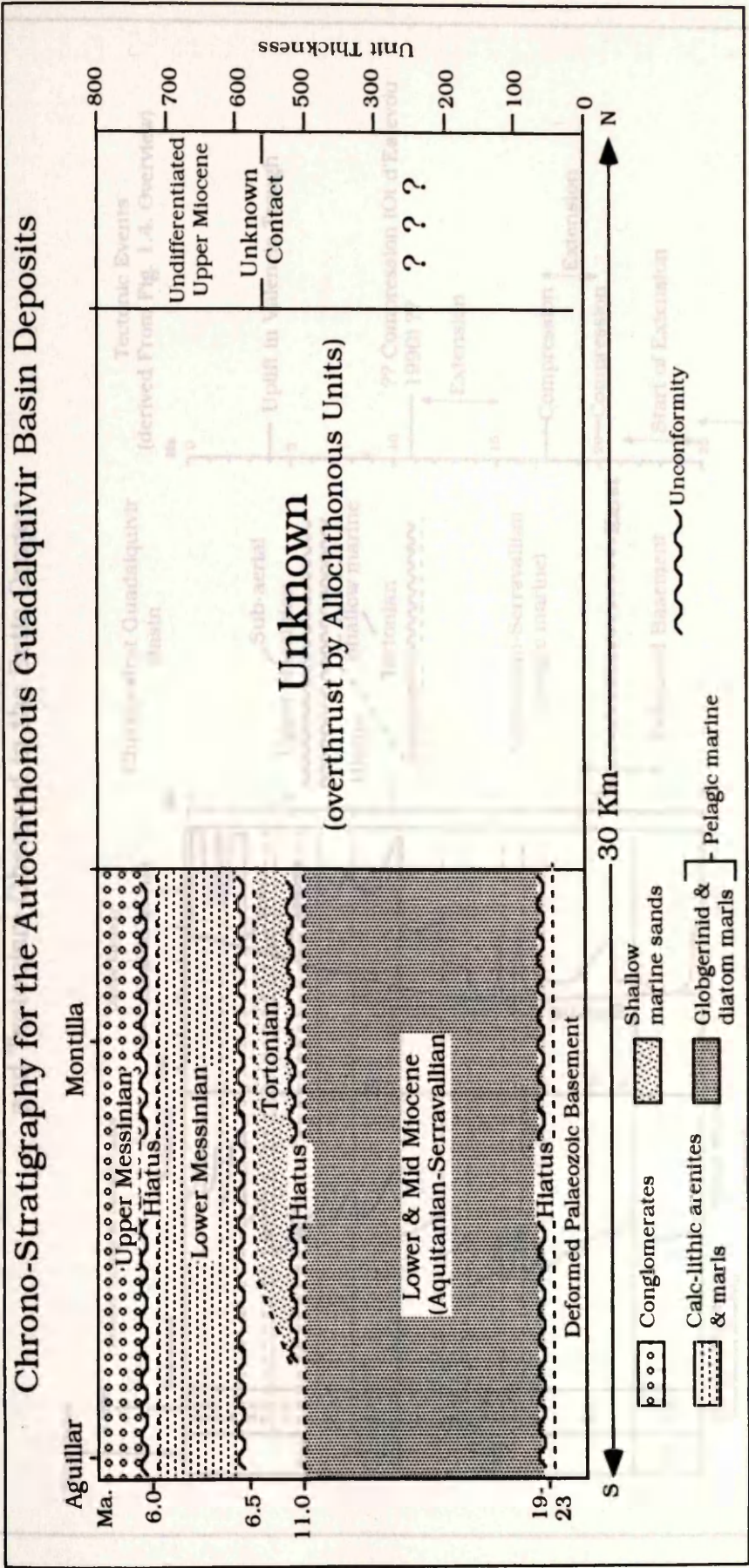


Figure 2.10. Chronostratigraphy of the Guadalquivir Basin. Stratigraphic units are plotted in terms of their vertical and lateral continuity through time. Relative time is given on the left y axis and stratigraphical thickness on the right y axis. The time scale is adjusted to thickness. A hiatus represents a space-time value of non-deposition.



Figure 2.11. Chrono-stratigraphy plotted against global eustasy and tectonism.

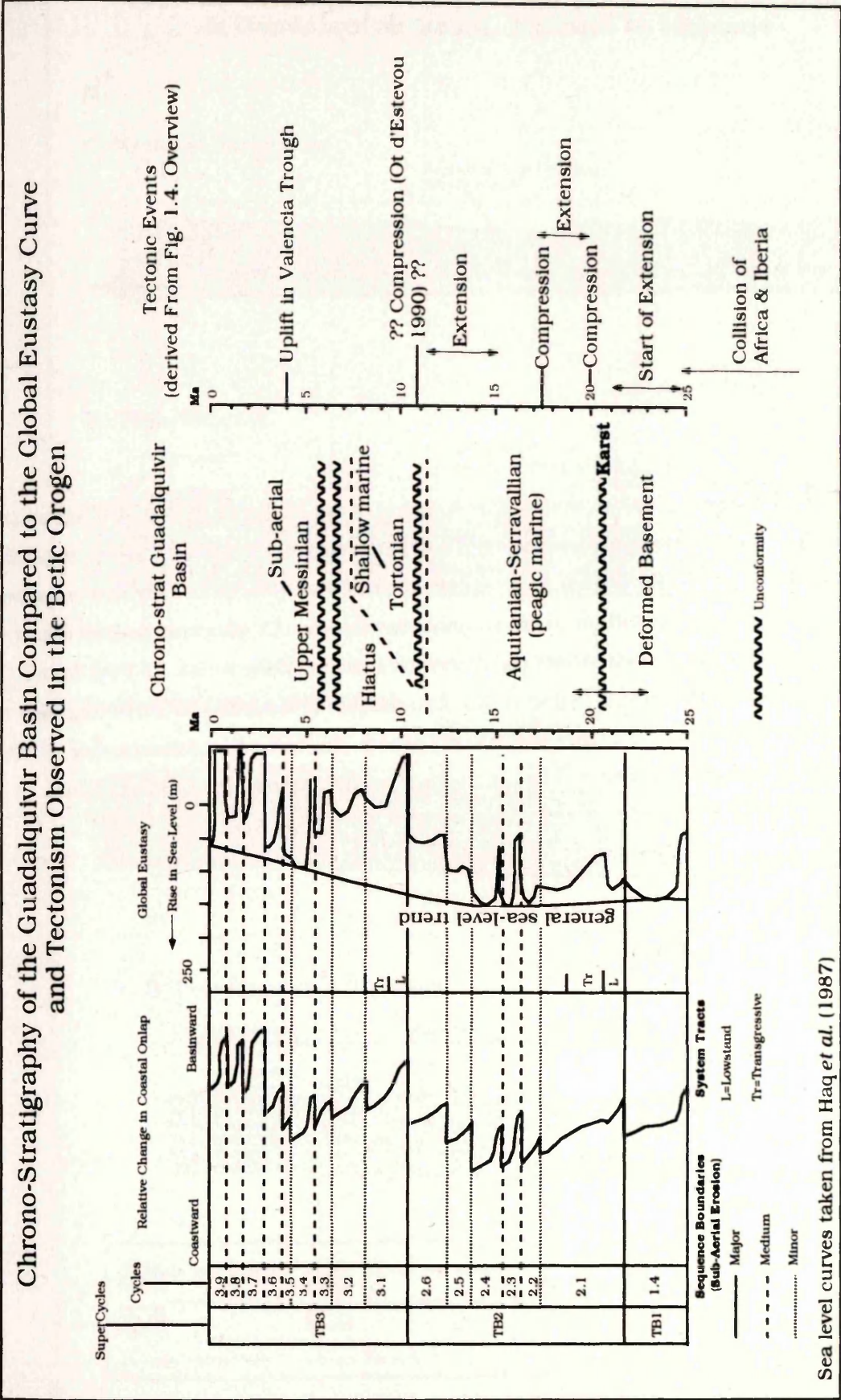


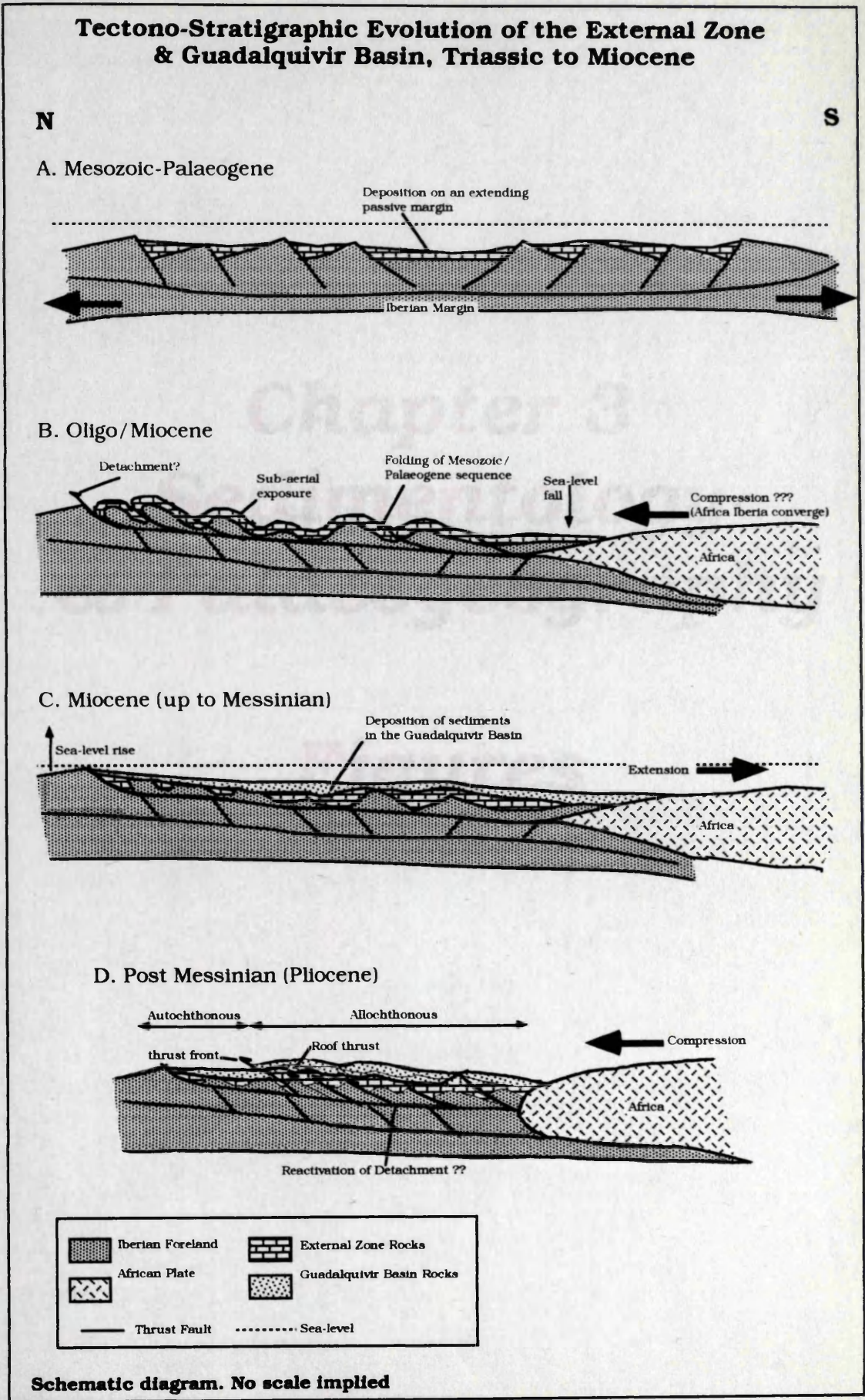
Figure 2.11. Chrono-stratigraphy plotted against global eustasy (Haq et al., 1987) and tectonism observed in the Betic Orogen. The unconformity that marks the base of the Guadalquivir Basin is driven by a tectonism the effects of which was amplified by a major sea-level fall at the base of super cycle TB2. Other unconformities appear to have been driven by eustasy rather than tectonism.



Figure 2.12 The tectonic and stratigraphic evolution of the External Zone and Guadalquivir Basin. A: Mesozoic-Palaeogene; External Zone sediments are deposited on an extending passive margin. B: Oligo-Miocene; rocks of the External Zone are deformed and sub-aerial exposure led to the karstification of Palaeogene limestones. C: Miocene; sediments of the Guadalquivir Basin are deposited over the deformed External Zone rocks. D: Post-Messinian (Pliocene); Compression in the region of the Guadalquivir basin led to thrusting and the division of the basin into an allochthon and autochthon. The inferred relative motion of Africa is shown, although this may be subject to further modification in later discussions.



Figure 2.12 Tectonic and stratigraphic evolution.



**Chapter 3**  
**Sedimentology**  
**& Palaeogeography**

**Figures**



Figure 3.1 Lithostratigraphy of the Guadalquivir Basin.

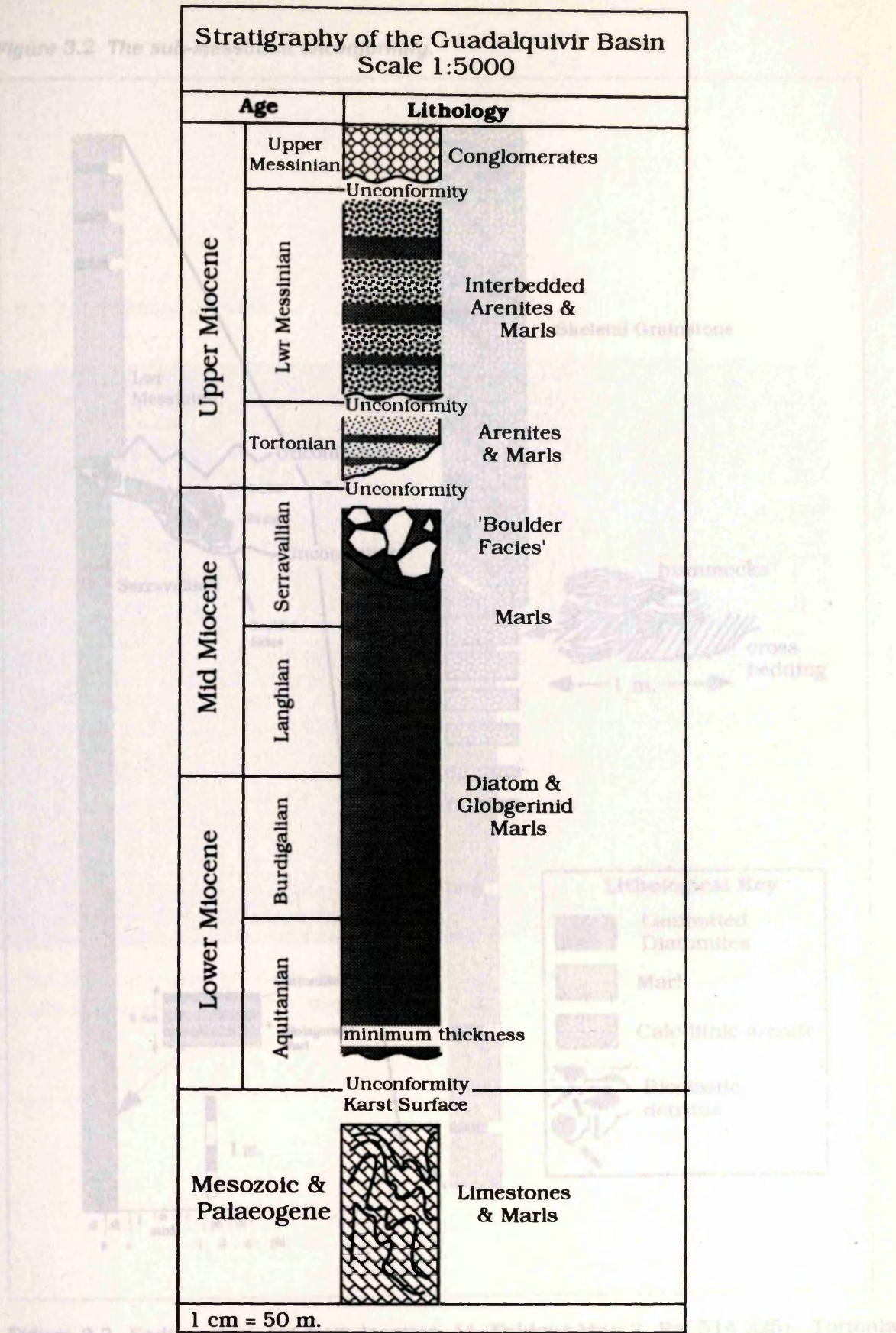


Figure 3.1 Lithostratigraphy of the Guadalquivir Basin, modified from Roldan Garcia *et al.*, (1985a,b)



Figure 3.2 The sub-Messinian unconformity.

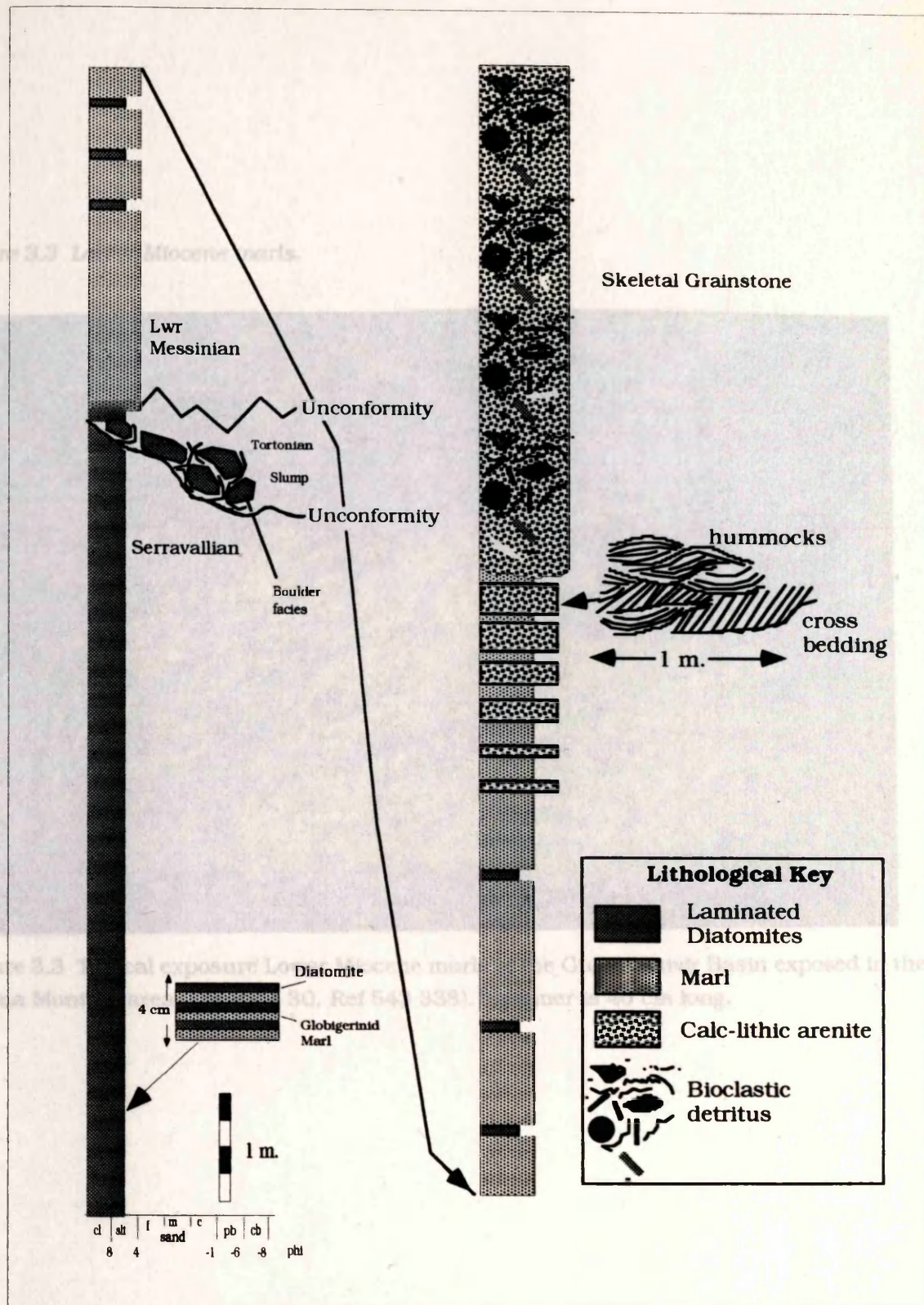


Figure 3.2 Sedimentary log from location 44 (Foldout Map 2, Ref 514 325). Tortonian sedimentary rocks are cut out by the sub-Messinian unconformity.



Figure 3.3 Lower Miocene marls.

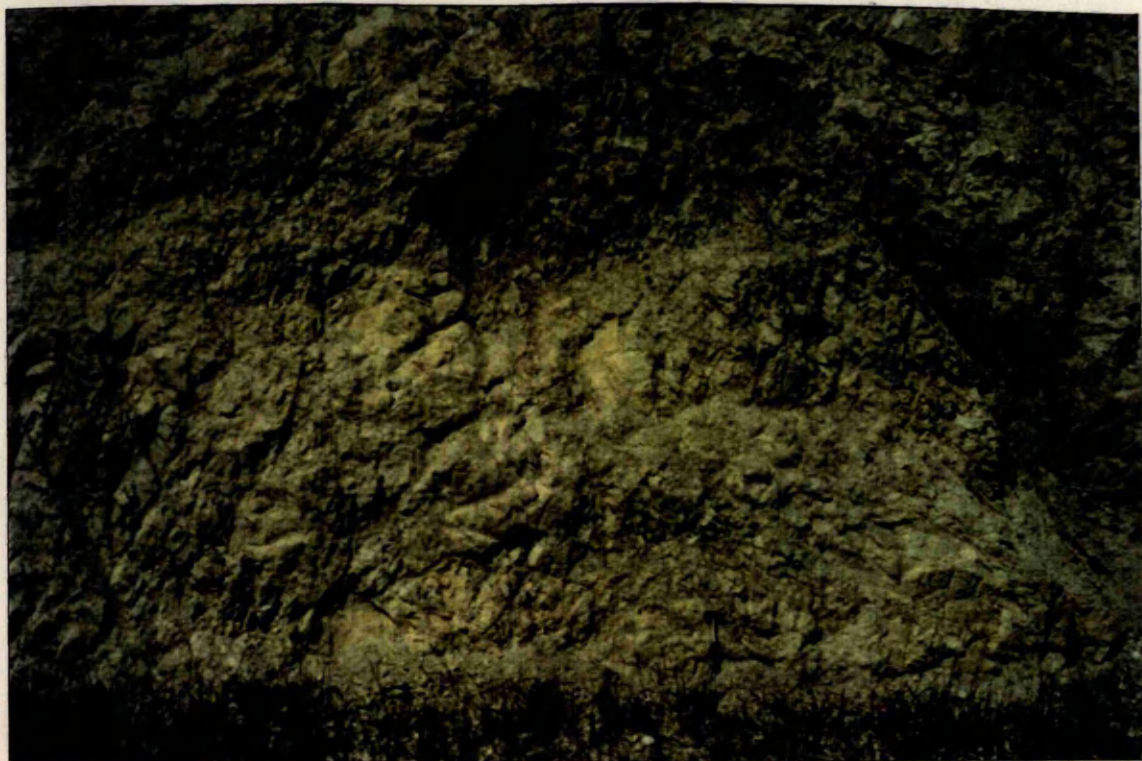


Figure 3.3 Typical exposure Lower Miocene marls of the Guadalquivir Basin exposed in the Baena Montilla area (Location 30, Ref 543 338). Hammer is 40 cm long.



Figure 3.4 Photo montage and derived line diagram of the boulder facies that belong to Lower Miocene rocks of the Guadalquivir Basin. Photo montage from exposure found at location 40 (Foldout Map 1, Ref. 530 334)



Figure 3.4. Lower Miocene boulder facies.

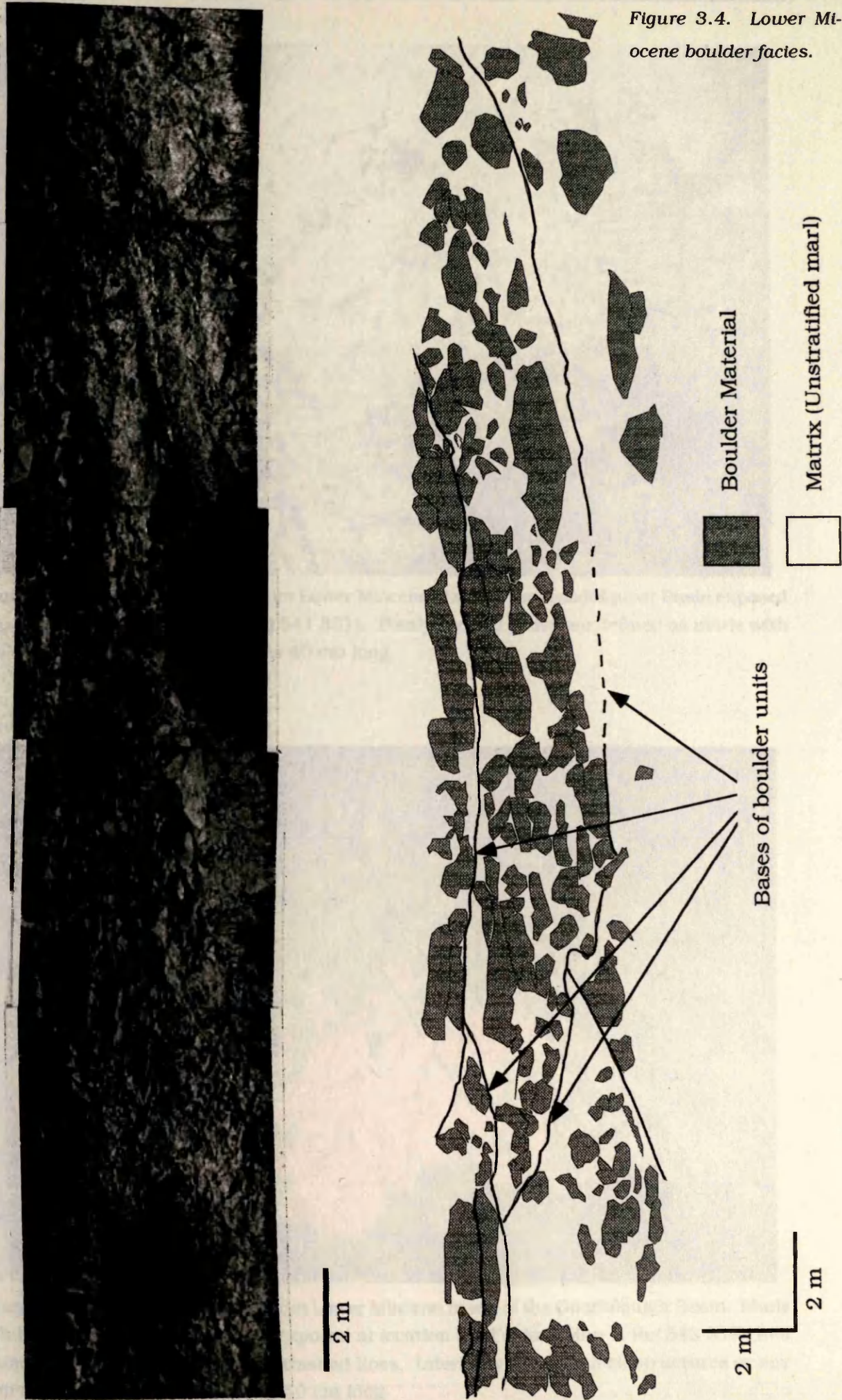




Figure 3.5 Thinly bedded facies.

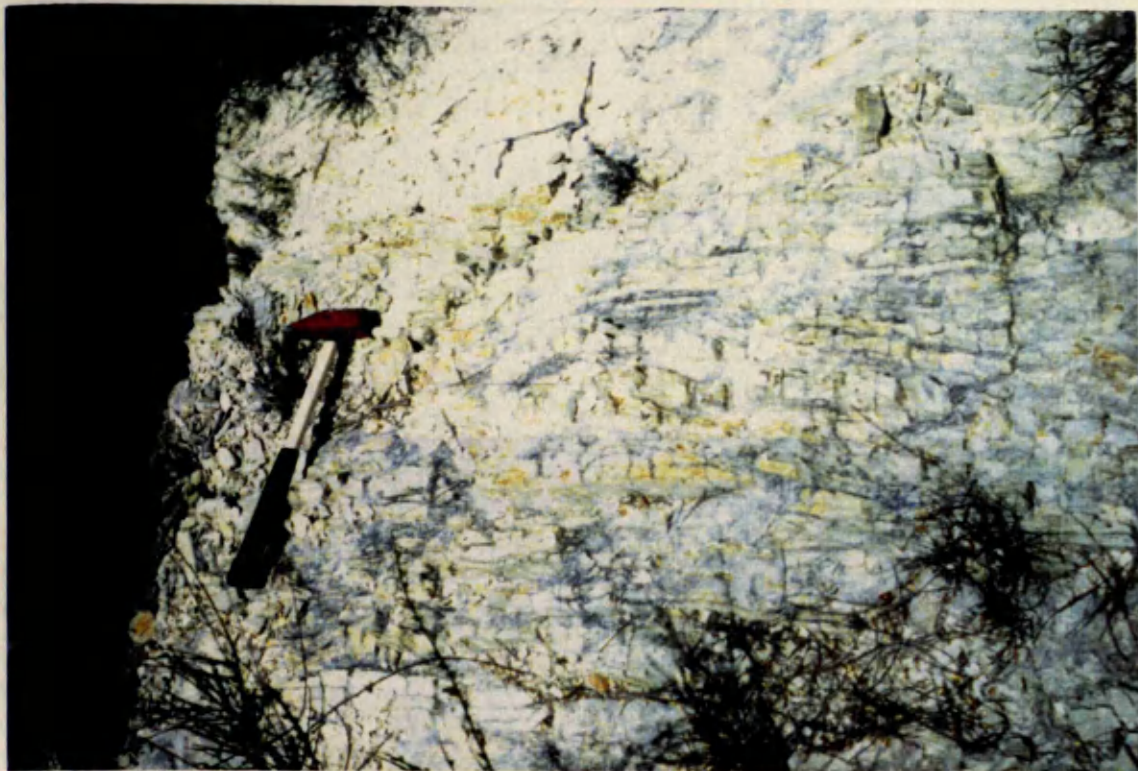


Figure 3.5 Thinly bedded facies from Lower Miocene Marls of the Guadalquivir Basin exposed at location 23 (Foldout Map 1, Ref 541 331). Thinly bedded facies are defined as marls with less than 10 cm beds. Hammer is 40 cm long.

Figure 3.6 Thickly bedded marls.



Figure 3.6 Thickly bedded marls from Lower Miocene marls of the Guadalquivir Basin. Marls with beds thicker than 50 cm are exposed at location 31 (Foldout Map 1, Ref 543 339) Bed bounding surfaces are marked by dashed lines. Internally the beds lack structures or any form of stratification. Hammer is 40 cm long.



Figure 3.7 Laminated diatomites.



Figure 3.7 Laminated diatomites from the Lower Miocene Guadalquivir Basin exposed at location 44 (Foldout Map 2, Ref 514 325). (Cy) Clay rich laminae. (Ca) Carbonate rich laminae. Penknife is 12 cm long.



Figure 3.8(a) Diatom ooze.



Figure 3.8(a) Diatom ooze from the clay rich laminae of the laminated diatomite (Fig 3.7) showing Diatoms (D) and Radiolaria (R).

Figure 3.8(b) *Concinodiscus* sp.

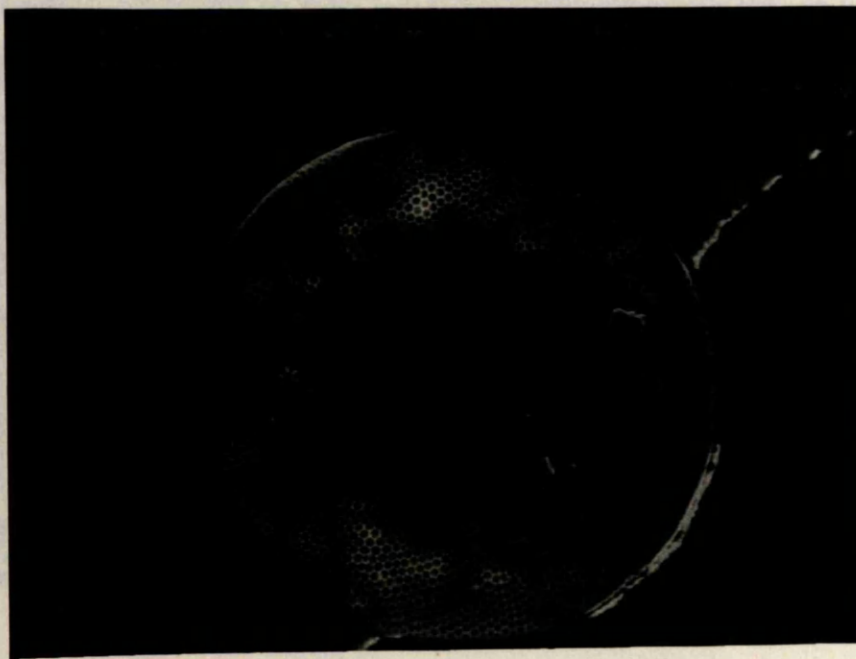


Figure 3.8(b) *Concinodiscus* sp., location 44 (Ref. 514 325), Lower Miocene laminated Diatomite facies. The diatom flora from the clay rich laminae is monospecific, dominated by *Concinodiscus*.



Figure 3.9 Lenticular units in the boulder facies

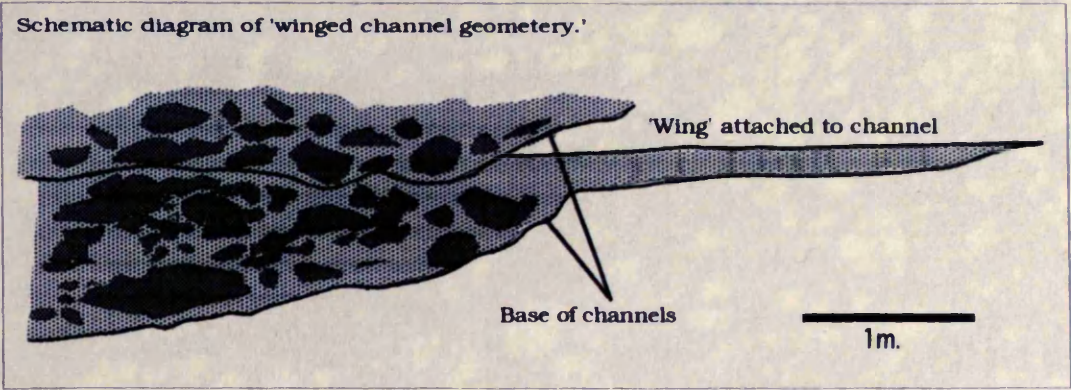


Figure 3.9 Schematic diagram of lenticular units found in the boulder facies at locality 40 (Foldout Map 1, Ref. 530 334). The lenticular units have a winged channel type of geometry.

Figure 3.10 Photomicrograph of calc-lithic arenite.

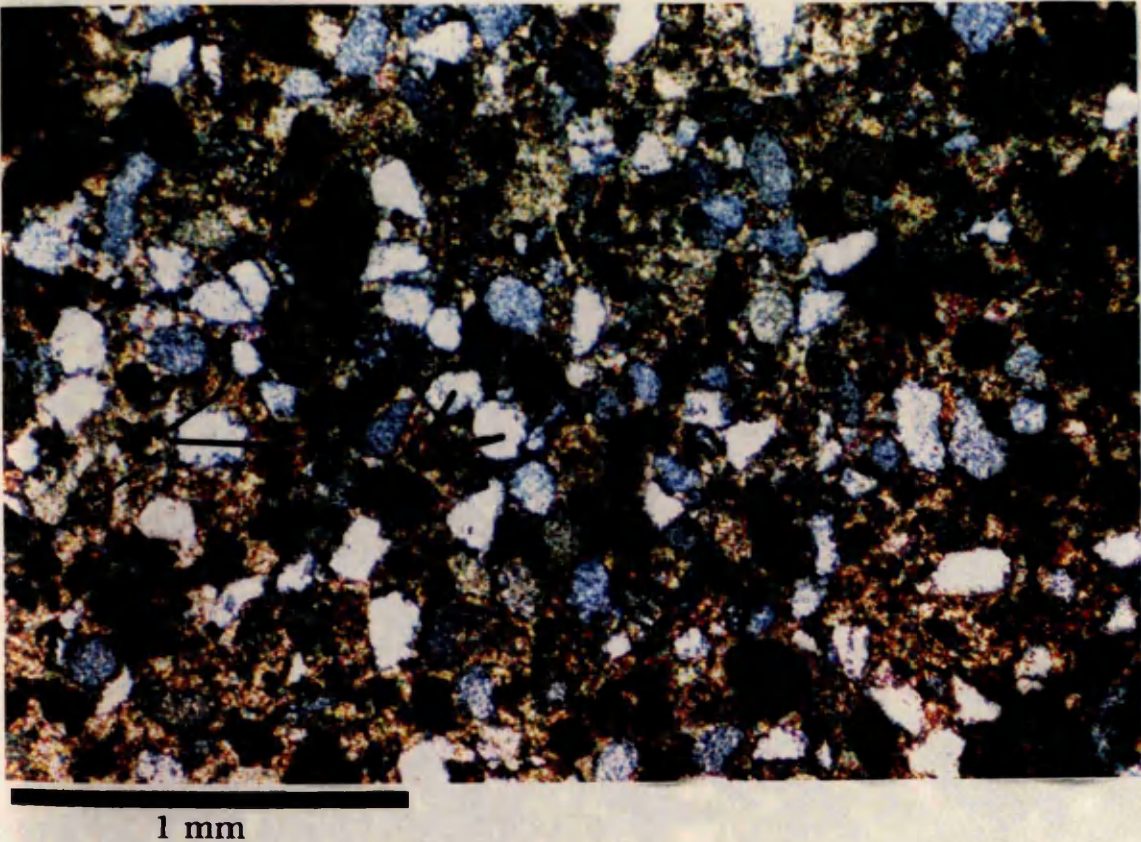
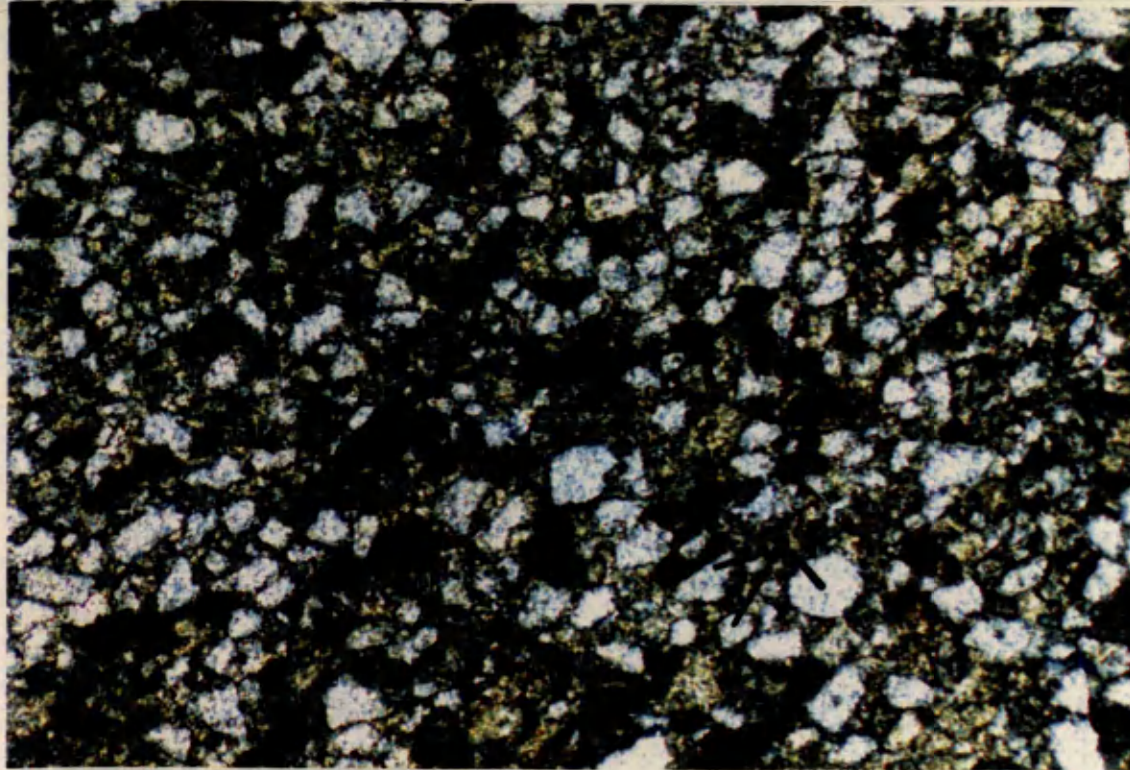


Figure 3.10 Photomicrograph of calc-lithic arenite from Tortonian sandstones of the Guadalquivir Basin. (Q) quartz clast. (C) carbonate clast.



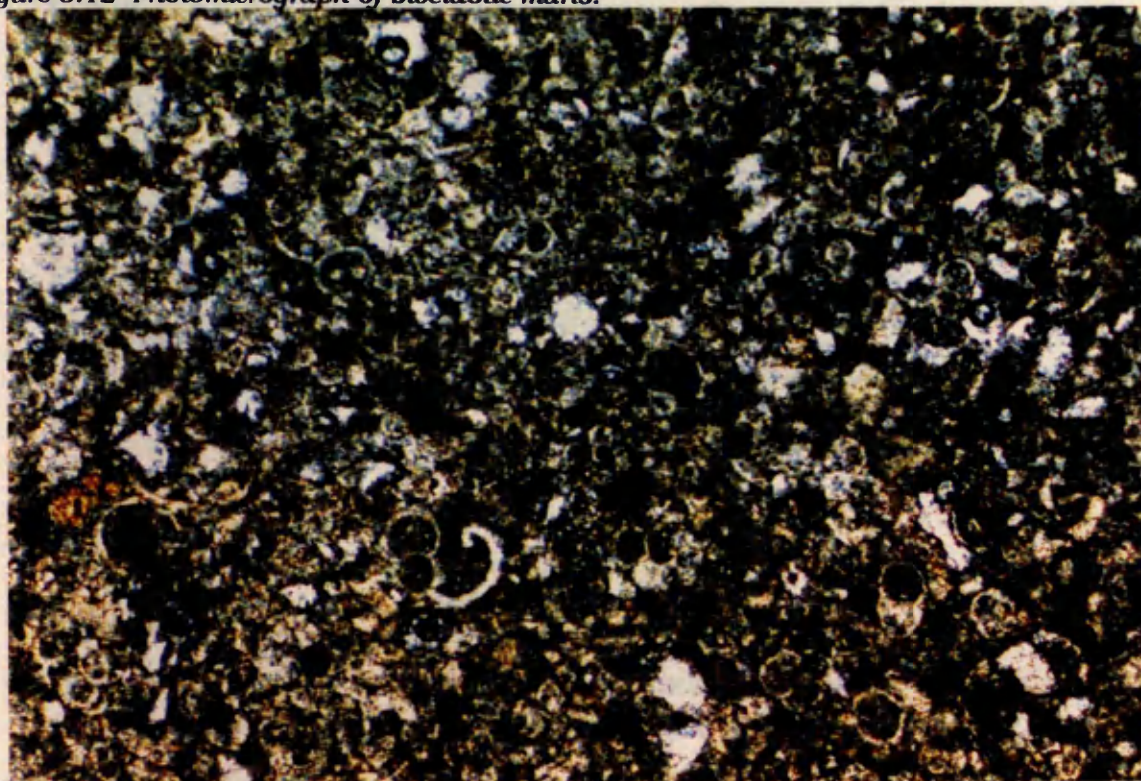
Figure 3.11 Photomicrograph of fine grained calc-lithic arenite.



1 mm

Figure 3.11 Photomicrograph of fine grained calc-lithic arenite from sandstone beds found in Tortonian thin bedded facies of the Guadalquivir Basin. (Q) quartz clasts. (C) carbonate clasts.

Figure 3.12 Photomicrograph of bioclastic marls.



1 mm

Figure 3.12 Photomicrograph of bioclastic marls that are found interbedded with calc-lithic arenites in the thin bedded facies, Tortonian sediments of the Guadalquivir Basin. Bioclasts are dominated by planktonic Foraminifera, but may also include Pelmatozoa and Radiolaria.



Figure 3.13 Thin bedded and thick bedded, Tortonian sedimentary cycles.

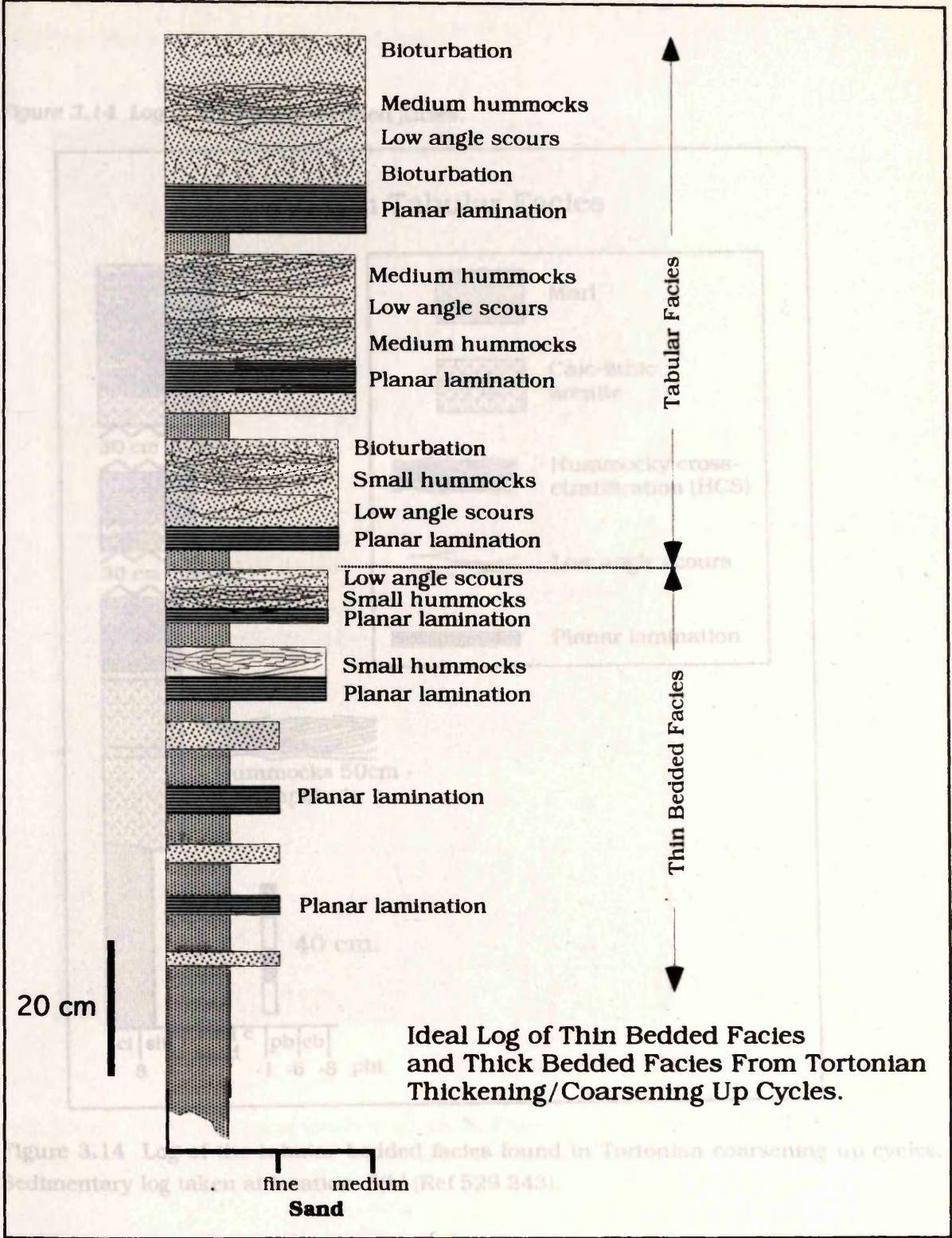


Figure 3.13 Ideal log of thin bedded and thick bedded facies found in the Tortonian sedimentary cycles, the ideal log is inferred from logs given in Appendix I.



Figure 3.15(a). Photo of thick bedded sandstones.

Figure 3.14 Log of the tabular bedded facies.

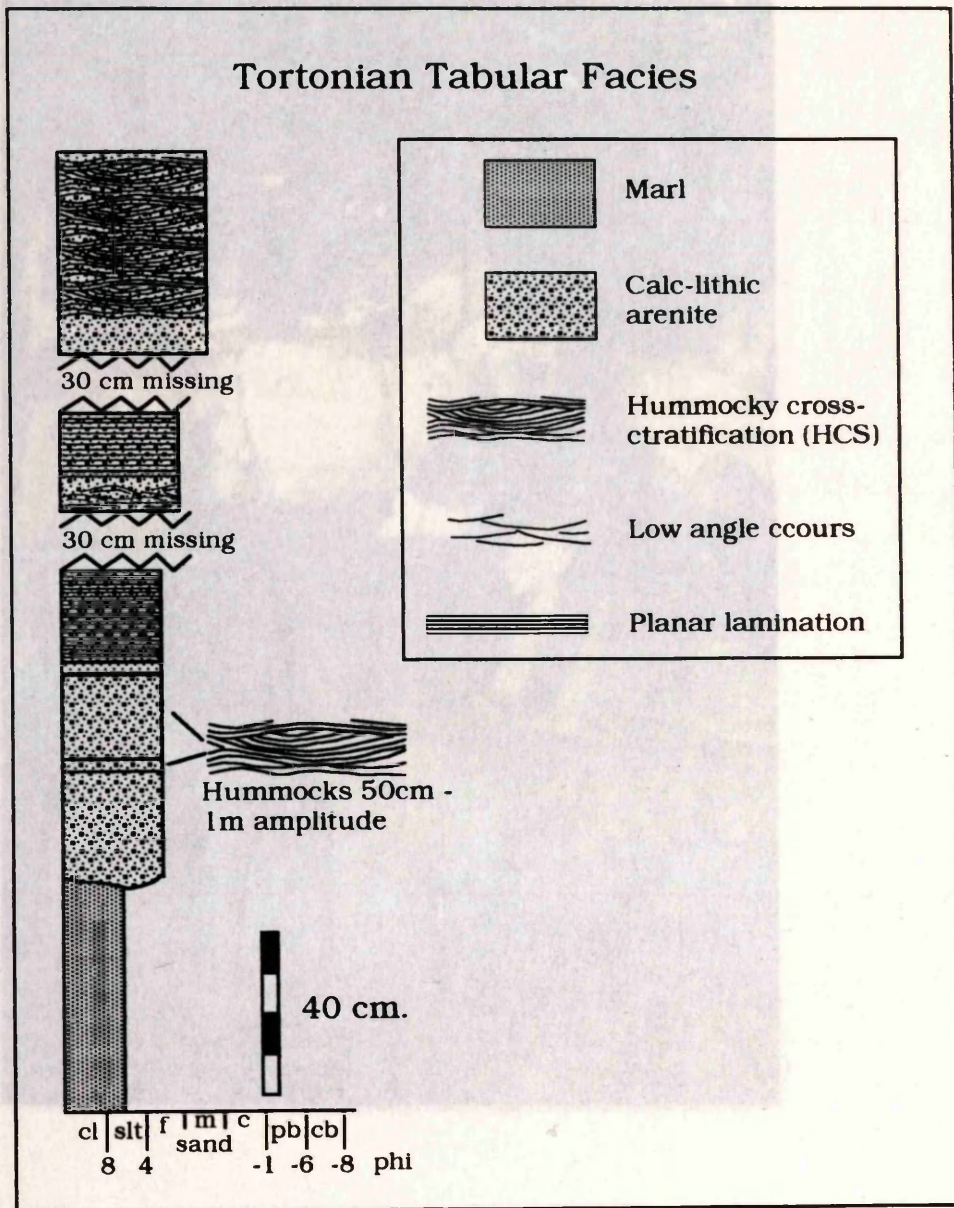


Figure 3.15(a). Photo of logged section given in Figure 3.15(b) showing thick bedded

Figure 3.14 Log of the tabular bedded facies found in Tortonian coarsening up cycles. Sedimentary log taken at location 5(b) (Ref 529 343).



Figure 3.15(a). Photo of thick bedded sandstones.



Figure 3.15(a). Photo of logged section given in Figure 3.15(b) showing thick bedded sandstones, Tortonian Guadalquivir Basin. Hammer is 40 cm long.



**Figure 3.15(b) Sedimentary log of the thick bedded facies from the Tortonian sedimentary succession. Sedimentary log taken from location 93 (Foldout Map 2, Ref 521 343)**



Figure 3.15(b). Sedimentary log of the thick bedded facies.

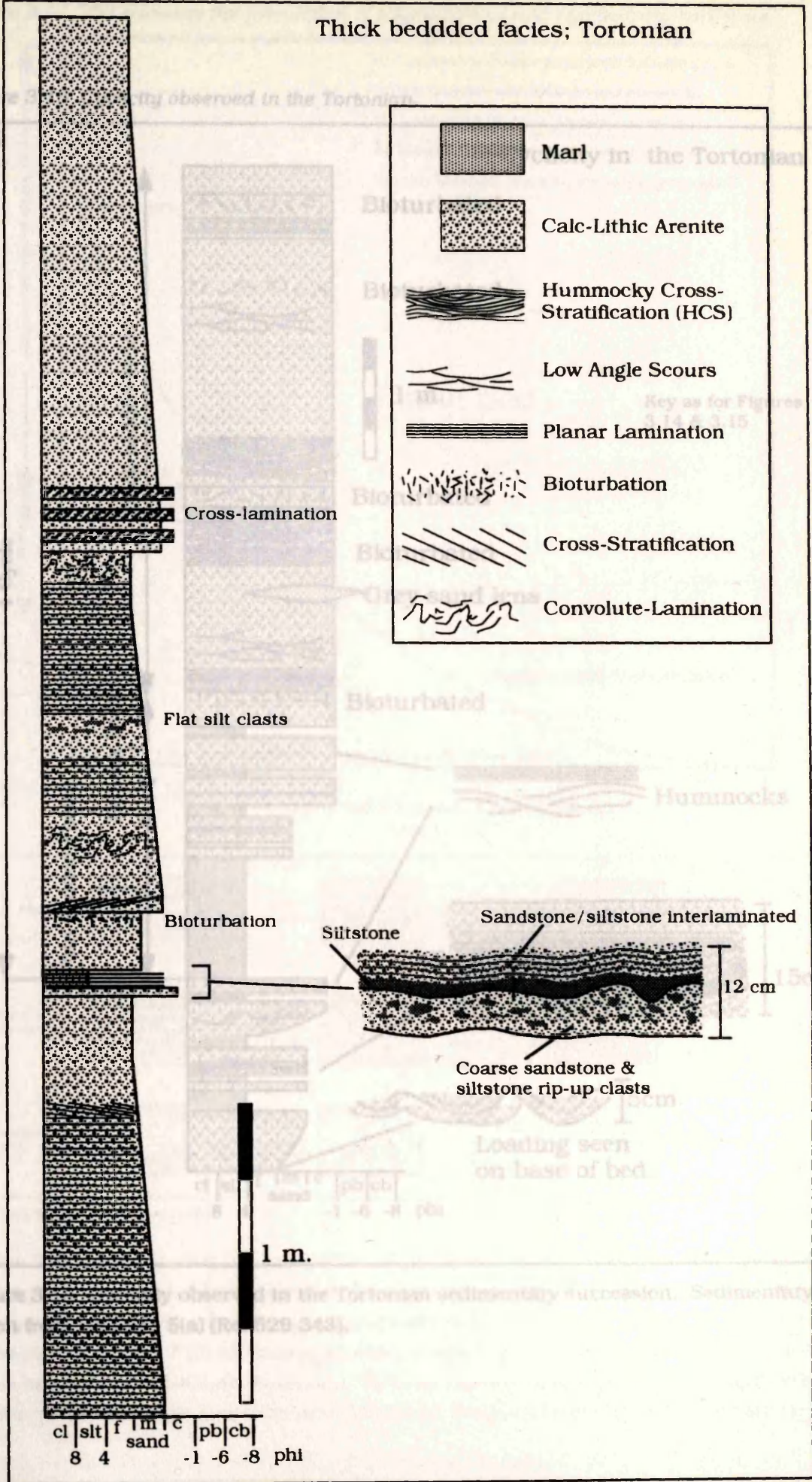




Figure 3.17 Plot showing the production of asymmetrical and symmetrical bedforms.

Figure 3.16 Cyclicity observed in the Tortonian.

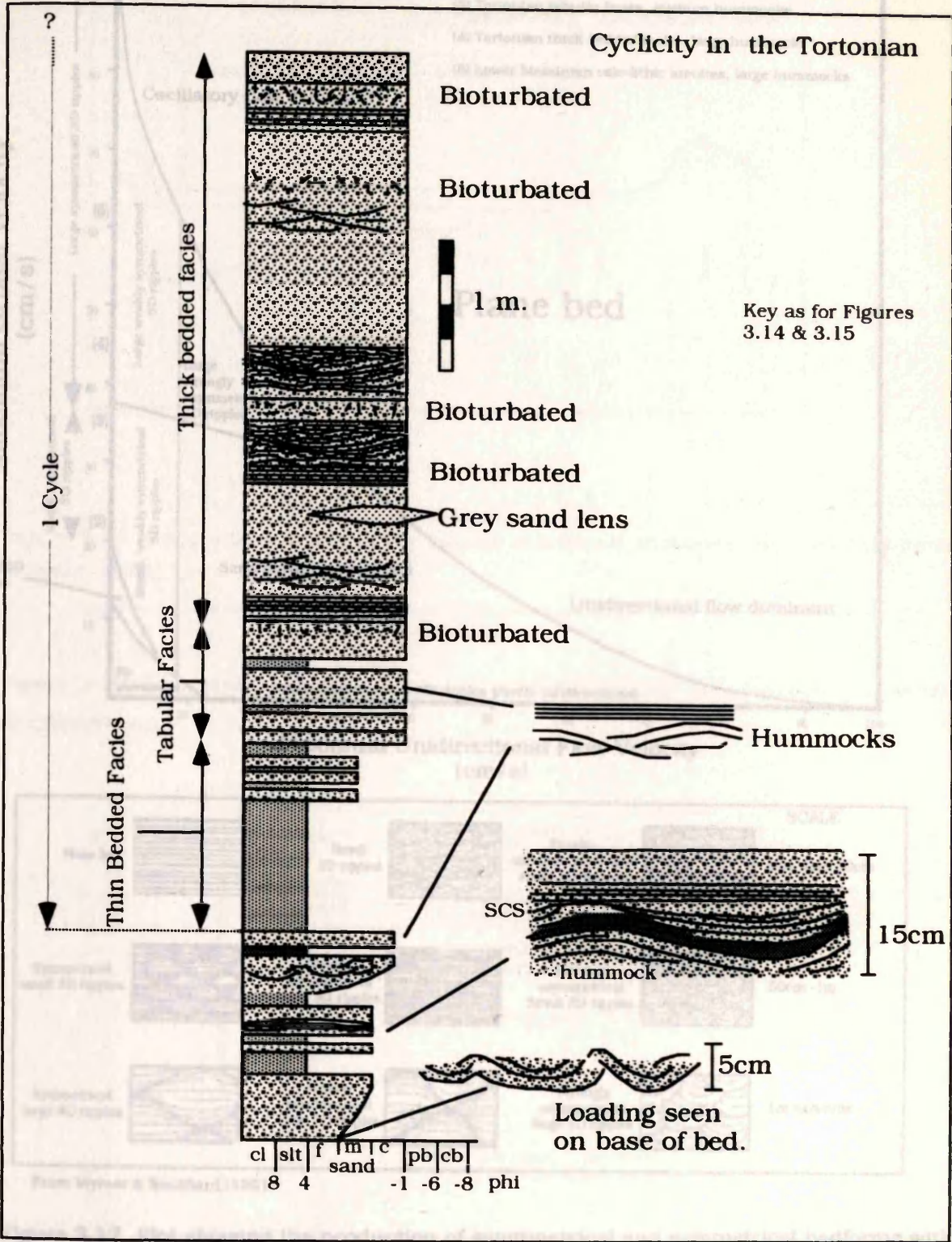
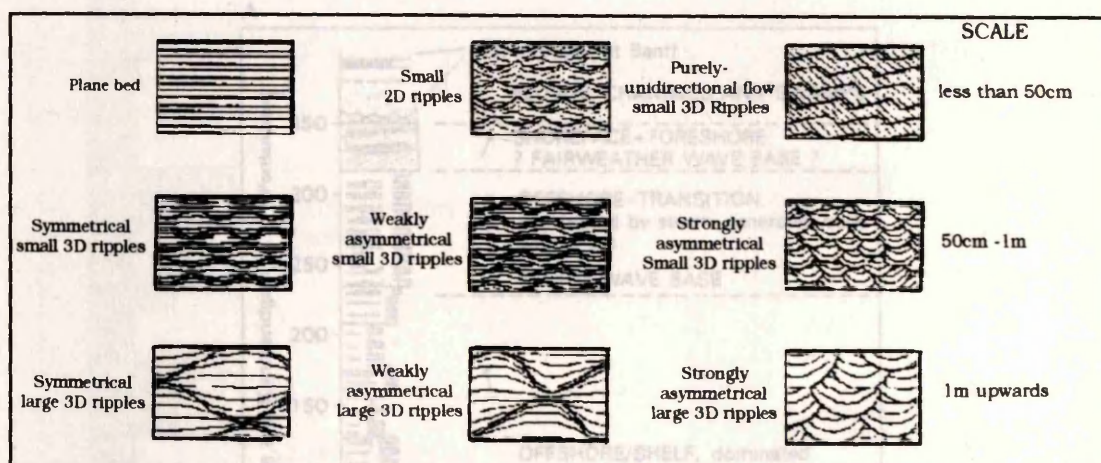
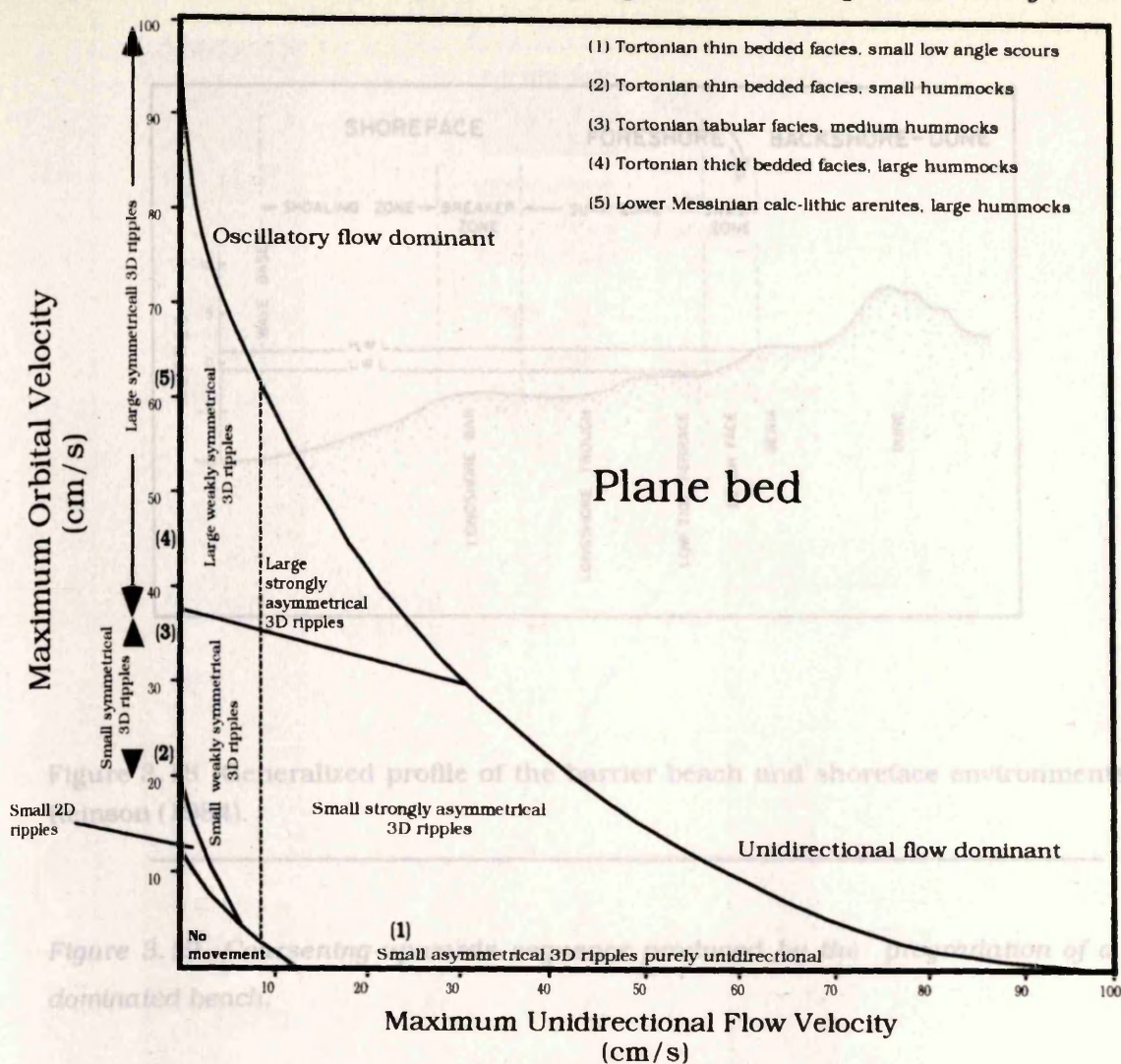


Figure 3.16 Cyclicity observed in the Tortonian sedimentary succession. Sedimentary log taken from Location 5(a) (Ref 529 343).



**Figure 3.17** Plot showing the production of asymmetrical and symmetrical bedforms.



From Myrow & Southard (1991)

**Figure 3.17 Plot showing the production of asymmetrical and symmetrical bedforms with varying combinations of unidirectional and oscillatory flow velocity. 3D asymmetrical ripples are equivalent to low-angle scours and symmetrical 3D ripples are equivalent to hummocky cross-stratification. With increasing oscillatory flow symmetrical bedforms (i.e. hummocky cross-stratification) become dominant. With increasing unidirectional flow asymmetrical bedforms (i.e. low angle scours) become dominant. Diagram from Myrow & Southard (1991).**



Figure 3.18 Profile of a barrier beach.

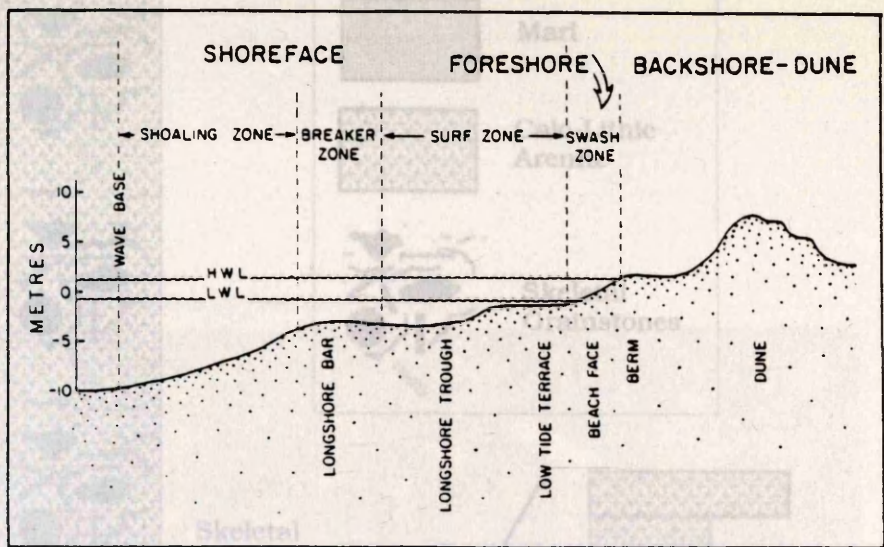


Figure 3.18 Generalized profile of the barrier beach and shoreface environments From Reinson (1984).

Figure 3.19 Coarsening-upwards sequence produced by the progradation of a storm-dominated beach.

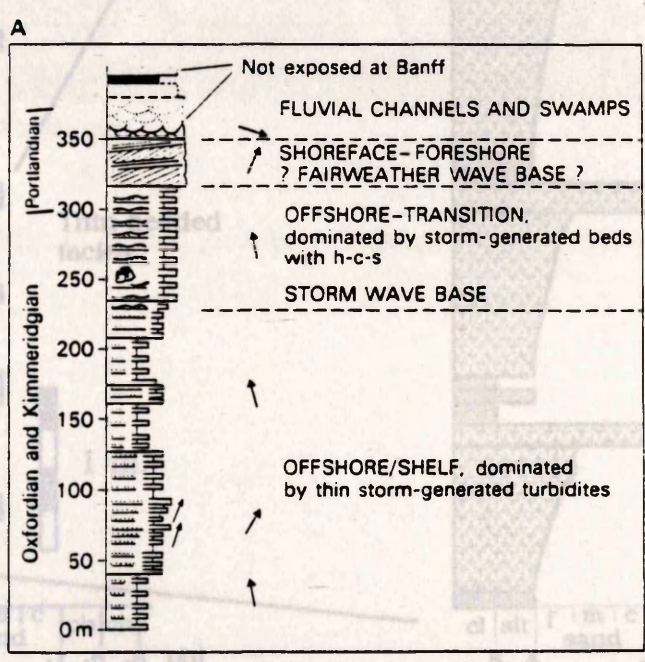


Fig. 3.19. Jurassic Fernie-Kootenay Formations. Alberta, Canada (After Hamblin & Walker, 1979). Large scale coarsening-upwards sequence produced by the progradation of a storm-dominated beach face in a wave dominated delta (Diagram from Elliot, 1978).



Figure 3.20 Sedimentary log of Lower Messinian sedimentary rocks.

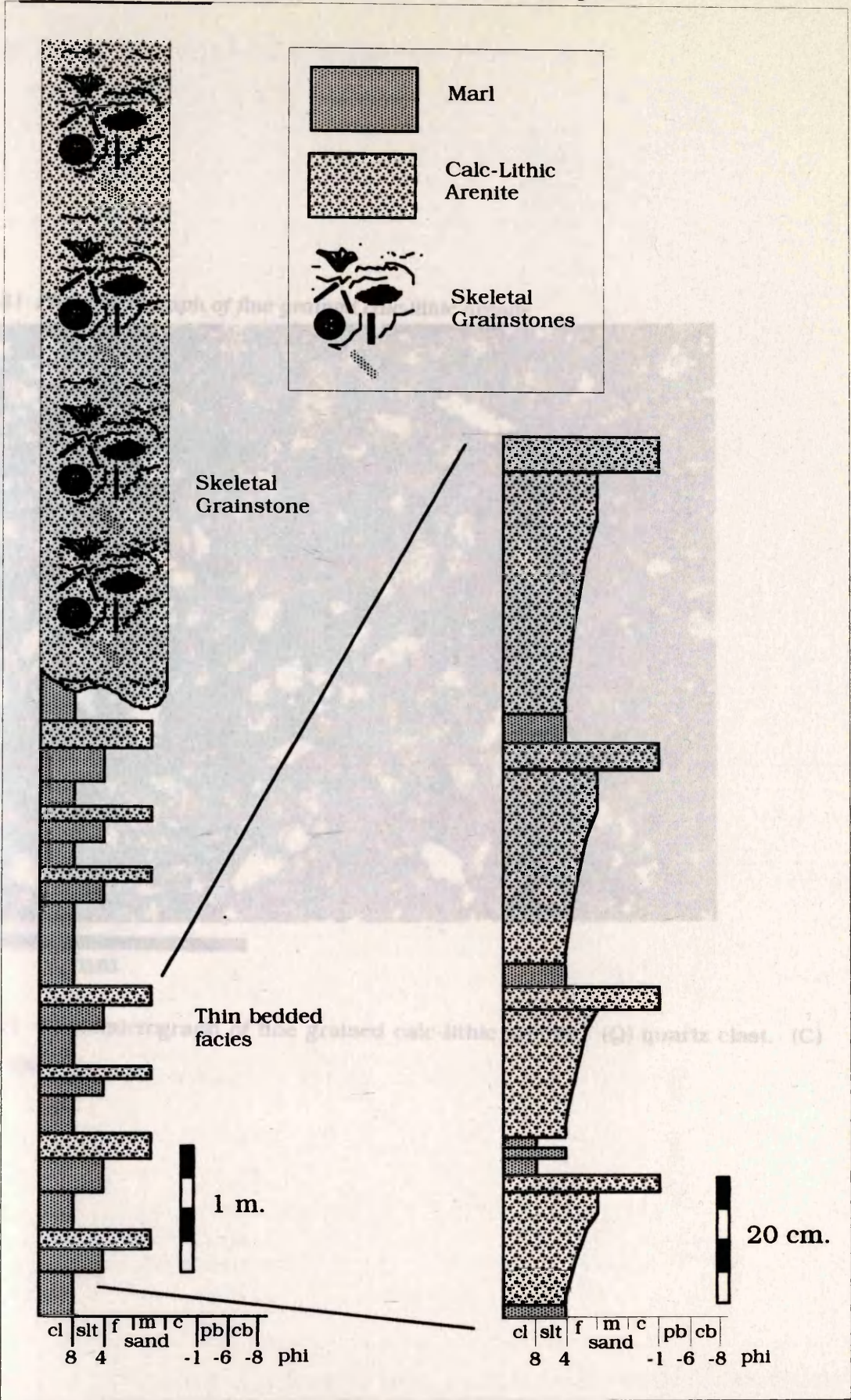
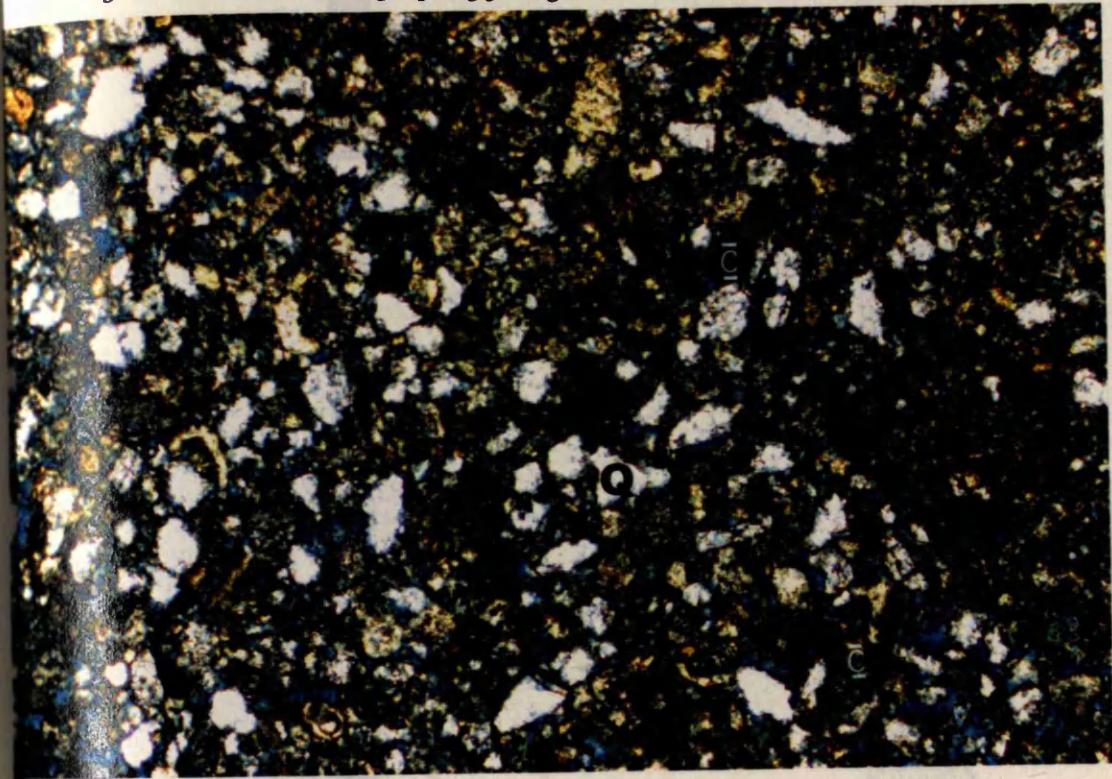


Figure 3.20 Sedimentary log of Lower Messinian sedimentary rocks found at location 61 (Foldout Map 2, Ref 514 325). Log shows thin bedded and skeletal grainstone facies.





1 mm

Figure 3.21 Photomicrograph of fine grained calc-lithic arenite. (Q) quartz clast. (C) carbonate clast.



Figure 3.22 Sedimentary log of lower Messinian fining up cycles.

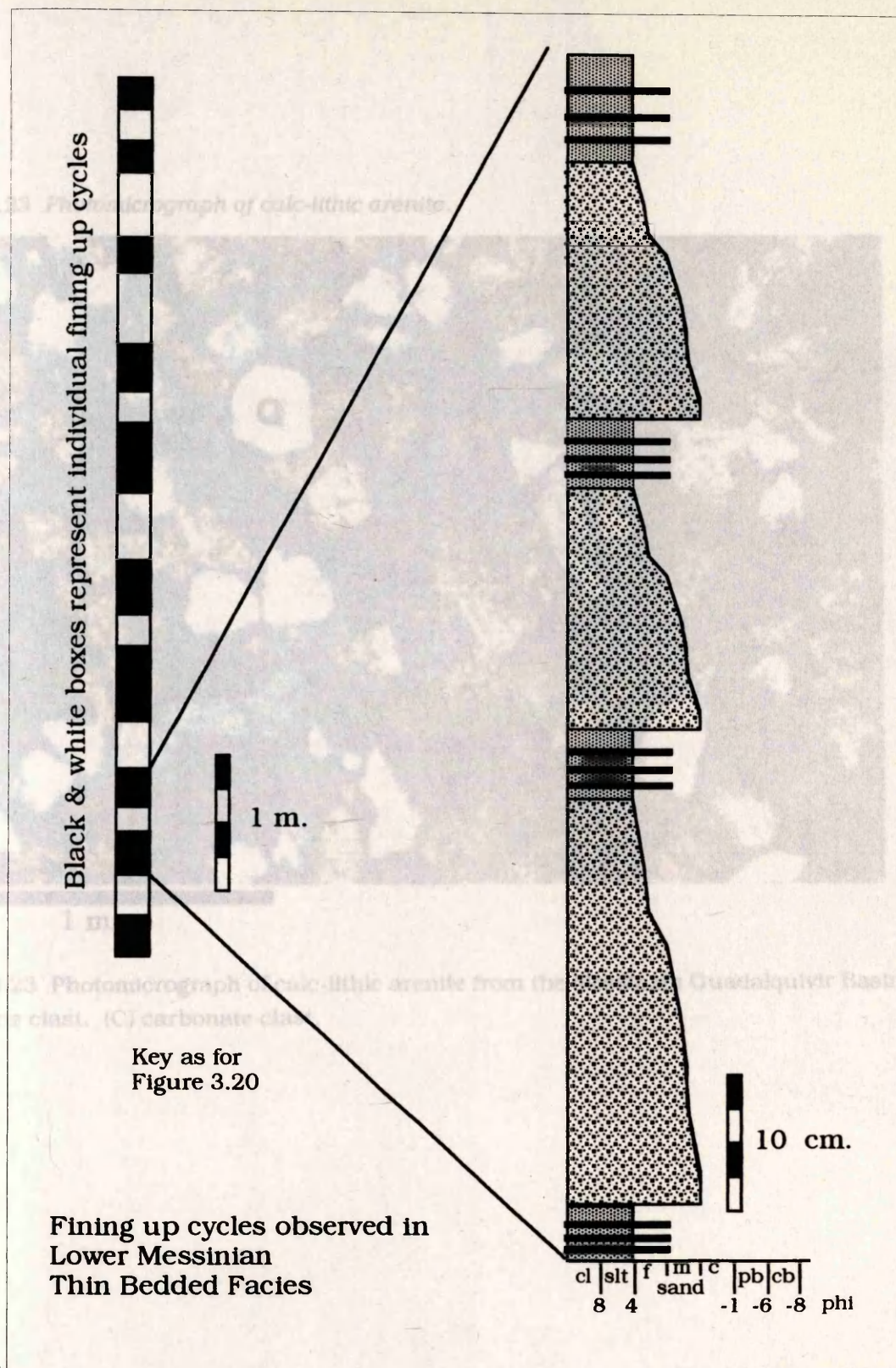
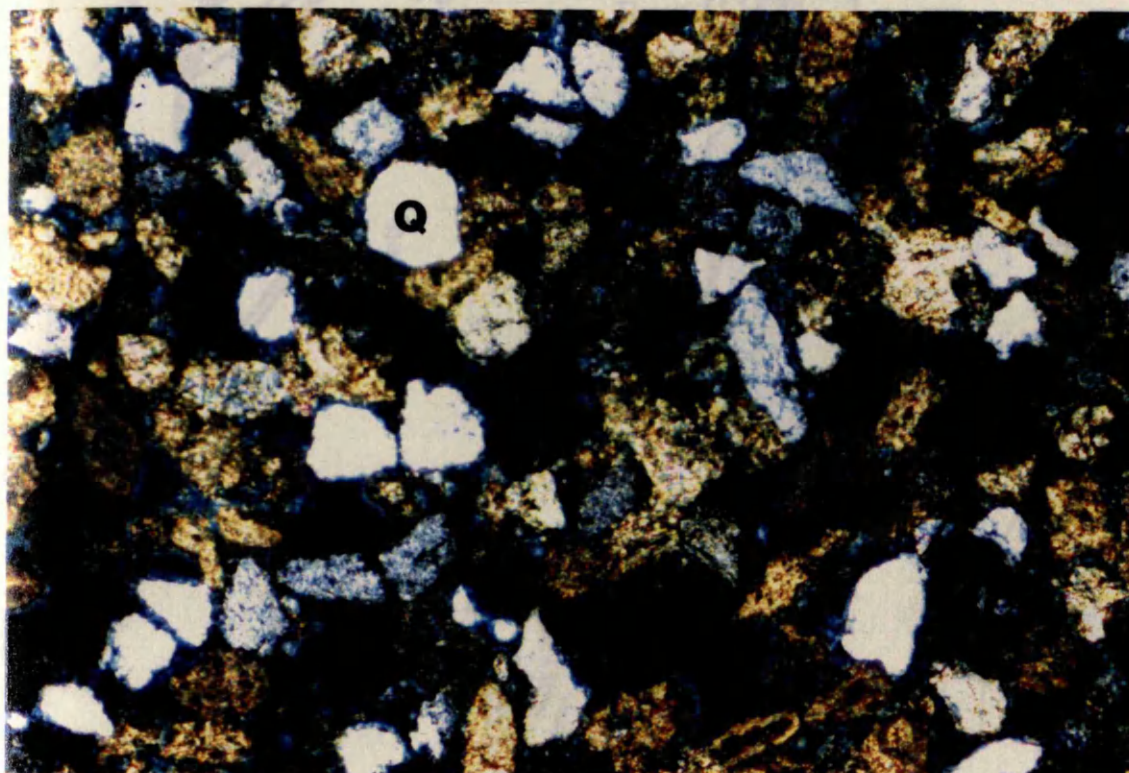


Figure 3.22 Sedimentary log of fining up cycles found in the thin bedded facies of the Lower Messinian sedimentary succession. Black and white boxes represent individual fining up cycles, one box represents one cycle. From location 75 (Foldout Map 2, Ref 500 339)



Figure 3.23 Photomicrograph of calc-lithic arenite.



1 mm

Figure 3.23 Photomicrograph of calc-lithic arenite from the Messinian Guadalquivir Basin.  
(Q) quartz clast. (C) carbonate clast.



Figure 3.24 Diagram of mega-ripple bed

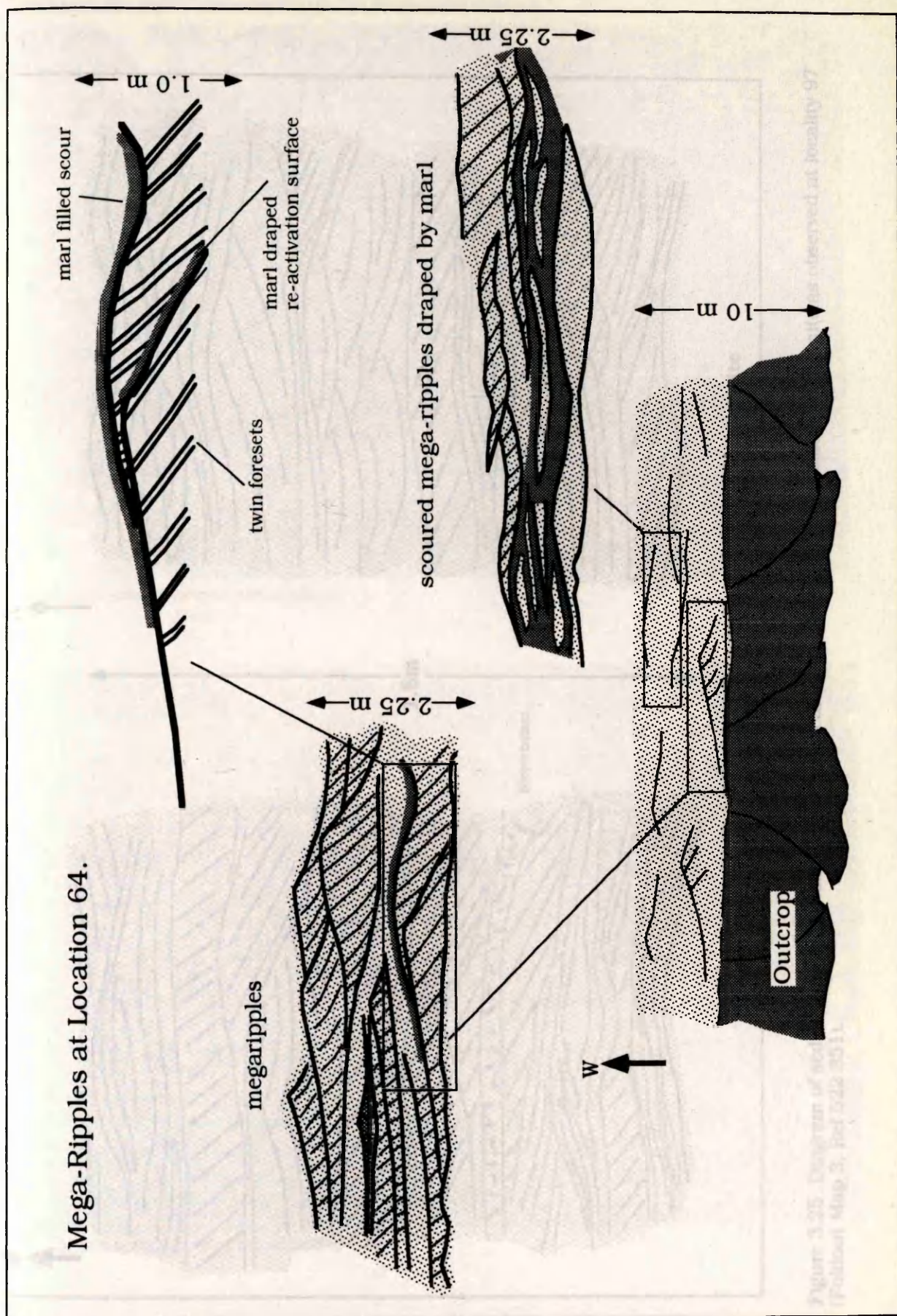


Figure 3.24 Diagram of mega-ripple bed forms observed at location 64 (Foldout Map 2, Ref 514 330).



Figure 3.25 Sedimentary structures in calc-lithic arenite.

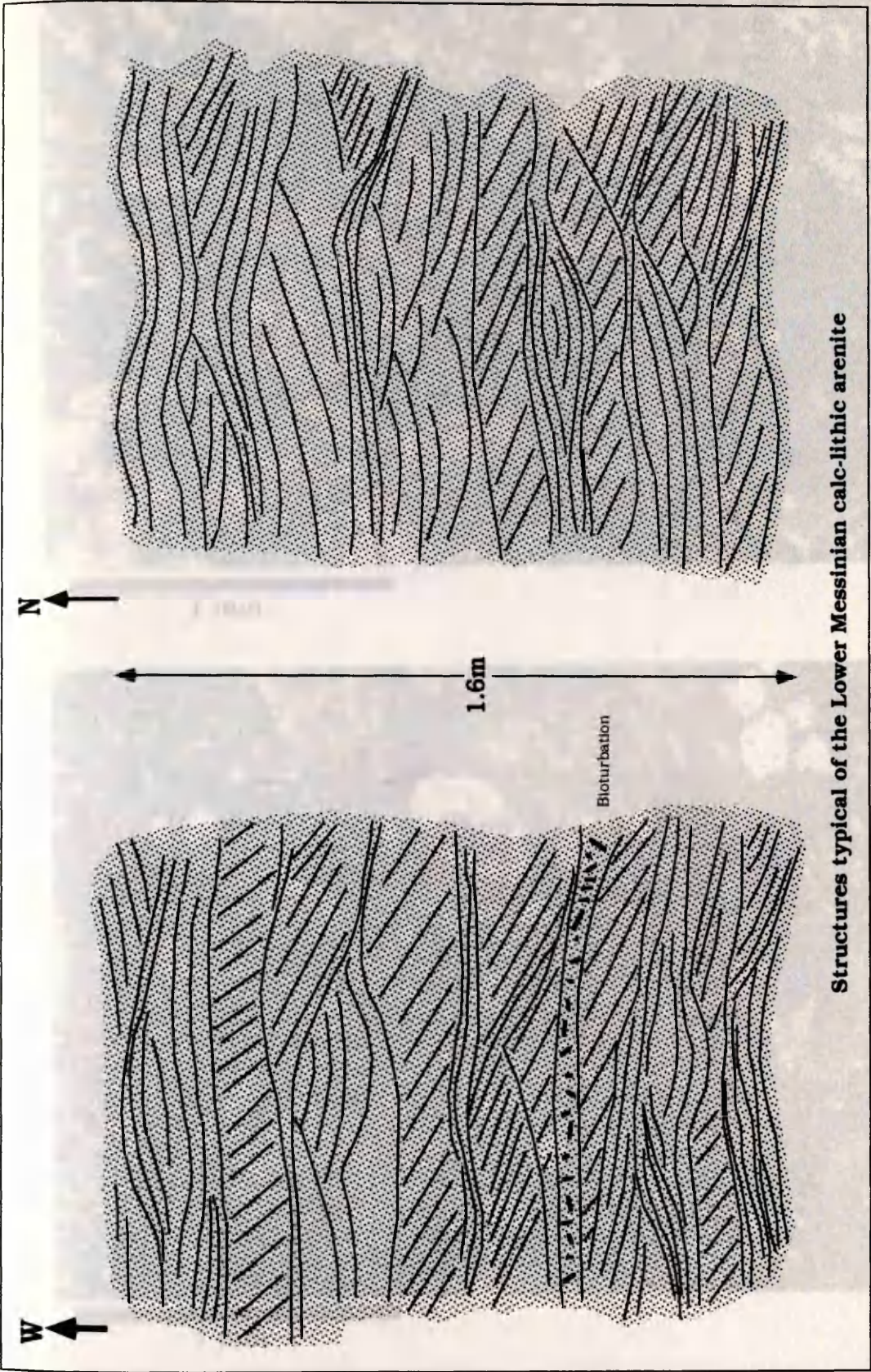


Figure 3.25 Diagram of sedimentary structures that are typical of the Lower Messinian calc-lithic arenite as observed at locality 97 (Foldout Map 3, Ref 522 351).

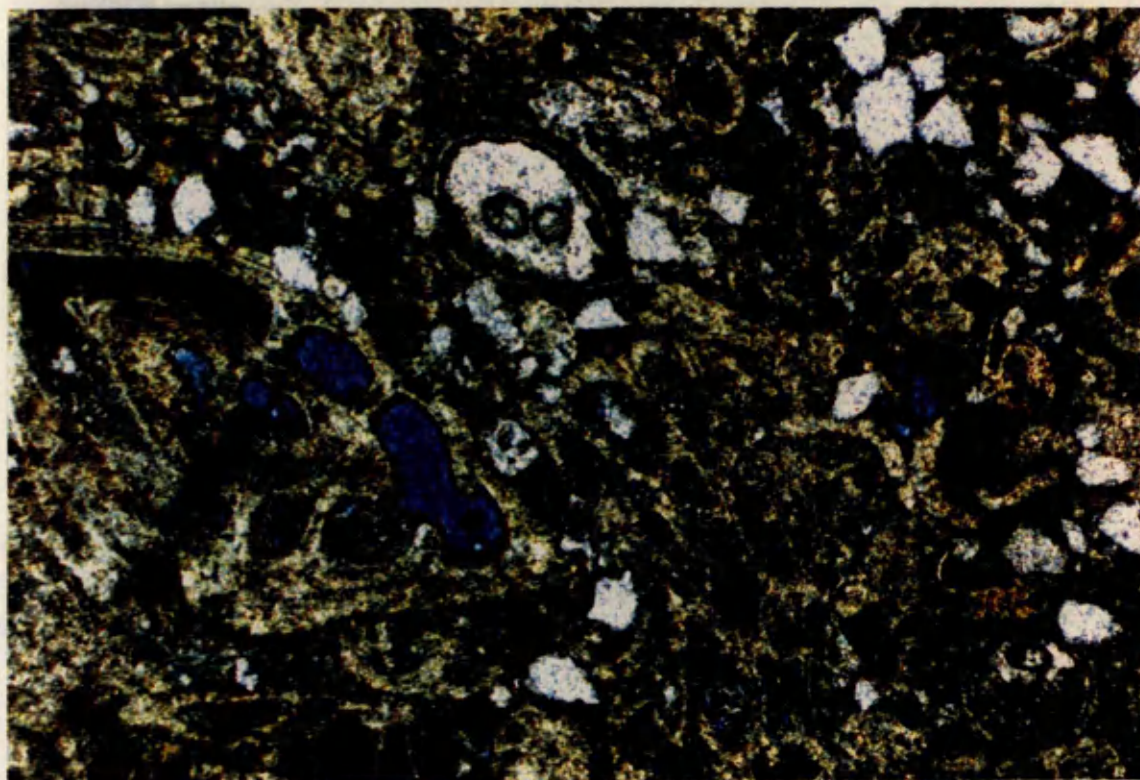
Figure 3.26 Photomicrographs of Bioclastic grainstones from the Messinian Guadalquivir Basin.



Figure 3.26 Photomicrographs of Bioclastic grainstones.



1 mm



1 mm

Figure 3.26 Photomicrographs of Bioclastic grainstones from the Messinian Guadalquivir Basin.



Figure 3.27 Log of channelised matrix supported conglomerate.

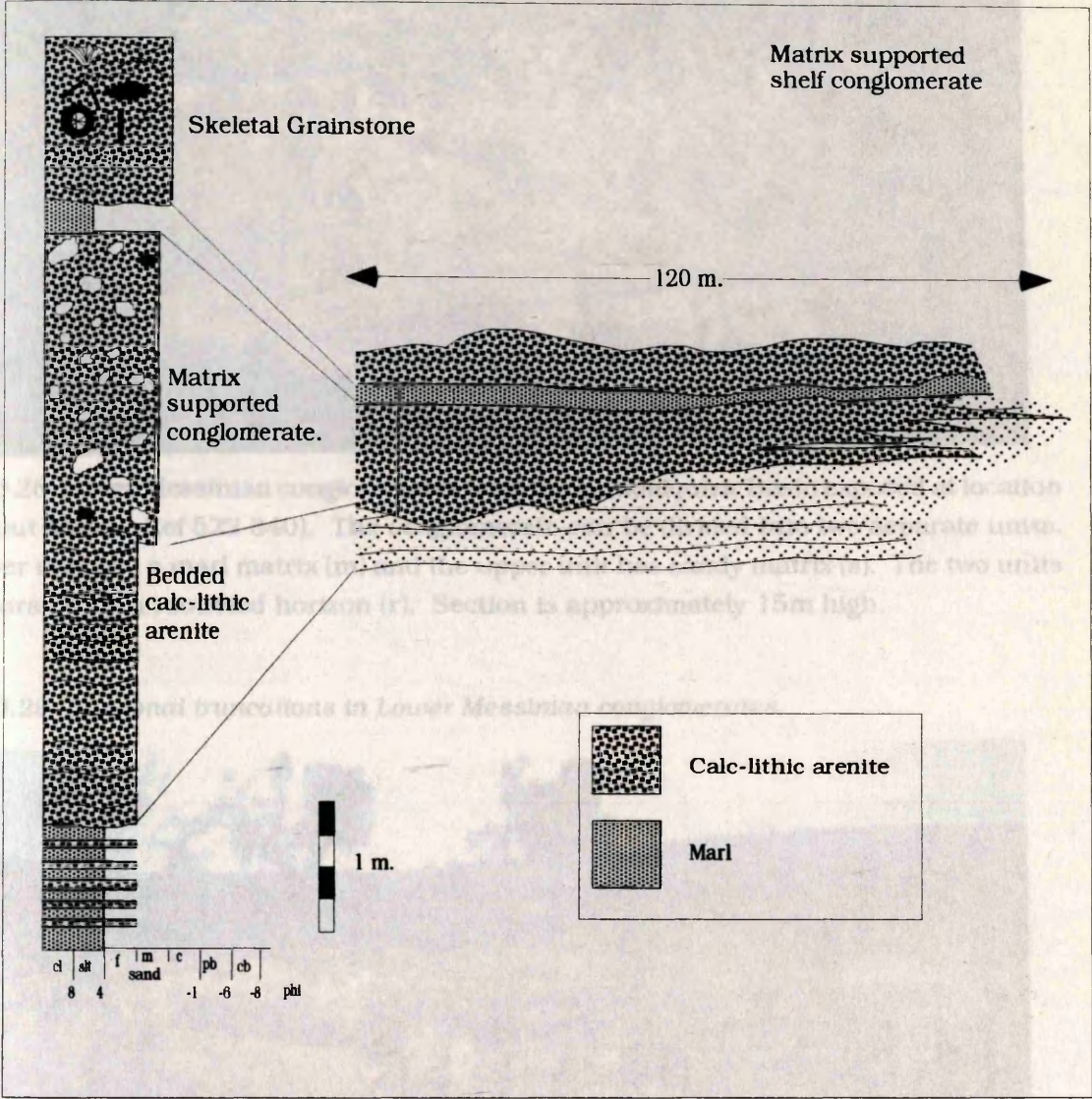


Figure 3.27 Sedimentary log taken from Lower Messinian rocks exposed at location 99 (Foldout Map 3, Ref 510 344). Log shows the channelised matrix supported conglomerate that is observed to be interbedded with marine calc-lithic arenites.



Figure 3.28 Lower Messinian conglomerates.



Figure 3.28 Lower Messinian conglomerates from the Guadalquivir Basin exposed at location 9 (Foldout Map 2, Ref 522 340). The conglomerate can be divided into two separate units. The lower unit has a marl matrix (m) and the upper unit has sandy matrix (s). The two units are separated by a rootlet horizon (r). Section is approximately 15m high.

Figure 3.29 Erosional truncations in Lower Messinian conglomerates.

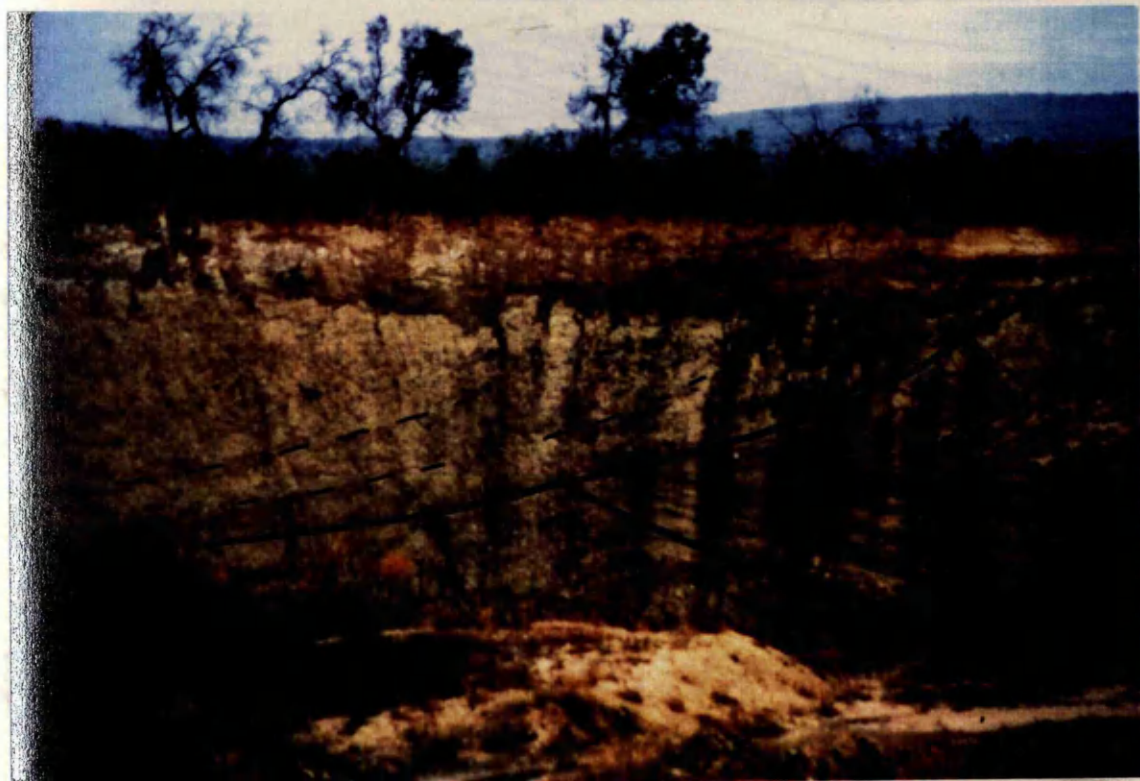


Figure 3.29 Erosional truncations in Lower Messinian conglomerates exposed at location 9 (Foldout Map 2, Ref 522 340). Section is approximated 15m high.



Figure 3.30 The formation of low-angle reactivation surfaces in sand waves

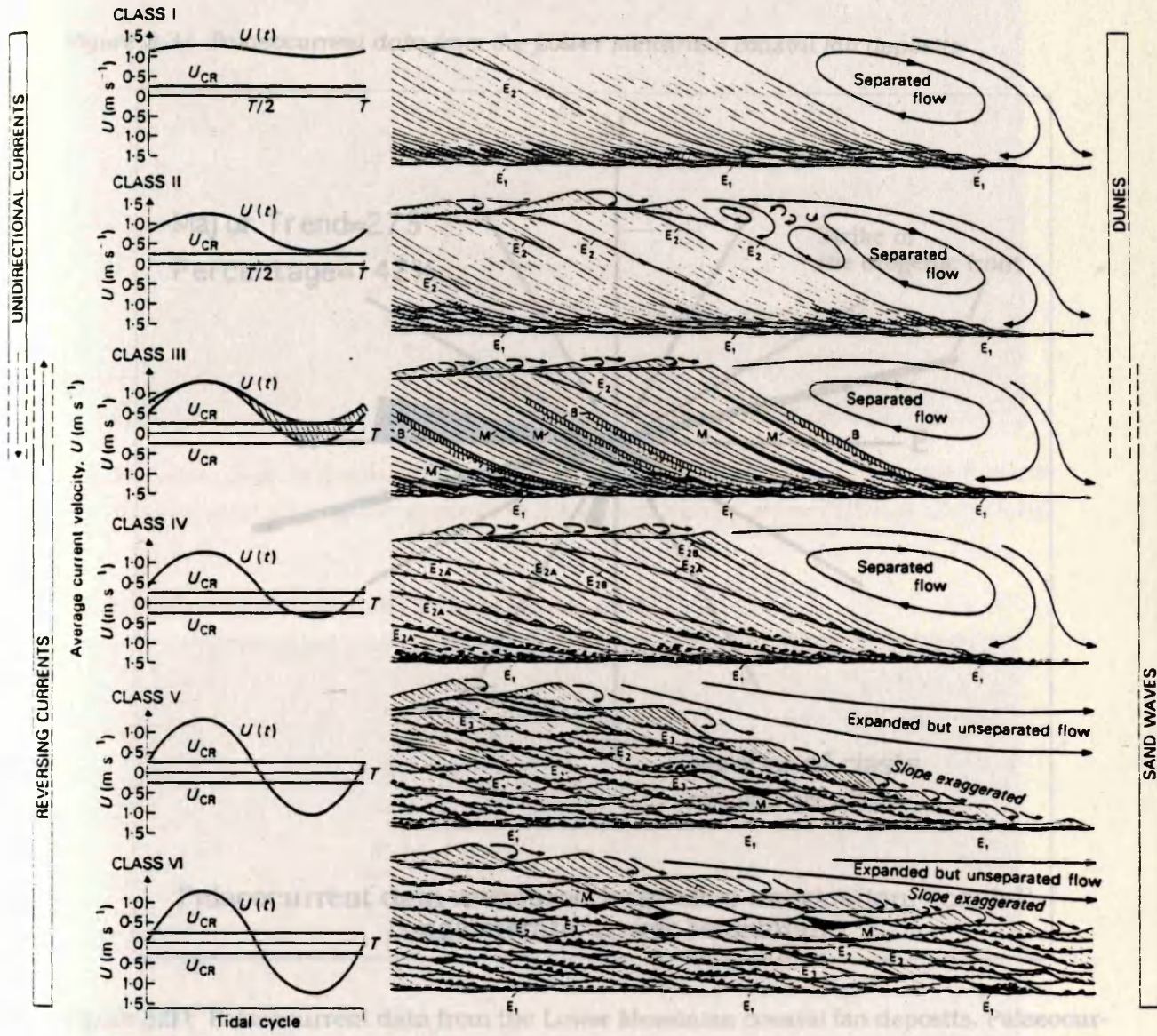


Figure 3.30 A theoretical model; to explain the formation of low-angle reactivation surfaces in sand waves formed by reversing currents. Diagram from Allen (1980).



Figure 3.31 Palaeocurrent data from the Lower Messinian coastal fan deposits

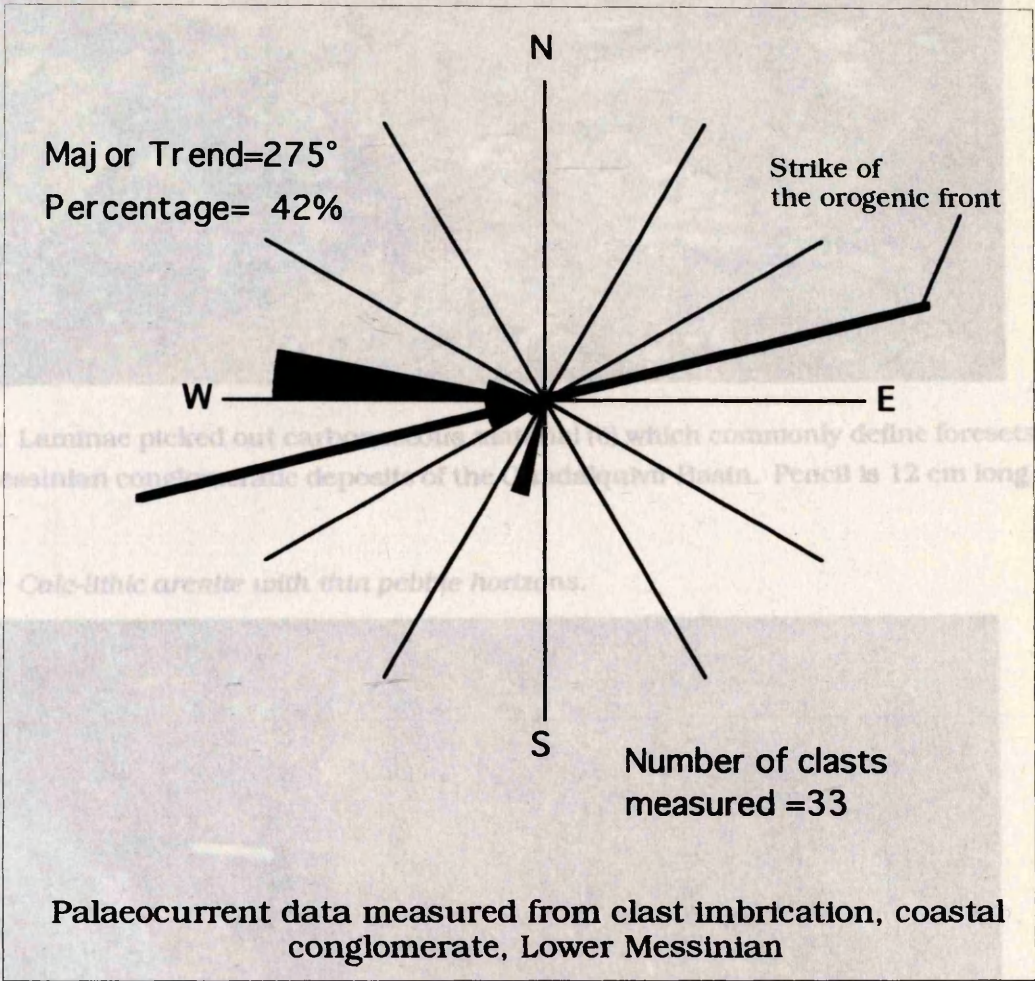


Figure 3.31 Palaeocurrent data from the Lower Messinian coastal fan deposits. Palaeocurrents derived from the dip direction of imbricate clasts. The approximate strike of the orogenic (External Zone) front is also shown



Figure 3.32 Laminae picked out carbonaceous material (c) which commonly define foresets in Upper Messinian conglomeratic deposits of the Guadalquivir Basin. Pencil is 12 cm long.



Figure 3.32 Laminae picked out carbonaceous material (c) which commonly define foresets in Upper Messinian conglomeratic deposits of the Guadalquivir Basin. Pencil is 12 cm long.

Figure 3.33 Calc-lithic arenite with thin pebble horizons. Photo from location 46 (Foldout Map 2). Hammer is 40 cm long.

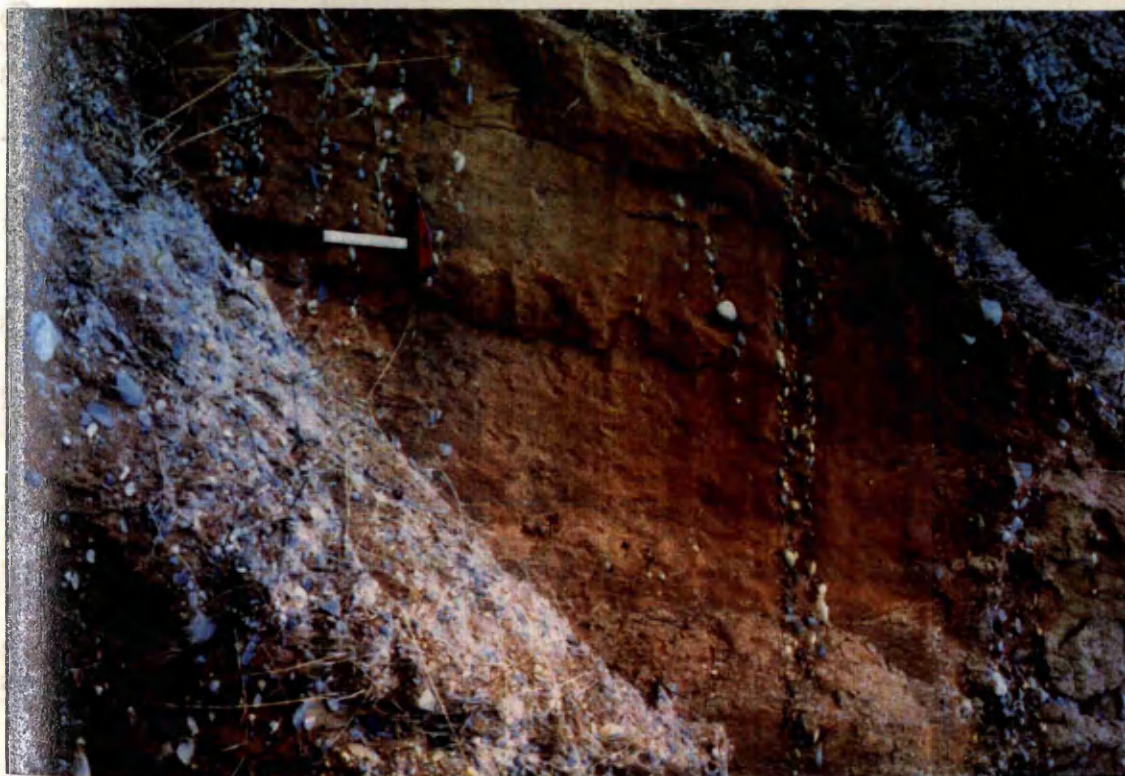


Figure 3.33 Calc-lithic arenite with thin pebble horizons that are common in Lower Messinian conglomerates of the Guadalquivir Basin. Photo from location 46 (Foldout Map 2). Hammer is 40 cm long.



Figure 3.34 Sedimentary log of Upper Messinian conglomerates.

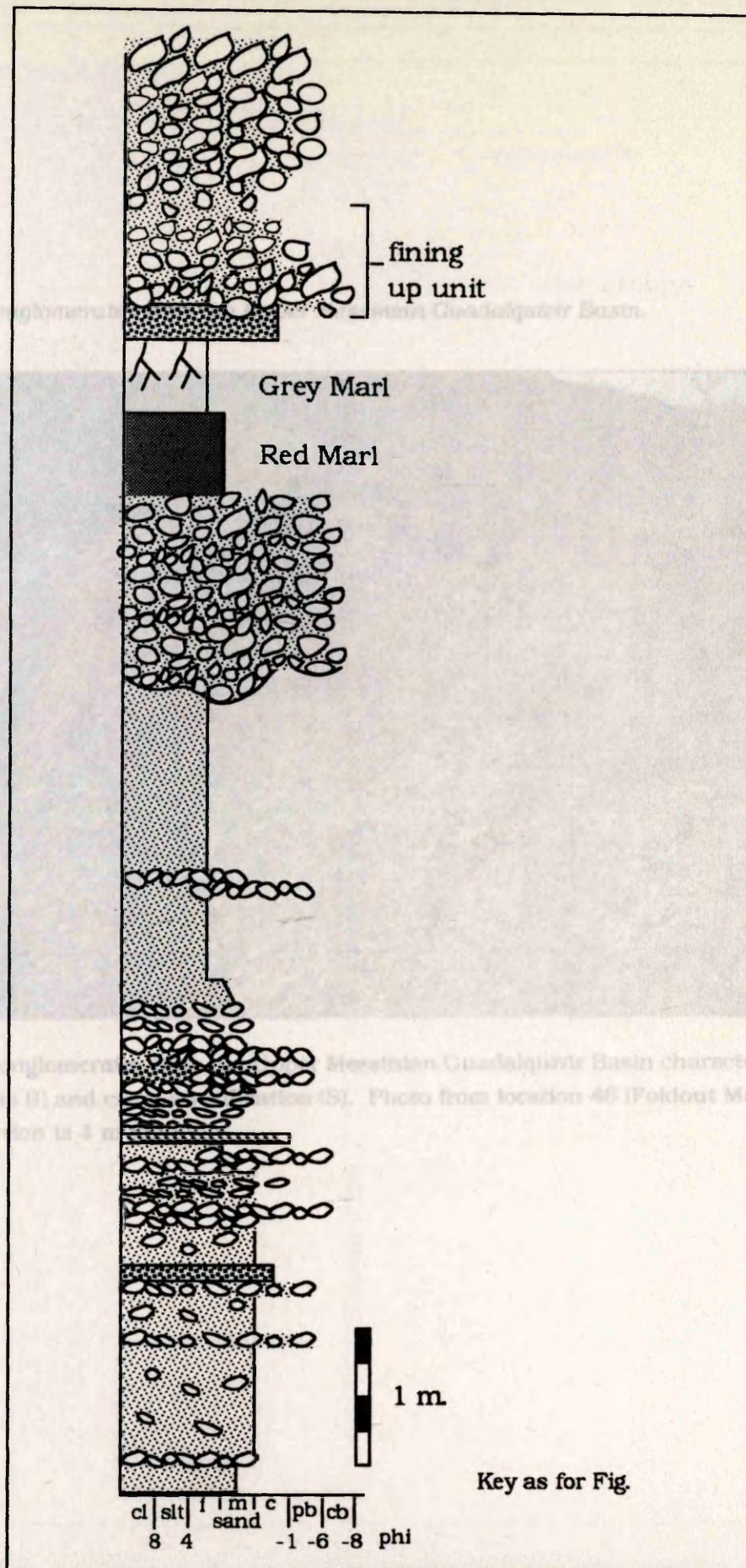


Figure 3.34 Sedimentary log of Upper Messinian conglomerates showing colour stratified marls and fining up units. Log taken from location 46 (Foldout Map 2, Ref 511 338)





Figure 3.35 Conglomerates from the Upper Messinian Guadalquivir Basin characterised by imbricate clasts (I) and cross stratification (S). Photo from location 46 (Foldout Map 2, Ref 511 338). Section is 4 m high.



Figure 3.36 Sedimentary log of Upper Messinian conglomerates.

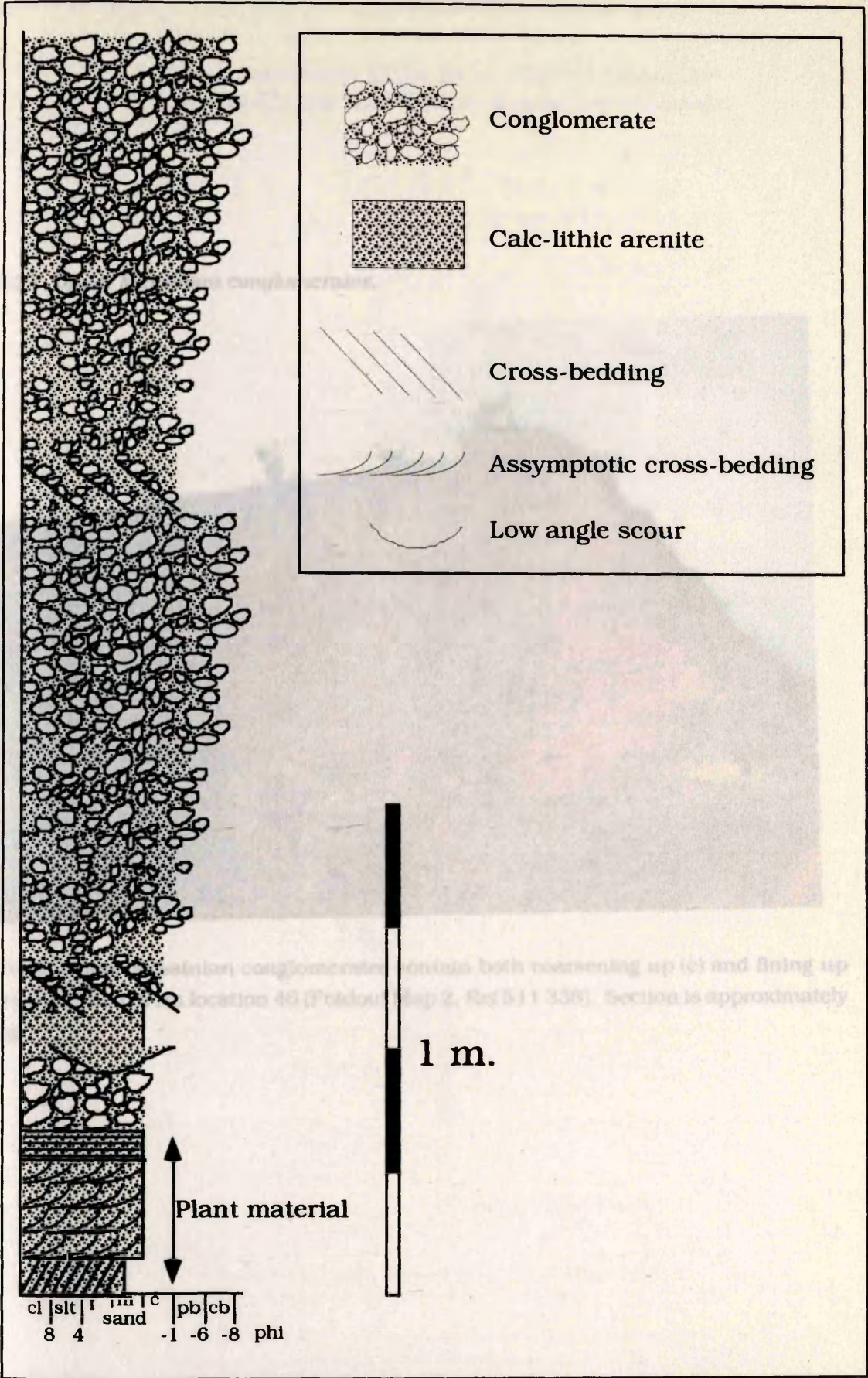


Figure 3.36 Sedimentary log of Upper Messinian conglomerates showing coarsening up sequences and pebble draped cross-strata. Log taken from location 47, Foldout Map 2 (Ref 510 340).



Figure 3.37 Upper Messinian conglomerates.



Figure 3.37 Upper Messinian conglomerates contain both coarsening up (c) and fining up (f) sequences. Photo from location 46 (Foldout Map 2, Ref 511 338). Section is approximately 10 m high.



Figure 3.38. Palaeocurrent data taken from Upper Messinian fluvial deposits.

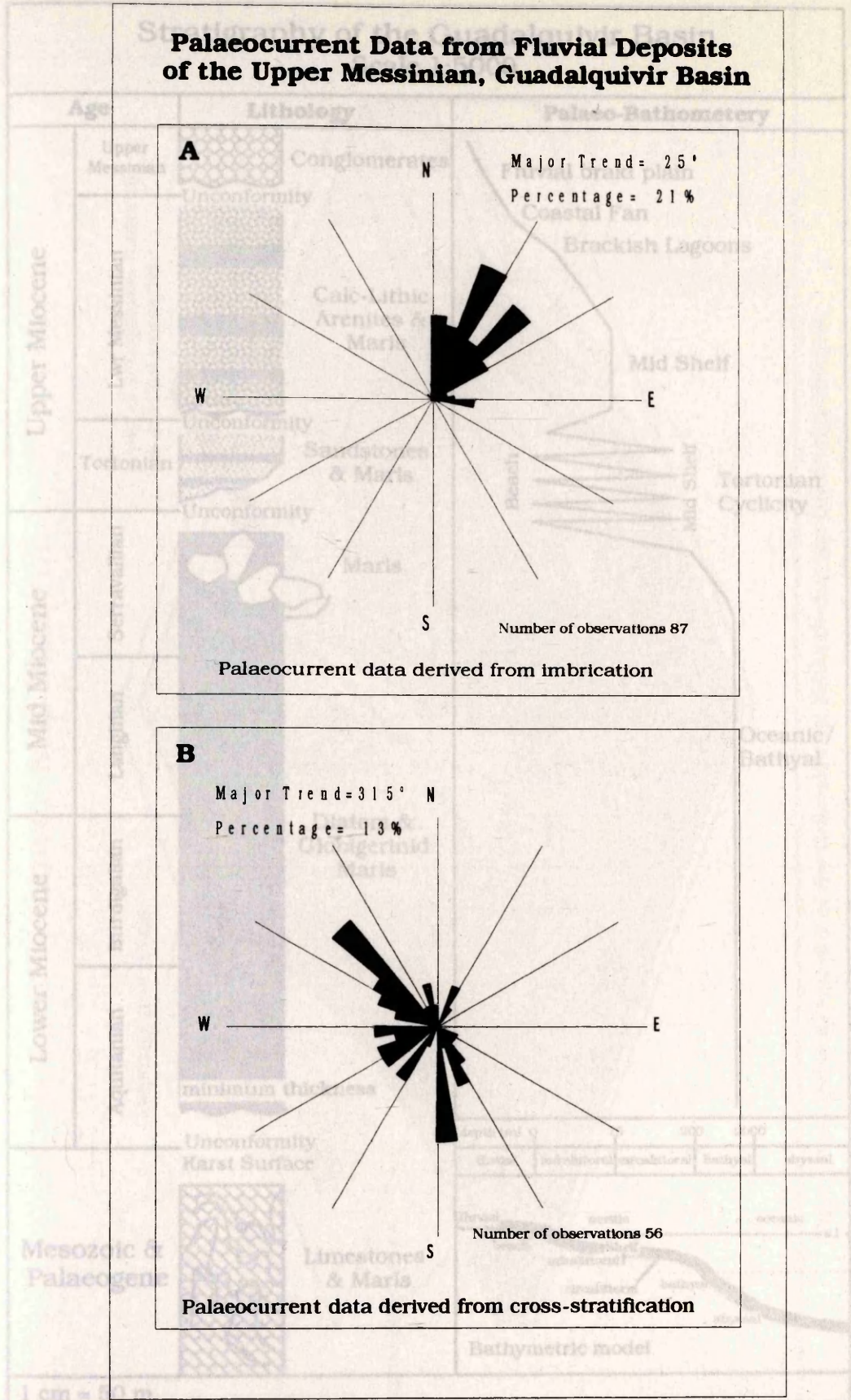


Figure 3.38 Palaeocurrent data taken from Upper Messinian fluvial deposits. A) palaeocurrent data derived from the dip direction of imbricate clasts. B) palaeocurrent data derived the dip direction of cross-stratification.



Figure 3.39 Palaeo-bathymetry of the Guadalquivir Basin succession.

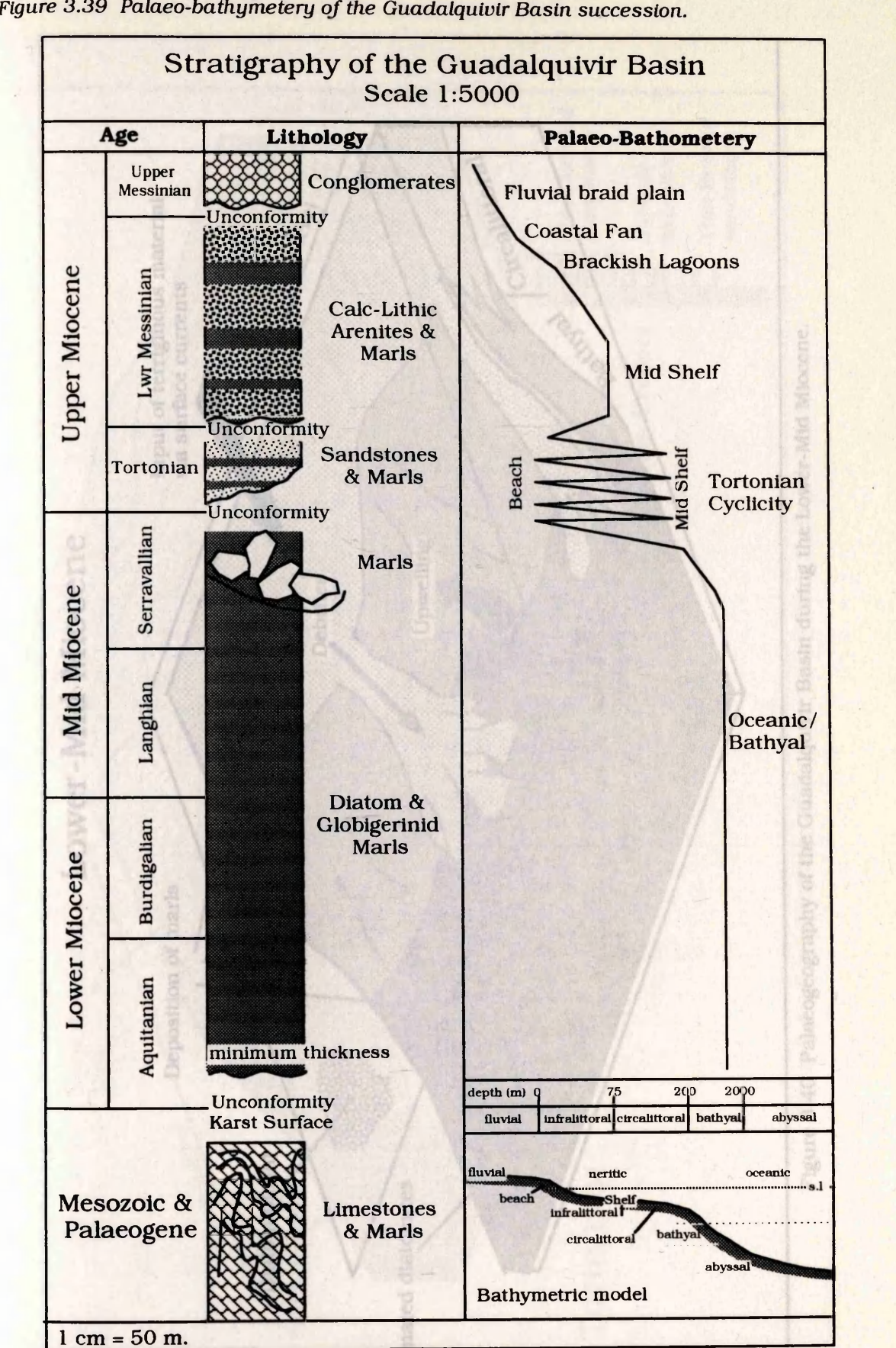


Figure 3.39 Palaeo-bathymetry of the Guadalquivir Basin succession, derived from facies analysis and micro-palaeontology (Appendix 2).



Figure 3.40 Palaeogeography during the Lower-Mid Miocene.

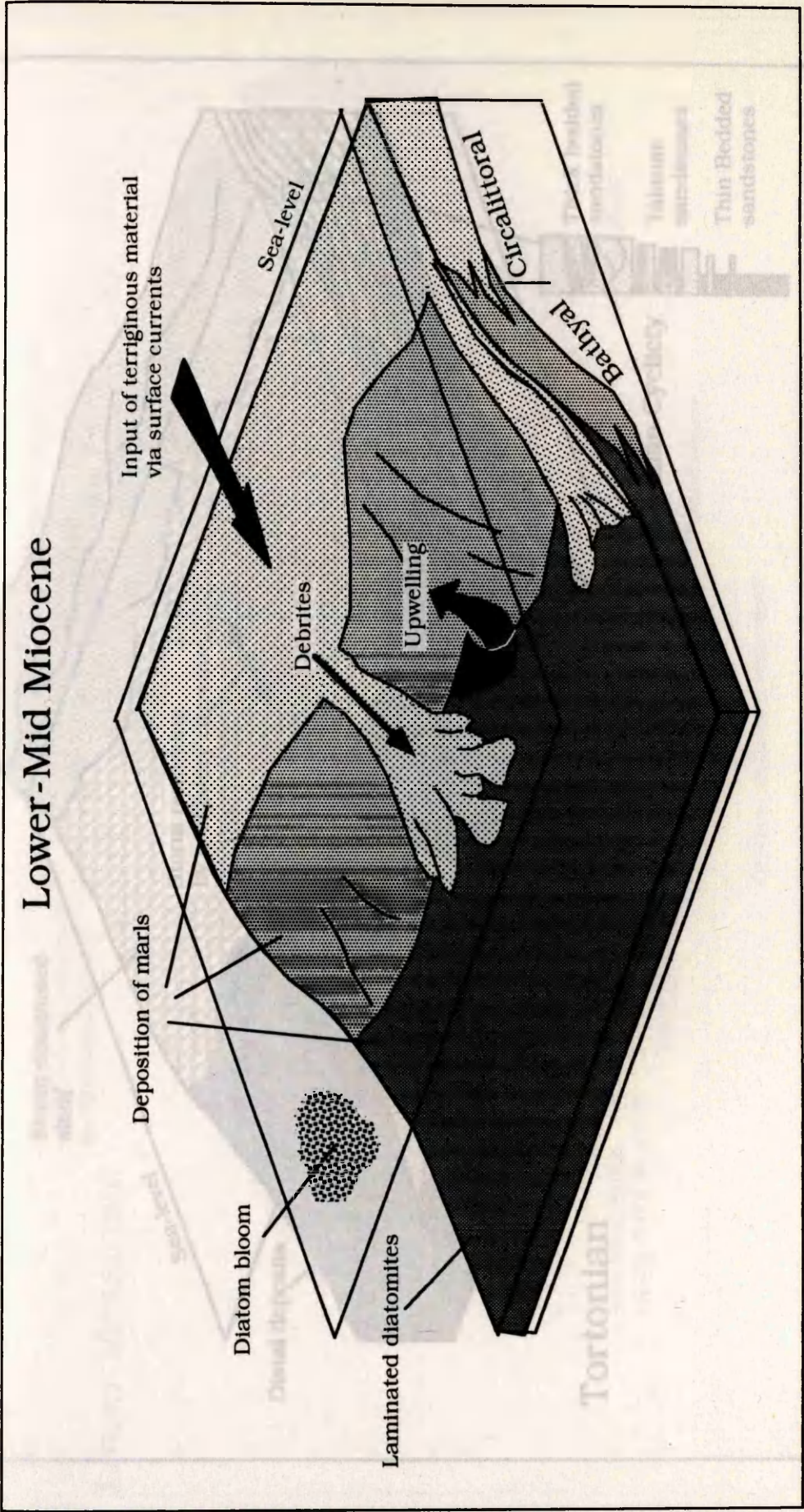


Figure 3.40 Palaeogeography of the Guadalquivir Basin during the Lower-Mid Miocene.



Figure 3.41 Palaeogeography during the Tortonian.

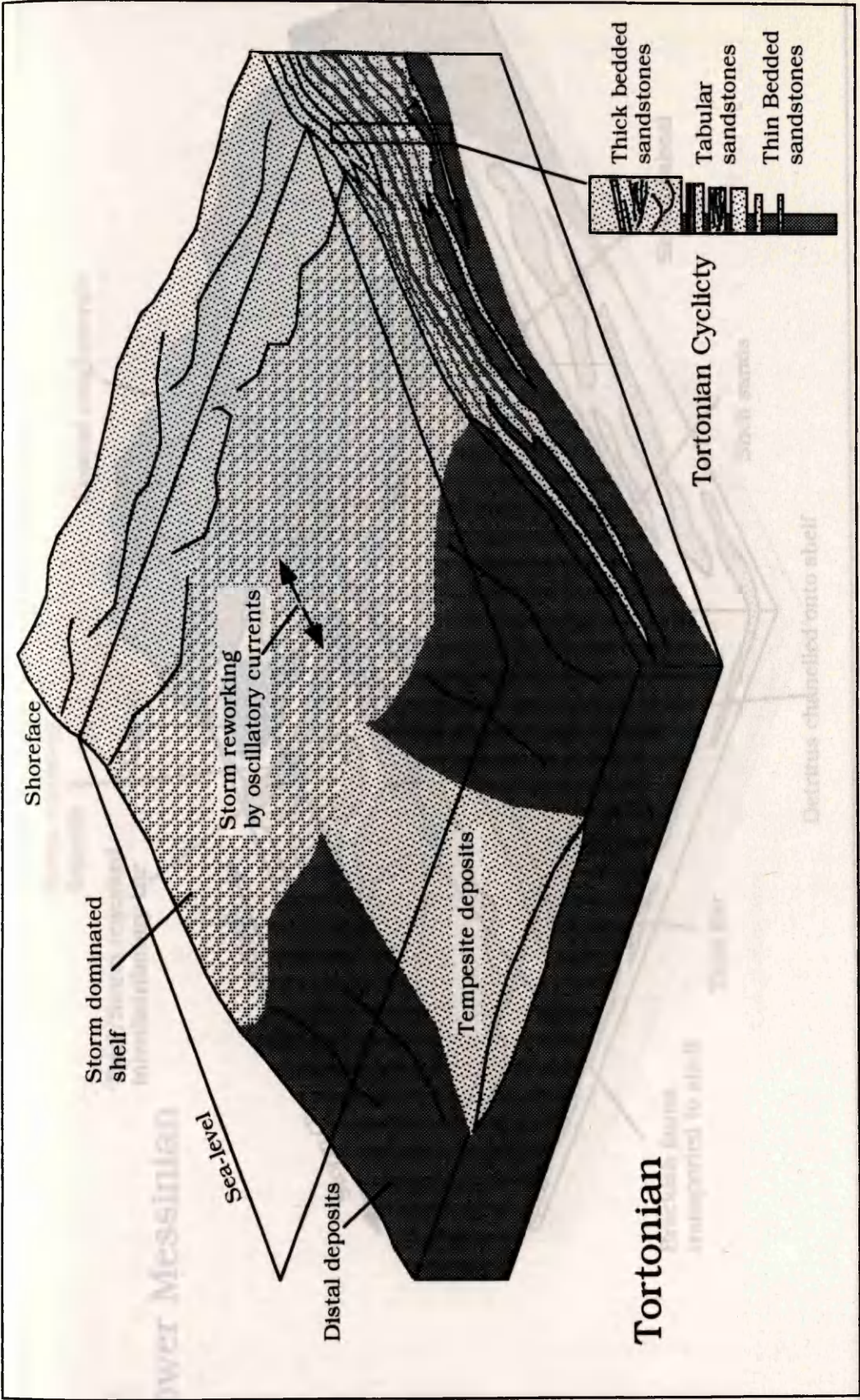


Figure 3.41 Palaeogeography of the Guadalquivir Basin during the Tortonian.



Figure 3.42 Palaeogeography during the Lower Messinian.

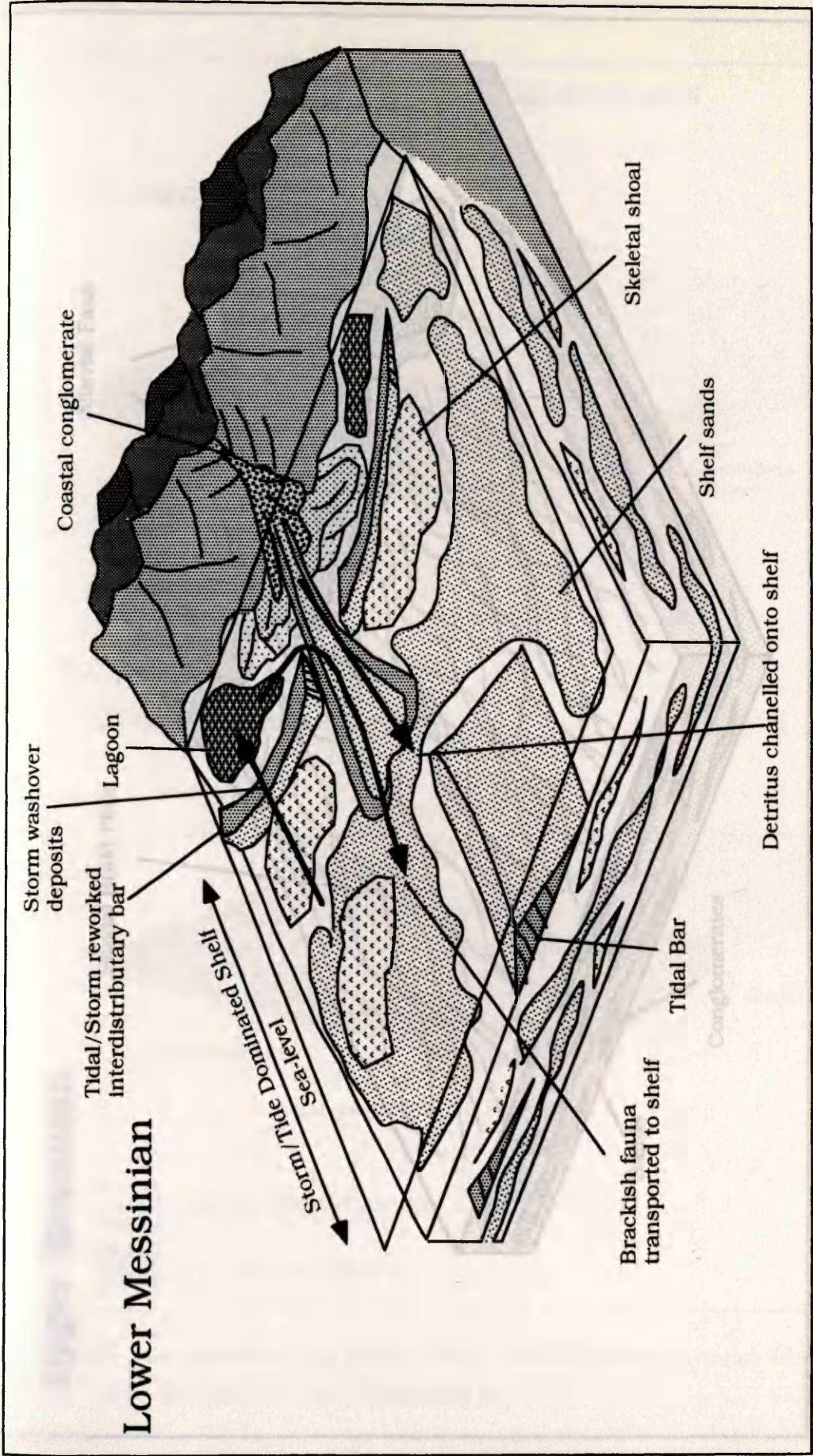


Figure 3.42 Palaeogeography of the Guadalquivir Basin during the Lower Messinian.



Figure 3.43 Palaeogeography during the Upper Messinian.

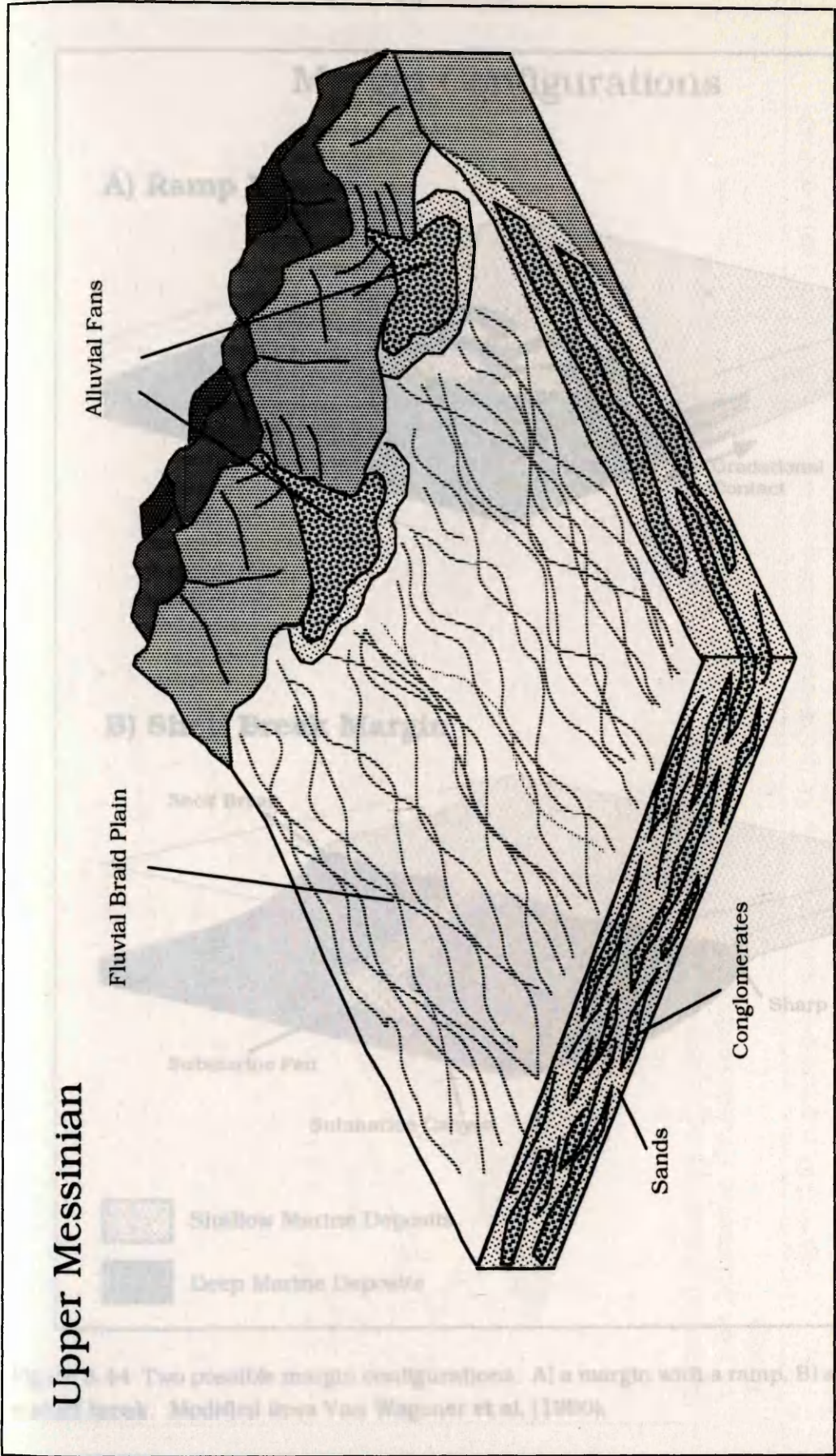


Figure 3.43 Palaeogeography of the Guadalquivir Basin during the Upper Messinian.



Figure 3.45 A generalized paleogeography.

Figure 3.44 Two possible margin configurations.

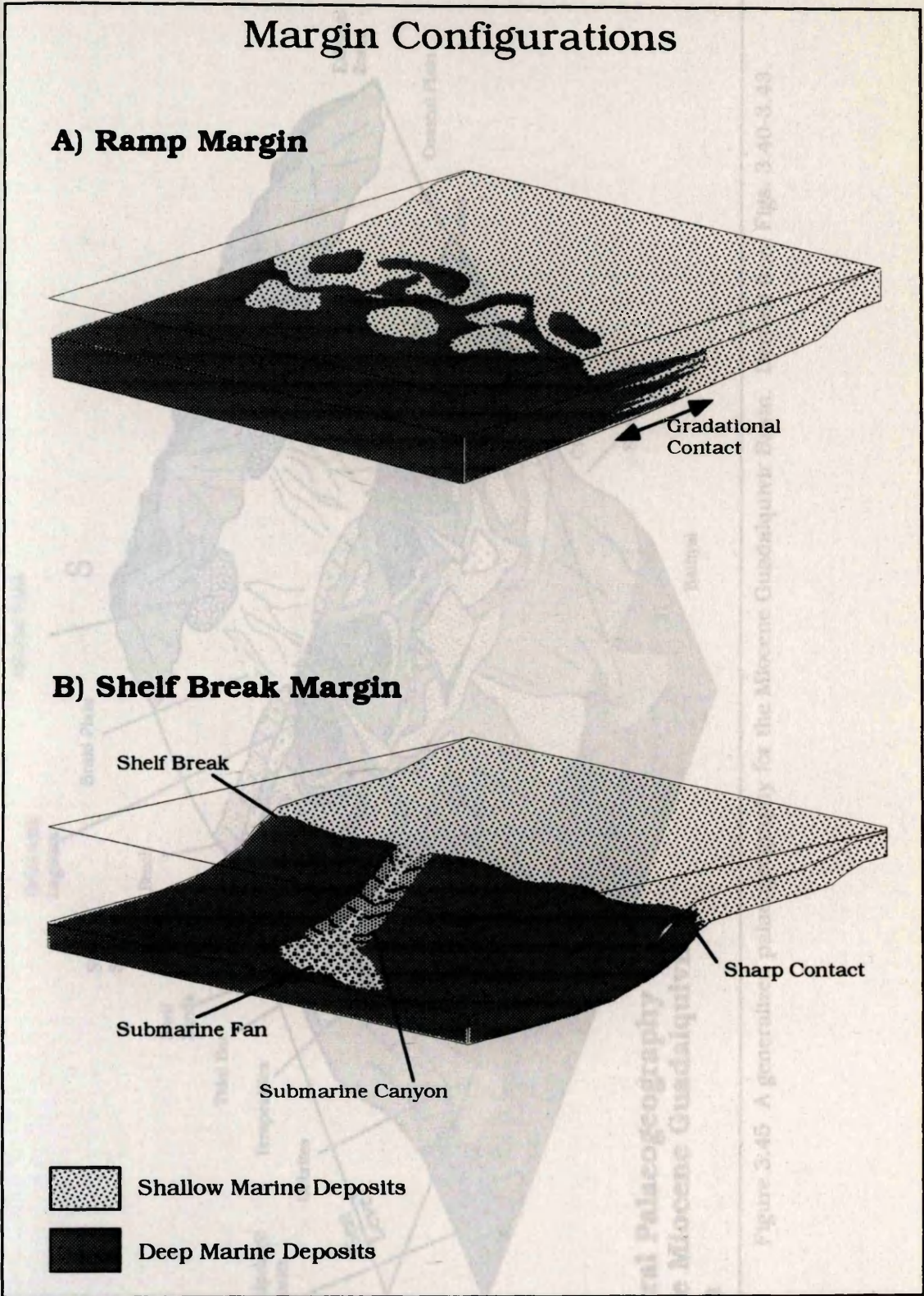


Figure 3.44 Two possible margin configurations. A) a margin with a ramp, B) a margin with a shelf break. Modified from Van Wagoner et al. (1990).



Figure 3.45 A generalized palaeogeography.

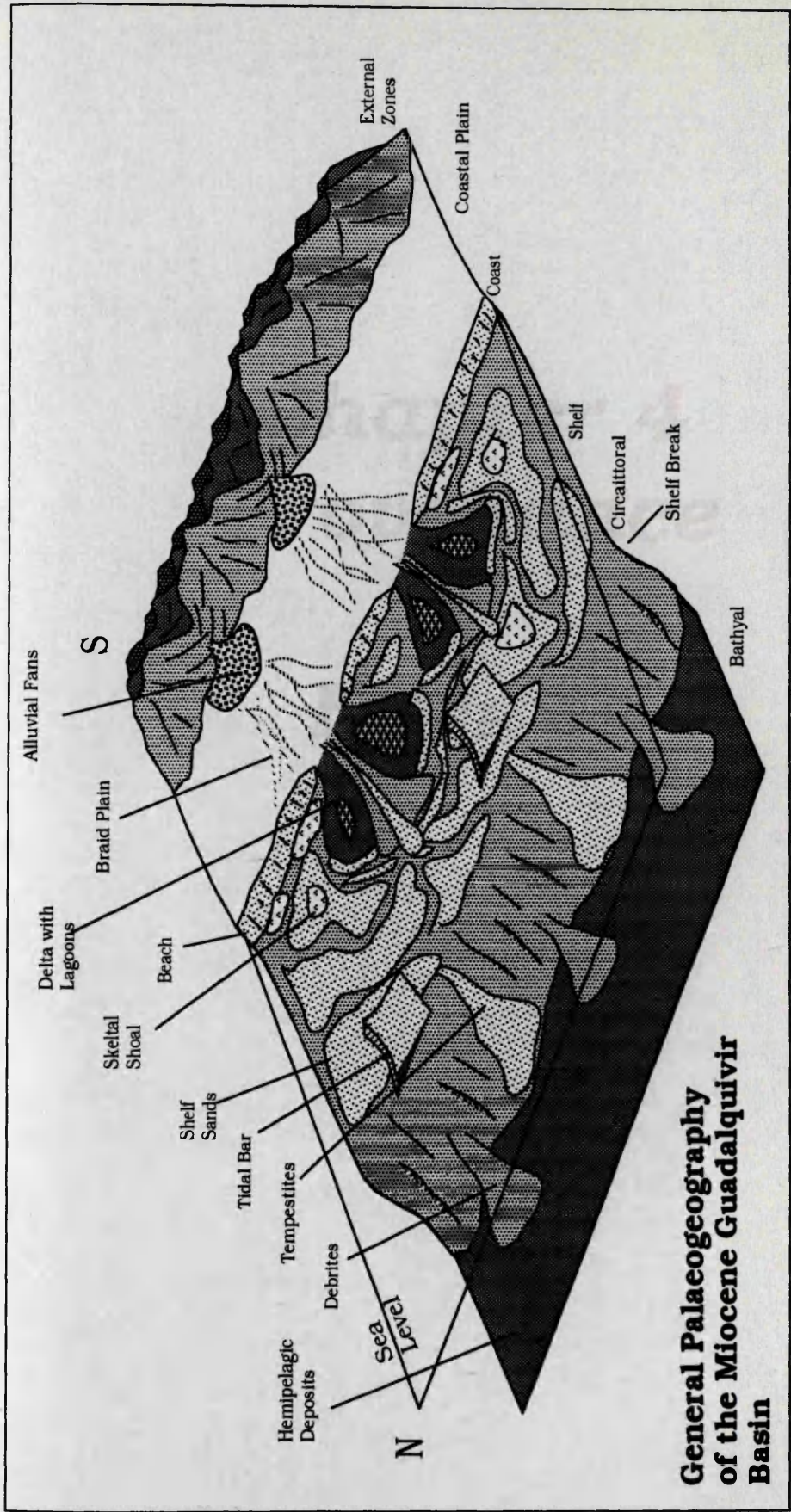


Figure 3.45 A generalized palaeogeography for the Miocene Guadalquivir Basin. Derived from Figs. 3.40-3.43.



# ***Chapter 4***

## ***Provenance***

### ***Figures***



Figure 4.1 Candidate source rocks.

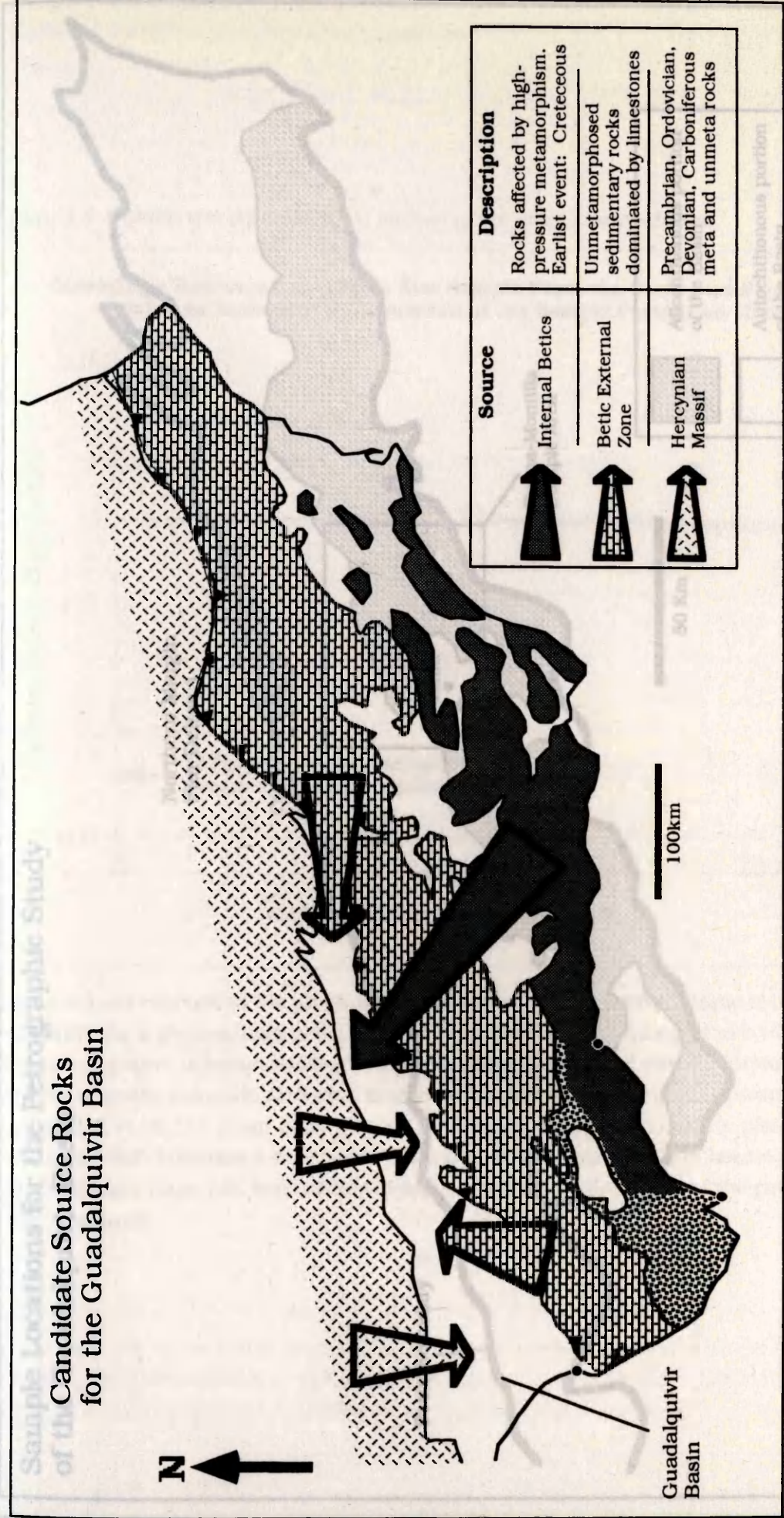


Figure 4.1 Candidate source rocks for Miocene sediments of the Guadalquivir Basin. Possible sources are the Hercynian Massif, the Betic External Zone and the Betic Internal Zone



Figure 4.2 Sample locations.

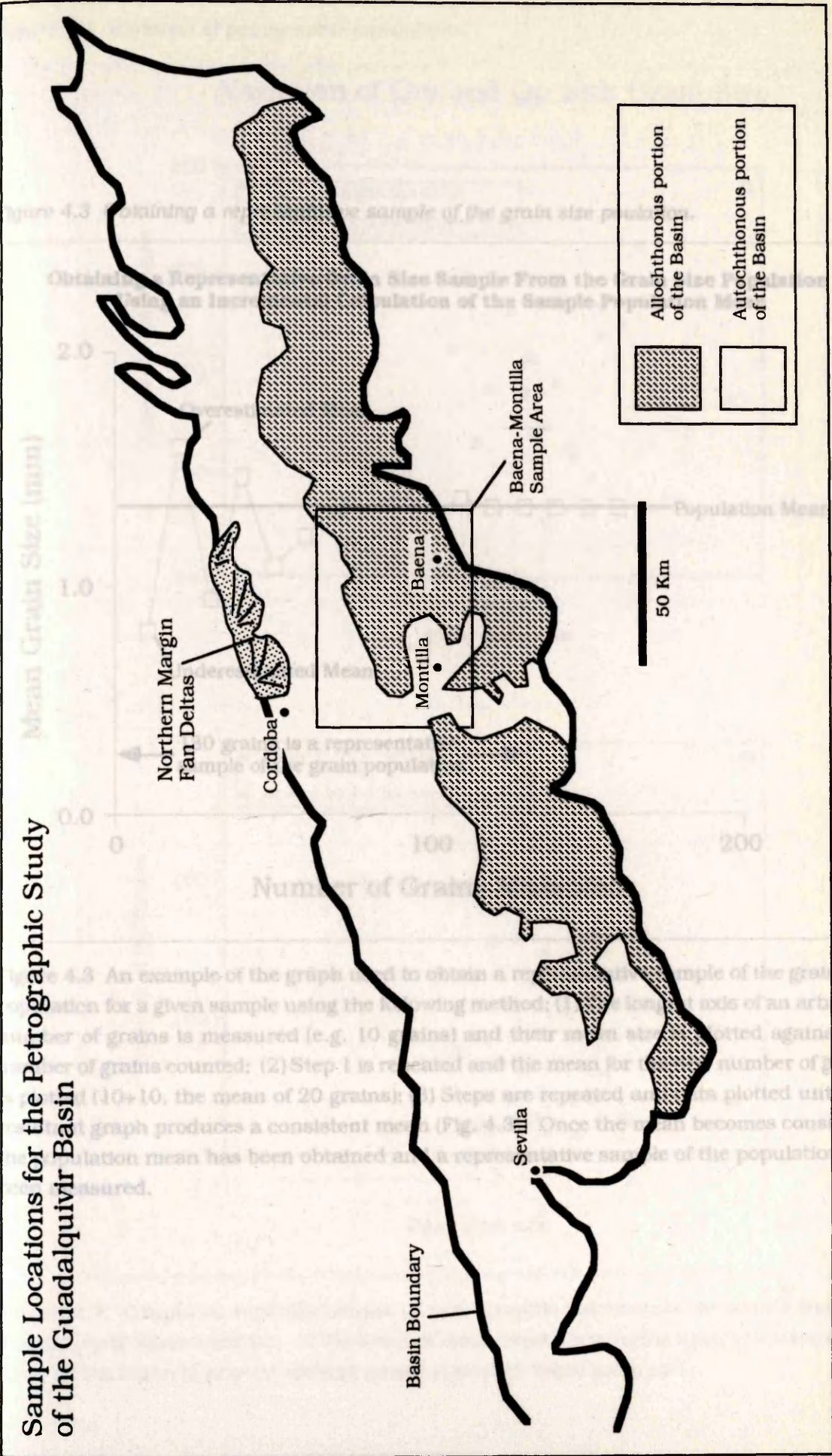


Figure 4.2 Schematic map showing the general locations from which samples were collected for the petrographic study of the Guadalquivir Basin Miocene sediments. Two main areas were collected from; the Baena-Montilla are on the southern margin and the northern margin fan delta deposits.



Figure 4.4 Variation of petrographic parameters.

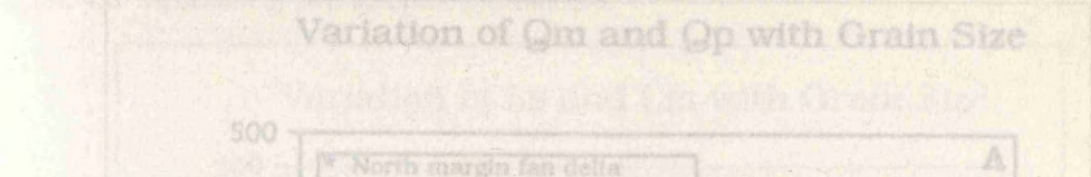


Figure 4.3 Obtaining a representative sample of the grain size poulation.

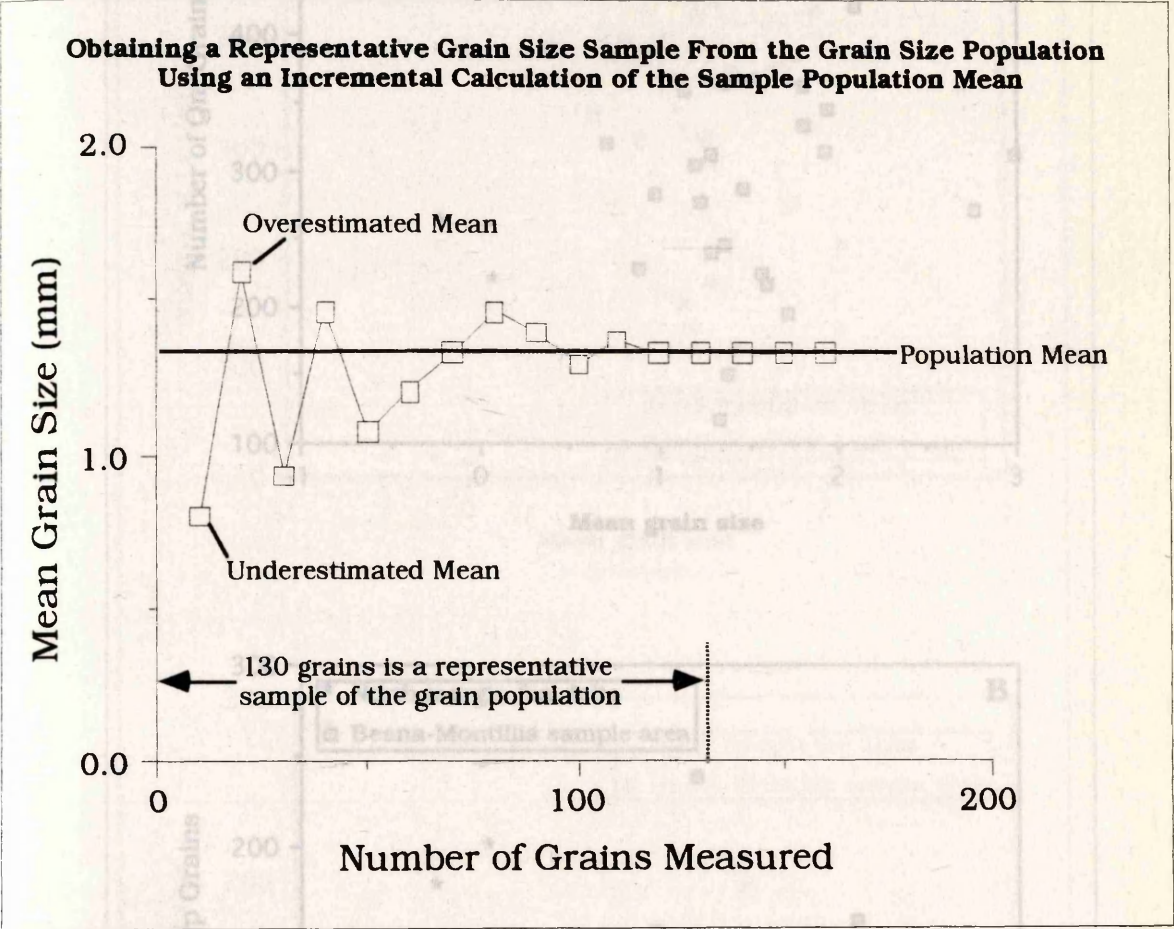


Figure 4.3 An example of the graph used to obtain a representative sample of the grain size population for a given sample using the following method; (1) The longest axis of an arbitrary number of grains is measured (e.g. 10 grains) and their mean size is plotted against the number of grains counted; (2) Step 1 is repeated and the mean for the new number of grains is plotted (10+10, the mean of 20 grains); (3) Steps are repeated and data plotted until the resultant graph produces a consistent mean (Fig. 4.3). Once the mean becomes consistent the population mean has been obtained and a representative sample of the population has been measured.

Figure 4.4 Graphical representations of petrographic parameters measured from the Guadalquivir Basin samples: A) Variation of mono-crystalline quartz (Qm) with mean grain size; B) Variation of poly-crystalline quartz (Qp) with mean grain size.



Figure 4.4 Variation of petrographic parameters.

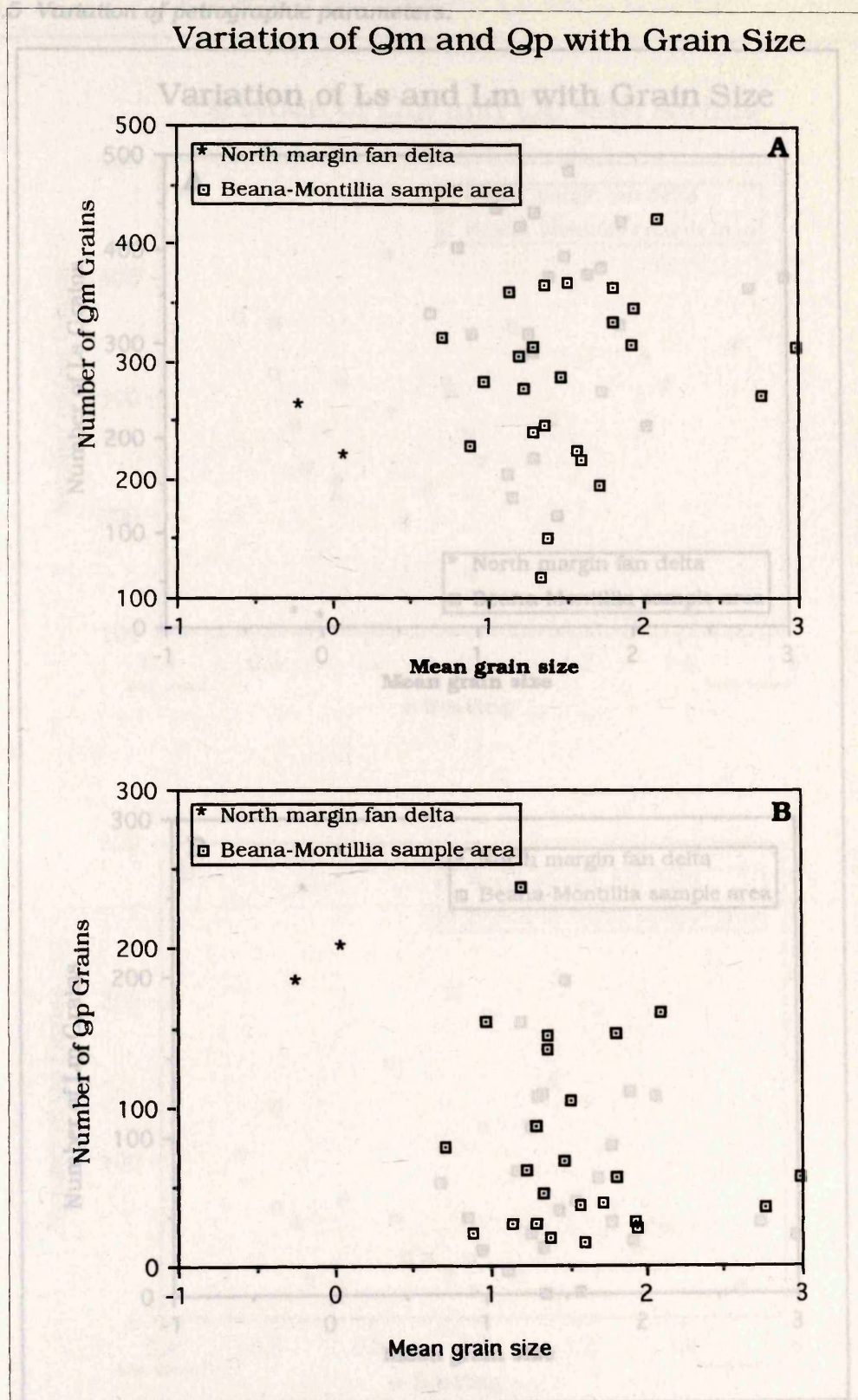


Figure 4.4 Graphical representations of petrographic parameters measured from the Guadalquivir Basin samples; A) Variation of mono-crystalline quartz (Qm) with mean grain size, B) Variation of poly-crystalline quartz (Qp) with mean grain size.



Figure 4.5 Variation of petrographic parameters.

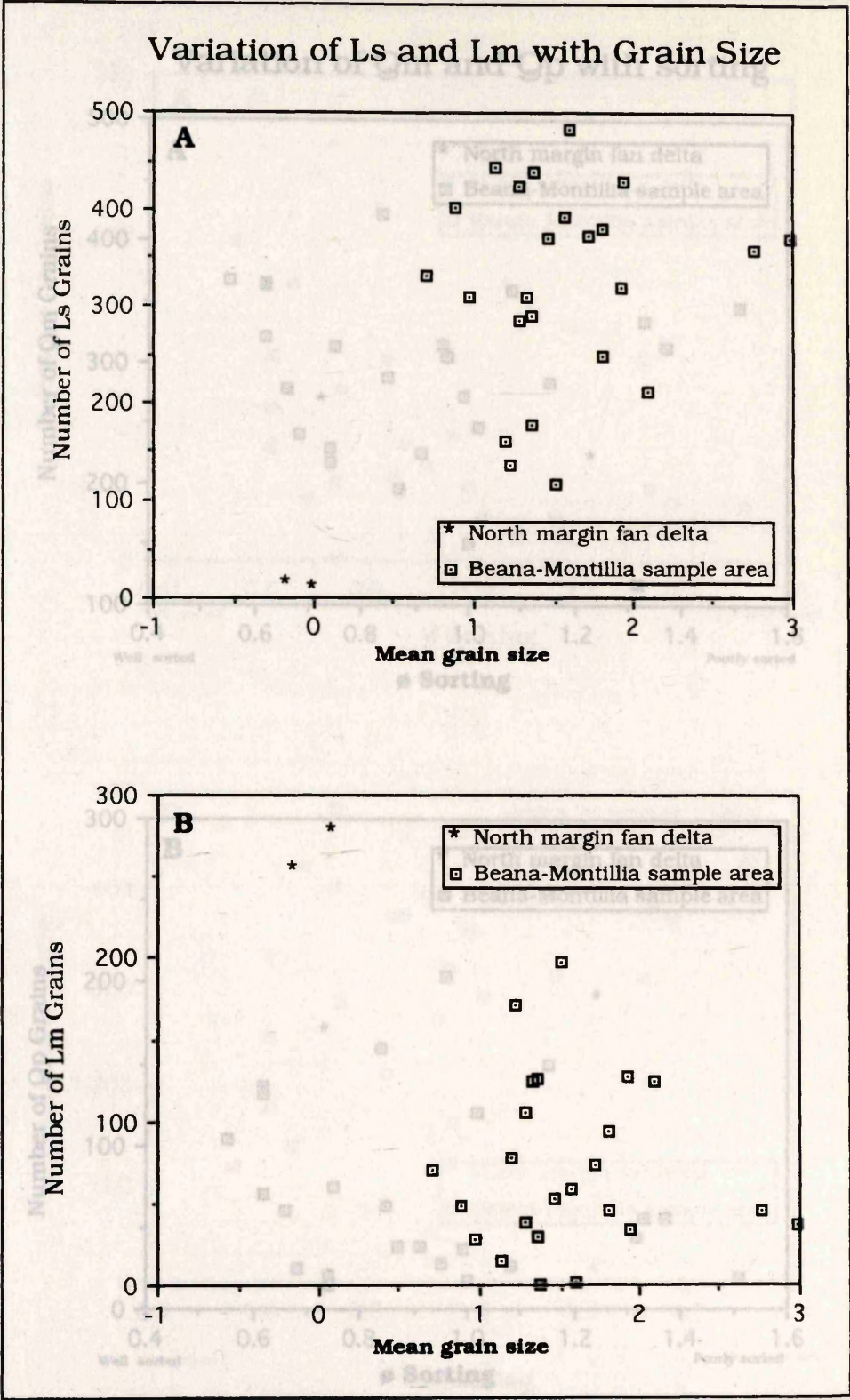


Figure 4.5 Graphical representations of petrographic parameters measured from the Guadalquivir Basin samples; A) Variation of sedimentary lithics (Ls) with mean grain size, B) Variation of metamorphic lithics (Lm) with mean grain size.



Figure 4.7 Variation of petrographic parameters.

Figure 4.6 Variation of petrographic parameters.

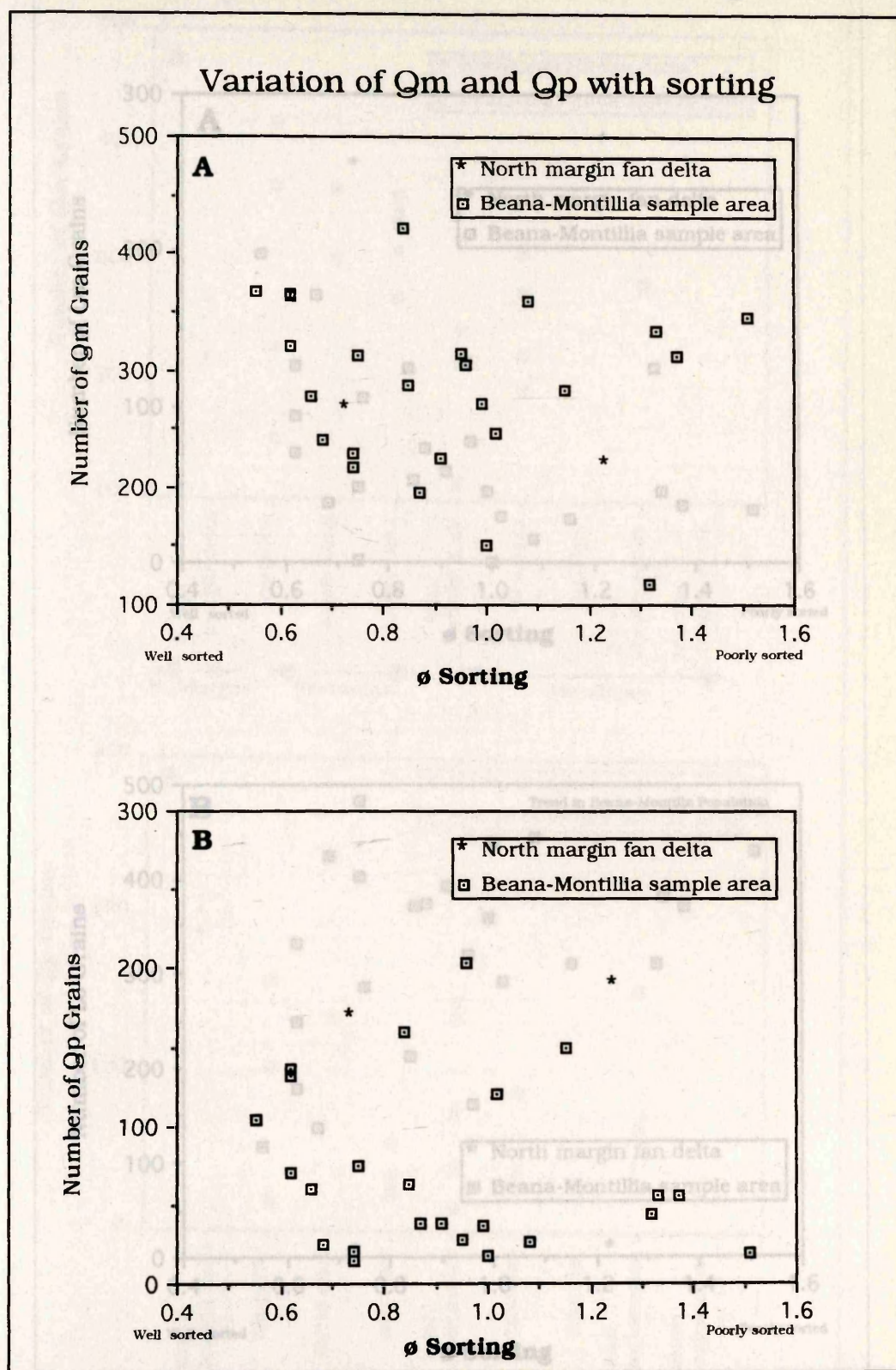


Figure 4.6 Graphical representations of petrographic parameters measured from the Guadalquivir Basin samples; A) Variation of mono-crystalline quartz (Qm) with sorting, B) Variation of poly-crystalline quartz (Qp) with sorting.



Figure 4.7 Variation of petrographic parameters.

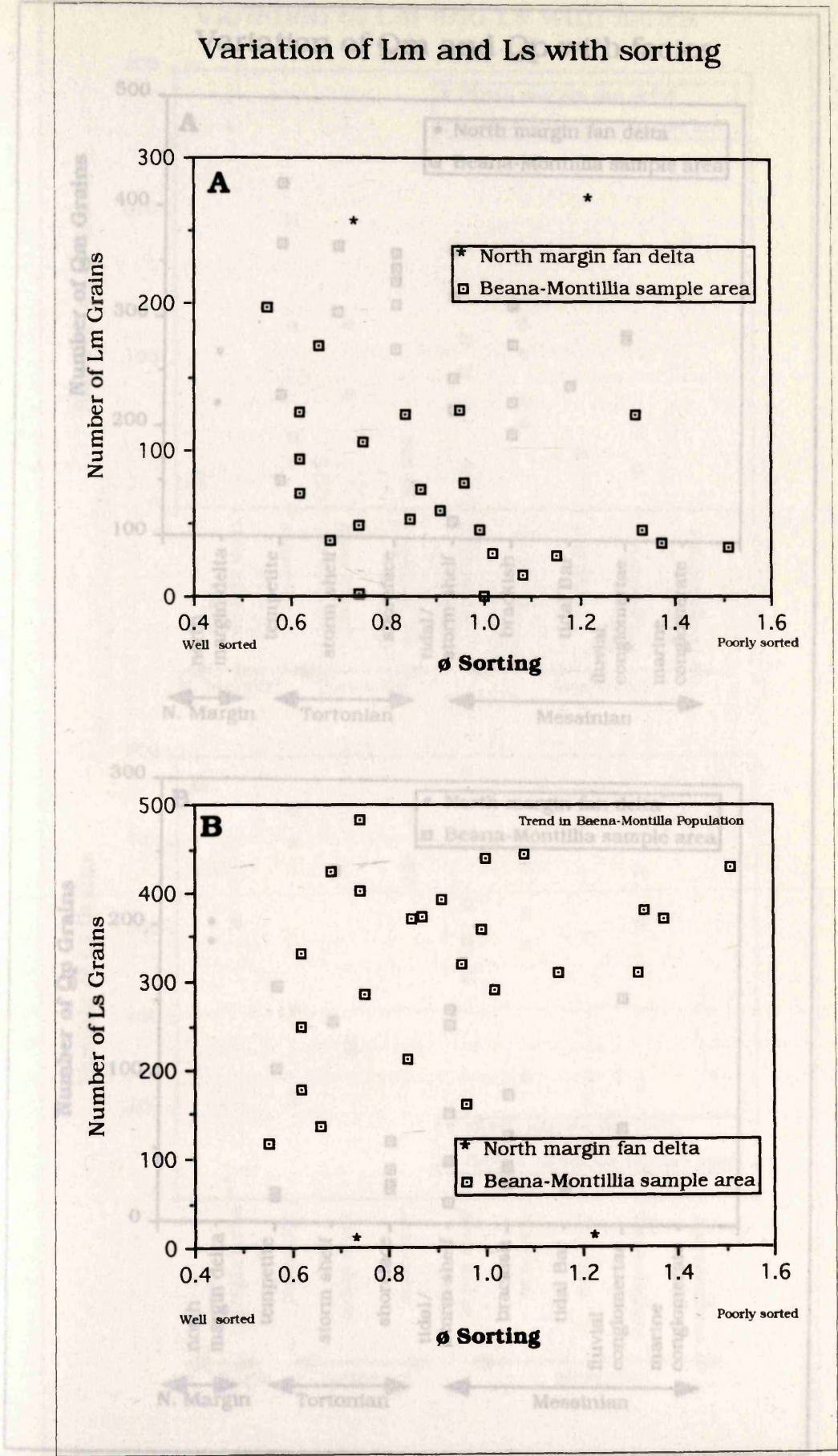


Figure 4.7 Graphical representations of petrographic parameters measured from the Guadalquivir Basin samples; A) Variation of sedimentary lithics (Lm) with sorting. B) Variation of metamorphic lithics (Ls) with sorting.



Figure 4.8 Variation of petrographic parameters.

Figure 4.8 Variation of petrographic parameters.

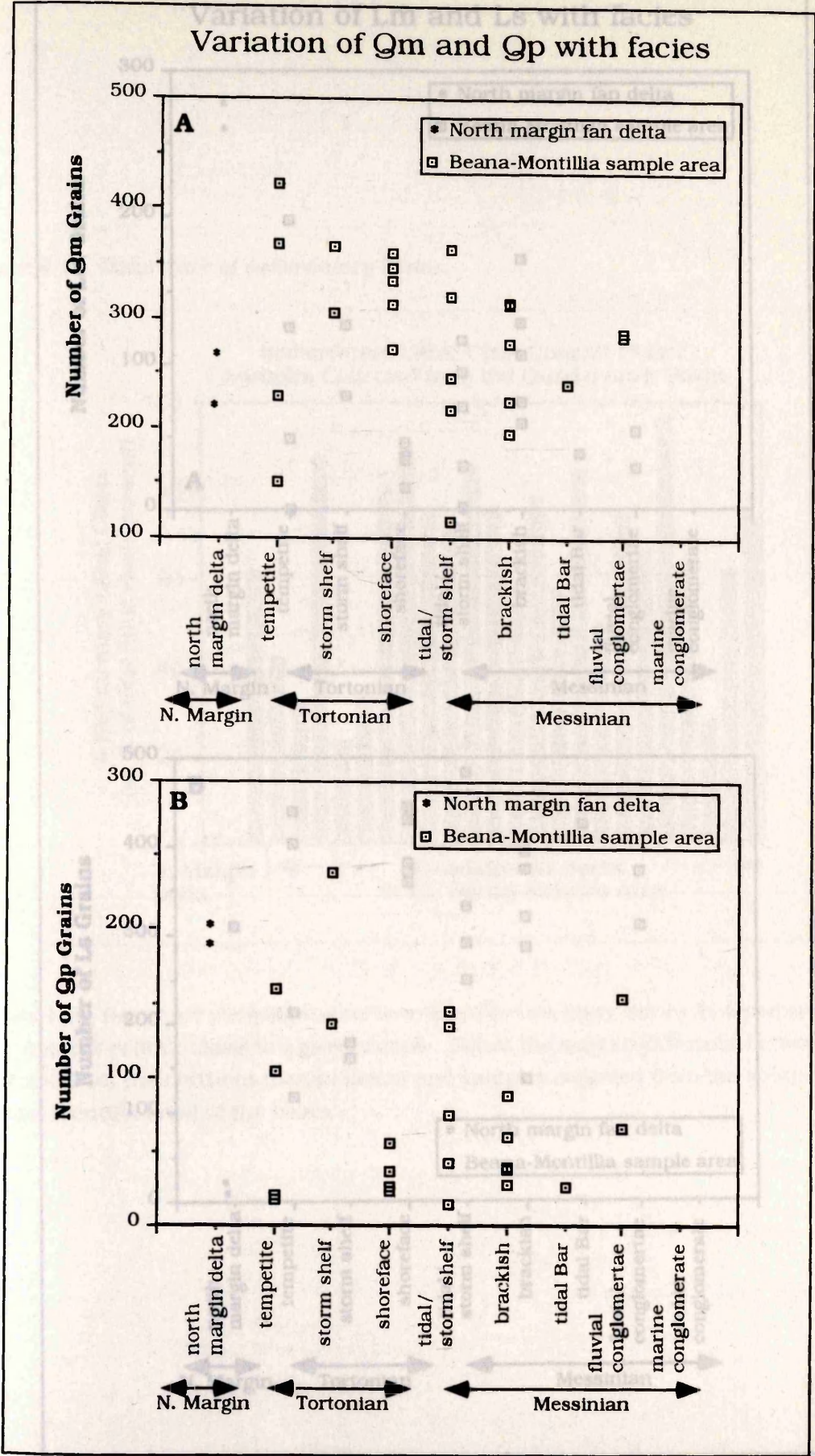


Figure 4.8 Graphical representations of petrographic parameters measured from the Guadalquivir Basin samples; A) Variation of mono-crystalline quartz (Qm) with facies type, B) Variation of poly-crystalline quartz (Qp) with facies type.



Figure 4.9 Variation of petrographic parameters.

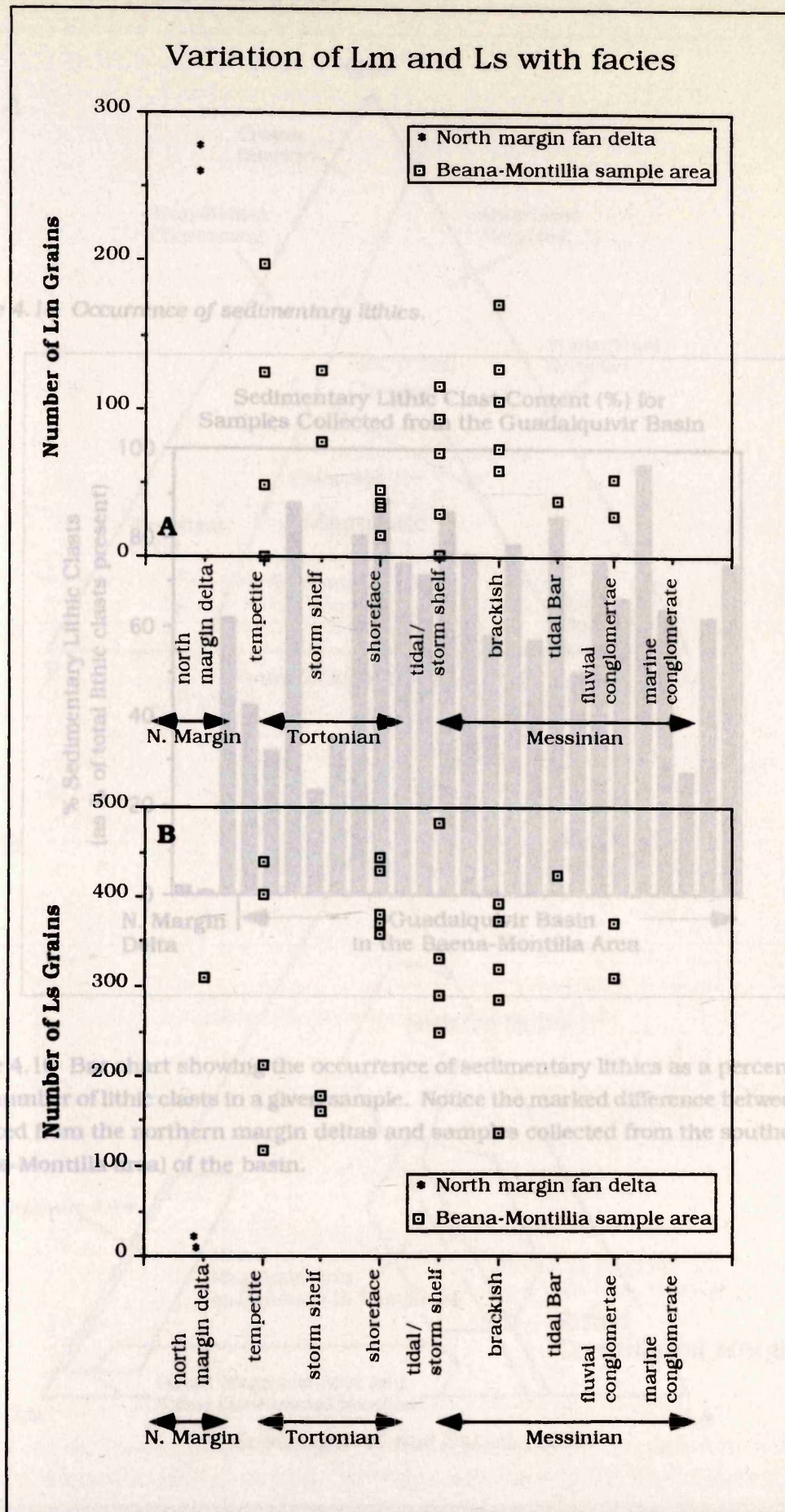


Figure 4.9 Graphical representations of petrographic parameters measured from the Guadalquivir Basin samples; A) Variation of sedimentary lithics (Ls) with facies type, B) Variation of metamorphic lithics (Lm) with facies type.



Figure 4.11 Petrographic ternary plots.

Figure 4.10 Occurrence of sedimentary lithics.

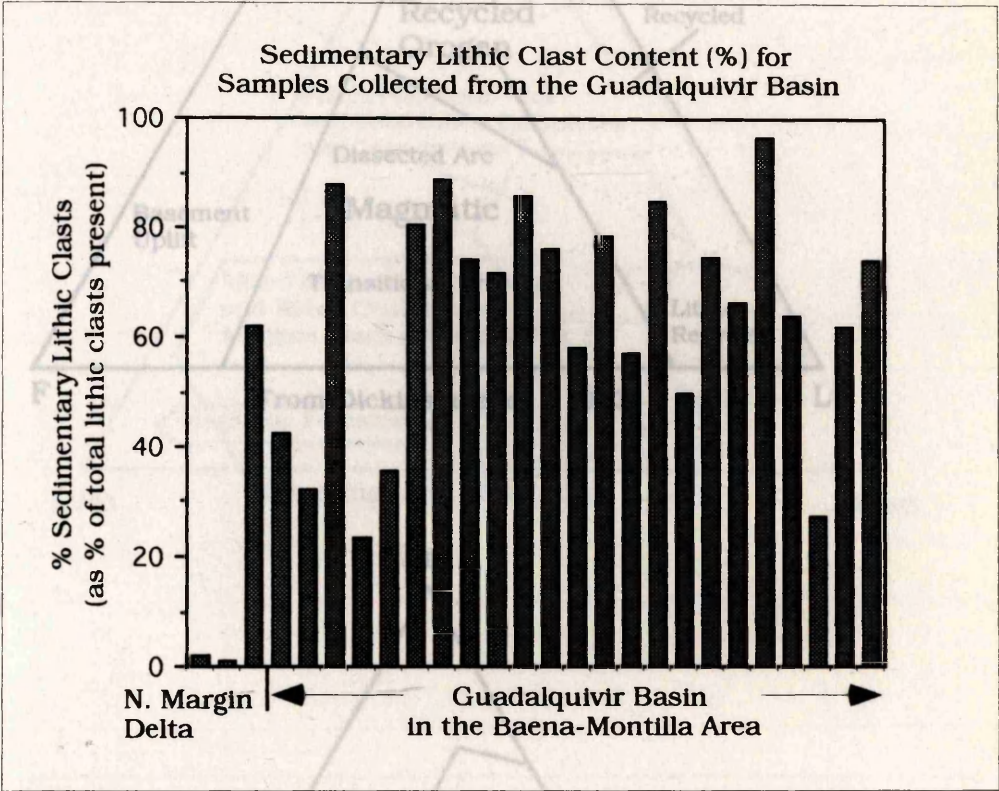


Figure 4.10 Bar chart showing the occurrence of sedimentary lithics as a percentage of the total number of lithic clasts in a given sample. Notice the marked difference between samples collected from the northern margin deltas and samples collected from the southern margin (Baena-Montilla area) of the basin.

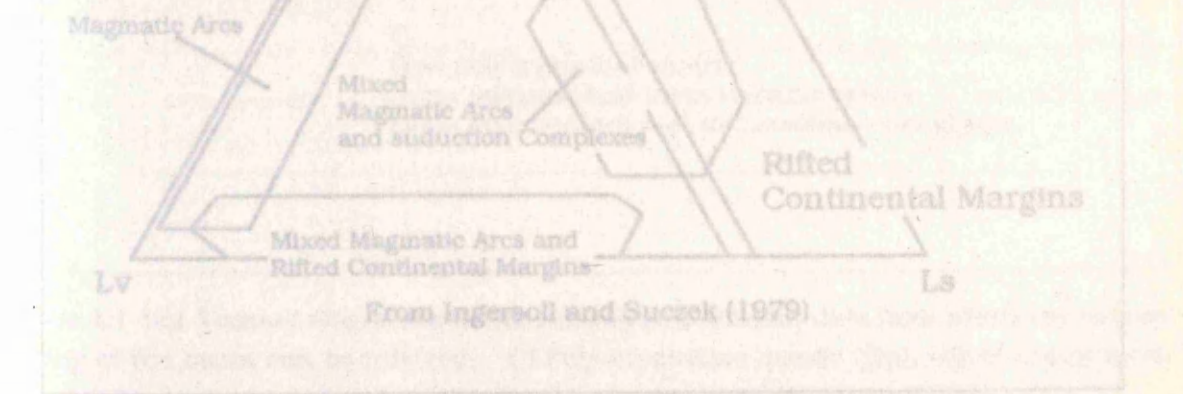


Figure 4.11 Ternary diagrams used for plotting petrographic data from which the tectonic setting of the basin can be inferred. A) Mono-crystalline quartz (Qm), feldspar (F) and lithic fragments (Lt). B) Metamorphic lithics (Lm), volcanic lithics (Lv) and sedimentary lithics (Ls).



Figure 4.11 Petrographic ternary plots.

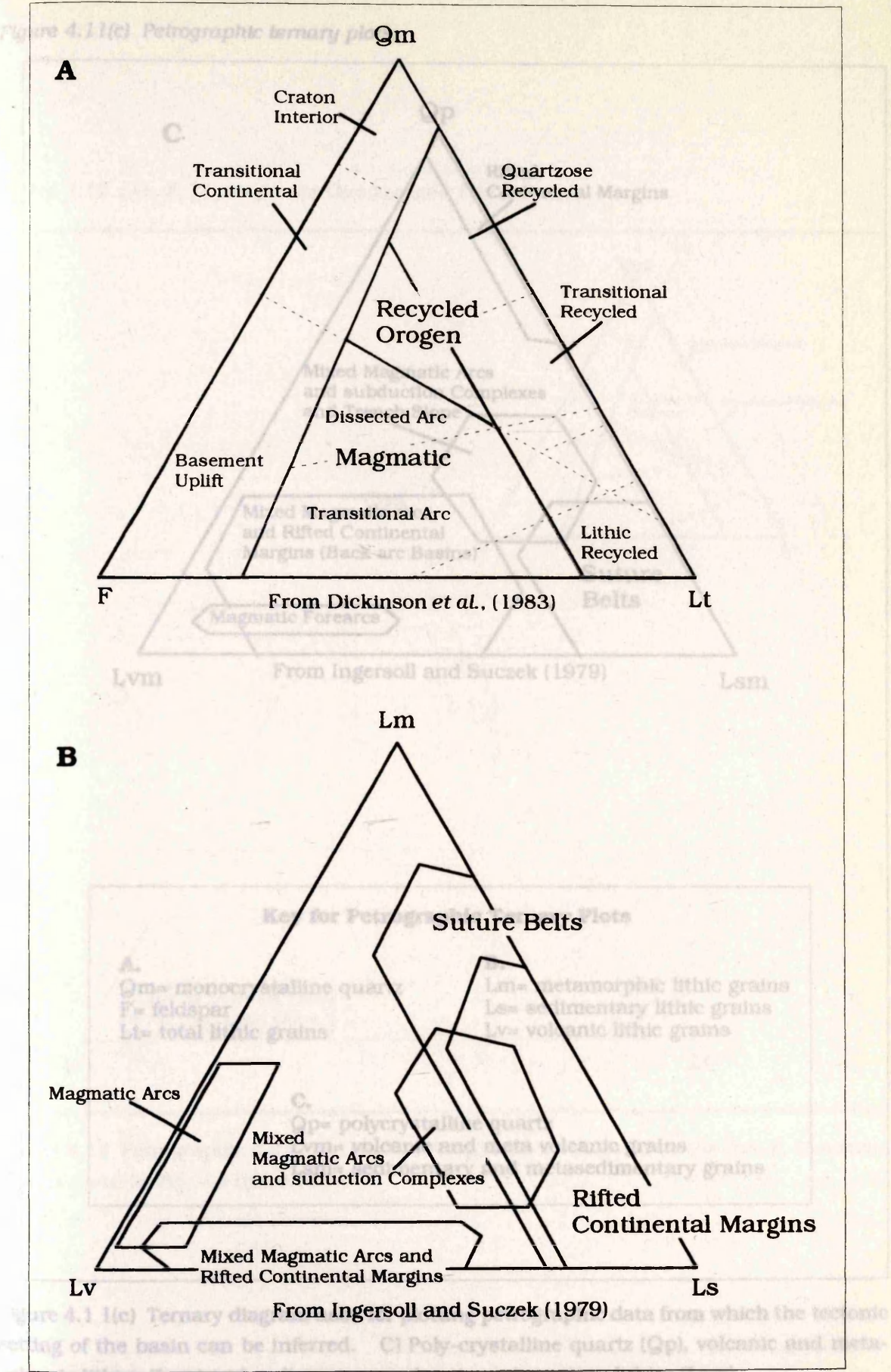
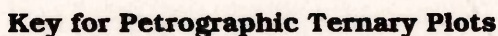


Figure 4.11 Ternary diagrams used for plotting petrographic data from which the tectonic setting of the basin can be inferred. A) Mono-crystalline quartz (Qm), feldspar (F) and lithic fragments (Lt). B) Metamorphic lithics (Lm), volcanic lithics (Lv) and sedimentary lithics (Ls).



Figure 4.12 Qm, F, Lt plot for the Guadalquivir



Lt= total lithic grains

Lv= volcanic lithic grains

Lsm= sedimentary and metasedimentary grains

### Part I The Guadalquivir Basin: Figures

Figure 4.13 Qp, Lvm, Lsm plot for the Guadalquivir Basin.

Figure 4.12 Qm, F, Lt plot for the Guadalquivir Basin.

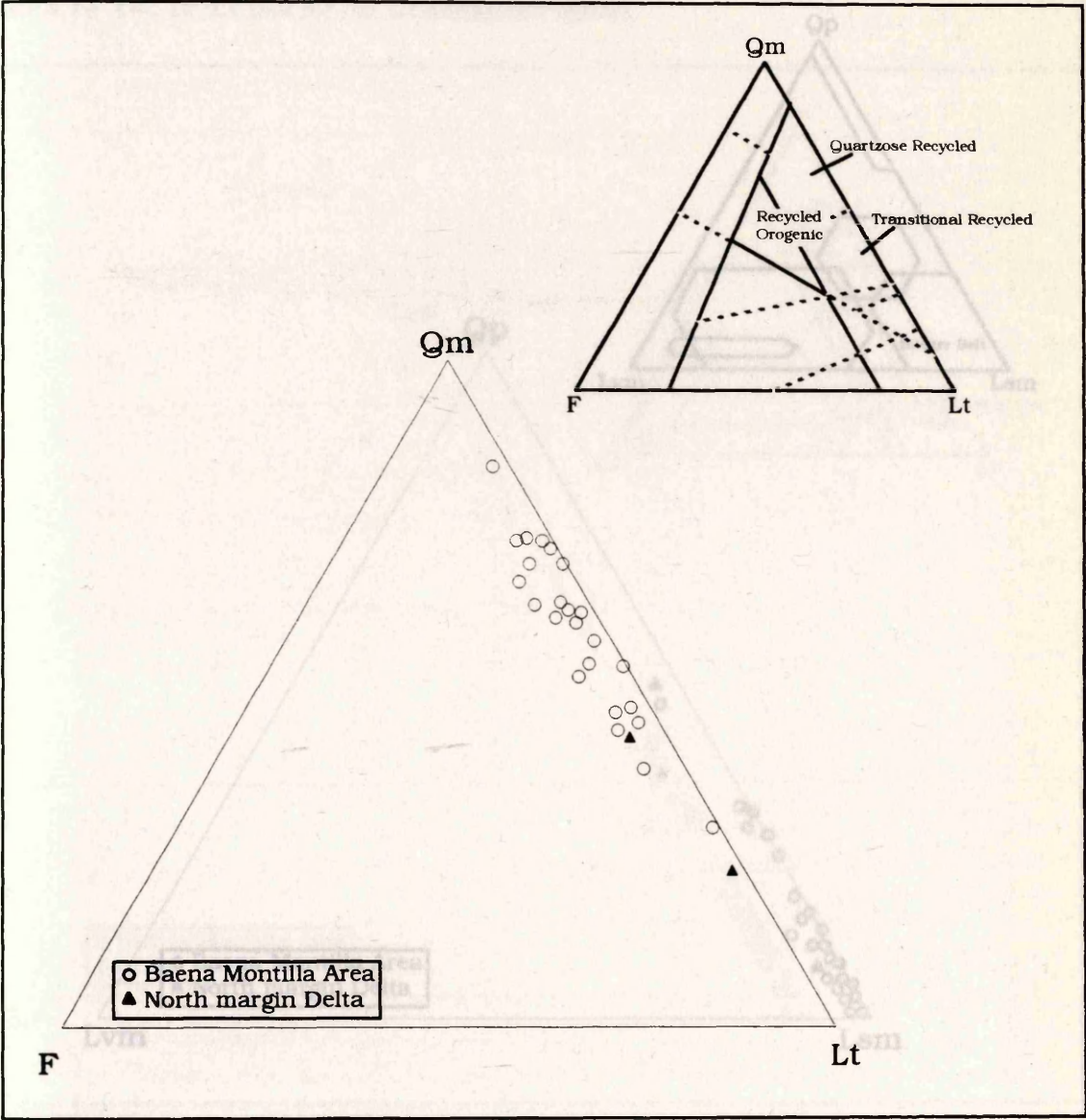


Figure 4.12 Petrographic data from the Guadalquivir Basin plotted on the Qm, F, Lt ternary plot as given in Fig. 4.11(a).



Figure 4.13 Qp, Lvm, Lsm plot for the Guadalquivir Basin.

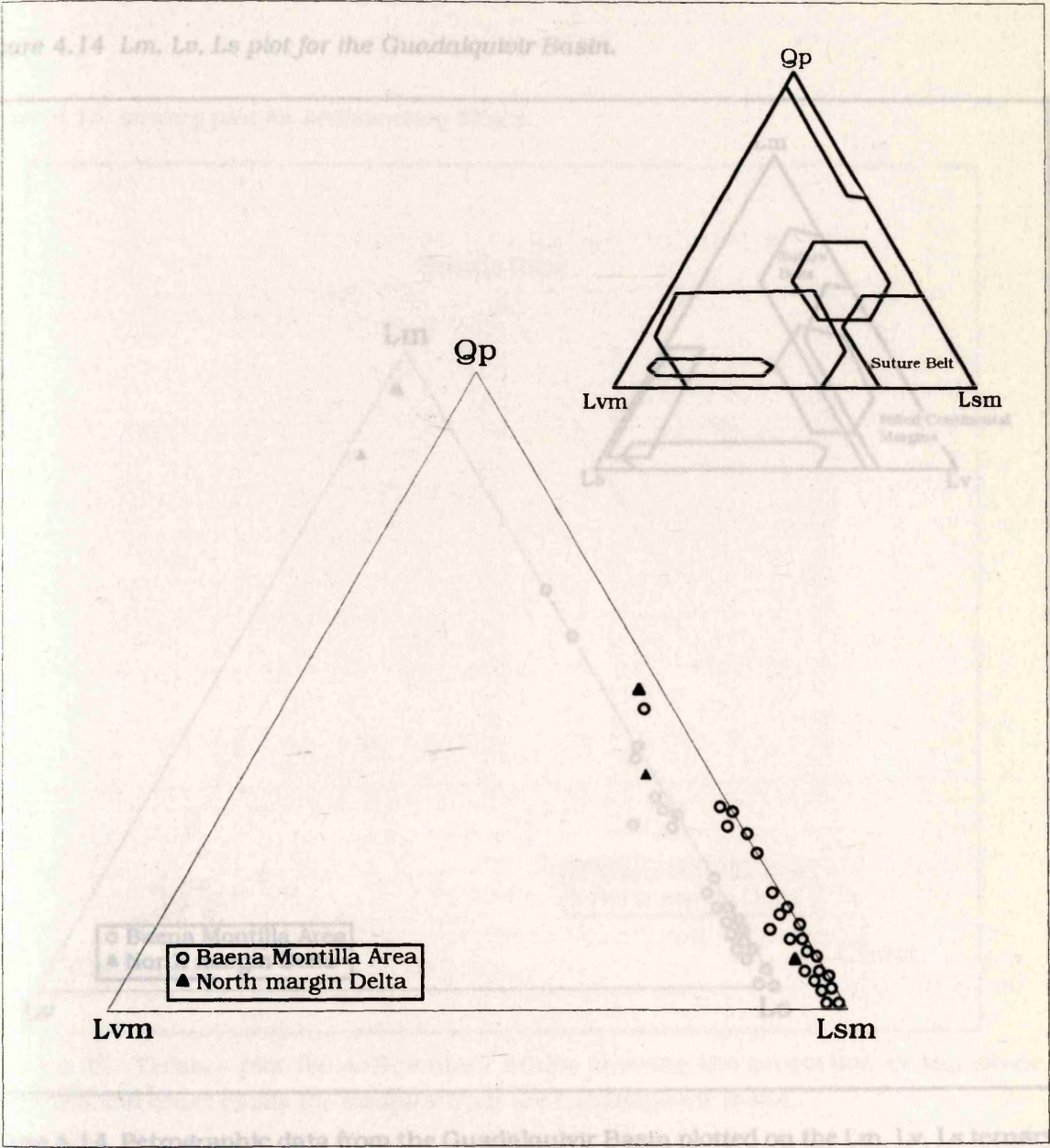


Figure 4.13 Petrographic data from the Guadalquivir Basin plotted on the Qp, Lvm, Lsm ternary plot as given in Fig. 4.11(c).

Figure 4.14 Lm, Lv, Ls plot for the Guadalquivir Basin.

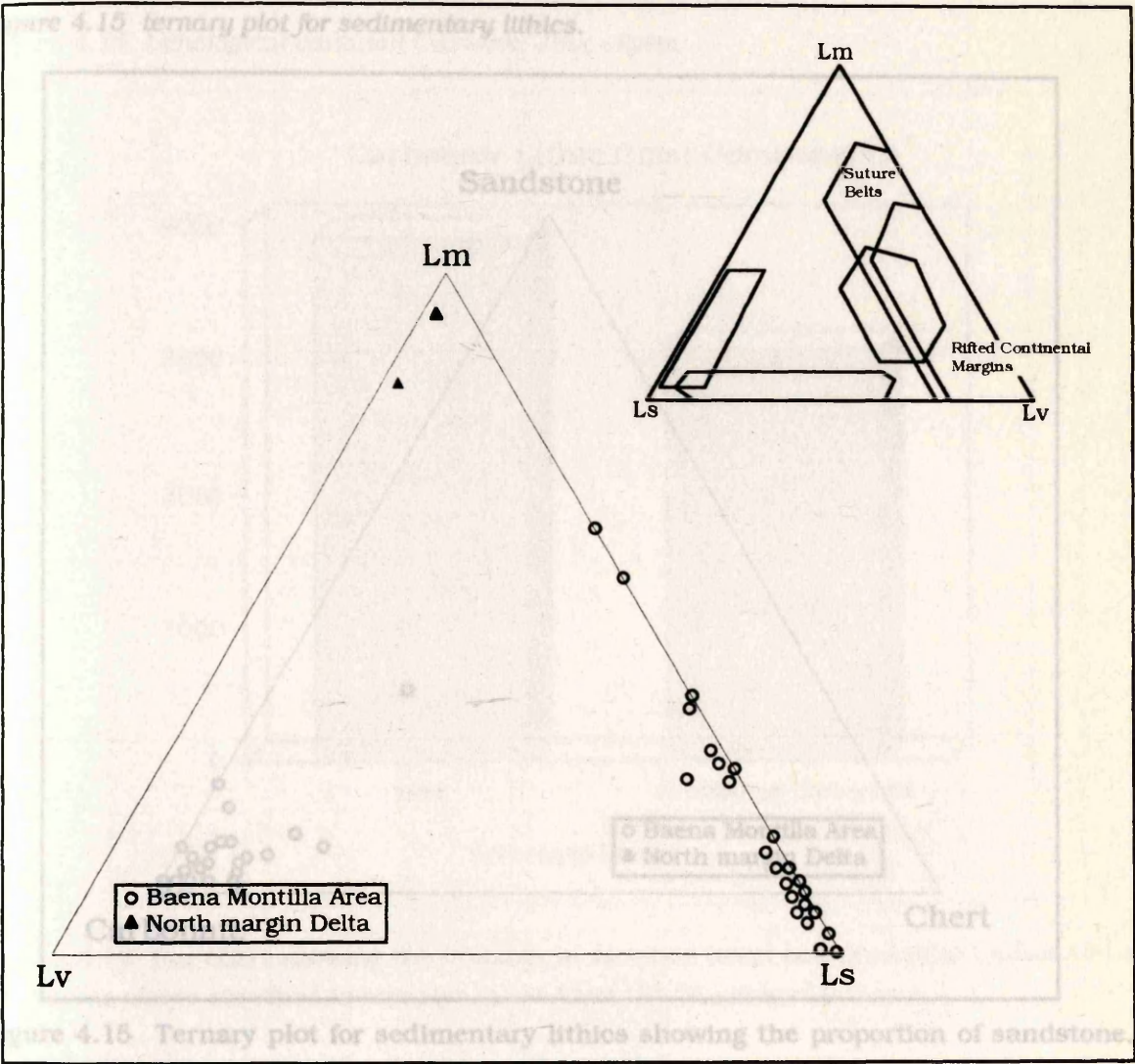


Figure 4.14 Petrographic data from the Guadalquivir Basin plotted on the Lm, Lv, Ls ternary plot as given in Fig. 4.11(b).



Figure 4.15 ternary plot for sedimentary lithics.

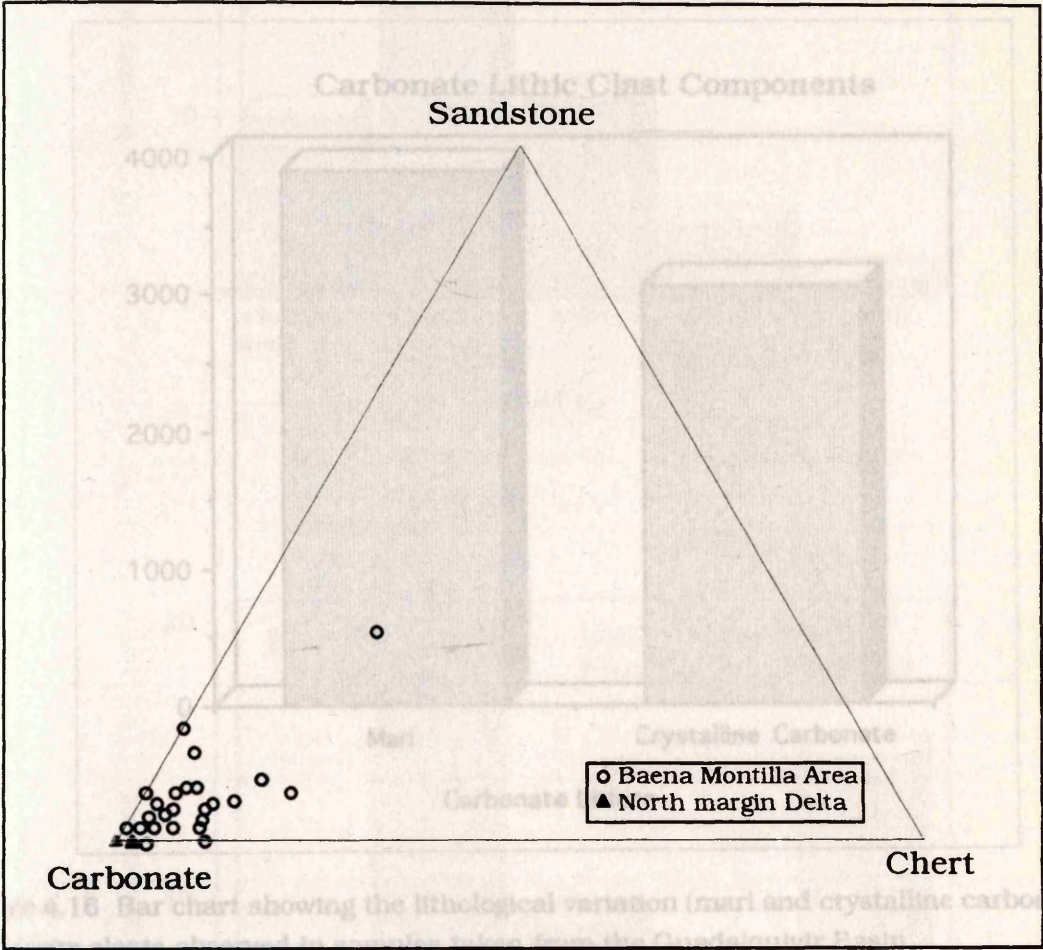


Figure 4.15 Ternary plot for sedimentary lithics showing the proportion of sandstone, carbonate and chert clasts for samples from the Guadalquivir Basin.



Figure 4.17 Composition of clasts found in Messinian deposits.

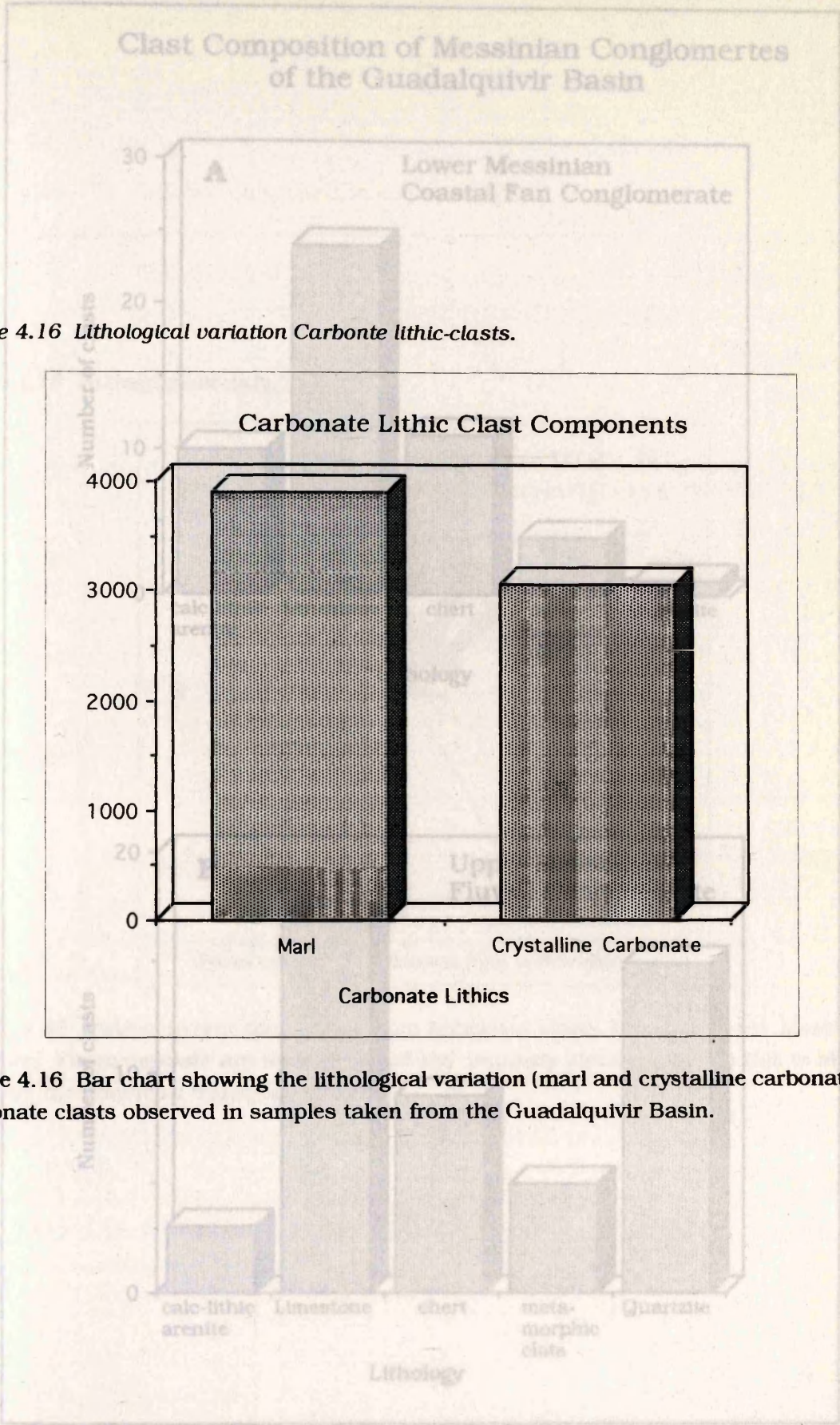


Figure 4.16 Lithological variation Carbonte lithic-clasts.

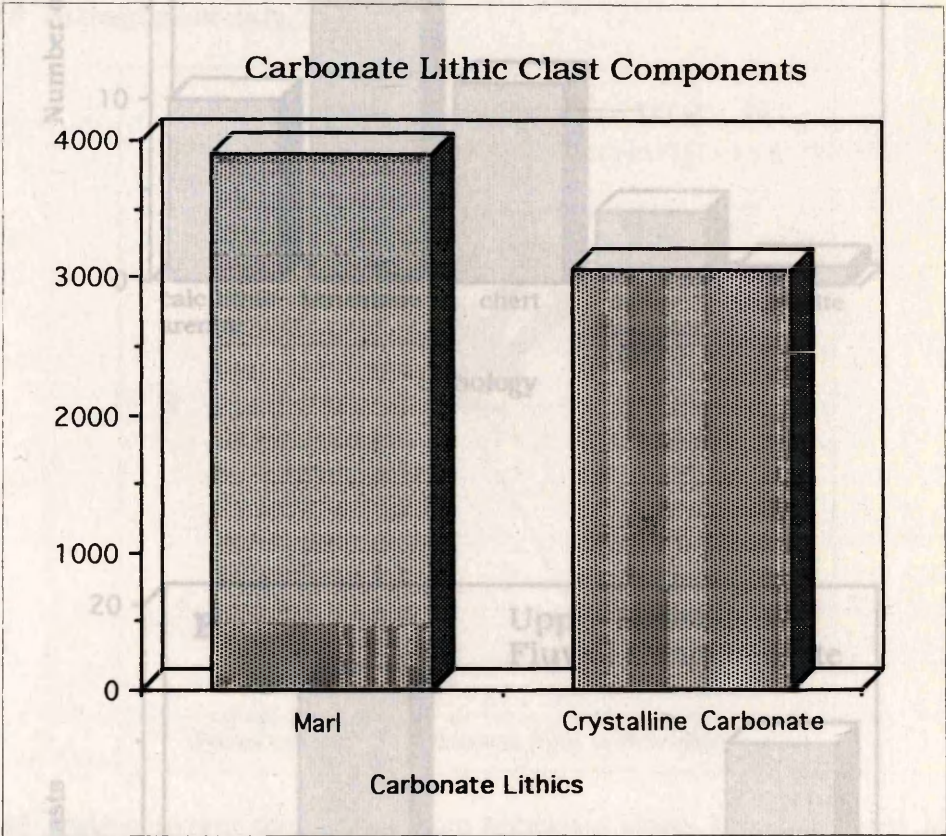


Figure 4.16 Bar chart showing the lithological variation (marl and crystalline carbonate) of carbonate clasts observed in samples taken from the Guadalquivir Basin.



Figure 4.17 Composition of clasts found in Messinian deposits.

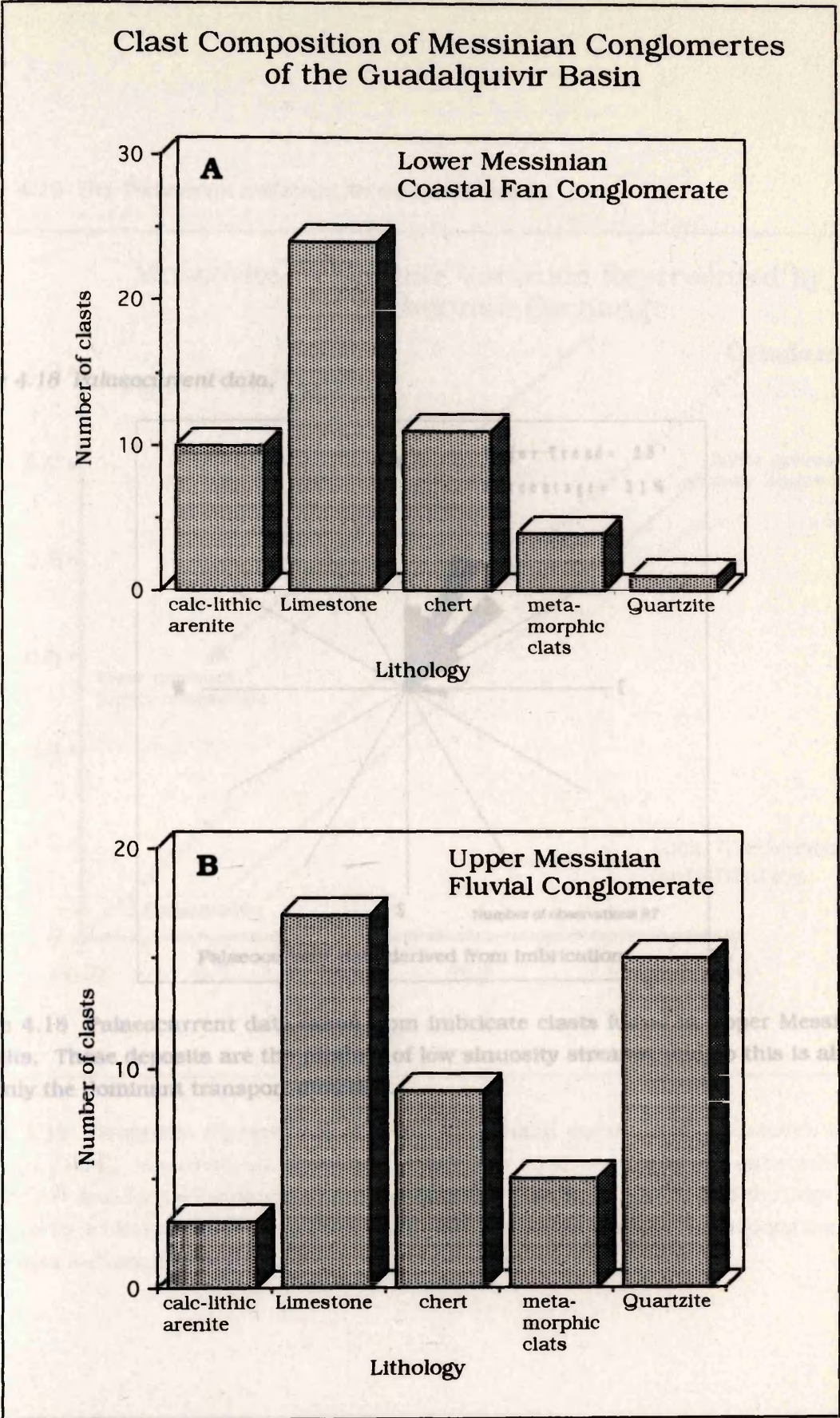


Figure 4.17 Lithological composition of clasts found in Messinian deposits of the Guadalquivir Basin. A) Clasts from lower Messinian fluvial deposits, B) Clasts from upper Messinian fluvial deposits. Full data set can be found in Appendix IV.



Figure 4.19 The Tschermak exchange for muscovite micas.

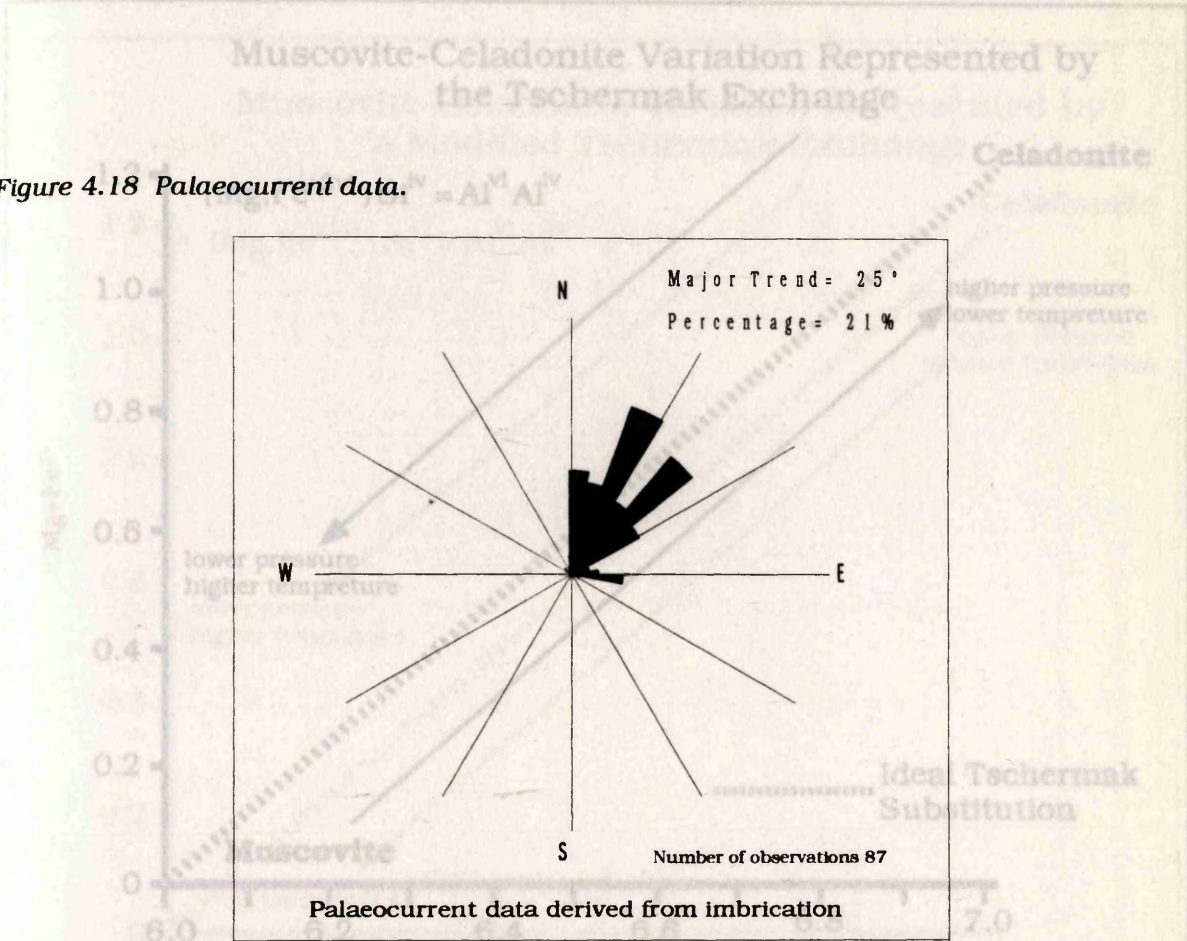


Figure 4.18 Palaeocurrent data taken from imbricate clasts found in upper Messinian deposits. These deposits are the product of low sinuosity streams, and so this is almost certainly the dominant transport direction.

Figure 4.19 Graphical representation of the Tschermak exchange for muscovite micas (Frost, 1984). Muscovite varies towards celadonite compositions by the substitution of  $Al^{IV}$  for  $Al^{VI}$  and by the Tschermak exchange  $(Mg, Fe^{2+}, Ti)Si^{IV} = Al^{VI} Al^{IV}$ . If all the  $(Mg, Fe^{2+}, Ti)$  in muscovite is charge-balanced by Si replacing  $Al^{IV}$ , the points should cluster along the ideal Tschermak substitution line.



Figure 4.19 The Tschermak exchange for muscovite micas.

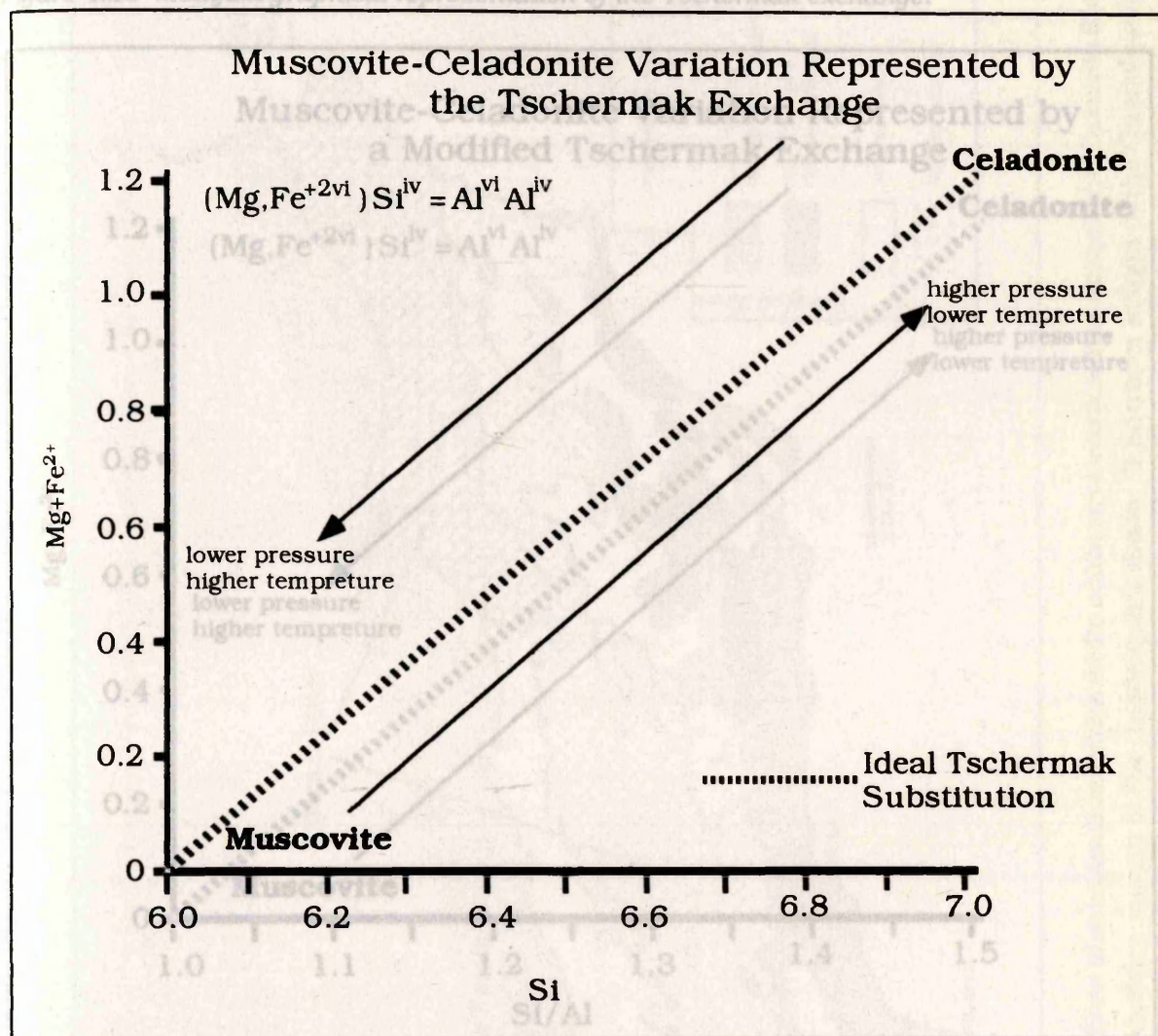


Figure 4.19 Graphical representation of the Tschermak exchange for muscovite micas (Guidotti, 1984). Muscovite varies towards celadonite compositions by the substitution of  $\text{Fe}^{3+}$  for  $\text{Al}^{\text{iv}}$  and by the Tschermak exchange  $(\text{Mg}, \text{Fe}^{2+})\text{Si}^{\text{iv}} = \text{Al}^{\text{vi}}, \text{Al}^{\text{iv}}$ . If all the  $(\text{Mg} + \text{Fe}^{2+})$  in muscovite is charge-balanced by Si replacing  $\text{Al}^{\text{iv}}$ , the points should cluster along the ideal Tschermak substitution line.



Figure 4.20 Modified graphical representation of the Tschermak exchange.

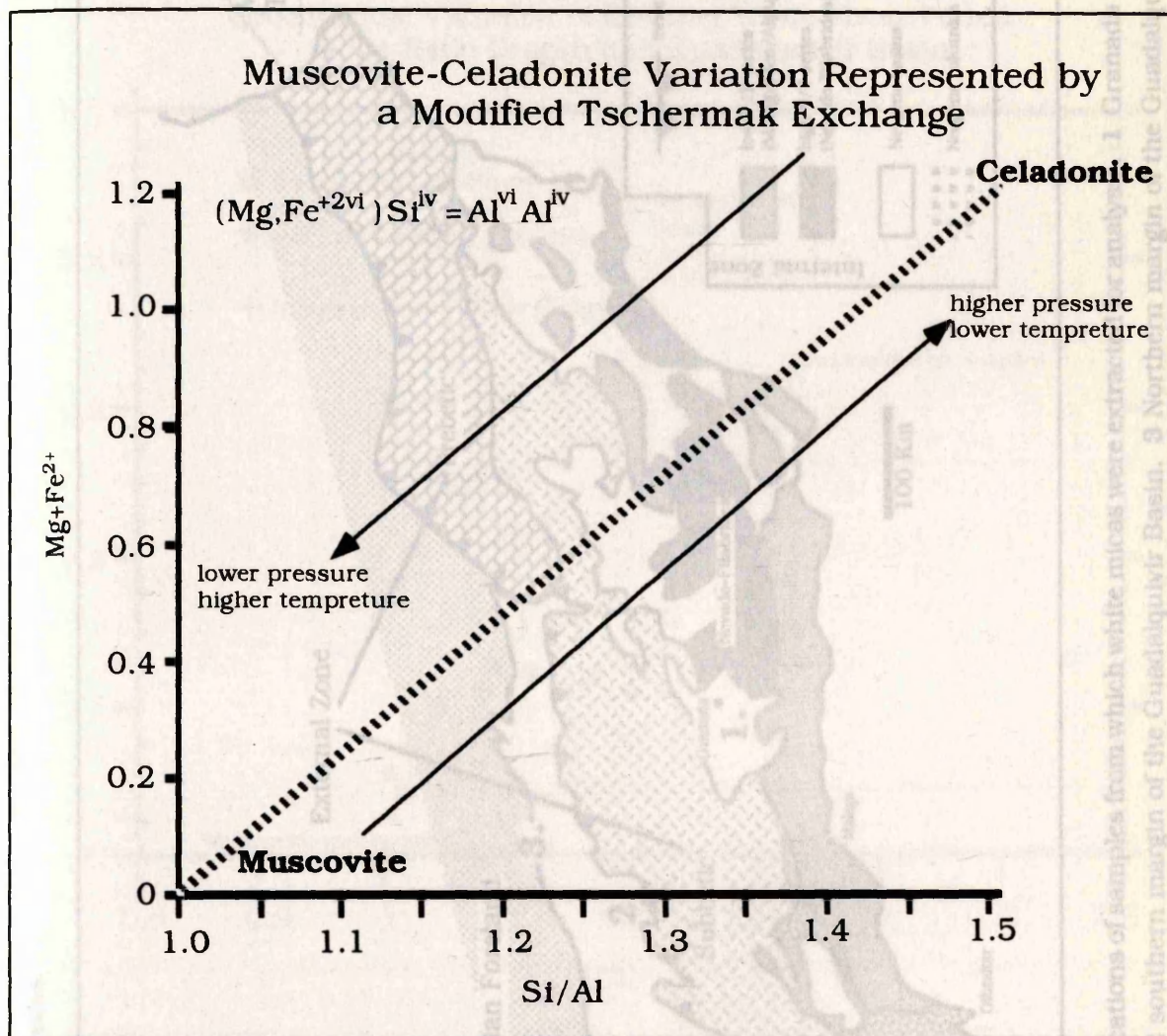


Figure 4.20 Graphical representation of the Tschermak exchange modified by plotting the Si/Al ratio in preference to Si on the X-axis. Since Si substitutes for  $\text{Al}^{\text{vi}}$  the Si/Al ratio should increase towards celadonite end member-compositions.



Figure 4.21 Sample locations for white micas.

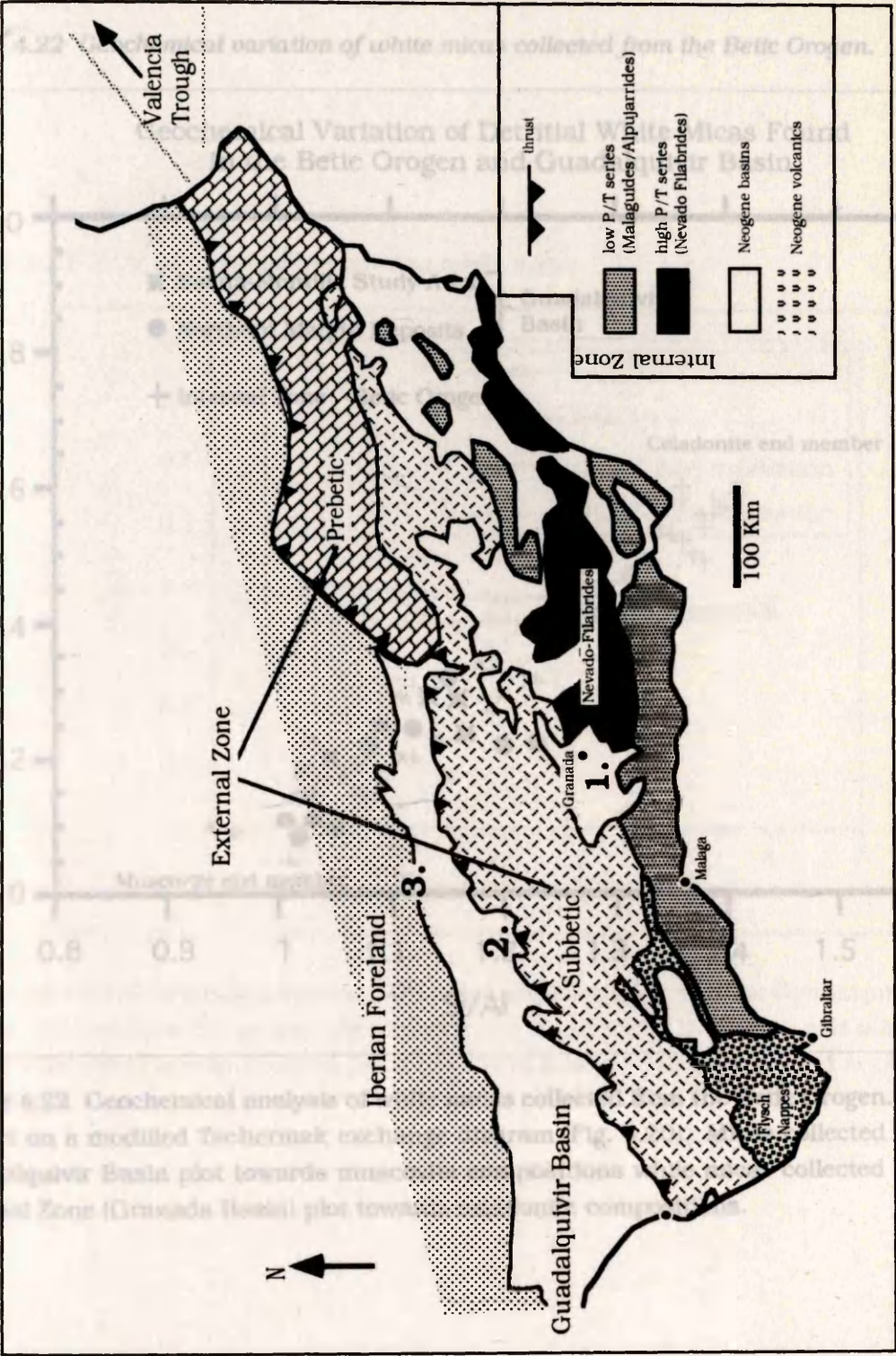


Figure 4.21 Map of the Betics showing locations of samples from which white micas were extracted for analysis. **1** Granada Basin, sediment sourced directly from the Betic Internal Zones. **2** southern margin of the Guadalquivir Basin. **3** Northern margin of the Guadalquivir Basin.



Figure 4.22 Geochemical variation of white micas collected from the Betic Orogen.

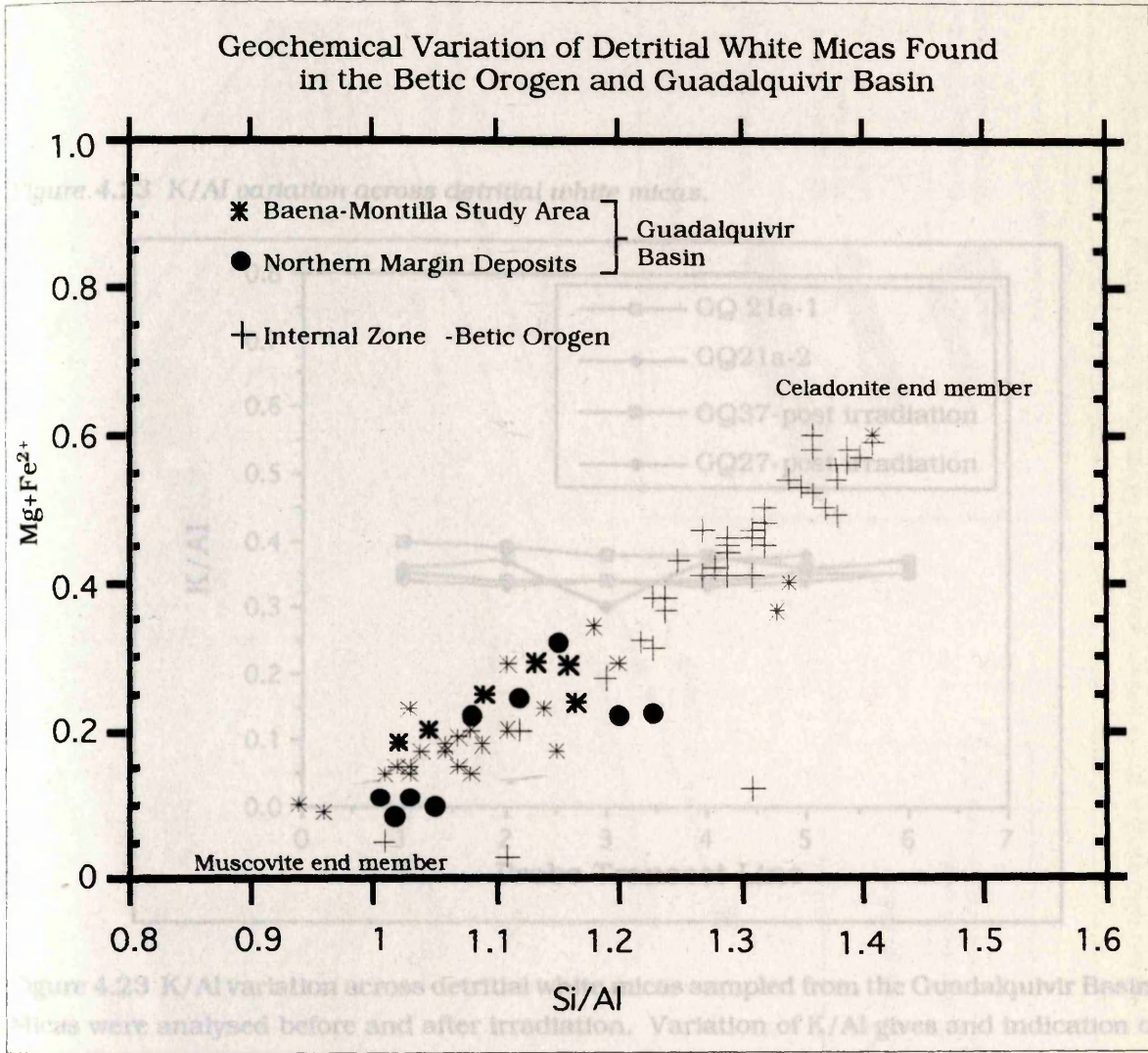


Figure 4.22 Geochemical analysis of white micas collected from the Betic Orogen. Results plotted on a modified Tschermak exchange diagram (Fig. 4.20). Micas collected from the Guadalquivir Basin plot towards muscovite compositions while micas collected from the Internal Zone (Granada Basin) plot towards celadonite compositions.



Figure 4.24 Provenance model.

Figure 4.23 K/Al variation across detrital white micas.

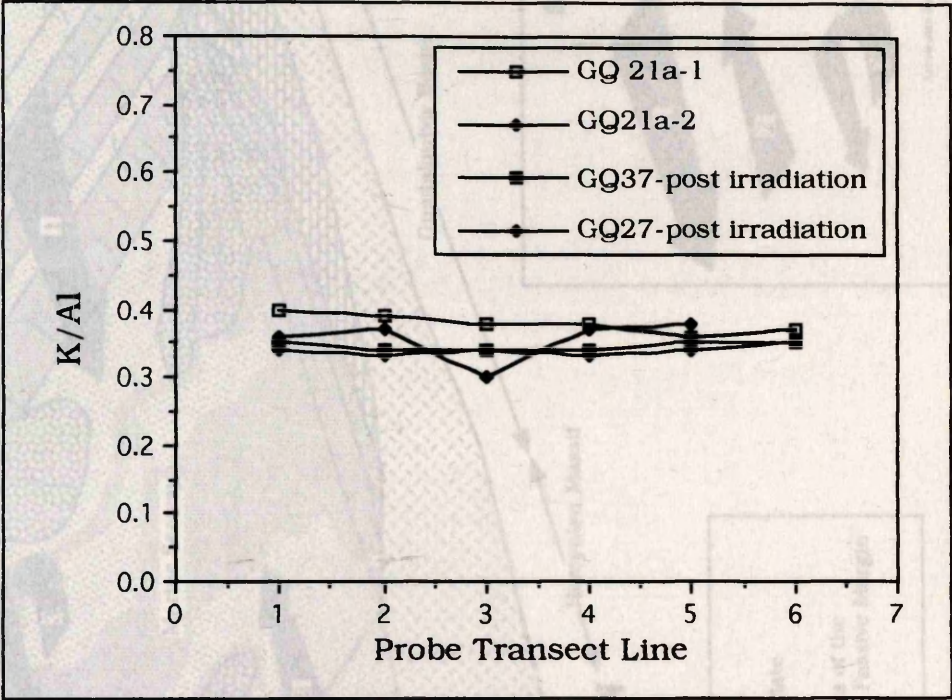


Figure 4.23 K/Al variation across detrital white micas sampled from the Guadalquivir Basin. Micas were analysed before and after irradiation. Variation of K/Al gives an indication of K loss from the grains from which the reliability of isotopic dating (K/Ar and Ar/Ar) can be assessed.



Figure 4.24 Provenance model.

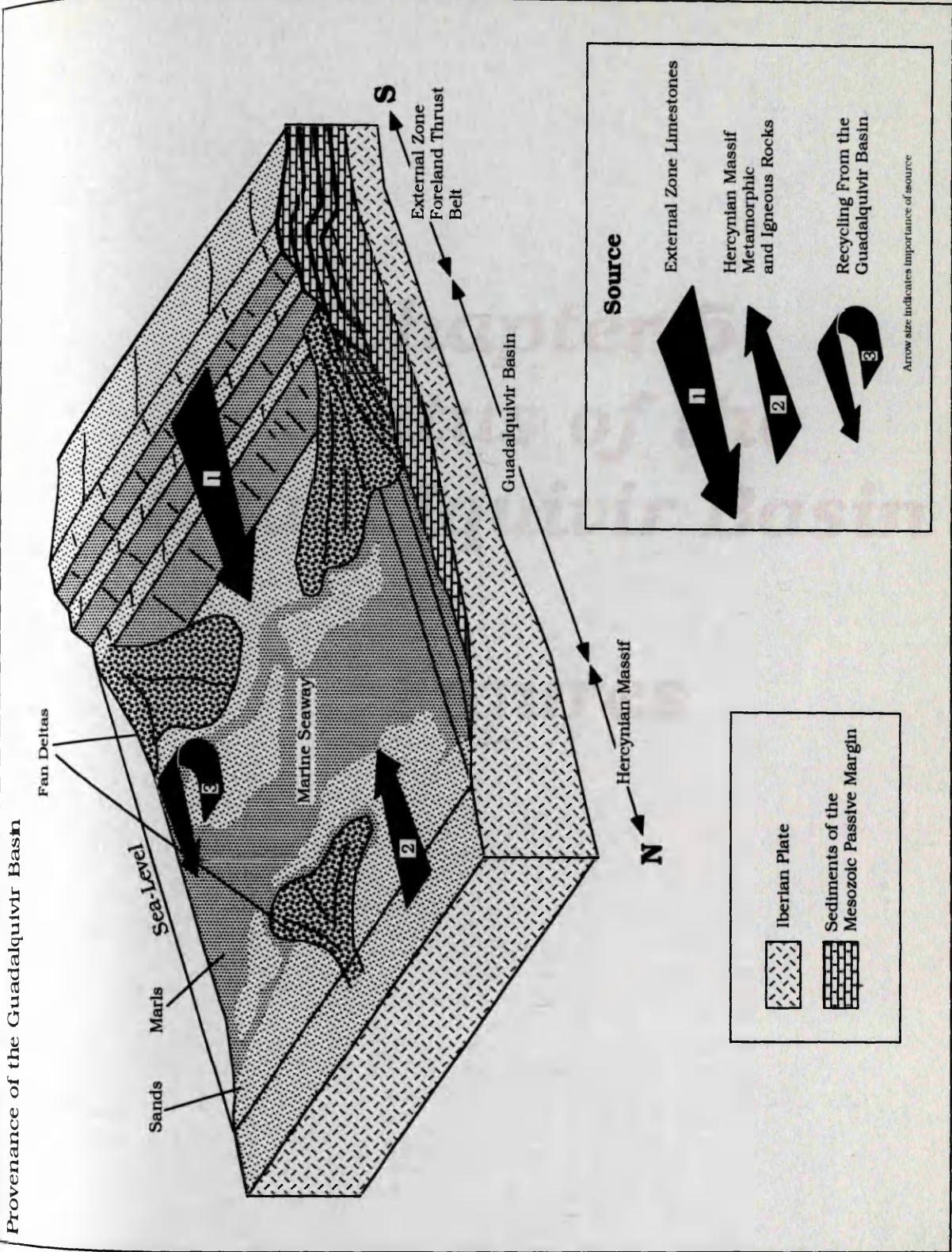


Figure 4.24 Schematic diagram showing a provenance model for Miocene sediments of the Guadalquivir Basin.



**Chapter 5**  
**Status of the**  
**Guadalquivir Basin**

**Figures**

Figure 5.2 Early 'flysch' stage of a foreland basin.

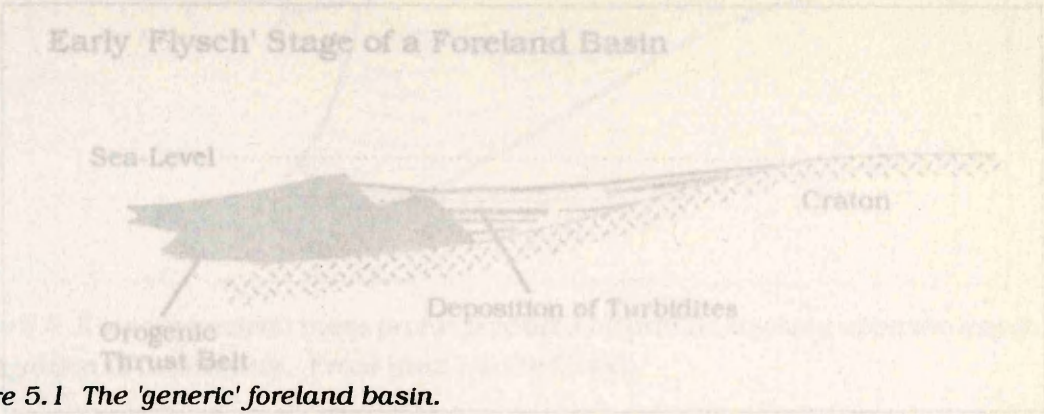


Figure 5.1 The 'generic' foreland basin.

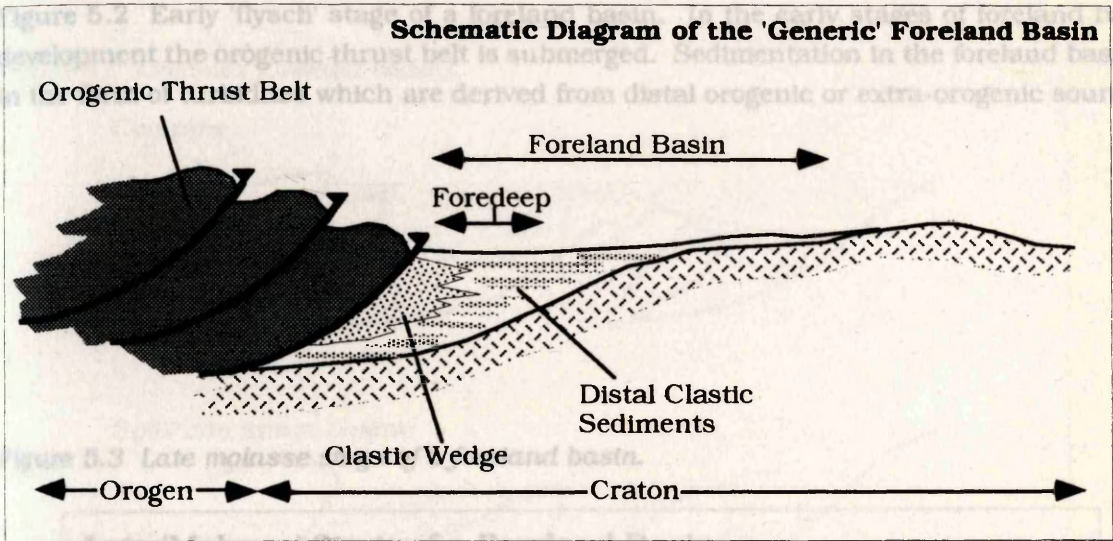


Figure 5.1 The 'generic' foreland basin can be defined as a basin that exists between an orogenic mountain belt and adjacent craton. The deepest part of a foreland basin is always adjacent to the orogenic wedge.

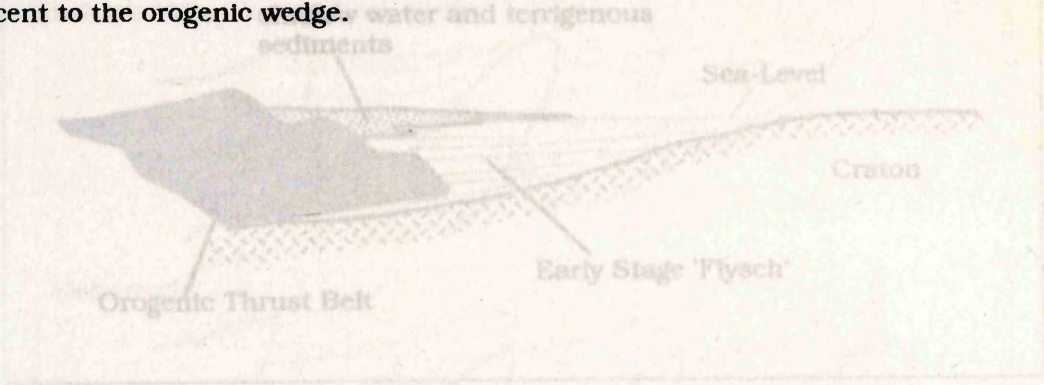


Figure 5.3 Late molasse stage of a foreland basin. Following the emergence of the orogenic thrust belt, shallow water and terrigenous sediments are deposited as a clastic wedge in the foreland basin. Detritus is sourced from the orogenic thrust belt.



Figure 5.4 A simple foreland basin profile.

Figure 5.2 Early 'flysch' stage of a foreland basin.

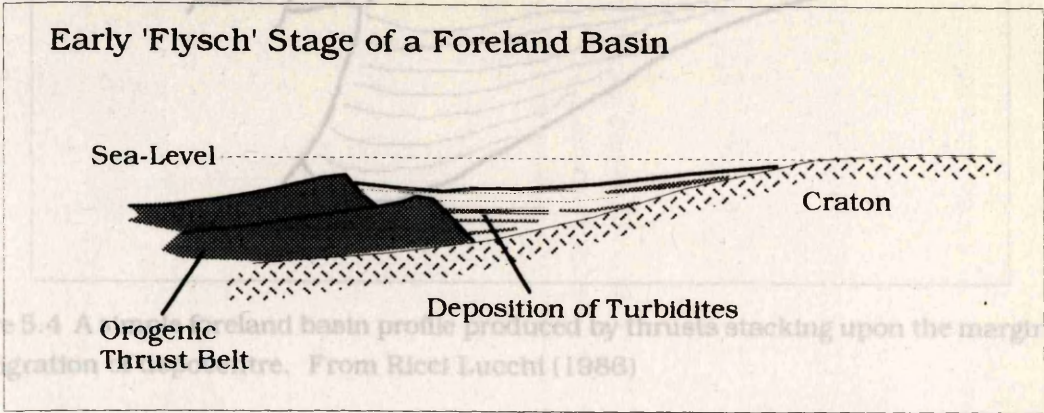


Figure 5.2 Early 'flysch' stage of a foreland basin. In the early stages of foreland basin development the orogenic thrust belt is submerged. Sedimentation in the foreland basin is in the form of turbidites which are derived from distal orogenic or extra-orogenic sources.

Figure 5.3 Late molasse stage of a foreland basin.

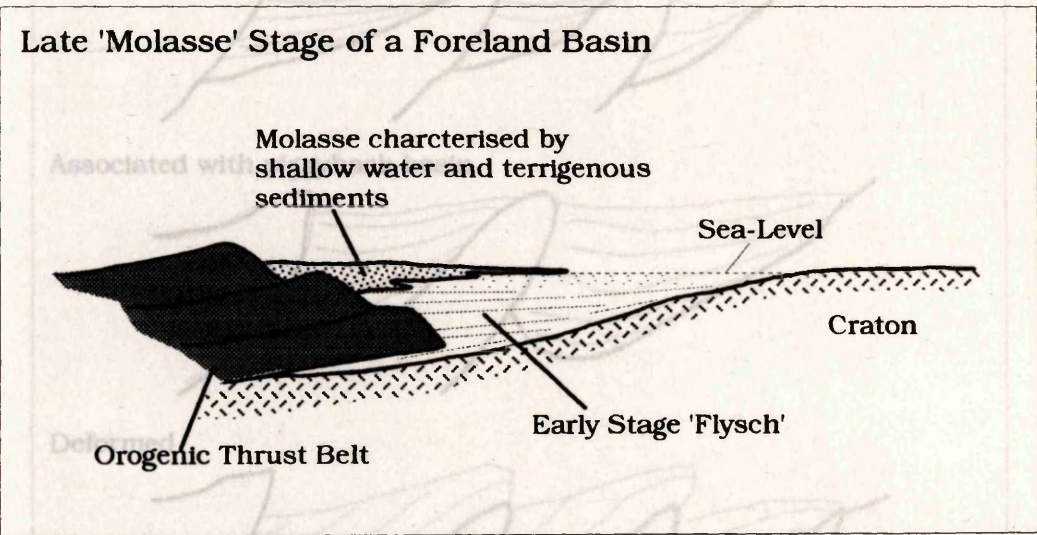


Figure 5.3 Late molasse stage of a foreland basin. Following the emergence of the orogenic thrust belt, shallow water and terrigenous sediments are deposited as a clastic wedge in the foreland basin. Detritus is sourced from the orogenic thrust belt

Figure 5.5 Complex foreland basins produced as the thrust front and depocentre migrate into the foreland basin. From Ricci Lucchi (1986)



Figure 5.4 A simple foreland basin profile.

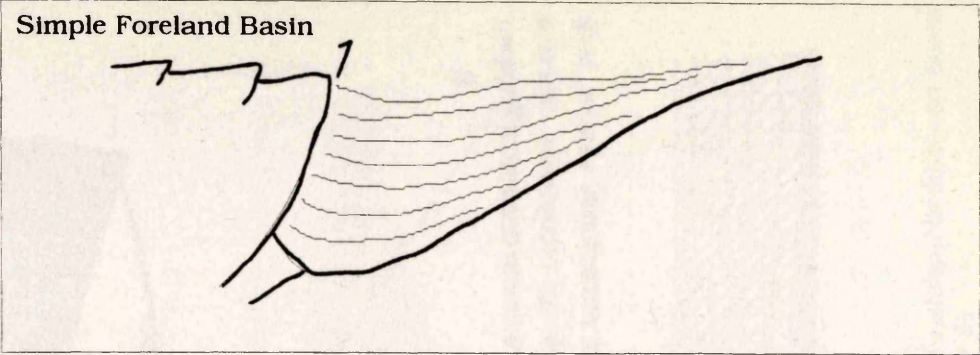


Figure 5.4 A simple foreland basin profile produced by thrusts stacking upon the margin and no migration of depocentre. From Ricci Lucchi (1986)

Figure 5.5 Complex foreland basins.

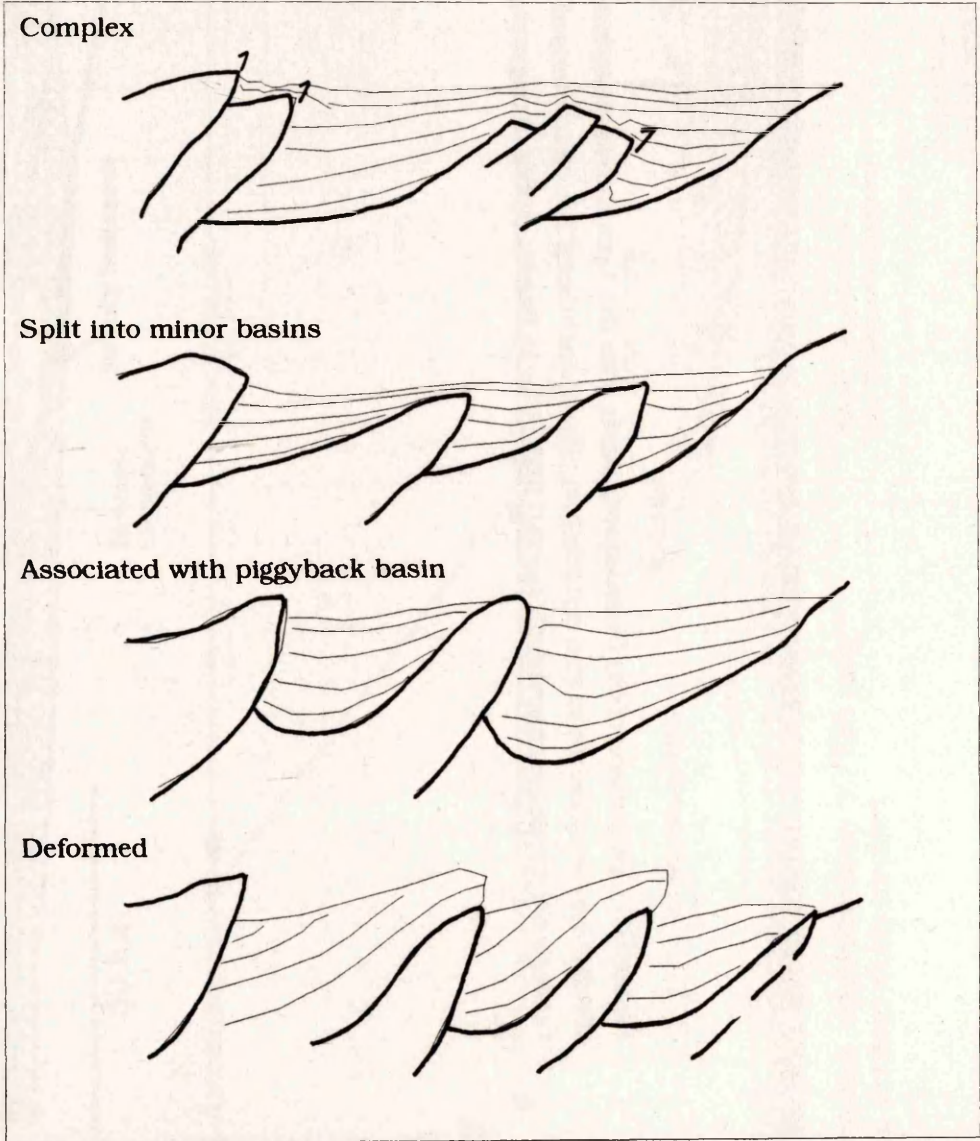


Figure 5.5 Complex foreland basins produced as the thrust front and depocentre migrate into the foreland basin. From Ricci Lucchi (1986)

Figure 5.6 Comparison of the Guadalquivir Basin with the Apennine foreland basin. The two basins are remarkably similar, both divided into an allochthon and autochthon. The autochthons are characterised by thrusting and melange complexes. Section through the Apennines from Ricci Lucchi (1986) (after D. Roeder, 1980). Section through the Guadalquivir Basin derived in Chapter 2.



Figure 5.6 Comparison of the Guadalquivir Basin with the Apennine foreland basin.

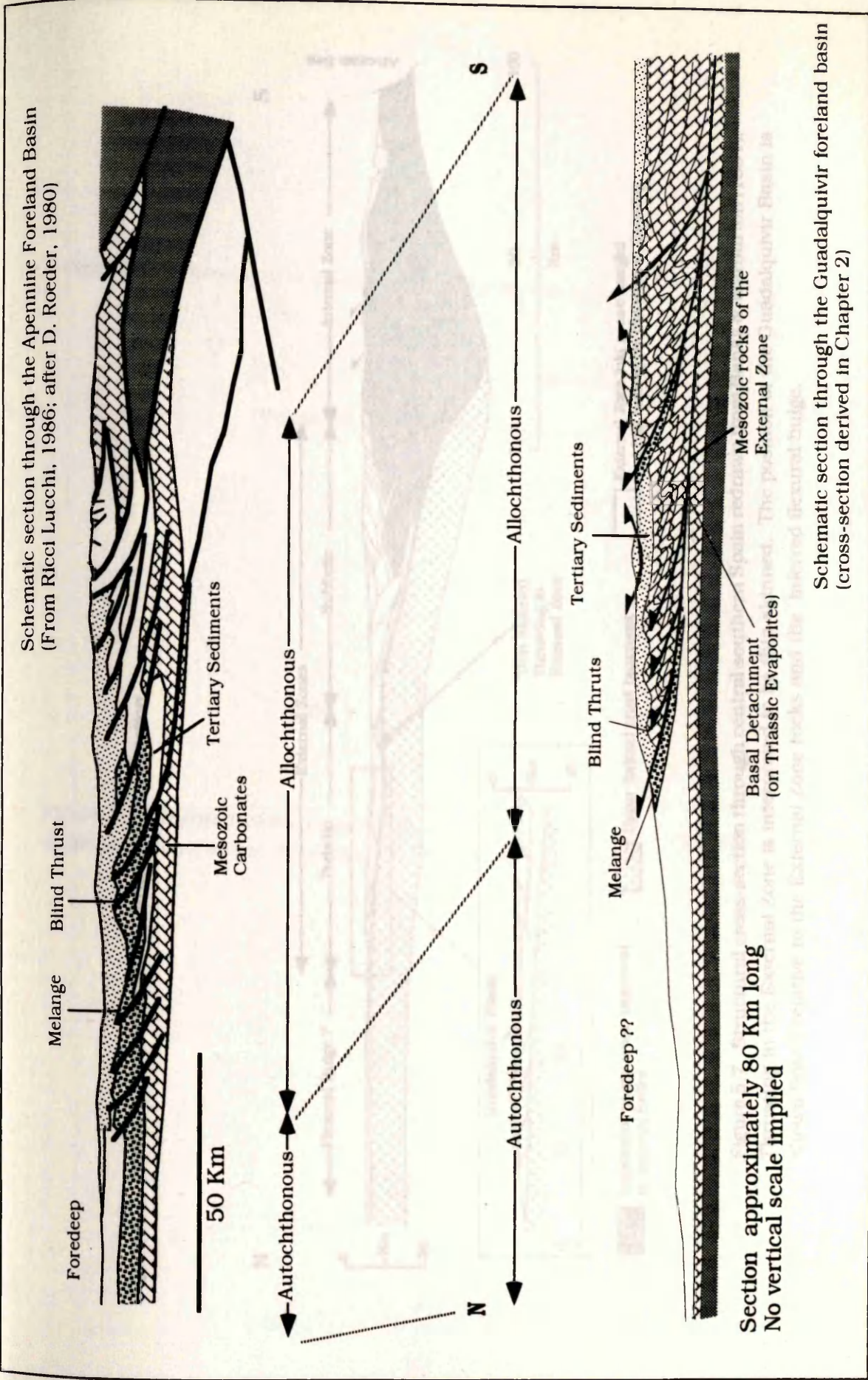




Figure 5.7. Banks & Warburton (1991) Structural cross-section.

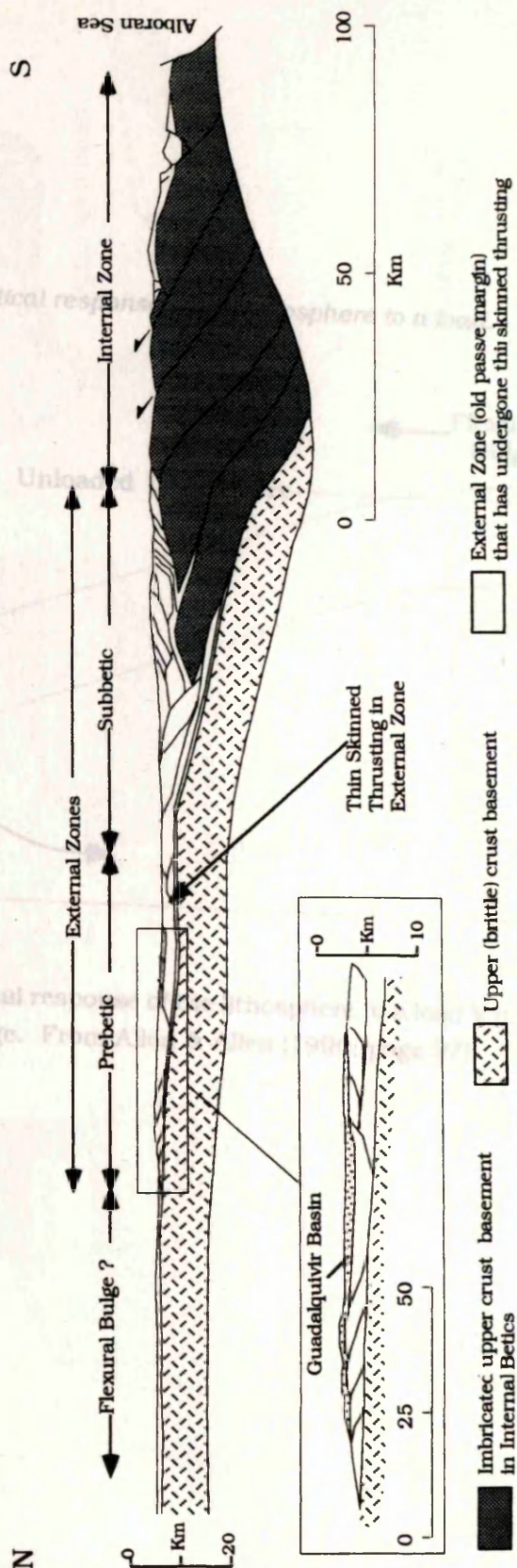


Figure 5.7. Structural cross-section through central southern Spain redrawn from Banks & Warburton (1991). Thrusting in the External Zone is interpreted to be thin skinned. The position of the Guadalquivir Basin is shown (inset) relative to the External Zone rocks and the inferred flexural bulge.

Figure 5.8. Theoretical response of the lithosphere to a load.

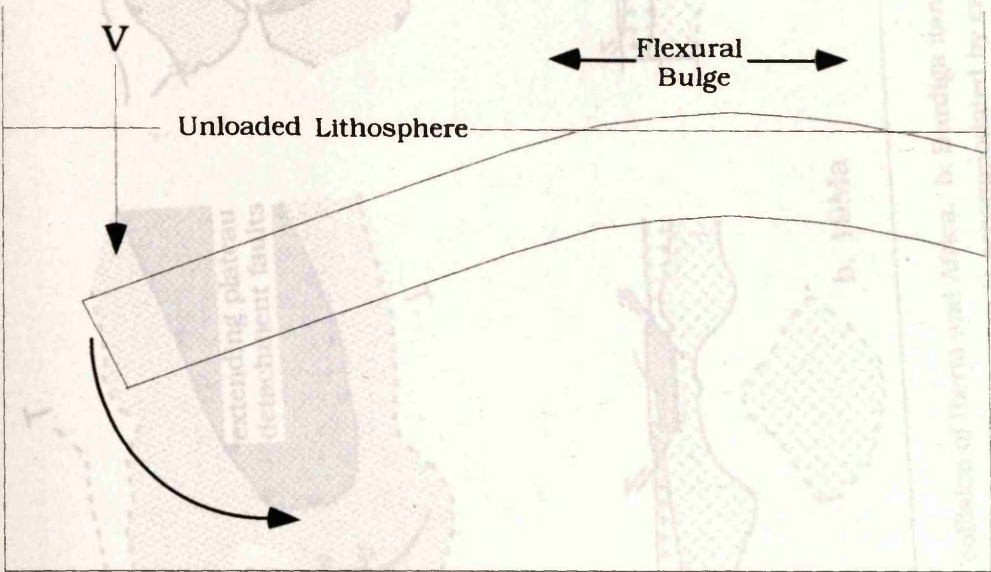


Figure 5.8. Theoretical response of the lithosphere to a load V (i.e. an orogenic wedge). Note uplift at flexural bulge. From Allen & Allen (1990; page 97).



Figure 5.9 Tectonic evolution of the Betic Orogen.

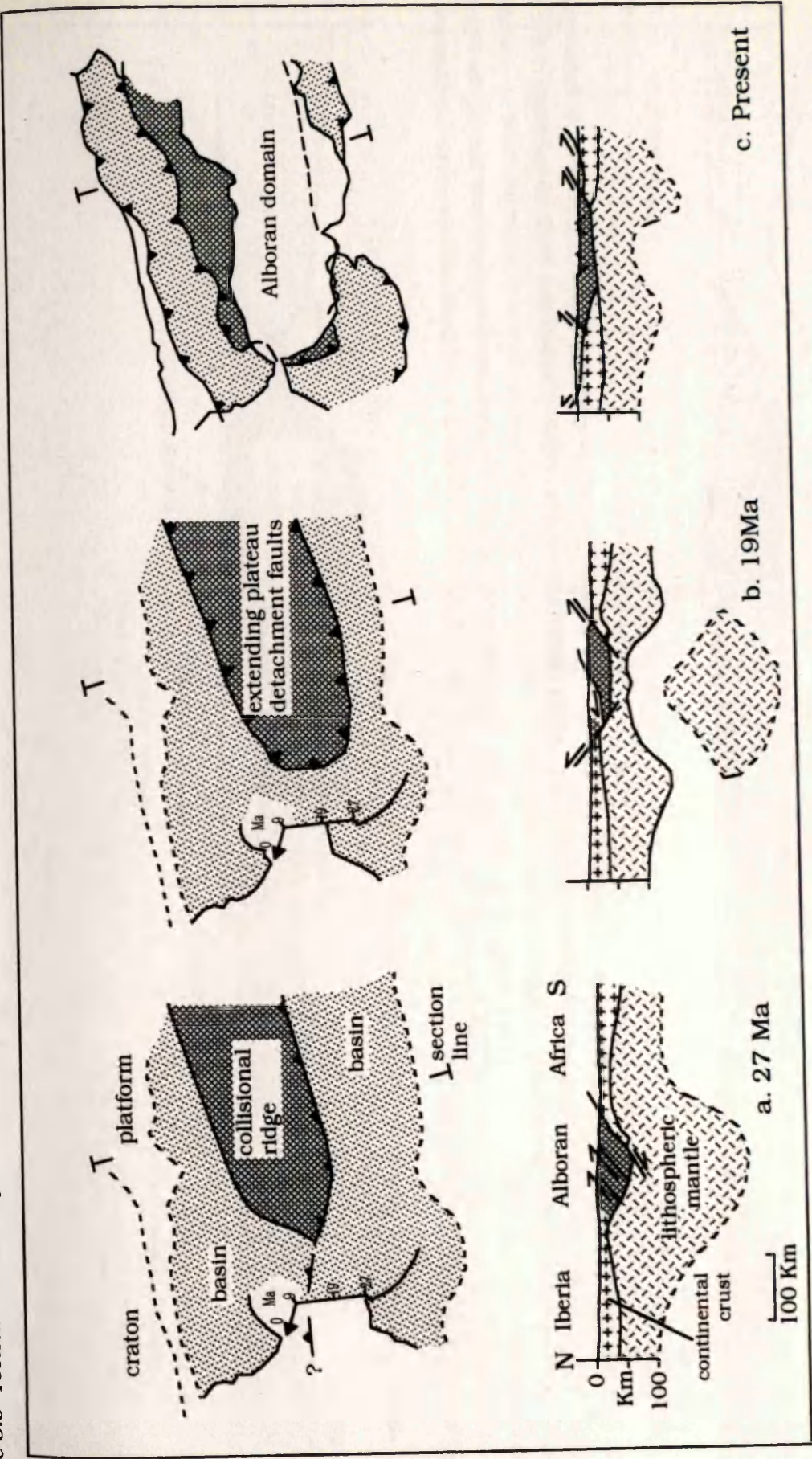


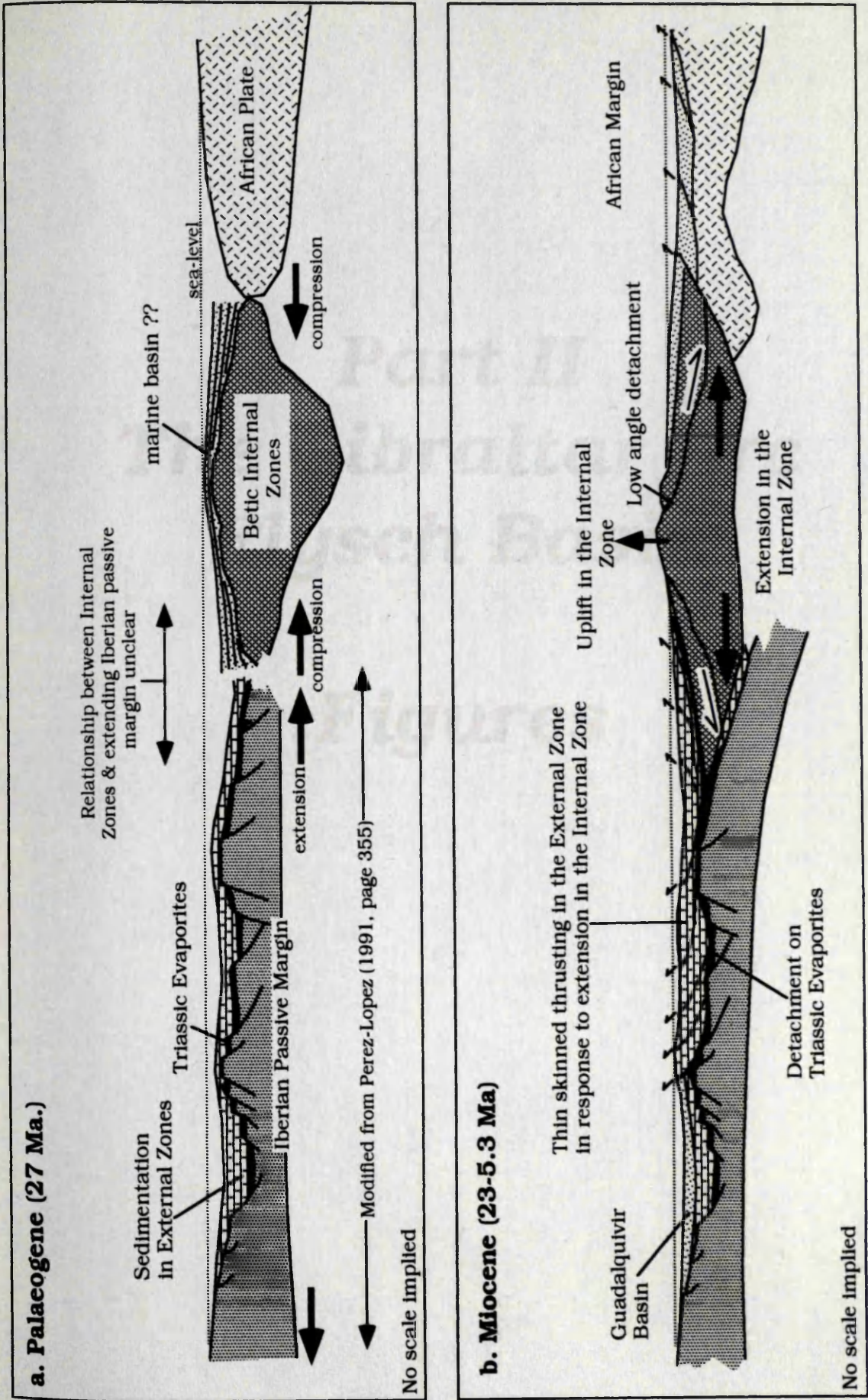
Figure 5.9 Tectonic evolution of the Betic Orogen. a: Mid-Oligocene, collision of Iberia and Africa. b: Burdiga llan. Convective removal of lithospheric root has caused uplift, increase in potential energy of collisional ridge, and extension. Extension is accommodated by crustal shortening and radial thrusting in the External Zones and Gibraltar Arc. c: Extending Alboran Domain has been emplaced onto surrounding continental margins; centre subsides as lithosphere thickens by cooling and continued slow convergence Maps show coastline around Gibraltar and Tangiers, and plate motion vectors for Africa relative to Europe (Dewey et al., 1989). Figure from Platt & Vissers (1989; Figure 6; page 542)



Figure 5.10. Schematic diagram showing the evolution of the Internal Zone, External Zone and Guadalquivir Basin of the Betic Orogen. a: Palaeogene, the External Rocks were deposited on an extending passive margin (Blankenship, 1992; Garcia Hernandez, 1980). Graben and basin morphology of the Iberian Margin taken from Perez-Lopez (1991). At the same as deposition was taking place on the Iberian Margin the Internal Zones are known to have been undergoing compression and metamorphism (Bakker et al., 1989; Moliné et al., 1991). The relationship between the Internal and External Zones during the Palaeogene is unclear. b: During the Miocene extension in the Internal Zone was accommodated by thin skinned thrusting in the External Zone. The Guadalquivir Basin formed as a part of the destruction of the Iberian passive margin (External Zone).



Figure 5.10. Schematic diagram showing the evolution of the Betics.





**Part II**  
**The Gibraltar Arc**  
**Flysch Basin**

**Figures**



**Chapter 1**  
**Introduction &**  
**Tectono-Stratigraphic**  
**History**

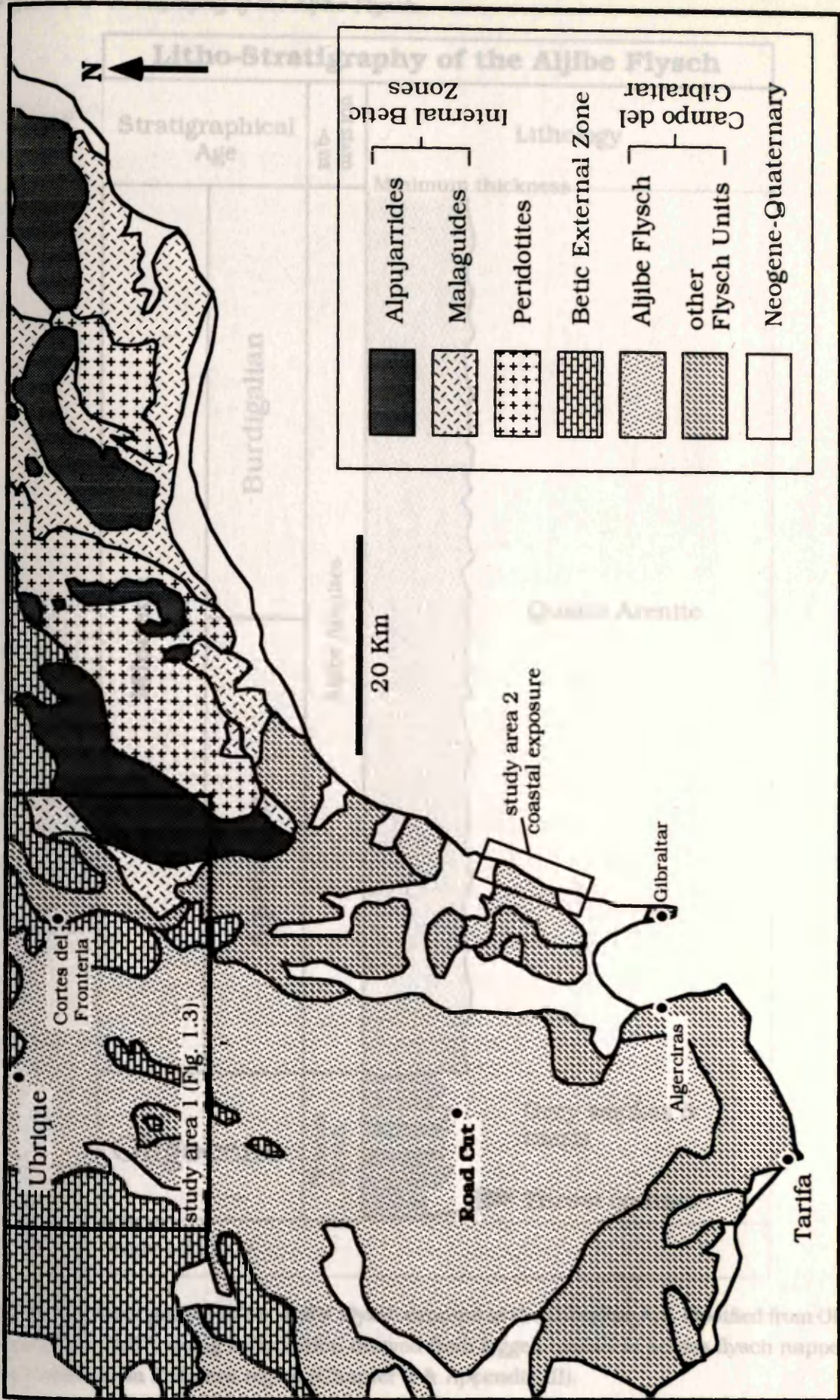
**Figures**

Figure 1.1 Geology of the Gibraltar Arc. The Aljibe Flysch, which is the subject of this thesis, has been studied in two areas; Study Area 1 is the Cortes de la Frontera region and Study Area 2 is based on well exposed, wave washed rocks found on the southern coast of Spain. Study Area 1 is shown in Figure 1.3. Diagram redrawn from Geological Map 1.200.000, sheet 87, Instituto Geológico y Minero de España, Madrid.



Figure 1.1 Geology of the Gibraltar Arc

Geology of the Gibraltar Arc, Betic Orogen, Southern Spain



redrawn from Geological Map 1.200.000, sheet 87, Instituto Geológico y Minero de España, Madrid.



Figure 1.2 Stratigraphy of the Aljibe Flysch.

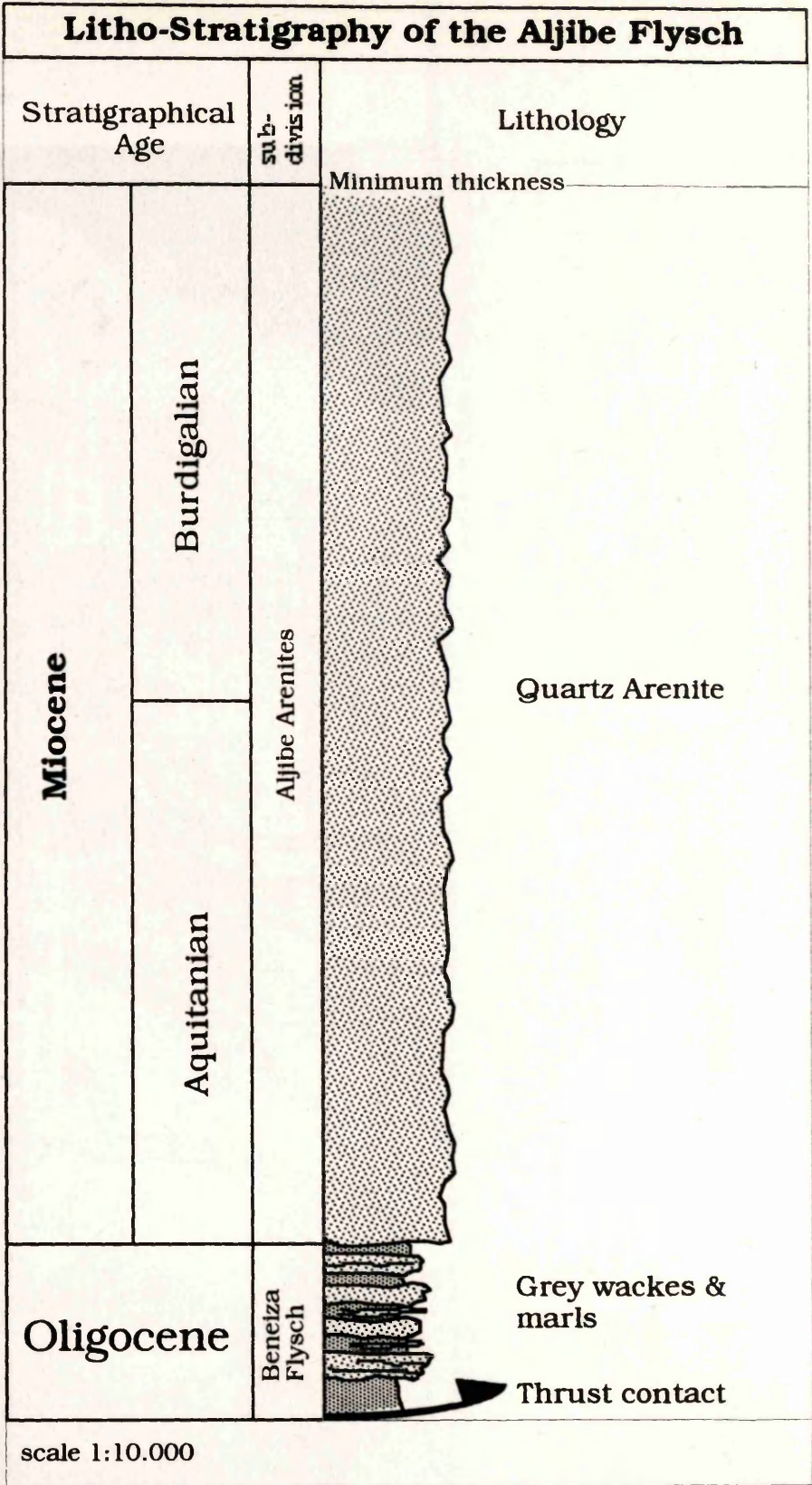


Figure 1.2 Stratigraphy of the Aljibe Flysch exposed in the Gibraltar Arc. Modified from Olmo-Sanz et al. (1987) using information derived from logged transects across flysch nappes in the Cortes de la Frontera region (Chapter 2 & Appendix III).

Figure 1.3 Study Area 1 for the Aljibe Flysch. Logged transects across the Flysch Nappes are shown in Figures 1.4-1.6, the locations of which are shown in this Figure



Figure 1.3 Study Area 1 for the Aljibe Flysch.

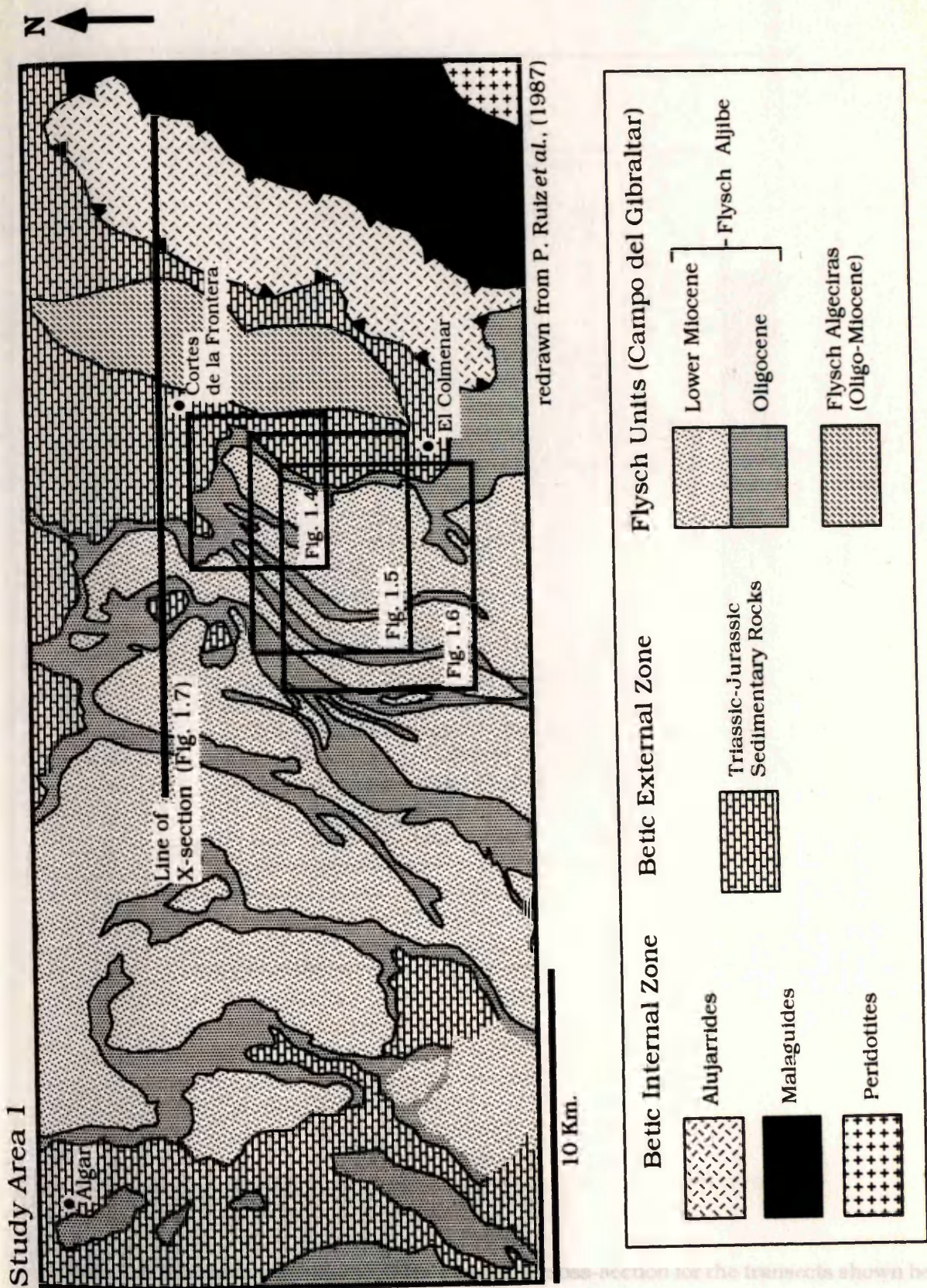
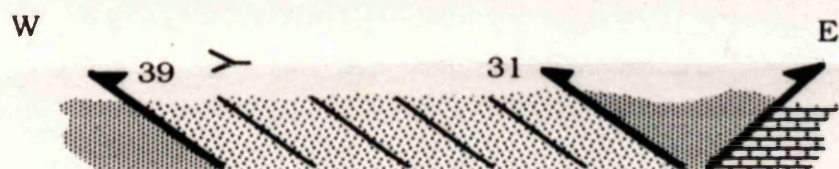
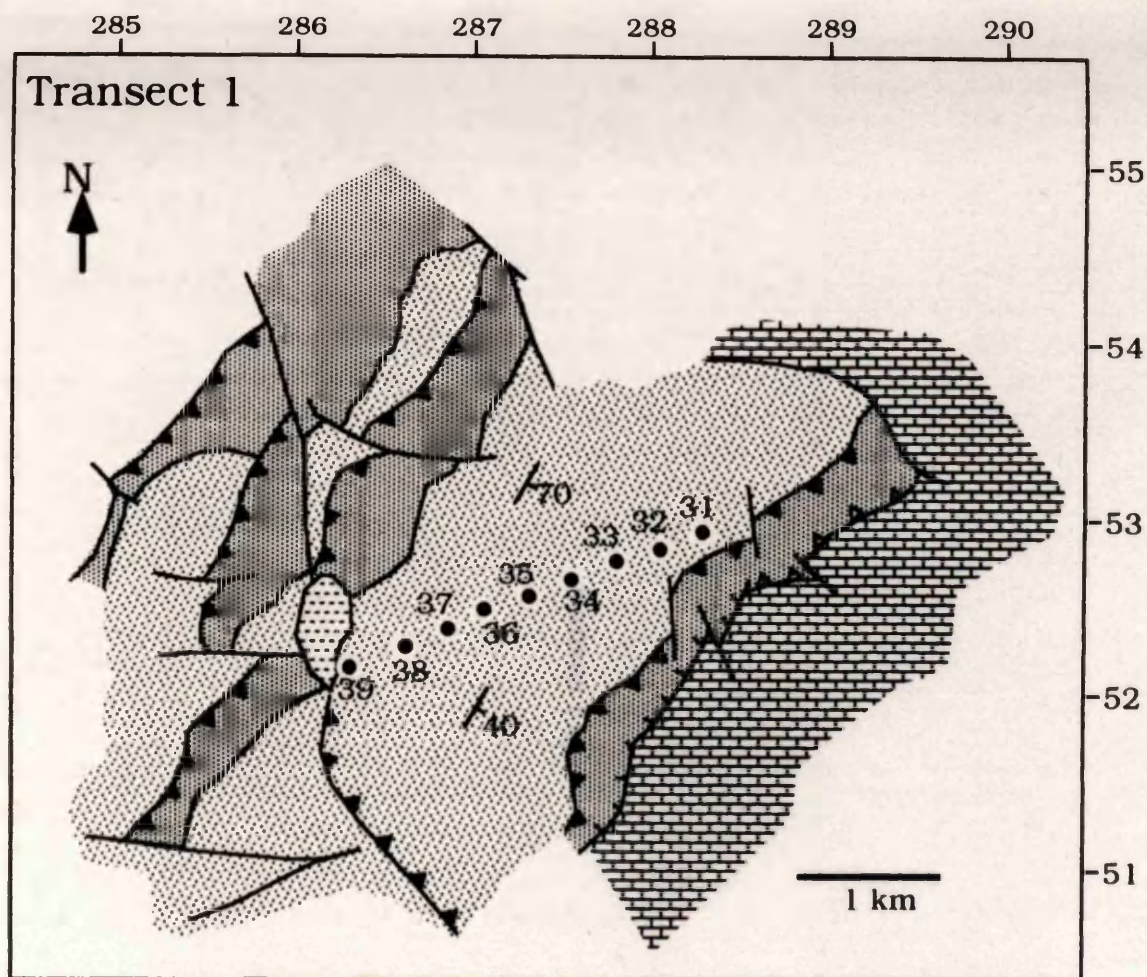




Figure 1.4 Transect 1 across the Aljibe Flysch.

Canvas Fig.

Figure 1.4 Transect 1 across the Aljibe Flysch. A cross-section for the transects shown below the map. Location numbers refer to sample and sedimentary log locations. A sample of the logs is given in Appendix III



schematic cross-section of transect 1

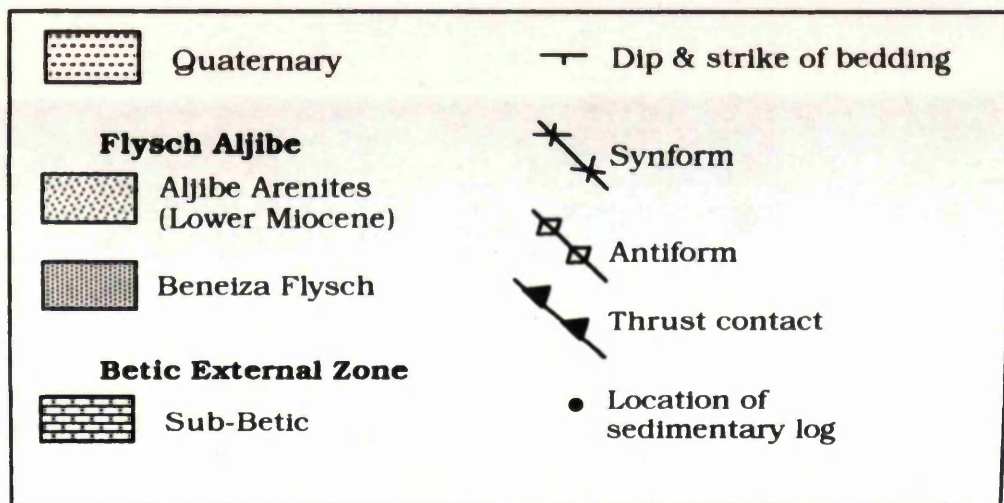
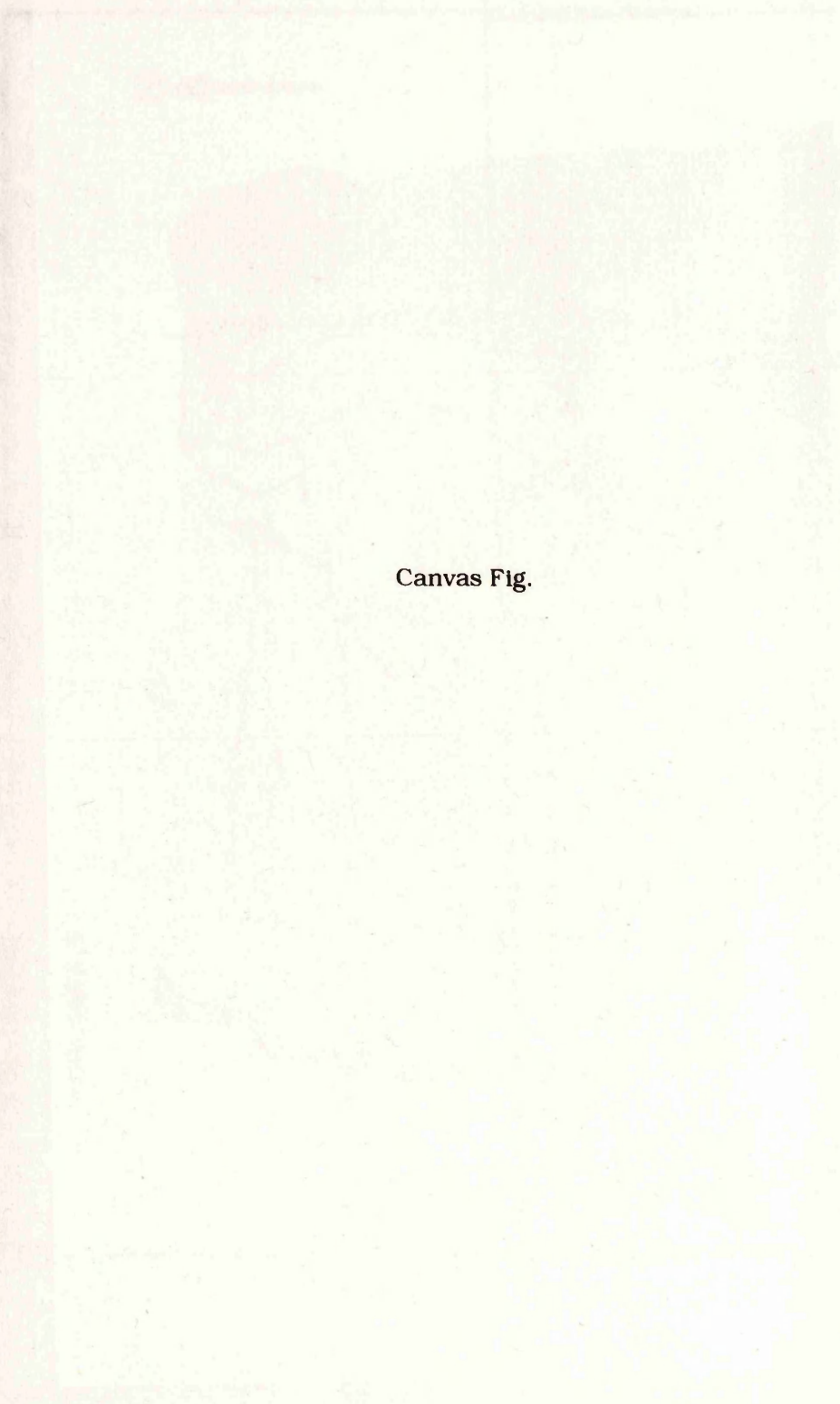




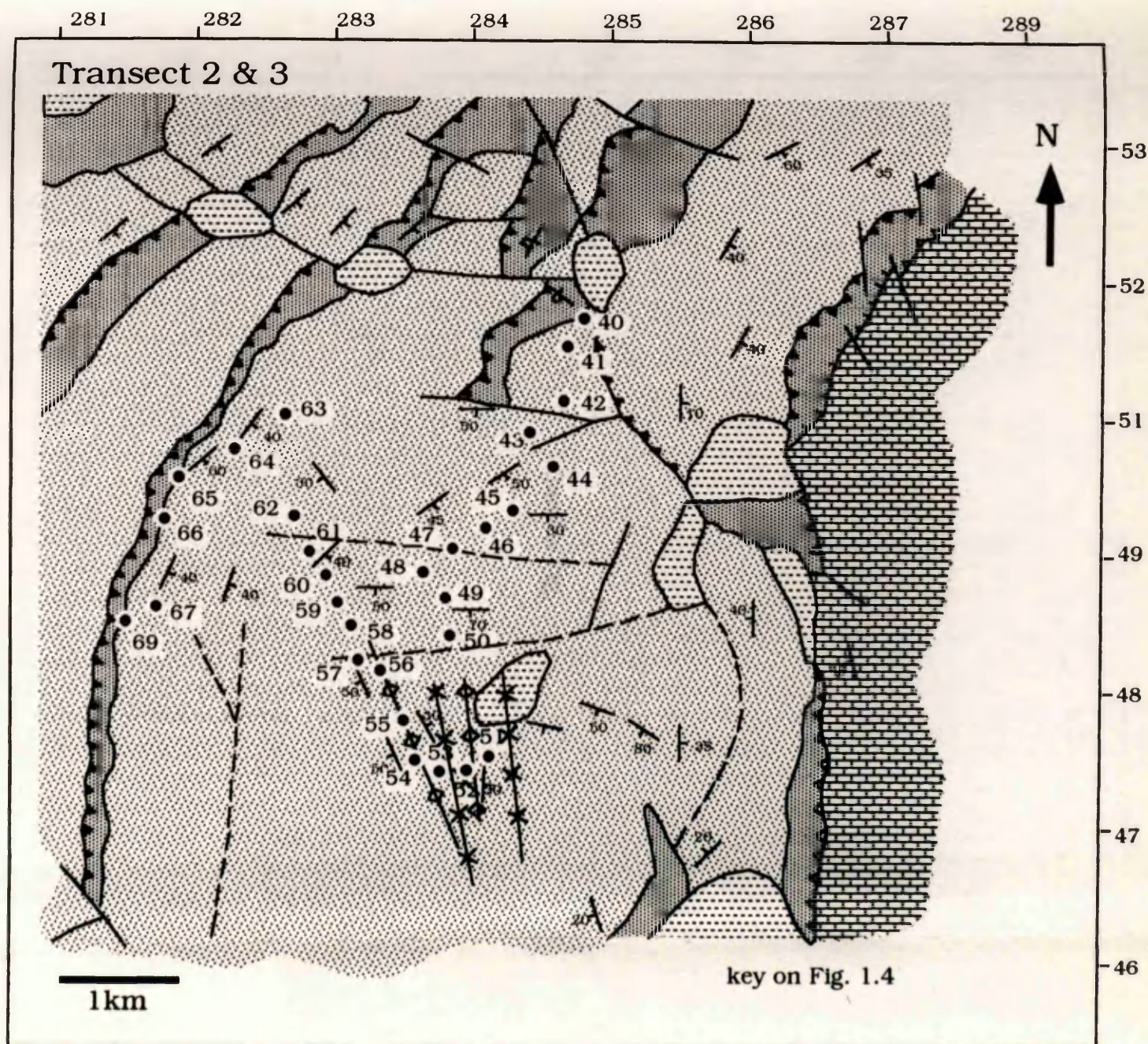
Figure 1.5 Transects 2 & 3 across the AljibeFlysch.



Canvas Fig.

Figure 1.5 Transects 2 & 3 across the AljibeFlysch. A cross-section for the transects is shown below the map. Location numbers refer to sample and sedimentary log locations. A sample of the logs is given in Appendix III





### Schematic Cross-Section

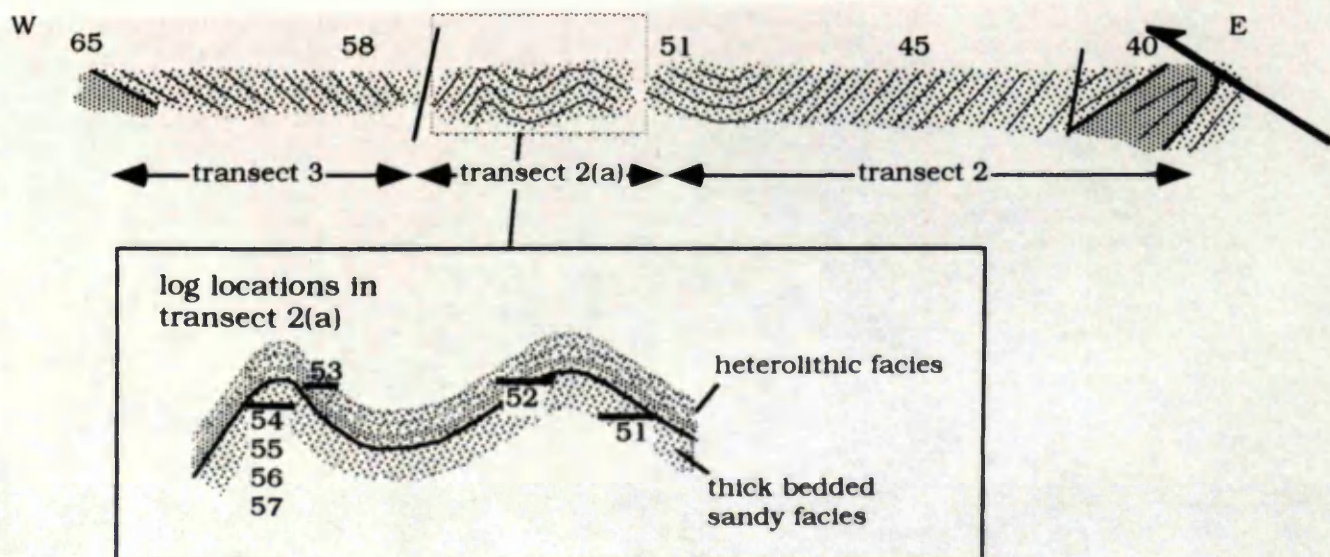
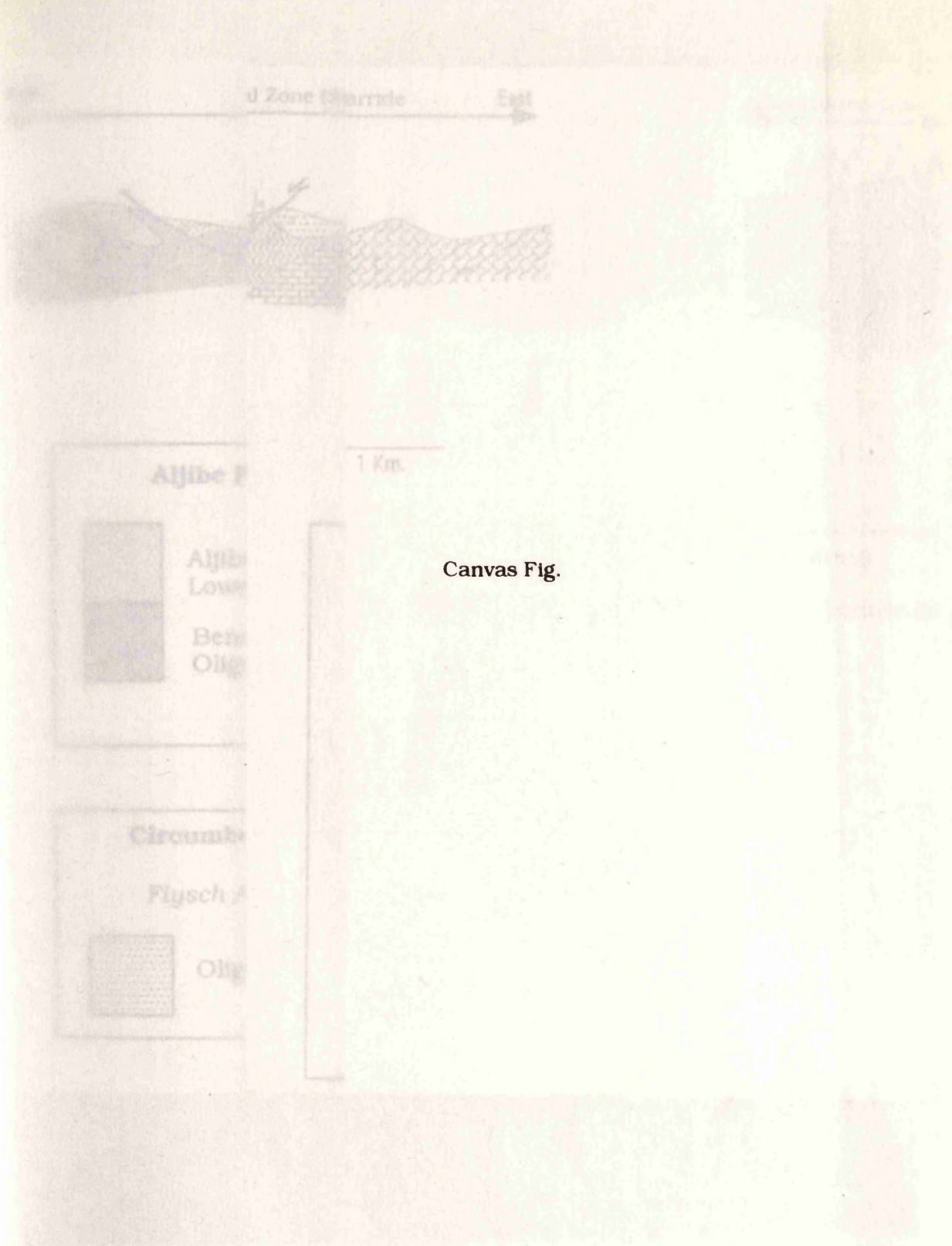




Figure 1.6 Transect 4 across the Aljibe Flysch.



Canvas Fig.

Figure 1.7 Cross-section across Study Area 1 (Cortés de la Frontera region). Cross-section  
Figure 1.6 Transect 4 across the Aljibe Flysch. Location numbers refer to sample and sedimentary log locations. A sample of the logs is given in Appendix III



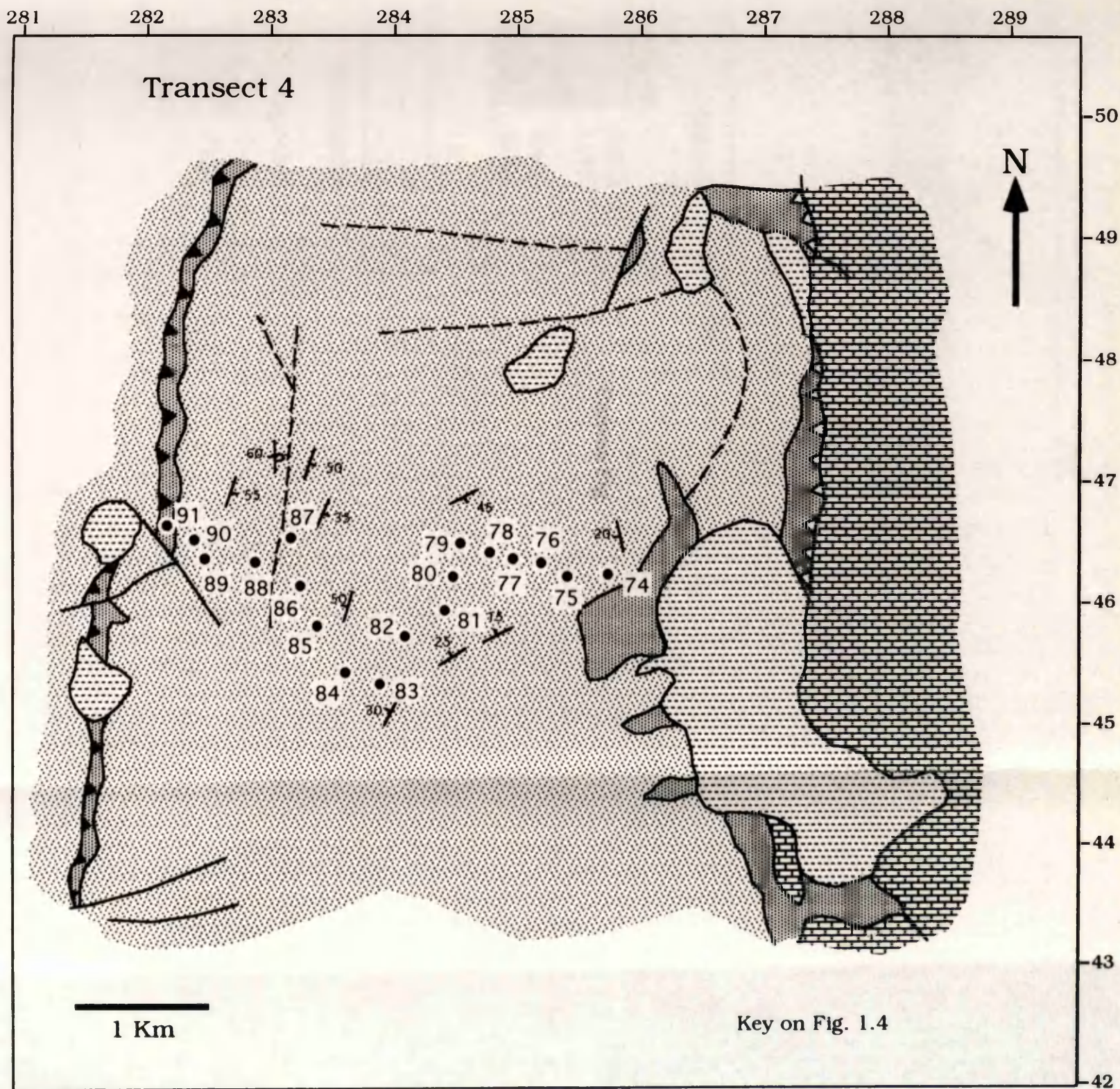




Figure 1.7 Cross-section across Study Area 1.

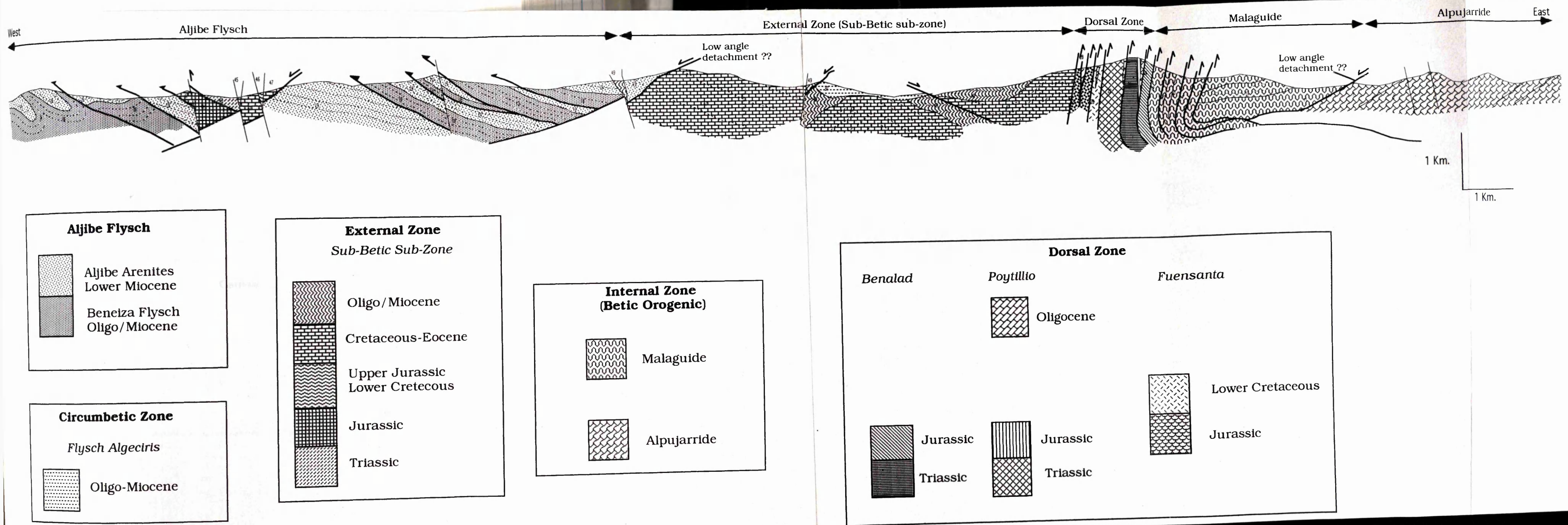


Figure 1.7 Cross-section across Study Area 1 (Cortes de la Frontera region). Cross-section derived from published maps (Olmo-Sanz et al., 1987), sedimentary logs (Appendix III), and other field observations.



Figure 1.8 Flysch nappes of the Gibraltar Arc.

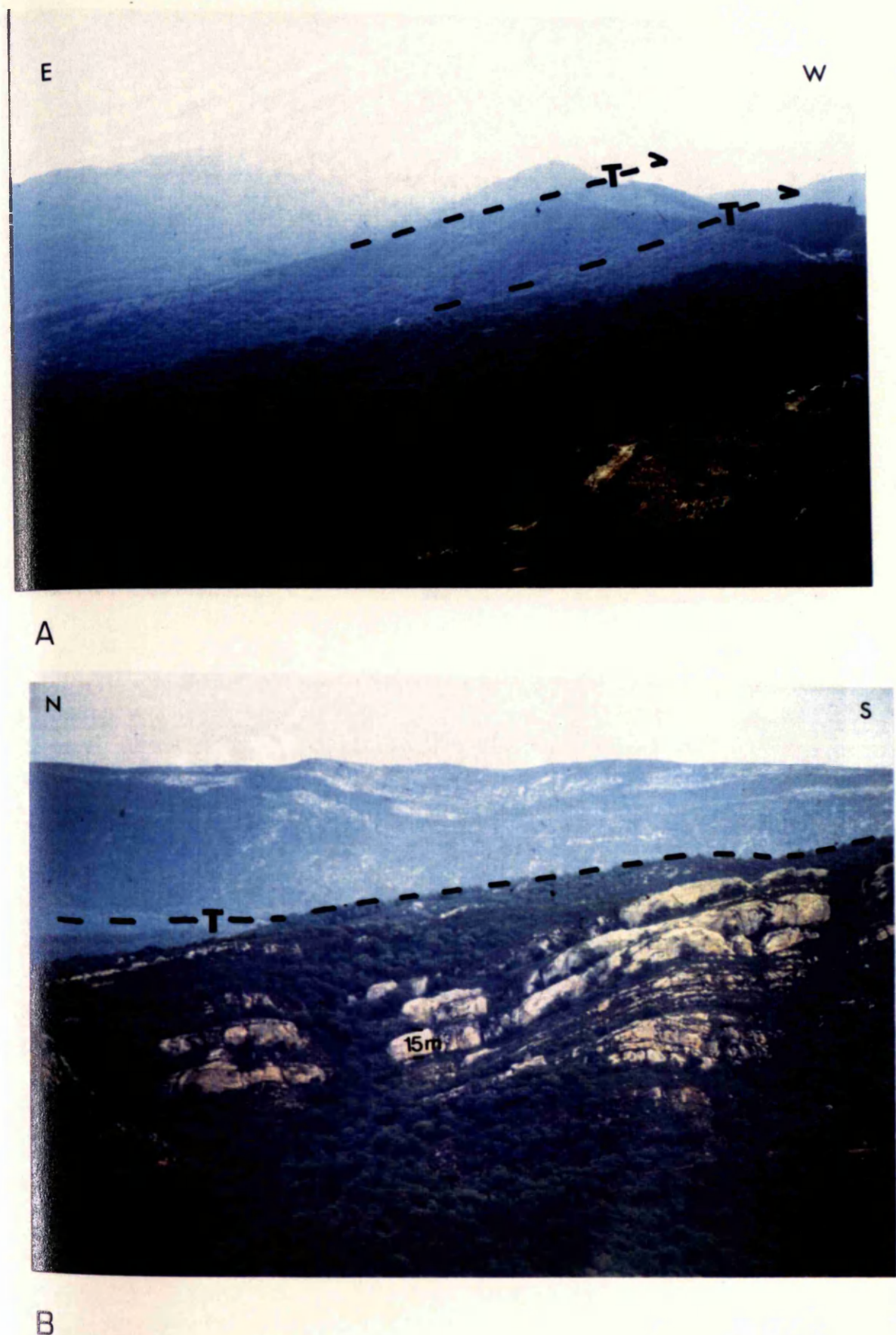


Figure 1.8 Flysch nappes of the Gibraltar Arc with thrust contacts marked (T). (a) E-W cross-section through nappes. (b) N-S strike section. Sandstone beds in (b) proximately 15m high.



Figure 1.9 Tectonic contacts in the Gibraltar Arc.



(a)



(b)

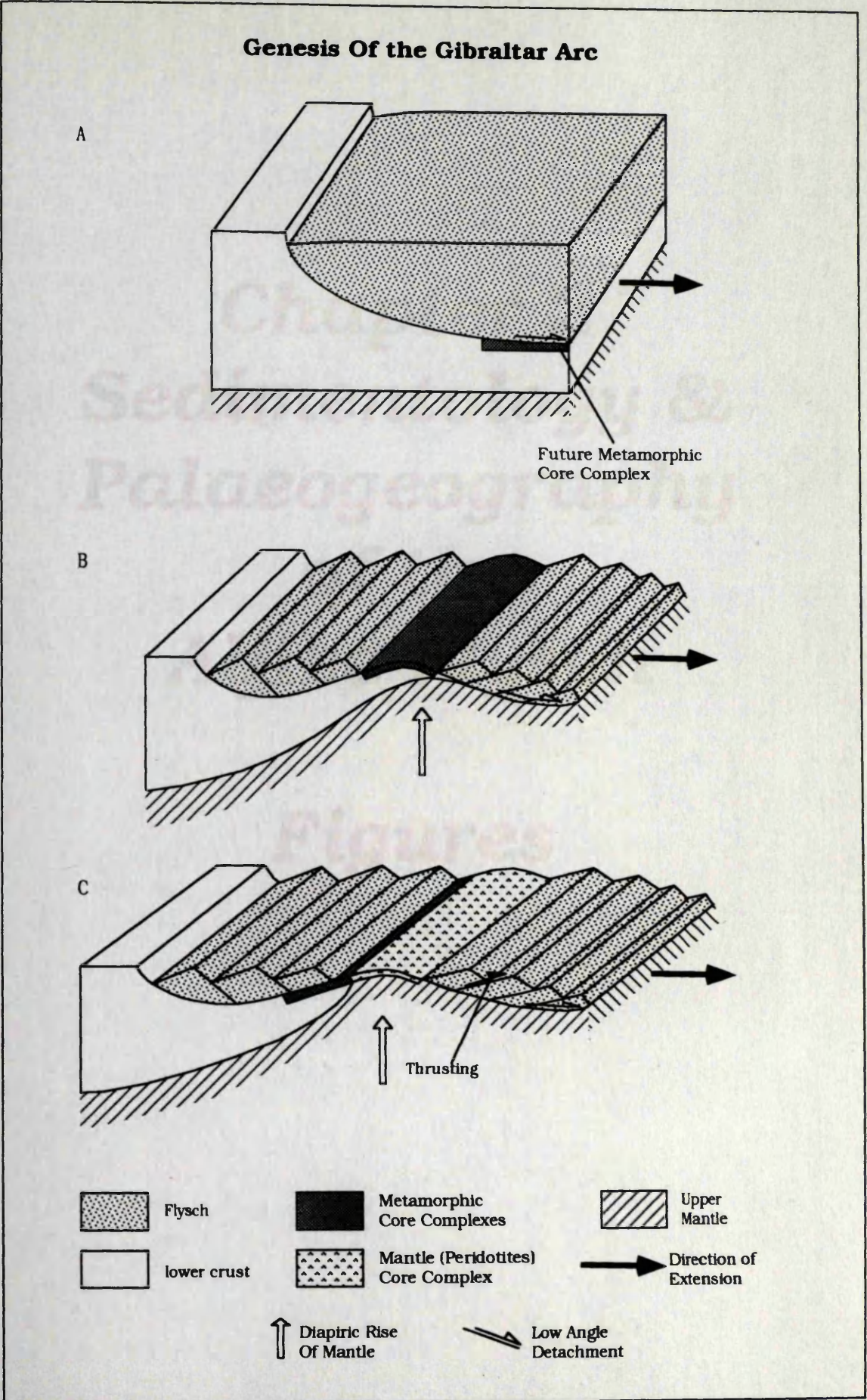
Figure 1.9 Tectono-stratigraphic units within the Gibraltar Arc are often separated by low angle tectonic contacts. (a) the Miocene Aljibe Arenites (AA) are juxtaposed against Triassic deposits of the External Zone (EZ). (b) thrust contacts are often characterised by thin slices of Triassic material that contains halite and gypsum (HG) evaporite horizons. Camera lens in centre of outcrop is 7cm in diameter.



Figure 1.10 Schematic diagram showing the genesis of the Gibraltar Arc. Low angle detachments form in response to crustal extension (A). Extension of the crust is coeval with the diapiric rise of the mantle (B). Extension is considered to have progressed far enough to allow the exposure of mantle peridotite bodies (C). Diagram from Doblas & Oyarzun (1989).



Figure 1.10 Genesis of the Gibraltar Arc.



Modified from Doblas & Oyarzun (1989)



**Chapter 2**  
**Sedimentology &**  
**Palaeogeography**  
**of the**  
**Aljibe Flysch**

**Figures**



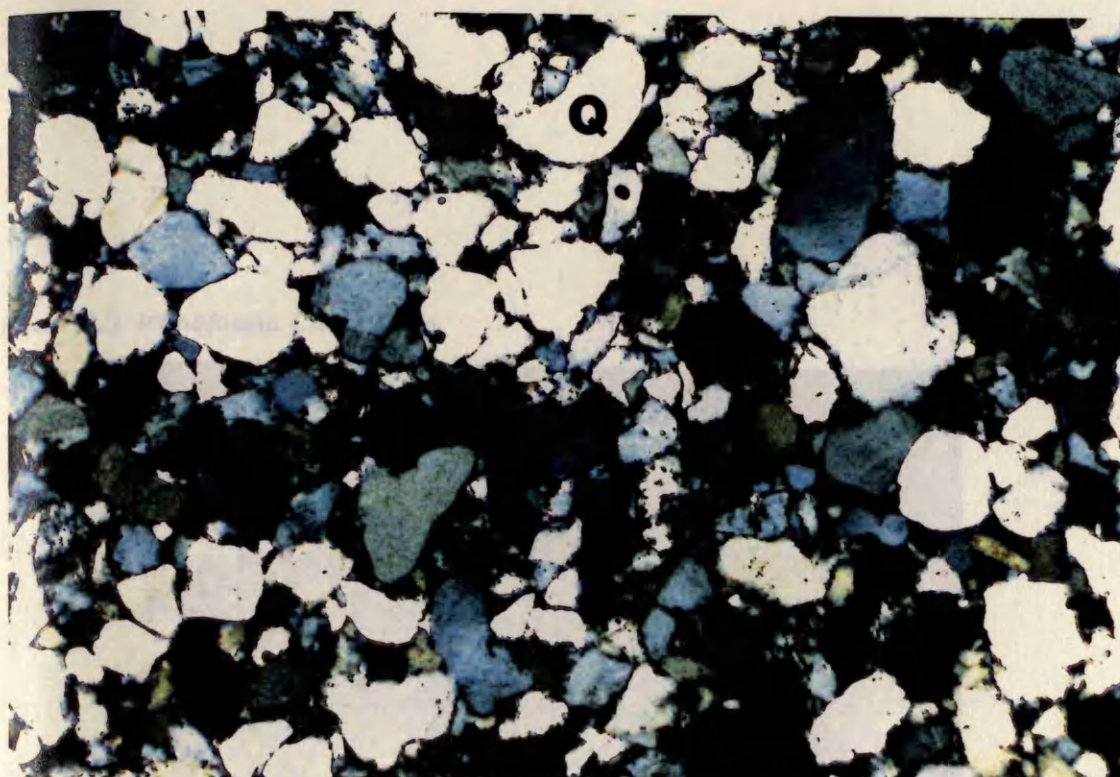
Figure 2.1 The Beneiza Flysch and the Aljibe Arenites.



Figure 2.1 Outcrop showing the stratigraphic contact between the Beneiza Flysch (F) and the Aljibe Arenites (AA). The Beneiza Flysch consists of thin (<20cm) siltstones and fine grained sandstones intercalated with marls. Photo taken at road cutting located on Fig. 1.3 (Study Area 1).

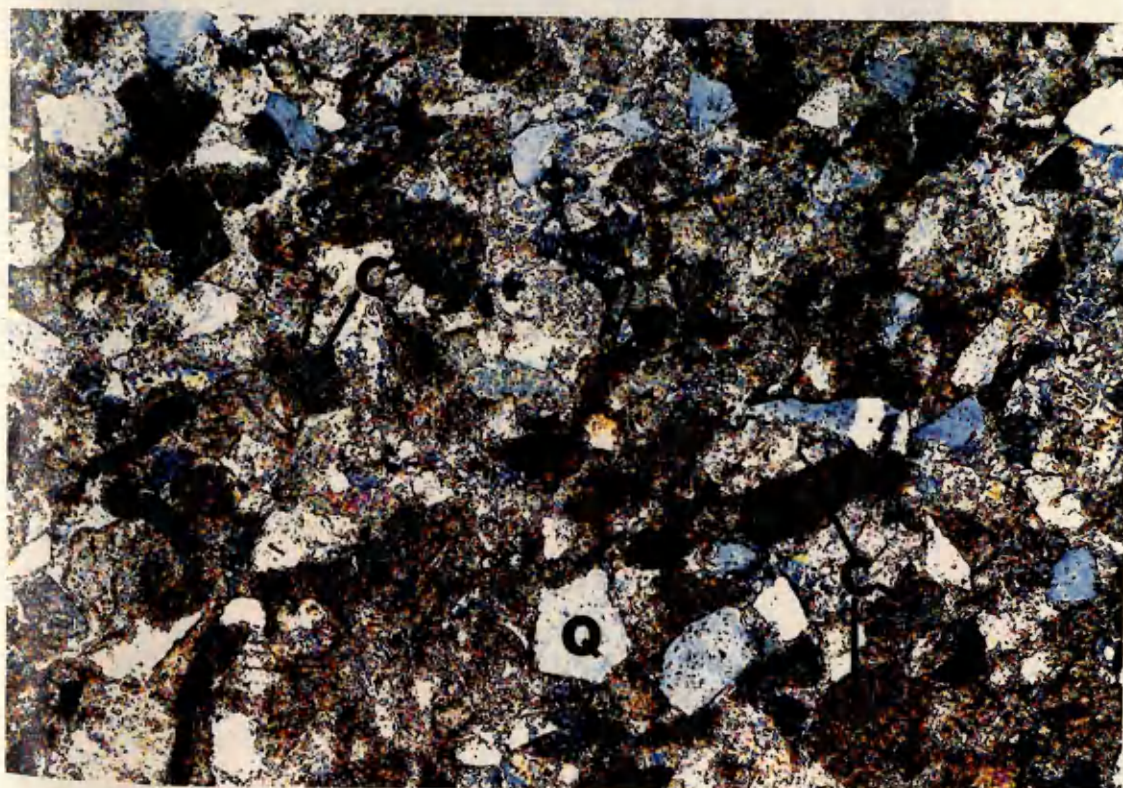


Figure 2.2 Photomicrographs of sandstones from the Beneiza Flysch



a

1 mm



b

1 mm

Figure 2.2 Photomicrographs of sandstones from the Beneiza Flysch.

a: Quartz arenites.

b: Lithic arenites containing both quartz (Q) and Carbonate (C) lithoclasts.



Figure 2.3 Ichnofauna Chondrites.

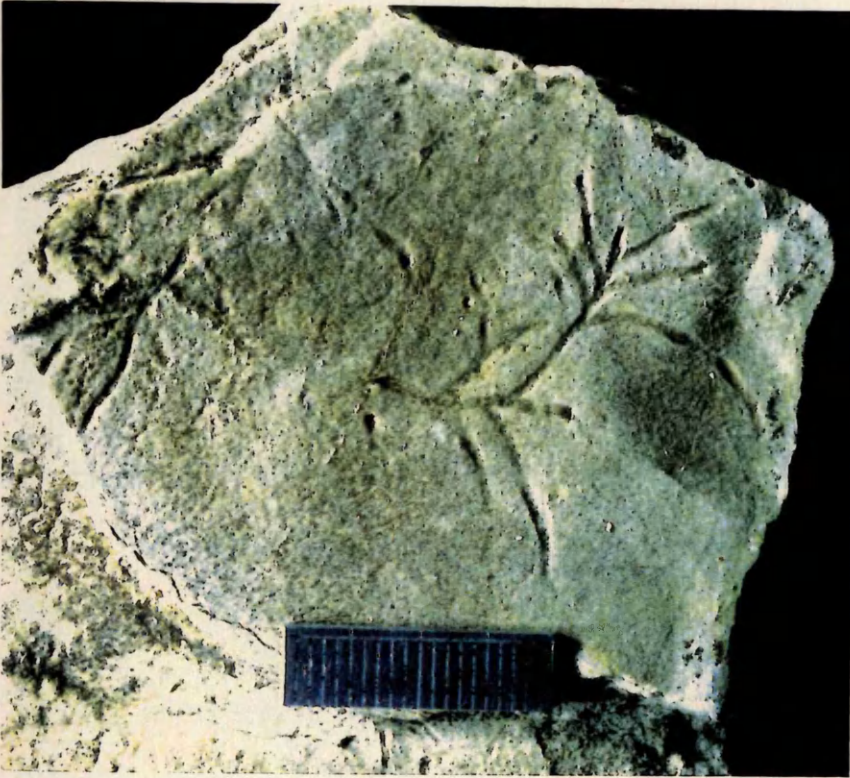


Figure 2.3 Ichnofauna, Chondrites found on bedding surfaces in the Beneiza Flysch, sub-unit of the Aljibe Flysch. Scale bar is 2cm long.



Figure 2.4 Sedimentary log of part of the Beneiza Flysch, a sub-unit of the Aljibe Arenites.  
Log from location 66 (Fig. 1.5, Ref 282 051).



## Logged Section of the Beneiza Flysch (Sub-Unit of the Aljibe Arenites)

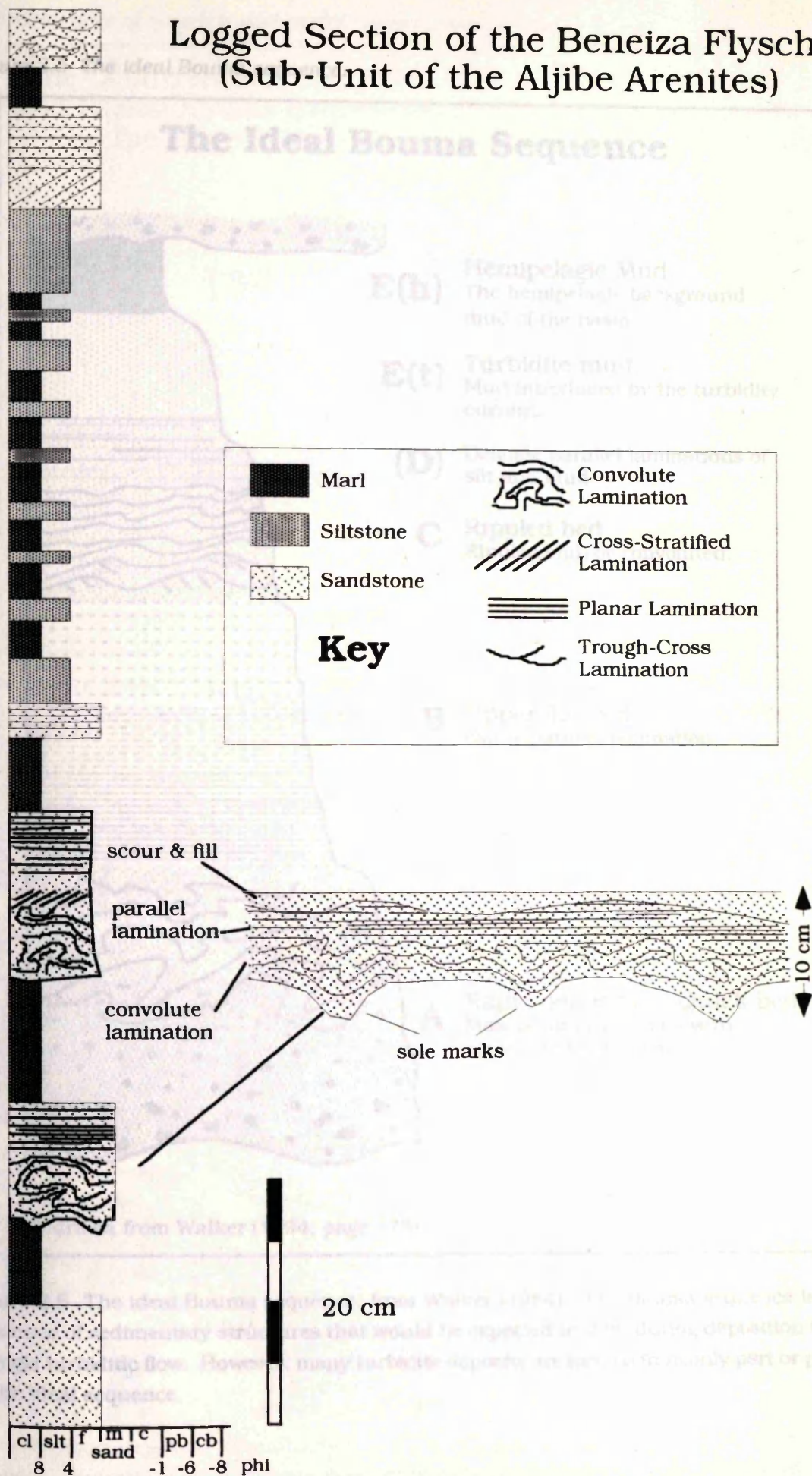


Figure 2.4 Sedimentary log of part of the Beneiza Flysch



Figure 2.5 The ideal Bouma sequence.

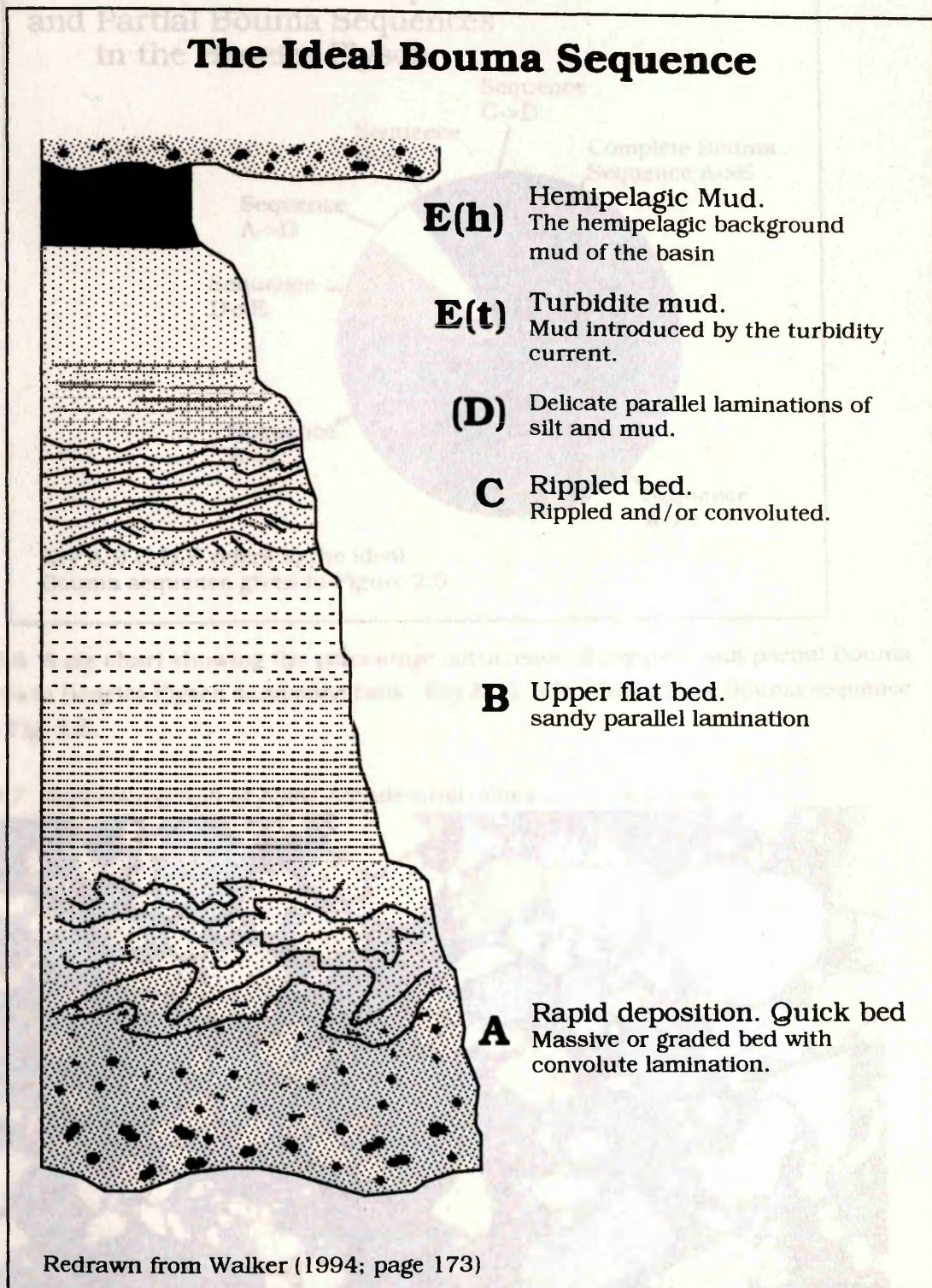


Figure 2.5 The ideal Bouma sequence, from Walker (1984). The Bouma sequence is the sequence of sedimentary structures that would be expected to form during deposition from a single turbiditic flow. However, many turbidite deposits are formed from only part or parts of the ideal sequence.



Figure 2.6 Occurrence of complete and partial Bouma sequences.

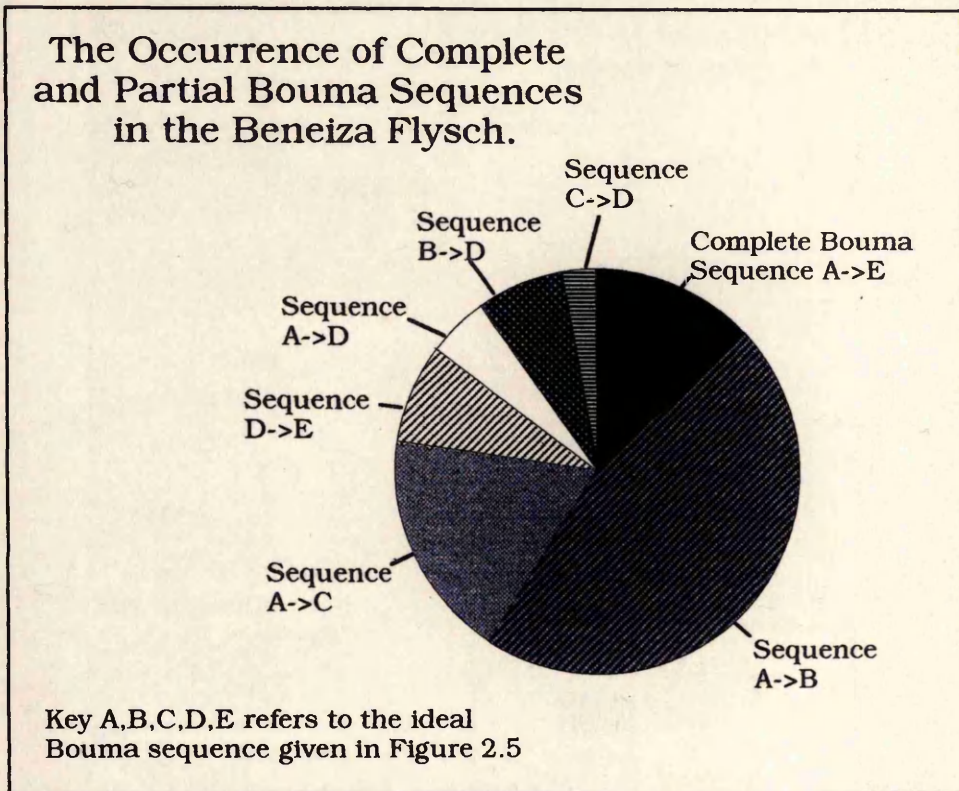


Figure 2.6 A pie chart showing the percentage occurrence of complete and partial Bouma sequences in Beneiza Flysch sandstone beds. Key A->E refers to the Ideal Bouma sequence given in Fig. 2.5.

Figure 2.7 Photomicrograph of Aljibe Arenite sandstones.

5cm = 1mm

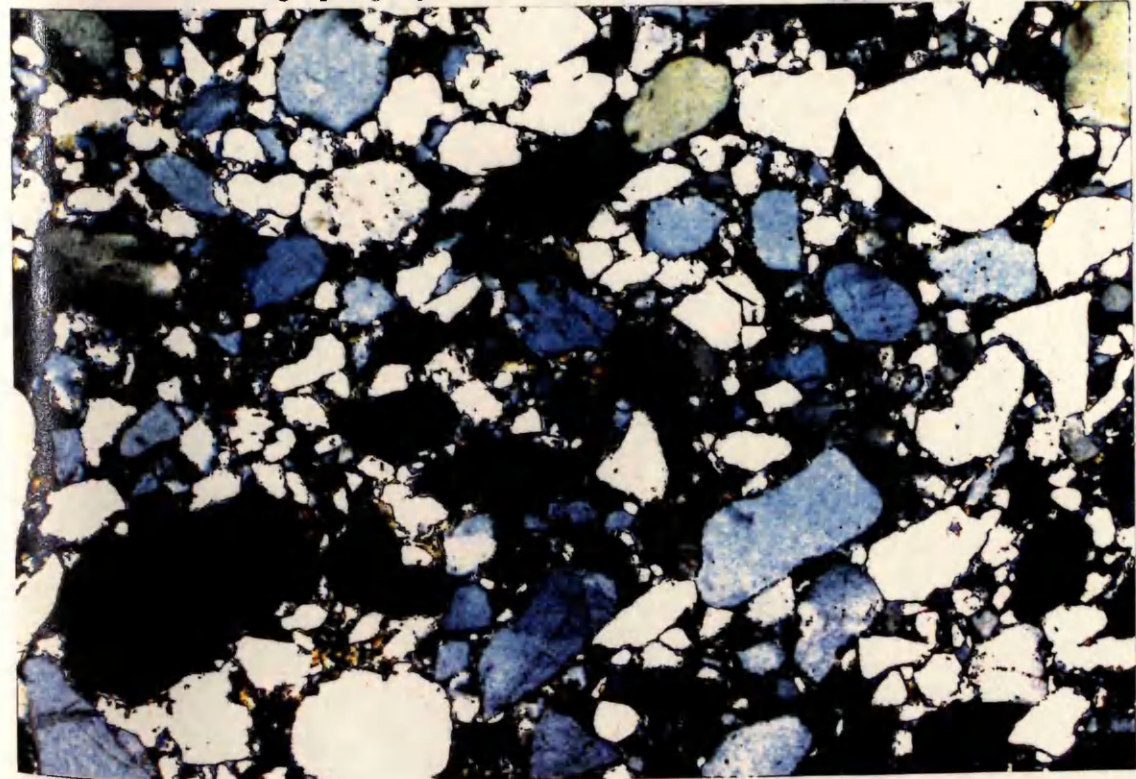


Figure 2.7 Photomicrograph of sandstones that are representative of the Aljibe Arenites. Quartz clasts generally constitute more than 98 percent of the framework grains and are usually well rounded.



Figure 2.8 Sedimentary log of part of the Aljibe Arenites. Log shows thick, apparently massive sandstones and displays both coarsening and fining up sequences. Log from location 32 (Fig. 1.4, Ref 287 052).

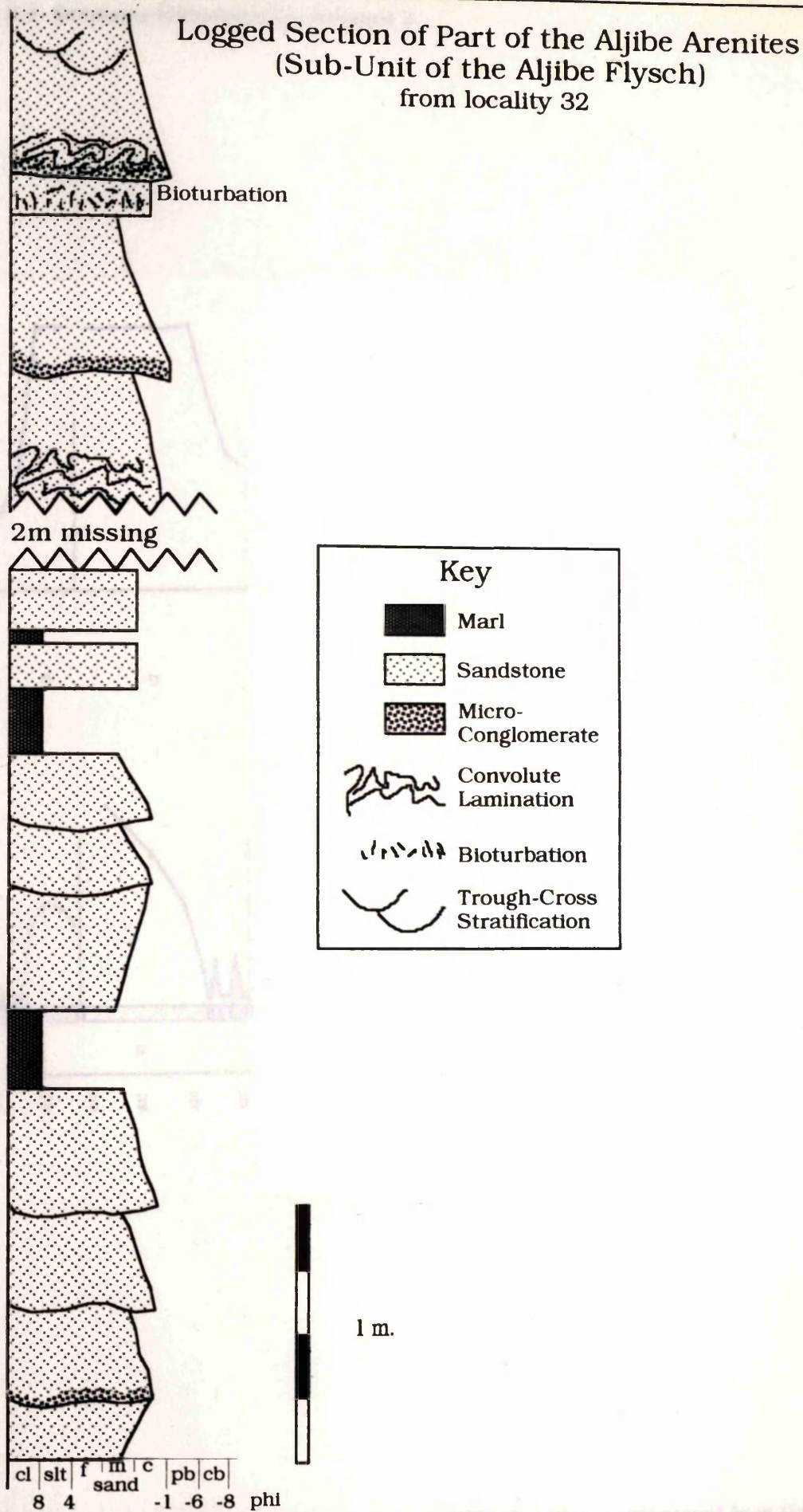


Figure 2.8 Sedimentary log of part of the Aljibe Arenites.



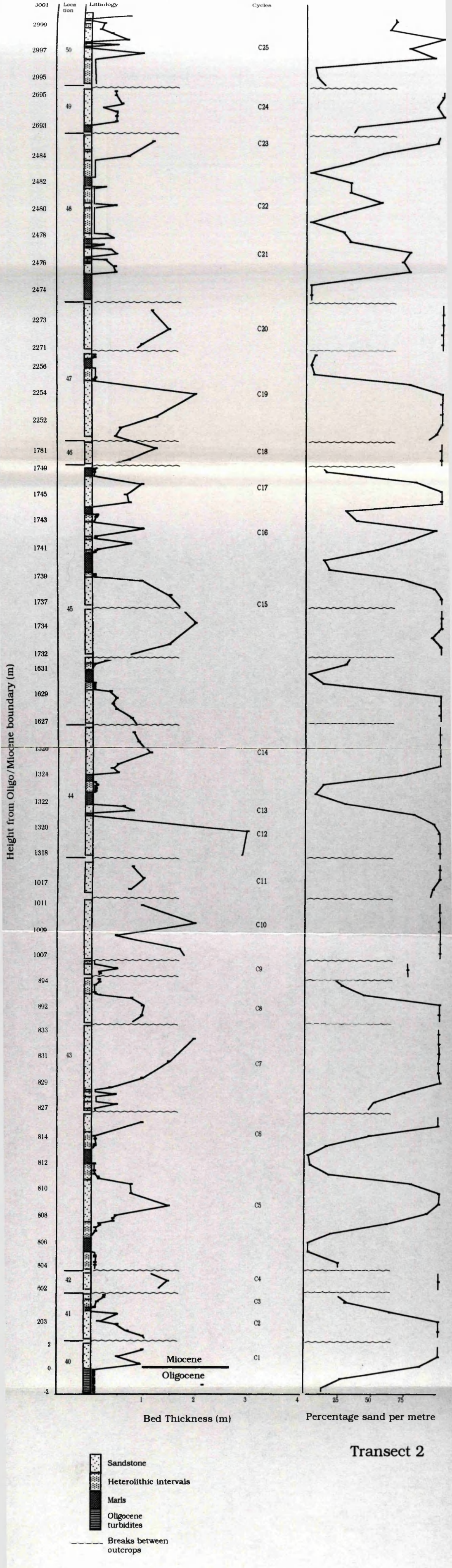




Figure 2.9 Summary lithological log, transect 2.

Figure 2.9 Summary lithological log of part of the Aljibe Arenites, constructed from transect 2 (Fig. 1.5). Approximate coarsening/thickening up cycles are shown as C1, C2, C3.....etc.

Figure 2.10 Summary lithological log, transect 3.

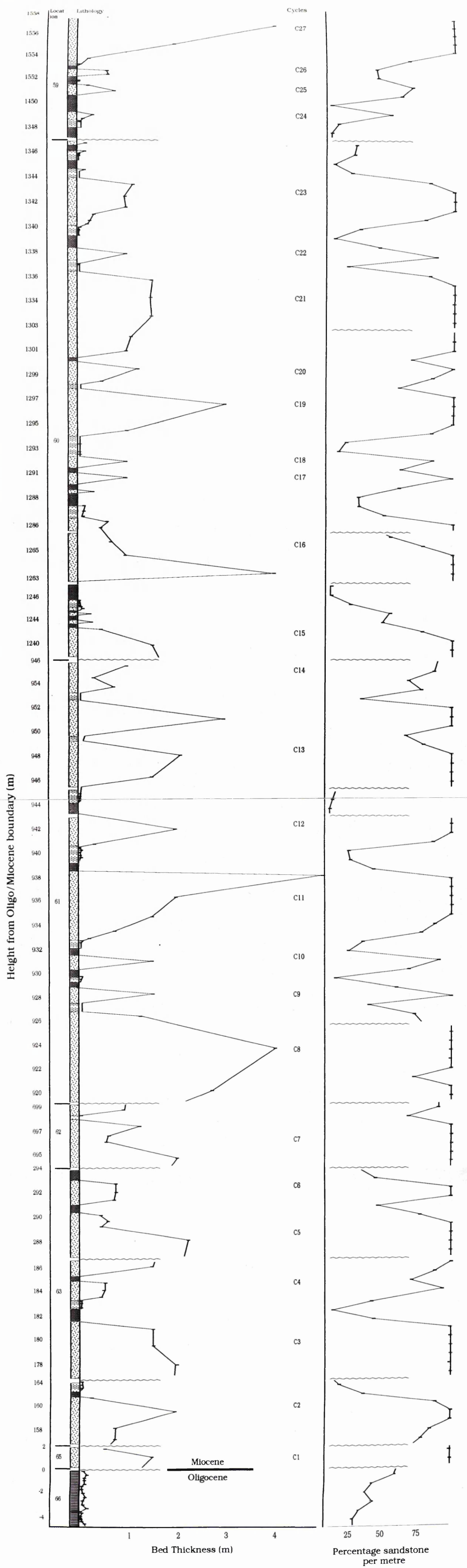


Figure 2.10 Summary lithological log of part of the Aljibe Arenites, constructed from transect 3 (Fig. 1.5). Approximate coarsening/thickening up cycles are shown as C1, C2, C3.....etc.



Figure 2.11 Dark laminae (D) in the Aljibe Arenites are picked out by heavy minerals, clays and micas forming characteristic dark streaks. The dark laminae are often overlain by lighter bands (L) of quartz and feldspar. Scale at base of photo is 3cm long.

Figure 2.11 Dark laminae in the Aljibe Arenites.



Figure 2.12 Dish structured laminae found in the Aljibe Arenites. Dishes (marked by arrows) are formed by discontinuous concave upwards laminae. Scale is 3cm long.



Figure 2.12 Dish structured laminae.

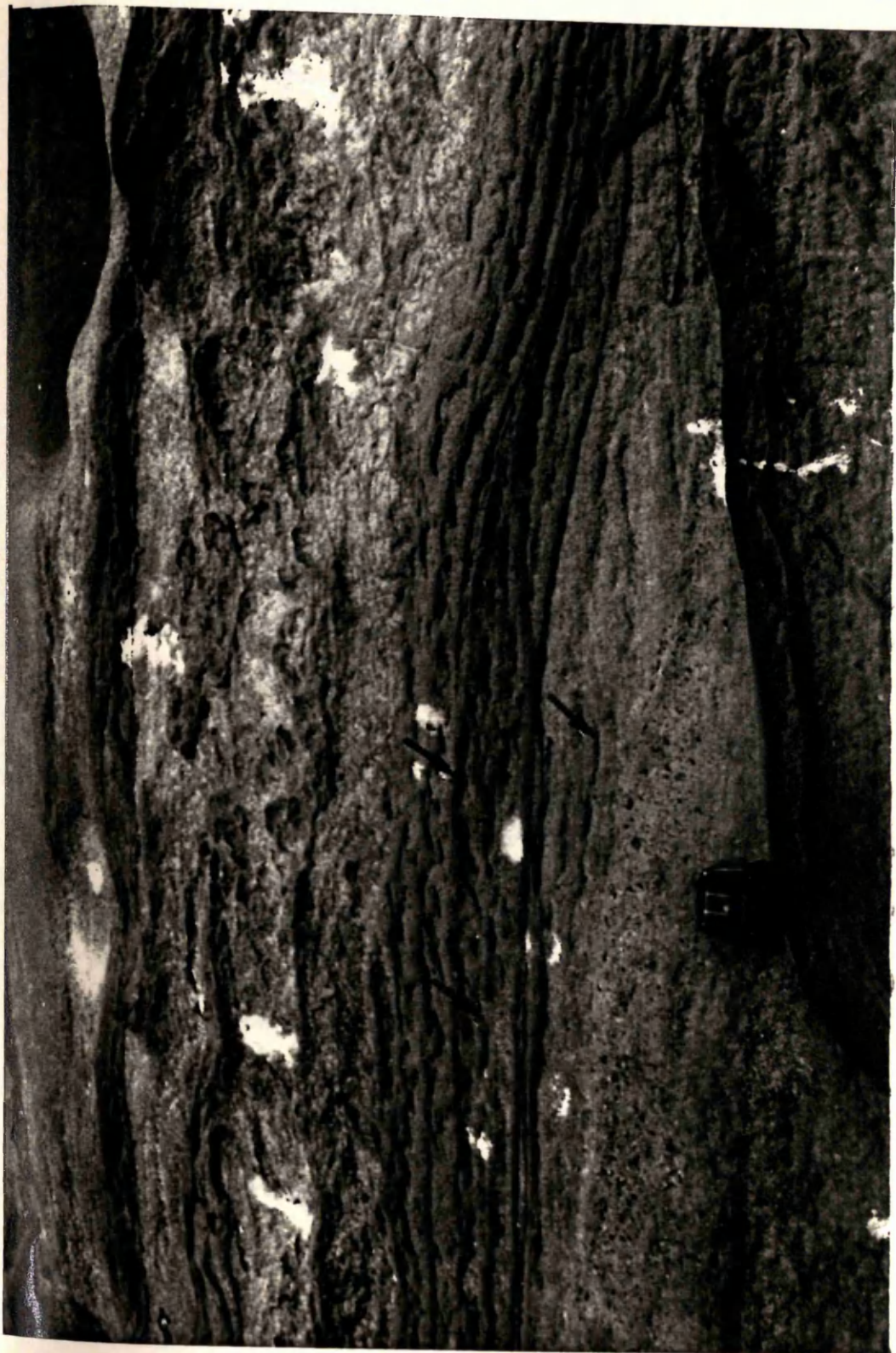


Figure 2.13 Mega-dishes and associated vertical pillars.

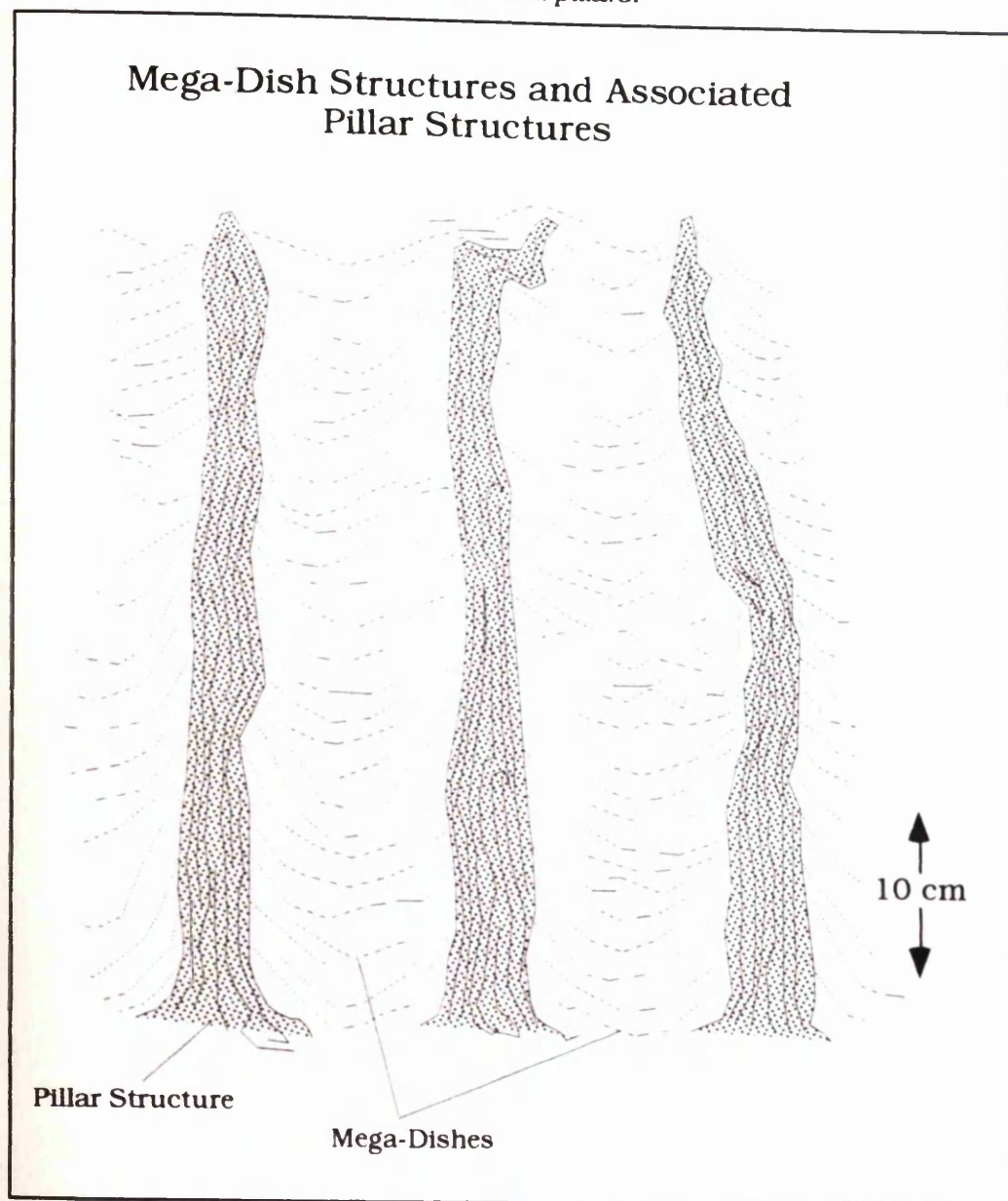


Figure 2.13 Diagram of mega-dishes and associated vertical pillars. Mega-dishes are defined as deep upward curving dishes that are 4-5cm deep.

Figure 2.14 Dish structured laminae (D) can often be found in medium grained sandstones that overlie microconglomerates (M). Photo from the Aljibe Arenites. Scale at base of photo is 3cm long.



Figure 2.14 Dish structured laminae that overlie micro-conglomerates.



Figure 2.15 Convolute overturned folds (F) observed in the Aljibe Arenites. Coin in centre of photo is 2cm in diameter.



Figure 2.15 Convolute overturned folds.





Figure 2.16 Convolute diapirs (D) emanating from a pillar (P). Photo from the Aljibe Arenites.  
Coin in centre of photo is 2cm in diameter.

Figure 2.16 Convolute diapir emanating from a pillar.



Figure 2.17 Diapirs (picked out by dashed lines) with discontinuous or disrupted tops (T).  
From the Aljibe Arenites. Scale is 3cm long.



Figure 2.17 Diapirs with disrupted tops.



Figure 2.18 Type A pillars (P) and associated mega-dishes (D). Photo from the Aljibe Arenites.  
Ruler is 25cm long.



Figure 2.18 Type A pillas and associated mega-dishes.

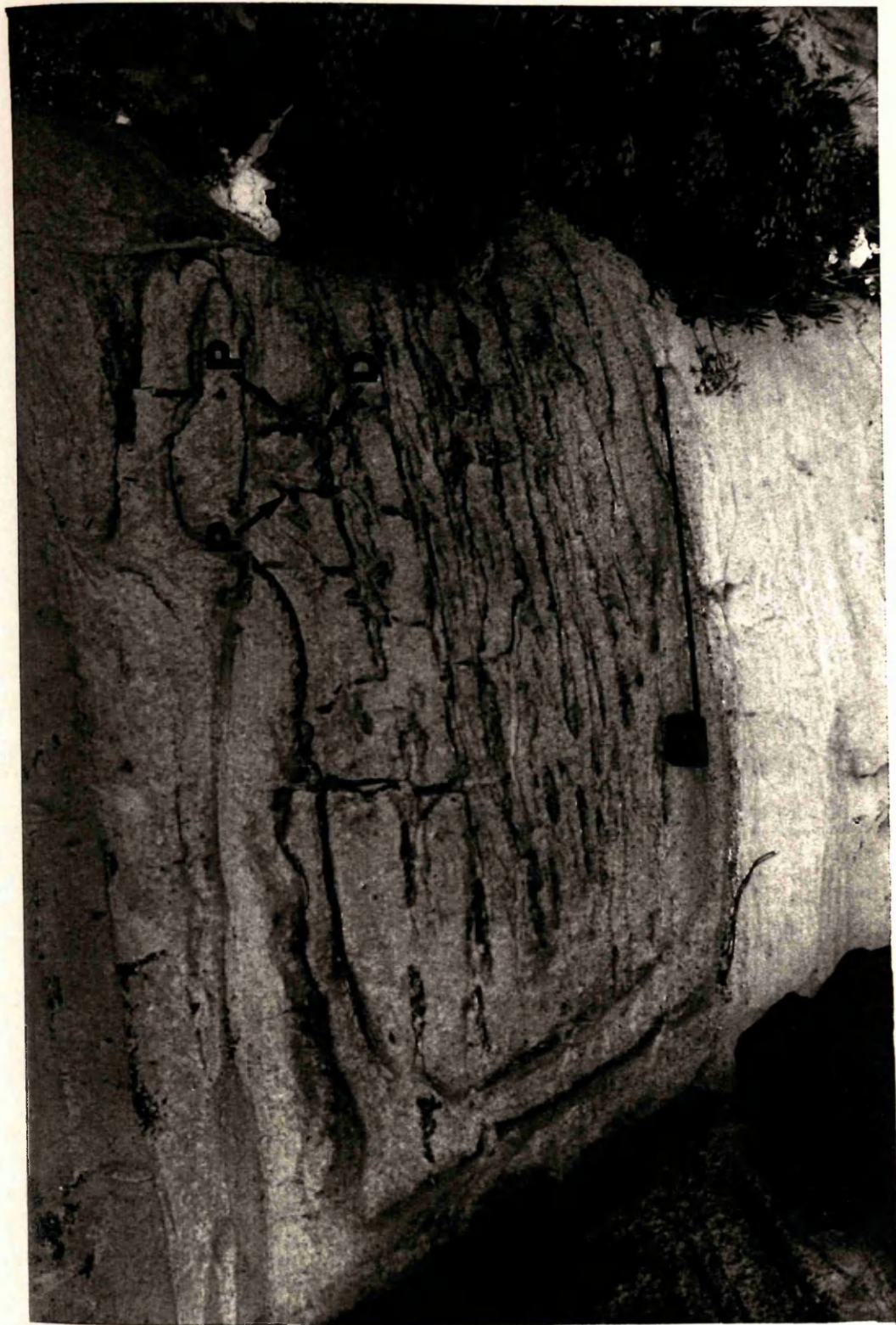




Figure 2.19 Sinuous pillar, found in the Aljibe Arenites. Top of coke can is 6cm wide.

Figure 2.19 Sinuous pillar.



**Figure 2.20 Bifurcating pillar from the Aljibe Arenites. Ruler is 10 cm long.**



Figure 2.20 Bifurcating pillar.

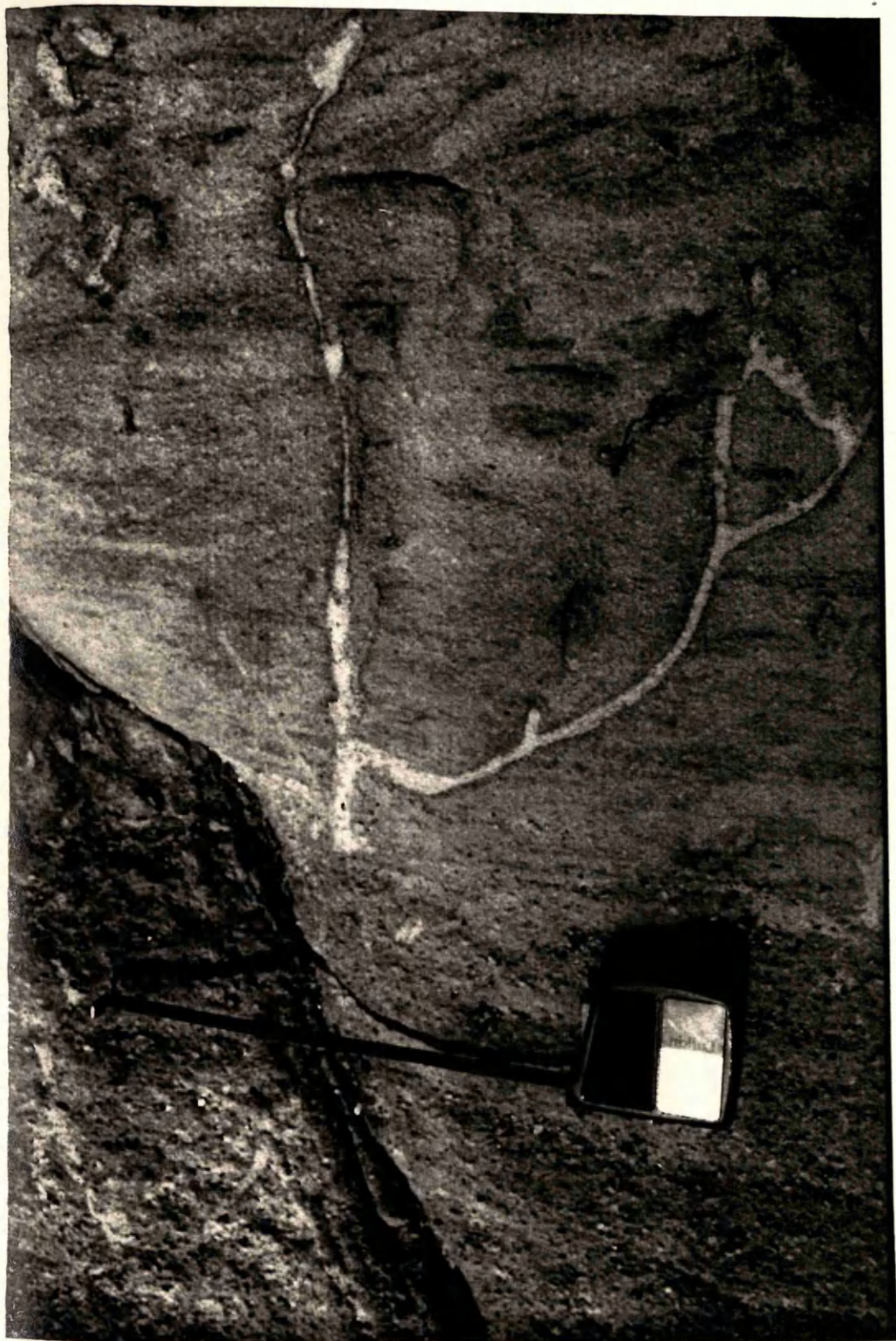


Figure 2.21 Type C pillars formed by diffuse lenticular streaks. These pillars are associated with the upper layers of beds. Bedding surface is marked by arrows. Bottle is 15cm long.



Figure 2.21 Type C pillars.

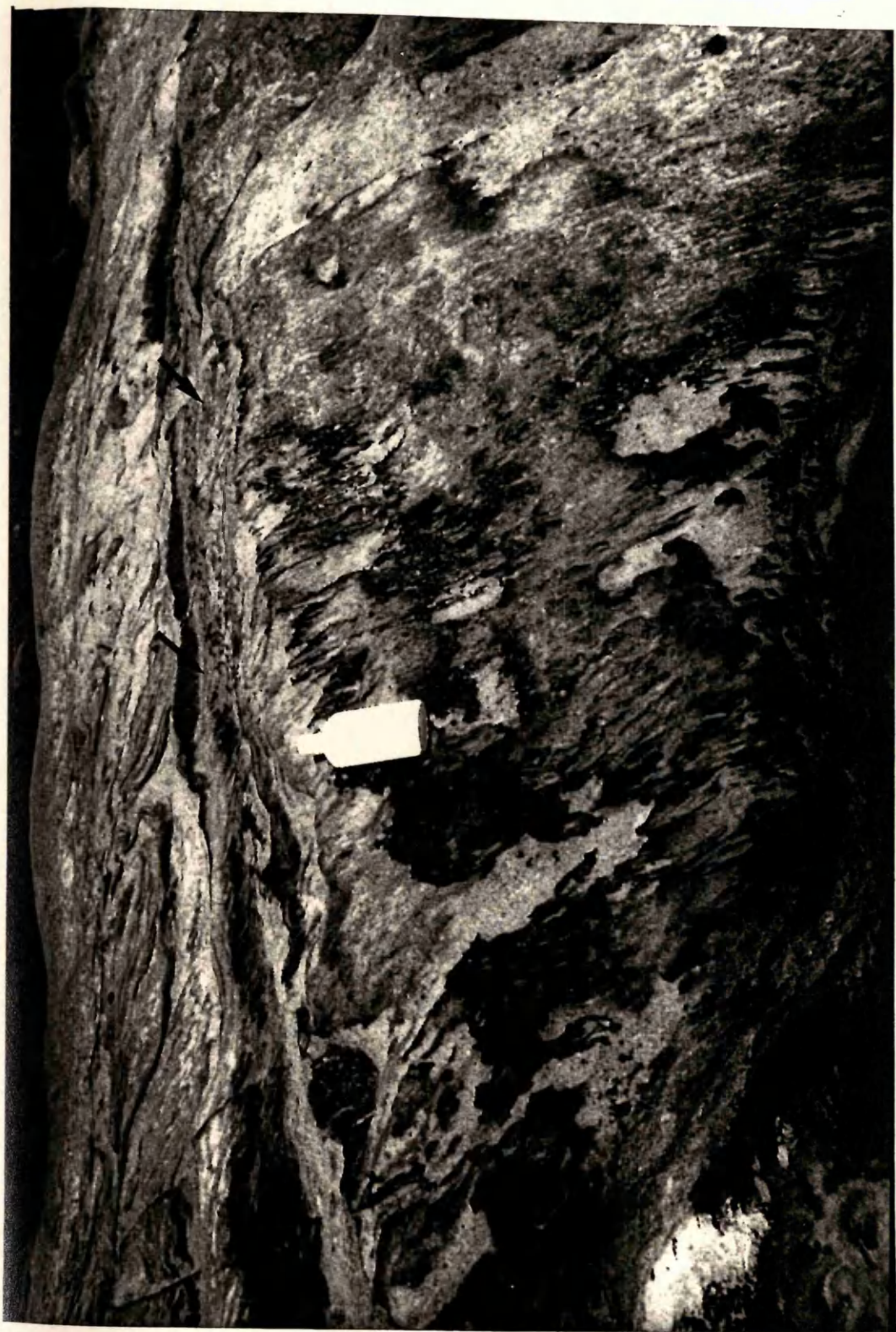




Figure 2.22 Type D pillars (D) exposed on a bedding surface where they form echelon sets. Type D pillars are termed 'stress pillars' (Lowe, 1975). Bottle is 15cm long.

Figure 2.22 Type D pillars.



Figure 2.23 Type E pillar, or sandstone intrusion (I). Photo from the Aljibe Arenites. Scale is 3cm in length.



Figure 2.23 Sandstone intrusion.



Figure 2.24 Downwards descending pillar (DP) in the Aljibe Arenites. Scale is 3cm long.



Figure 2.24 Downwards descending pillar.





Figure 2.25 Pillar (P) found in the core of a diaplir (D). Photo from the Aljibe Arenites. Ruler at the base of photo is 10cm long.

Figure 2.25 Pillar found in the core of a diapir.



Figure 2.26 A sand mound (M) exposed on a bedding surface. The sand mound is surrounded by concentric rings of heavy minerals (R). Mound is 50 cm wide.



Figure 2.26 Sand mound.



Figure 2.27 Diffuse streaks found in zones of complete mixing of dark and light sandstones that give a mottled appearance. Photo from the Aljibe Arenites. Bottle is 15cm long.



Figure 2.27 Diffuse streaks found in zones of complete mixing.





Figure 2.28 Typical sequence of structures found in the Aljibe Arenites. The sequence featured in this photo is: microconglomerate (A), dark laminae (B), dish structured laminae (C), mega-dishes (D), diapires (E) and diffuse streaks (F). The idealised sequence (Fig. 2.29) is constructed from this sequence and other similar sequences. Bottle is 15cm long.

Figure 2.28 Typical sequence of structures found in the Aljibe Arenites.

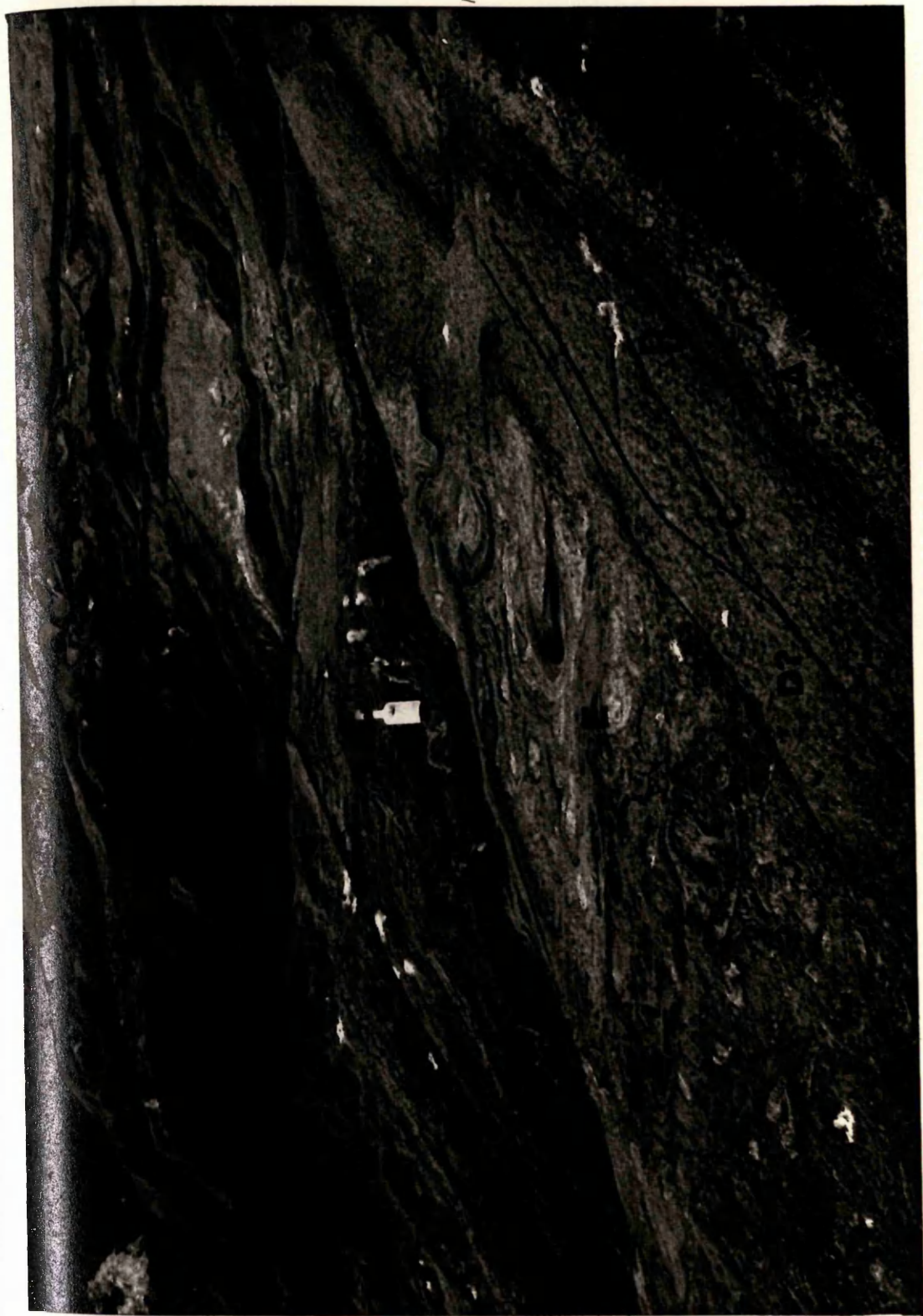




Figure 2.29 The idealised sequence of water escape structures.

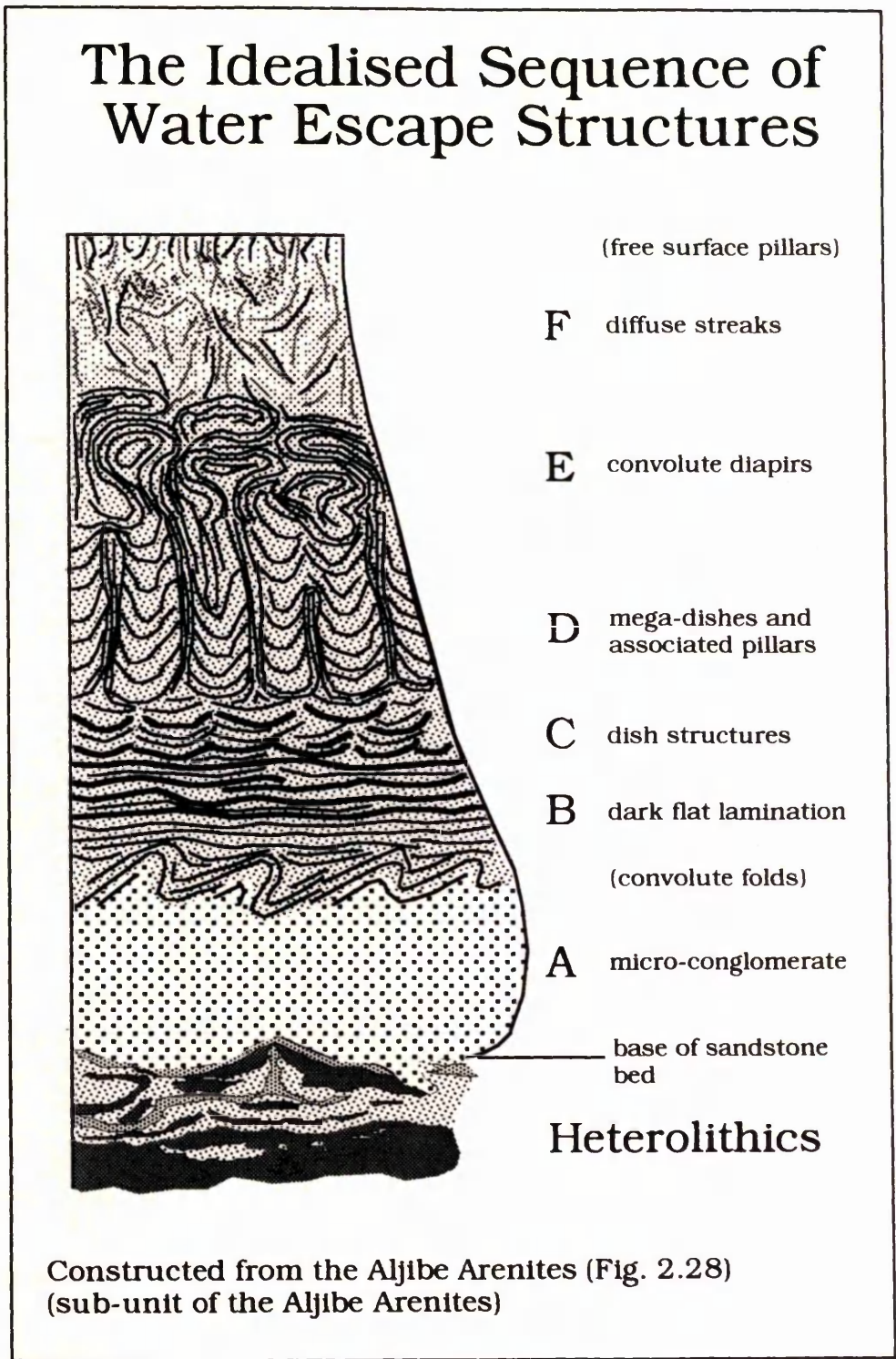


Figure 2.29 The idealised sequence of water escape structures constructed from sequences exposed in the Aljibe Arenites.



Figure 2.30 Coarse sandstone (S) passing directly into type B pillars (P) into which coarse sandstone may be injected (I).  
Photo from the Aljibe Arenites. Ruler is 10cm long.

Figure 2.30 Coarse sandstone passing directly into type B pillars.



Figure 2.31 Pillars (P) passing directly into convolute diapiers (D). Photo from the Aljibe Arenites. Ruier is 25cm long.



Figure 2.31 Pillars passing directly into convolute diapirs

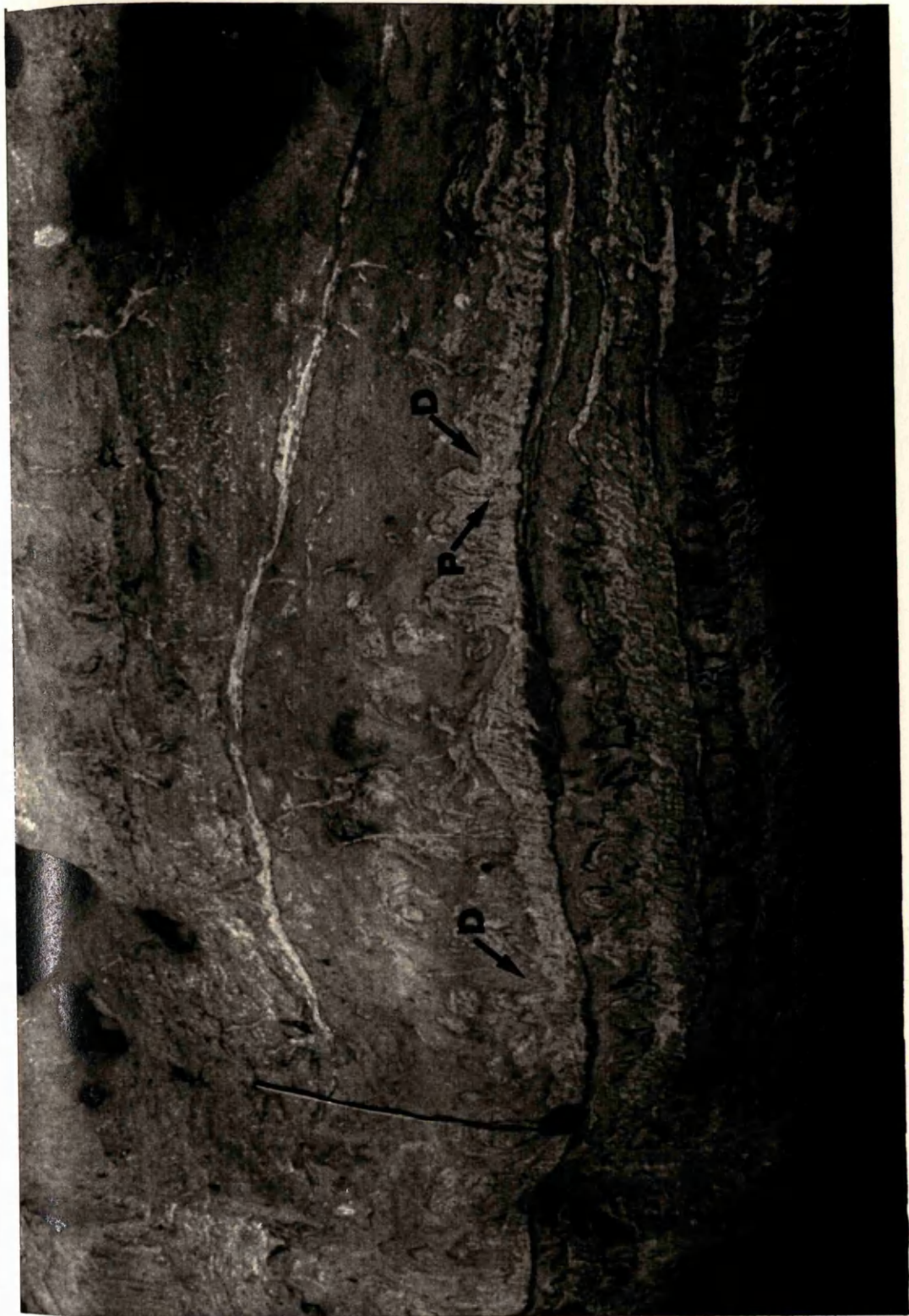


Figure 2.32 Dish structured laminae (L) passing directly into convolute diapirs (D). Photo from the Aljibe Arenites. Bottle is 15cm long.



Figure 2.32 Dish structured laminae passing directly into convolute diapirs.





Figure 2.33 Overturned pillars (O) in the Aljibe Arenites. Scale is 3cm long.

Figure 2.33 Overturned pillars.





Figure 2.34 Heterolithic intervals, Aljibe Arenites.

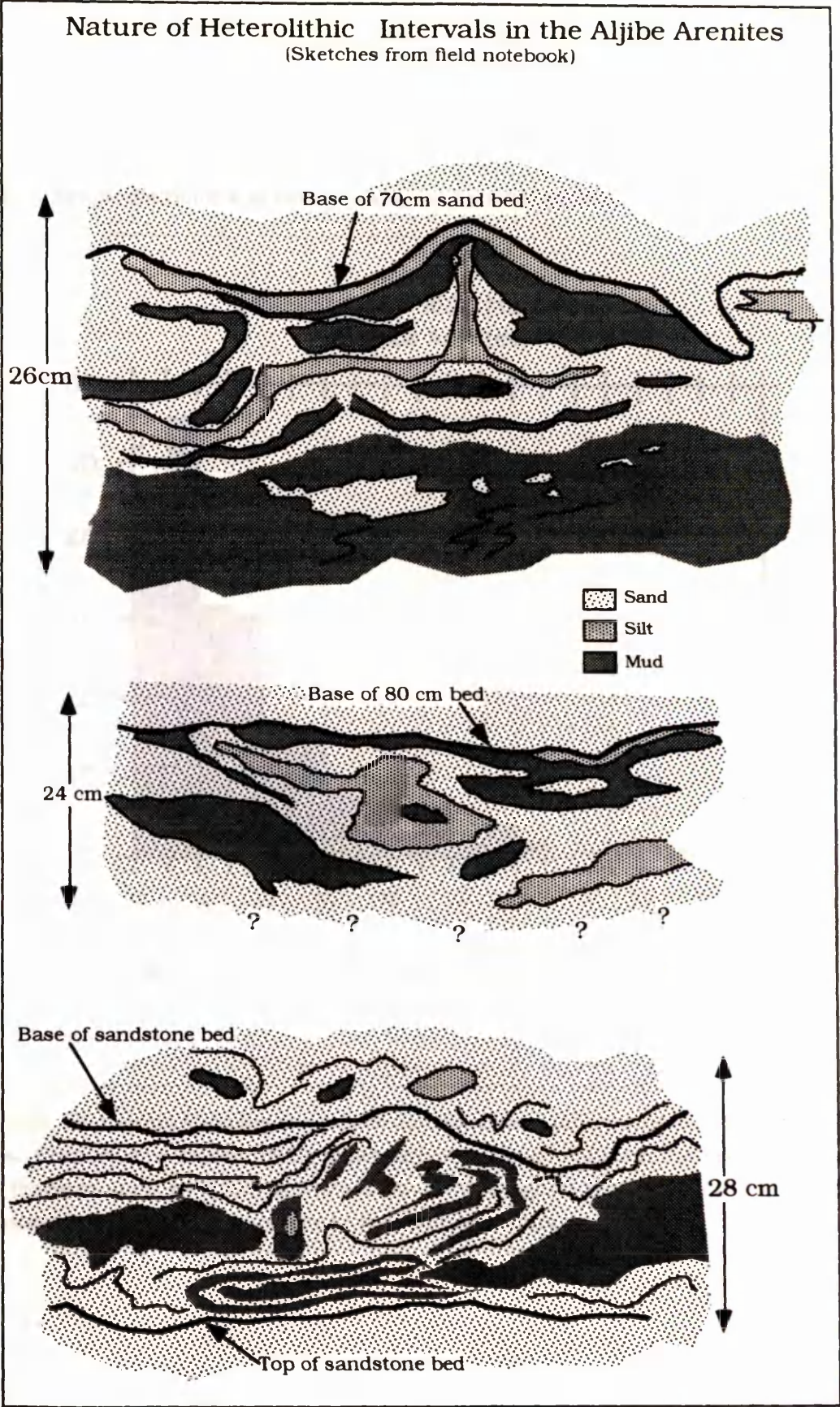


Figure 2.34 Diagrams of heterolithic intervals found in the Aljibe Arenites. Heterolithics are pervasively mixed and display injection structures.



Figure 2.35 Height distribution of pillars measured from the Aljibe Arenites.

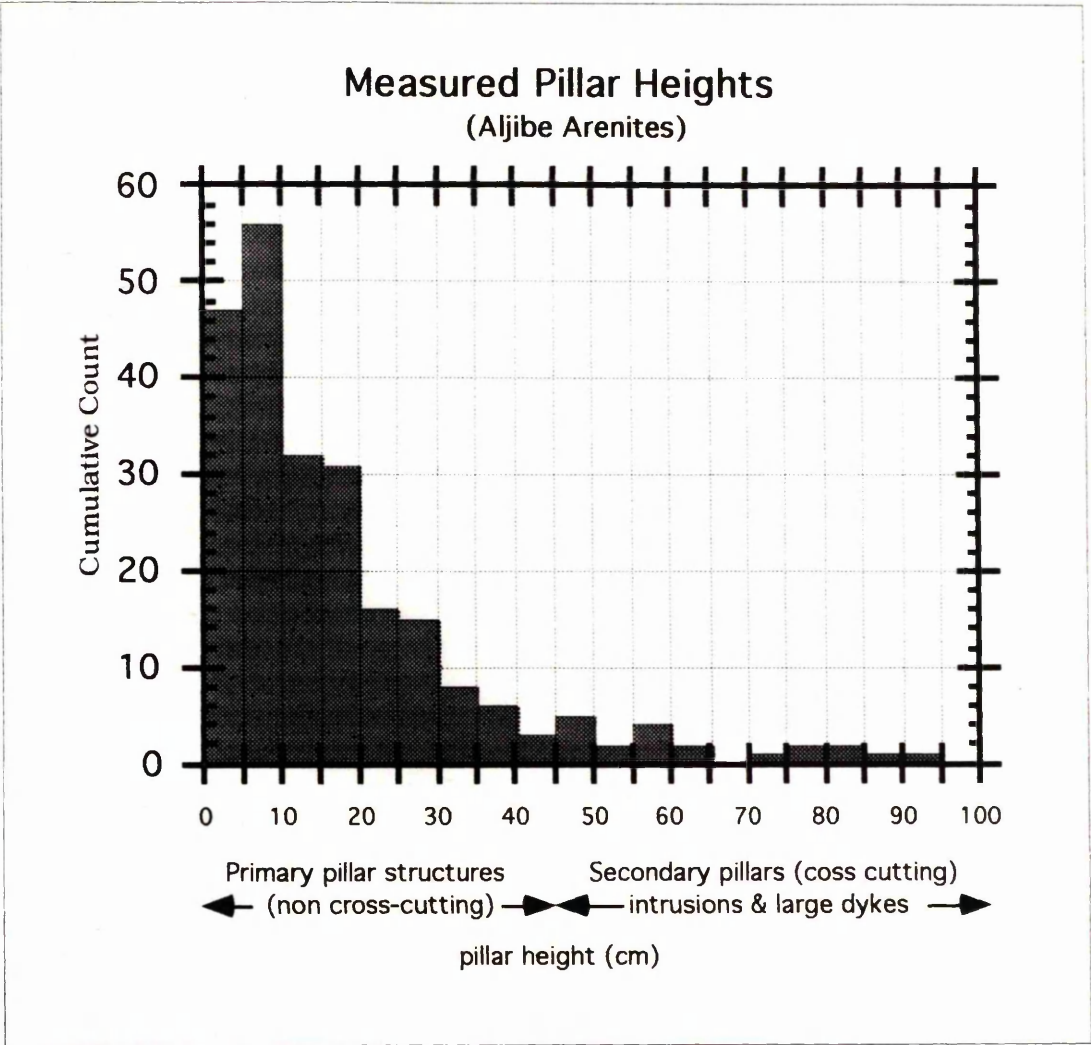


Figure 2.35 Histogram showing the height distribution of pillars measured from the Aljibe Arenites. Primary non-cross-cutting pillars are much more common than secondary cross-cutting features such as dykes or intrusions. This suggests that cross-cutting pillars are rarely formed relative the occurrence of fluidisation events.

Figure 2.36 The Beneiza Flysch to Aljilbe Arenites transition. The boundary between the Beneiza Flysch (F) and Aljilbe Arenites (AA) is a sharp non-gradational boundary (C). Across this contact there is a dramatic change of thin bedded turbidites in the Beneiza Flysch to thick and dewatered sandstones in the Aljilbe Arenites. Section is approximately 30m high.

Figure 2.36 The Benetza Flysch to Aljibe Arenites transition.





# ***Part III***

## ***Figures***



Figure 1 The Alboran domain

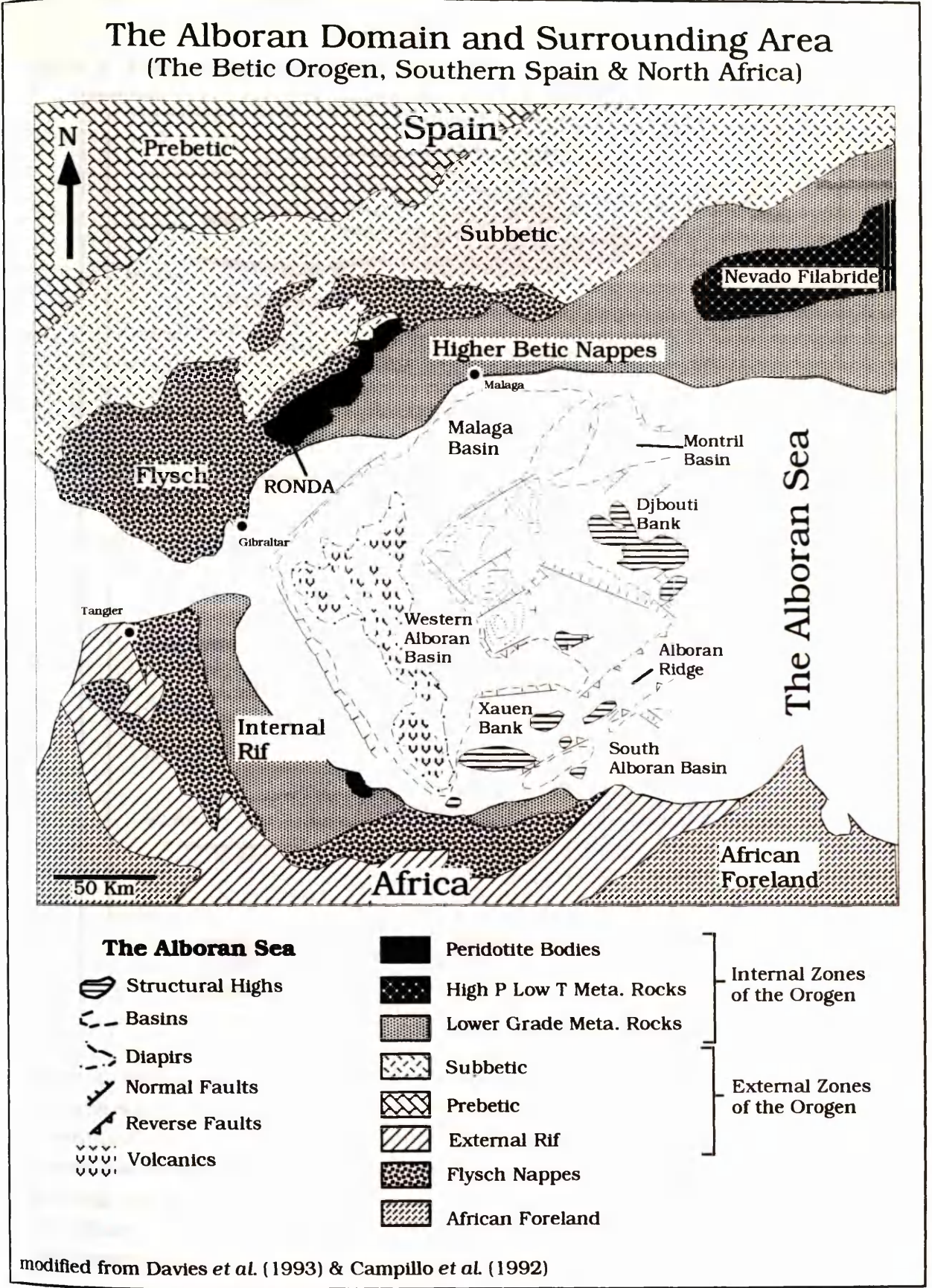


Figure 1 A summary geological map for the Alboran domain and surrounding area. Figure modified from Davies *et al.* (1993) and Campillo *et al.* (1992).

Figure 2 Model for emplacement of the peridotites.

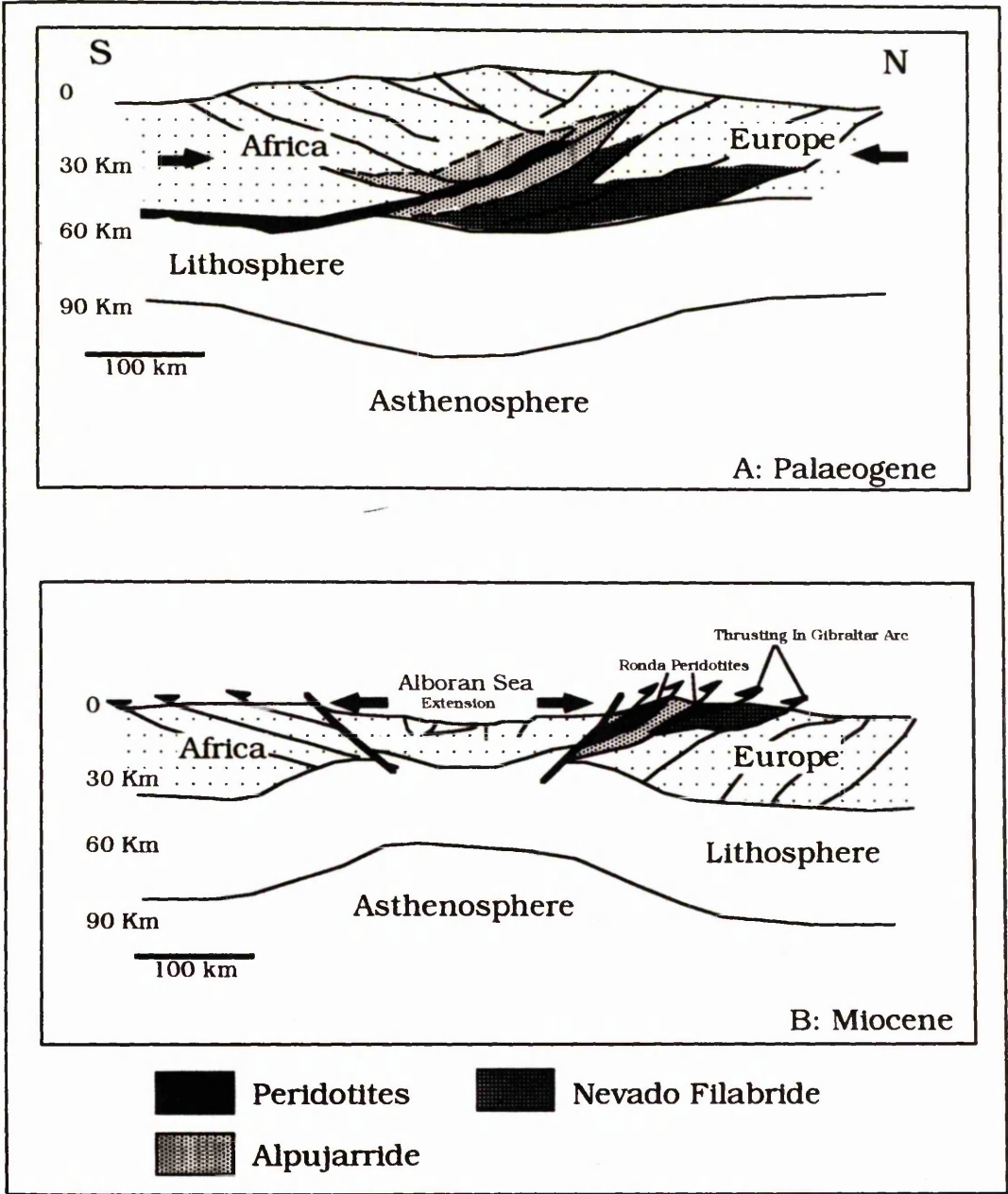


Figure 2. Model for emplacement of the peridotites. Diagram inferred from explanation given by Torné et al. (1989). (A) peridotites initially emplaced during Palaeogene, at which time they constituted a slab of lithospheric mantle within units of the Alpujarride. How this was achieved is not made clear but presumably Torné et al. (1989 ) envisaged a phase of thrust stacking. (B) During the Miocene crustal stacking, related to thrusting in the Gibraltar Arc and rifting in the Alboran sea, unrooted and dismembered the peridotites placing, them in their present position.



Figure 3 Proposed evolution of the western Mediterranean. A: Formation of high-P, low-T metamorphic facies during continental collision at ~85 Ma. and subsequent nappe emplacement. These events caused uplift of diamondiferous eclogites, diamond graphitization, and the first stage of nappe emplacement. B: Slab detachment at ~20 Ma. resulted in rapid uplift of hot asthenosphere and emplacement of second generation of nappes. C: cooling of hot asthenospheric mantle caused rapid subsidence of orogen core and a topographic inversion. Margins of fold belt returned to lithostatic equilibrium, unroofing peridotite massifs. Figure from Davies et al. (1992)

Figure 3 Proposed evolution of the western Mediterranean

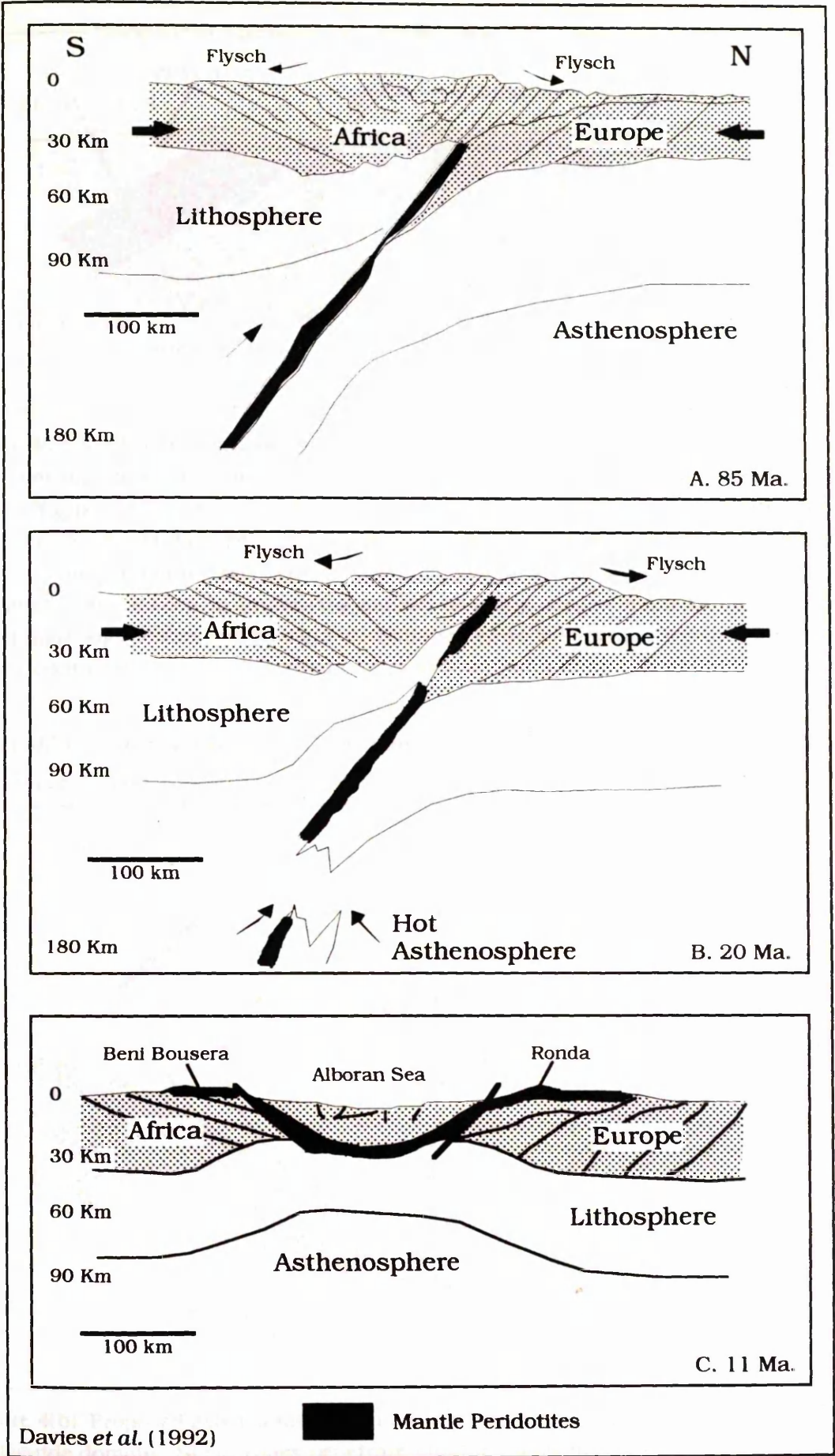


Figure 4(a) Schematic cross-section across the Maláguide Complex and Los Reales Nappe.

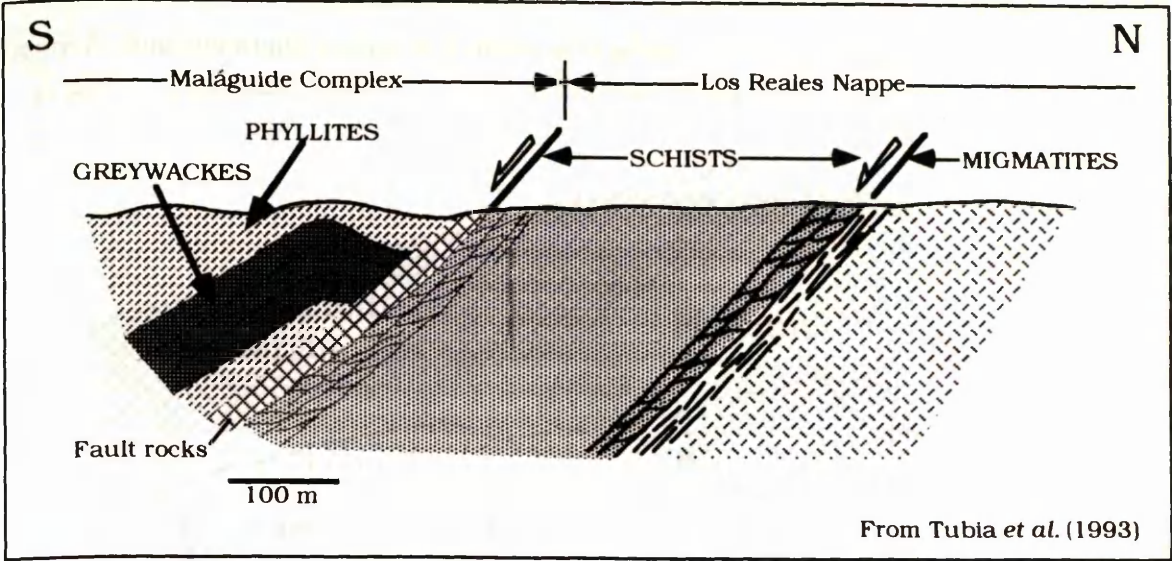


Figure 4(a) Schematic cross-section showing structures related to extensional deformation. Roll-over anticlines develop when the contact between the Maláguide Complex and Los Reales Nappe cuts across competent layers of the Malaguide Complex. Restoring the slope of the Los Reales-Maláguide contact to the horizontal, this structure reflects a hangingwall ramp. Gouge and fault breccias mark out the Maláguide-Los Reales contact, whereas S-C mylonites can be seen in underlying schists or along deeper contacts. This structural variation along the same extensional deformation episode suggests that the Maláguide-Los Reales contact is an extensional fault. Figure from Tubia et al. (1993).

Figure 4(b) Proposed geodynamic model for the extensional deformation in the Los Reales-Maláguide domain.

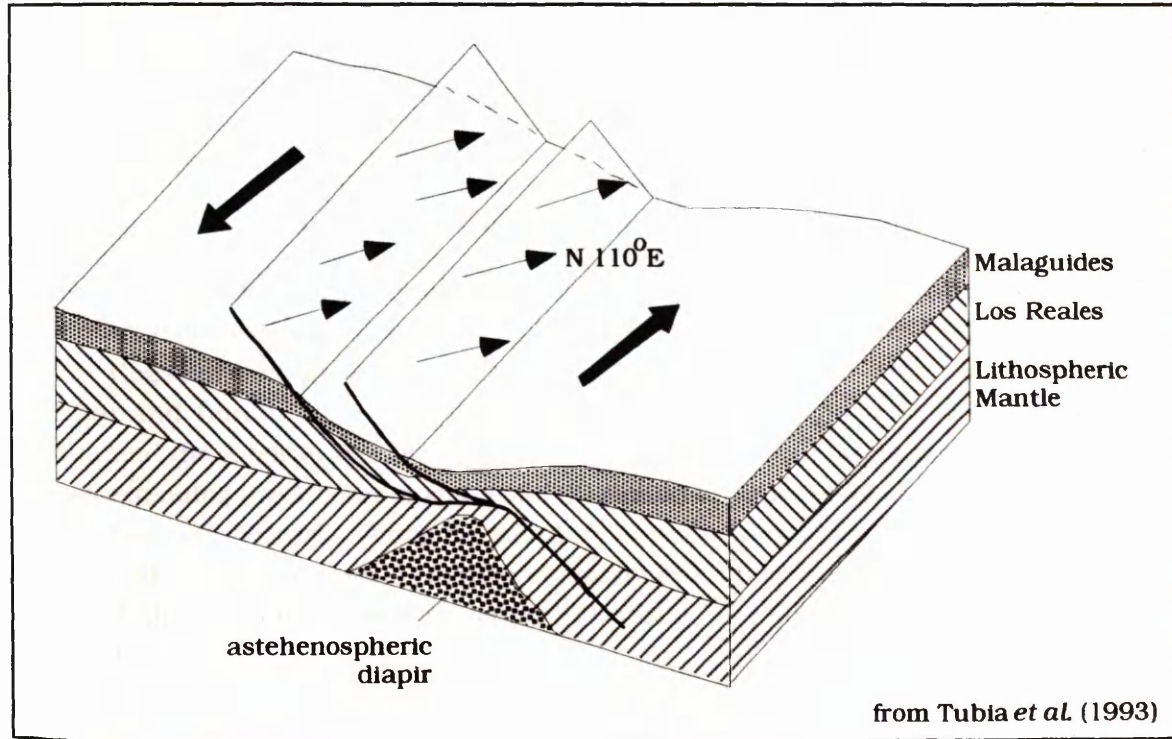


Figure 4(b) Proposed geodynamic model for the extensional deformation in the Los Reales-Maláguide domain. Shear zones penetrate into the lithosphere mantle, in accordance with the mylonitization of upper levels of the Ronda peridotites. Stretching lineations (thin arrows) are oblique to the rift axis, marked by plagioclase peridotites, suggesting a transtensional



Figure 5 Time-averaged motion of Eurasia and Africa.

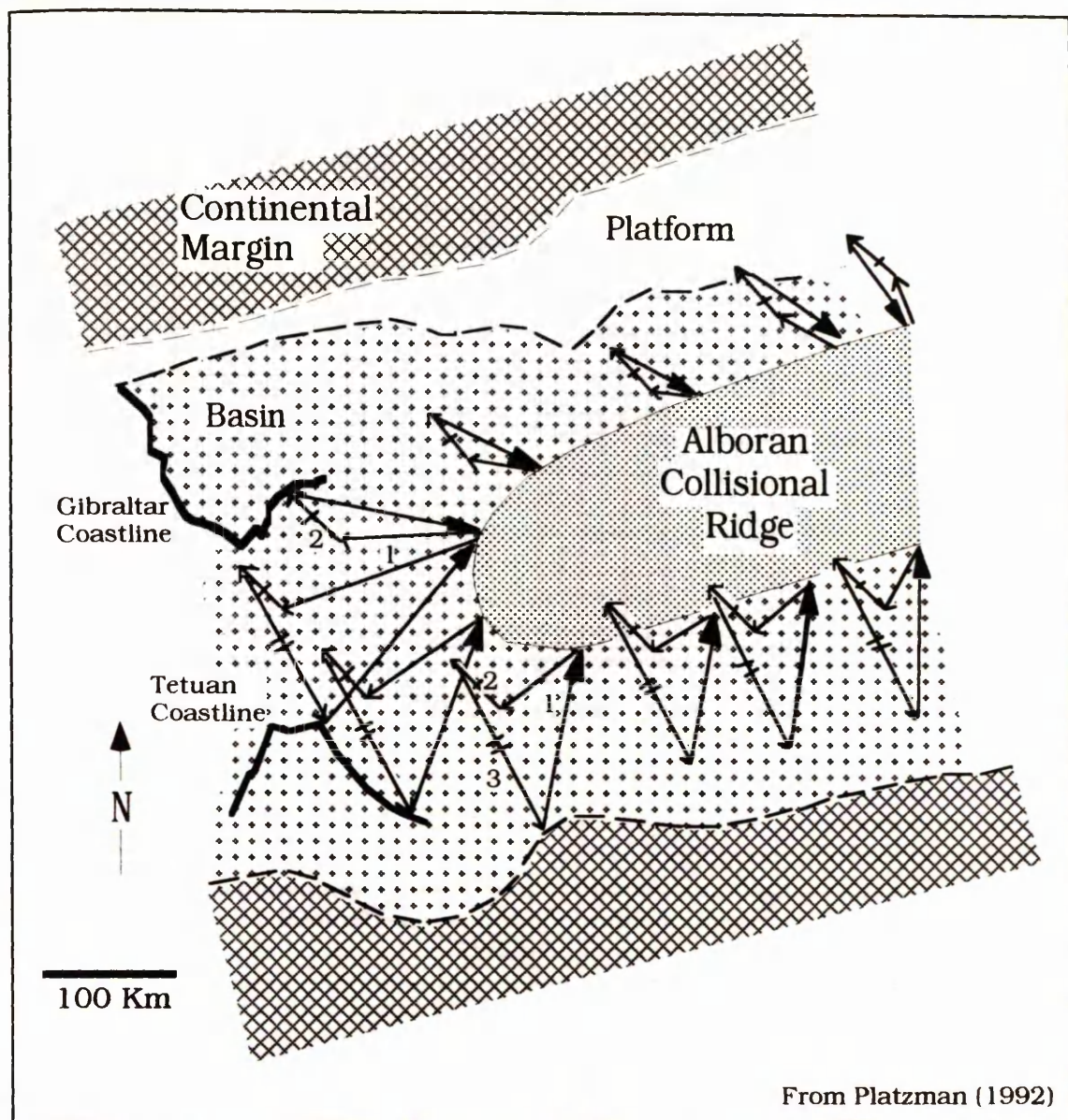


Figure 5. Schematic diagram illustrating time-averaged motion of Eurasia and Africa relative to the margin of the Alboran domain from 27 Ma. to the present (modified from Platt & Vissers, 1989). Regional configuration during mid-Oligocene is shown with coastlines around Gibraltar and Tetuan for reference. Along the northern margin relative motion between Eurasia and the Alboran margin is derived from (1) motion of margin relative to the centre of mass extending the Alboran domain and (2) motion of centre of mass of extending Alboran domain relative to Eurasia. Along the southern Alboran margin, the motion of Africa relative to the margin is derived from (1) motion of margin relative to the Alboran center of mass (2) motion of Alboran centre of mass relative to Eurasia, and (3) motion of Eurasia relative to Africa (from Dewey et al., 1989)

Figure 6 Rotation in simple shear zone.

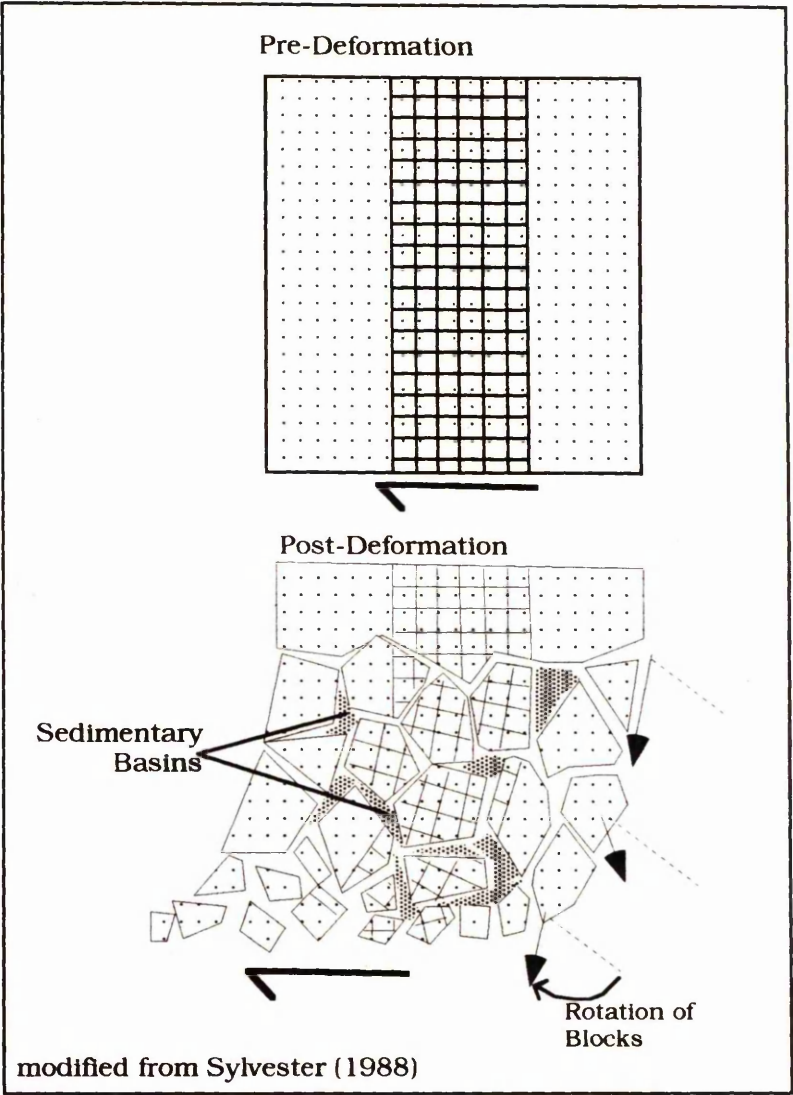


Figure 6 Mechanism of rotation in simple shear zone. Small block model (i.e. terrain blocks) with variable internal rotation. Sedimentary Basins may open up between blocks, and this may be the mechanism by which the internal basins of the Betic Orogen formed (Diagram modified from Sylvester (1988)).



Figure 7 Structural sections through the Betic Movement Zone.

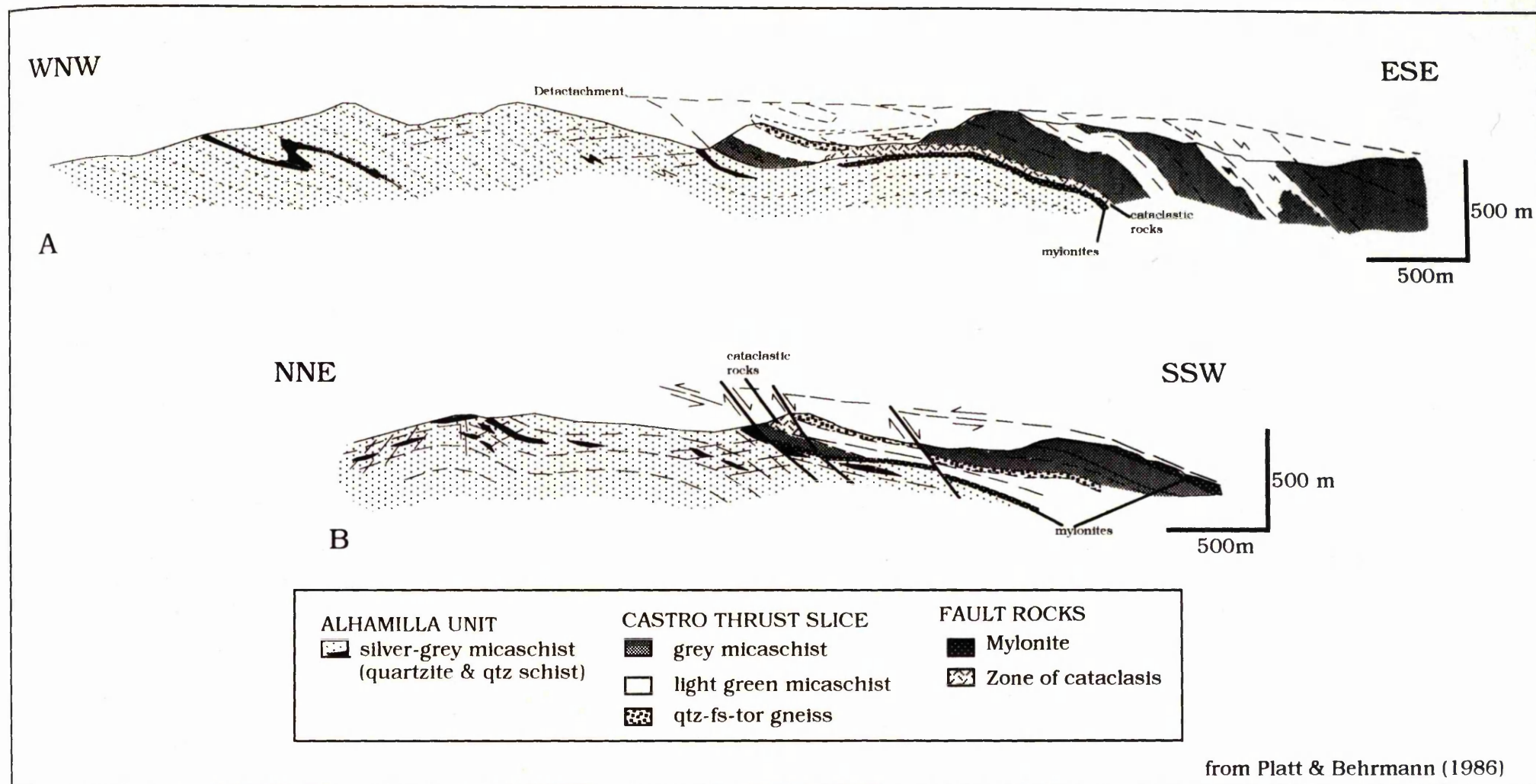


Figure 7 Structural sections through the Betic Movement Zone. (A) section normal to main phase folds and stretching lineation. (B) section parallel to the main phase stretching lineation, and hence probable direction of nappe transport. Figure modified from Platt & Behrmann (1986).



Figure 8(a) Iberian margin 65-27 Ma.

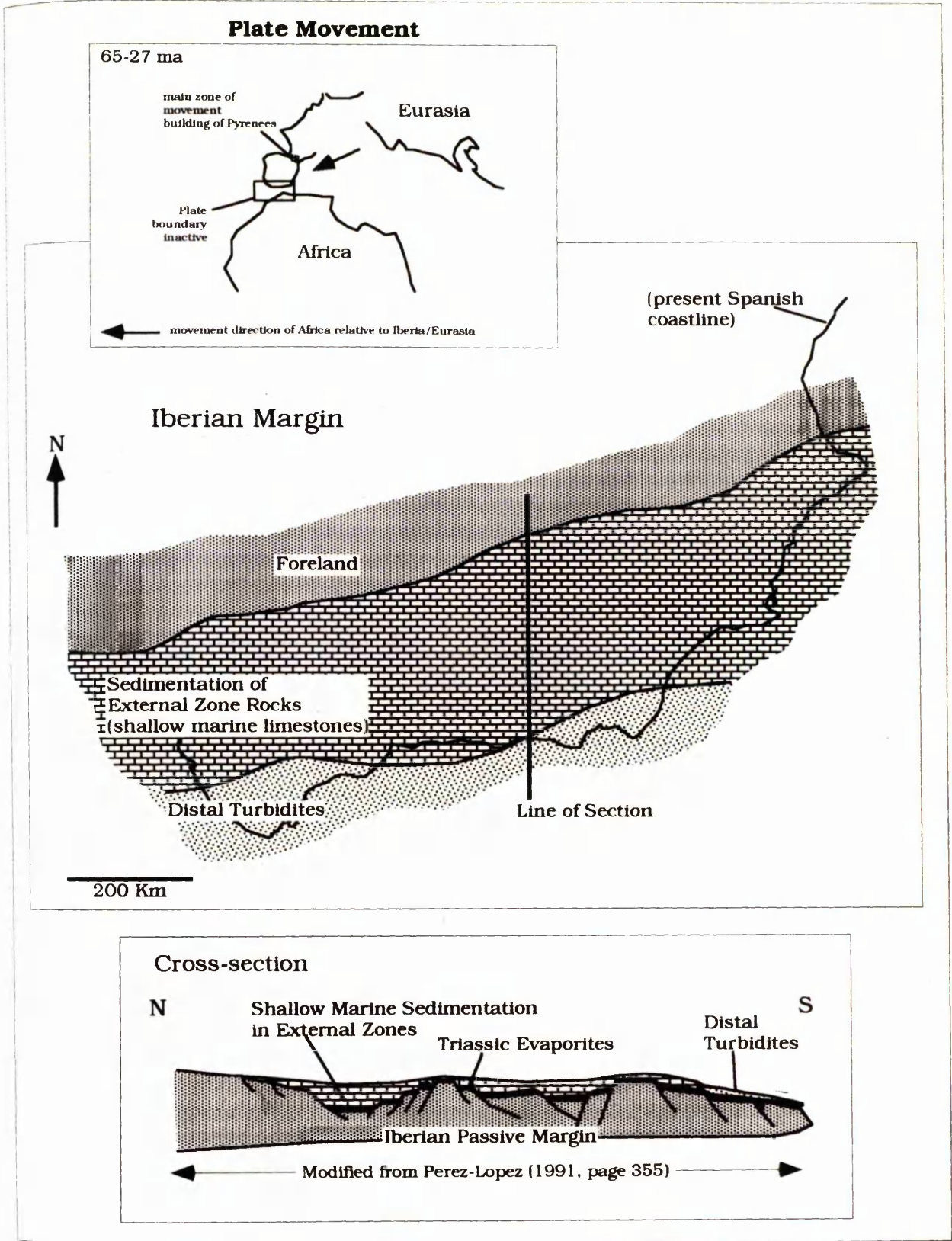


Figure 8(a) Iberian margin 65-27 Ma. Plate boundary inactive between Iberia & Africa (Sirvastava, et al., 1990a), with main plate movements at this time accommodated between Iberia & Eurasia leading to the building of the Pyrenean mountain chain. During this inactive period sedimentation of the External Zone rocks took place on an extended Iberian Margin. Plate movement model modified from Dewey et al. 1973) using data from Sirvastava, et al. (1990a).

Figure 8(b) During the Miocene the plate boundary became active as Africa rotated into Iberia (Sirvastava et al., 1990a). The first events recorded were extension in the Alboran Domain and compression along the northern margin of the External Zones (in the region now occupied by the Guadalquivir Basin). Extension in the Alboran Domain led to the break up of the western parts of the External Zone and the formation of small and confined pull-apart basins into which sediment, mobilised from the External Zone, was rapidly deposited. Compression along the northern margin of the External Zone is more difficult to explain but may have been induced by the arrival of metamorphic terranes which required deflection of the plate boundary to accommodate them. These terranes, which now form the Internal Zones, are interpreted to have been emplaced by lateral movement along strike slip faults. Plate movement model modified from Dewey *et al.* 1973) using data from Sirvastava, et al. (1990a).



Figure 8(b) Miocene evolution of the Betic Orogen.

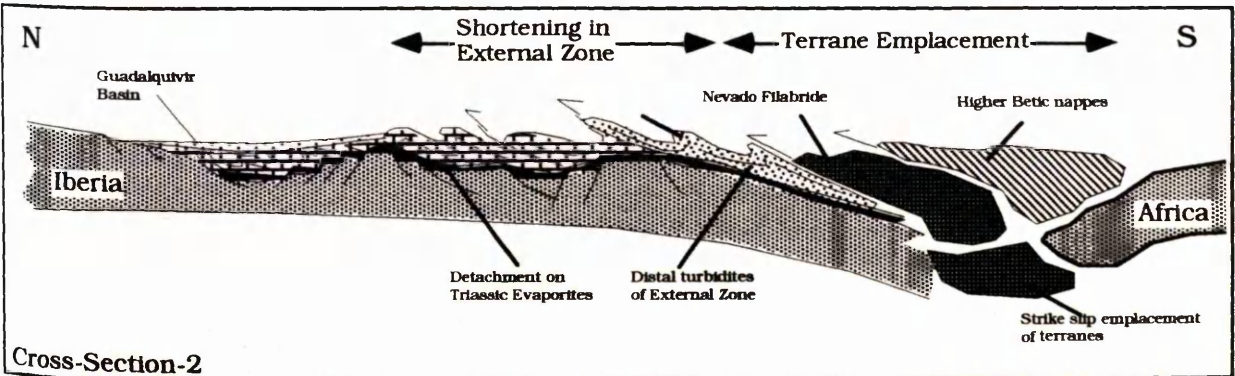
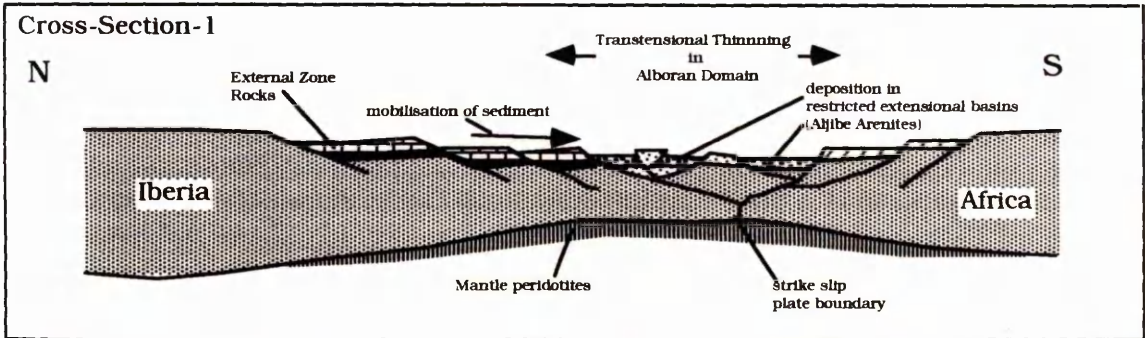
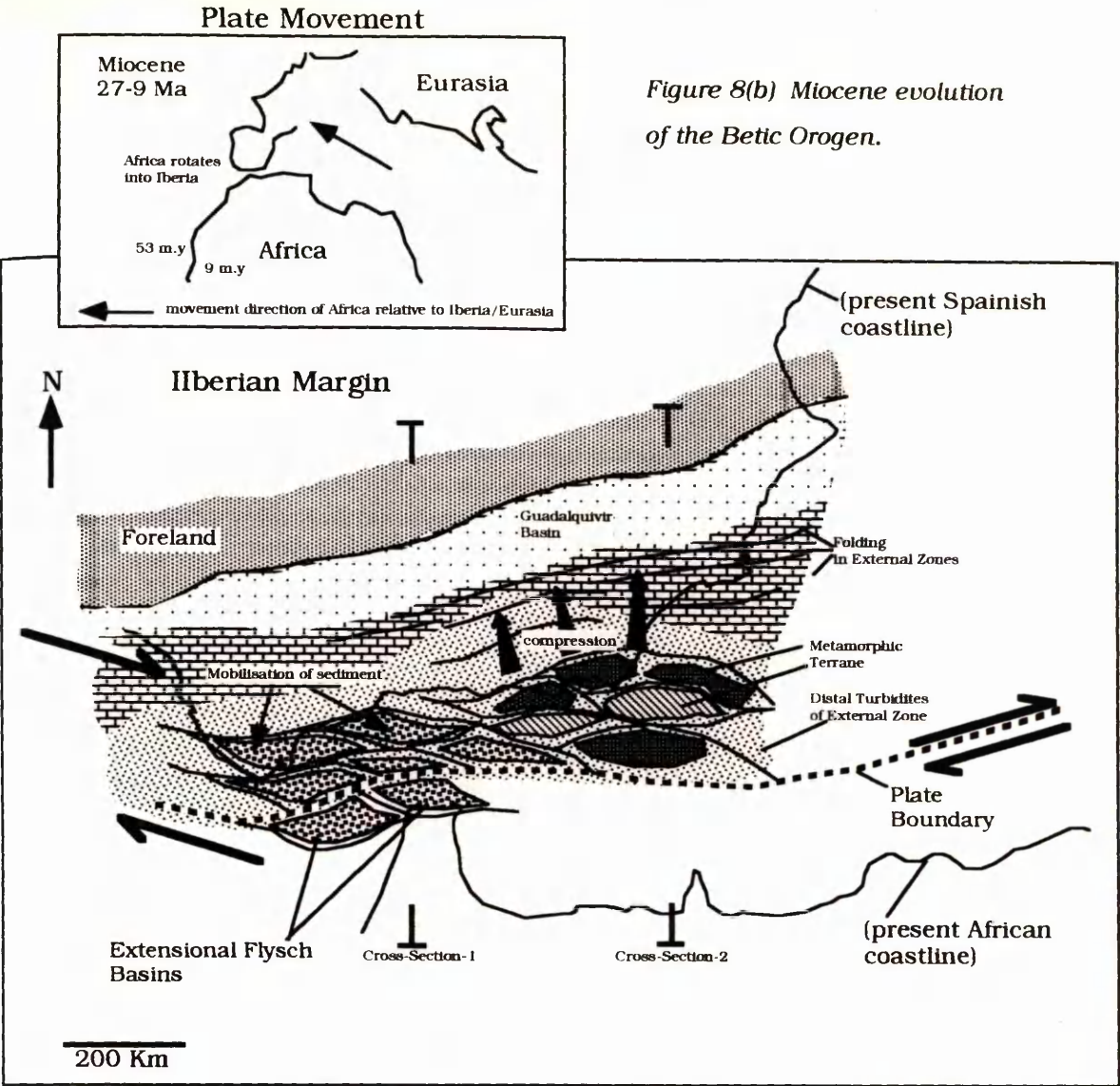




Figure 8(c) Towards the end of the Pliocene the convergence of Africa and Iberia became less oblique, as Africa began to move in a more northerly direction (Campillo et al., 1992). This resulted in the mainly transtensional regime becoming more transpressional. Related compression resulted in tectonic inversions, movements including the thrusting and the emplacement of peridotites into their present position and the destruction of the Guadalquivir Basin, which became subdivided into the allochthonous and autochthonous zones present today. Plate movement model modified from Dewey et al. 1973) using data from Sirvastava, et al. (1990a).

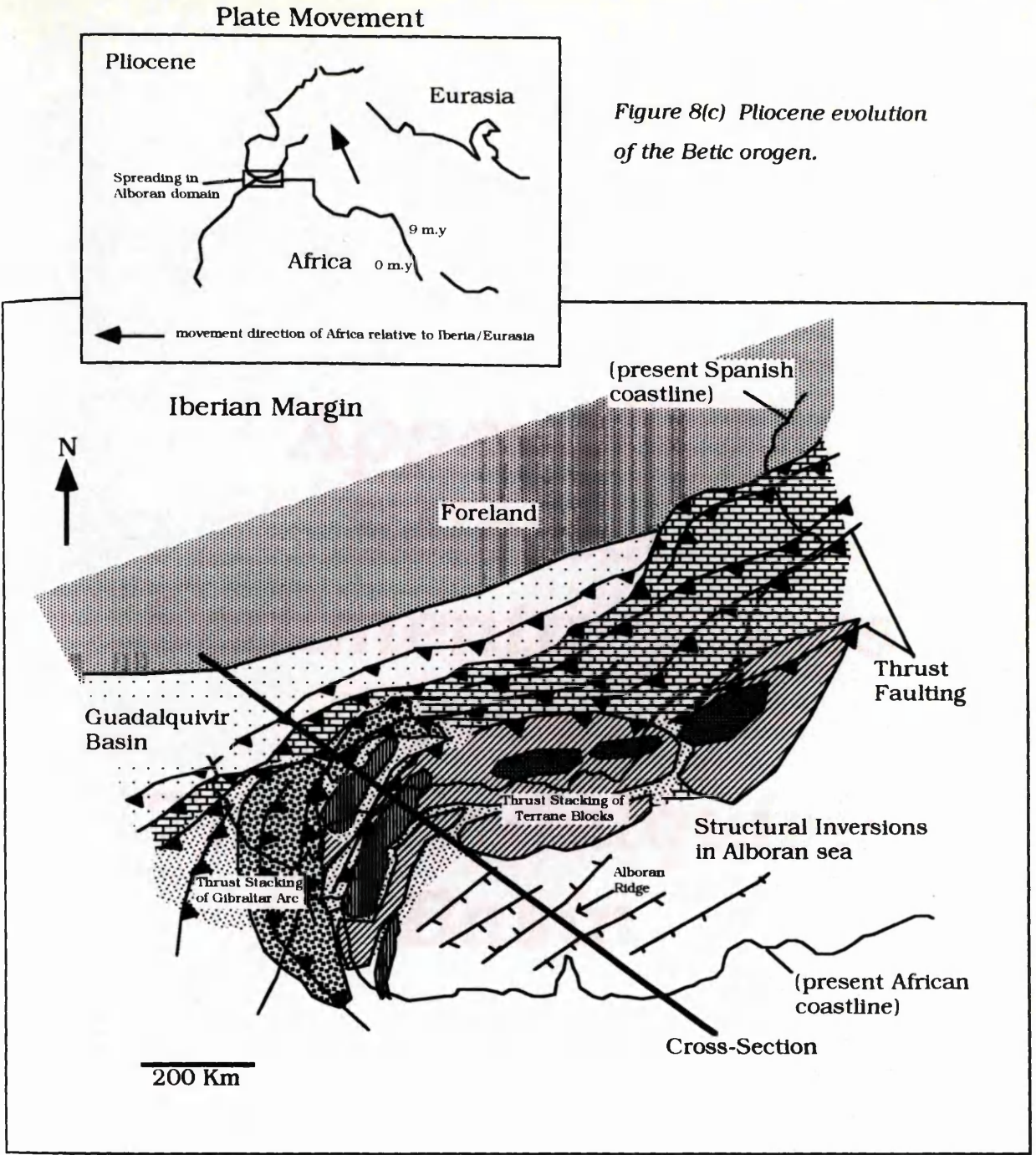
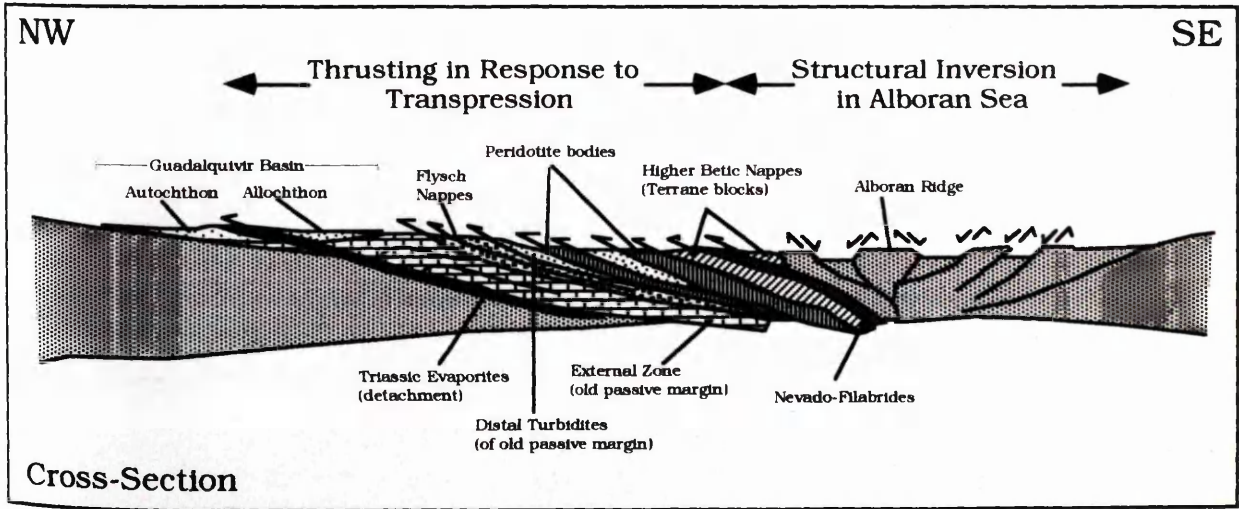


Figure 8(c) Pliocene evolution of the Betic orogen.





**Appendix I**  
**Selected**  
**Sedimentary Logs**  
**From**  
**The Guadalquivir**  
**Basin**



The following appendix gives a representative sample of sedimentary logs taken from the Guadalquivir Basin. For each log the location numbers are given. For each location there is a corresponding grid reference and relevant thesis map which are given in Appendix V. Thesis maps are can be found in Foldouts 1,2 &3 (Maps).

# Key to Logs Taken From the Guadalquivir Miocene Basin

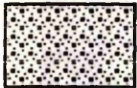
## Lithology



Marl



Laminated  
Diatomite Clay/  
Globgerinid Marls



Calc-Lithic  
Arenite



Siltstone



Skeletal  
Grainstones



Carbonaceous  
Detritus



Conglomerate



Rootlets



Conglomerate  
with Algal Bound  
Clasts & Oyster  
Shell Fragments

## Sedimentary Structures



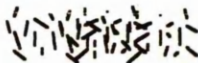
Hummocky Cross-  
Stratification (HCS)



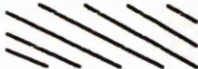
Swaley Cross-  
Stratification (SCS)



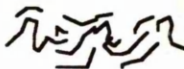
Planar Lamination



Bioturbation



Cross-Stratification



Convolute-Lamination



Ripple Cross-  
Lamination

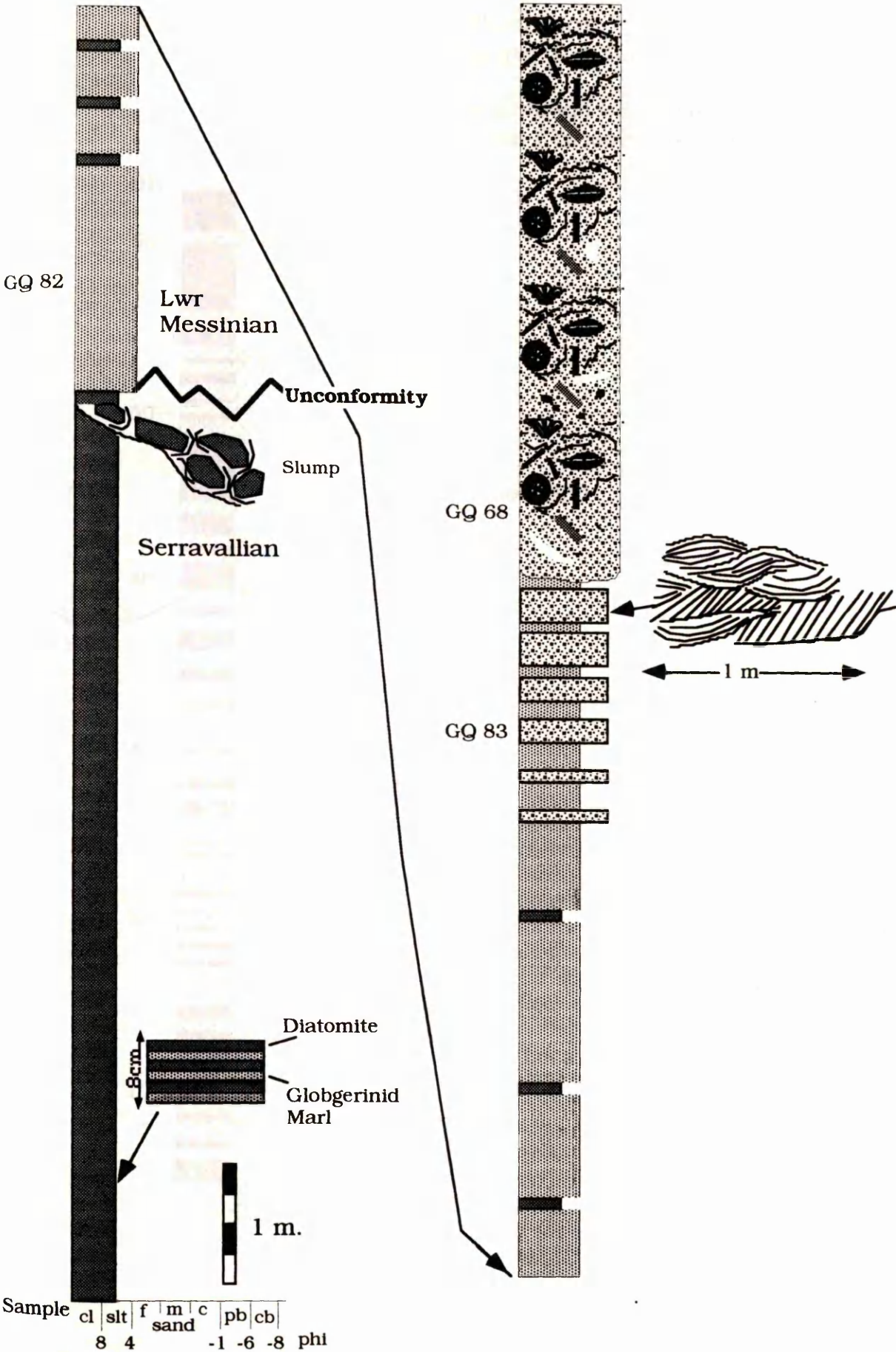


Asymptotic X-lamination



Palaeocurrent vector

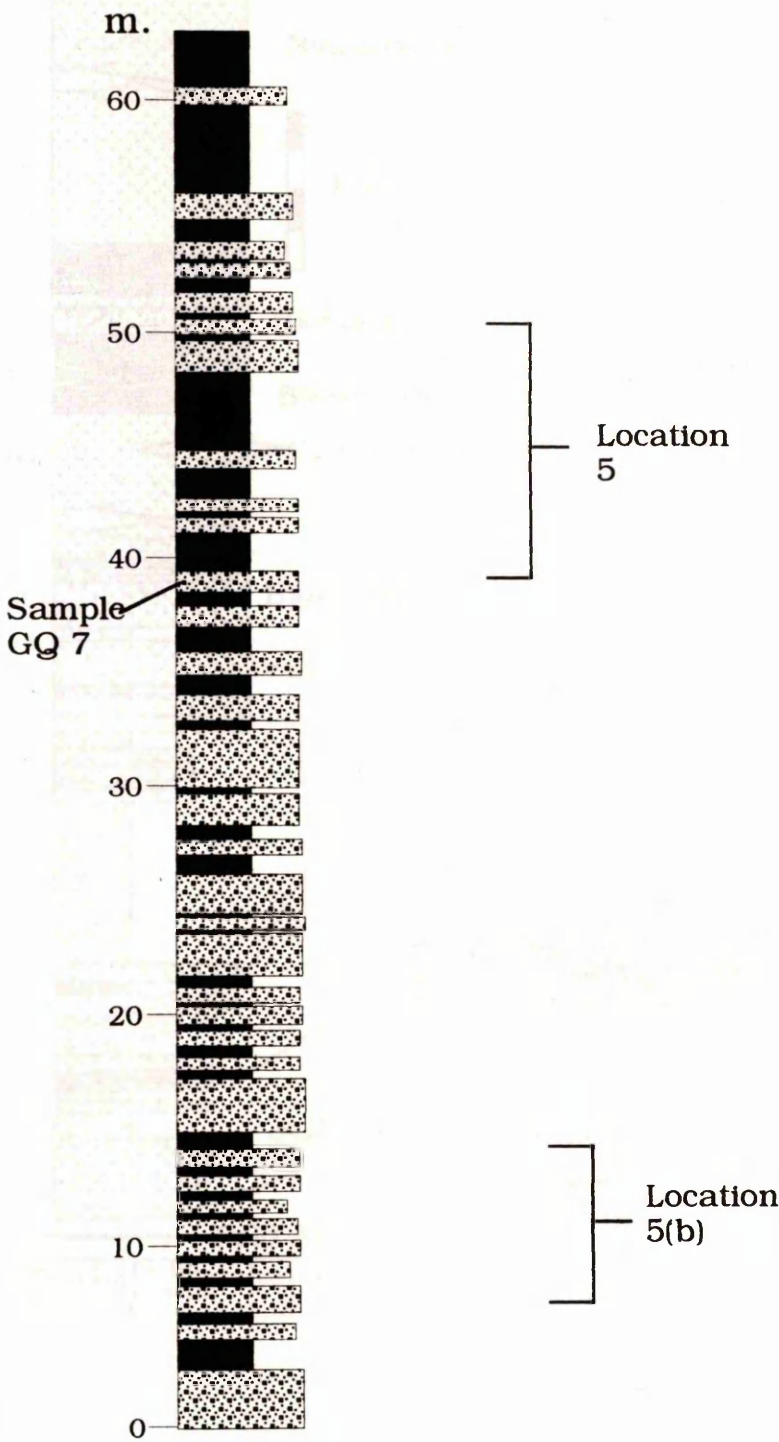
Serravallian-Lwr Messinian  
Location 44





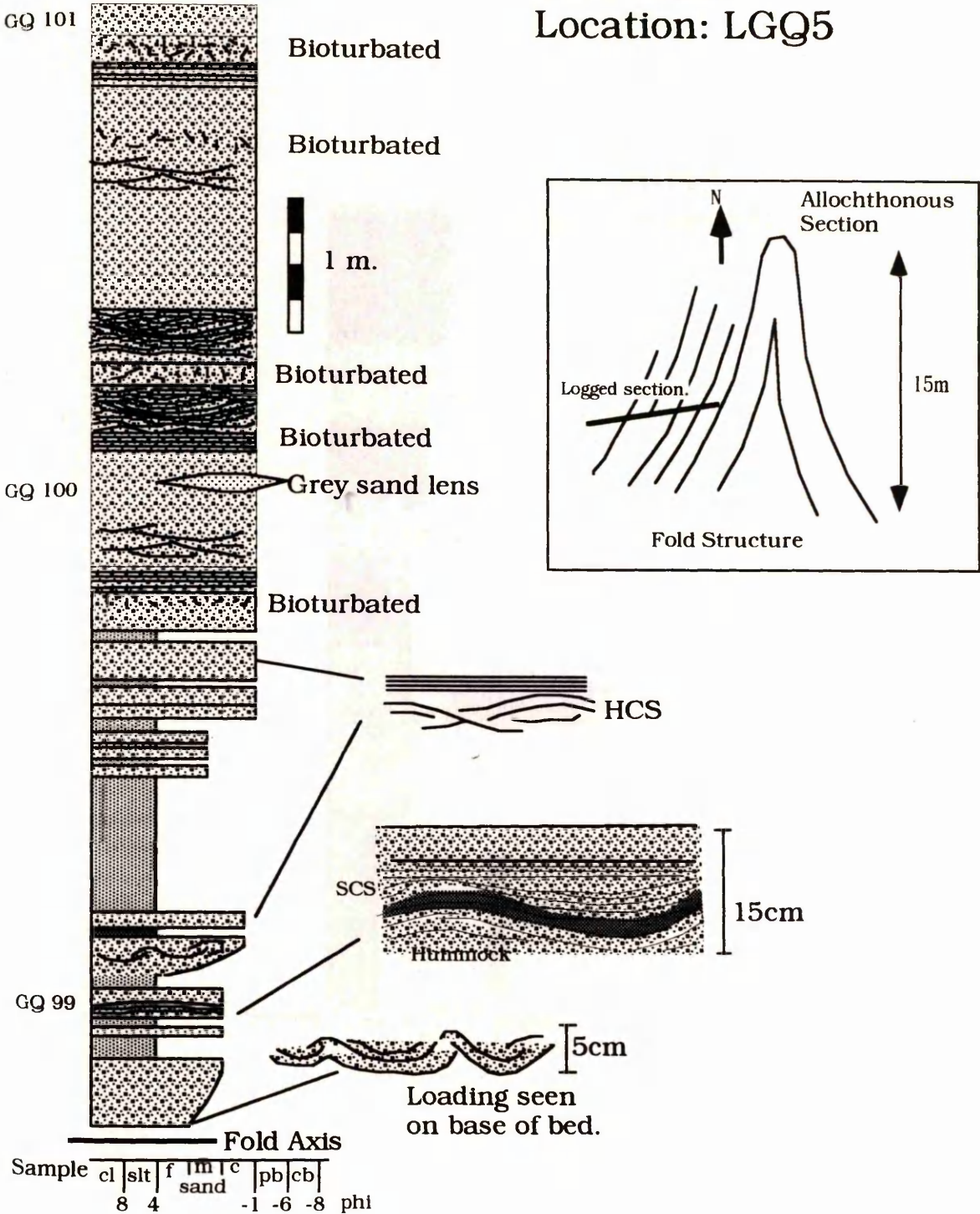
Tortonian  
Location 5 & 5(b)

(Logged by Granada University  
Dept of Geology; Juan-Fernandez pers. comm.)

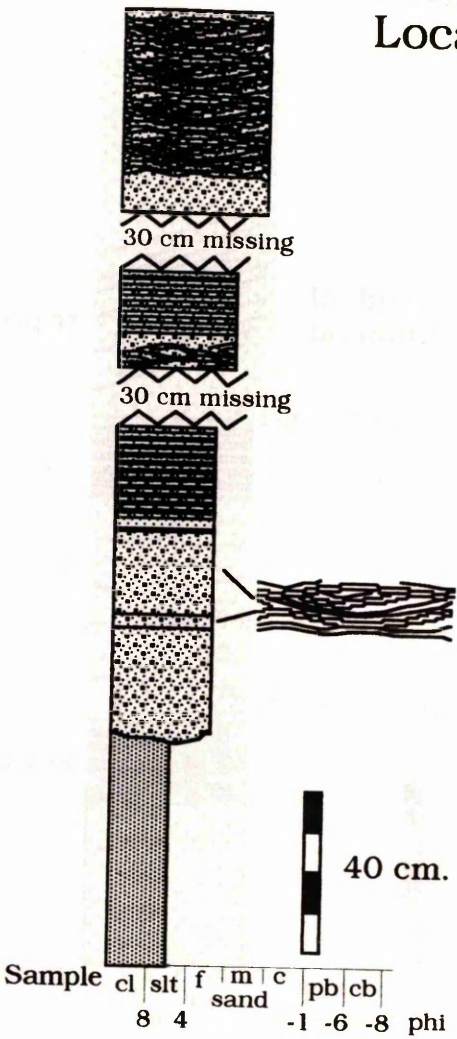


Tortonian

Location: LGQ5

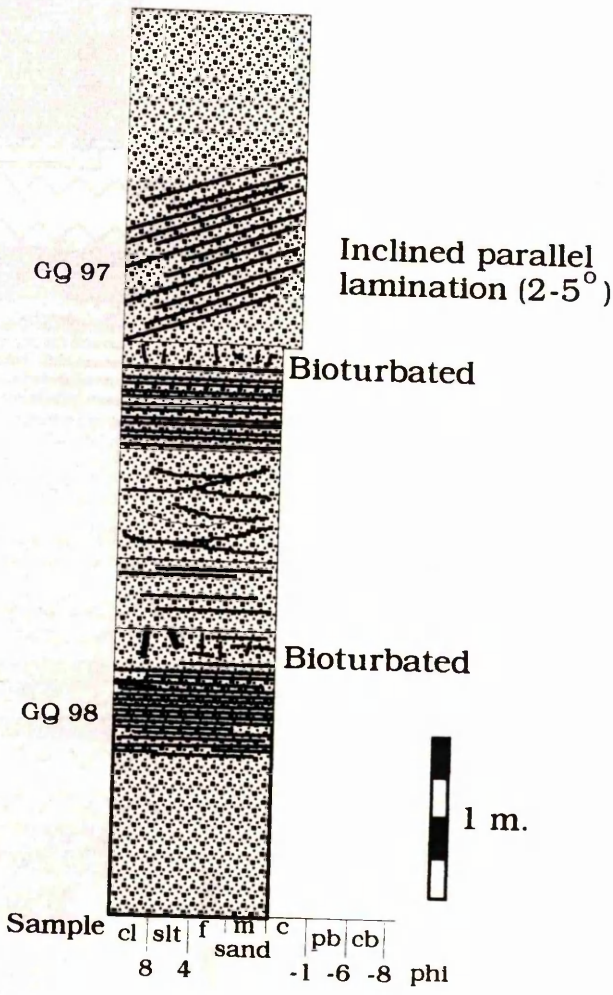


Tortonian  
Location: 5(b)

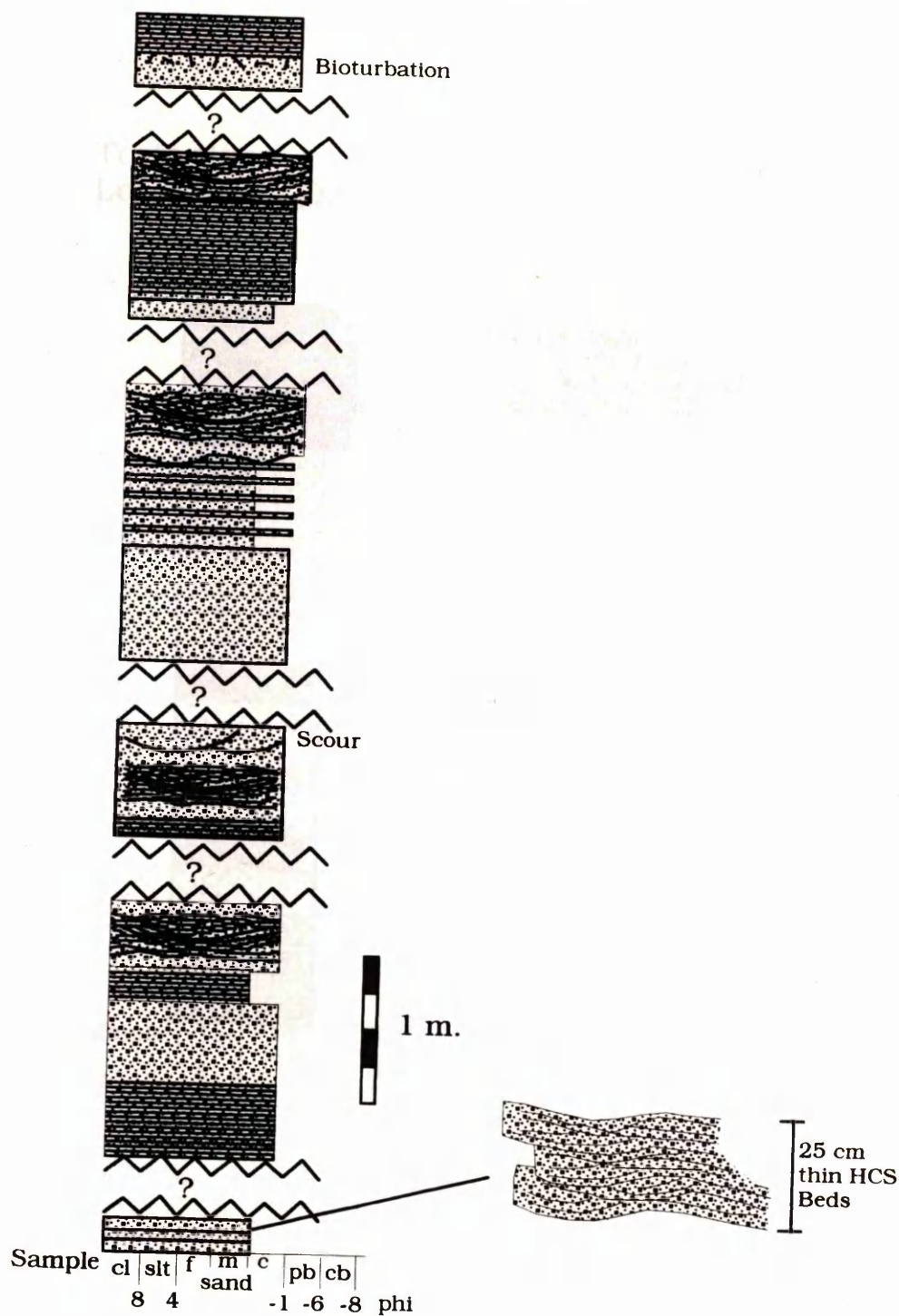




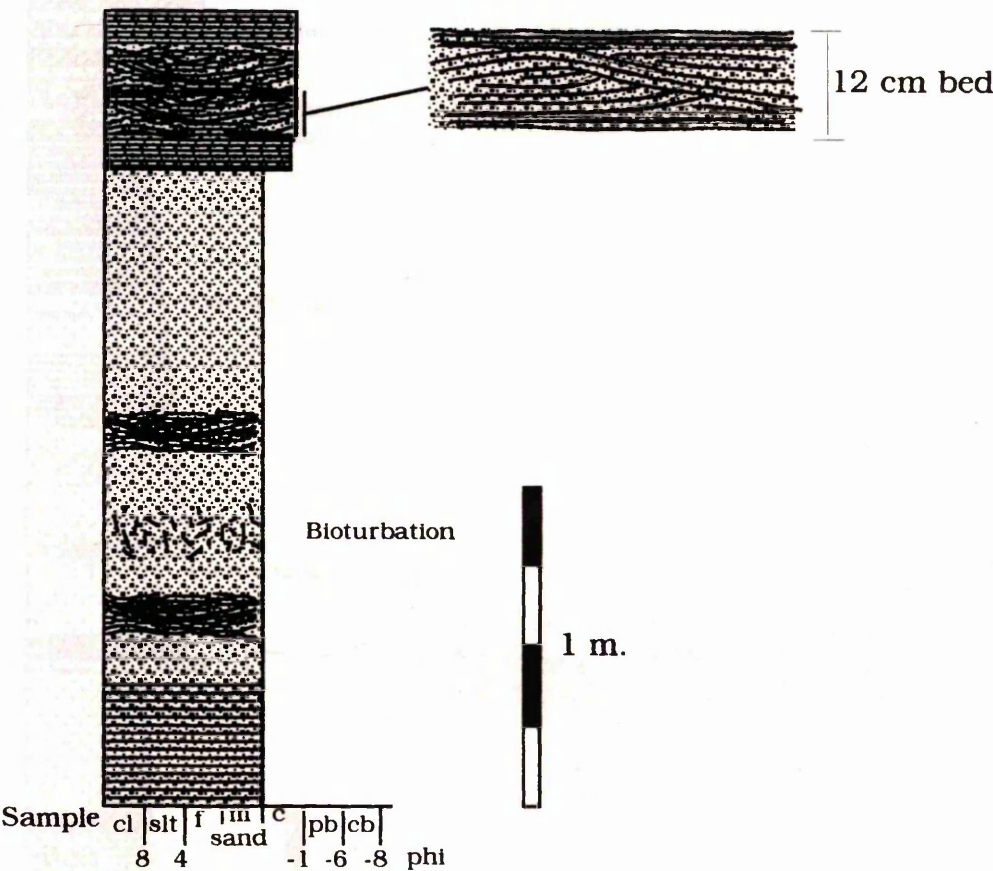
Tortonian  
Location: 80



# Tortonian Location: 81

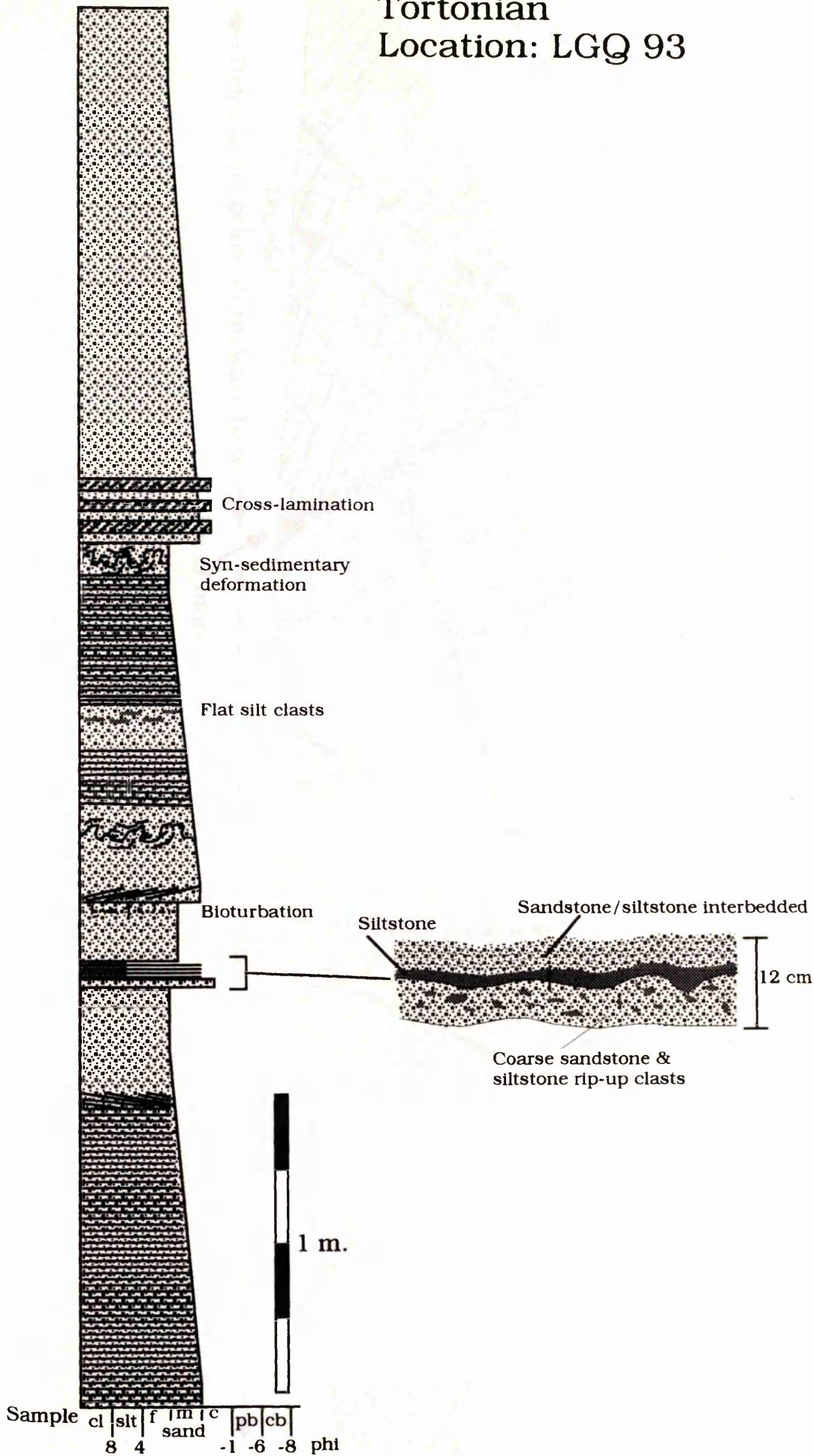


Tortonian  
Location LGQ92

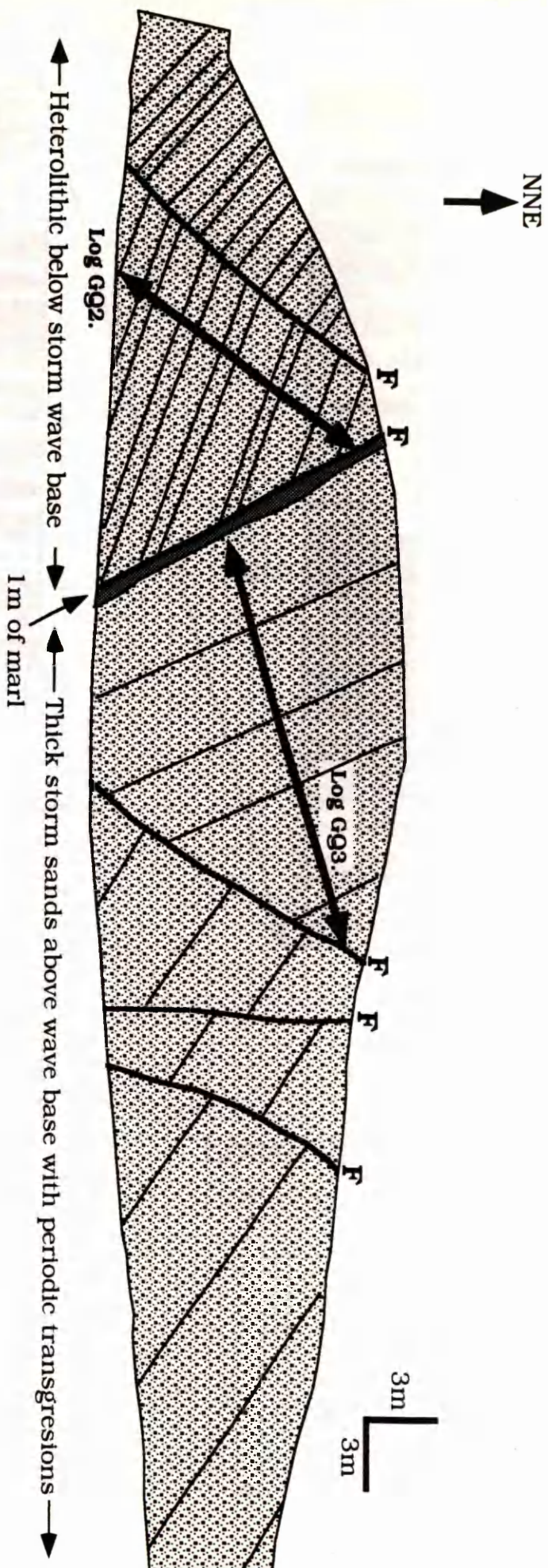




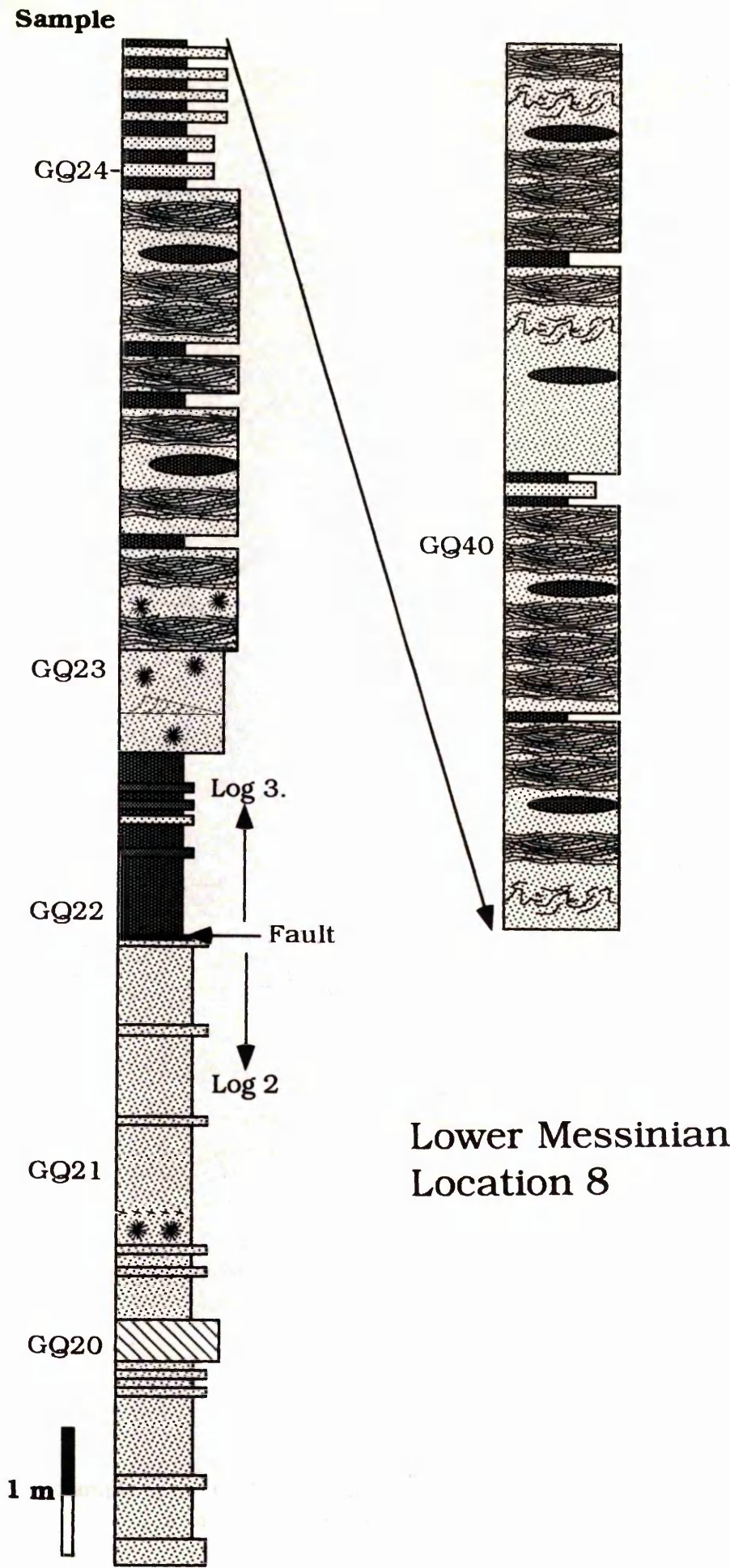
Tortonian  
Location: LGQ 93



# Location LGQ 8: Road Cut at Montilla

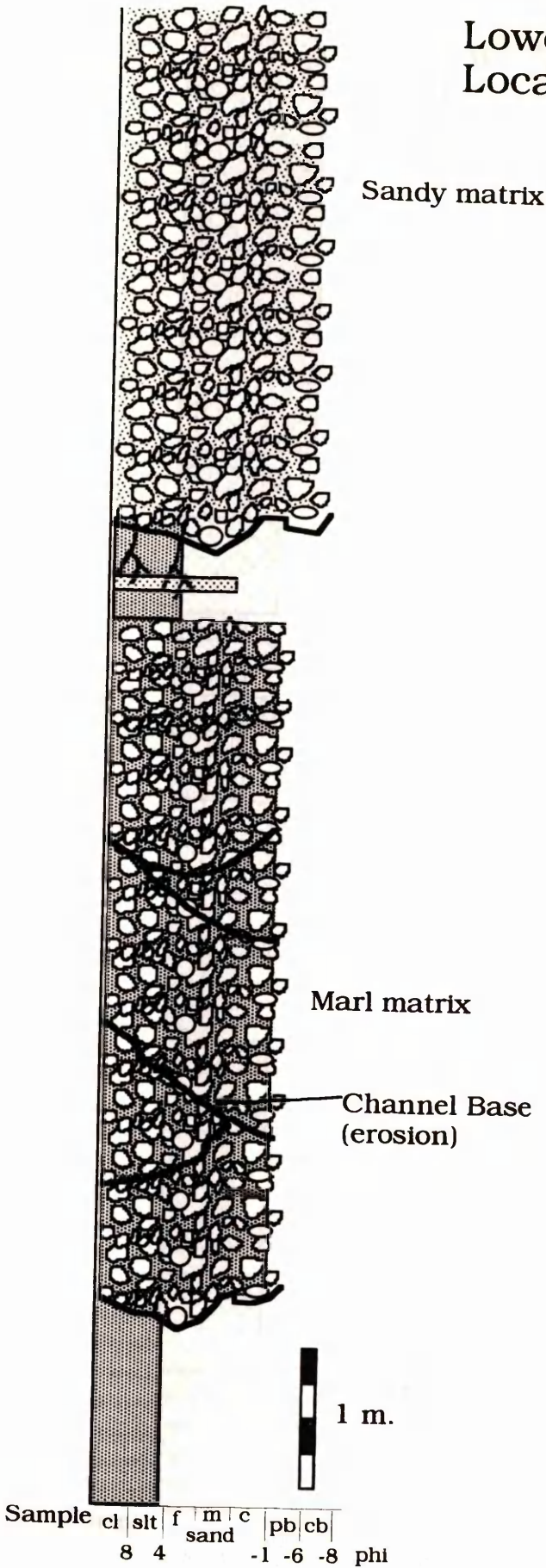




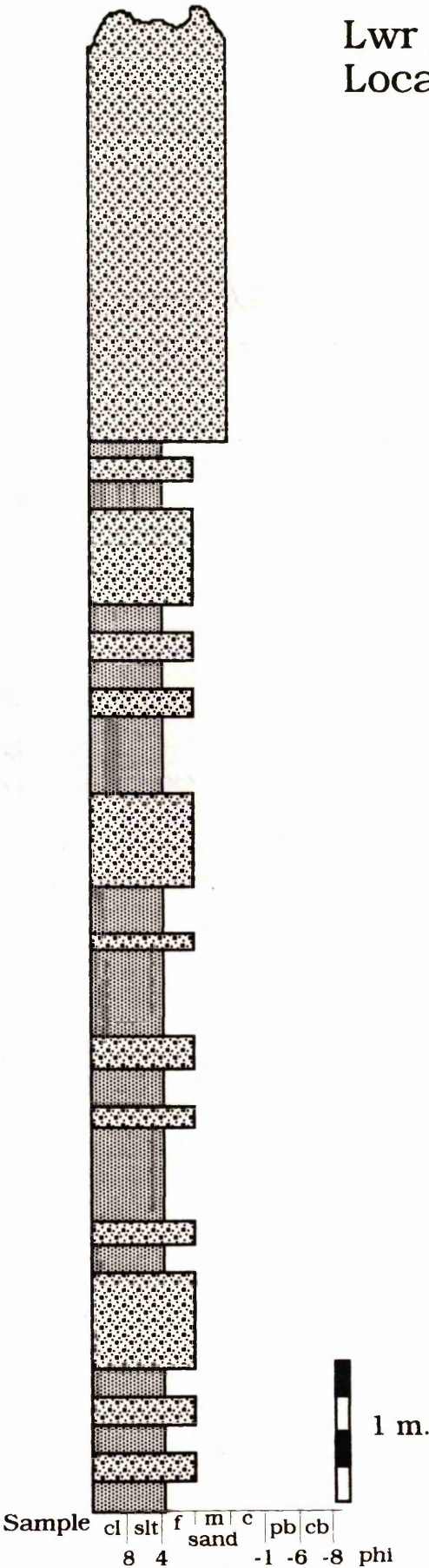




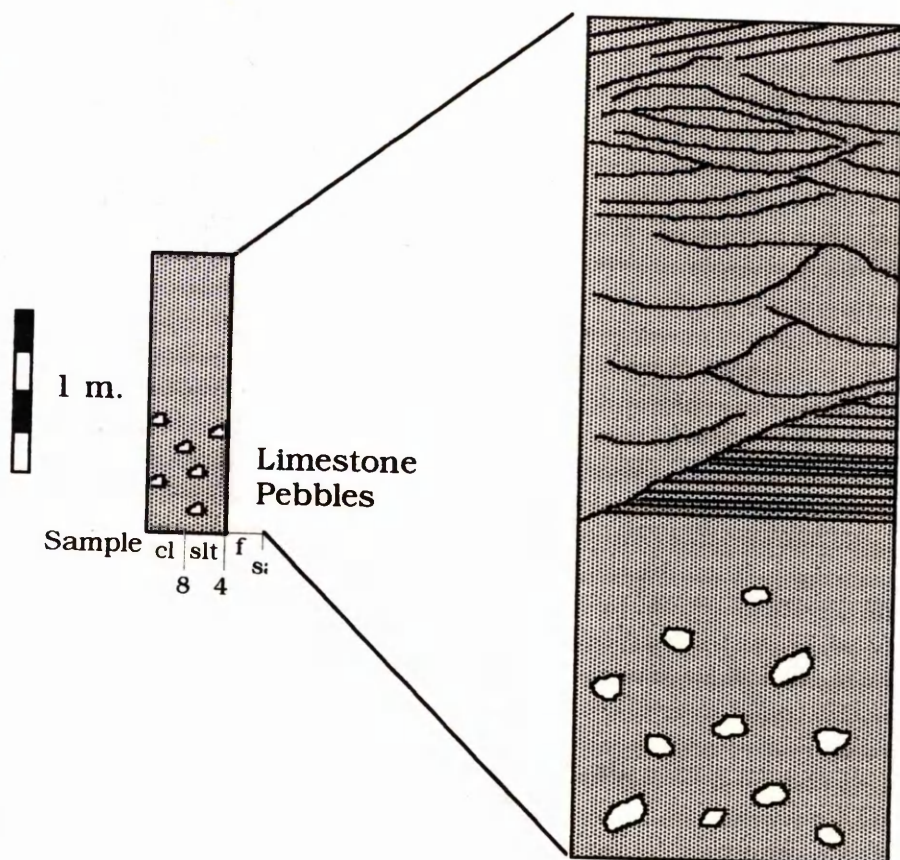
Lower Messinian  
Location: 9



Lwr Messinian  
Location: 49

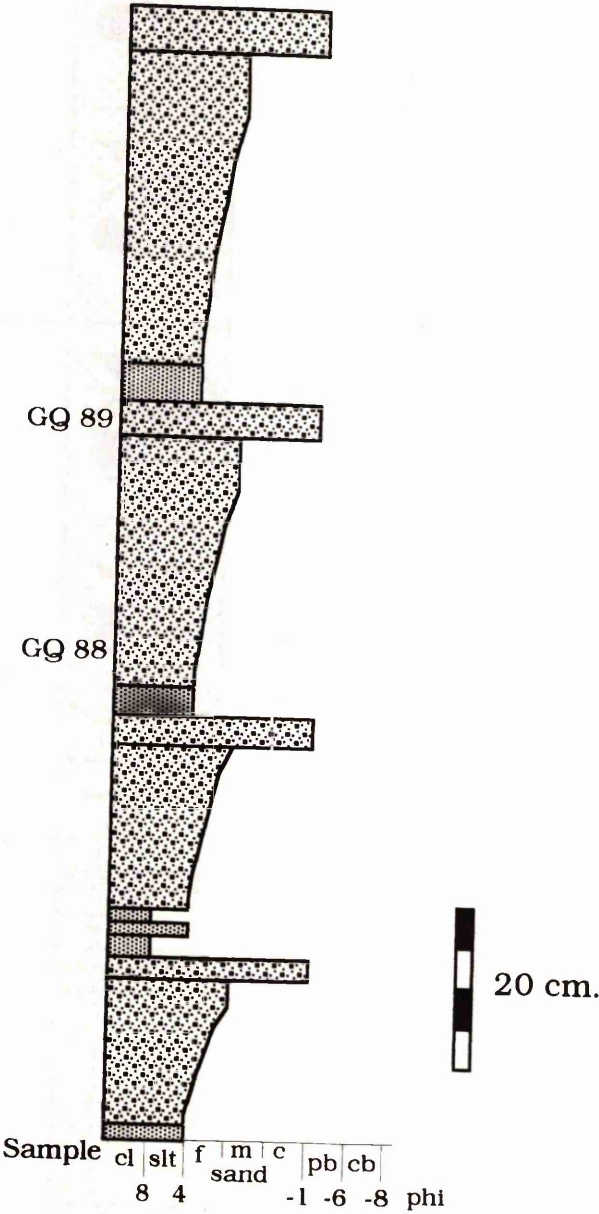


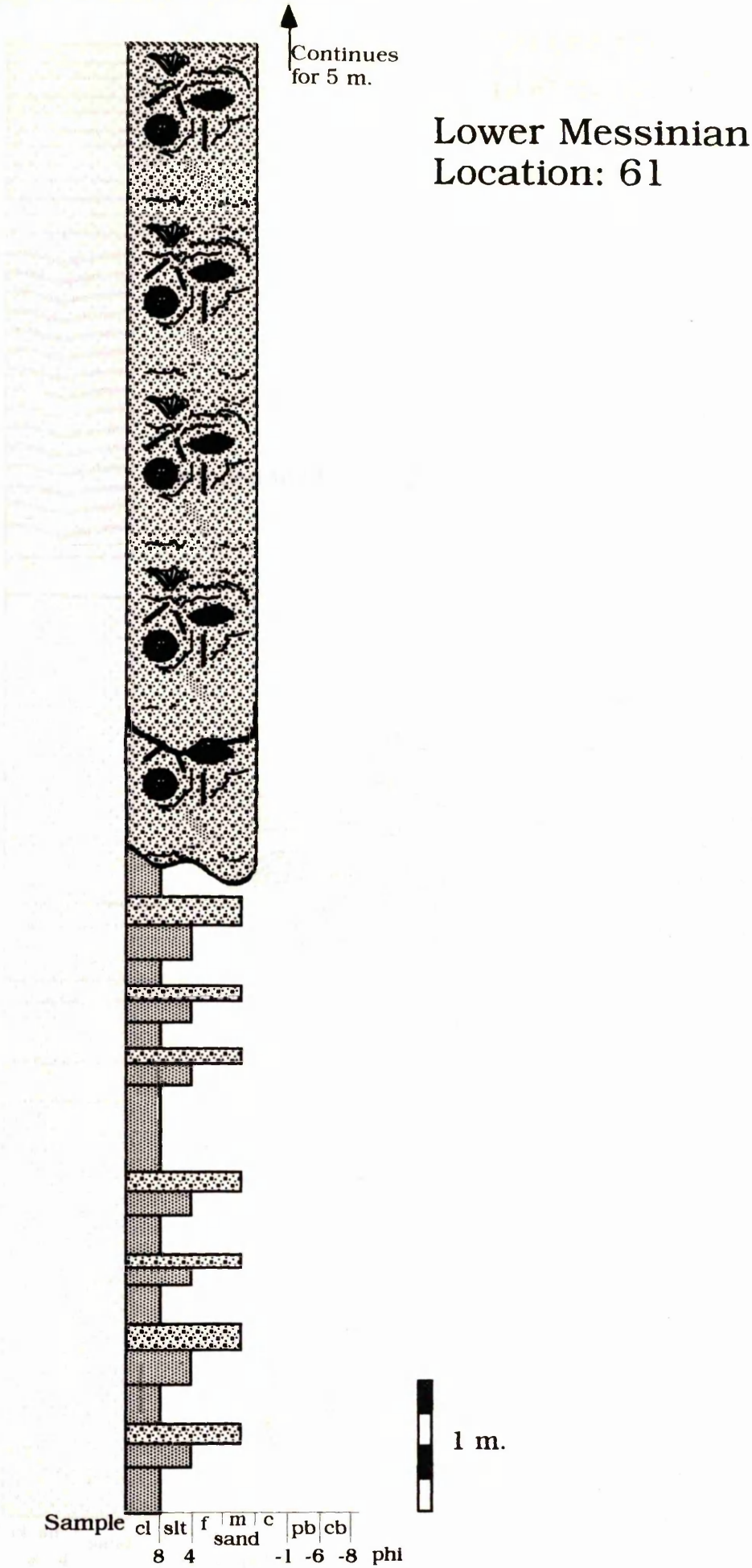
# Lower Messinian Location: 52





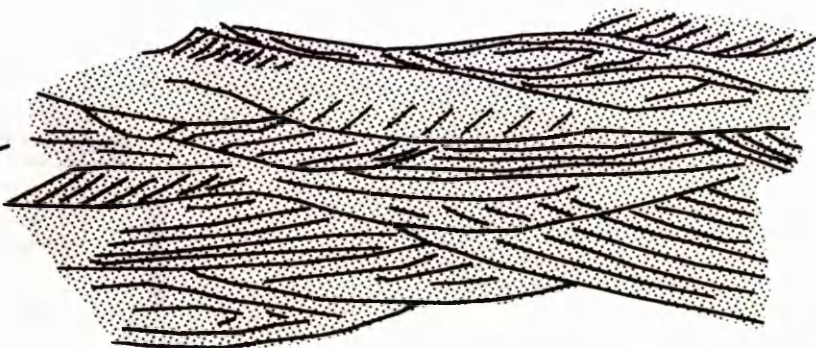
Lower Messinian  
Location: 58



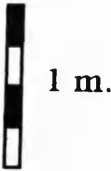


Lower Messinian  
Location: 65

well defined bedding



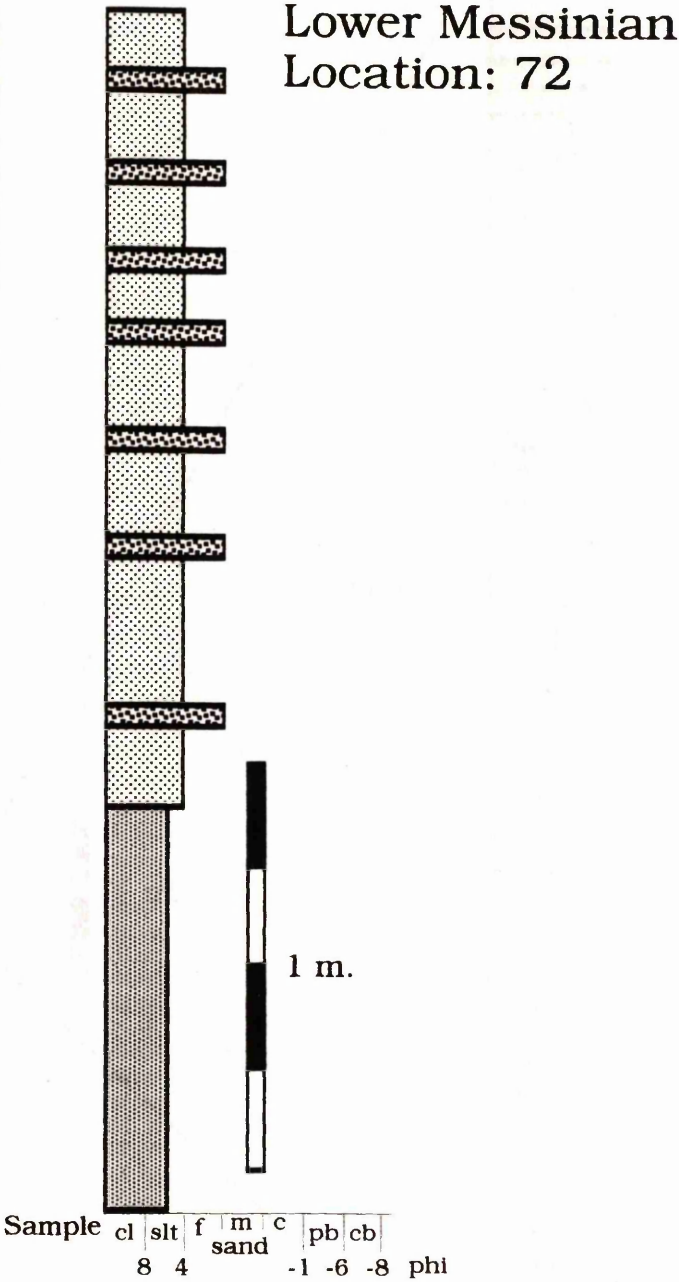
Typical structures seen throughout logged section



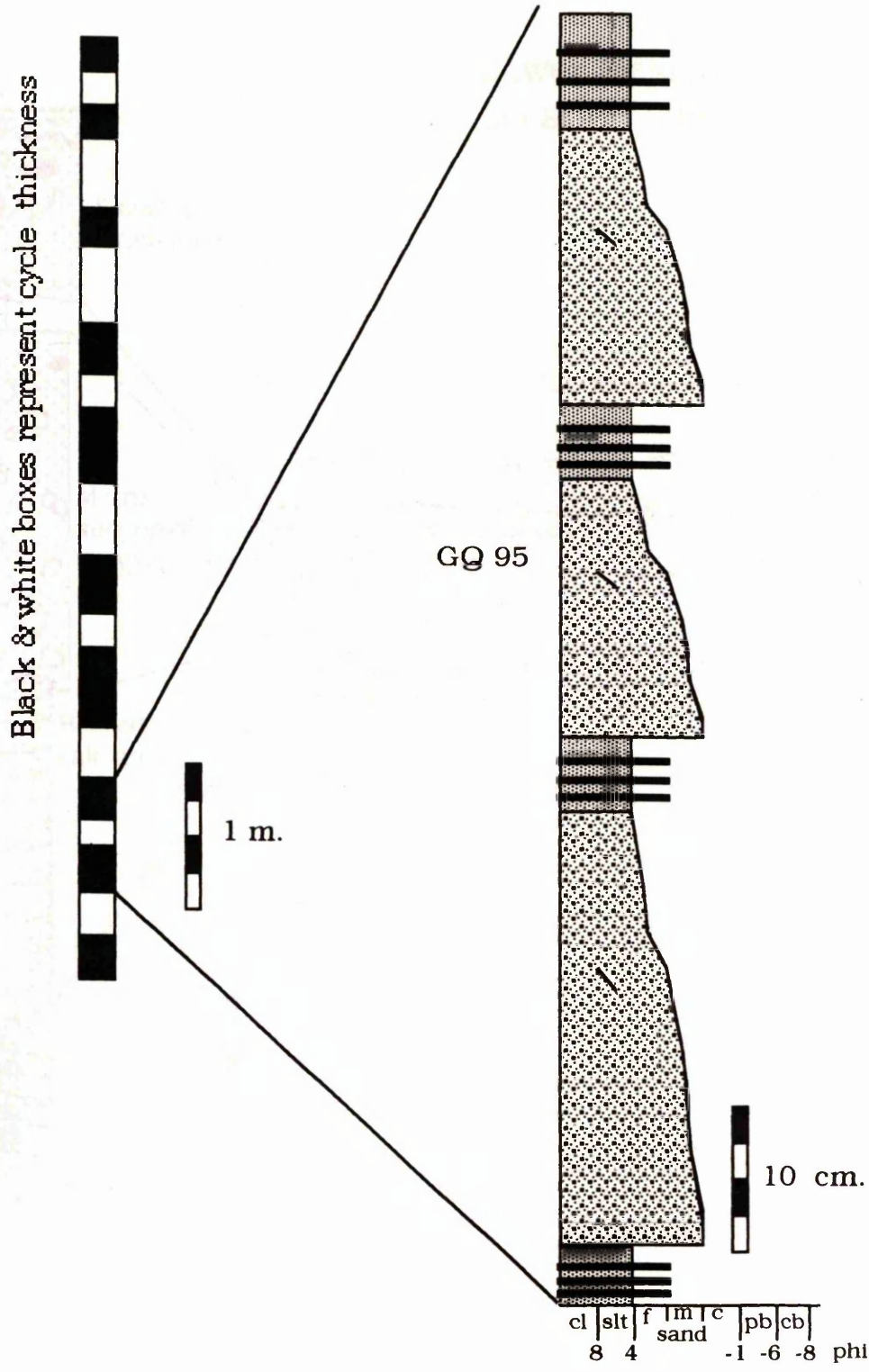
1 m.

Sample	cl	slt	f	m	c	pb	cb	
	8	4		sand		-1	-6	-8 phi

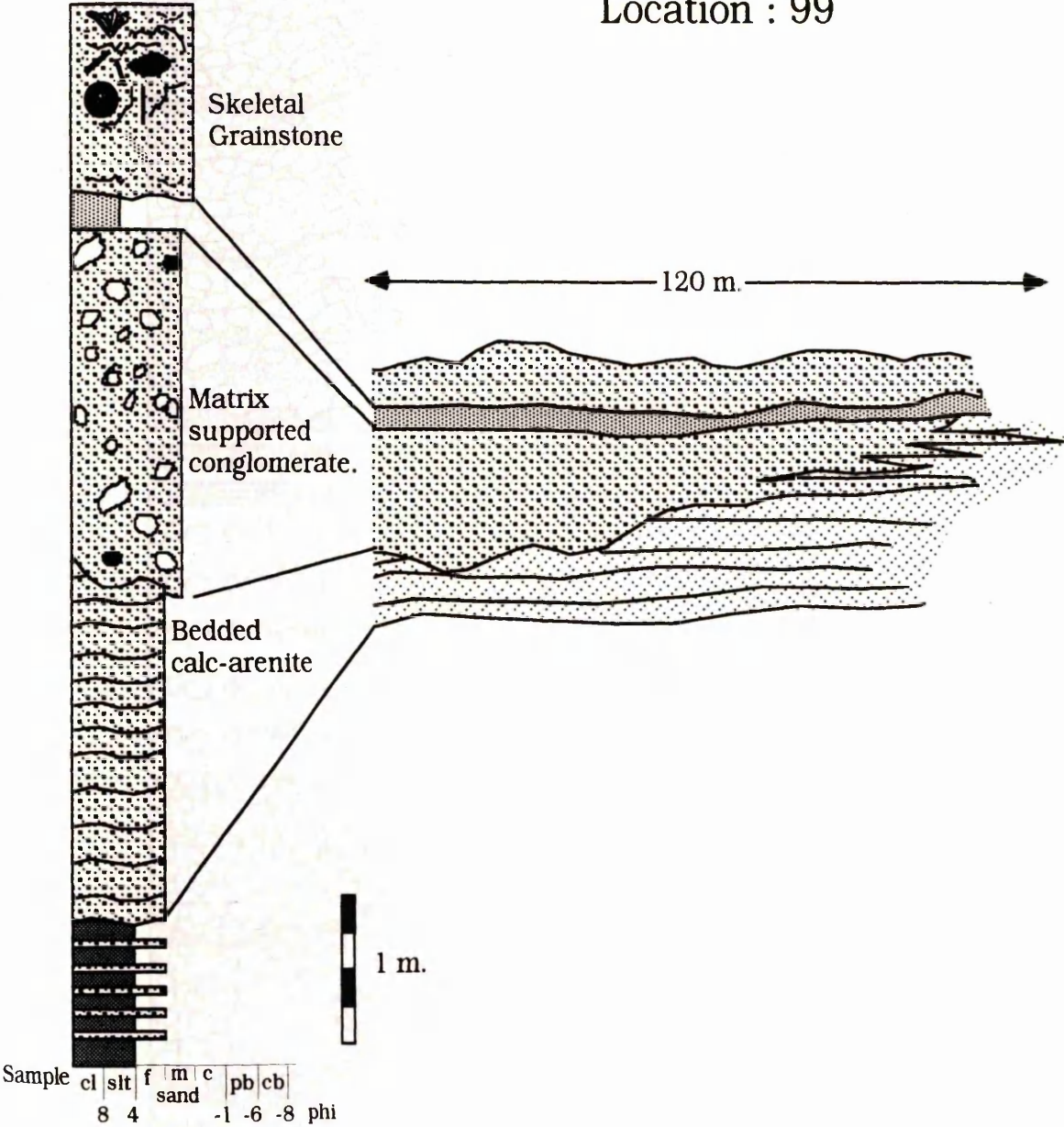




Lwr Messinian  
Location. GQ75

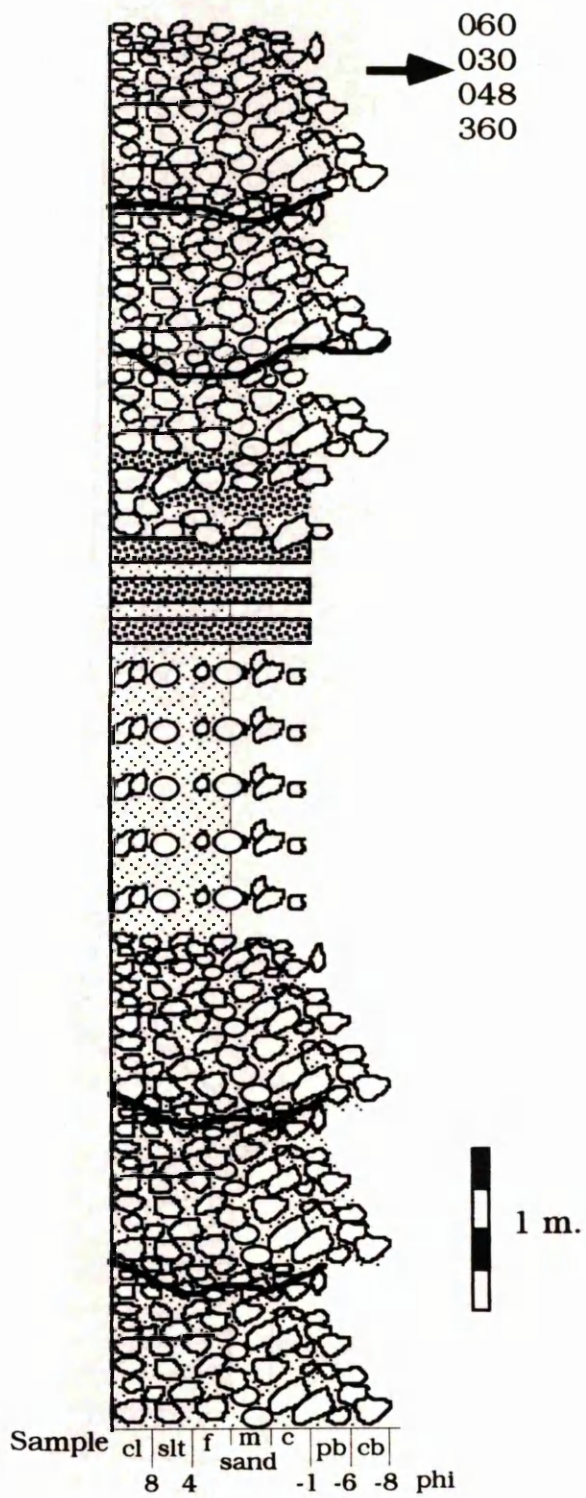


Lower Messinian  
Location : 99

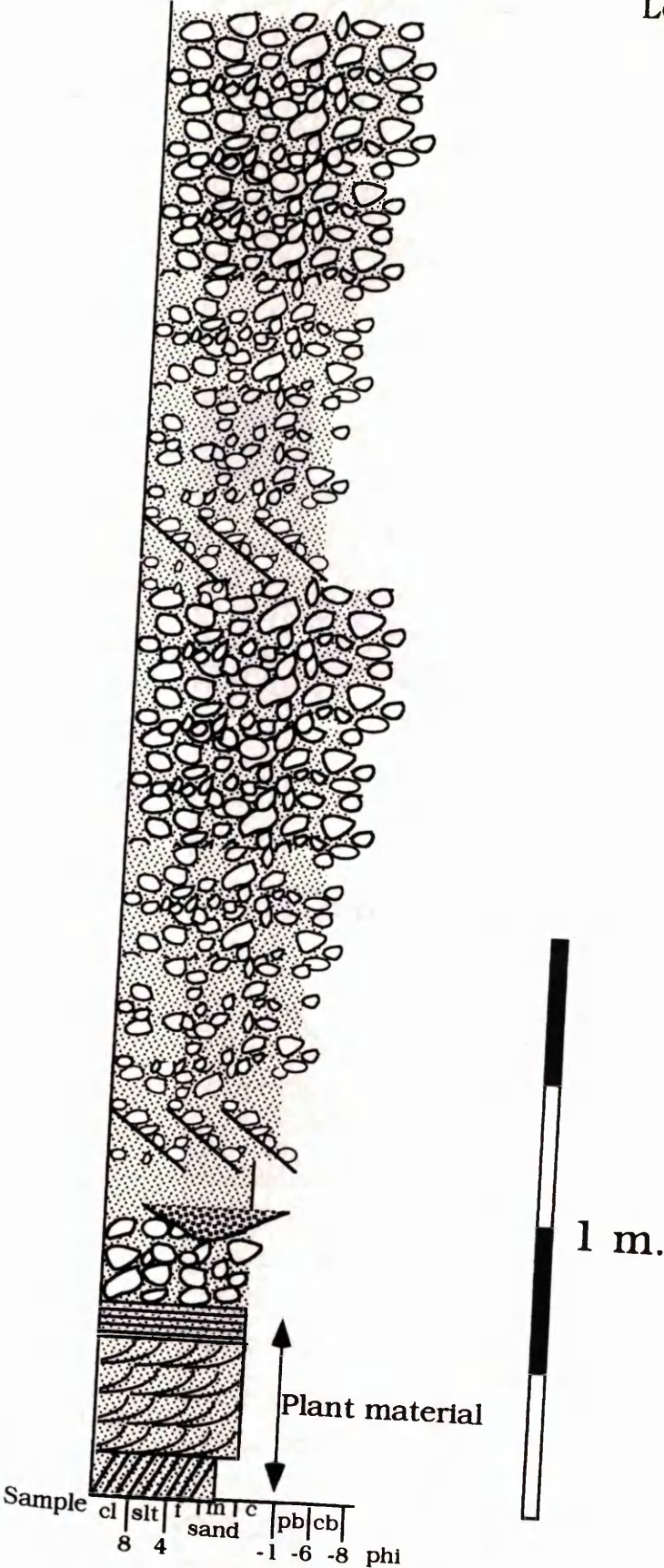




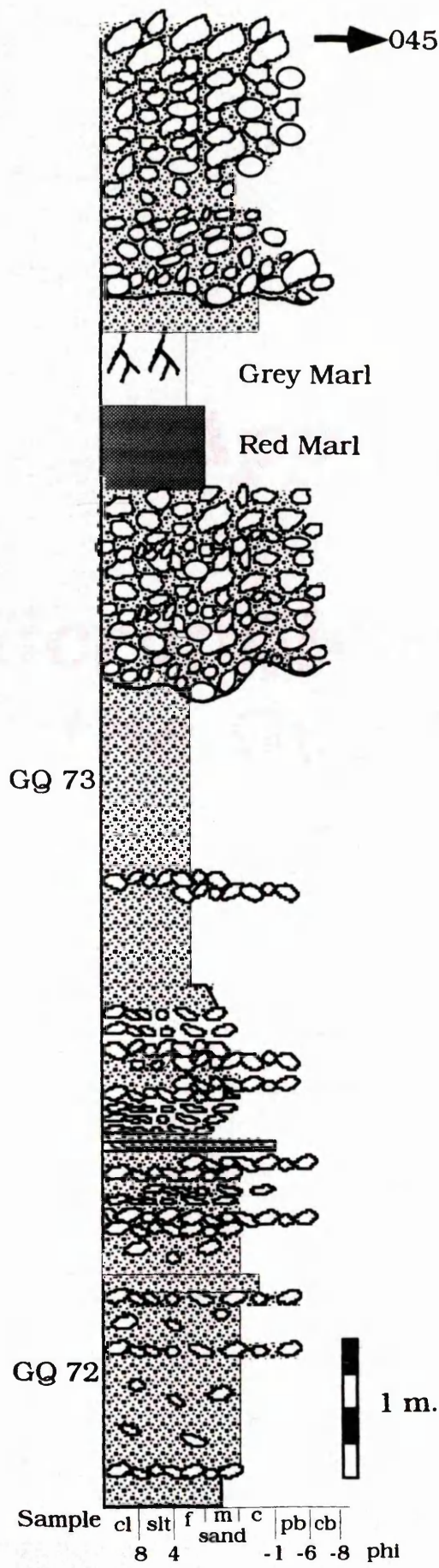
Upper Messinian  
Location: 46(a)



Upper Messinian  
Location: 47



Upper Messinian  
Location: 46(b)





## ***Appendix II***

# ***Micropalaeontology of the Guadalquivir Basin***



## Appendix II

### Micropalaeontology of the Guadalquivir Basin

#### Introduction

Microfossils have been separated from samples taken from the Aquitanian to Lower Messinian succession of the Guadalquivir Basin. The ostracods and foraminifera have been studied in detail and specimens identified as far as possible. Diatoms and Radiolaria are also present although they have not been studied in detail. Attention has been focussed on the benthonic faunas as they provide the most reliable environmental indicators. Planktonic foraminifera have not been subject to detailed identification, but the percentage of each assemblage which they represent is recorded. Identification of the specimens was carried out by M. Keen at the University of Glasgow.

The ostracods and foraminifera have been identified, and their environments interpreted, using general micropalaeontological references; Several papers have been published on various aspects of the palaeo-ecology of Miocene foraminifera (Berggren & Haq, 1976; Van de Poel, 1992; Cita *et al.*, 1978; Wright, 1978a,b). Murray (1991) deals with foraminiferal ecology in general, with relevant descriptions of Mediterranean and adjacent Atlantic living benthonic faunas. There are no such general works dealing with ostracods and the environmental details are scattered through the literature. The general technique of using ostracods in palaeo-environmental studies can be seen in Keen (1993). Aranki (1987) and Pari (1968) list ecological data for many of the species recorded here, while several chapters of De Dekker *et al.* (1988) deal with palaeo-environmental aspects.

This appendix aims to outline the methods of separation, the micropalaeontology of Lower/Mid Miocene, Tortonian and Lower Messinian sedimentary rocks and the palaeobathymetry inferred. The data is presented in the form of tables and plates of the most important species are given at the end of the appendix.

#### Methods

Samples were collected from each of the lithofacies identified in the Miocene succession of the Guadalquivir Basin. The samples were disaggregated by treatment for 3 days in 10% hydrogen peroxide solution. They were then washed through a series of mesh sieves to separate 90  $\mu\text{m}$ , 125  $\mu\text{m}$  and 250  $\mu\text{m}$  size fractions. The residues were dried in an oven at 70 °C and examined under a binocular microscope.

#### Micropalaeontology

##### *Problems Associated With Allochthonous Specimens*

In many of the samples the planktonic foraminifera were found to be most abundant in the fine (90mm) size fraction, common in the medium (125mm) fraction but absent from the coarse (250mm) fraction. The finer fraction is not dominated by small species but by small specimens of species that would normally be distributed across all the size fractions in an in-situ assemblage. Planktonic forms are more easily transported and the dominance of small planktonic specimens in the assemblages suggests that the planktonic foraminiferal

fraction of many of the samples is allochthonous. Therefore the planktonic specimens are considered to be an unreliable palaeo-environmental indicator. An exception to this is the Tortonian samples dominated by deepwater forms, in both the benthonic and planktonic assemblages. In these samples the planktonic and benthonic forms are both considered to be in-situ as both the planktonics and benthonics are dominated by deepwater forms. In the Messinian samples the benthonic forms show a more normal size distribution, with a population structure that contains both juvenile and adult specimens. In these cases the benthonic specimens are considered to be autochthonous, and are therefore a reliable palaeo-environmental indicator.

Because the planktonic assemblages may contain allochthonous specimens, and because the benthonic assemblages are considered more likely to be autochthonous, the benthonic specimens have been studied in more detail. The benthonic assemblages have consequentially been used to infer the palaeo-environment of deposition for the Guadalquivir Basin sedimentary rocks.

#### *Lower to Mid Miocene*

In samples from the Lower/Mid Miocene marls the ostracod and foraminiferal assemblages are dominated by circalittoral, upper bathyal and bathyal forms. By contrast samples taken from clay laminae found in laminated clay/carbonate rocks were found to be dominated by radiolaria and diatoms. The Diatom assemblage of one sample (GQ 67) is monospecific, characterised by *Concinodiscus*.

Overall the Lower/Mid Miocene faunal assemblage indicates outershelf to bathyal environments of deposition, with a few samples from the laminated facies, indicating bathyal depths in excess of 1000m

#### *Tortonian*

Three Tortonian samples from the thin bedded, and tabular facies contain no ostracods and are dominated by a planktonic foraminiferal assemblage indicative of open ocean waters. Benthonic foraminifera are also found to be present, but in much smaller numbers than the Planktonic forms. The benthonic species indicate upper bathyal to bathyal environments and depths in excess of 200m. The thin bedded facies also contain radiolaria indicating a bathyal environment and depths probably in excess of 1000m.

By contrast, the thick bedded facies contain both ostracods such as *Cyamocytheridea meniscus*, *Cypridels* *gp. torosa* and *Cytheridea* *cf. expansa* and foraminifera such as *Ammonia* *gp. becarri*, *Elphidium crispum* and *Elphidium "excavatum"* typical of present coastal and brackish waters. The ostracods show a population structure of adults and several moult stages which is usually thought to indicate an autochthonous assemblage. Foraminifera and ostracods typical of open shelf environments are also present, but in much smaller numbers than the brackish forms. The open shelf fauna may have been transported into the protected environments.



### Lower Messinian

Ostracods from the Lower Messinian include elements from several different coastal facies including:

- (1) freshwater (*Ilocypris*, and large *Cyprideis*);
- (2) Hypohaline (i.e "brackish water") (*Cyprideis* *gp. torosa* );
- (3) polyhaline to euhaline (i.e. coastal bays) (*Cyamocytheridea*, *Pontocythere* and *Cytheridea* *cf. expansa*);

Species typical of shoreline open marine environments are also present, including *Nonurocythereis*, *Loxoconcha* and *Hemicythere*., but in much smaller numbers. Some open marine ostracod are deformed and this is thought to indicate that they have been transported.

The general implication of the ostracod assemblage is that faunas from several environments, ranging from coastal to open marine have been transported and mixed together. The population structure indicates that mixing probably occurred in near coastal waters.

The benthonic foraminifera are dominated by *Ammonia* *gp becarri* and *Elphidium* which together constitute over 80% of individuals present. These forms are associated with coastal environments and mild hyper-salinity. *Ammonia* is commonly infaunal in muddy sands in brackish hyposaline inner shelf waters while *Elphidium* is epifaunal, living on sand substrates on the inner shelf in depths of no more than 50m. An *Ammonia becarri* association is well known in the Mediterranean and Atlantic provinces and is found in marshes and lagoons of variable salinity (Murray, 1991).

Other foraminifera in the Lower Messinian samples are more typical of infralittoral, circalittoral and upper bathyal environments. These occur in much smaller numbers than brackish forms and are interpreted as allochthonous and have been transported into coastal waters.

Like the ostracods, the foraminifera indicate more than one environment, confirming that sediments from different parts of the shelf were mixed together by transport processes.

Thus, the Lower Messinian foraminiferal and ostracod assemblages differentiate four main coastal facies although various degrees of mixing are recognised. Sample GQ21 (from the thin bedded facies) has the strongest freshwater influence, samples GQ 88 and GQ89 (also from the thin bedded facies) indicate a strong brackish influence but lack the freshwater forms. Finally Samples GQ22 and GQ21, (taken from calc-lithic arenites), are more typical of shallow coastal waters and but contain a mixture brackish and open marine forms.

### Palaeo-bathymetry

The species of the ostracod assemblages have been examined quantitatively and can be used to give a general palaeo-bathymetry for the Guadalquivir basin (Fig ApII.1). The Lower/Mid Miocene is characterised by fauna from circalittoral and bathyal environments indicating depths of deposition below 200m. The Tortonian thick bedded facies and Lower Messinian samples show a mixing of faunas from brackish, shelf and circalittoral environments with

varying proportions of forms from each environment (Fig. ApII.1).

The foraminiferal assemblage, assessed in a more qualitative manner, supports this inferred palaeo-bathymetry, with the addition of faunas from Tortonian thin bedded and tabular facies which are more typical of bathyal environments. The faunal assemblages have been combined with lithofacies interpretations and derived stratigraphy to produce a bathymetry curve for the Guadalquivir Basin (Fig. ApII.2). This clearly shows a shallowing through the Miocene succession from bathyal conditions in the Lower Miocene to coastal waters in the Lower Messinian. In the Tortonian there was some fluctuation between near shore and outer shelf environments indicating rapid relative sea-level changes. This cyclicity is reflected in the sedimentary cycles in the Tortonian succession (Part I, Chapter 3).

Tabulation of data

The data from analysis of ostracods and foraminifera have been tabulated, and these data have been incorporated into the sedimentary interpretations given in Part I, Chapter 3. In these tables samples are shown in terms of lithofacies and environmental interpretations derived prior to the incorporation of the micropalaeontological data. The environmental association of each group or species is usually associated is given in column 2 of the tables. The ostracod data have been quantified and the numbers indicate the number of specimens of each species or group that were found in any given sample. The Foraminiferal data are qualitative and specimen abundance is classified as;

- Dominant

species that make up more than 50% of the assemblage of a given sample.
- Abundant

species that make up 20-50% of the assemblage of a given sample.
- √

species present, but make up less than 20% of the assemblage

Plates

Plates I, II and III show a selection of the most important microfossils identified in sedimentary rock samples taken from the Guadalquivir Basin. The location numbers refer to locations given in Foldout Maps 1,2 & 3 (contained in the back of this Thesis).

## REFERENCES

- Aranki, J. F. (1987) Marine lower Pliocene ostracoda of southern Spain with notes on the recent fauna. *Bulletin of the Geological Institutions of the University of Uppsala* , **13** 144pp.
- Berggren, W. A. and Haq, B. U. (1976) The Andalusian Stage (Late Miocene): Biostratigraphy, biochronology and paleoecology. *Palaeogeography, Palaeoclimatology, Palaeoecology* , **20** (67-129),
- Cita, M. B., Wright, R. C., Ryan, W. B. F. and Longinelli, A. (1978) Messinian Palaeoenvironments. *Initial Reports of the Deep Sea Drilling Project* , **42** (1), 1003-1035.
- De-Dekker, P., Colin, J. P. and Peypoquet, J. P. (1988) *Ostracoda in the Earth Sciences*. Elsevier, Amsterdam, pp
- Keen, M. C. (1993) Ostracods as palaeoenvironmental indicators examples from the Tertiary and Early Cretaceous. In: *Applied Micropalaeontology* (Ed. by Jenkins), Kluwer,
- Murray, J. W. (1991) *Ecology and Palaeoecology of Benthic Foraminifera*. Longman, London, pp 397.
- Pari, H. S. (1968) Ecologic distribution of recent Ostracoda. *Proc. SympCrustacea, pt. I. Marine Biol. Ass. India.* , (457-495),
- Van-de-Poel, H. M. (1992) Foraminiferal biostratigraphy and palaeoenvironments of the Miocene-Pliocene Carbaneras-Nijar Basin (SE Spain). *Scripta Geol.* , **102** 32pp.
- Wright, R. (1978a) Neogene paleobathymetry of the Mediterranean based on benthic foraminifera from DSDP Log 42A. *Initial Reports of the Deep Sea Drilling Project* , **42** (1), 837-846.
- Wright, R. (1978b) Neogene benthic foraminifera from DSDP Leg 42A Mediterranean SEa. *Initial Reports of the Deep Sea Drilling Project* , **42** (1), 209-726.



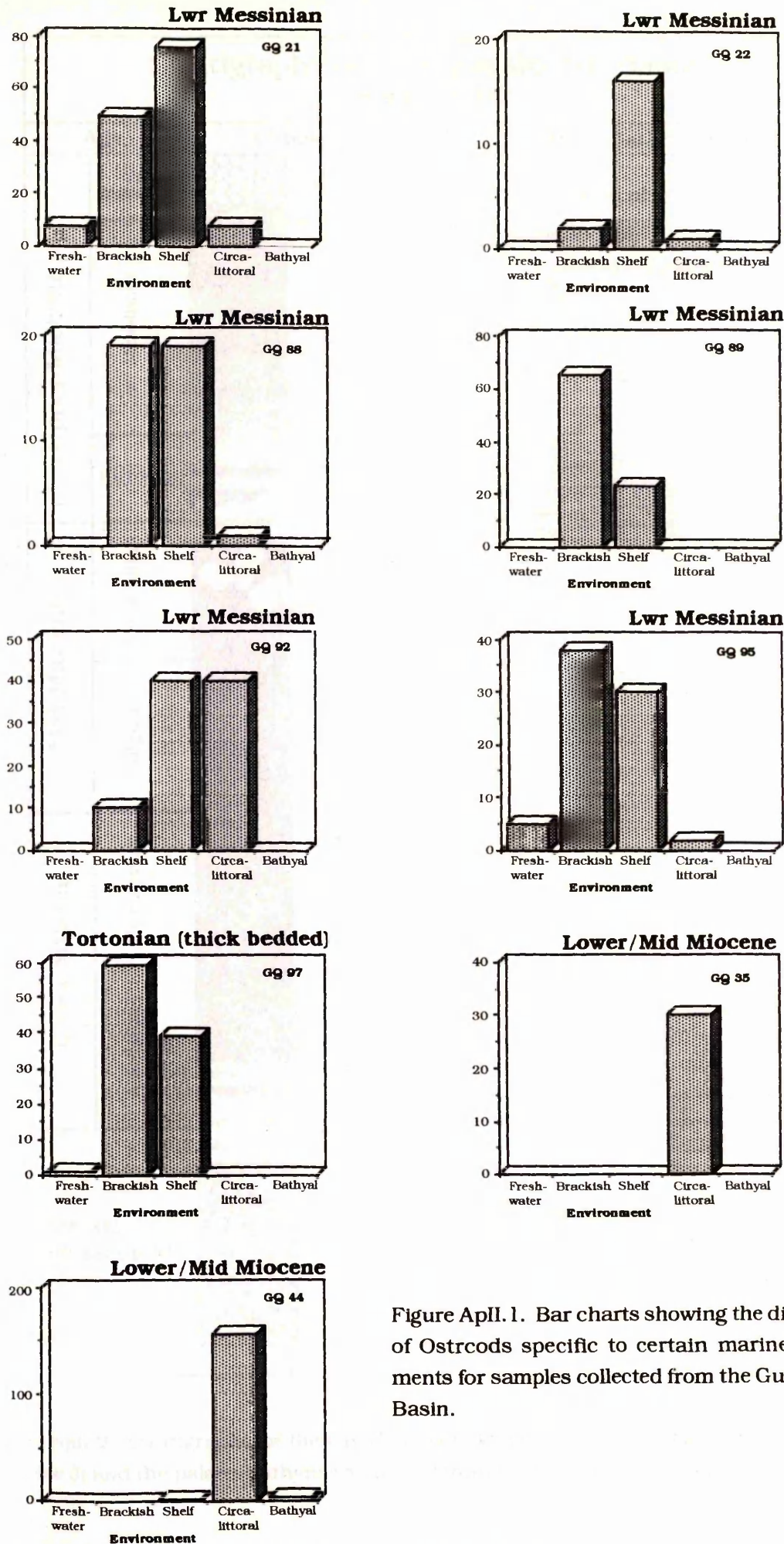


Figure ApII.1. Bar charts showing the distribution of Ostracods specific to certain marine environments for samples collected from the Guadalquivir Basin.

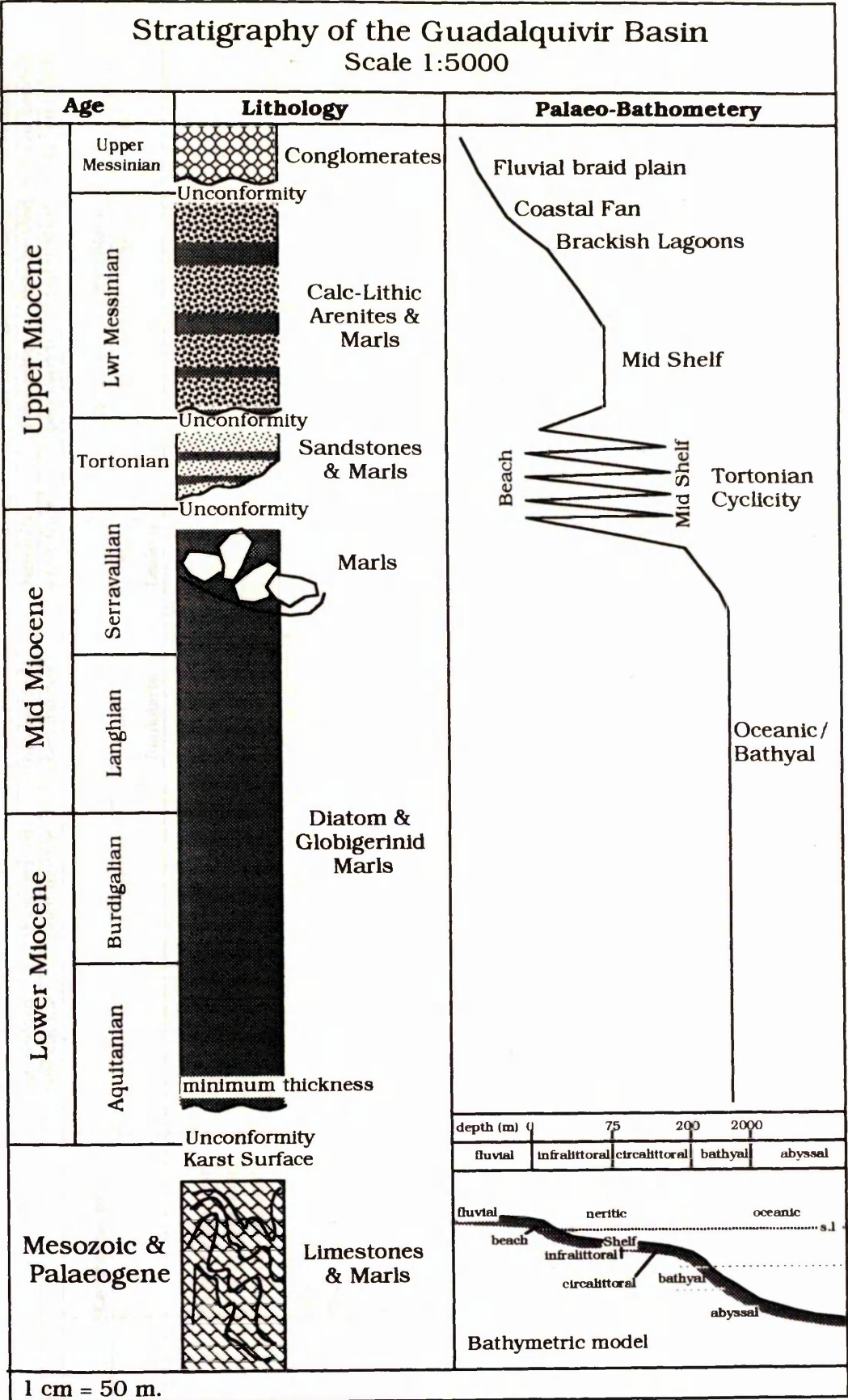


Figure ApII.2 Stratigraphy of the Guadalquivir Basin showing lithofacies interpretations (Chapter 3) and the palaeo-bathymetry derived from faunal assemblages present in samples.







Sample Location	GG35	GG44	GG83	GG87	GG82	GG107	GG79
Stratigraphical age	9	18	30	44	44	98	49
Facies	Lwr/Mid Miocene thin bedded	Lwr/Mid Miocene thick bedded	Lwr/Mid Miocene thin bedded	Lwr/Mid Miocene Diatomite	Lwr/Mid Miocene Diatomite	Tortonian thin bedded	Tortonian tabular bedded
Lithofacies Interpretation	open marine	open marine	open marine	open marine	open marine	outer shelf	outer/mid shelf
Environment					Diatoms	Radiolaria	
<i>Quinquecostulina</i>	✓	✓					
<i>Bullimina aculeata</i>		✓					
<i>Uvigerina gp. boninaensis</i>		✓					
<i>Bigenerina sp. [agg.]</i>		✓					
<i>Planulina</i>		✓					
<i>Lagenid</i>		✓					
<i>Pyrgo</i>		✓					
<i>Cyclammina</i>		✓					
<i>Uniseriat Bullminid</i>		✓					
<i>Spiroplectammina</i>		✓					
<i>Uvigerina sp.</i>		✓	✓				
<i>Textularia</i>							
<i>Uvigerina rotula</i>							
<i>Heterolipa subhaulingeri</i>							
<i>Siphonka reticulata</i>							
<i>Trifarina</i>							
<i>Cibicides cf. wuellerstorfi</i>						✓	

	G997	G921	G922	G988	G989	G992	G995
	80	8	8	88	88	64	75
<b>Stratigraphical age</b>	Tortonian	Lwr Messinian	Lwr Messinian	Lwr Messinian	Lwr Messinian	Lwr Messinian	Lwr Messinian
<b>Facies</b>	thick bedded	calc-lithic arenite	calc-lithic arenite	thin bedded	thin bedded	mega-ripples	thin bedded
<b>Lithofacies Interpretation</b>	Beach	open shelf	open shelf	???	???	Tidal bar	???
<b>Environment</b>							
% Planktonic	40	78	90	10	10	40	10
Other fauna & flora							
<i>Annonia</i> sp. beccarii	abundant	dominant	dominant	abundant	abundant	abundant	✓
<i>Elphidium crispum</i>	abundant	✓		dominant	dominant	abundant	dominant
<i>Elphidium</i> sp. "excavatum"		abundant	✓	✓	✓	abundant	✓
<i>Stilostomella</i>	✓	✓					✓
<i>Bolivina</i>		✓					
<i>Cibicides</i>		✓	✓	✓	✓		✓
<i>Fronicularia</i>	✓	✓					✓
<i>Nodosaria</i>		✓				✓	✓
<i>Nonion boueanum</i>	✓	✓	abundant				
<i>Orthomorphina</i>		✓					
<i>Nonionella</i>		✓					
<i>Bullimina costata</i>		✓					✓
<i>Uvigerina hispidula</i>		✓					
<i>Uvigerina striatissima</i>		✓					
<i>Lenticulina</i>			✓				✓
<i>Millammina</i>			✓				
<i>Uvigerina auberlana</i>							✓
<i>Gyroidina</i> sp. cf. <i>altiformis</i>							
<i>Uvigerina peregrina</i>							
<i>Cibicides</i> cf. <i>pachydelmis</i>							
<i>Bullimina</i> cf. <i>alazanensis</i>							
<i>Melonis</i>							
<i>Multifidella</i>							
<i>Stilostomella</i>							
<i>Astacelus</i>							
<i>Karrerilla</i>							
	Outer shelf/Bathyal						





Sample Location	GG 35	GG 44	GG 97	GG 21	GG 22	GG 88	GG 89	GG 95	GG 92
	9	18	80	8	8	88	88	75	64
Stratigraphical age	Lwr/Mid Miocene	Lwr/Mid Miocene	Tortonian	Lwr Messinian	Lwr Messinian	Lwr Messinian	Lwr Messinian	Lwr Messinian	Lwr Messinian
Facies	thin bedded	thick bedde	thick bedded	calc-lithic arenite	calc-lithic arenite	thin bedded	thin bedded	thin bedded	mega-ripples
Lithofacies interpretation	open marine	open marine	Beach	open shelf	open shelf	???	???	???	Tidal bar/shelf
<b>Environment</b>									
<i>Xestoleris</i> sp. a									
<i>Xestoleris</i> sp. b						2	1	1	1
<i>Caudites</i> sp.			1						
<i>Loculicytherella</i> cf. <i>morkhoveni</i>			3						
<i>Henricocythere triangularis</i>			6		13			1	
<i>Aurila</i> sp. c				4					
<i>Henryhowella asperlimma</i>	6	1		7		1	1		1
<i>Cytherella</i> sp.			2	2					
<i>Eucytheruana</i> sp.									
<i>Bairdia</i> sp. a.				1					2
<i>Candonia</i> sp.						1			1
<i>Large cyprid</i>				2					
<i>Cytherura</i> sp.								1	
<i>Callistocythere</i> sp. c								1	
<i>Bairdia</i> sp. b	5	3							1
<i>Cytherella</i> cf. <i>postidenticulata</i>	11	126							
<i>Paleobittocythere</i>	1								
<i>Agrenocythere hazelae</i>		5							
<i>Trachyleberidea</i> sp.		4							
<i>Macrocyparis</i> cf. <i>bathyalensis</i>		1							
<i>Echinocythereis</i> cf. <i>szscaabra</i>		1							
<i>Schizocythere</i> sp.		2							
<i>Krithe</i> sp.		22							

Sample Location	GG 35 9	GG 44 18	GG 97 80	GG 21 8	GG 22 8	GG 88 88	GG 89 58	GG 95 75	GG 92 64
Stratigraphical age	Lwr/Mid Miocene	Lwr/Mid Miocene	Tortonian	Lwr Messinian	Lwr Messinian	Lwr Messinian	Lwr Messinian	Lwr Messinian	Lwr Messinian
Facies	thin bedded	thick bedded	thick bedded	calc-lithic arenite	calc-lithic arenite	thin bedded	thin bedded	thin bedded	mega-ripples
Lithofacies interpretation	open marine	open marine	Beach	open shelf	open shelf	???	???	???	Tidal bar/shelf
Environment									
<i>Acanthocythereis</i> <i>gp hystrix</i>							1	1	
<i>Aurilia</i> <i>gp convexa</i>				3		1	2		
<i>Aurilia</i> <i>sp. a</i>			3	5	1	5	8	7	2
<i>Aurilia</i> <i>sp. e</i>				3					
<i>Callistocythere</i> <i>sp. a</i>				2	1				
<i>Callistocythere</i> <i>cf. panol</i>									
<i>Carinocythereis</i> <i>carinata</i>				1		2			
<i>Carinovalva</i> <i>aquila</i>				1					
<i>Chrysocythere</i> <i>paradisus</i>				1					
<i>Costa</i> <i>batei</i> <i>batei</i>			4	7	1	2		3	
<i>Cyamocytheridea</i> <i>meriscus</i>			24	4		4	5		
<i>Cyprideis</i> <i>gp. torosa</i>			12	35		10	22	10	
<i>Cytheridea</i> <i>cf. expansa</i>			14	6	2		16	4	
<i>Grapocythere</i> <i>h-scripta</i>							1		
<i>Hiltermannicythere</i> <i>rubra</i>				2					
<i>Hiltermannicythere</i> <i>cephalontica</i>				2					
<i>Ilyocypris</i> <i>sp. a</i>				6				5	
<i>Ilyocypris</i> <i>sp. b</i>			1	1				1	
<i>Kirithe</i> <i>langhiana</i>	3				1				
<i>Kirithe</i> <i>clatae</i>	4								
<i>Kirithe</i> <i>sp. c</i>								1	
<i>Krommelbeinella</i> <i>cf. caoe</i>			2			1	1	8	
<i>Loxoconcha</i> <i>trirectangularis</i>			4	3					
<i>Loxoconcha</i> <i>gp. rhomboida</i>			2	1					
<i>Loxoconcha</i> <i>sp. c</i>									
<i>Neocytherideis</i> <i>cf. senescens</i>			2	1					
<i>Nonurocytheris</i> <i>gp. laevigata</i>				16		2	2	2	
<i>Nonurocytheris</i> <i>seminulum</i>				10					
<i>Pontocythere</i> <i>cf. elongata</i>			9	4		5	22	24	1
<i>Pontocythere</i> <i>sp. b</i>				8					
<i>Urocytheris</i> <i>gp. favosa</i>			10	2		3	7	4	
<i>Vejerla</i> <i>tricolatula</i>				1					

## **Plate I: Foraminifera**

- 1** *Elphidium crispum* (Linné), diameter 1000  $\mu\text{m}$ , Lower Messinian, location 89.
- 2** *Elphidium* gp "*excavatum*", diameter 450  $\mu\text{m}$ , Lower Messinian, location 21
- 3** *Florilus boueanum* (d'Orbigny), diameter 650  $\mu\text{m}$ , Lower Messinian, location 22.
- 4** *Ammonia* gp. *becarri* (Linné), diameter 1250  $\mu\text{m}$ , Lower Messinian, location 22.
- 5** *Ammonia* gp. *becarri* (Linné), diameter 1250  $\mu\text{m}$ , Lower Messinian, location 21.
- 6** *Cibicides* cf. *wullerstorfi* (Schawager), diameter 600  $\mu\text{m}$ , Tortonian, location 107.
- 7** *Heterolipa subhaidingeri* (Parr), diameter 250  $\mu\text{m}$ , Lower Messinian, Location 95.
- 8** *Cibicides* sp., diameter 500  $\mu\text{m}$ , Lower Messinian, location 95.
- 9** *Heterolipa subhaidingeri* (Parr), diameter 500  $\mu\text{m}$ , Lower Messinian, location 95.

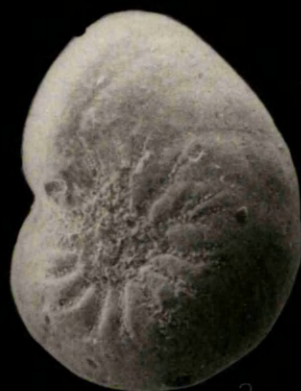




1



2



3



4



5



6



7



8



9

## Plate II: Foraminifera

- 1 *Nodosariid* height 1000  $\mu\text{m}$ , Lower Messinian, location 21.
- 2 *Bolivina* sp., height 900  $\mu\text{m}$ , Lower Messinian, location 21.
- 3 *Orthomorphina* sp., height 900  $\mu\text{m}$ , Lower Messinian, location 21.
- 4 *Bigenerina* sp., height 2000  $\mu\text{m}$ , Lower Messinian, location 21
- 5 *Uvigerina hispida* (Schwager), height 1000  $\mu\text{m}$ , Lower/Mid Miocene, location 35.
- 6 *Uvigerina peregrina* (Cushman), height 400  $\mu\text{m}$ , Lower/Mid Miocene, location 44.
- 7 *Uvigerina* sp. *bonineasis* (Fornasini), height 850  $\mu\text{m}$ , Lower Mid/Miocene, location 44.
- 8 *Orbulina Universia* (d'Orbigny), diameter 450  $\mu\text{m}$ , Tortonian, location 79.
- 9 *Lenticulina* sp., height 500  $\mu\text{m}$ , Lower/Mid Miocene, location 35.
- 10 *Lenticulina* sp., height 850  $\mu\text{m}$ , Lower/Mid Miocene, location 35.
- 11 *Globigerrinid* sp., height 450  $\mu\text{m}$ , Lower/Mid Miocene, location 35.
- 12 *Globigerrinid* sp., height 250  $\mu\text{m}$ , Lower/Mid Miocene, location 35.



1



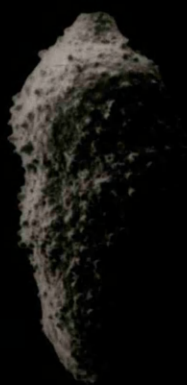
2



3



4



5



6



7



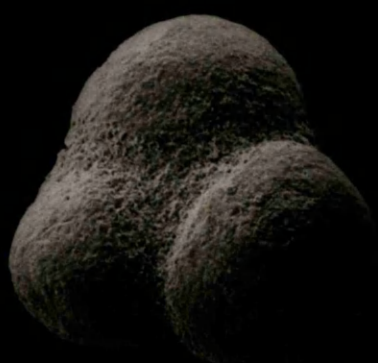
8



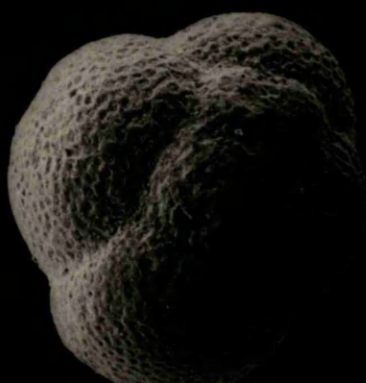
9



10



11



12



### Plate III: Ostracods

- 1 *Nonurocythereis* gp. *laevigata* (Pievi & Russo), length 500  $\mu$ m, Lower Messinian, location 95.
- 2 *Nonurocythereis* *seminulum* (Sequenza), length 500  $\mu$ m, Lower Messinian, location 21.
- 3 *Paleoblitocythere* sp., length 500  $\mu$ m, Lower/Mid Miocene, location 35.
- 4 *Krithe* sp., length 500  $\mu$ m, Lower/Mid Miocene, location 44.
- 5 *Krithe* sp., length 500  $\mu$ m, Lower/Mid Miocene, location 44.
- 6 *Cyamocytheridea* *meniscus* (Dorak), left valve, length 500  $\mu$ m, Lower Messinian, location 89.
- 7 *Cyprideis* gp. *torosa* (Jones), female, left valve, length 500  $\mu$ m, Lower Messinian, location 89.
- 8 *Cyprideis* gp. *torosa* (Jones), male, left valve, length 1000  $\mu$ m, Lower Messinian, location 89.
- 9 *Urocythereis* gp. *favosa* (Roemer), right valve, length 900  $\mu$ m, Lower Messinian, location 89.
- 10 *Cytherella* cf. *postdenticulata* (Oertli), length 1000  $\mu$ m, Lower/Mid Miocene, location 35.
- 11 *Cytherella* sp. length 1000  $\mu$ m, Lower/Mid Miocene, location 44.
- 12 *Henryhowella* *asperimma* (Reuss), length, 1000  $\mu$ m, Lower Messinian, location 95.
- 13 *Ilyocypris* sp. b, length 550  $\mu$ m, Lower Messinian, location 95.
- 14 *Ilyocypris* sp. a, length 700  $\mu$ m, Lower Messinian, location 95.
- 15 *Aurila* sp. a, length 500  $\mu$ m, Lower Messinian, location 88.
- 16 *Cytheridea* cf. *expansa* (Carbonnelli), left valve, length 500  $\mu$ m, Lower Messinian, location 95.
- 17 *Henricythere* *triangularis* (Oertli), left valve, length 650  $\mu$ m, Lower Messinian, location 95.
- 18 *Pontocythere* cf. *elongata* (Brady), left valve, length 550  $\mu$ m, Lower Messinian, location 95.
- 19 *Acanthocythereis* gp. *hystrix* (Reuss), length 500  $\mu$ m, Lower Messinian, location 95.
- 20 *Costa batel batel* (Brady), right valve, length 550  $\mu$ m, Lower Messinian, location 95.
- 21 *Macrocypris* cf. *bathyalensis* (Halings), length 1500  $\mu$ m, Lower/Mid Miocene, location 44.



1



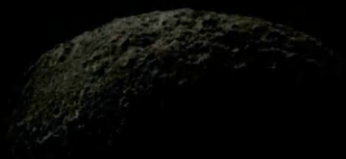
2



3



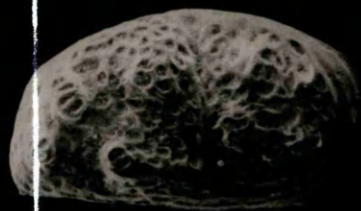
4



5



6



7



8



9



10



11



12



13



14



15



16



17



18



19



20



21



**Appendix III**  
**Selected**  
**Sedimentary Logs**  
**From**  
**The Aljibe Flysch**  
**(Gibraltar Arc)**





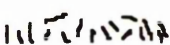
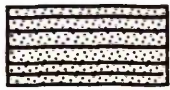

The following appendix gives a representative sample of sedimentary logs taken from the Aljibe Arenites (Gibraltar Arc). For each log the location numbers are given. For each location there is a corresponding grid reference and relevant thesis map which are given in Appendix V. Thesis maps can be found in Part II, Figures 1.4, 1.5 & 1.6.

# Key

## Lithology

	Marl
	Siltstone
	Sandstone
	Micro-conglomerate

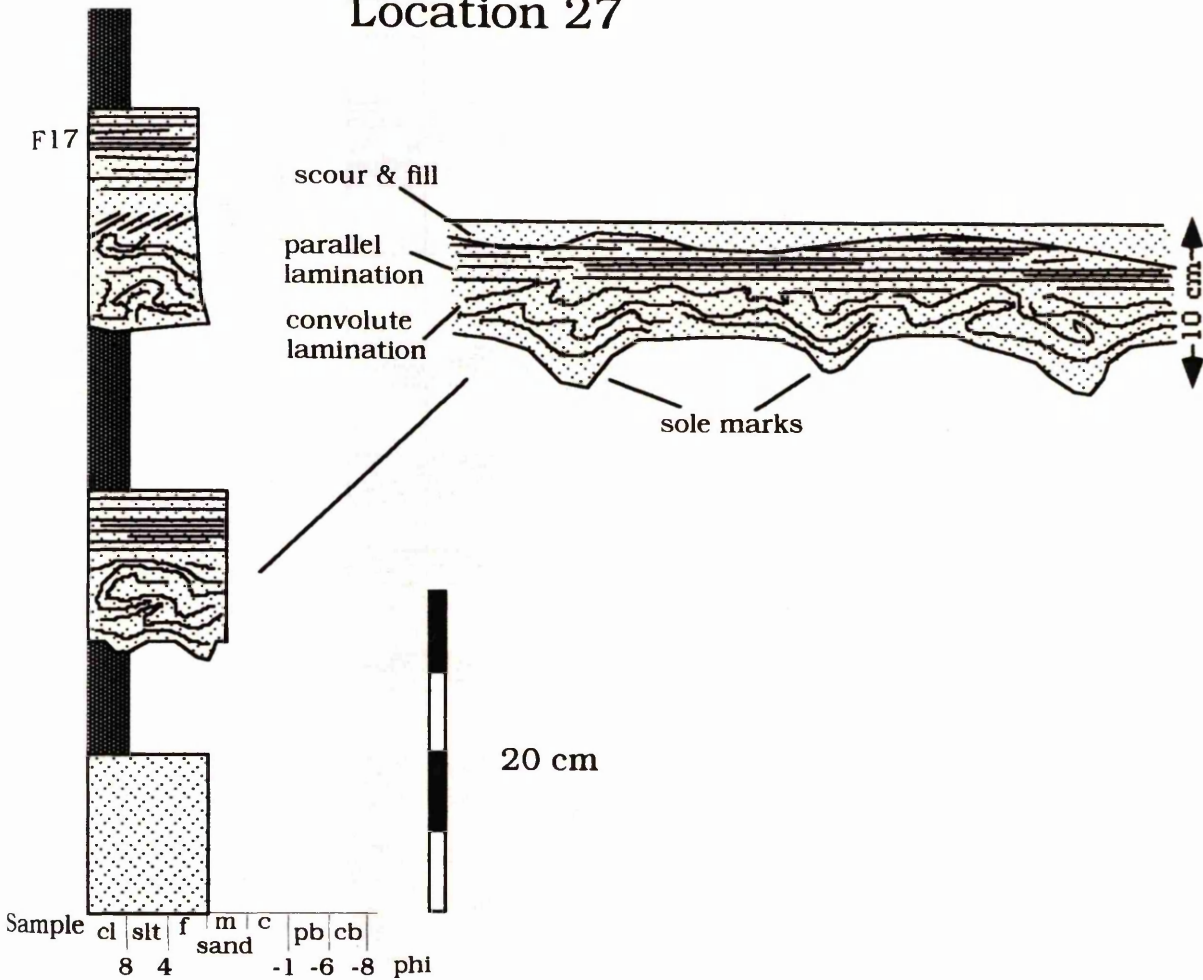
## Sedimentary Structures

	Trough cross-lamination
	Convolute lamination
	Diffuse streaks, lighter coloured sand (Bioturbation ??)
	Planar lamination
	Cross-lamination

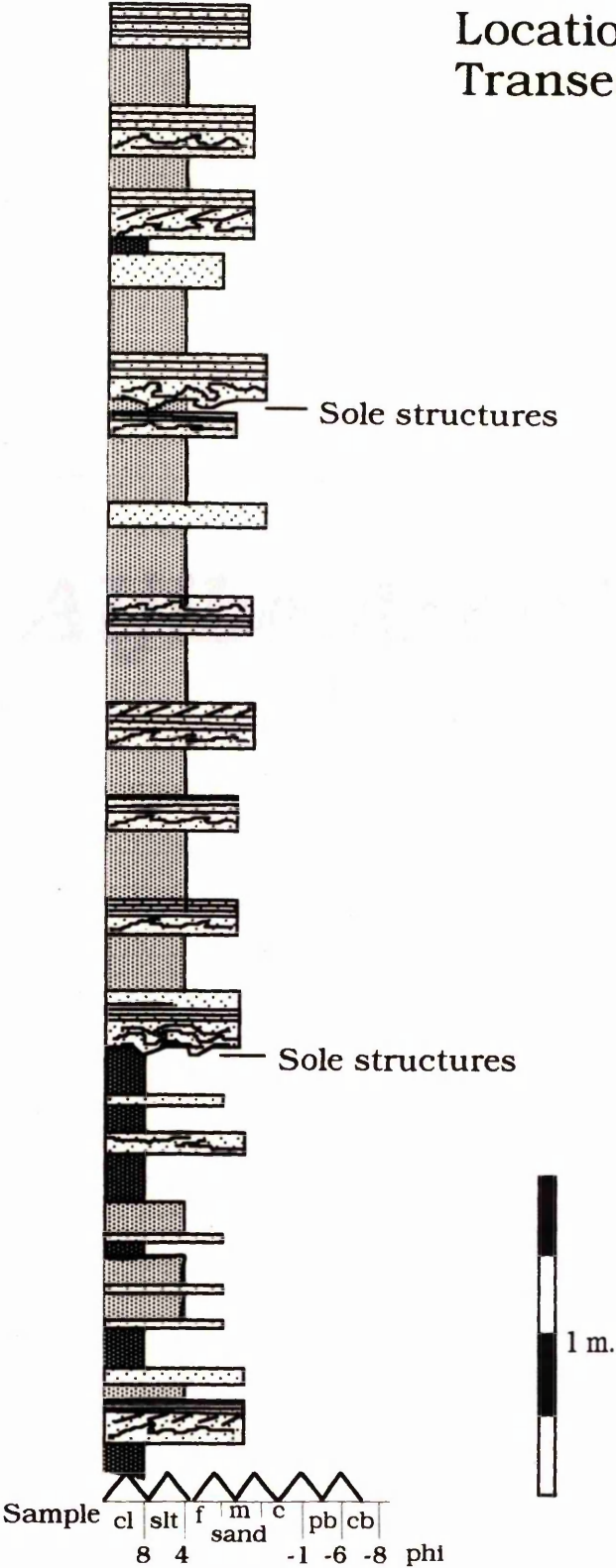
***Beneiza Flysch***



Location 27

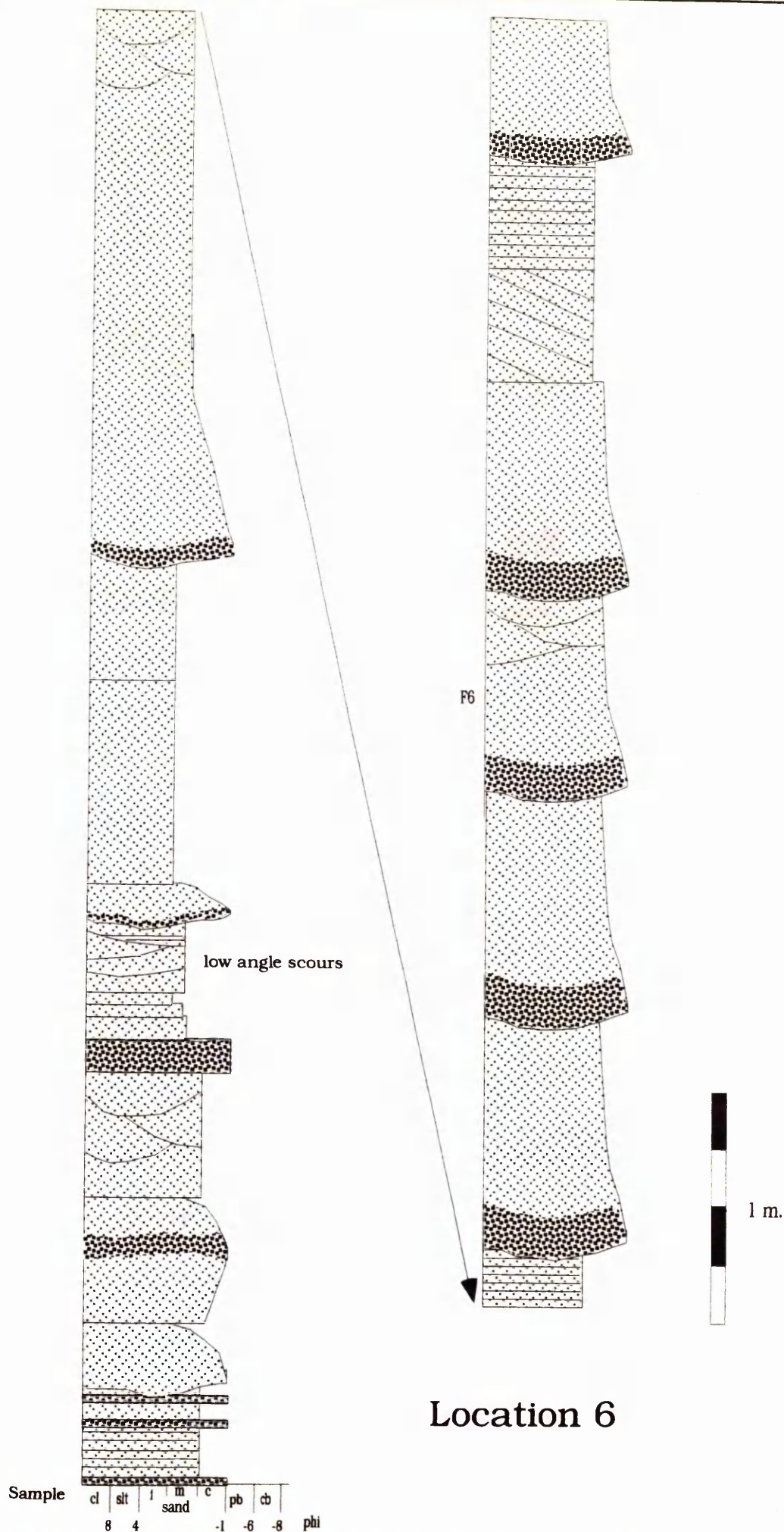


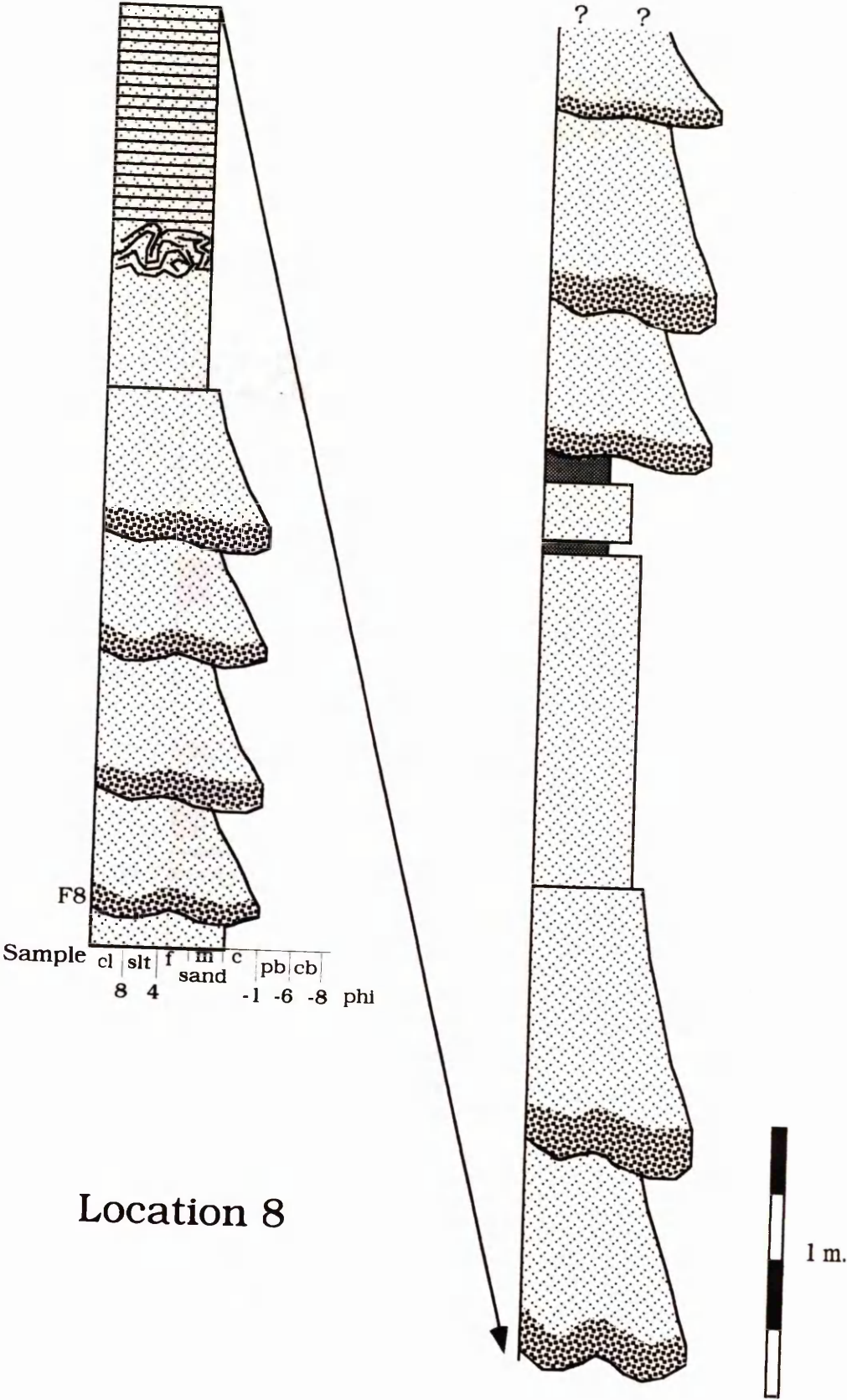
Location 66  
Transect 3



# ***Aljibe Arenites***

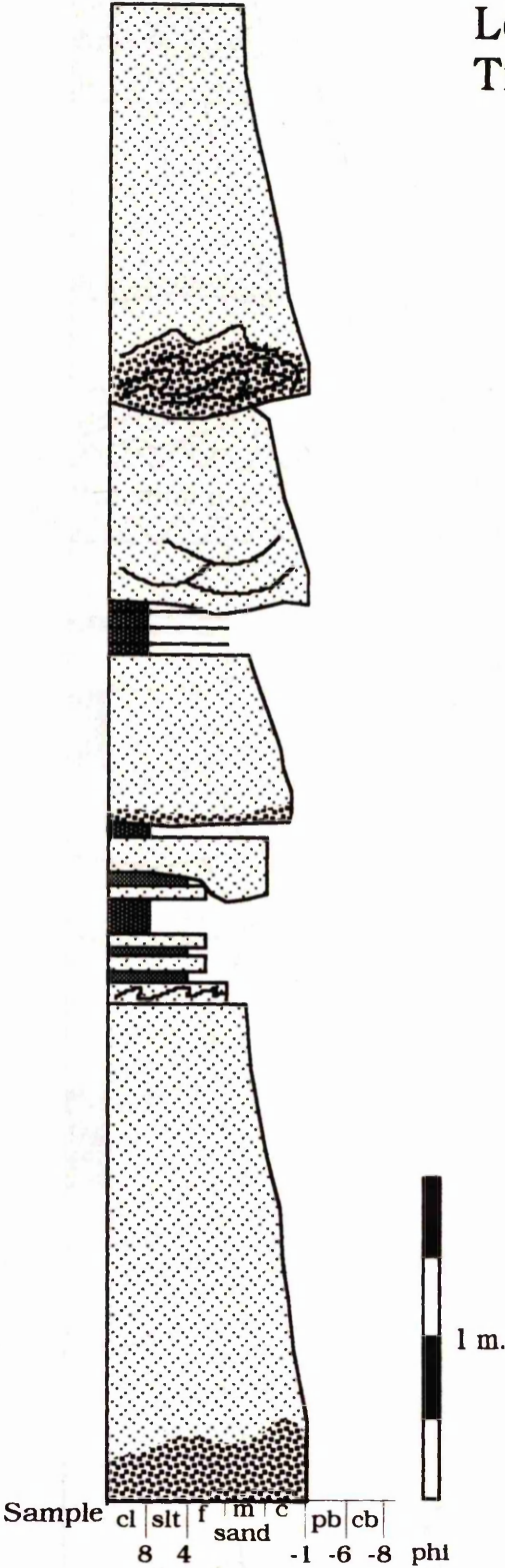




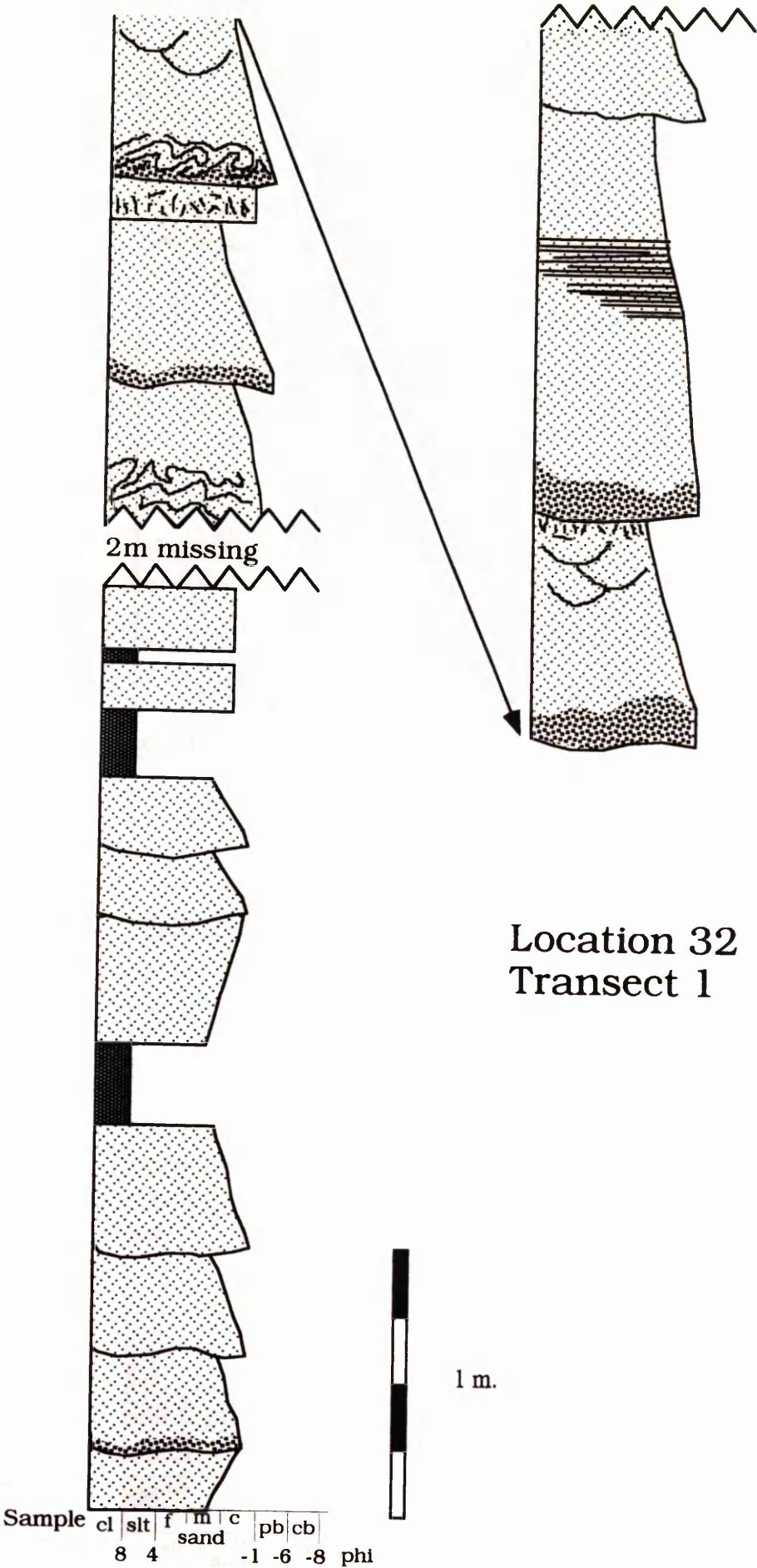


Location 8

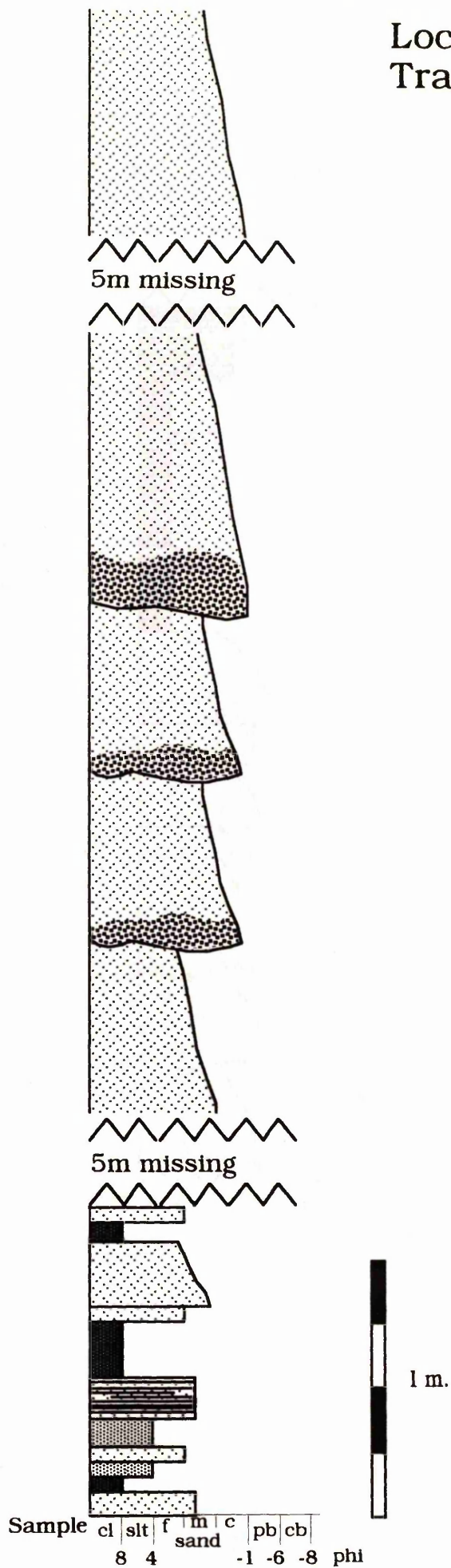
Location 31.  
Transect 1

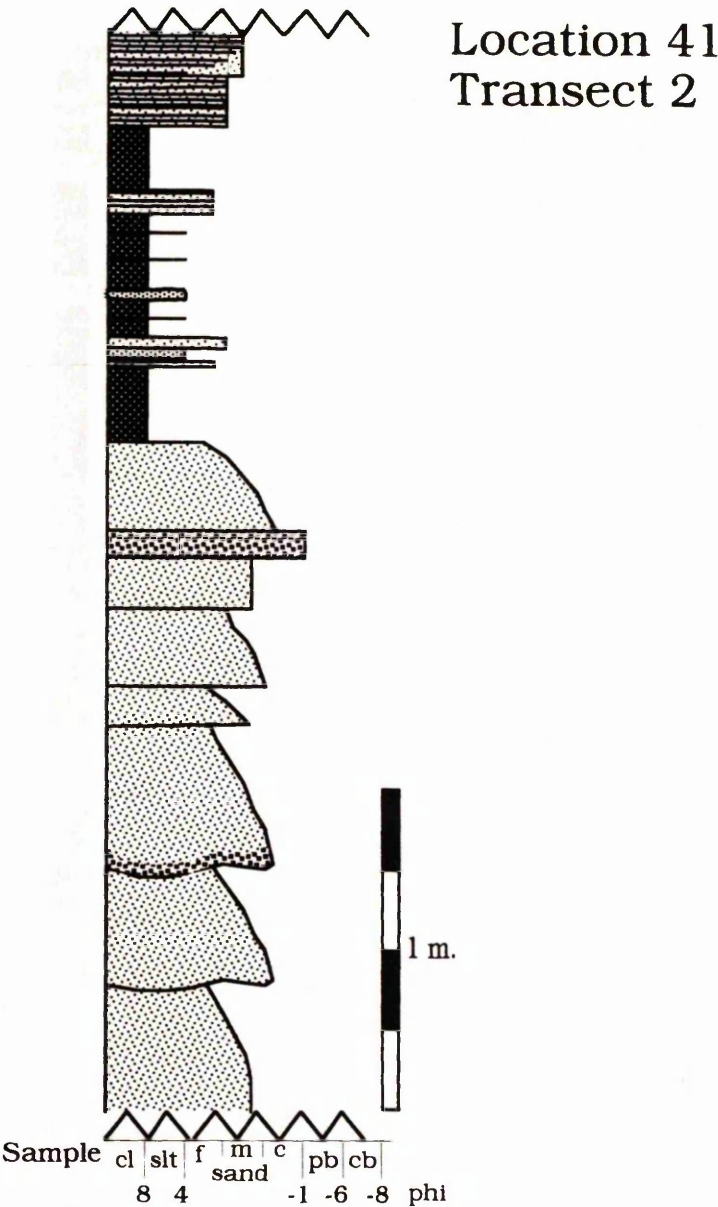






Location 34  
Transect 1

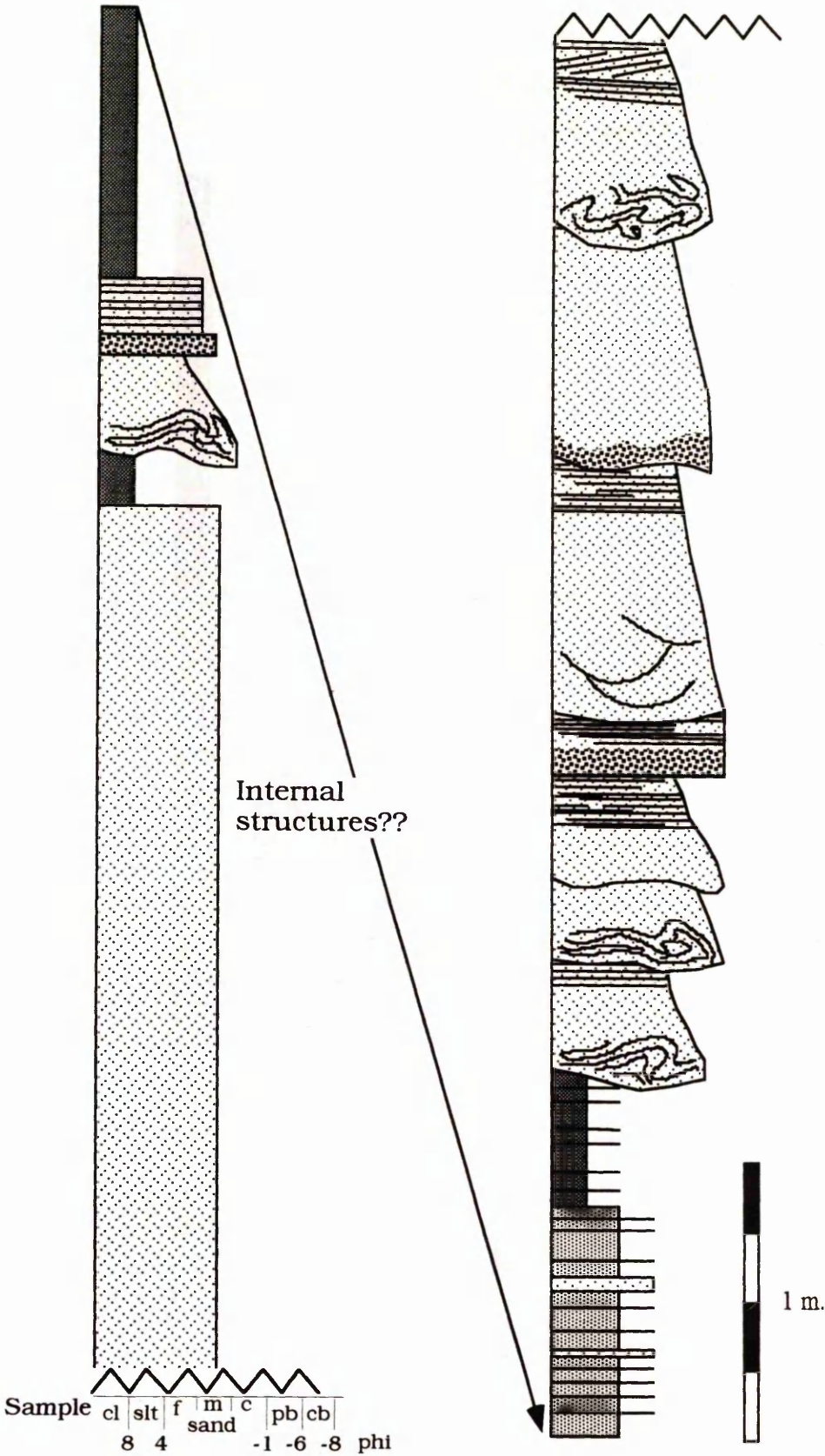






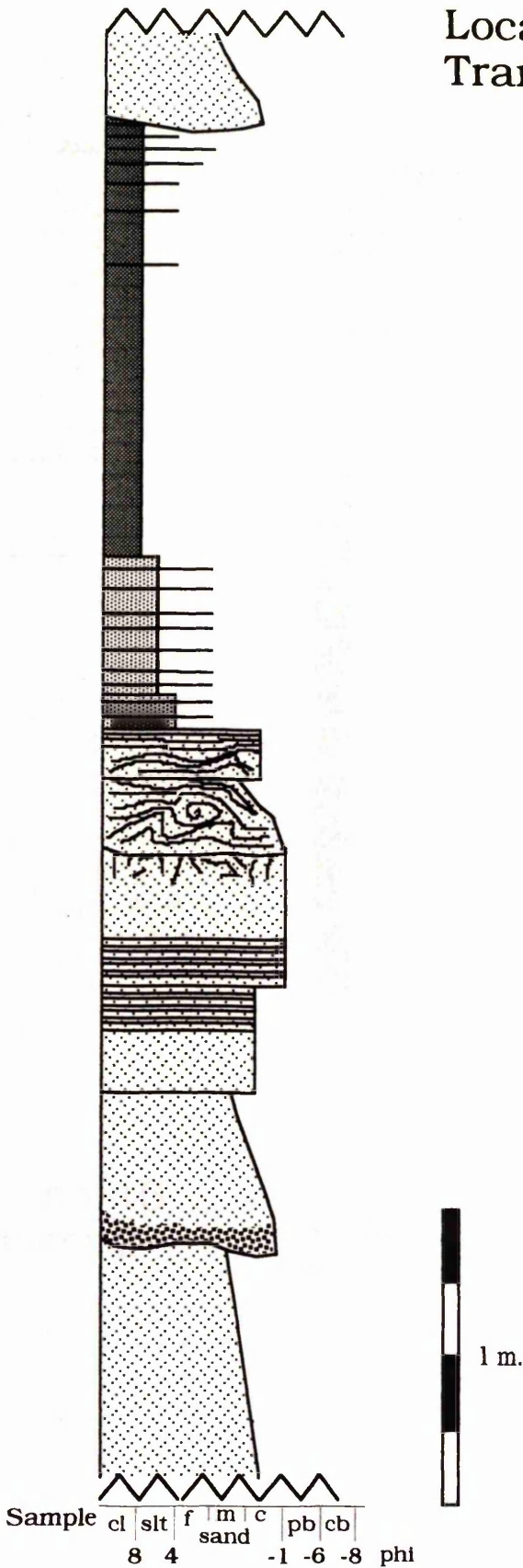


Location43  
Transect 1

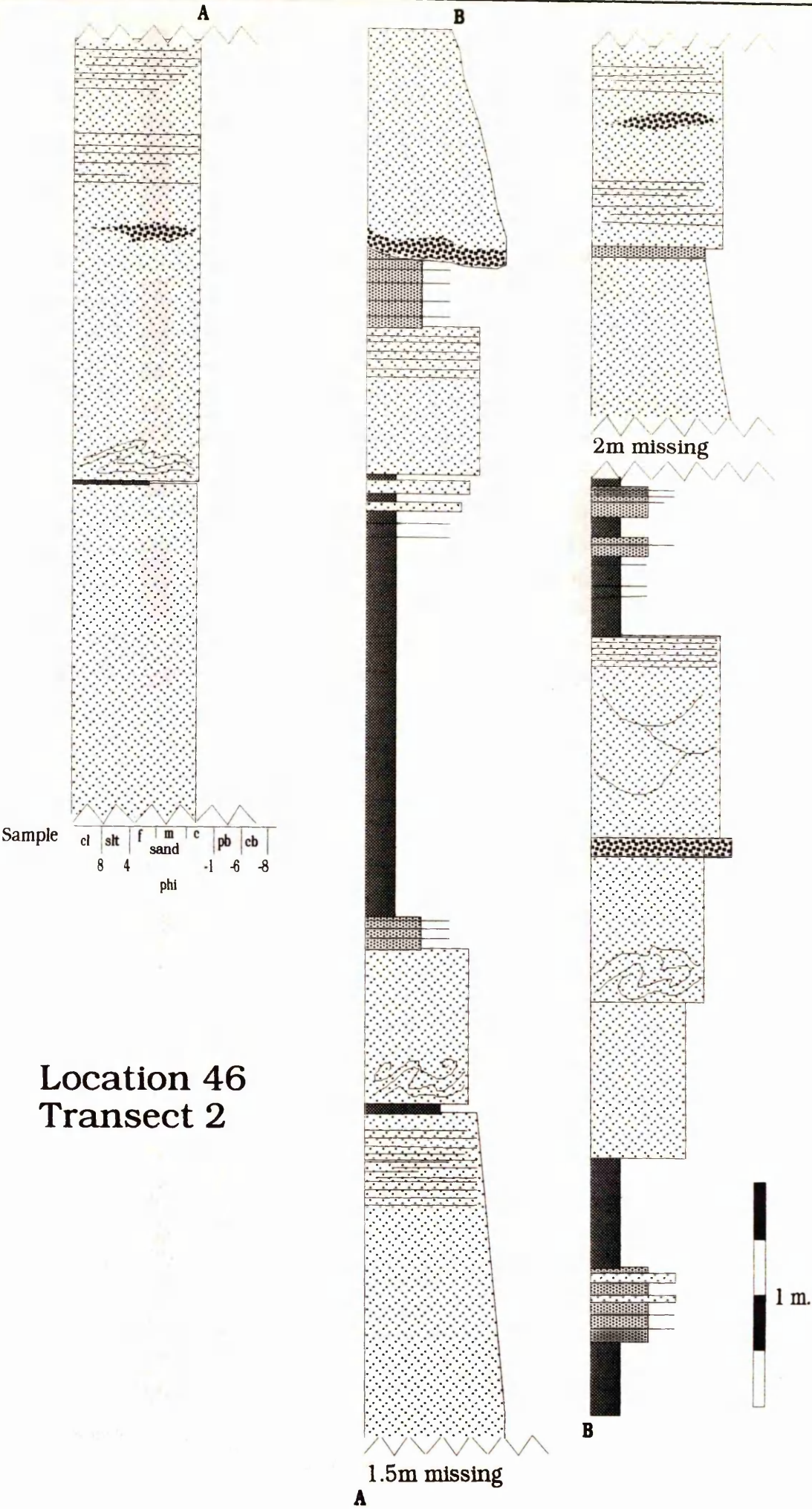


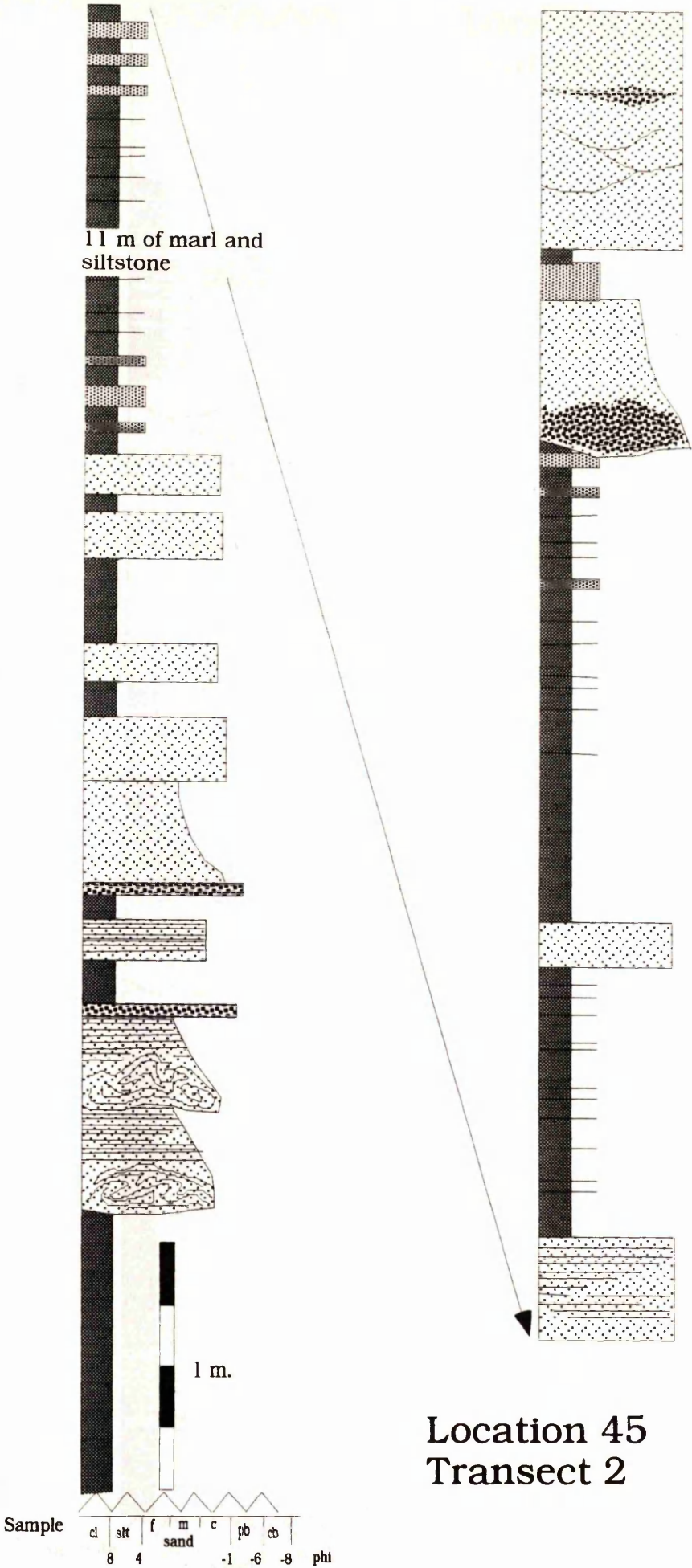
Location 44  
Transect 2

Location 45  
Transect 2

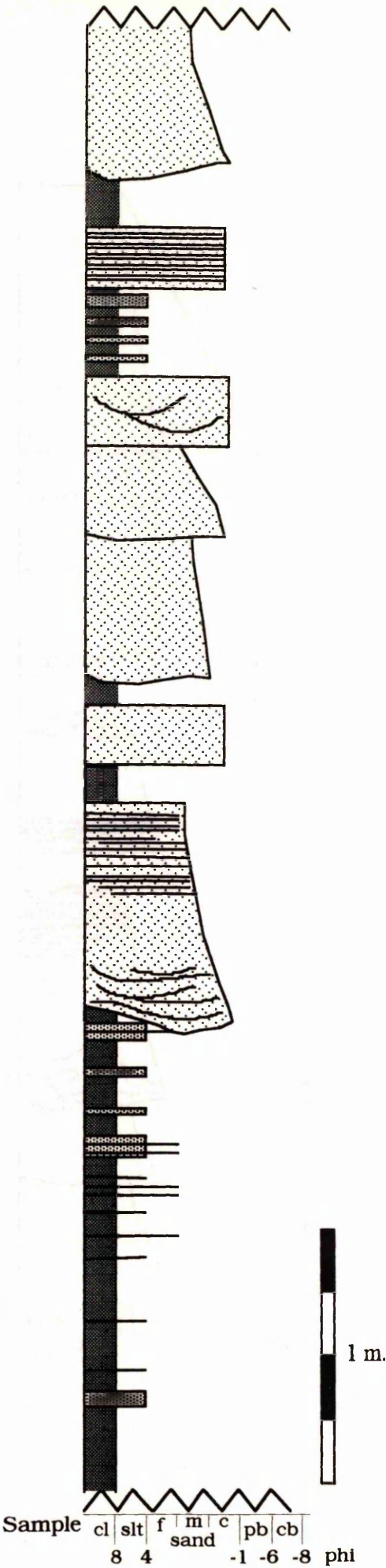




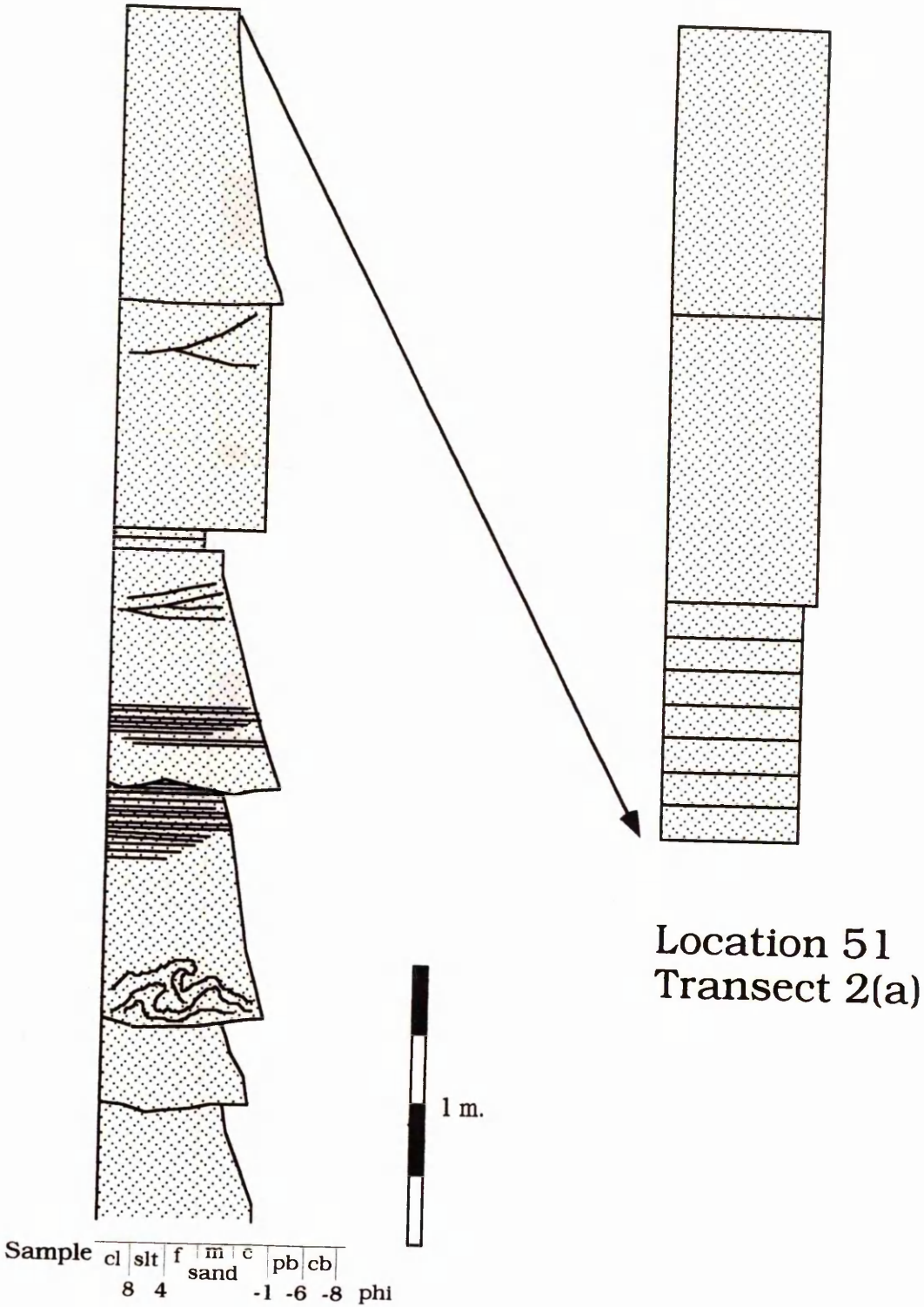




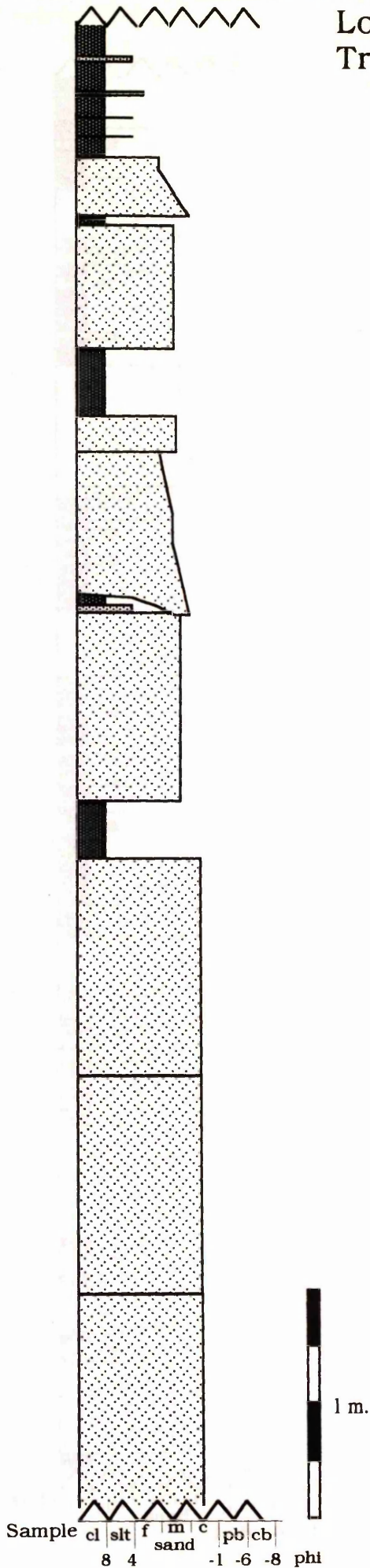
Location 50  
Transect 2



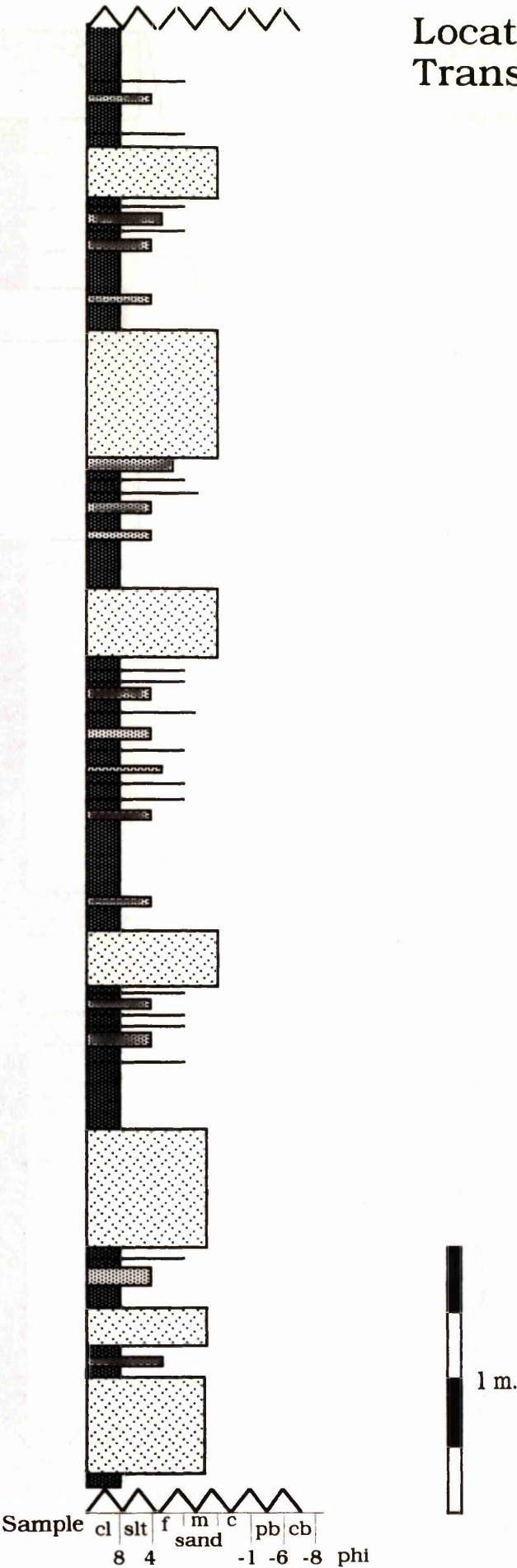




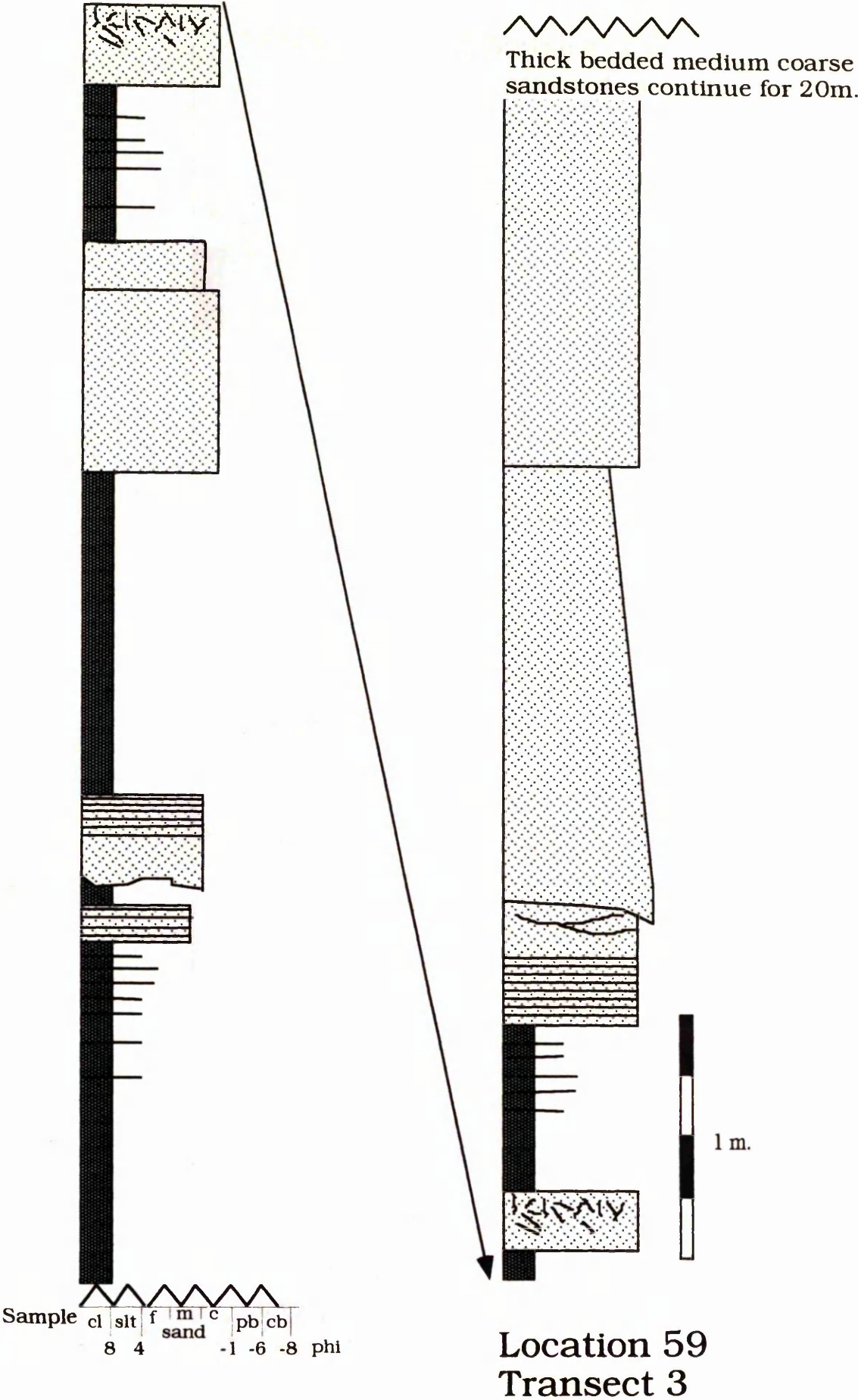
Location 52  
Transect 2(a)



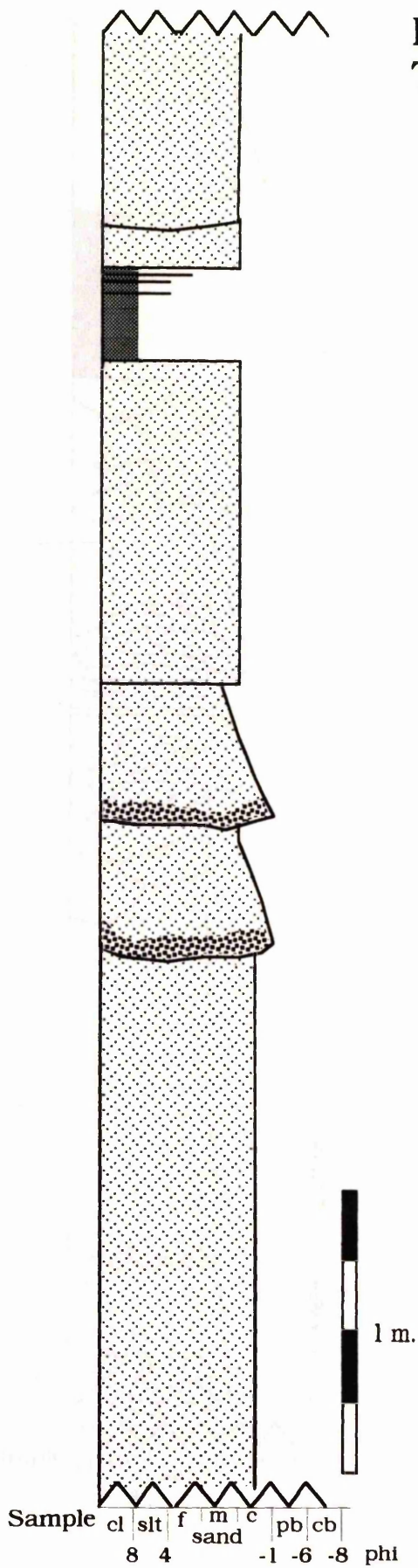
Location 53  
Transect 2(a)

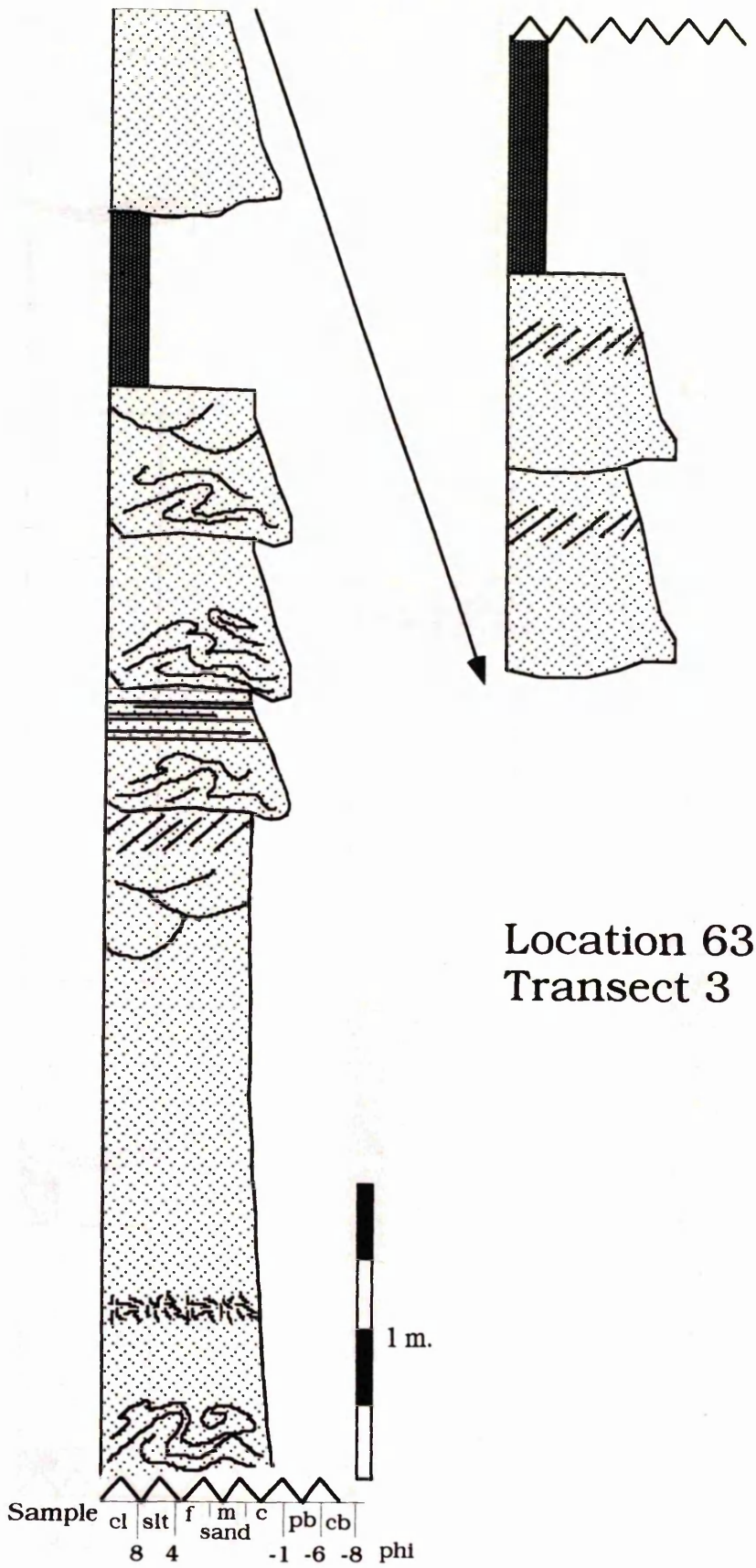




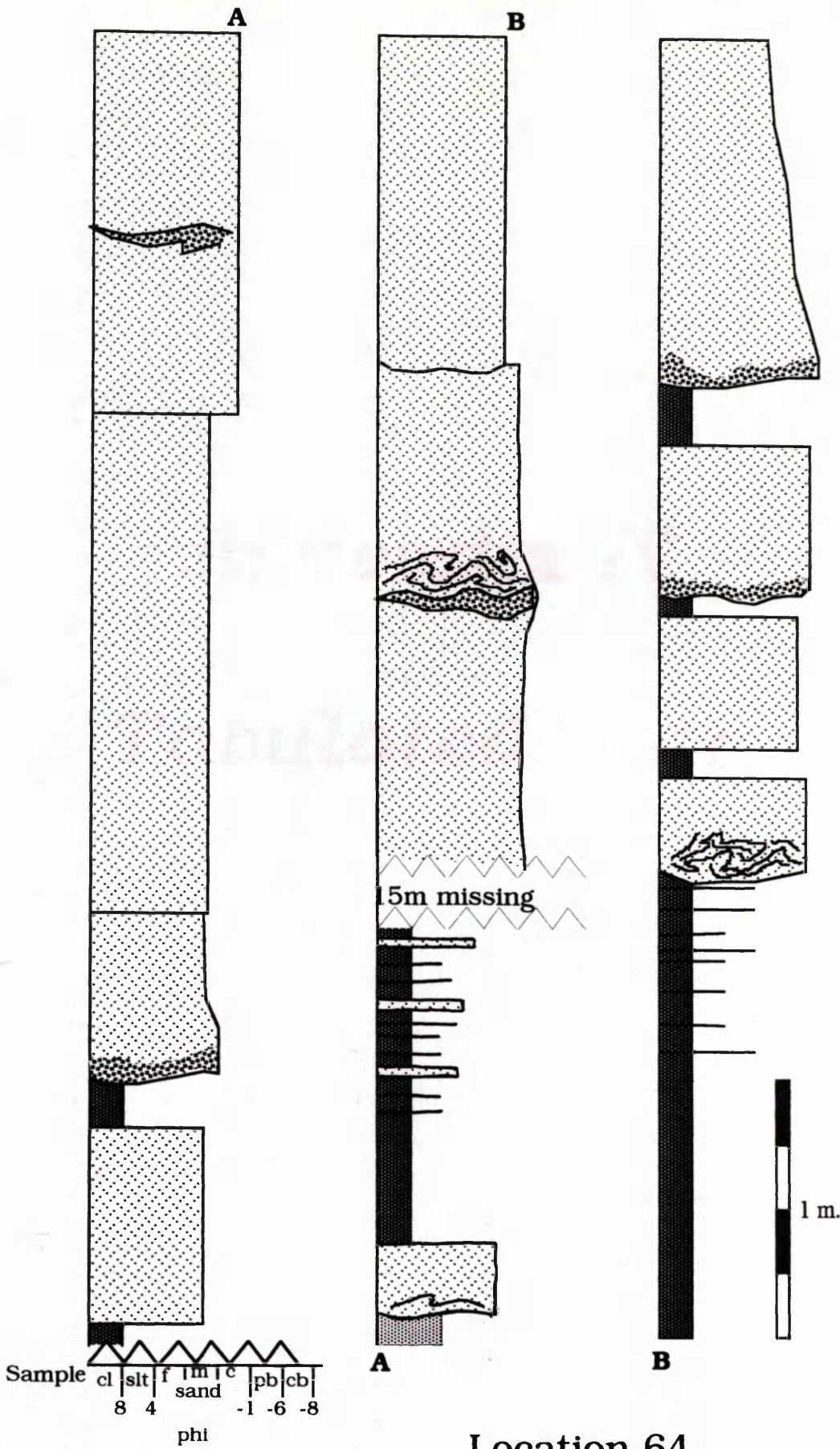


Location 62  
Transect 3









Location 64  
Transect 3

# ***Appendix IV***

## ***Tabulated Data***



## **Lower Miocene Boulder Facies From the Guadalquivir Basin**

The following data sets represent a detailed survey of the boulder facies found at location 40 (Ref. 530 334) in the Lower Miocene Guadalquivir Basin.

The data set is in two parts, lenticular unit dimensions, and a detailed survey of the clasts present within the lenticular units. The lenticular units are figured in Volume 2, Part I (Fig. 3.9).

### **Lenticular Unit Dimensions**

The lenticular units are recognised where erosional bounding surfaces form stacked lenticular units which occasionally have a winged geometry. Nine units are recognised at location 40, exposed in a N-S orientated section. Measurements made of these unit were as follows:

#### *Ht of Base*

This is the height (m) measured from the base of the section to the lowest part of the basal bounding surface of the lenticular unit. The base of the section is defined by a road.

#### *Width*

This is the maximum horizontal width (length), in metres, of the lenticular unit.

#### *Max Depth*

This is the maximum vertical depth (thickness) of the lenticular unit and is measured in metres.

#### *Min Depth*

This is the minimum vertical depth (thickness) of the lenticular unit. This thickness was measured only where it was maintained for a distance of at least 0.5 m and was at least 0.5 m away from the end (termination) of the unit.

### **Clast Survey**

This data set represents a detailed survey of the clasts (boulders) found within the lenticular units of the boulder facies. The clasts were classified as follows:

#### *Unit No.*

This refers to the unit number, as is given in the lenticular unit data set, within which the clast was found. E.g. Unit 1, Clast 1 is the first clast in unit number 1.

#### *Clast*

A reference number given to the clast. Clasts were numbered within each lenticular unit.



### *Lithology*

The lithology of the clast. Lithologies were defined as follows;

#### *Marl*

*Calcite*, crystalline calcite clasts in which individual crystals can be recognised

*Reworked* clasts are conglomeratic clasts that are interpreted to have been reworked from the underlying lenticular units

*Type I* is a lithology that is characterised by brown stained, indurated limestone (dolomite ??). These clasts commonly contain fractures that are filled by calcite.

### *Long Axis*

This is a measurement (in cm) of the long axis of the clast and is defined by the maximum diameter of the clast.

### *Short Axis*

A measurement of the short axis (in cm) of the clast and is defined by the minimum diameter of the clast.

### *Long Axis Orien*

The orientation of the clast was measured as a dip and dip direction in the N-S section. This is a 2 dimensional measurement only. An orientation of 18 N means that the long axis of the clast dips 18 degrees towards the northern end of the section.

### *Ht from Ch Base*

This the vertical measured distance from the base of the lenticular unit to the approximate centre of the clast.

### *Sample*

A reference number for samples taken of the clasts.

Lower Miocene Boulder Facies  
Lenticular Unit Dimensions

Unit No.	Ht of Base (m)	Width (m)	Max Depth (m)	Min Depth(m)
1	0.00	15.00	2.00	0.20
2	0.00	6.00	2.00	0.30
3	0.68	3.00	1.15	0.33
4	0.60	3.50	2.00	0.30
5	0.00	7.00	2.00	0.20
6	1.80	8.50	1.50	30.00
7	0.00	15.00	2.50	0.20
8	0.00	8.00	1.50	0.40
9	0.00	6.00	1.44	0.20

# Survey of Clasts Found in Lower Miocene Boulder Facies

Unit No.	Clast	Lithology	Long Axis (cm)	Short Axis(cm)	Long Axis Orien	Ht fom Ch Base	Sample
1	1	marl	0.26	0.19	22 N	0.10	
	2	marl	0.22	0.10	18 N	0.53	
	3	marl	0.20	0.05	20 N	0.47	
	4	calcite	0.14	0.06	38 S	0.41	
	5	marl	0.15	0.06	2 S	0.78	
	6	marl	0.17	0.06	3 S	0.72	
	7	marl	0.33	0.17	30 S	1.20	
	8	marl	0.26	0.20	35 S	0.97	
	9	marl	1.14	0.70	15 S	0.15	GQ 69
	10	marl	0.22	0.14	10 S	1.52	
	11	reworked	0.55	0.30	70 N	0.69	
	12	reworked	0.35	0.20	20 S	0.79	
	13	marl	0.38	0.20	20 S	1.05	
	14	marl	0.17	0.13	20 S	1.05	
	15	marl	0.29	0.18	20 S	1.09	
	16	marl	0.40	0.15	0	1.20	
	17	marl	0.42	0.15	15 N	1.30	
	18	marl	0.30	0.30	0	0.00	
	19	marl	1.20	0.37	30 S	0.80	
	20	marl	0.31	0.20	45 S	0.63	
	21	type I	0.24	0.10	80 S	1.07	GQ 70
	22	type I	0.36	0.70	10 S	0.20	
	23	type I	0.54	0.22	0	0.84	GQ 71
	24	type I	1.30	0.70	10 S	1.02	
	25	type I	0.35	0.18	0	0.00	
	26	type I	0.80	0.62	0	0.00	
	27	marl	0.60	0.52	5 S	0.30	
	28	type I	0.50	0.30	0	2.00	
	29	type I	0.40	0.20	80 S	2.00	
	30	reworked	0.65	0.60	85 S	0.00	
2	1	marl	0.50	0.26	10 S	1.30	
	2	reworked	0.40	0.36	90	1.20	
	3	reworked	0.50	0.30	15 S	1.10	
	4	type I	0.60	0.43	0	0.00	
	5	type I	0.30	0.30	0	0.84	
	6	type I	0.70	0.32	15 S	1.64	
	7	type I	0.85	0.66	0	0.52	
	8	type I	0.20	0.15	0	0.89	
	9	reworked	1.20	1.10	0	0.40	
	10	marl	0.15	0.05	5 N	1.05	
	11	marl	0.20	0.15	90	1.11	
	12	marl	0.30	0.22	25 N	1.20	
3	1	marl	0.40	0.28	0	0.68	
	2	marl	0.44	0.15	5 S	1.07	
	3	marl	0.25	0.10	0	1.22	
	4	marl	0.50	0.15	0	0.90	
	5	marl	0.24	0.16	5 N	1.24	
	6	marl	0.40	0.26	0	0.90	
	7	marl	0.68	0.10	0	1.17	
4	1	reworked	1.50	0.70	0	0.80	
5	1	reworked	1.10	0.38	0	0.60	
	2	type I	0.80	0.33	0	0.20	
	3	type I	0.50	0.40	0	1.80	
	4	type I	0.50	0.40	0	1.80	
	5	type I	0.33	0.18	0	0.56	
	6	marl	0.27	0.10	0	0.81	
	7	marl	0.23	0.16	90	1.22	
	8	marl	0.54	0.29	30 N	0.10	
	9	marl	0.90	0.55	20 N	0.10	
	10	marl	1.00	0.76	28 N	0.30	



6	1	marl	0.31	0.23	90	2.02
	2	marl	0.30	0.13	90	2.02
	3	reworked	0.32	0.18	90	1.93
	4	marl	0.15	0.11	90	2.01
	5	marl	0.34	0.26	90	1.98
	6	marl	0.30	0.29	90	1.98
	7	marl	0.25	0.28	0	1.98
	8	marl	0.74	0.44	0	2.04
	9	reworked	0.35	0.14	0	2.20
	10	reworked	0.20	0.15	30 S	2.02

7	1	reworked	0.44	0.26	85 N	0.74
	2	type I	1.18	0.61	0	0.00
	3	type I	1.02	0.64	10 S	0.15
	4	type I	0.53	0.26	12 S	0.00
	5	reworked	0.28	0.50	60	0.95
	6	marl	0.40	0.21	0	0.99
	7	marl	0.85	0.20	0	2.00
	8	type I	0.20	0.16	60 S	0.80
	9	reworked	0.60	0.40	5 N	0.65
	10	reworked	0.70	0.44	0	1.31
	11	reworked	0.80	0.70	0	1.10

8	1	marl	1.00	0.46	15 N	0.69
	2	reworked	0.80	0.42	85 S	0.98
	3	marl	0.61	0.42	85 S	0.98
	3	marl	0.61	0.42	90	0.90
	4	reworked	0.31	0.32	0	0.85
	5	marl	0.50	0.33	0	0.75
	6	marl	0.60	0.20	35 S	0.84
	7	marl	0.33	0.15	80 S	0.90
	8	marl	0.26	26.00	0	0.85
	9	type I	0.33	0.24	10 N	0.92
	10	type I	0.88	0.33	5 N	1.02
	11	type I	0.44	0.26	0	1.15
	12	marl	0.40	0.33	0	1.50
	13	marl	0.45	0.35	0	1.55

9	1	marl	0.50	0.30	80 S	0.00
	2	marl	0.60	0.42	70 S	0.00
	3	marl	0.44	0.40	0	0.00
	4	marl	0.83	0.74	0	0.00
	5	type I	0.60	0.32	0	0.20
	6	type I	0.47	0.40	76 S	0.30
	7	type I	0.44	0.26	62 S	0.38
	8	type I	0.32	0.34	90 N	0.24
	9	marl	0.48	0.30	85 N	0.00
	10	marl	0.60	0.24	0	0.26

	1	marl	0.28	0.16	38 S	0.46
	2	type I	0.40	0.25	20 S	2.12
	3	type I	0.50	0.14	0	1.82
	4	marl	0.50	0.47	0	0.00
	5	marl	0.44	0.33	85 N	0.34
	6	marl	0.26	0.17	0	0.88
	7	marl	0.93	0.82	45 S	1.14
	8	reworked	0.44	0.29	15 S	0.52
	9	marl	0.83	0.44	0	0.00
	10	marl	1.45	0.77	20 S	0.75
	11	type I	0.82	0.70	80 N	0.79
	12	type I	0.77	0.77	0	1.92
	13	type I	0.99	0.80	30 S	0.45
	14	marl	0.68	0.36	45 S	1.45
	15	marl	1.23	0.40	0	2.45
	16	marl	0.40	0.30	0	0.68
	17	marl	1.92	1.00	44 S	0.00
	18	type I	0.58	0.24	44 S	0.45
	19	marl	0.90	0.60	90	0.34
	20	type I	1.35	0.85	60 S	0.00

## Quantitative Petrography of Samples from The Guadalquivir Basin

The following data set represents the results of petrographic point counts conducted on samples from the Guadalquivir Basin.

Point-counts of the framework modes of each thin section were conducted using a mechanised point-counting stage. The stage-advance was set to increment a distance equal to the average grain size. Two counts were conducted on each thin section. The first quantified the proportion of monocrystalline quartz (**Qm**), plagioclase (**P**), K-feldspar (**K**) and lithic fragments (**Lt**) in each sample. A total of 500 grains was counted. The second count was designed to provide a detailed inventory of the lithic fragments in terms of their metamorphic, volcanic and sedimentary components. The metamorphic component was split into metamorphic grain types, based on the method outlined by Rapson (1965) and Ingersoll & Suczek (1979). A total of 500 lithic fragments were counted and classified for each sample. Metamorphic grain types were recognised as follows;

**phyllitic schist (Ph.Sch)** fragments of micaceous with a distinct schistose fabric, (i.e. a well developed, finely spaced cleavage);

**quartz, mica and feldspar aggregate (Q-M-F Ag)** fragments of quartz mica and feldspar aggregates lacking a distinct fabric;

**quartz, mica and feldspar tectonite (Q-M-F Tect)** fragments composed of quartz mica and feldspar with a distinct fabric such as grain flattening, elongation or alignment;

**quartz and mica aggregate (Q-M Ag)** fragments containing only quartz and mica lacking a distinct fabric;

**quartz mica tectonite (Q-M Tect)** fragments containing quartz and mica with a distinct fabric such as grain flattening, elongation or alignment;

**polycrystalline quartz tectonite (Qp Tect)** fragments of polycrystalline quartz in which grains are flattened, elongated or aligned to form a distinct fabric;

**Micas (Micas)** single mica grains;

**polycrystalline micas (Micas p)** fragments containing more than one mica grain, but without a schistose fabric;

**polycrystalline quartz** fragments of polycrystalline quartz lacking a distinct fabric;

**quartz and feldspar aggregate (Q-F Ag)** fragments containing quartz and feldspar but lacking a distinct fabric and

**contact metamorphic minerals (Contact meta)** minerals associated with the contact metamorphism of country rocks. The commonest is cordorite.

Sedimentary lithic fragments were also divided into generic lithic fragment types which are as follows;

**sandstone (Sand)** fragments containing identifiable quartz, feldspar and lithic grains of sedimentary origin;

**argillite other than marls (Argillite)** mud-rock fragments, excluding carbonate;  
**polycrystalline carbonates (Carb pc)** carbonate fragments in which grains are identifiable;  
**Marl (Marl)** carbonate mud rock in which separate grains could not be identified and  
**Chert (Chert)** cryptocrystalline quartz fragments.

Framework modes, outlined above, were used to derive other modal values characterizing the rock sample, including the total number polycrystalline quartz grains ( $Q_p$ ), the total number of metamorphic lithic fragments ( $L_m$ ), the total number of volcanic lithic fragments ( $L_v$ ) the total number of sedimentary lithics ( $L_s$ ), the total number of volcanic and meta-volcanic lithic fragments ( $L_{vm}$ ) and the the total number of sedimentary and meta-sedimentary lithic fragments ( $L_{sm}$ ). These variables were calculated as follows;

$$Q_p = Q_p \text{ Tect} + Q_p$$

$$L_m = \text{Ph.Sch} + Q\text{-M-F Ag} + Q\text{-M-F Tect} + Q\text{-M Ag} + Q\text{-M Tect} + \text{Micas} + \text{Mica p} + Q\text{-F Ag} + \text{Contact Meta}$$

$$L_v = \text{Total number of hypabyssal volcanic grains}$$

$$L_s = \text{Sand} + \text{Argillite} + \text{Carb pc} + \text{Marl} + \text{Chert}$$

$$L_{vm} = L_v$$

$$L_{sm} = L_m + L_s$$



[illegible]

	Age Facies	Q-F 104		Q-F 88		Q-F 79(a)		Q-F 77(b)		Q-F 78(b)		Q-F 88		Q-F 89		Q-F 92		Q-F 20		Q-F 95		Q-F 106		Q-F 40
		Tortonian	4	92	Tortonian	80	4	Messinian	49	46	Messinian	47	Messinian	88	Messinian	58	Messinian	64	Messinian	8	Messinian	75	Messinian	
		%matrix	26				resin		0		0	resin		resin		resin		44		15		42	resin	
		% Bloclasts	13		<1		<1		92		84	4		<2		8		0		10		16	<1	
Q-F-Lt (500 points)	1	Qm	346		334		247		n/a		n/a	224		313		240		364		195		320	217	
	2	P	2		30		20		n/a		n/a	18		12		13		3		18		12	21	
	3	K	0		8		1		n/a		n/a	12		5		0		5		10		6	8	
	4	Lt	152		128		184		n/a		n/a	246		170		247		127		277		162	254	
		Total F (2+3)	2		38		21		n/a		n/a	30		17		13		8		28		18	29	
Lt (500 points) Meta Lithics	5	Ph. Sch	0		0		0		n/a		n/a	0		0		0		0		0		0	0	
	6	Q-M-F Ag	6		14		10		n/a		n/a	20		19		15		13		19		8	0	
	7	Q-M-F Tect	0		0		0		n/a		n/a	0		0		0		0		0		0	0	
	8	Q-M Ag	9		22		20		n/a		n/a	20		73		12		28		27		25	0	
	9	Q-M Tect	0		0		0		n/a		n/a	0		0		3		9		3		0	0	
	10	Qp Tect	5		0		25		n/a		n/a	0		13		2		16		2		5	0	
	11	Micas	2		10		0		n/a		n/a	18		0		6		25		18		37	2	
	12	Mica p	16		0		0		n/a		n/a	0		13		2		19		6		0	0	
	13	Qp	19		56		120		n/a		n/a	38		75		25		131		38		70	14	
	14	Q-F Agg	0		0		0		n/a		n/a	0		0		0		0		0		0	0	
	Contact Meta		0		0		0		n/a		n/a	0		0		0		0		0		0	0	
	Volcanic			0		0		0		n/a		n/a	0		0		1		0		0		0	0
		Hypabysall																						
	Sediment		19		16		80		n/a		n/a	n/a	14		15		0		5		26		10	10
Sand		3		0		25		n/a		n/a	n/a	0		0		0		0		0		1	0	
Argillite (other than marls)		58		144		125		n/a		n/a	n/a	184		160		188		79		229		102	235	
Carb pc		331		188		60		n/a		n/a	n/a	170		85		228		142		105		190	210	
Marl		19		32		0		n/a		n/a	n/a	24		26		9		22		13		29	28	
Chert																								
	Unknown Lt	13		18		35		n/a		n/a	n/a	12		21		9		11		14		21	1	
	Qp (13+10)	24		56		145		n/a		n/a	n/a	38		88		27		147		40		75	14	
	Lm(5...9+11+12+14+16+17)	33		46		30		n/a		n/a	n/a	58		105		38		94		73		70	2	
	Lv(17)	0		0		0		n/a		n/a	n/a	0		0		1		0		0		0	0	
	Ls(18...22)	430		380		290		n/a		n/a	n/a	392		286		425		248		373		332	483	
	Lvm(17)	0		0		0		n/a		n/a	n/a	0		0		1		0		0		0	0	
	Lsm(Ls+Lm)	463		426		320		n/a		n/a	n/a	450		391		463		342		446		402	485	
		1.94		1.36		1.02		1.56		1.29	1.28	0.91		1.56		1.28		1.8		1.72		0.7	1.6	
		1.51		1.02		1.02		0.91		0.75	0.68	0.91		0.75		0.68		0.62		0.87		0.62	0.74	

# Class Surveys for Geology 101 Found in the Marginaly Green Bay Area

## FACIES KEY

- Northern Margin**  
 1. Northern margin delta
- Tortonian**  
 2. Tempestite  
 3. Storm dominated shelf  
 4. Shoreface
- Messinian**  
 5. Tidal/Storm shelf  
 6. Brackish  
 7. Tidal bar  
 8. Conglomerate matrix (fluvial)  
 9. Conglomerate matrix (marine)

Sample Location		Q3 84	Q3 85	Q3 72	Q3 73
Age		Messinian	Messinian	Upper Mess	Upper Mess
Facies		6	6	8	8
Q-F-Lt (500 points)	%matrix	40	60	11	resin
	% Bloclasts	28	8	0	0
	Qm	314	278	284	288
	P	8	16	29	9
	K	6	4	4	3
Lt (500 points)	Lt	164	102	130	197
	Total F (2+3)	14	20	33	12
Meta Lithics	Ph. Sch	0	0	0	0
	Q-M-F Ag	0	28	4	4
	Q-M-F Tect	0	0	0	0
	Q-M Ag	22	55	12	30
	Q-M Tect	0	0	12	0
	Qp Tect	0	0	4	3
	Micas	106	88	0	19
	Mica p	0	0	0	0
	Qp	28	60	150	63
	Q-F Agg	0	0	0	0
Contact Meta	Contact Meta Minerals	0	0	0	0
Volacanic	Hypabysall	0	0	0	0
	Sand	0	22	27	0
Sediment	Argillite (other than marls)	0	0	10	0
	Carb pc	150	0	127	221
	Marl	136	115	106	139
	Chert	34	0	40	11
	Unknown Lt	14	132	7	10
Contact Meta	Qp (13+10)	28	60	154	66
	Lm(5...9+11+12+14+15)	128	171	28	53
	Lv(16)	0	0	0	0
	Ls(17...21)	320	137	310	371
	Lvm(17)	0	0	0	0
Volacanic	Lsm(Ls+Lm)	448	308	338	424
	Average Grain Size (Phi)	1.93	1.23	0.97	1.47
Sediment	Sorting	0.95	0.66	1.15	0.85



## **Clast Surveys for Conglomerates Found in the Messinian Guadalquivir Basin**

The following data sets represent the results of surveys carried out for the clast population of Messinian conglomerates found in the Guadalquivir Basin. Clasts were sampled at location 9 (Ref. 522 340), location 47 (Ref. 510 340) and location 48 (Ref. 510 340). The parameters measured for each clast were as follows:

### *Long Axis*

The long axis (measured in cm) is defined as the maximum diameter of the clast.

### *Short Axis*

The short axis (measured in cm) is defined as the maximum diameter of the clast.

### *Lithology*

The clast lithologies are defined as follows;

**c.a** Calc-lithic arenites. This lithology is typical of Miocene rocks exposed in the Guadalquivir Basin,

**L** Limestone clasts,

**Ch** Chert clasts (cryptocrystalline quartz),

**m** Any metamorphic clast,

**Dol** Dolomitic limestone clasts,

**i** Any igneous clast,

**q** Quartzite clasts.

### *Angularity*

The angularity of the clasts was estimated in the field and is defined as follows:

**a** Angular and sub-angular clasts,

**r** Rounded and well rounded clasts.

Angularity was not estimated at location 47.

Clast Survey: Lower Messinian Location 9 (Fan Delta)

**Clast No. Long Axis (cm) Short Axis (cm) Lithology Angularity**

1	13	7	c.a	a
2	6	5	c.a	a
3	2	1	l	r
4	5	2	l	a
5	4	3	ch	r
6	4	3	c.a	r
7	6	3	l	r
8	5	3	m	r
9	4	2	m	r
10	5	6	ch	r
11	3	3	ch	r
12	2	1	l	r
13	3	2	dol	a
14	7	4	l	r
15	3	9	ch	r
16	4	2	c.a	r
17	9	2	ch	r
18	3	2	l	r
19	4	1	m	r
20	7	4	ch	r
21	3	3	l	a
22	7	2	ch	r
23	3	4	l	r
24	3	4	l	r
25	4	3	c.a	a
26	7	6	c.a	a
27	3	3	l	a
28	2	1	l	a
29	3	3	l	r
30	1	3	l	r
31	2	4	l	r
32	3	3	ch	r
33	4	5	l	r
34	6	3	l	r
35	2	4	l	r
36	4	4	l	r
37	6	4	c.a	a
38	4	3	c.a	r
39	2	4	c.a	r
40	1	1	m	r
41	4	3	l	a
42	3	2	ch	r
43	2	6	l	a
44	4	3	l	a
45	4	3	l	a
46	5	4	l	a
47	6	4	ch	r
48	6	4	c.a	r
49	3	2	ch	a
50	4	4	l	r

Clast survey: Upper Messinian Location 47 (Fluvial)

Clast No.	Long Axis (cm)	Short Axis (cm)	Lithology
1	11.00	3.00	Q
2	5.00	4.00	Q
3	5.00	4.00	L
4	3.00	1.00	m
5	2.00	2.00	ch
6	6.00	2.00	c.a
7	0.20	0.10	Q
8	0.20	0.10	L
9	0.30	0.20	Q
10	4.00	2.00	ch
11	0.50	0.30	m
12	2.00	1.00	Q
13	3.00	2.00	L
14	2.00	1.00	L
15	2.00	2.00	Q
16	2.00	2.00	L
17	4.00	2.00	L
18	4.00	2.00	L
19	1.00	1.00	Q
20	0.30	0.10	ch
21	2.00	2.00	ch
22	3.00	2.00	m
23	4.00	4.00	Q
24	5.00	5.00	Q
25	3.00	5.00	ch
26	4.00	2.00	Q
27	3.00	5.00	L
28	3.00	3.00	L
29	6.00	4.00	Q
30	3.00	3.00	L
31	2.00	1.00	Q
32	0.10	0.10	ch
33	0.20	0.10	m
34	4.00	4.00	Q
35	8.00	4.00	Q
36	1.00	2.00	L
37	2.00	2.00	L
38	4.00	4.00	L
39	9.00	4.00	m
40	4.00	4.00	ch
41	3.00	2.00	L
42	3.00	1.00	L
43	4.00	3.00	L
44	4.00	2.00	Q
45	3.00	3.00	ch
46	4.00	3.00	ch
47	2.00	2.00	c.a
48	3.00	2.00	c.a
49	4.00	3.00	L
50	5.00	4.00	c.a



Clast Survey: Upper Messinian Location 48 (Fluvial)

Clast No.	Long Axis (cm)	Short Axis (cm)	Lithology	Angularity
1	4	3	ch	r
2	3	3	ch	r
3	2	1	m	r
4	2	2	m	r
5	1	1	Q	r
6	1	1	Q	r
7	1	1	Q	r
8	5	1	s	a
9	20	13	c.a	r
10	4	4	m	r
11	5	9	Q	a
12	6	4	L	r
13	4	2	i	r
14	3	4	ch	a
15	12	8	c.a	r
16	4	2	i	a
17	9	5	c.a	r
18	4	4	ch	a
19	4	3	m	a
20	4	7	c.a	r
21	6	3	m	r
22	2	2	s	r
23	8	4	Q	a
24	7	7	ma	
25	6	5	s	r
26	3	5	Q	a
27	4	2	ch	r
28	8	4	m	r
29	4	4	ch	r
30	3	4	ch	r
31	5	3	b	a
32	4	6	m	r
33	3	9	m	r
34	4	1	i	r
35	9	4	c.a	a
36	4	2	ch	a
37	3	1	ch	a
38	4	1	s	a
39	3	2	s	a
40	3	4	m	a
41	7	9	ch	a
42	14	4	i	a
43	3	2	c.a	a
44	19	14	c.a	a
45	4	6	m	s
46	3	2	ch	s
47	1	1	i	s
48	3	1	ch	s
49	1	1	i	s
50	2	1	i	s

## Palaeocurrent Data

The following data represent the results of palaeocurrent measurements from Messinian conglomerate deposits in the Guadalquivir Basin. Palaeocurrents were measured at location 9 (Ref. 522 340) location 47 (Ref. 510 340) and location 48 (Ref. 510 340).

Palaeocurrents were measured from imbricate clasts at location 9 and from cross-stratification and imbricate clasts at locations 47 & 48. Palaeocurrents are given as a bearing representing direction to which the current flowed

# Palaeocurrent Data

Age Location Facies Source	Lwr Messinian Loc. 9 Fan Delta Imbricate Clasts	Upper Messinian Loc. 47, 48 Fluvial Braided Cross Stratification	Upper Messinian Loc. 47, 48 Fluvial Braided Imbricate Clasts	
	270	220	45	27
	278	180	60	28
	280	210	360	23
	260	240	60	22
	262	240	30	21
	265	220	50	20
	280	180	48	19
	285	240	55	2
	290	250	360	3
	244	260	30	2
	255	260	25	3
	233	220	45	5
	222	360	60	6
	275	350	20	7
	278	348	28	8
	279	33	3	94
	276	320	5	95
	275	270	16	96
	274	268	5	100
	273	25	30	55
	245	245	35	88
	243	246	45	100
	191	150	45	103
	190	158	48	12
	192	149	32	45
	193	180	60	82
	194	180	72	80
	198	178	35	43
	274	120	36	42
	273	124	58	22
	274	330	69	25
	280	300	32	28
	285	301	45	
		310	32	
		320	65	
		160	89	
		160	50	
		140	42	
		170	18	
		270	17	
		300	16	
		300	15	
		312	33	
		180	34	
		313	323	
		314	33	
		315	55	
		340	45	
		310	48	
		290	46	
		290	20	
		22	22	
		310	23	
		311	29	
			25	
			24	
			26	



Mica Analysis

The following data set represents the results of the geochemical analysis of white micas collected from the Guadalquivir Basin and Internal Zones of the Betic Orogen (Granada Basin). The data from the Internal Zones was collected by John Hughes at the University of Glasgow.

All the micas were analysed at the University of Glasgow using a Cameca SX50 electron microprobe. The data was reduced using ZAF techniques and cations per formula unit calculated on the basis of 22 oxygens. The  $Fe^{2+} / Fe^{3+}$  ratio was estimated by ratio, following the methods of Schumacher (1991)

Sample GQ21M.2 GQ21M.6 GQ21M.9 GQ21M.12 GQ5M.3 GQ5M.4 GQ5M.8 GQ37M.8 GQ40M.1 GQ40M.4 GQ40M.5 GQ40M.7 GQ40M.9															
Location	8	8	8	8	8	N.Margin	N.Margin	64	8	8	8	8	8	8	8
SiO2	44.35	59.44	43.47	43.91	46.03	44.79	44.99	44.57	46.53	46.2	44.56	45.44	42.61		
TiO2	0.12	0.44	0.11	0.3	0.26	0.22	0.15	0.12	0.21	0.13	0.26	0.14	0.12		
Al2O3	36.93	19.63	37.22	37.94	35.39	36.43	36.18	36.25	34.67	36.72	36.63	36.23	38.49		
Cr2O3	0	0.05	0.04	0	0.03	0.05	0	0.01	0	0.025	0	0.02	0		
MgO	0.78	0.56	0.83	0.36	0.86	0.76	1.01	0.57	0.99	0.84	0.58	0.76	0.32		
CaO	0.01	0.03	0.44	0.01	0.06	0.02	0	0.01	0.01	0.15	0.07	0	0.12		
MnO	0.03	0.05	0	0	0.02	0	0.02	0.02	0.06	0	0.02	0.01	0.04		
Fe2O3	0.9	0.9	1.35	0.85	1.03	1.19	1.15	1.72	1.46	1.27	1.69	1.27	1.41		
FeO	0.14	0.14	0.21	0.14	0.16	0.19	0.18	0.27	0.23	0.2	0.27	0.2	0.22		
Na2O	1.95	0.14	3.02	0.41	0.7	0.4	0.43	0.52	1.08	3.84	2.47	0.56	6.15		
K2O	5	8.75	3.48	6.24	5.49	6.21	6.08	6.22	4.87	2.94	4.03	6.24	1.04		
Total	90.21	90.13	90.17	90.16	90.03	90.26	90.19	90.28	90.11	92.315	90.58	90.87	90.52		
Si	6.03	8.12	8.15	5.92	6.2	6.09	6.07	6.03	6.31	6.12	6.04	6.15	5.77		
Ti	0.01	0.01	0	0.03	0.03	0.02	0.02	0.01	0.02	0.01	0.03	0.01	0.01		
Al	5.96	3.12	3.06	6.18	5.74	5.88	5.89	5.92	5.54	5.73	5.85	5.78	6.14		
Cr	0	0.01	0	0	0	0.01	0	0	0	0	0	0	0		
Mg	0.12	0.11	0.11	0.07	0.18	0.15	0.21	0.12	0.2	0.17	0.12	0.15	0.07		
Ca	0	0	0.01	0	0.01	0	0	0	0	0.02	0.01	0	0.02		
Mn	0	0.01	0	0	0	0	0	0	0.01	0	0	0	0.01		
Fe3	0.09	0.09	0.12	0.09	0.1	0.12	0.12	0.18	0.15	0.13	0.17	0.13	0.14		
Fe2	0.02	0.02	0.02	0.02	0.02	0.02	0.02	0.03	0.03	0.02	0.03	0.02	0.03		
Na	0.52	0.04	0.04	0.11	0.19	0.11	0.11	0.14	0.29	0.99	0.65	0.15	1.62		
K	0.87	1.53	1.53	1.1	0.96	1.08	1.07	1.1	0.84	0.5	0.7	1.08	0.18		
Total	13.62	13.06	13.04	13.52	13.43	13.48	13.51	13.53	13.39	13.69	13.6	13.47	13.99		

Mica Analysis: Guadalquivir Basin

Sample GQ40M.11 GQ40M.13 F2M.1 F2M.3 F2M.7 F2M.8 GQ7M.3 GQ7M.9 GQ91M.2 GQ91M.3 GQ91M.4 GQ91M.6 GQ91M.9 GQ91M.10															
Location	8	8	93	93	93	93	93	93	5	64	64	64	64	64	64
SiO2	46.42	49.61	69.844	48.44	50.14	46.92	41.94	44.68	45.76	44.02	44.75	45.55	45.58	45.84	
TiO2	0.59	0.23	0.167	0.1	2.28	0.51	7.3	0.51	0.18	0.7	0.17	0.13	0.28	0.2	
Al2O3	35.48	31.54	19.13	30.13	30.37	34.66	33.26	28.47	34.89	36.45	32.11	36.28	32.32	36.16	
Cr2O3	0.02	0.05	0.02	0.04	0.01	0.08	0.14	0.05	0	0.07	0.07	0.02	0.03	0.03	
MgO	0.8	1.64	0.43	2.66	1.55	0.72	0.62	1.45	0.83	0.59	1.37	0.73	1.23	0.64	
CaO	0	0.09	0.08	0.02	0.09	0.11	0	0.06	0	0.04	0.06	0.07	0.04	0	
MnO	0	0.089	0.17	0	0.02	0.05	0.03	0.05	0.01	0.03	0.04	0.03	0.01	0	
Fe2O3	1.08	1.9	0.98	2.75	2.21	1.83	0.9	4.95	1.37	0.86	3.44	1.51	2.25	0.8	
FeO	0.17	0.3	0.16	0.44	0.35	0.29	0.14	0.79	0.22	0.14	0.55	0.24	0.36	0.13	
Na2O	0.52	0.92	1.11	0.11	0.82	1.08	1.29	0.94	0.75	0.95	1.21	2.15	0.68	0.13	
K2O	5.51	4.76	2.18	6.1	3.78	4.48	4.68	8.55	9.12	9.46	7.75	7.22	8.44	8.6	
Total	90.59	91.129	94.271	90.79	91.62	90.73	90.3	90.5	93.13	93.31	91.52	93.93	91.22	92.53	
Si	6.2	6.64	8.62	6.66	6.65	6.31	5.76	6.33	6.18	5.96	6.18	6.06	6.29	6.13	
Ti	0.06	0.02	0.02	0.01	0.23	0.05	0.75	0.06	0.02	0.07	0.02	0.01	0.03	0.02	
Al	5.71	4.98	2.78	4.72	4.75	5.5	5.39	4.73	5.55	5.81	5.23	5.7	5.25	5.7	
Cr	0	0.01	0.01	0	0	0.01	0.02	0.01	0	0.01	0.01	0	0	0	
Mg	0.16	0.33	0.08	0.55	0.31	0.14	0.13	0.31	0.17	0.12	0.28	0.15	0.25	0.13	
Ca	0	0.01	0.01	0	0.01	0.02	0	0.01	0	0.01	0.01	0.01	0.01	0	
Mn	0	0.01	0.02	0	0	0.01	0	0.01	0	0	0.01	0.03	0	0	
Fe3	0.11	0.19	0.1	0.29	0.22	0.19	0.09	0.53	0.14	0.09	0.36	0.15	0.23	0.08	
Fe2	0.02	0.03	0.02	0.05	0.04	0.03	0.02	0.094	0.03	0.02	0.06	0.03	0.04	0.01	
Na	0.14	0.24	0.27	0.03	0.21	0.28	0.34	0.26	0.2	0.25	0.32	0.55	0.18	0.29	
K	0.96	0.81	0.34	1.07	0.64	0.77	0.82	1.56	1.57	1.63	1.37	1.23	1.49	1.47	
Total	13.36	13.27	12.27	13.38	13.06	13.31	13.32	13.904	13.86	13.97	13.85	13.92	13.77	13.83	



Sample	GQ2M.2	GQ2M.4	GQ2M.5	GQ2M.6	GQ2M.7	GQ2M.8	GQ1M.3	GQ1M.4	GQ1M.6	GQ1M.7	GQ1M.10
Location	N.Margin	N.Margin	N.Margin	N.Margin	N.Margin	N.Margin	N.Margin	N.Margin	N.Margin	N.Margin	N.Margin
SiO2	45.43	46.59	44.99	56.35	47.43	44.6	44.56	44.97	44.98	37.21	45.58
TiO2	0.33	0.87	0.25	0.2	0.46	0.24	0.41	0.39	0.59	0	0.05
Al2O3	36.84	32.29	36.92	26.1	32.63	37.54	34.98	37.82	33.98	20.2	33.7
Cr2O3	0.09	0.02	0	0.06	0.08	0.01	0.02	0.02	0	0	0.03
MgO	0.47	0.92	0.43	0.62	0.81	0.45	0.94	0.37	1.03	6.71	1.38
CaO	0.05	0.01	0	0.07	0.16	0.01	0	0.02	0	0.3	0
MnO	0.02	0.04	0.02	0.02	0.05	0	0.06	0	0.03	0.12	0.02
Fe2O3	1.07	1.62	0.96	1.57	2.73	1.089	1.45	0.91	1.84	20.52	2.42
FeO	0.17	0.26	0.15	0.25	0.43	0.17	0.23	0.14	0.29	3.25	0.38
Na2O	0.43	0.52	0.61	1.04	0.79	0.62	0.79	0.57	0.7	0.09	0.53
K2O	6.13	7.13	9.56	4.5	5.71	10.39	9.83	8.48	10.18	2.41	10.35
Total	91.03	90.27	93.89	90.78	91.28	95.119	93.27	93.69	93.62	90.81	94.44
Si	6.13	6.34	6.03	7.54	6.41	5.94	6.05	5.99	6.11	5.45	6.15
Ti	0.03	0.09	0.03	0.02	0.05	0.02	0.04	0.04	0.06	0	0.01
Al	5.86	5.29	5.83	3.96	5.2	5.89	5.6	5.94	5.44	3.59	5.36
Cr	0.01	0	0	0.01	0.01	0	0	0	0	0	0
Mg	0.09	0.19	0.09	0.12	0.16	0.09	0.19	0.07	0.21	1.51	0.28
Ca	0.01	0	0	0.01	0.02	0	0	0	0	0.05	0
Mn	0	0.01	0	0	0.01	0	0.01	0	0	0.02	0
Fe3	0.11	0.17	0.1	0.16	0.28	0.11	0.15	0.092	0.19	2.33	0.25
Fe2	0.02	0.03	0.02	0.03	0.05	0.02	0.03	0.016	0.03	0.41	0.04
Na	0.11	0.14	0.16	0.27	0.21	0.16	0.21	0.146	0.18	0.03	0.14
K	1.06	1.27	1.63	0.77	0.99	1.77	1.7	1.44	1.76	0.46	1.78
Total	13.43	13.53	13.89	12.89	13.39	14	13.98	13.734	13.98	13.85	14.01

	D2-1B	D2-1C	D2-1D	D2-2A	D2-2B	D2-2C	D2-3A	QR2-2D	D2-3B	D2-3C	D2-4A	D2-4B	A3-4	A3-5	A3-6	A3-7	A3-8	A3-9	QR1-6	QR1-2
SiO <sub>2</sub>	45.81	48.76	48.3	48.86	49.66	49.71	49.53	49.95	47.83	49.73	49.01	50.11	45.9	45.6	45.7	46.8	46.9	46.2	50.03	40.25
TiO <sub>2</sub>	0.52	0.58	0.53	0.43	0.45	0.45	0.466	0.44	0.48	0.04	0.53	0.45	0.33	0.33	0.08	0.37	0.24	0.31	0.31	1
Al <sub>2</sub> O <sub>3</sub>	30.2	31.97	31.3	30.96	30.83	30.83	30.4	30.4	29.45	30.34	31.49	30.13	34.8	34.7	38.6	32.4	32.3	33	32.48	26.32
Fe <sub>2</sub> O <sub>3</sub>	1.58	1.49	1.39	1.8	2.04	1.53	1.62	1.62	3.92	1.64	1.7	1.66	1.23	1.14	0.42	1.19	1.25	1.07	0.92	11.95
FeO	0.25	0.23	0.22	0.28	0.32	0.24	0.25	0.25	0.62	0.26	0.27	0.26	0.19	0.18	0.06	0.18	0.19	0.17	0.14	1.89
MnO	0.04	0.6	0	0	0	0.04	0	0	0	0.04	0	0	0	0.98	0.02	0.04	0	0.02	0	0.03
MgO	2.11	2.23	1.96	2.63	2.83	2.49	2.83	2.83	2.147	2.84	2.42	2.96	0.94	0.09	0.29	1.51	1.47	1.31	0.55	5.41
CaO	0	0.04	0.1	0.03	0.09	0.04	0.063	0.06	1.159	0.01	0.06	0.1	0.1	0.09	0.19	0	0.01	0.01	0.01	0.01
Na <sub>2</sub> O	0.76	0.95	1.05	0.75	0.82	0.82	0.822	0.82	0.87	0.05	1.07	0.94	2.27	2.52	6.55	0.95	0.68	0.8	1.52	0.76
K <sub>2</sub> O	9.33	9.74	9.5	9.51	9.52	9.68	9.75	9.75	9.48	9.6	9.56	9.56	6.61	6.96	1.46	9.06	8.89	8.67	7.86	8.47
Total	90.6	96.59	94.35	95.25	96.56	95.83	95.73	96.12	95.96	94.55	96.11	96.17	92.3	92.6	93.3	92.5	92	91.5	93.82	96.09
Si	6.38	6.4	6.45	6.44	6.47	6.52	6.53	6.53	6.38	6.57	6.42	6.56	6.18	6.16	5.97	6.34	6.39	6.31	6.61	5.59
Ti	0.05	0.05	0.53	0.04	0.04	0.04	0.04	0.04	0.04	0.04	0.05	0.04	0.03	0.03	0	0.03	0.02	0.03	0.03	0.1
Al	4.96	4.95	4.93	4.81	4.74	4.76	4.68	4.68	4.63	4.73	4.86	4.65	5.52	5.54	5.94	5.18	5.19	5.31	5.06	4.31
Fe <sub>3</sub>	0.16	0.14	0.14	0.17	0.2	0.15	0.16	0.16	0.39	0.16	0.16	0.16	0.12	0.11	0.04	0.12	0.12	0.11	0.09	1.25
Fe <sub>2</sub>	0.02	0.02	0.02	0.03	0.03	0.02	0.02	0.02	0.07	0.02	0.03	0.02	0.02	0.02	0	0.02	0.02	0.01	0.01	0.22
Mn	0	0	0	0	0	0	0	0	0	0	0	0	0	0.11	0	0	0	0	0	0
Mg	0.44	0.43	0.39	0.51	0.55	0.48	0.55	0.55	0.42	0.56	0.47	0.57	0.18	0.01	0.05	0.3	0.29	0.26	0.11	1.12
Ca	0	0	0.01	0	0.01	0	0	0	0.16	0	0	0.01	0.01	0.01	0.02	0	0	0	0	0
Na	0.2	0.24	0.27	0.19	0.2	0.21	0.2	0.2	0.22	0.01	0.27	0.24	0.59	0.66	1.66	0.25	0.18	0.21	0.38	0.2
K	1.65	1.63	1.62	1.6	1.58	1.62	1.62	1.62	1.61	1.62	1.6	1.59	1.13	1.2	0.24	1.56	1.54	1.51	1.32	1.5
Total	13.86	13.86	14.36	13.79	13.82	13.8	13.8	13.8	13.92	13.71	13.86	13.84	13.8	13.9	13.9	13.8	13.8	13.8	13.61	14.29

cations per formula unit calculated on the basis of 22 oxygens

Mica Analysis: Internal Zones (Granada Basin).



	QR2-1	QR2-2B	QR2-2B	QR2-3A	QR2-4B	QR2-4C	D2-5C	D2-5D	D2-5E	D2-6A	D2-6B	D2-6D	D2-7A	D2-7B	D2-7C	D2-8B	D2-8C	D2-8D
SiO2	47.66	47.4	47.4	47.3	46.53	46.71	49.32	48.74	48.78	48.01	49.01	49.31	46.12	47.01	47.32	46.22	48.77	48.6
TiO2	0.47	0.49	0.48	0.49	0.35	0.25	0.55	0.5	0.49	0.49	0.58	0.43	0.56	0.48	0.59	0.37	0.37	0.35
Al2O3	29.65	29.05	29.45	31.61	29.99	30.89	30.79	31.28	31.43	32.46	32.3	30.9	31.77	32.19	31.71	31.7	30.02	29.76
Fe2O3	3.7	4.05	3.92	1.72	3.1	3.14	1.73	1.6	1.56	1.53	1.56	1.62	1.31	1.41	1.38	1.51	1.7	1.8
FeO	0.59	0.64	0.62	0.27	0.49	0.49	0.27	0.25	0.24	0.24	0.24	0.25	0.2	0.22	0.21	0.24	0.27	0.28
MnO	0	0.04	0	0	0.05	0.02	0	0	0	0	0	0.04	0.06	0.02	0	0.01	0	0
MgO	2.34	2.36	2.14	2.24	2.039	1.86	2.93	2.17	2.35	2.09	2.03	2.62	1.77	1.79	1.96	1.68	2.66	2.68
CaO	0.053	0	0	0.05	0.12	0.02	0.07	0	0.06	0.04	0.06	0.06	0.04	0.04	0	0.09	0	0.03
Na2O	0.95	0.89	1.15	1.05	1.38	1.25	1.06	0.89	0.88	0.88	1.14	0.89	0.95	0.96	1.01	1	0.85	0.86
K2O	9.74	9.67	9.48	9.22	9.27	9.2	9.76	9.67	9.64	9.81	9.64	9.89	9.31	9.41	9.45	9.43	9.56	9.65
Total	95.15	94.59	94.64	93.95	93.319	93.83	96.48	95.1	95.43	95.55	96.56	96.01	92.09	93.53	93.63	92.25	94.2	94.01
Si	6.4	6.41	6.4	6.35	6.35	6.32	6.46	6.46	6.44	6.34	6.39	6.48	6.3	6.33	6.37	6.33	6.52	6.53
Ti	0.04	0.05	0.04	0.05	0.03	0.02	0.05	0.05	0.04	0.04	0.05	0.04	0.05	0.04	0.06	0.03	0.03	0.03
Al	4.69	4.63	4.68	5	4.83	4.93	4.75	4.89	4.89	5.06	4.96	4.79	5.12	5.11	5.03	5.12	4.73	4.71
Fe3	0.37	0.41	0.39	0.175	0.31	0.32	0.17	0.16	0.15	0.15	0.15	0.16	0.13	0.14	0.14	0.15	0.17	0.18
Fe2	0.06	0.07	0.07	0.031	0.05	0.05	0.03	0.02	0.02	0.02	0.02	0.02	0.02	0.02	0.02	0.02	0.03	0.03
Mn	0	0	0	0	0	0	0	0	0	0	0	0	0	0	0	0	0	0
Mg	0.46	0.47	0.43	0.44	0.41	0.37	0.57	0.43	0.46	0.41	0.39	0.51	0.36	0.36	0.39	0.34	0.53	0.53
Ca	0	0	0	0	0.01	0	0.01	0	0	0	0	0	0	0	0	0.01	0	0
Na	0.24	0.23	0.3	0.27	0.36	0.33	0.27	0.23	0.22	0.22	0.28	0.22	0.25	0.25	0.26	0.26	0.22	0.22
K	1.66	1.67	1.63	1.58	1.61	1.59	1.63	1.63	1.62	1.65	1.6	1.66	1.62	1.61	1.62	1.64	1.63	1.65
Total	13.92	13.94	13.94	13.896	13.96	13.93	13.94	13.87	13.84	13.89	13.84	13.88	13.85	13.86	13.89	13.9	13.86	13.88

Mica Analysis: Internal Zones (Granada Basin).



	D2-9A	D2-9B	D2-9C
SiO2	47.41	47.09	46.4
TiO2	0.47	0.45	0.44
Al2O3	31.07	30.56	30.44
Fe2O3	1.48	1.44	1.55
FeO	0.23	0.22	0.24
MnO	0.83	0	0
MgO	2.21	2.22	2.06
CaO	0	0.01	0.02
Na2O	0.84	0.94	0.84
K2O	9.47	9.38	9.37
Total	94.01	92.31	91.36
Si	6.41	6.43	6.41
Ti	0.04	0.04	0.04
Al	4.95	4.92	4.95
Fe3	0.15	0.14	0.16
Fe2	0.02	0.02	0.02
Mn	0.01	0	0
Mg	0.44	0.45	0.42
Ca	0	0	0
Na	0.22	0.24	0.22
K	1.63	1.63	1.65
Total	13.87	13.87	13.87

Mica Analysis: Internal Zones (Granada Basin).

### **Measured Pillar Height from the Aljibe Arenites**

The following data is the result of measurements made in the Aljibe Arenites in the Gibraltar Arc (Study Area 2; Part II, Fig. 1.1)

The vertical heights of pillar structures were measured. Pillars are defined in Part II. Chapter 2 (Section 2.3.4)

Measured Pillar Height (cm) in the Aljibe Arenites

---

46	3	30	10	14
13	5	9	10	15
62	32	65	37	25
20	80	37	120	13
4	23	52	3	25
3	5	15	7	21
4	6	13	17	10
5	4	17	10	18
4	4	45	8	6
3	33	28	9	12
9	35	32	22	15
16	18	49	9	14
5	16	83	7	35
7	5	88	95	19
3	14	16	12	17
4	7	18	12	9
20	7	22	8	9
8	7	16	13	8
5	12	18	11	16
26	15	29	15	37
14	39	27	10	8
60	28	21	57	8
14	5	21	12	5
60	5	3	4	25
15	7	3	7	33
13	8	3	19	6
22	4	85	3	15
20	5	29	11	18
30	7	27	22	12
48	27	19	11	34
113	15	80	12	
163	15	45	27	
163	9	15	38	
5	29	58	17	
4	20	25	11	
8	24	10	18	
4	3	30	6	
5	2	47	28	
8	5	10	7	
16	7	8	31	
4	45	17	4	
4	6	16	6	
8	7	24	7	
2	18	23	18	
2	5	46	7	
3	4	38	7	
2	28	10	7	
6	15	55	8	
7	14	71	4	
8	9	16	10	
22	17	3	20	
8	3	18	6	

---



# ***Appendix V***

## ***Locations, Grid References & Maps***

The following pages give the most important localities and their grid references for the Guadalquivir Basin and Gibraltar Arc Flysch study areas. Grid references refer to the grids given in 1:50000 geological maps. Where appropriate the maps included in this thesis, which display the location numbers, are also cited. The geological maps are published by the Instituto Geologico Minero de Espana, Madrid, Spain. These maps can be obtained from most government book-sellers in Spain.

The geological maps have topographic base maps, which are as follows:

#### **Guadalquivir Basin**

<b>1:50.000 Geological Map</b>	<b>Topographic Map</b>
Sheet 944 (16-38)	Geografica dibujo y reproduccion: Instituto Geografico y Industria (16-38)
Sheet 945 (17-38)	A.M.S Serie M 781 (17-38)
Sheet 966 (16-39)	A.M.S Serie M 781 (16-39)
Sheet 967 (17-39)	A.M.S Serie M 781 (17-39)

#### **Gibraltar Arc Flysch**

<b>1:50.000 Geological Map</b>	<b>Topographic Map</b>
Sheet 1.064 (14-45)	Servicio Geografico del Ejercito (14-45)

**Note:** Not all topographic maps are available to the public.



## Guadalquivir Basin Locations

Location Grid Ref.		Geological Map	Publisher	Thesis Map
5	529 343	1:50,000, Sheet 945 (17-38)	IGME, Spain	n/a
8	515 331	1:50,000, Sheet 966 (16-39)	IGME, Spain	Foldout 2 (map)
9	522 340	1:50,000, Sheet 966 (16-39)	IGME, Spain	Foldout 2 (map)
10	515 331	1:50,000, Sheet 966 (16-39)	IGME, Spain	Foldout 2 (map)
18	543 334	1:50,000, Sheet 967 (17-39)	IGME, Spain	Foldout 1 (map)
19	540 431	1:50,000, Sheet 967 (17-39)	IGME, Spain	Foldout 1 (map)
20	540 431	1:50,000, Sheet 967 (17-39)	IGME, Spain	Foldout 1 (map)
21	541 331	1:50,000, Sheet 967 (17-39)	IGME, Spain	Foldout 1 (map)
22	541 331	1:50,000, Sheet 967 (17-39)	IGME, Spain	Foldout 1 (map)
23	541 331	1:50,000, Sheet 967 (17-39)	IGME, Spain	Foldout 1 (map)
27	540 329	1:50,000, Sheet 967 (17-39)	IGME, Spain	Foldout 1 (map)
28	540 329	1:50,000, Sheet 967 (17-39)	IGME, Spain	Foldout 1 (map)
28b	540 329	1:50,000, Sheet 967 (17-39)	IGME, Spain	Foldout 1 (map)
29	543 329	1:50,000, Sheet 967 (17-39)	IGME, Spain	Foldout 1 (map)
30	543 338	1:50,000, Sheet 967 (17-39)	IGME, Spain	Foldout 1 (map)
31	543 339	1:50,000, Sheet 967 (17-39)	IGME, Spain	Foldout 1 (map)
32	543 340	1:50,000, Sheet 967 (17-39)	IGME, Spain	Foldout 1 (map)
33	531 330	1:50,000, Sheet 967 (17-39)	IGME, Spain	Foldout 1 (map)
34	531 329	1:50,000, Sheet 967 (17-39)	IGME, Spain	Foldout 1 (map)
35	531 330	1:50,000, Sheet 967 (17-39)	IGME, Spain	Foldout 1 (map)
36	531 331	1:50,000, Sheet 967 (17-39)	IGME, Spain	Foldout 1 (map)
37	530 330	1:50,000, Sheet 967 (17-39)	IGME, Spain	Foldout 1 (map)
38	532 333	1:50,000, Sheet 967 (17-39)	IGME, Spain	Foldout 1 (map)
39	530 334	1:50,000, Sheet 967 (17-39)	IGME, Spain	Foldout 1 (map)
40	530 334	1:50,000, Sheet 967 (17-39)	IGME, Spain	Foldout 1 (map)
41	532 340	1:50,000, Sheet 967 (17-39)	IGME, Spain	Foldout 1 (map)
42	532 339	1:50,000, Sheet 967 (17-39)	IGME, Spain	Foldout 1 (map)
43	534 338	1:50,000, Sheet 967 (17-39)	IGME, Spain	Foldout 1 (map)
44	514 325	1:50,000, Sheet 966 (16-39)	IGME, Spain	Foldout 2 (map)
46	511 338	1:50,000, Sheet 966 (16-39)	IGME, Spain	Foldout 2 (map)
47	510 340	1:50,000, Sheet 966 (16-39)	IGME, Spain	Foldout 2 (map)
48	510 340	1:50,000, Sheet 966 (16-39)	IGME, Spain	Foldout 2 (map)
49	510 335	1:50,000, Sheet 966 (16-39)	IGME, Spain	Foldout 2 (map)
50	503 332	1:50,000, Sheet 966 (16-39)	IGME, Spain	Foldout 2 (map)
51	503 332	1:50,000, Sheet 966 (16-39)	IGME, Spain	Foldout 2 (map)
52	508 335	1:50,000, Sheet 966 (16-39)	IGME, Spain	Foldout 2 (map)
52(a)	508 336	1:50,000, Sheet 966 (16-39)	IGME, Spain	Foldout 2 (map)
53	513 323	1:50,000, Sheet 966 (16-39)	IGME, Spain	Foldout 2 (map)
54	513 324	1:50,000, Sheet 966 (16-39)	IGME, Spain	Foldout 2 (map)
55	511 324	1:50,000, Sheet 966 (16-39)	IGME, Spain	Foldout 2 (map)
56	510 324	1:50,000, Sheet 966 (16-39)	IGME, Spain	Foldout 2 (map)
58	502 329	1:50,000, Sheet 966 (16-39)	IGME, Spain	Foldout 2 (map)
59	497 333	1:50,000, Sheet 966 (16-39)	IGME, Spain	Foldout 2 (map)
60	597 335	1:50,000, Sheet 966 (16-39)	IGME, Spain	Foldout 2 (map)
61	506 334	1:50,000, Sheet 966 (16-39)	IGME, Spain	Foldout 2 (map)
62	514 325	1:50,000, Sheet 966 (16-39)	IGME, Spain	Foldout 2 (map)
63	515 324	1:50,000, Sheet 966 (16-39)	IGME, Spain	Foldout 2 (map)
64	514 330	1:50,000, Sheet 966 (16-39)	IGME, Spain	Foldout 2 (map)
65	517 332	1:50,000, Sheet 966 (16-39)	IGME, Spain	Foldout 2 (map)
66	517 332	1:50,000, Sheet 966 (16-39)	IGME, Spain	Foldout 2 (map)
67	517 334	1:50,000, Sheet 966 (16-39)	IGME, Spain	Foldout 2 (map)
68	517 333	1:50,000, Sheet 966 (16-39)	IGME, Spain	Foldout 2 (map)
69	519 335	1:50,000, Sheet 966 (16-39)	IGME, Spain	Foldout 2 (map)



70	519 335	1:50,000, Sheet 966 (16-39)	IGME, Spain	Foldout 2 (map)
71	523 341	1:50,000, Sheet 966 (16-39)	IGME, Spain	Foldout 2 (map)
72	505 336	1:50,000, Sheet 966 (16-39)	IGME, Spain	Foldout 2 (map)
73	504 336	1:50,000, Sheet 966 (16-39)	IGME, Spain	Foldout 2 (map)
74	337 502	1:50,000, Sheet 966 (16-39)	IGME, Spain	Foldout 2 (map)
75	500 339	1:50,000, Sheet 966 (16-39)	IGME, Spain	Foldout 2 (map)
76	507 336	1:50,000, Sheet 966 (16-39)	IGME, Spain	Foldout 2 (map)
77	507 336	1:50,000, Sheet 966 (16-39)	IGME, Spain	Foldout 2 (map)
78	508 338	1:50,000, Sheet 966 (16-39)	IGME, Spain	Foldout 2 (map)
79	500 327	1:50,000, Sheet 966 (16-39)	IGME, Spain	Foldout 2 (map)
80	505 328	1:50,000, Sheet 966 (16-39)	IGME, Spain	Foldout 2 (map)
81	524 345	1:50,000, Sheet 944 (16-38)	IGME, Spain	Foldout 3 (map)
82	524 343	1:50,000, Sheet 944 (16-38)	IGME, Spain	Foldout 3 (map)
83	524 344	1:50,000, Sheet 944 (16-38)	IGME, Spain	Foldout 3 (map)
84	524 343	1:50,000, Sheet 944 (16-38)	IGME, Spain	Foldout 3 (map)
85	524 344	1:50,000, Sheet 944 (16-38)	IGME, Spain	Foldout 3 (map)
86	523 344	1:50,000, Sheet 944 (16-38)	IGME, Spain	Foldout 3 (map)
87	521 346	1:50,000, Sheet 944 (16-38)	IGME, Spain	Foldout 3 (map)
88	521 346	1:50,000, Sheet 944 (16-38)	IGME, Spain	Foldout 3 (map)
89	522 346	1:50,000, Sheet 944 (16-38)	IGME, Spain	Foldout 3 (map)
90	523 347	1:50,000, Sheet 944 (16-38)	IGME, Spain	Foldout 3 (map)
91	521 348	1:50,000, Sheet 944 (16-38)	IGME, Spain	Foldout 3 (map)
92	522 343	1:50,000, Sheet 944 (16-38)	IGME, Spain	Foldout 3 (map)
93	521 343	1:50,000, Sheet 944 (16-38)	IGME, Spain	Foldout 3 (map)
94	518 352	1:50,000, Sheet 944 (16-38)	IGME, Spain	Foldout 3 (map)
95	358 520	1:50,000, Sheet 944 (16-38)	IGME, Spain	Foldout 3 (map)
96	523 353	1:50,000, Sheet 944 (16-38)	IGME, Spain	Foldout 3 (map)
97	522 351	1:50,000, Sheet 944 (16-38)	IGME, Spain	Foldout 3 (map)
98	512 345	1:50,000, Sheet 944 (16-38)	IGME, Spain	Foldout 3 (map)
99	510 344	1:50,000, Sheet 944 (16-38)	IGME, Spain	Foldout 3 (map)
100	508 349	1:50,000, Sheet 944 (16-38)	IGME, Spain	Foldout 3 (map)



## Gibraltar Arc Flysch Locations

Location Grid Ref.		Geological Map	Publisher	Thesis Map
6	274 052	1:50000, Sheet 1.064 (14-45)	IGME Spain	n/a
7	275 052	1:50000, Sheet 1.064 (14-45)	IGME Spain	n/a
8	275 052	1:50000, Sheet 1.064 (14-45)	IGME Spain	n/a
9	275 053	1:50000, Sheet 1.064 (14-45)	IGME Spain	n/a
10	275 053	1:50000, Sheet 1.064 (14-45)	IGME Spain	n/a
11	276 053	1:50000, Sheet 1.064 (14-45)	IGME Spain	n/a
12	276 053	1:50000, Sheet 1.064 (14-45)	IGME Spain	n/a
13	275 054	1:50000, Sheet 1.064 (14-45)	IGME Spain	n/a
14	275 054	1:50000, Sheet 1.064 (14-45)	IGME Spain	n/a
15	275 054	1:50000, Sheet 1.064 (14-45)	IGME Spain	n/a
16	278 054	1:50000, Sheet 1.064 (14-45)	IGME Spain	n/a
17	279 055	1:50000, Sheet 1.064 (14-45)	IGME Spain	n/a
18	280 055	1:50000, Sheet 1.064 (14-45)	IGME Spain	n/a
19	280 055	1:50000, Sheet 1.064 (14-45)	IGME Spain	n/a
20	281 055	1:50000, Sheet 1.064 (14-45)	IGME Spain	n/a
21	283 054	1:50000, Sheet 1.064 (14-45)	IGME Spain	n/a
22	283 055	1:50000, Sheet 1.064 (14-45)	IGME Spain	n/a
23	284 055	1:50000, Sheet 1.064 (14-45)	IGME Spain	n/a
24	284 055	1:50000, Sheet 1.064 (14-45)	IGME Spain	n/a
25	284 055	1:50000, Sheet 1.064 (14-45)	IGME Spain	n/a
26	285 066	1:50000, Sheet 1.064 (14-45)	IGME Spain	n/a
27	286 054	1:50000, Sheet 1.064 (14-45)	IGME Spain	n/a
28	286 053	1:50000, Sheet 1.064 (14-45)	IGME Spain	n/a
31	287 052	1:50000, Sheet 1.064 (14-45)	IGME Spain	Part II, Fig. 1.4
32	287 052	1:50000, Sheet 1.064 (14-45)	IGME Spain	Part II, Fig. 1.4
33	287 052	1:50000, Sheet 1.064 (14-45)	IGME Spain	Part II, Fig. 1.4
34	287 052	1:50000, Sheet 1.064 (14-45)	IGME Spain	Part II, Fig. 1.4
35	286 052	1:50000, Sheet 1.064 (14-45)	IGME Spain	Part II, Fig. 1.4
36	286 052	1:50000, Sheet 1.064 (14-45)	IGME Spain	Part II, Fig. 1.4
37	286 052	1:50000, Sheet 1.064 (14-45)	IGME Spain	Part II, Fig. 1.4
38	286 052	1:50000, Sheet 1.064 (14-45)	IGME Spain	Part II, Fig. 1.4
39	286 052	1:50000, Sheet 1.064 (14-45)	IGME Spain	Part II, Fig. 1.4
40	285 051	1:50000, Sheet 1.064 (14-45)	IGME Spain	Part II, Fig. 1.5
41	285 051	1:50000, Sheet 1.064 (14-45)	IGME Spain	Part II, Fig. 1.5
42	285 051	1:50000, Sheet 1.064 (14-45)	IGME Spain	Part II, Fig. 1.5
43	285 051	1:50000, Sheet 1.064 (14-45)	IGME Spain	Part II, Fig. 1.5
44	285 050	1:50000, Sheet 1.064 (14-45)	IGME Spain	Part II, Fig. 1.5
45	285 050	1:50000, Sheet 1.064 (14-45)	IGME Spain	Part II, Fig. 1.5
46	284 050	1:50000, Sheet 1.064 (14-45)	IGME Spain	Part II, Fig. 1.5
47	284 050	1:50000, Sheet 1.064 (14-45)	IGME Spain	Part II, Fig. 1.5
48	284 050	1:50000, Sheet 1.064 (14-45)	IGME Spain	Part II, Fig. 1.5
49	284 049	1:50000, Sheet 1.064 (14-45)	IGME Spain	Part II, Fig. 1.5
50	284 049	1:50000, Sheet 1.064 (14-45)	IGME Spain	Part II, Fig. 1.5
51	284 048	1:50000, Sheet 1.064 (14-45)	IGME Spain	Part II, Fig. 1.5
52	284 048	1:50000, Sheet 1.064 (14-45)	IGME Spain	Part II, Fig. 1.5
52	284 048	1:50000, Sheet 1.064 (14-45)	IGME Spain	Part II, Fig. 1.5
53	284 048	1:50000, Sheet 1.064 (14-45)	IGME Spain	Part II, Fig. 1.5
54	284 048	1:50000, Sheet 1.064 (14-45)	IGME Spain	Part II, Fig. 1.5
55	284 048	1:50000, Sheet 1.064 (14-45)	IGME Spain	Part II, Fig. 1.5
56	284 049	1:50000, Sheet 1.064 (14-45)	IGME Spain	Part II, Fig. 1.5
57	283 049	1:50000, Sheet 1.064 (14-45)	IGME Spain	Part II, Fig. 1.5
58	283 049	1:50000, Sheet 1.064 (14-45)	IGME Spain	Part II, Fig. 1.5
59	283 049	1:50000, Sheet 1.064 (14-45)	IGME Spain	Part II, Fig. 1.5

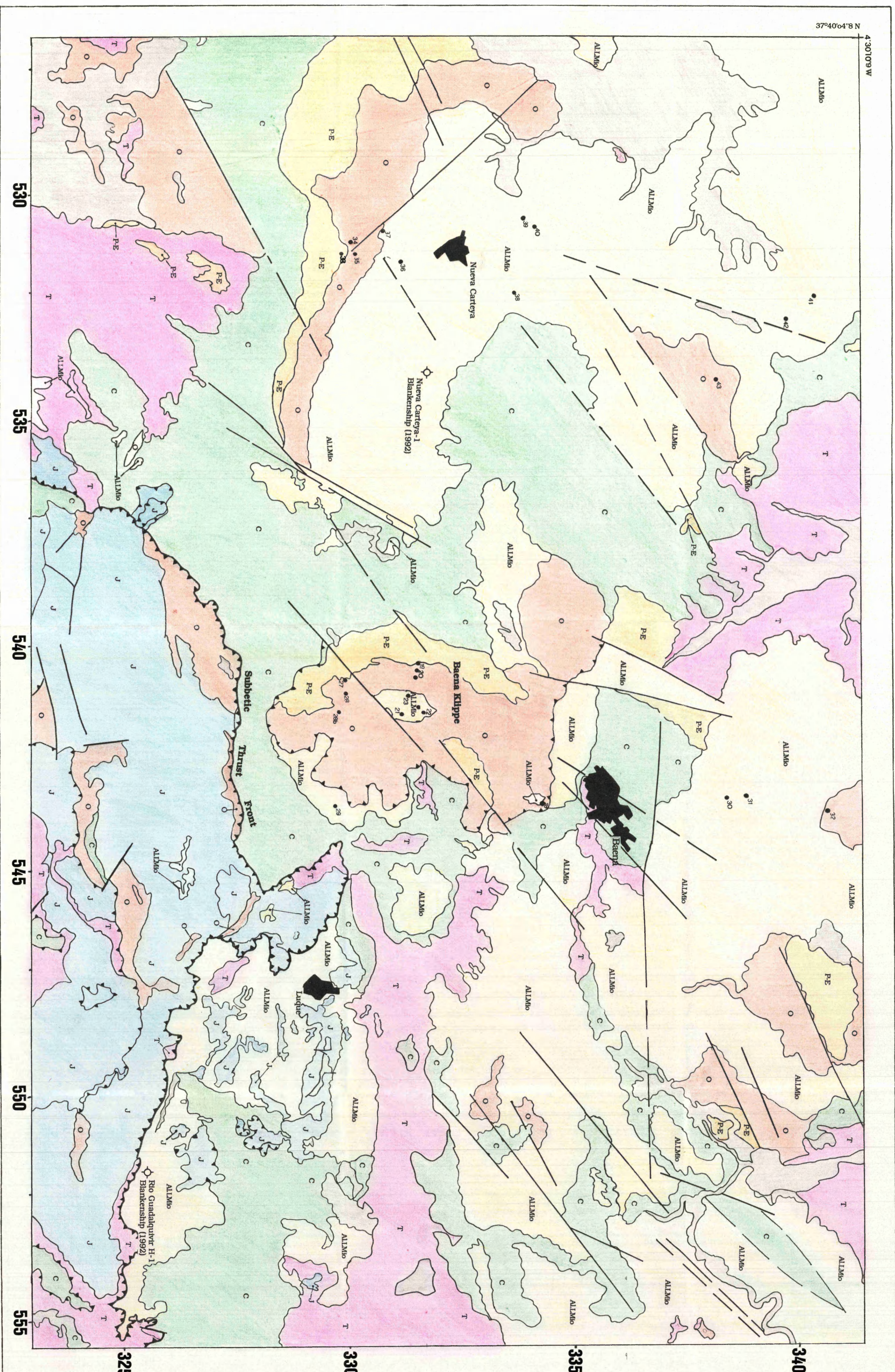
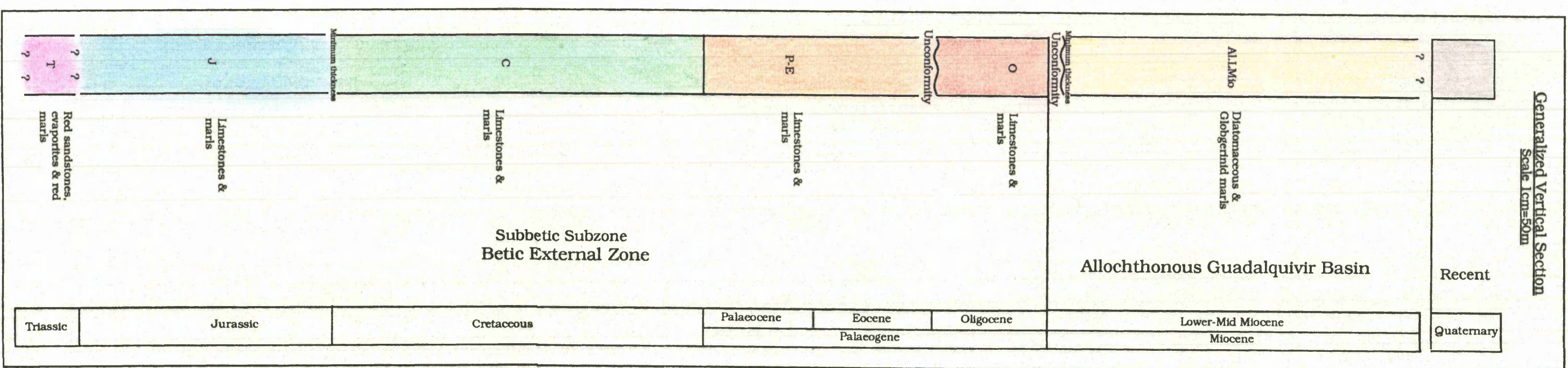


60	283 050	1:50000, Sheet 1.064 (14-45)	IGME Spain	Part II, Fig. 1.5
61	283 050	1:50000, Sheet 1.064 (14-45)	IGME Spain	Part II, Fig. 1.5
62	283 050	1:50000, Sheet 1.064 (14-45)	IGME Spain	Part II, Fig. 1.5
63	283 051	1:50000, Sheet 1.064 (14-45)	IGME Spain	Part II, Fig. 1.5
64	282 051	1:50000, Sheet 1.064 (14-45)	IGME Spain	Part II, Fig. 1.5
65	282 050	1:50000, Sheet 1.064 (14-45)	IGME Spain	Part II, Fig. 1.5
66	282 050	1:50000, Sheet 1.064 (14-45)	IGME Spain	Part II, Fig. 1.5
67	282 050	1:50000, Sheet 1.064 (14-45)	IGME Spain	Part II, Fig. 1.5
68	282 049	1:50000, Sheet 1.064 (14-45)	IGME Spain	Part II, Fig. 1.5
69	281 049	1:50000, Sheet 1.064 (14-45)	IGME Spain	Part II, Fig. 1.5
70	280 049	1:50000, Sheet 1.064 (14-45)	IGME Spain	n/a
71	280 049	1:50000, Sheet 1.064 (14-45)	IGME Spain	n/a
72	279 048	1:50000, Sheet 1.064 (14-45)	IGME Spain	n/a
73	286 047	1:50000, Sheet 1.064 (14-45)	IGME Spain	n/a
74	285 047	1:50000, Sheet 1.064 (14-45)	IGME Spain	Part II, Fig. 1.6
75	285 047	1:50000, Sheet 1.064 (14-45)	IGME Spain	Part II, Fig. 1.6
76	285 047	1:50000, Sheet 1.064 (14-45)	IGME Spain	Part II, Fig. 1.6
77	284 047	1:50000, Sheet 1.064 (14-45)	IGME Spain	Part II, Fig. 1.6
78	284 047	1:50000, Sheet 1.064 (14-45)	IGME Spain	Part II, Fig. 1.6
79	284 047	1:50000, Sheet 1.064 (14-45)	IGME Spain	Part II, Fig. 1.6
80	284 047	1:50000, Sheet 1.064 (14-45)	IGME Spain	Part II, Fig. 1.6
81	284 047	1:50000, Sheet 1.064 (14-45)	IGME Spain	Part II, Fig. 1.6
82	283 046	1:50000, Sheet 1.064 (14-45)	IGME Spain	Part II, Fig. 1.6
83	283 046	1:50000, Sheet 1.064 (14-45)	IGME Spain	Part II, Fig. 1.6
84	283 046	1:50000, Sheet 1.064 (14-45)	IGME Spain	Part II, Fig. 1.6
85	283 046	1:50000, Sheet 1.064 (14-45)	IGME Spain	Part II, Fig. 1.6
86	282 047	1:50000, Sheet 1.064 (14-45)	IGME Spain	Part II, Fig. 1.6
87	282 047	1:50000, Sheet 1.064 (14-45)	IGME Spain	Part II, Fig. 1.6
88	282 047	1:50000, Sheet 1.064 (14-45)	IGME Spain	Part II, Fig. 1.6
89	282 047	1:50000, Sheet 1.064 (14-45)	IGME Spain	Part II, Fig. 1.6
90	282 047	1:50000, Sheet 1.064 (14-45)	IGME Spain	Part II, Fig. 1.6
91	281 047	1:50000, Sheet 1.064 (14-45)	IGME Spain	Part II, Fig. 1.6

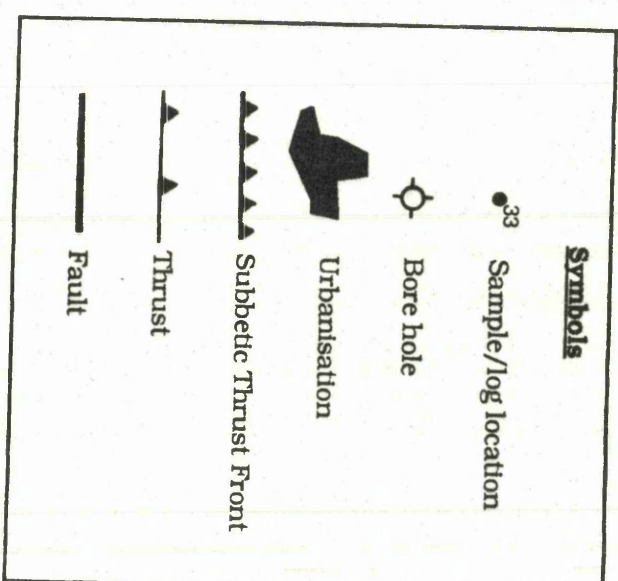


GUADALQUIVIR BASIN (BAENA MONTILLA REGION) MAP 1

SCALE 1:50,000



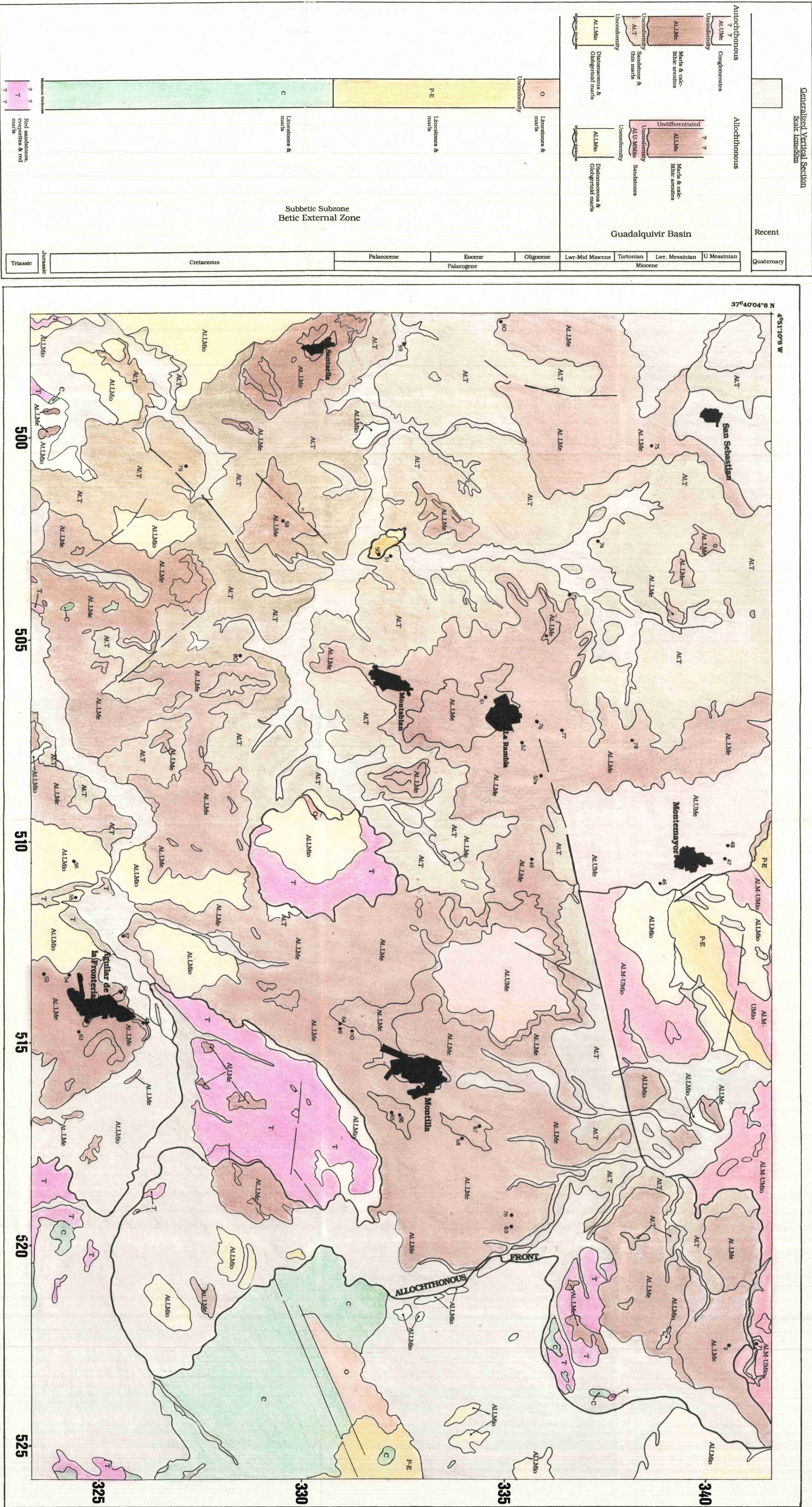
Modified from Roldán García (1985)





GUADALQUIVIR BASIN (BAENA-MONTILLA REGION) MAP 2

SCALE 1:50,000



Modified from Roldán García (1985)

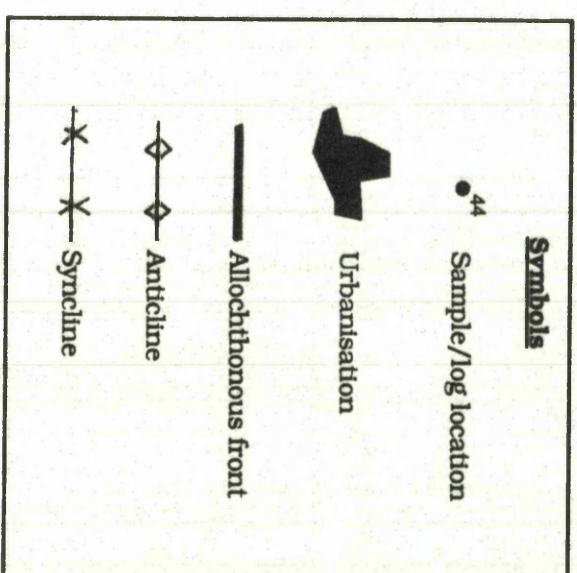
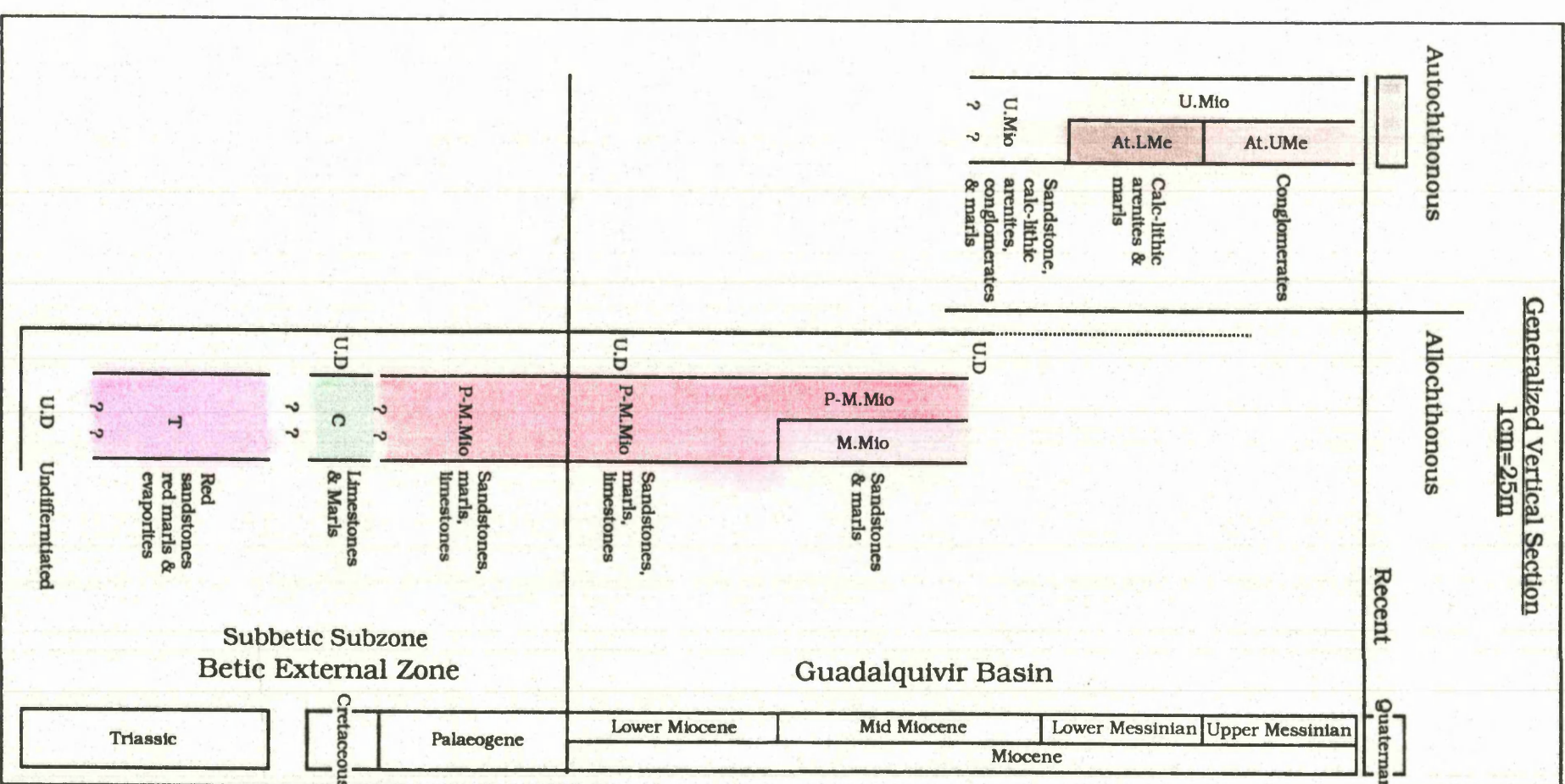


Guadalquivir Basin (Baena Montilla Region) Map 3

Scale 1:50,000

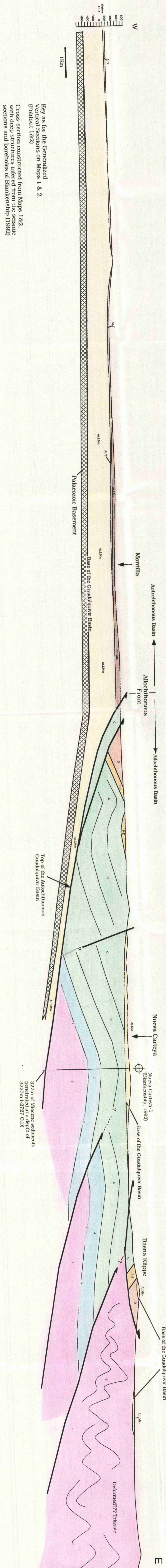


Modified from Leyva Cabello (1973)





E-W Cross Section Across Maps 1 & 2 of the Guadalquivir Basin (Baena Montilla Region).  
Scale 1:50,000



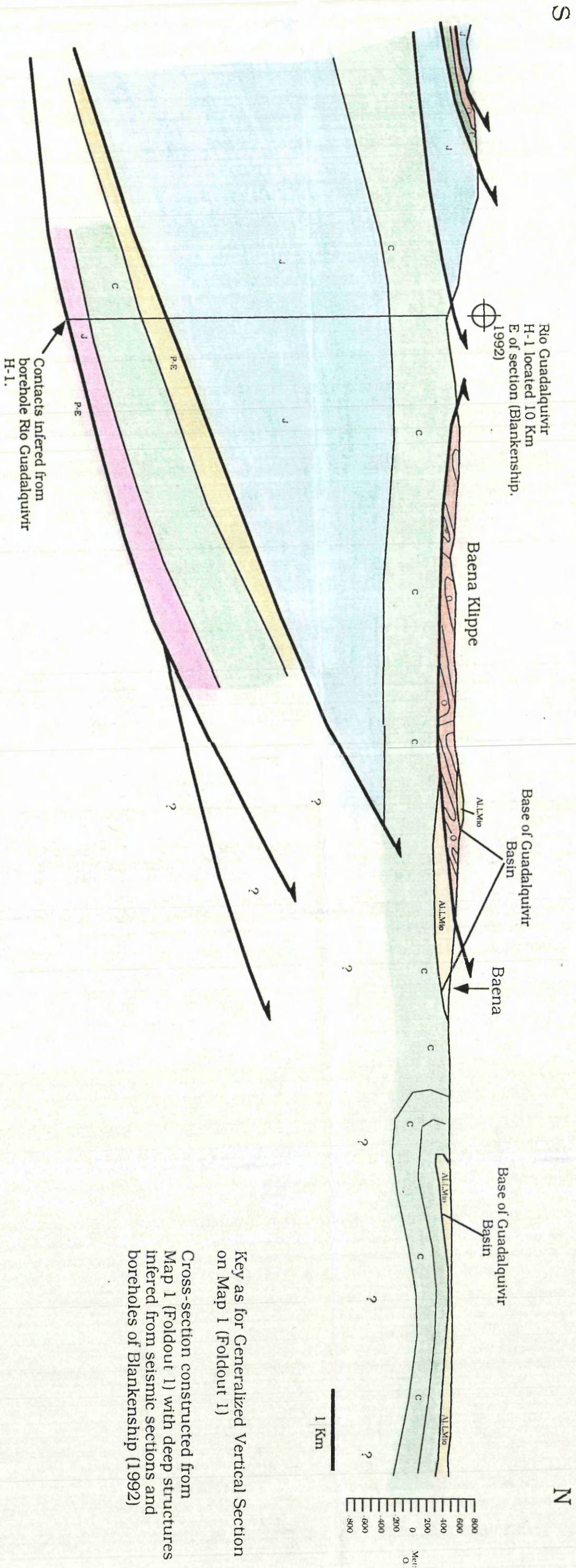
Key as for the Generalized Vertical Sections on Maps 1 & 2. (Foldout 182)

Cross-section constructed from Maps 182 with deep structures inferred from the seismic sections and boreholes of Blankenship (1992)



# S-N Cross-Section Across Map 1 of the Guadalquivir Basin (Baena-Montilla Region)

Scale 1:50,000

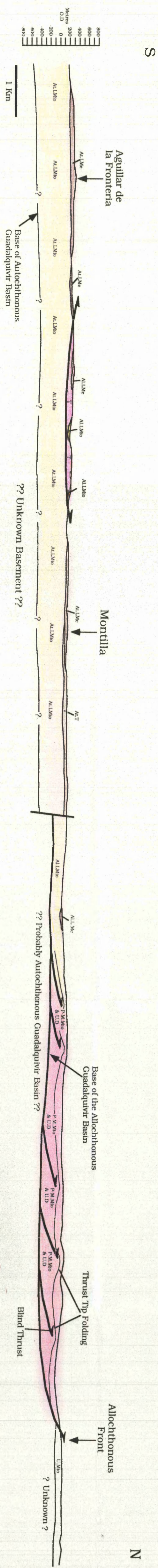


Key as for Generalized Vertical Section on Map 1 (Foldout 1)

Cross-section constructed from Map 1 (Foldout 1) with deep structures inferred from seismic sections and boreholes of Blankenship (1992)



S-N Cross-Section Across Maps 2 & 3 of the Guadalquivir Basin (Baena-Montilla Region)  
Scale 1:50,000



Key as for Generalized Vertical  
Sections on Maps 2 & 3

Cross-section constructed from  
Maps 2 & 3 with thrusts inferred  
from E-W Cross-section (Foldout 4)  
and seismic sections of Blankenship  
(1992)